Synthesis of magnetic nanoparticles and nanocomposites via water-in-oil microemulsions

SYNTHESIS OF MAGNETIC NANOPARTICLES AND NANOCOMPOSITES VIA WATER-IN-OIL MICROEMULSIONS

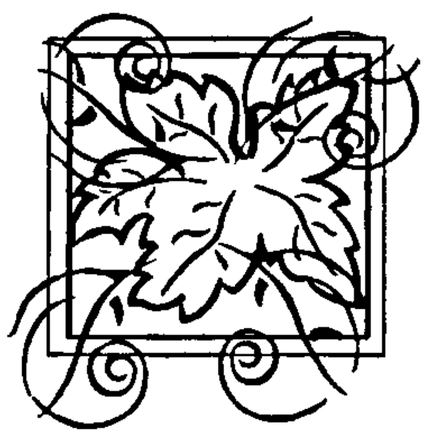

MIAN LIN

May 2006

A document submitted in partial fulfilment of the requirements of Loughborough University for Degree of Doctor of Philosophy

To DongDong,

For the skirts of the past time...

ACKNOWLEDGEMENTS

I am deeply indebted to my supervisor Dr. Xujin Bao, whose help, stimulating suggestions and encouragement, gave me invaluable support throughout the time of research, writing of this thesis and all my difficult days in this country.

Forever love to my dad and mum, my grandfather and grandmother... my pleasant, warm big family.

Special thanks goes to dear Lei & Li, current post-graduate students in Loughborough University, who brought me a colourful life during the last three years and shared with me a lovely story about "Once a takeaway".

Particularly, I would like to thank Lala, by whose company I experienced most amazing places and very moments.

Last but not least, I would like to express my gratitude to all those who helped me to complete this thesis.

ABSTRACT

The effects of surfactants, co-surfactants, aqueous phase and temperature on the solubilisation capability of microemulsion systems were investigated. Appropriate water-in-oil (w/o) microemulsion systems for the synthesis of nanomaterials were selected in consideration of the higher solubilisation and the better thermo-stability.

Mono-dispersed iron oxide nanoparticles with the size of 1-5 nm were synthesised via Igepal CO-520/cyclohexane w/o microemulsion at 25°C. The size of particles increased from 1 nm to 10 nm with the increase of the size of water pools. The original particles as prepared were identified as magnetite, which transformed into maghemite after 2-hour hydrothermal at 120°C and into hematite after 2-hour hydrothermal at 140°C, accompanied with the increased crystallite size. Precipitation was employed for basic studies of starting materials, reaction time and temperature. Compared with precipitation-derived particles, microemulsion-derived nanoparticles show smaller particle size, are less aggregated and exhibit higher activities and a lower saturation magnetisation and coercivity both at 5K and 300K.

Poly-(methacrylic acid) (PMAA), Polyacrylamide (PAM) nano-spheres were synthesised via Triton X-114/cyclohexane and Brij 97/cyclohexane w/o microemulsions at 60°C, respectively. The size of PMMA spheres is 30-100nm while the size of PAM spheres increased from 50 nm to 200 nm with the increase of surfactant concentration from 19.3% to 28.9%. The increased size of water pools from 2.43 to 4.32 also resulted in the increased size of PAM from 50 nm to 500 nm. The effects of reaction time and temperature, and reagent concentration on PAM polymerisation in microemulsion were investigated in terms of the conversion, molecular weight and morphology of polymers produced.

Core-shell structured silica coated iron oxide nanoparticles were synthesised via Igepal CO-520/cyclohexane systems at 25°C, with 5 nm core and 5 nm shell. Nanocomposites of PAM embedded with iron oxide were synthesised in Brij 97/cyclohexane at 60°C, with the size of 120 nm. The crystallinity of magnetic nanoparticles was affected by the coating process.

CONTENTS

ACKNOWLEDGEMENTS
ABSTRACT
ABBREVIATIONS

1. INTRODUCTION 1

2. LITERATURE SURVEY 4

2.1 Nanotechnology 4

2.2 Applicable methods 6
2.2.1 Properties of nano-structured materials 6
2.2.2 Applied methods in fabricating nano-structured materials ... 9
2.2.3 Comparison and limitation 12

2.3 Dressing up 15
2.3.1 What is core-shell structure 15
2.3.2 Applicable method into core-shell 18

2.4 Microemulsions 18
2.4.1 Internal structure of microemulsions 18
2.4.2 Water-in-oil microemulsions 21
2.4.3 Analysis on behaviours of microemulsion 22
2.4.4 Applications 27

2.5 Novel approach 28
2.5.1 Synthesis of magnetic nanoparticles via w/o microemulsions 30
2.5.2 Synthesis of core-shell structured nanocomposites via microemulsion 40

3. EXPERIMENTAL DETAILS 60

3.1 Materials 60

3.2 Investigation of w/o microemulsions 61

3.3 Synthesis of nanomaterials via w/o microemulsions 63
3.3.1 Synthesis of iron oxide nanoparticles 64
3.3.2 Synthesis of polymer nano-spheres 65
3.3.3 Synthesis of silica nano-spheres 66
3.3.4 Synthesis of nanocomposites of iron oxide with ceramics/polymer 66

3.4 Synthesis of iron oxide nanoparticles by other methods 67

3.5 Characterisation 68

4. APPROPRIATE W/O MICROEMULSION SYSTEMS 71

4.1 INVESTIGATION OF W/O MICROEMULSIONS 71
4.1.1 Studies on different surfactants 71
4.1.2 Studies on addition of co-surfactants 75
4.1.3 Studies on aqueous phases 77
4.1.4 Studies on temperature 79

4.2 DISCUSSIONS 81
4.2.1 Effect of surfactant (co-surfactant) and oil 82
4.2.2 Effect of aqueous phase 90
4.2.3 Effect of temperature 93
4.2.4 Non-ionic and ionic surfactants 95
SUMMARY 96

5. SYNTHESIS OF NANO-MAGNETS 97

5.1 PREPARATION OF IRON OXIDE NANOPARTICLES 97
5.1.1 Preparation by precipitation method 98
5.1.2 Preparation by w/o microemulsion 104
5.1.3 Studies on post-heat treatment 110
5.1.4 Magnetism characterisation 122

5.2 DISCUSSIONS 124
5.2.1 Investigation of reaction parameters by precipitation 124
5.2.2 Synthesis of nano-magnets via w/o microemulsions 131
5.2.3 Investigation of post-heat-treatments 133
SUMMARY 140

6. POLYMERISATION IN W/O MICROEMULSIONS 141

6.1 PREPARATION OF POLYMER NANO-SPHERES 141
6.1.1 Acrylamide partitioning in oil and water 141
6.1.2 Studies on different surfactants 142
6.1.3 Studies on initiator in AM polymerisation 144
6.1.4 Studies on reaction temperature and time of AM polymerisation 146
6.1.5 Studies on crosslinking 149
6.1.6 Studies on AM concentration in polymerisation 151
6.1.7 Studies on microemulsion system control 154
6.1.8 Preparation of PMAA nano-spheres 158

6.2 DISCUSSIONS 161
6.2.1 General consideration of AM polymerisation via w/o microemulsions 163
6.2.2 Effect of initiator 166
6.2.3 Effect of crosslinking 168
6.2.4 Effect of monomer concentration 170
6.2.5 Investigation of system-controlled polymerisation 173
6.2.6 Investigation of the synthesis of PMAA 176
SUMMARY 180

7. SYNTHESIS OF NANOCOMPOSITES **181**

7.1 PREPARATION OF SILICA/IRON OXIDE NANOCOMPOSITES **181**

7.1.1 Preparation of silica nano-spheres 182

7.1.2 Preparation of silica coated nanocomposites 185

7.2 PREPARATION OF PAM/IRON OXIDE NANOCOMPOSITES **190**

7.3 DISCUSSIONS **193**

7.3.1 Free-water in synthesis of silica coated nano-composites ... 193

7.3.2 Comparison between different nanocomposites synthesised .. 198

SUMMARY 199

8. CONCLUSIONS AND PERSPECTIVES **200**

REFERENCE

APPENDICES

I. Preparation of magnetic nanocomposition via water-in-oil microemulsion

Preparation of nanometer-sized polymethacrylic acid particles in water-in oil microemulsions

II. Structures & properties of materials used in experiments

III. Characteristic values of iron oxide samples

ABBREVIATIONS

α:	Mark-Houwink parameter
γ:	Surface tension of solid-solvent
η:	Viscosity
η_{red}:	Reduced viscosity
η_{rel}:	Relative viscosity
η_{sp}:	Specific viscosity
$[\eta]$:	Intrinsic viscosity
θ:	Diffraction angle
λ:	Wavelength of monochromatic X-ray beam
σ_o:	Lattice yield stress
σ_s:	Saturation magnetisation
σ_y:	Yield strength
τ:	Time
Φ:	Volume fraction of surfactant
ω_o:	Molar ratio of water to surfactant
a_o:	The head group area of surfactant molecule
ab:	nucleation period
AIBN:	Azobisisobutyronitrile
ABCN:	1,1'-Azobiscyclohexane-1-carbonitrile
AM:	Acrylamide
[AM]:	Mol concentration of acrylamide
bc:	Growth period
BP:	Boiling point
BPO:	Benzoyl peroxide
c:	Solution concentration
C:	Average mean curvature of interface in microemulsion
cd:	re-crystallisation period
CMC:	Critical Micelle Concentration
CP:	Cloud Point
C_s:	Solute concentration
CVD:	Chemical Vapour Deposition
d:	Average grain size
d_c:	Critical grain size
D:	Diameter of particles
D_h:	Hydrodynamic radius (the radius of water core)
EO:	Ethylene oxide
f	Initiator efficiency
FTIR:	Fourier Transform Infrared spectrometry (FTIR)
H:	Hardness
H:	Enthalpy
H_o:	Single crystal hardness
Hc:	Coercivity
HLB:	Hydrophile-Lipophile Balance
[I]:	Initiator concentration

k_d:	Decomposition rate
K:	Mark-Houwink parameter
K:	Constant
k_p:	Rate constant of propagation
k_t:	Rate constant of termination
KP:	Krafft Point
KPS:	Potassium persulfate
L:	Isotropic liquid phase (microemulsion structure)
L_α:	lamellar liquid crystalline phase
l:	Effective length of the surfactant molecule
MBA:	N, N'-methylen-bisacrylamide
M:	Molarity
[M]:	Monomer concentration
M_o:	Molecular weight of surfactant molecule
MAA:	methacrylic acid
M_m:	Molecular weight of micelle
$\overline{M_n}$:	Number average molecular weight
$\overline{M_v}$:	Viscosity average molecular weight
M_s:	Spontaneous magnetisation
M_T:	Remnant magnetisation MT
[MBA]:	Mol concentration of crosslinking agent
n:	Aggregation number
O:	oil phase
PE:	Petroleum ether
PMMA:	polymethylmethacrylate
POE:	Polyoxyethylenated
PVD:	Physical Vapour Deposition
r_l:	Radius of large particles
r_s:	Radius of small particles
R:	Packing ratio of surfactant molecules
R_p:	Polymerisation rate
RHT:	Molar ratio of H_2O to TEOS
S:	Entropy
S_{max}:	Maximum solubilisation of aqueous phase
S-w_{max}:	Maximum solubilisation of water
SQUID:	Superconducting quantum interference device
STM:	Scanning Tunnelling Microscope
$t_{1/2}$:	Half-life
T_c:	Curie Temperature
TEM:	Transmission Electron Microscope
$v_{c\text{-}max}$:	Maximum crystallisation rate
V_m:	Molar volume of the solute molecules
V_s:	Molecular volume of the hydrocarbon chain
W:	Water phase
w/o:	Water-in-oil
X_s:	Crystallite size
XRD:	X-ray diffractometry

INTRODUCTION

Nano-scaled materials can be defined as those whose characteristic length scale lies within the range between one and several hundreds of nanometers, which exhibit novel electrical, mechanical, chemical, optical and magnetic properties, compared with their corresponding bulk materials.

With the development of nanotechnology, the fabrication of magnetic nanoparticles attracts more attentions due to their wide applications in information storage, colour imaging, magnetic refrigeration [1], bio-processing [2], medical diagnosis [3] and controlled drug delivery [4]. Various techniques have been developed to prepare iron oxide nanoparticles. Having the promising control of the particles' size and morphology with high homogeneity, the water-in-oil (w/o) microemulsion, as a spatially and geometrically restricted media, is advancing more rapidly in the synthesis of nano-scaled particles including magnetic metal oxides such as magnetite [6-7] and maghemite [8-9] and organic polymers [10]. The superiority of w/o microemulsion systems in nano-synthesis area arises from its featured structure in which the aqueous droplets of the system can be used as a nano-reaction vessel for the preparation of finely divided materials [5].

However, nano-structured particles posses large surface areas and often form agglomerates as a result of attractive van der Waals forces [11] of minimising the total surface or interfacial energy. On the other hand, magnetic nanomaterials would undergo rapid biodegradation when being directly exposed to the biological system which limits their applications in biotechnology and biomedical engineering. Therefore, a coating process should be applied not only to avoid the aggregation, but also to prevent the biodegradation. For instance, silica-coated magnetic nanoparticles can be immobilised with the antibody to deliver them into a specific target via the antibody-antigen recognition. The

polymer/magnet nanocomposites can be more easily dispersed in organic solutions, which would be very useful for efficient bio-molecule separation and magnetically guided biosensor applications [12]. Since the restricted environment offered by the w/o microemulsion system provides better control over the particle morphology and inter-particle spacing, it was also employed as a novel technique in the synthesis of nanocomposites, especially the core-shell structured nanomaterials.

The main objectives of this project are to synthesise iron oxide nanoparticles, poly-(methacrylic acid) (PMAA) and poly-acrylamide (PAM) nano-spheres, silica coated nanocomposites and PAM/iron oxide nanocomposites via w/o microemulsion systems. The studies will include the systematic investigation of w/o microemulsions and the effect of reaction parameters, especially the microemulsion-dependent factors on the properties of synthetic nanomaterials.

The morphology of nanoparticles and nanocomposites, including the size, shape and the inter-structure was characterised by transmission electron microscope (TEM). Silica-coated iron oxide nanoparticles were further examined using a TEM equipped with thin window energy dispersive X-ray analysis (EDX). The crystallinity of magnetic nanomaterials was identified by X-ray diffractometry (XRD). The magnetism of iron oxide nanoparticles was measured by a superconducting quantum interference device (SQUID). Fourier transform infrared spectrometry (FTIR) was employed in the characterisation of polymer nano-spheres and polymer/iron oxide nanocomposites. The molecular weight of polymer nano-spheres was calculated by dilute solution viscosity measurements with an Ostwald viscometer.

THESIS OUTLINE

Chapter 2 is the literature survey about the topic-related content of this thesis covering: the development of nanotechnology and nano-synthesis; the definition and properties of the w/o microemulsion and the synthesis of magnetic nanomaterials via w/o microemulsion systems.

Chapter 3 provides an insight to the details of the synthesis and the characterisation of samples.

Chapter 4 investigates the influence of various factors, i.e. the effect of surfactants, co-surfactants, component ratio and temperatures on behaviours of w/o microemulsions, to find out an appropriate system for the further fabrication. Different behaviours of microemulsions in different circumstances are discussed in terms of the structure-derived interactions and geometrically packing considerations.

Chapter 5 presents the synthesis of iron oxide nanoparticles via w/o microemulsion systems. Precipitation was also involved to make comparisons and systematic investigations of reaction conditions. Hydrothermal and calcinations were employed as post-heat-treatments. The magnetic nanoparticles synthesised by different methods were studied through the mechanism of crystal growth and the thermodynamically dependent phase transition happening on iron oxide nanoparticles synthesised from a macro- and a nano- environment, respectively.

Chapter 6 deals with the microemulsion polymerisation of acrylamide and methacrylic acid. The effects of reaction time and temperature, initiator, crosslinking and microemulsion-dependent factors were investigated. The mechanism of microemulsion polymerisation of AM was mainly studied in terms of the morphology of polymer nano-spheres.

Chapter 7 summarises the synthesis of silica/iron oxide and PAM/iron oxide nanocomposites via w/o microemulsions. The effect of coating process on the properties of original magnetic nanoparticles was discussed in terms of the particular interactions exists in the core-shell structure.

Chapter 8 describes the main conclusions and future work of this project.

2 LITERATURE SURVEY

2.1 NANOTECHNOLOGY: HISTORY AND DEVELOPMENT

A nanometre is one billionth of one metre (10^{-9} m, about 3-4 atoms wide). The term "nano-structured" describes materials with structure on length scales from 1 to 100 nm [13]. Nano-structured materials often have unique electrical, chemical, structural, and magnetic properties [14-17], which is so important that it gradually directs scientists' traditional research towards the nano-scale exploration. Nanotechnology, the science and technology of precisely controlling the structure of matter at the molecular level (nano-scale), is widely viewed as the most significant technological frontier currently being explored in the 21st century.

In 1958, the great physicist Richard Feynman [18] suggested that it should be possible to build machines small enough to manufacture objects with atomic precision. This was the first vision of the possibilities of science and technology at the nano-scale [19]. The term "nanotechnology" was coined in 1974 by Norio Taniguchi of the University of Tokyo [18] to denote "production technology to get the extra high accuracy and ultra fine dimensions, i.e. the preciseness and fineness on the order of 1 nanometre". Taniguchi predicted that within 15 years there would be machining methods capable of sub-100 nm dimensional precision which was largely proven correct.

What is most amazing about the development of nanotechnology is the pace at which it has advanced. By the early 1990s, nano-technology's capabilities could not only image and probe atomic structures, but also move individual atoms, one at a time, around on a substrate. One early demonstration of the power came in 1990 when team of IBM physicists revealed that they had, the year before, spelled out

the letters "IBM" using 35 individual atoms of xenon **[Figure 2.1-1]**. In 1991, the same research team built an "atomic switch" likely to be an important development in the future of computing [18]. The "Quantum Stadium" image generated by IBM researchers provides another poignant example of the ability of controlling the position of atoms **[Figure 2.1-2]**. The image consists of 76 iron atoms on a copper substrate. Wave patterns in the interior are from the density distribution of trapped electrons [21].

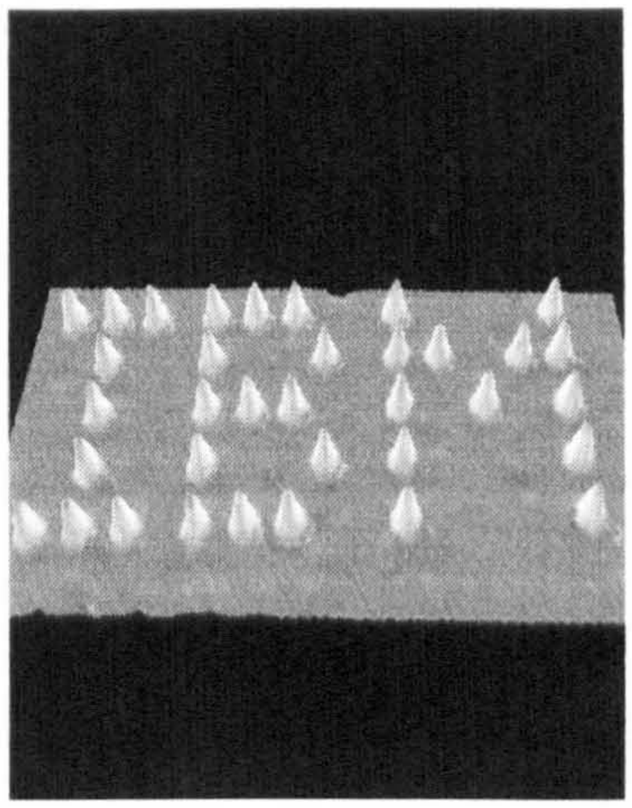

Figure 2.1-1 The IBM logo on atomic scale. All right reserved [20].

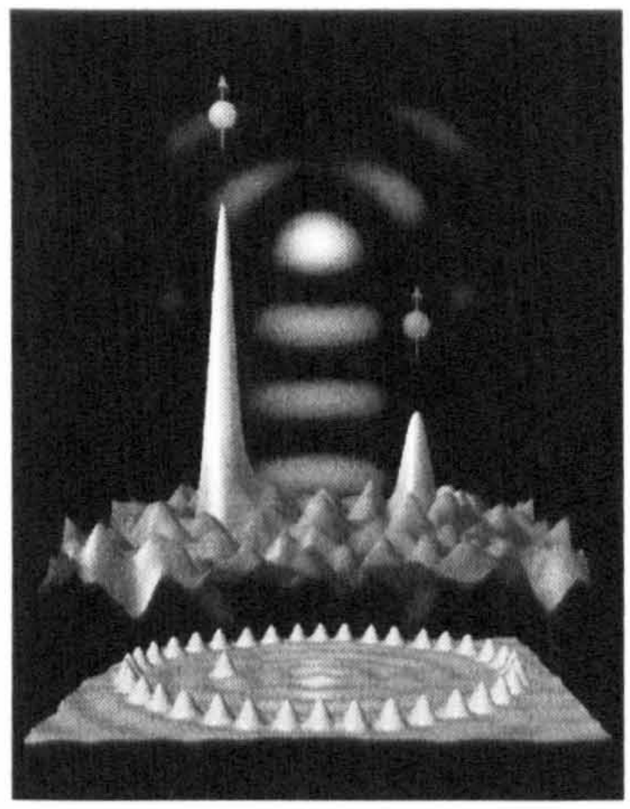

Figure 2.1-2 Quantum Stadium. Courtesy: IBM, Almaden Research Center. All right reserved [20].

Having recognised the potential of nanotechnology, governments started to support the development in their economies by directing special funding to the area. The leading countries today are USA and Japan. The scale of funding is large, up to several hundred million USD per annum in these two countries. At the same time governmental research and development decision makers all over the world are setting up new nanotechnology-specific research programs aiming at putting their respective countries in a favourable position for the future. There are more than 4000 companies and research institutes are dealing with nano-technique all over the world [22]. The global spending was 7.4 billion USD in 2002 and will increase up to 26.0 billion USD by 2006. The total markets for nanotechnology worldwide will grow from 110.6 billion USD in 2003 to 299.9 billion USD in 2006 and 891.1 billion USD in 2015 [22]. This growth rate is very rapid and it does not show signs of slowing down. The sales to date have been largely domestic, but with the increasing global interest on the development of

nanotechnology and with the advantage of modern communication we can safely speculate that this could be a very profitable investment in the near future.

Nanotechnology is a cross-section technology and will redefine all known technologies and markets in the 21st century. On a short-term basis, nanotechnology will complement and change life science, pharmacy, diagnostic, medicine technology, food, environmental technology, water, energy, electronics, and mechanical engineering and so on. Although in the past twenty years, nano-science has truly made a big progress, and some nanotechnology-based products are already on the market and others will follow, nanotechnology as a whole is still an emerging area. The world markets for pure nanotech products only come to a few billions USD, markets and products using nanotech are already many times bigger. The global growth rates will, according to branch and application, amount to 8-21% per annual in the next 15 years [22].

2.2 APPLICABLE METHODS: SYNTHESIS OF NANO-STRUCTURED MATERIALS

There are a number of processes currently used for producing nanomaterials. Before introducing these methods, the novel properties of nano-structured materials will be briefly described in advance.

2.2.1 Properties of nano-structured materials

The promise of nanotechnology is based upon the ability to create nano-structured materials that will produce novel properties on the macro scale [21]. However, in many cases, the mechanisms behind these observed properties are not yet clearly understood, it is still possible to attribute, by inference, the novel qualities of these nanomaterials to the following changes in internal structure.

1. When the diameter of grain falls into nano-scale, the fraction of surface atoms becomes dominant

with the ratio of atoms on the surface to the total increased [**Figure 2.2-1**]. The increased surface areas will alter the physical properties of nanomaterials.

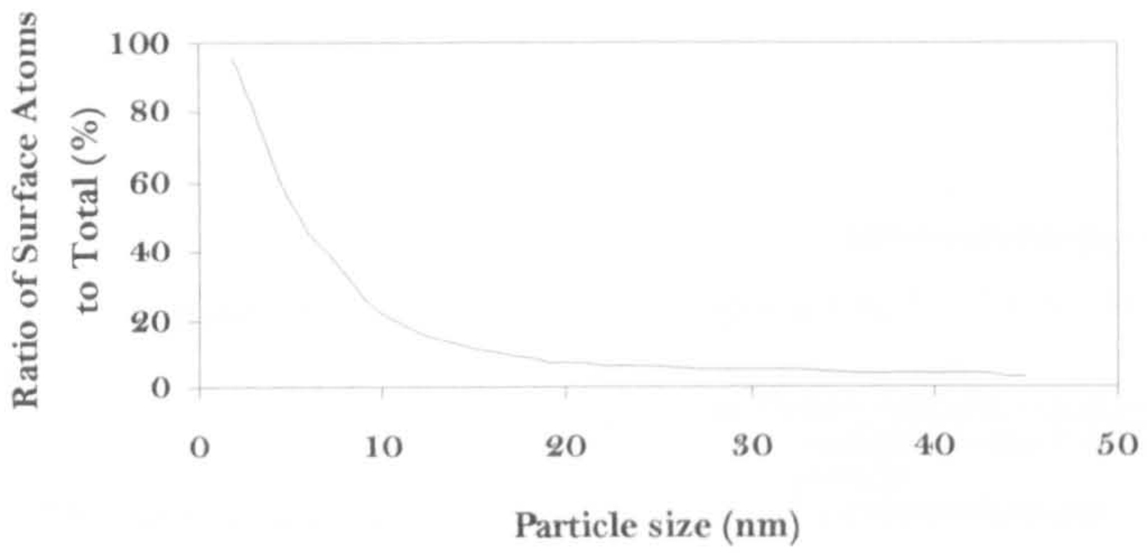

Figure 2.2-1 The relationship between the number of surface atoms and particle size.

2. Discrete electronic levels (quantum behaviour) will alter the electrical and optical properties of nanomaterials as grain size approach the nano-scale. The discrete energies associated with electron orbits become more evident as grain size < 5 nm, creating non-linear property effects [21].

- **Magnetic Properties**

The fundamental motivation for the fabrication and study of nano-scaled magnetic materials is the dramatic change in magnetic properties when the critical length is comparable to the nanoparticles or nano-crystal size. For example, the ultra fine alloy particles of iron series exhibit much stronger magnetism comparing with bulk materials. It also has superior thermal conductivity especially at the low temperature [21]. The magnetisation of ferromagnetic materials is very sensitive to the size and structure of the sample [23]. If the sample consists of small particles, its magnetisation decreases with the particle sizes, because small particles finally reach a super-paramagnetic state with reduced exchange inter-particle interactions [24-25].

- **Mechanical Properties**

The mechanical properties of nanomaterials is that the strength and hardness follow the Hall-Petch relationship, i.e. they increase with the increase of the grain size, up to a critical dimension (~10 nm)

and decreased after that [**Figure 2.2-2**] [26]. In practice, nano-structured metals and ceramics generally show super-plasticity at 200°C which is lower than micro-structured materials. The improved formability is of much importance to ceramics [21].

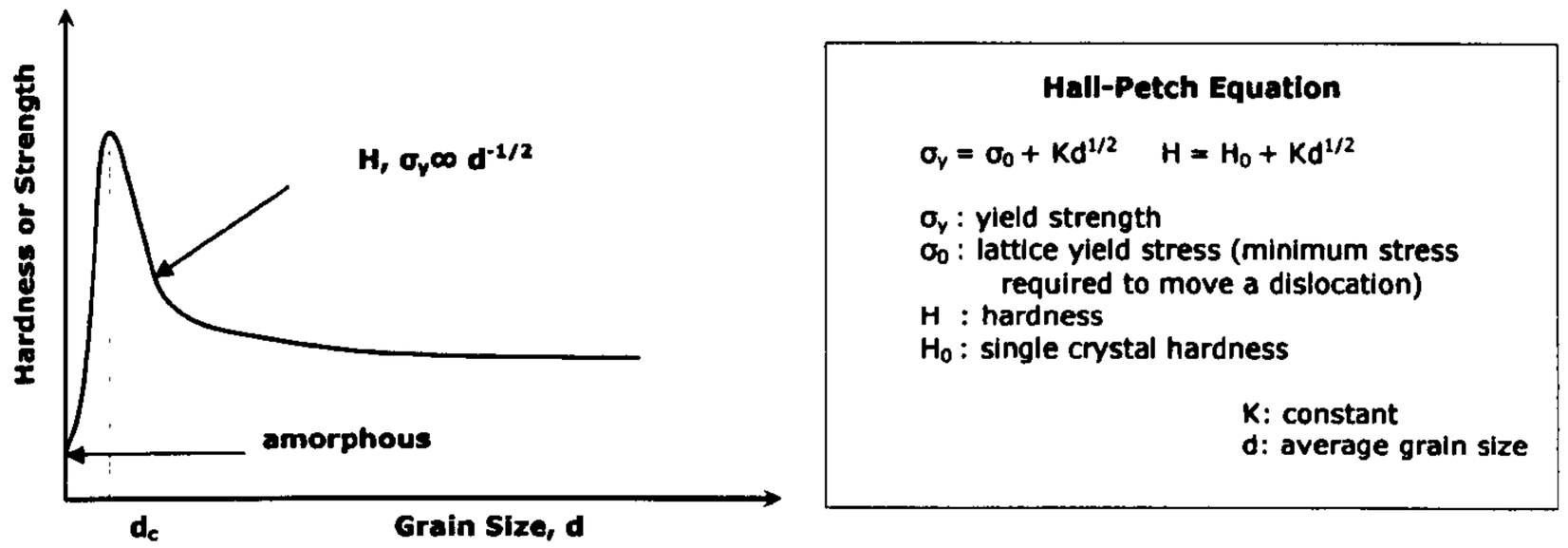

Figure 2.2-2 Strength/Hardness of nano-structured materials [26]

- **Chemical Reactivity & Electrical Properties**

Large numbers of atoms on the surface of nano-crystallites provide active sites for reactions leading to an increased chemical activity. Quantum effect in nanomaterials produces a non-linear dependence of electrical conductivity on electric field and can produce electron tunnelling characteristics [26].

- **Thermal Properties**

The decreased thermal conductivity and melting point of nano-structured metals might be observed (such as a 27°C lower melting point for gold), which is attributed to the enhanced diffusibility, meanwhile an increased thermal expansion coefficient might be obtained.

- **Optical Properties**

As having the ultra small size of grains in nano-structured materials, the absorbance of the light by the particulates can be different. For example, the colour of larger cadmium selenide particles is black, however with the crystallite size of ~1.5 nm, the materials appears yellow and if the size was increased to 4 nm, the materials will appear red [27].

2.2.2 Applied methods in fabricating nano-structured materials

Over the past 15 years nano-sized materials have been prepared from a variety of physical or chemical methods. Mechanical grind is one of the most fundamental physical methods, which could be regarded as a "top-down" process, involving re-structuring a bulk material in order to create a nanostructure [28]. Another physical process commonly used to produce nano-structured materials is **Physical vapour deposition** (PVD).

As one of chemical methods, **Chemical vapour deposition** (CVD) involves a gas-phase chemical reaction which forms a solid material on a substrate, which is commonly used to produce nano-structured ceramics and composites. **Precipitation Method**, **Sol-Gel Process** and **Hydrothermal** are another three major chemical methods. Further discussing about them will be given in this chapter. **Electro-deposition** has been used to form nano-crystalline materials with the grain size of 5 nm. Pascal C *et al.* [29] reported the synthesis of maghemite nanoparticles by **electro-deposition process**. Besides the methods mentioned above, Ziolo *et al.* [30-31] also reported the **Matrix-Mediated Synthesis** of maghemite nano-crystallites in aqueous solution using $FeCl_2 \cdot 4H_2O$ as raw material. Recently Vollath *et al.* [32] have synthesised the maghemite nanoparticles by the **Microwave Plasma Method**. Hyeon *et al.* [33] prepared iron-oleic acid metal complex by the **Thermal Decomposition** of iron pentacarbonyl in the presence of oleic acid at 100°C followed by 300°C aging to synthesise highly crystalline and mono-dispersed maghemite nanoparticles. **Sonochemical method** was studied by Shafi *et al.* [1] to produce magnets coating.

2.2.2.1 Precipitation method

Precipitation is the process by which aqueous solutions of reagents are mixed together to introduce precipitation through chemical reactions and the desired materials would be obtained after post-treatments, such as filtering, washing, drying and pyrolysis.

The final product of the precipitation process depends on the concentration of reactants, pH value, temperature, time of aging, the nature of the anions present, and other topochemical transformations [34].

Hence the nature of precipitated particles could be controlled by different reaction conditions.

2.2.2.2 Sol-Gel process

Sols and gels have been known to exist naturally for a long time but were only of pure scientific interests. Since the 1970's, an increasing number of publications published in the field of gels and inorganic colloids led to an increasing number of potentially interesting applications in high technology ceramics [35]. Now, high purity sub-micro powders, nuclear fuels, electronic and ionic conductors and magnetic materials can be produced by sol-gel techniques.

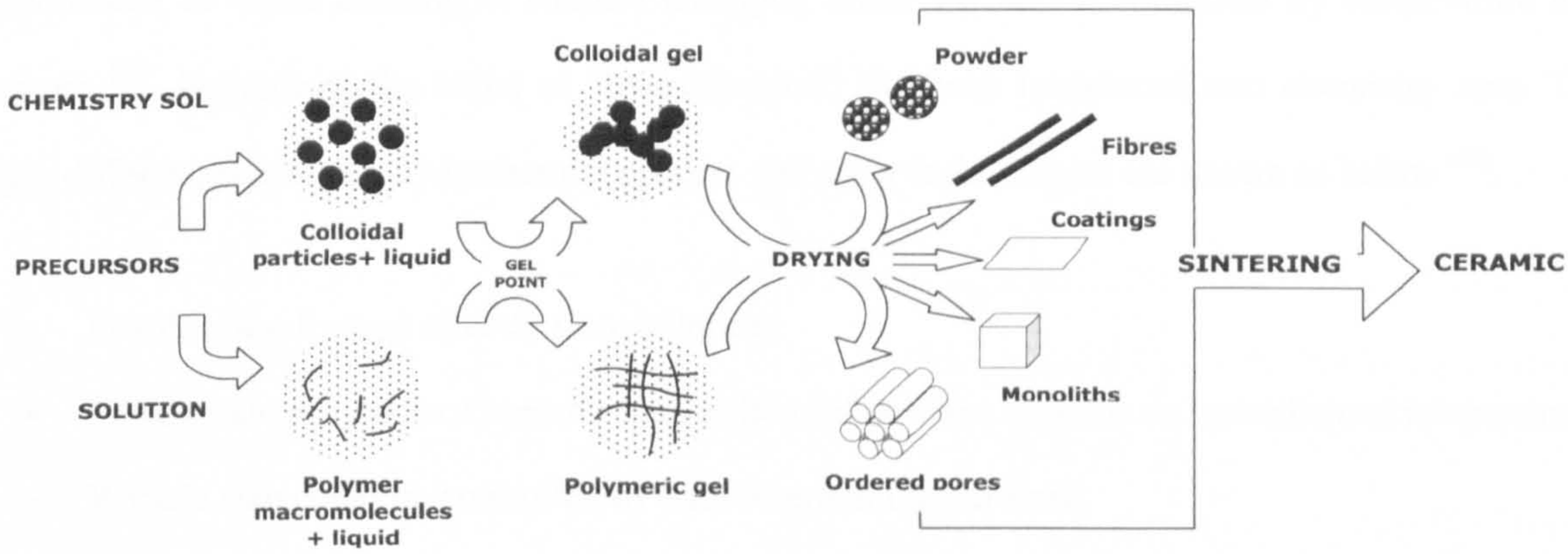

Figure 2.2-3 Schematics of sol-gel process.

A sol is a stable suspension of colloidal solid particles within a liquid [36]. In order to keep dynamic stability of a sol and make it exist longer, the solid particles in it must be small enough for the forces responsible of dispersion to be greater than gravity. Generally the particle size between 2 nm and 0.2 μm is necessary in a colloidal sol. A gel is a porous 3-dimensionally interconnected solid network that expands in a stable fashion throughout a liquid medium and is only limited by the size of the container [35].

As shown in **Figure 2.2-3**, the sol-gel process is a colloidal method used to synthesise ceramics with an intermediate stage including a sol and/or a gel state [35]. The homogeneous solution phase and the elastic, gel-like, solid phase are essentially two phases presenting in sol-gel processing. The solution is dried then transformed into a gel, while maintaining a constant volume. Subsequent drying leads to a

phase transformation with a reduction in volume, finally resulting in the desired phase. To obtain nano-structured materials using this process is to control the processing parameters. The properties of the materials depend on the hydrolysis catalyst, the pH value of the gelling solution, the nature of the impurities added before gelling and the thermal treatment [35]. The morphological properties were largely determined by the gelation and ageing process, which are strongly influenced by the pH value and water content of the sol.

2.2.2.3 Hydrothermal process

The term of "hydrothermal" appeared about 140 years ago. It was used initially to describe the phenomenon of water existing in stratum changing under the action combined by temperature and pressure [37]. Nowadays, the name of "hydrothermal" has been introduced into chemistry area. The major differences between hydrothermal process and other technologies are shown as below [38]:

- Powders are formed directly from solution;
- Powders are anhydrous. Crystalline/amorphous of powders depends on hydrothermal temperature;
- Particle size could be controlled by hydrothermal temperature;
- Particle shape could be controlled by starting materials;
- Powders are highly reactive in sintering;
- Many cases, powders do not need calcinations;
- Many cases, powders do not need milling process;

Basically, hydrothermal process is a wet-chemical technique, which is normally carried out in a sealed vessel between 130°C and 250°C. Higher hydrothermal temperature would result in the increased oxidation of the products. The increase of aging time usually induces the growth of particles [39].

2.2.2.4 Microemulsions

The preparation of nanomaterials via microemulsions attracted growing interests in recent years, especially the water-in-oil (w/o) microemulsion system.

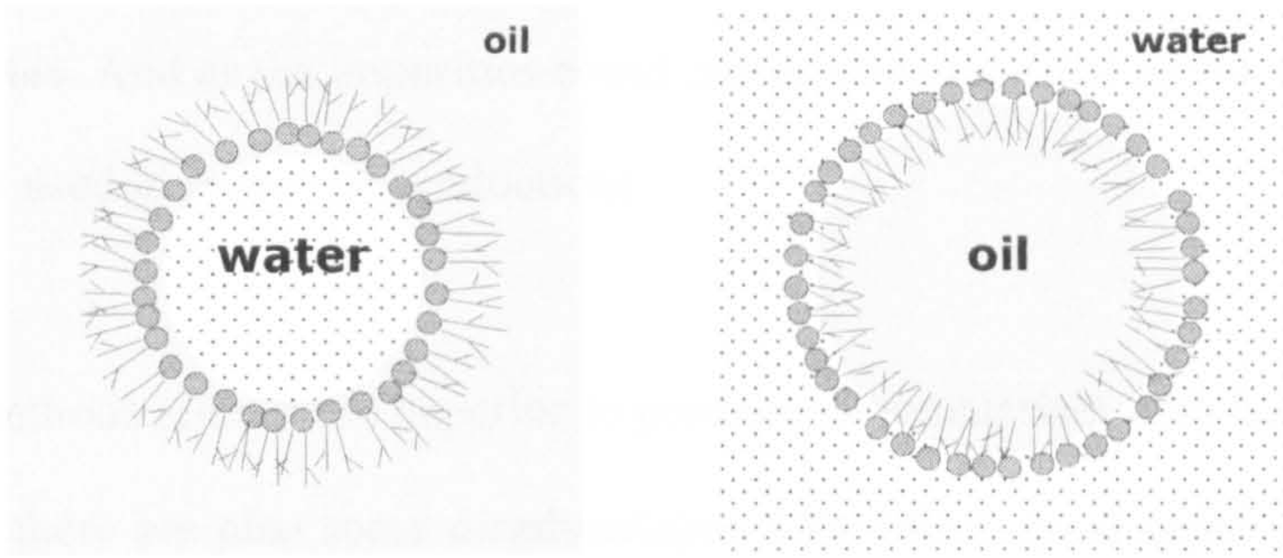

[A]. Water-in-oil microemulsion **[B]**. Oil-in-water microemulsion

Figure 2.2-4 Schematics of microemulsion system.

Figure 2.2-4 shows the schematics of microemulsion systems. Since a mono-layer of surfactant molecules surrounded at the interface of oil/water, the nano-droplets of the dispersed phase can be formed stably. In a w/o microemulsion system, the water droplets provide a reaction vessel for the preparation of finely divided particles. The growth and the aggregation of the precipitated "seeds" are partially restricted by the steric barrier provided by the surfactant mono-layer [40]. The most important feature for this method is that the size and the morphology of particles synthesised can be well controlled by varying the relative concentration of the surfactant, reactants, water and oil [8, 41]. More details of microemulsion system will be discussed in **2.4**.

2.2.3 Comparison and Limitation

Material properties depend on its atomic structure, composition, microstructure, defects, and interfaces, which are controlled by the thermodynamics and kinetics of the synthesis [42]. With the increasing interests of the synthesis of nano-structured materials, looking for an appropriate method to well control the material properties under nano-scale, particularly, the desirable morphology and the low extent of aggregation is of more and more important in applications.

In the preparation of nanomaterials by **PVD**, the particle size could be controlled by changing the pressure of inert gas. The ultra-fine particles are mono-dispersed and the surface of them is smooth.

However, the control of the morphology of prepared particles is difficult. The same problem also exists in **Mechanical Grind**. And as the impurities could contaminate the final product during processing, **Mechanical Grind** is not used in industrial productions.

Although chemical methods seem more superior to produce nanomaterials with homogeneous particle size and high purity, there are also some disadvantages. **CVD** offers good control over the chemical used for catalytic reactions and gas absorption applications. However, there is a problem of collection and storage of powders produced by this processing.

The main advantages of **Precipitation Method** are chemical homogeneity, the possibility of obtaining fine particles with a narrow size distribution and the good reactivity of products which allows the decrease in calcinations and sintering temperature [43]. However, in the hydrolysis of metal alkoxides in alcohols and water mixture, as reported by Bogush *et al.* [44], when the size of particle is less than 100 nm, the high poly-dispersity is unavoidable.

One of advantages of using **Sol-Gel Process** is the possibility to obtain large amounts of powders with high purity and the preparation of multi-component nanoparticles with mixing of the elements on a nano-scale. The synthesis of metallic oxides by the sol-gel process is a widely accepted method, particularly when it is desired to incorporate other metallic ions in the gels [45-48]. However, an inherent problem of sol-gel-derived materials is that it is difficult to mix the constituents on the molecular scale and the resultant structures are often meta-stable, prone to restructuring [49-50].

Comparing with other wet-chemical techniques, one obvious advantage of **Hydrothermal Process** is that crystalline powders could be prepared without calcinations at elevated temperature. It was reported that maghemite particles prepared by the hydrothermal process showed lower agglomeration compared with the spray pyrolysis method [51].

The most distinguished feature of **W/O Microemulsion** from other methods is the water-droplets in the

Table 2.2-1 Preparation of ideal ultra fine powders [54] and real powders by precipitation, sol-gel, hydrothermal and microemulsion methods are shown.

	Ideal Powder	Precipitation	Sol-gel	Hydrothermal [54]	Microemulsion
Particle size	Fine powder less than 1 μm	< 2 μm	< 1 μm	< 1 μm	< 100 nm
Coagulation	Soft or no agglomeration	Weak	Weak	No or weak	No
Diversity	Narrow particle size distribution	A bit wide relatively	Narrow	Narrow	Much Narrow
Chemical composition	controllable	controllable	Controllable	Controllable	controllable
Microstructure	controllable	controllable	Controllable	Controllable	Well controllable
Morphology	controllable	Poor Controllable	Poor Controllable	Poor Controllable	Well controlled by water pool
Homogeneity	Uniformity	Good	Good	Good	Good
Reactivity, sinter ability	/	Good	Good	Good	Good
Crystallinity	/	Good	Good	Single crystal in general. It depends on preparation temperature	Ultra small size near single domain then difficult to define by x-Ray pattern

bulk oil phase serve as nano-reactors for the synthesis of nanoparticles. Normally the water pool is

spherical and the size of the pools could affect the size of the nanoparticles prepared, therefore the morphology of nanoparticles could be controlled by the water pools [23]. The surfactant stabilised nano-droplets introduce a cage-effect in the synthesis via microemulsions, which limits the growth [52] and the aggregation of particles. Additionally, the presence of the surfactant allows the formation of a remarkably ordered particle arrangement upon volatilisation of the solvent [53].

The "surfactant wall" in microemulsions, not only reduces the interfacial tension and stables the overall system but furthermore act like a spherical mould for particles growing within the water pools. That is why the microemulsion system shows superiority in the control of the morphology of nanoparticles prepared, comparing with precipitation method, sol-gel process and hydrothermal method **[Table 2.2-1]**. The size of nanoparticles synthesised by microemulsion systems is much close to the nano-scale (generally below 100 nm). The unique inter-structure of microemulsion systems also plays a significant role in the synthesis of core-shell structured nanocomposites by introducing the potential of tailor-making the morphology of particles in order to facilitate desired nano-products. Hence, the microemulsion is a novel system in the nano-synthesis area.

2.3 DRESSING UP: ADVANCED CORE-SHELL STRUCTURE

2.3.1 What is core-shell structure

The term core-shell nowadays can be defined by a core of matter that is surrounded by a shell of a different matter [55]. A schematics of a core-shell structure is illustrated in **Figure 2.3-1 A**. TEM micrographs of core-shell structured nanocomposites are shown in **Figure 2.3-1 B, C**, by the research work of Tarun K. *et al.* [56].

Although there is no clear cut definition of core-shell structured particles, the main prerequisite to

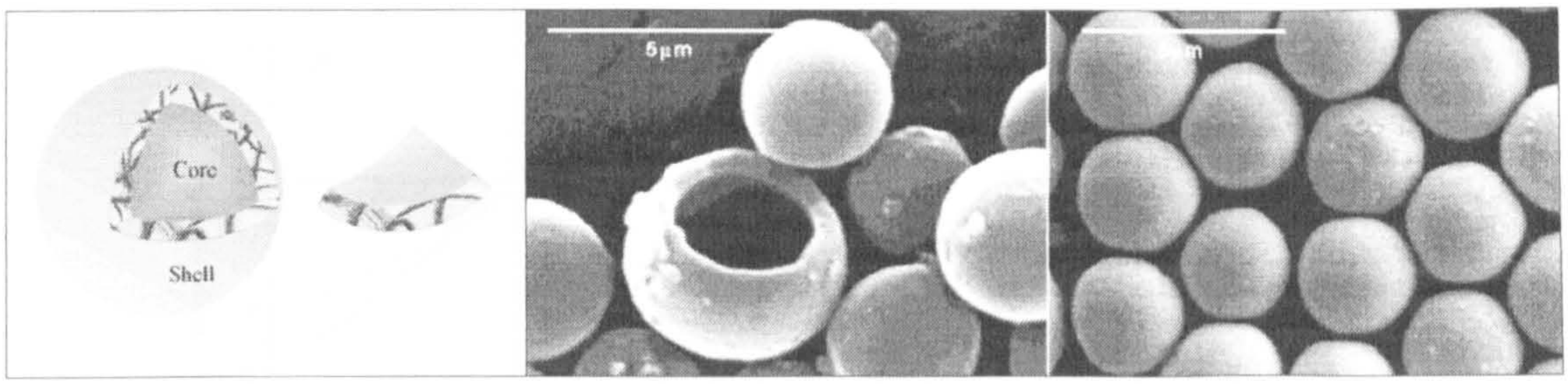

[A] Schematics of core-shell structure **[B]** Polymer shell **[C].** TEM micrographs of silica-poly-(benzl methacrylate) nanocomposites[56]

Figure 2.3-1 Schematics and TEM micrographs of core-shell structure.

interaction of the shell and the core which leads to an interaction between both shell and the core classify particles in that category is the intimate close connection in terms of physical and/or chemical compartments, creating synergistic effects [55].

Pure nanoparticles have the following limitations:

- they tend to form large aggregates,
- their original structure may change if they are not stable enough resulting in the alteration of chemical properties, such as the rapid biodegradation when nano-magnets are directly exposed to the biological system.

Therefore, a suitable coating is necessary to discard such limitations. Swadeshmukul *et al.* [23] found that the silica coating protects the magnetic particles from possible decomposition induced by the surrounding environment, prevents further aggregation, and reduces the inter-particle magnetic interference retaining the magnetic property of each particle intact. On the other hand encasing colloids in a shell of different composition may protect the core from extraneous chemical and physical changes [57-59]. The shell can also alter the charge, functionality, and reactivity of the surface, and can enhance the stability and dispersibility of the colloidal core. Magnetic, optical, or catalytic functions may be imparted to the dispersed colloidal core depending on properties of the coating.

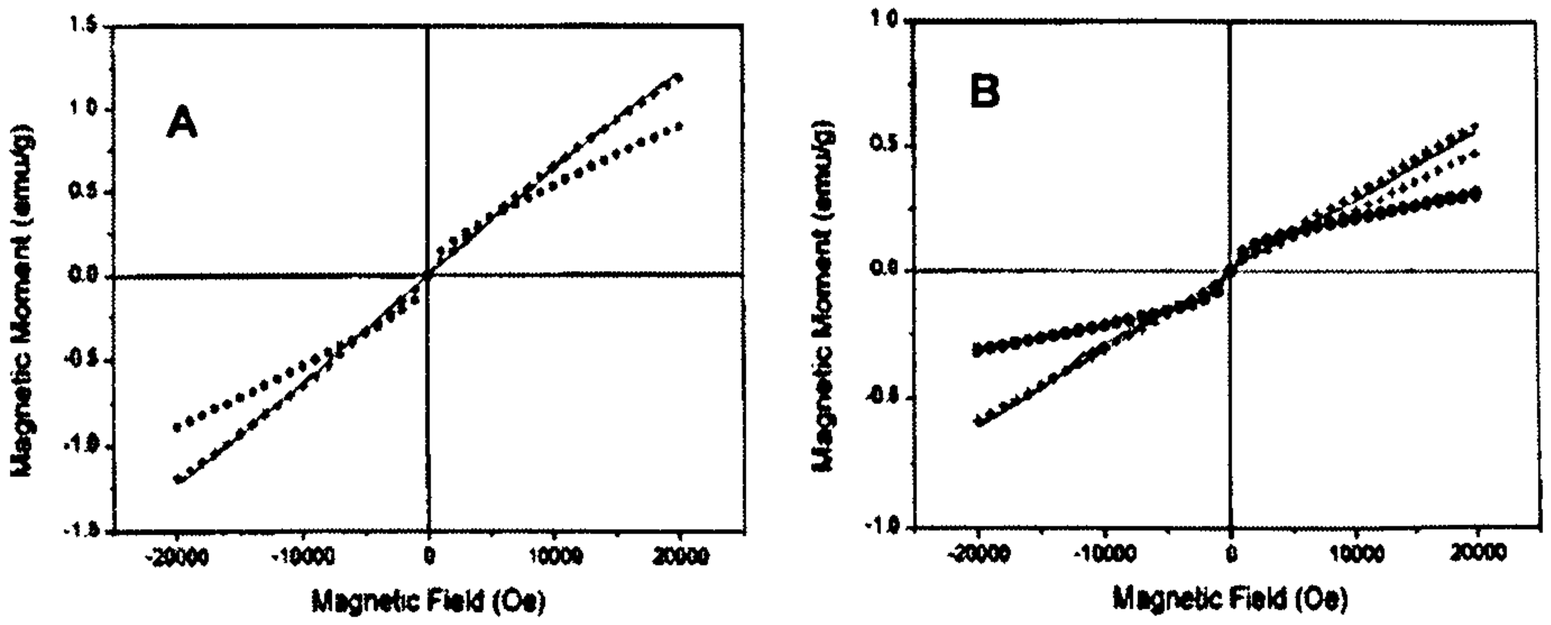

[A]. uncoated iron oxide nanoparticles **[B].** silica-coated iron oxide nanoparticles

Figure 2.3-2 Magnetisation curve for particles prepared in microemulsions with Brij-97 (•), Igepal CO-520 (+), and Triton X-100 (Solid line) [23] as surfactants.

Nanoparticles have different properties when dressed into core-shell structure. Core-shell structured nanocomposites often exhibit improved physical and chemical properties over their single-component counterparts, and hence are potentially useful in a broader range of applications. For examples, the magnetic nanocomposites with the core-shell structure could result in spin bias exchange at the boundary of the super-paramagnetic particles and, as a consequence of single domain characteristics, lead to enhanced coercivity and apparent ferromagnetic behaviour [60], as shown in **Figure 2.3-2.**

Santra *et al.* [61] reported that at any given magnetic field, the magnetisation for an uncoated sample is always higher than that for a coated sample. It is well known that below some critical size (<10 nm) magnetic particles become single domain because of the interplay between the energy of dipole field and domain wall creation. The decrease in the magnetisation when particles are coated with silica clearly distinguishes coated and uncoated particles [61] **[Table 2.3-1]**.

Table 2.3-1 SQUID data for iron oxide samples prepared by the w/o microemulsion, with and without coating. [61]

Sample	SQUID specific magnetisation [emu/g]	
	10 KOe	20 KOe
Bulk (uncoated) iron oxide	14.60	18.30
NaOH coated iron oxide	0.212	0.311
NaOH uncoated iron oxide	0.540	0.896

However, despite the fact that the advantages of uniformly coated and stable colloidal particles have been recognised for years [62-64], the controlled coating of colloids with recognised layers has for many years remained a technical challenge.

2.3.2 Applicable methods into core-shell

Sol-gel process is a widely accepted method for the preparation of nanoparticles and nanocomposites, for instance, to incorporate other metallic ions in the gels. However, the synthesis of nanoparticles using the restricted environment offered by w/o microemulsions provides much better control over the morphology of particles. The controlled environment also allows sequential synthesis to produce nano-particles with core-shell structure *in situ* [40]. Talham *et al.* [65] reported the nanocomposites with core-shell structure prepared by arrested precipitation of metal or semiconductor cluster in the w/o microemulsion system. The following section summarises the concepts and recent development in microemulsions which are enrolled as one of the most suitable system to synthesis nanoparticles.

2.4 MICROEMULSIONS: A STAGE BUILT IN A LITTLE WATER POOL

In 1959 J.H. Schulman [66] firstly introduced the term "microemulsions" for transparent solutions in a model four-component system; water, oil, surfactant and co-surfactant. Friberg and his group [67] stressed long-term stability of the microemulsions which was in fact a result of their thermodynamic stability. From a practical point of view microemulsions can be defined as thermodynamically stable liquid phases where the surfactants are optimised with regard to surface activity and the system with regard to water and oil content [68].

2.4.1 Internal structure of microemulsions

The internal structure of microemulsions may be complex and varied. Extensive theoretical and

experimental work has been devoted to different kinds of microemulsion systems in order to establish an unambiguous picture of these systems with regard to the structure. One of the most common models used to explain the different phase-forming situations for microemulsion systems was proposed by Winsor, who divided the system into four types: Winsor I, Winsor II, Winsor III and Winsor IV **[Figure 2.4-1]**.

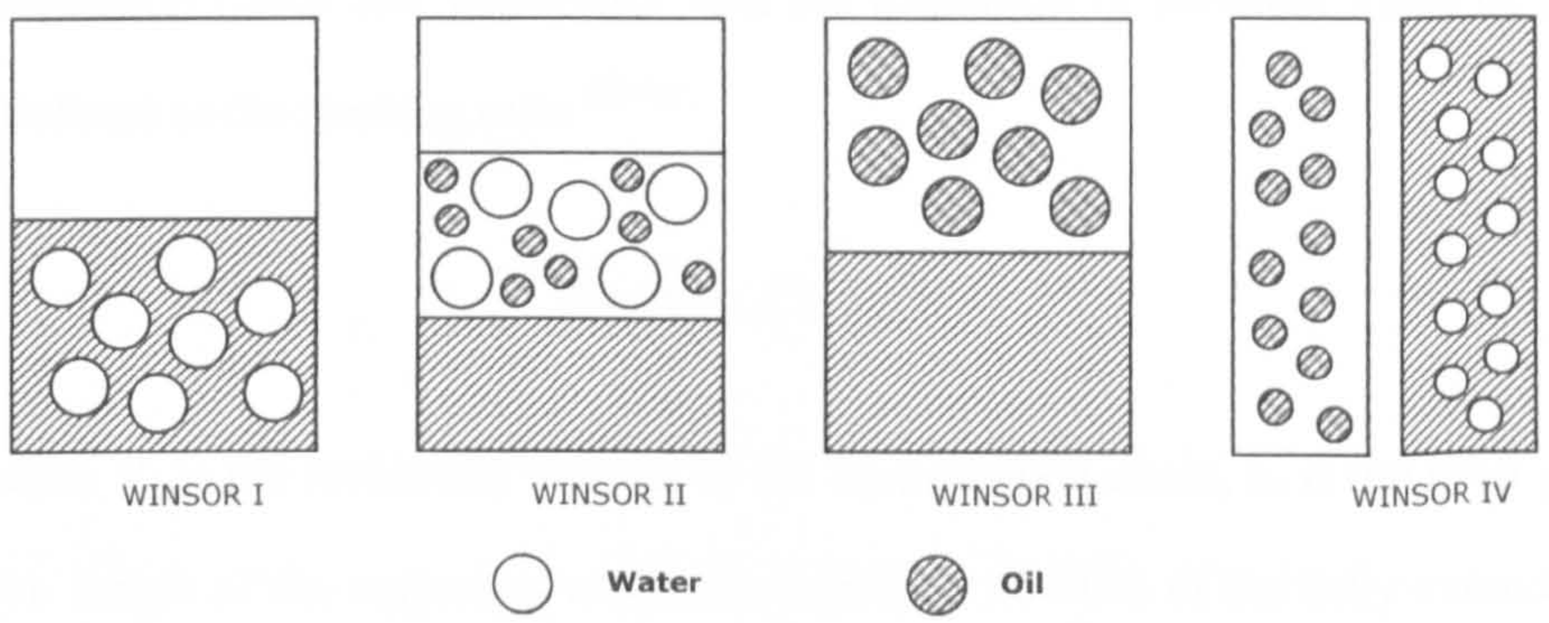

Figure 2.4-1 Winsor model of microemulsions.

It is physio-chemically conceived that on the higher end of water content, on the average, spherical dispersion of surfactant-coated oil micro-droplets exists in equilibrium with the excess water **[Winsor I]**. The increasing surfactant concentration ends up with increased droplet dimension together with distortion of the spherical shape; at comparable proportions of water and oil and irregular dispersions of both oil and water may simultaneously exist. This is called the "bi-continuous state" **[Winsor II]**, which is considered to be a sponge-like random network. As for compositions with a low percentage of water and a high percentage of oil, the situation like Winsor I is reverse **[Winsor III]**; a spherical dispersion of water micro-droplets coated with surfactant in equilibrium with excess oil. In **Winsor IV**, which is normally called as microemulsion, either the oil micro-droplets or the water micro-droplets homogeneously disperse in the continuous phase, which is a thermodynamic stable system with single phase.

As for the bi-continuous model, Lindman *et al.* [69-71] have shown that the microemulsion structure can be very intriguing for high amounts of water and oil, where these two components are free to diffuse

like in their pure states. In addition, the diffusion of the surfactant is generally low which indicates that this species is in an aggregated state. According to this model water and oil are supposed to have unrestricted diffusion in their respective channels inside the network, while the surfactant will constitute a mono-layer separating both the continuous domains.

In microemulsions, the aggregates of surfactant molecules are varied as well. A crucial parameter for surfactant association (ionic and non-ionic), and the formation of different kinds of structures is the steric factor defined as the packing ratio [72-74]:

$$R = V_s / (l \cdot a_0) \qquad \textbf{(2-1)}$$

In the expression V_s is the molecular volume of the hydrocarbon chain, a_0 is the head group area and l is the effective length of the surfactant molecule, normally 80-90% of the fully extended hydrocarbon chain. The geometries of aggregates will be restricted by the topology of the area of the end group and the volume of the hydrocarbon chain. Spherical aggregates will form when $R \leq \frac{1}{3}$. When the ratio is increased from $\frac{1}{3}$ to $\frac{1}{2}$ rod-shaped aggregates are favoured. The lamellar structures will formed when $\frac{1}{2} \leq R \leq 1$ and reversed structures appears when $R > 1$ **[Figure 2.4-2]**.

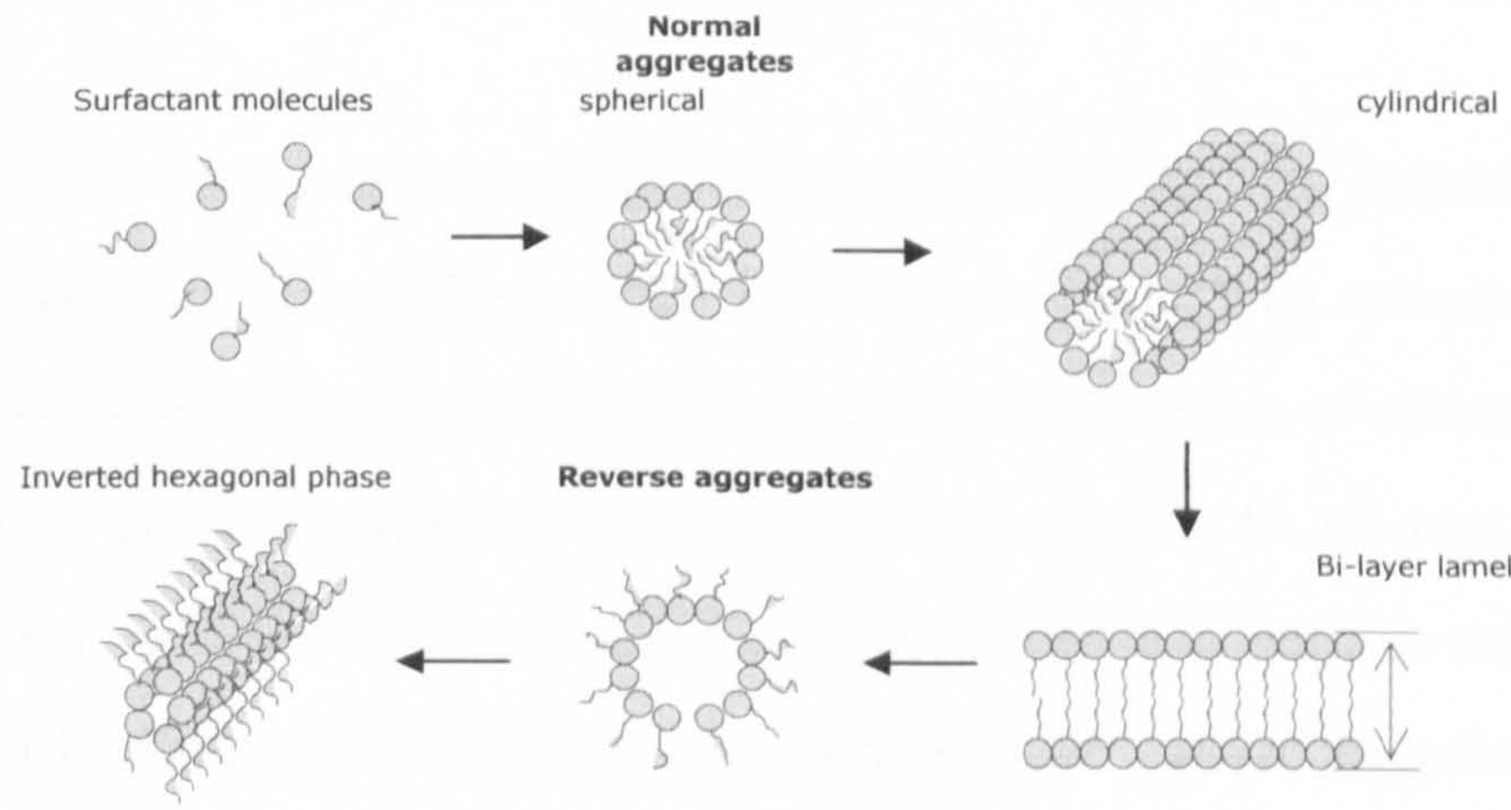

Figure 2.4-2 Schematic diagram of possible aggregate shapes expected for different geometries of the surfactant molecules according to $R = V_s / (l \cdot a)$ criteria.

2.4.2 Water-in-oil microemulsions

Microemulsion systems can be basically categorised into water-in-oil microemulsion system and oil-in-water microemulsion system. A water-in-oil (w/o) microemulsion is a transparent solution consisting of nano-sized water droplets, stabilised by a curved mono-layer of surfactant (and in some cases co-surfactant), and dispersed in a continuous hydrocarbon oil [75]. In the preparation of inorganic nanoparticles, these ultra-small water droplets could be regarded as a restricted reaction container, which appears more promising in controlling of particle size and its morphology in nano-synthesis.

In the w/o microemulsion, the polar heads of the surfactants are oriented inward and the non-polar tails orient towards the oil continuum. The availability of free water in the core called the "water-pool". The structure of the interfacial water in w/o microemulsion systems is different from bulk water.

Table 2.4-1 Nature of solubilised water in non-ionic surfactant

System	ω_0	No. of EO	H_2O/EO	Ref.
Triton X-100/Hexanol/Cyclohexane	5.8	9.5	0.50	[76-77]
$C_{12}EO_7$/Hexanol/Decane	1.4	7.0	0.20	[78]
NP-6/cyclohexane	4.0	6.0	0.67	[79]
NP-5/cyclohexane	1.2	5.0	0.25	[53]

When the amount of water in the organic phase is very low, most of the water molecules are hydrogen bonded to the surfactant polar groups and they are said to be bound. With an increase in the water content, unbound or free water molecules become available. The presence of surfactant head groups may significantly affect the water mobility. **Table 2.4-1** summarises the available results for the minimum water to surfactant molar ratio ω_0 and the water to polar head (ethylene oxygen, EO) molar ratio (H_2O/EO), by which free water is detected in the hydrophilic "core" of the surfactant aggregates. It was shown that less than one water molecule per EO unit is involved in the initial hydration shell. It seems that water may preferentially solvate some of the EO units along the polar chain, and that

further water addition results in the gradual formation of free water domains rather than in the complete hydration of all the EO units [73].

The knowledge of "free water" is very useful to the synthesis of nanoparticles via w/o microemulsions, especially the hydrolysis reaction in microemulsion, which is related to the kinetics of particle growth.

2.4.3 Analysis on behaviours of microemulsion

The different surfactants, different component ratio and temperature could all affect the stability of microemulsion systems.

2.4.3.1 Effect of ionic surfactant and non-ionic surfactant

Surfactant is a kind of amphiphiles with hydrophilicity and hydrophobicity simultaneously that could greatly reduce the interfacial tension. Which type of emulsions will be formed mainly depends on the nature of surfactants. Normally surfactants are classified according to their structure, into ionic, zwitterionic and non-ionic according to their charges. The structure and name of four classified specific surfactants are given in **Figure 2.4-3**.

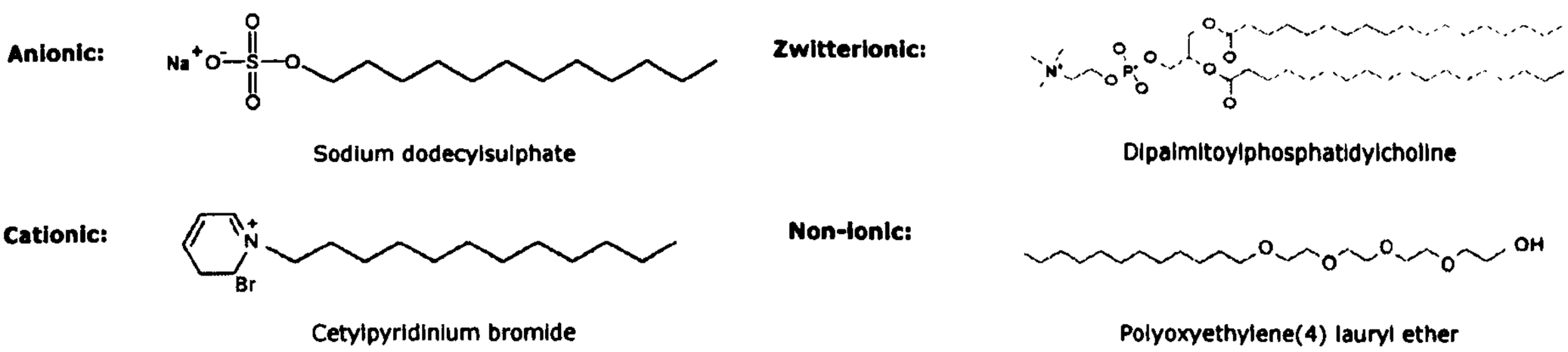

Figure 2.4-3 Classification of surfactants

Being the equibiliser of a thermodynamic stable system, surfactants play an important role. Different surfactants would yield different types of microemulsion systems. The first successful attempt to quantitatively correlate surfactant structures with their effectiveness as emulsifiers was the HLB system first developed by Griffin [80]. HLB means Hydrophile and Lipophile Balance [81-82].

Amphiphilic surfactants are characterised by the value of HLB, a relative ratio of polar and non-polar groups in the surfactant. The more hydrophilic surfactant normally has the higher value of HLB.

Table 2.4-2 The range of HLB of surfactants with different usage [81].

HLB	1 – 3.5	Antifoams
HLB	3.5 – 8	Water-in-Oil Emulsifiers
HLB	7 – 9	Wetting and Spreading Agents
HLB	8 – 16	Oil-in-Water Emulsifiers
HLB	13 – 16	Detergents
HLB	15 – 40	Solubilisers

The HLB values and corresponding different systems formed are showed in **Table 2.4-2** which gives an elementary principle to deal with so many kinds of surfactants. Although there is not an absolutely correct principle of choosing a surfactant for required applications, its HLB value partially provides a handy quantitative indication. At the higher end of the scale lies hydrophilic surfactants, which possess high water solubility and generally act as good solubilising agents, detergents, and stabilisers for oil-in-water emulsions; at the lower end there are surfactants with low water solubility, which act as solubilisers of water in oils and good w/o microemulsion stabilisers. The effectiveness of a given surfactant in stabilizing a particular emulsion system would depend on the balance between the HLB values of the surfactant and the oil phase involved [80].

2.4.3.2 Effect of temperature

It is well known that temperature generally affects the behaviour of surfactants and results in changing the microemulsion system. First, the change in temperature is known to affect the characteristics of the surfactant aggregates – size, shape, ionic nature, etc., and consequently affects the solubilising properties of surfactants. Second, the change in temperature might affect the intermolecular interactions between oil, water and surfactant, which would affect the structure of microemulsion systems. **Figure 2.4-4 A, B** shows the change of the structure of the microemulsion system with the

change of temperature. **Krafft point** (KP) and **Cloud point** (CP) are two characteristic factors of microemulsion system in terms of temperature dependence.

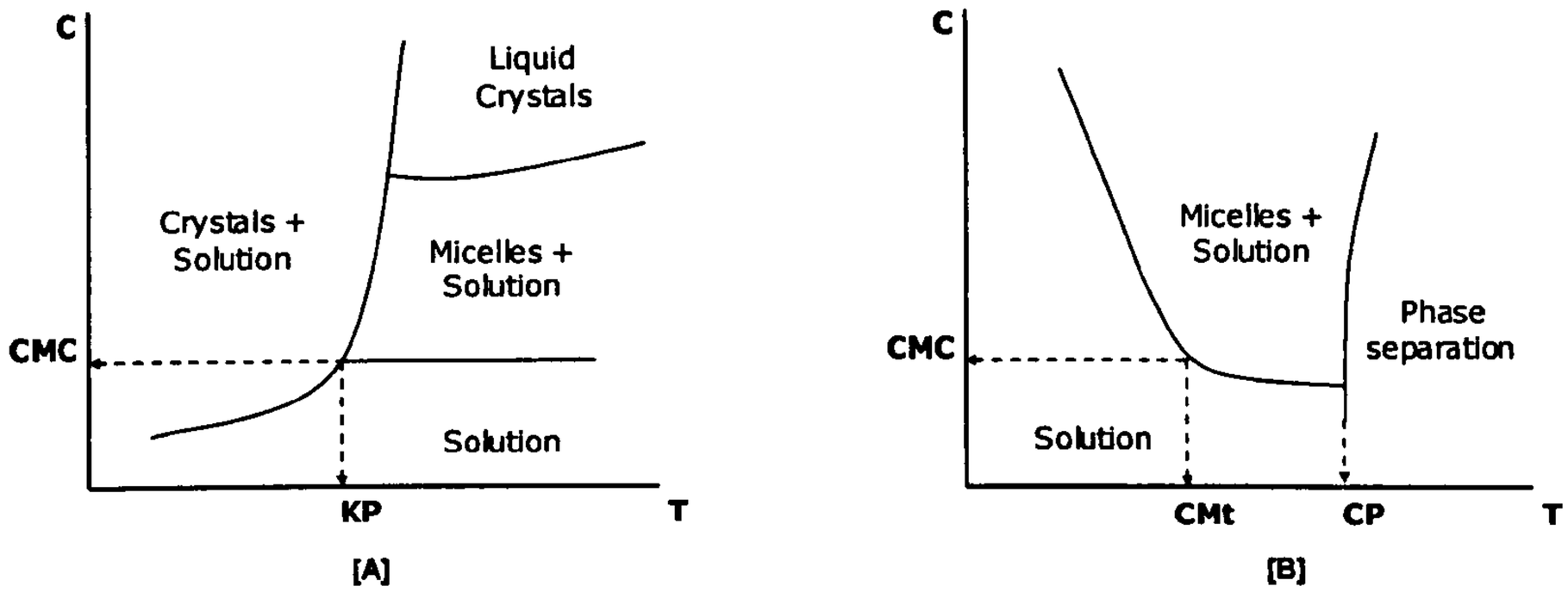

Figure 2.4-4 Effect of the temperature on the structure of microemulsions

- **Krafft Point (KP)**

The surface tension of a solution of an individual surfactant decreases steadily as the bulk concentration of surfactant is increased until the concentration reaches a value known as the **Critical Micelle Concentration (CMC)**. The temperature at which the solubility of an ionic surfactant becomes equal to the CMC is known as the **Krafft point (KP)** [80]. For surfactants being used below KP, the maximum reduction in surface tension will be determined by the concentration of surfactant at solution saturation and these materials may show lower effectiveness in reducing surface tension than similar materials that are being used above their KP.

- **Cloud Point (CP)**

The hydrophilicity of non-ionic surfactant basically depends on the hydration of EO units in the structure. The increase of temperature would normally result in the dehydration of EO units. Hence, the water solution of non-ionic surfactant will turn turbid with the increase of temperature, followed by phase separation. The temperature when non-ionic surfactant begins to separate from water is called **Cloud Point (CP).**

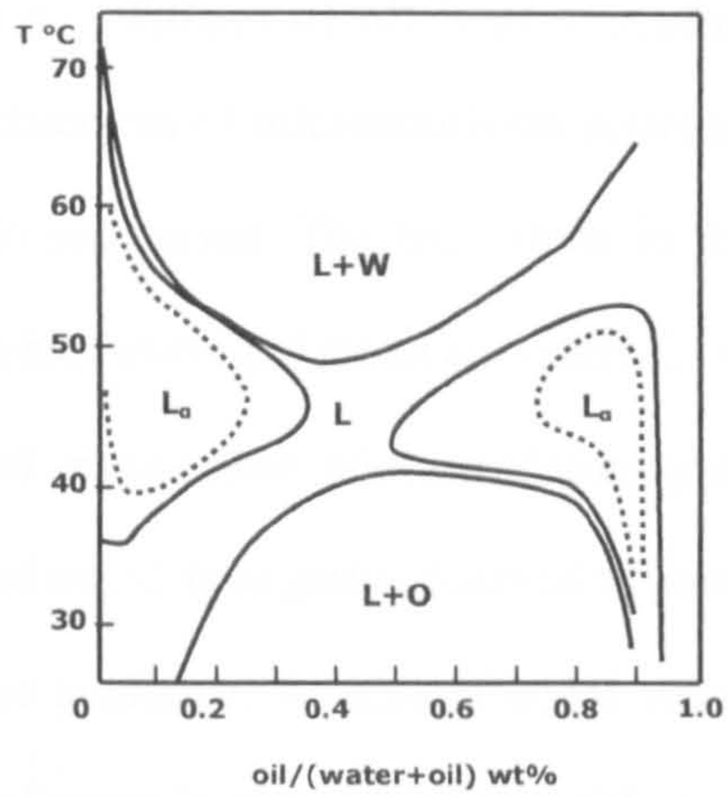

Figure 2.4-5 Phase diagrams at a constant surfactant concentration of 16.6% in the $C_{12}E_5/H_2O$/tetradecane system [85].

For a non-ionic surfactant, the phase equilibrium will be mostly governed by the cloud point [83]. The system based on $C_{12}E_5/H_2O$ ($C_{12}E_5$, the surfactant molecules in which the hydrocarbon chain is typically of the order C_{12} and the number of EO units is 5) has been investigate extensively with regard to phase diagram [84-86]. **Figure 2.4-5** is a typical cut of $C_{12}E_5/H_2O$/tetradecane system [85]. At low temperatures, w/o microemulsion phase (L) occur. An increase in temperature leads to the gradual formation of a bi-continuous phase (L_a), which transformed into a w/o microemulsion phase with excess water (L+W) at higher temperature.

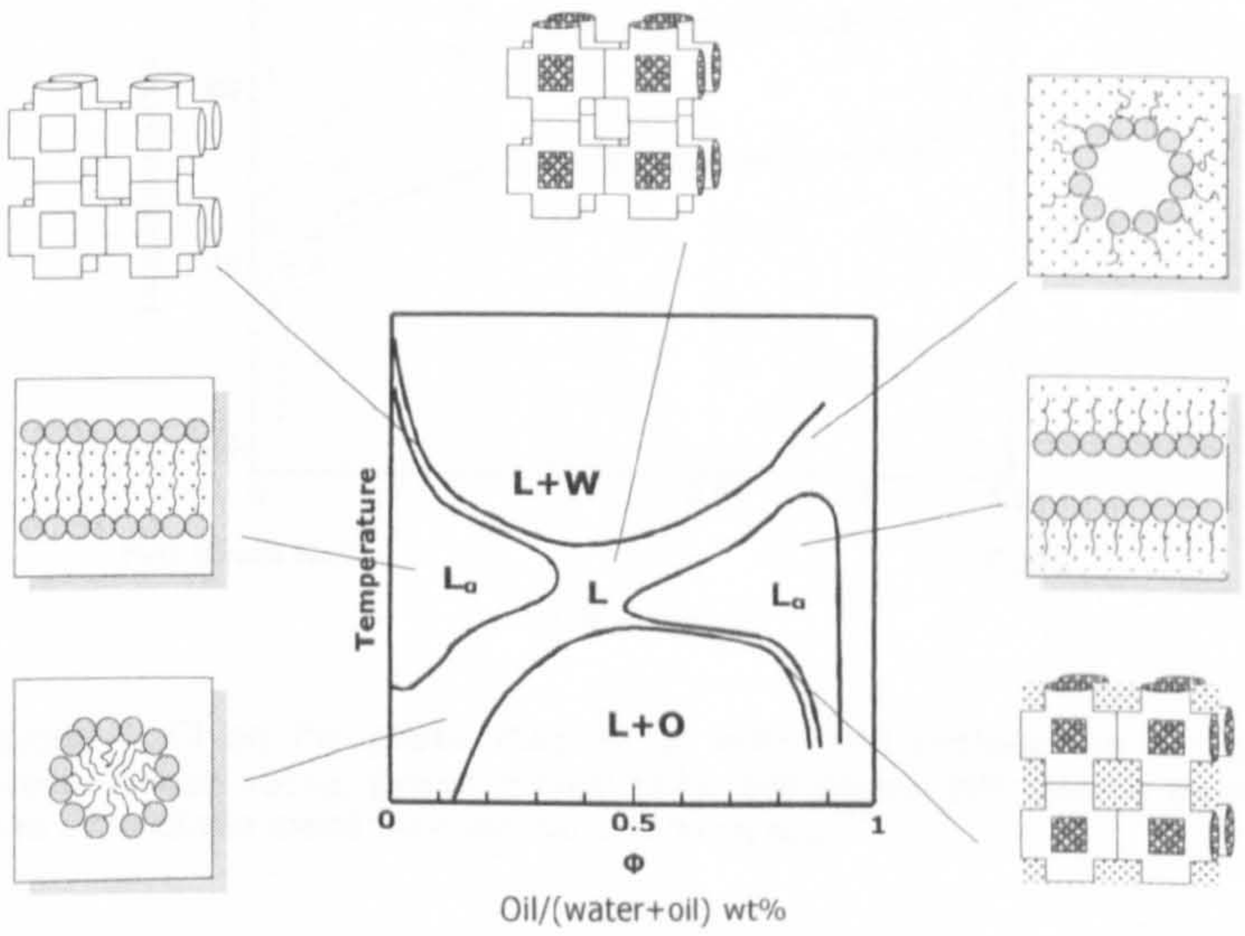

Figure 2.4-6 A schematic phase diagram and various micro-structures found in different regions of the liquid phase (microemulsion), L. At higher temperatures the liquid phase is in equilibrium with excess water (L+W), and at lower temperatures with excess oil (L+O) [85].

2.4.3.3 Effect of oil/water molar ratio

Figure 2.4-6 shows the different structures of microemulsion systems in such a two-dimensional cut as temperature and component ratio are varied. The transitions in this schematic drawing can also be interpreted as changes in the interface averaged mean curvature C. At low volume fractions of oil, C is positive (curved towards oil) and oil-in-water microemulsion systems might be formed as a result. While at high volume fractions of oil, C is negative (curved towards water) and the formation of w/o microemulsion systems would be available. At almost equal volume fractions of oil and water the mean average curvature of the surfactant is zero, which probably results in the bi-continuous structure.

2.4.3.4 Effect of co-surfactant and electrolyte

A surfactant mixed with a co-surfactant in a certain proportion is most used to further decrease the surface tension. Smaller alkanol (like butanol, pentanol and hexanol), and amines (like butylamine, hexylamine) can be profitably employed for this purpose. It is considered that their presence in the interface between water and oil imparts flexibility, in addition to lowering the interfacial tension, leading to easier surface bending for energetically favoured dispersion.

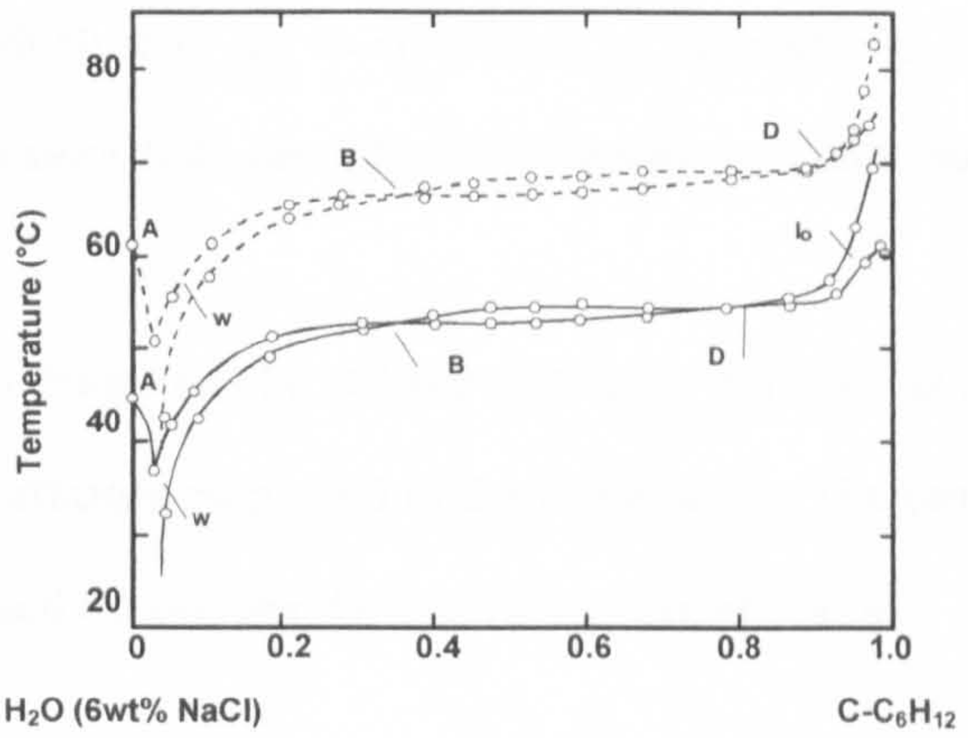

Figure 2.4-7 Effect of added NaCl on the phase diagram of water and cyclohexane containing 5 wt% $C_9H_{19}C_6H_4O\text{-}(CH_2CH_2O)_{9.7}H$. Dotted curves: no salt added. Drawn curves: 6wt% salt added. Not that the equilibrium compositions of the phases occurring in two- and three-phase areas may change on adding salt [87].

The influence of added electrolyte (Sodium chloride and calcium chloride etc.) on the phase equilibrium has also been investigated in several systems with non-ionic surfactant. Some

representative results from the system H_2O(6% NaCl)/C_6H_{12}/i-$C_9H_{19}C_6H_4O$-(CH_2CH_2O)(5%) are shown in **Figure 2.4-7**. The addition of NaCl systematically decreases the temperature of maximum solubilisation, but the extension of one-phase regions is otherwise not affected. Shinoda [87] has shown that by a very precise design of the balance between hydrophobic and hydrophilic properties of the surfactant and by a judicious choice of added salt, it is possible to obtain systems in which the one-phase regions extend almost continuously from aqueous solutions to oil solution at very low surfactant concentrations.

2.4.4 Applications

During the past decades there has been a complete revolution in utilizing microemulsion systems in a variety of chemical and industrial processes. With the evolution of science and technology, especially the rush of nanotechnology, some new applications in nano-synthesis area are carried out.

W/O microemulsions provide particularly favourable conditions for the preparation of mono-dispersed nanoparticles. The particle nucleation can be initiated simultaneously at a very large number of locations in the microemulsion with the nucleation sites well isolated from each other and in close contact with surfactants which may act as stabilisers of the particles formed. The structure and the solubilisation of microemulsions both can affect the formation of nanoparticles.

Polymerisation in microemulsions can be utilised to prepare polymer nano-spheres. The particle size is related to the amount of surfactant employed in the formulation. The molecular weight of the polymer can be decreased or increased by varying the emulsifier concentration.

Coating and encapsulation of particles to form core-shell structured materials are specialised technologies that impact a wide variety of products. This typically involves tailoring the surface properties of particles, often accomplished by coating or encapsulating them within a shell of a preferred material. Due to the unique internal structure, microemulsion system provides a novel environment for isolated cores forming and controlled shell.

2.5 NOVEL APPROACH: SYNTHESIS OF MAGNETIC NANOMATERIALS VIA MICROEMULSIONS

Synthesis of ultra small magnetic nanoparticles has been intensively studied with uniform size distribution because of their applications particularly in biology and medicine [88-91], such as **Magnetic Resonance Imaging (MRI)** contrast agent [92-94], magnetic separation of oligonucleotides [95] cells, and magnetically guided site specific drug delivery systems [96-97].

The exploration of commercial application of magnetic nanoparticles in biology and medicines is attributed to, first of all, their nano-scale size. As we know, living organisms are built of cells that are typically 10 μm across. However, the cell parts are much smaller and are in the sub-micron size domain. Even smaller are the proteins with a typical size of just 5 nm [98]. To work on the cellular machinery without introducing too much interference [99], the simple idea is using nano-scaled materials as ideally small implant, detector or carrier. The size and size distribution could be important especially in diagnostic applications. Applications in biology and medical diagnosis and therapy require the magnetic particles to be stable in water. The colloidal stability of the magnetic fluid will depend on the dimensions of the particles, which should be sufficiently small so that precipitation due to gravitation forces can be avoided [100]. On the other hand, different potential applications require the magnetic nanoparticles to have different properties. For biomedical applications the use of particles that present super-paramagnetic behaviour at room temperature is preferred [101-103]. That is the characteristic of magnetic materials exhibited only in nano-scale structure.

As discussed in previous sections, pure nanoparticles have some limitations when used directly, such as aggregation or the instability of chemical properties. Therefore, a coating layer would be necessary to give them a protection. Additionally, the coating also might be an important factor in consideration of material properties, including the considerably enhanced optical and magnetic properties. For example, the coated materials exhibit an increased absorption coefficient and an enhancement of the

third-order susceptibility [104]. Ferromagnetic particles in a non-magnetic host exhibit applications in magnetic recording heads. Diandra *et al.*[13] reported that the electrically insulating/conductive nature of the nonmagnetic matrix can also affect the magnetic properties of the nanocomposite.

There are some reports on the coating of ceramics or polymer on mono-disperse magnetic particles. López-Quintela and Rivas [105] reported that ferrite particles synthesised in reversed micelles have sizes approaching the magnetic domain size and then exhibit super-paramagnetic properties. Incorporation of these ferrite particles into the polymer-micro spheres confers super-paramagnetic properties to the composite. Such super-paramagnetic polymers were used in developing compositions for reprographic applications [106]. Polymer beads containing super-paramagnetic particles have also found commercial application in the field of biotechnology [107-108]. Furusawa *et al.* [109] used electrostatic and polymerisation processes to achieve the encapsulation of magnetic nanoparticle-coated polystyrene particles within a polystyrene shell. In the process, magnetic nanoparticles were heterocoagulated with larger polystyrene micro-spheres, followed by seed polymerisation to form a polystyrene layer around the composite particles. The advantage of this method is that the composite particles can be controlled by the diameter of the core latexes that are initially used. This study also shows the successful combination of multiple methods to form nanocomposite particles. Homola *et al.* [110-112] reported the coating of γ-Fe_2O_3 particles with preformed smaller silica particles by combining the particle mixtures under conditions where the two types of particles are oppositely charged. Rendering pure magnetic nanoparticles into nanocomposites with core-shell structure helpfully prevent the aggregation, and at the same time mostly maintain its original function. In some cases, there is possible interaction between core surface and coating layer. In other words, nanocomposites also assist in preventing agglomeration of magnetic particles by fixing them rigidly within the coating, which may provide a way of tuning interactions over a broader range possible than in ferro-fluids [13].

The main idea behind the microemulsion technique in the synthesis of nanomaterials is that by appropriate control of the synthesis parameters one can use these nano-reactors to produce tailor-made nano-scaled products with new special properties [113]. Furthermore, the ability to control the formation

of different core-shell nano-structures also became one of the main advantages of microemulsion over other preparation methods in nano-synthesis area. In the following sections, more attentions would be paid to review the synthesis of nanocomposites with core-shell structure via microemulsion systems.

2.5.1 Synthesis of magnetic nanoparticles via w/o microemulsions

Iron oxide such as magnetite (Fe_3O_4) and maghemite (γ-Fe_2O_3) are most commonly employed for biomedical applications [100]. They are similar in physical properties and crystalline structure [Table 2.5-1]. Both display ferromagnetism. Maghemite has slightly reduced magnetic response comparing with magnetite and could be obtained by controlled oxidation of magnetite or by heating one of modifications of FeO(OH) [114]. Magnetite has about 20% higher saturation magnetisation than maghemite. Furthermore, the coercivity of magnetite particles is usually higher by about 15% than the coercivity of maghemite particles of the same size and shape [114]. Due to its strong magnetic properties, magnetite was used first in biology and then in medicine for the magnetic separation of biochemical products [115] and cells [116] as well as the magnetic guidance of particles systems for drug delivery [117].

Table 2.5-1 Physical properties of magnetite and maghemite [118-119]

	Crystal system	Cell dimensions	Density	Colour	T_c
Magnetite	Cubic	0.839 nm	5.26 g/cm³	Black	850K
Maghemite	Cubic or tetragonal	0.834 nm	4.87 g/cm³	Reddish-brown	820-986K

2.5.1.1 Mechanism of magnetic nanoparticles formation by precipitation

It will be helpful to understand the reaction of synthesis of magnetic nanoparticles in w/o microemulsions by the investigation of the same reaction carried out in solution via precipitation. At the first stage, very small primary particles nucleate following the reaction, which aggregate and form the larger particles by a contact-re-crystallisation mechanism [120]. The adhesion of additional primary particles to the already re-crystallised particles leads to further growth. The coagulation of primary particles results from van der waals and magnetic forces under the condition of weak repulsion. In the

excess of ferrous/ferrite ions the electrostatic repulsion between the primary particles is small or negligible and consequently, the coagulation of very small primary particles would be expected to occur readily [121].

Due to the competition between the particles to already formed aggregates and the aggregation of the grown particles, the particle size and the increase of size distribution occurs as the excess concentration of ferrous/ferrite species increases. The large particles of various size-distributions are formed by fast diffusion/adhesion growth at the very low excess and at larger surplus iron concentrations the rate of iron oxide formation is slowed down; thus, simultaneous growth by adhesion and coagulation of the smaller clusters into larger particles may take place [121].

2.5.1.2 Magnetic properties of magnetic materials

Generally, the most used magnetic materials are ferro-magnets featured by spontaneous magnetisation. This magnetic property strongly depends on the temperature. The temperature-dependence of the ferro-magnets could be defined by Curie temperature T_C (the transition temperature between the ferromagnetic and super-paramagnetic state) [122] :

- Below the Curie temperature, materials possess a spontaneous magnetisation M_s, i.e. a magnetisation in the absence of an applied field.
- The magnitude of the spontaneous magnetisation M_s reaches to the maximum at 0K and decreases as the temperature increases, and is zero at the T_C.
- Heating magnets above T_C, the spontaneous magnetisation disappears and the materials become paramagnetic with effectively randomly oriented ionic magnetic moments.
- On cooling below T_C, the spontaneous magnetisation reappears with equal intensity, assuming that there have been no structural or chemical changes during the heating.

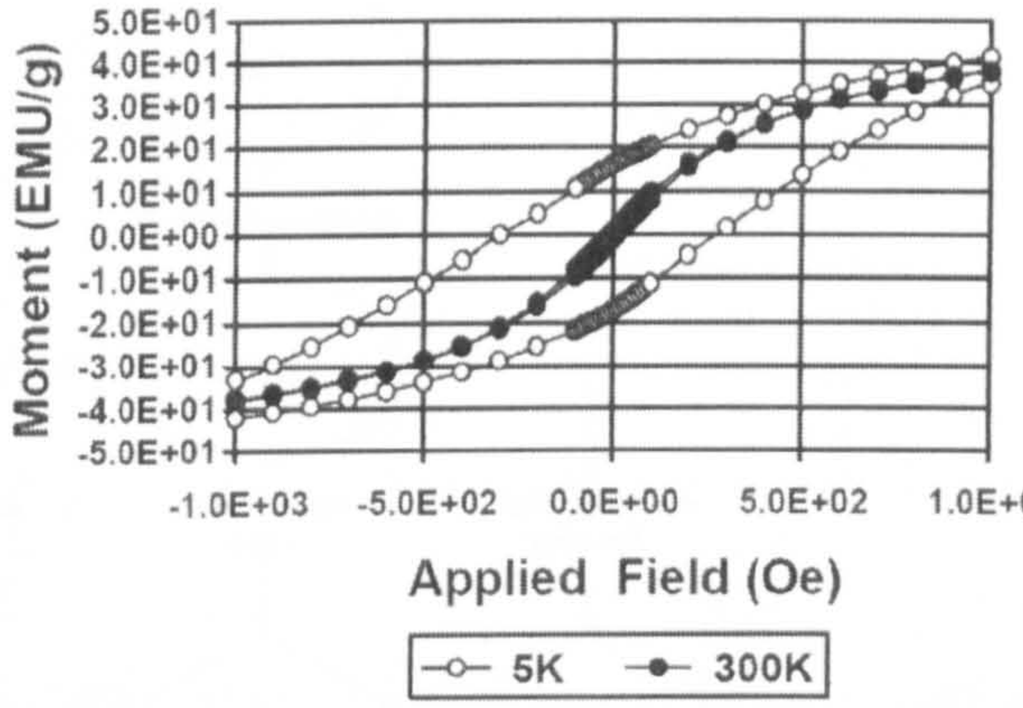

Figure 2.5-1 Applied field *vs.* magnetisation plot for the maghemite nanoparticles [123].

Figure 2.5-1 shows a magnetisation plot of γ-Fe_2O_3 nanoparticles as a function of magnetic field at 5K and 300K respectively. The T_C of this sample is about 100K. Below the T_C, particle showed ferromagnetic behaviour with an increase in remnant magnetisation M_T and coercivity H_C. At 5K, H_C was about 300Oe, and reduced to 30 Oe at 300K.

Many of the processes by which γ-Fe_2O_3 particles are prepared involve the preparation of particles of Fe_3O_4 as an earlier step, which are then converted to γ-Fe_2O_3 by carefully controlled oxidation. The transformation of $Fe_3O_4 \rightarrow \gamma$-$Fe_2O_3$ begins at 100°C and is completed at 250°C, while the transformation of $Fe_3O_4 \rightarrow \alpha$-$Fe_2O_3$ starts at 250°C and is finished at 500°C [124].A review of magnetite transformation studies is shown in **Figure 2.5-2**, and more details can be found in Cornell and Schwertmann's text [119].

Imaoka [125] used both acicular and non-acicular particles in his study of the transformations:

$$Fe_3O_4 \rightarrow \gamma - Fe_2O_3 \rightarrow \alpha - Fe_2O_3 \qquad \textbf{(2-2)}$$

Although the first step took place between 100°C and 250°C, (in agreement with Klimaszewski and Pietrzak [125]), for both particles, the second step occurred at 250-400°C for the non-acicular particles

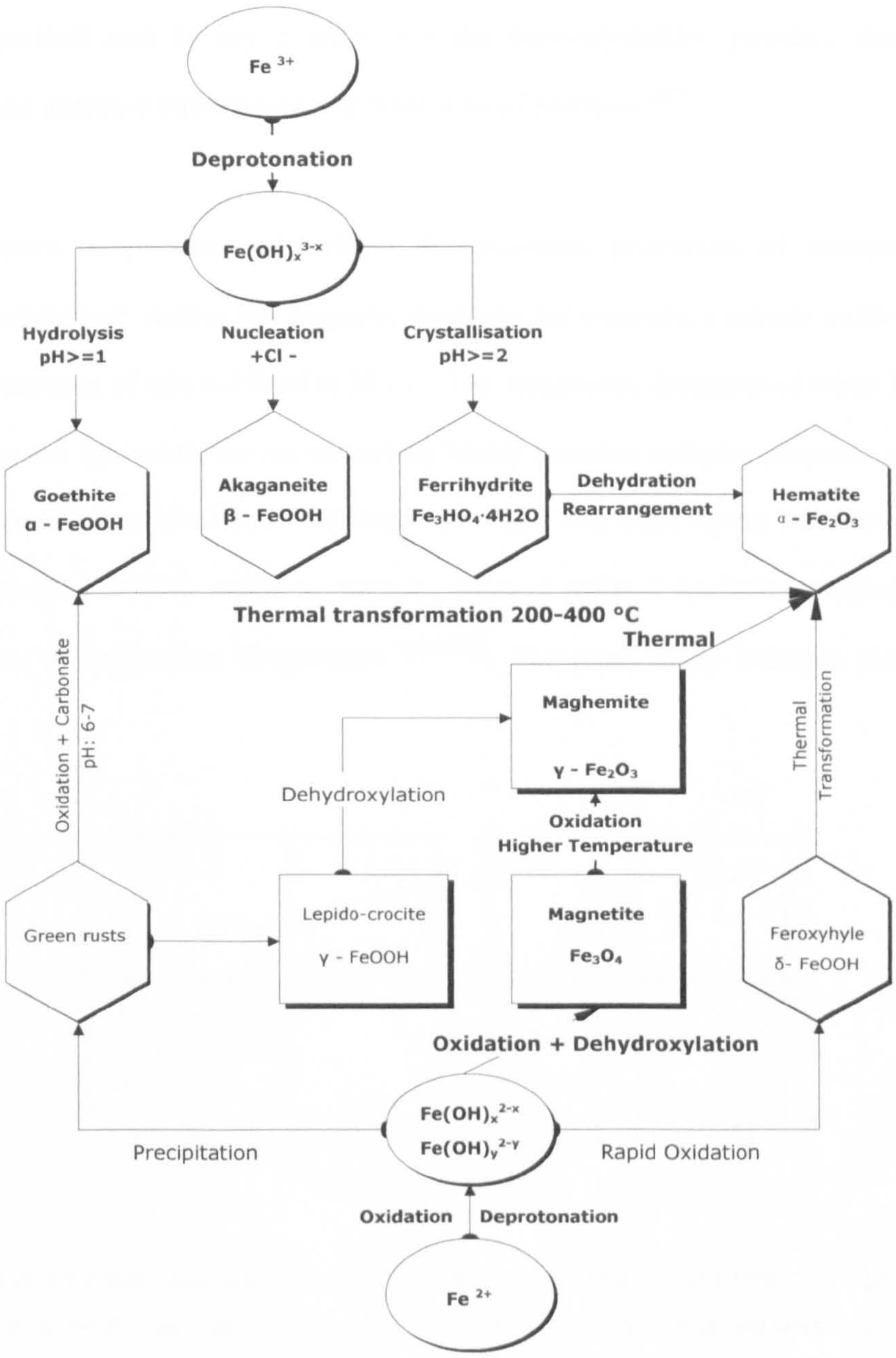

Figure 2.5-2 Transformation observed in iron oxides [125]

but at 560-650°C for the acicular ones. Bando *et al.* [126] determined that the $\gamma \rightarrow \alpha$ transformation took place in the temperature range of 400-500°C for non-acicular particles and 450-500°C for acicular particles. Gustard and Schuele converted acicular γ-Fe_2O_3 particles partially to α-Fe_2O_3 at temperatures of 525-650°C and found the remanence increased by a factor of three, (compared with

the initial value), when 90% conversion has been achieved. On the other hand, the temperature was subject to the particle size of any powder. For the nano-crystalline powders, the transformation temperature would decrease with decreasing mean size of particles [127].

The heat treatment temperature will affect the magnetic properties of nanoparticles. Higher temperatures progressively reduce the magnetic qualities; for example, a sample oxidised at 380°C has only half the remanence of one oxidised at 285°C. The remanence disappeared when heated at 665°C. **Figure 2.5-3** shows the hysteresis curves of barium ferrite powders samples prepared via two different co-precipitation methods (a: the ferrite solution was added into basic agent; b: basic agent was added into ferrite solution). For both methods, samples showed reduced intrinsic coercivity consequently with the increase of calcination temperature [128-129]. The relationship between the coercivity and

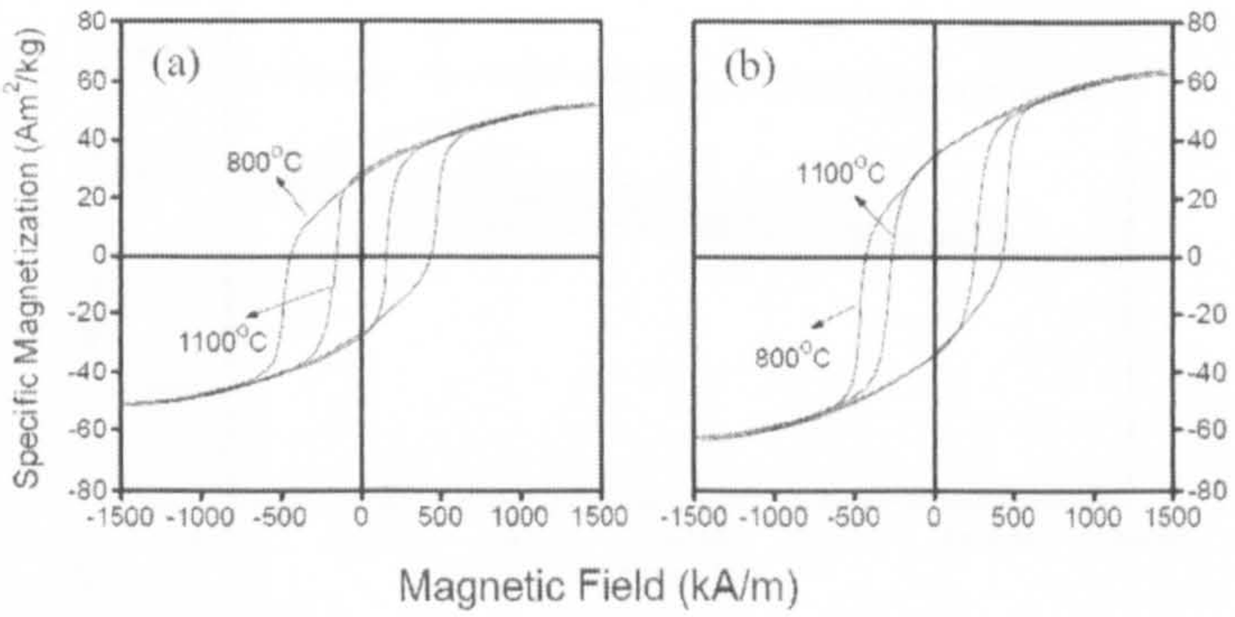

Figure 2.5-3 The Hysteresis curves of two samples calcined at 800°C and 1100°C for 1.5h [131]

a: Ferrite solution was added to the aqueous solution of sodium hydroxide and sodium carbonate;

b: The aqueous solution of sodium hydroxide and sodium carbonate was added to the ferrite solution

calcination temperature could be explained by the changing of particle size. It was reported that, with the increase of the calcination temperature, a growth of particles occurs. However, experimentally for ferromagnetic materials, the coercivity of small particles varies approximately as the inverse of the particle size [130]. Therefore the increased calcination temperature could result in the decrease of coercivity of ferro-materials.

Table 2.5-2 Magnetic properties of the barium ferrite powders [131]

Calcination temperature [°C]	Calcination time [Hour]	Intrinsic coercivity [kA/m]
800	1.5	440
1100	1.5	162
800	4.0	424
1100	4.0	142

On the other hand, the calcination time shows minor effect on the intrinsic coercivity of the barium ferrite powders. As shown in **Table 2.5-2**, with the increase of calcination time from 1.5 to 4.0 hours, the coercivity decreased by only about 2.5%. When the calcination temperature increased from 800°C to 1100°C, the decrease of the coercivity was nearly 3 times.

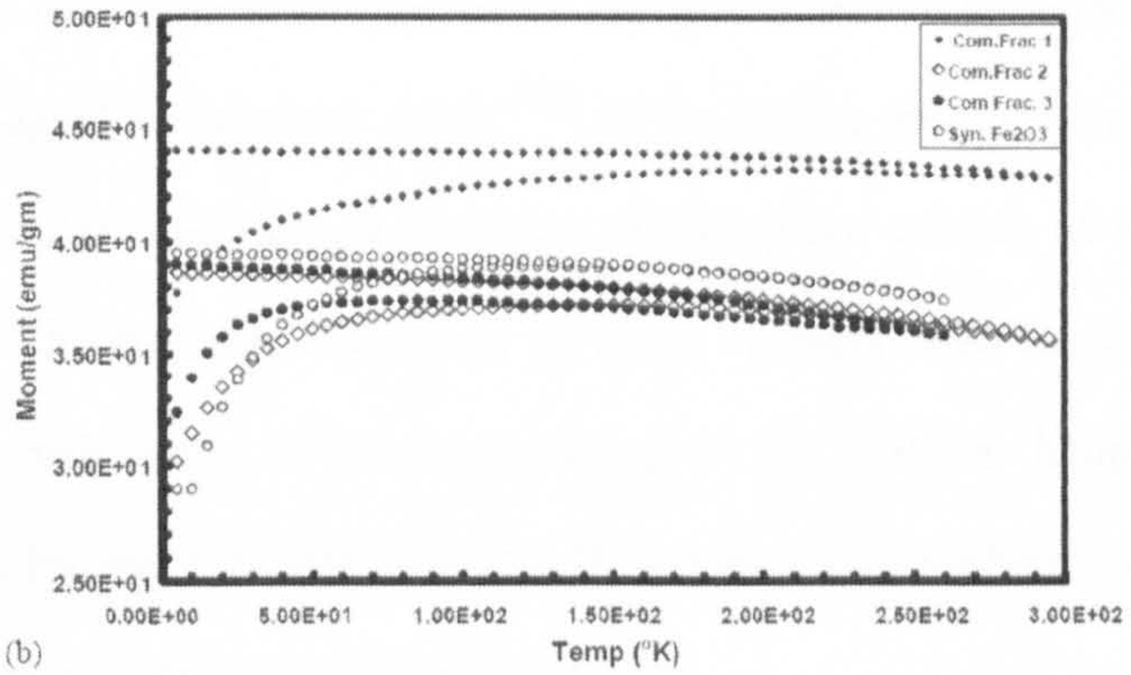

Figure 2.5-4 Temperature-moment plots for maghemite particle samples with different size [123].

Table 2.5-3 Comparison between the maghemite particle samples with different size [123].

Samples	Diameter [nm]	Curie Temperature [K]
1	130	205
2	20-30	130
3	10-12	100
4	5-11	75

It has been established by several groups that the abrupt change in magnetic properties takes place

when particles are in nanometre range. For example, nano-crystalline iron oxides are super-paramagnetic and they behave as ferromagnetic when the size is in micrometer range [123]. This kind of size-dependent magnetic property has been investigated by Chatterjee *et al.* [123]. In their study of nano-crystalline maghemite, it was found that with decrease of the particle size, the **Curie temperature** decreased. As shown in **Figure 2.5-4** and **Table 2.5-3**, the **Curie temperature** was 205K for the particles with 130 nm in size and deceased to 75 K when the particle size decreased to 5-11 nm.

2.5.1.3 Mechanism of magnetic nanoparticles formation in w/o microemulsions

The magnetic iron oxide nanoparticles can also be prepared using water-in-oil (w/o) microemulsion systems. W/O microemulsion technique was first used for the preparation of nanoparticles of metals such as Platinum [132] followed by the metal oxides such as magnetite [133] and maghemite [134].

Normally in the synthesis of magnetic nanoparticles via w/o microemulsion system, the precursor salts mixes with precipitating agent in the water cores [135], or by adding precipitating agent directly into w/o microemulsion, water droplets collide and coalesce, allowing the mixing of the reactants to produce the nanoparticles [136-138] The reactants dissolved in water droplets need to get through the surfactant layer before they meet each other. Hence, comparing to the reaction happening in bulk aqueous solution by precipitation, the reaction rate could be slower in microemulsion system. **Figure 2.5-5** shows the schematic of the reaction in the microemulsion system.

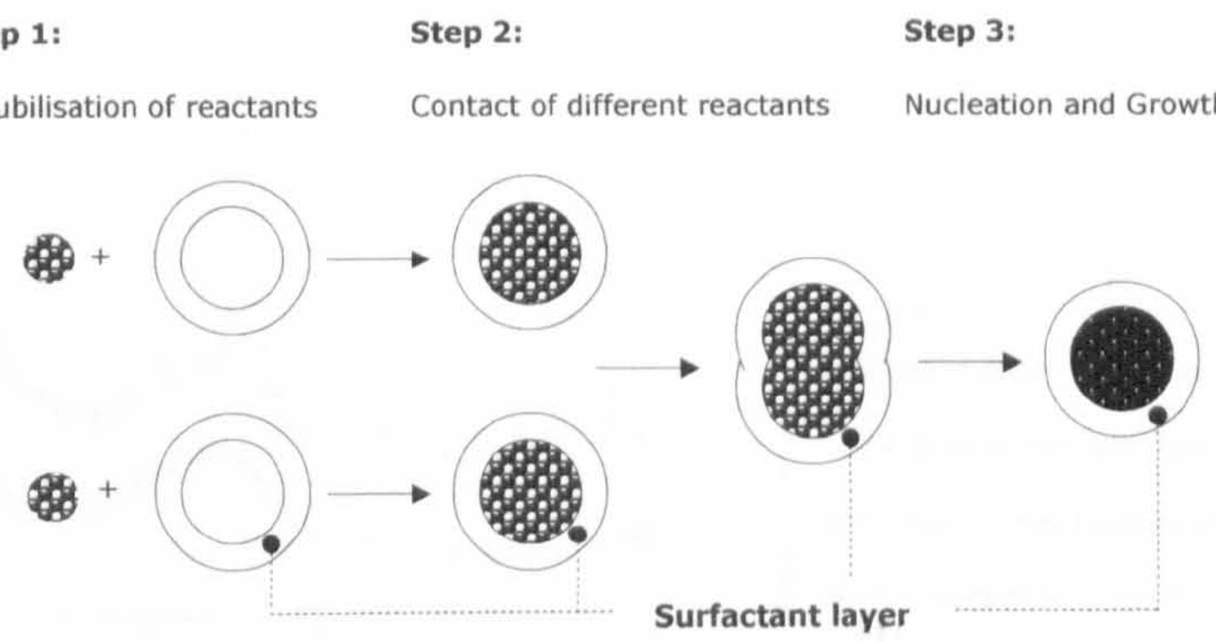

Figure 2.5-5 Schematic illustration of various stages in the growth of ultra fine particles in microemulsions.

The exchange of ions between the water-droplets by either diffusion or collision of them affects the particle formation. The surfactant walls act as barriers to the particle nucleation in synthesis via microemulsion. On the other hand, these walls of the micro-droplets act as cages for particle's growth. Consequently, the cage effect results in a narrow particle size distribution. The overall mechanism of particle nucleation and growth in w/o microemulsion involved both intra- and inter-micelle processes. Besides reactant diffusion to existing particles, the particle growth also involved aggregation of nuclei during micelle-micelle collisions.

2.5.1.4 System-dependent studies of magnetic properties of particles

As for the synthesis of nanomaterials via microemulsion, system-dependent properties of nanoparticles reveal the possibility of system-control in fabrication, which is actually a great motivation to introduce microemulsion method into the nano-synthesis area.

- **Effect of Molar ratio of water phase to surfactant ω_0**

The number of ω_0 has a direct correlation with the water pool radius, and the size of the water pool also correlates with the size of inorganic particles formed. Chhabra *et al.* [139] prepared iron oxide nanoparticles via water-in-oil microemulsion system with cyclohexane as the oil phase and the Triton X-100 as the surfactant. From a systematic XRD study of samples derived from different ω_0 values and calcined at different temperatures **[Figure 2.5-6]**, it was found that the single-phase γ-Fe_2O_3 was

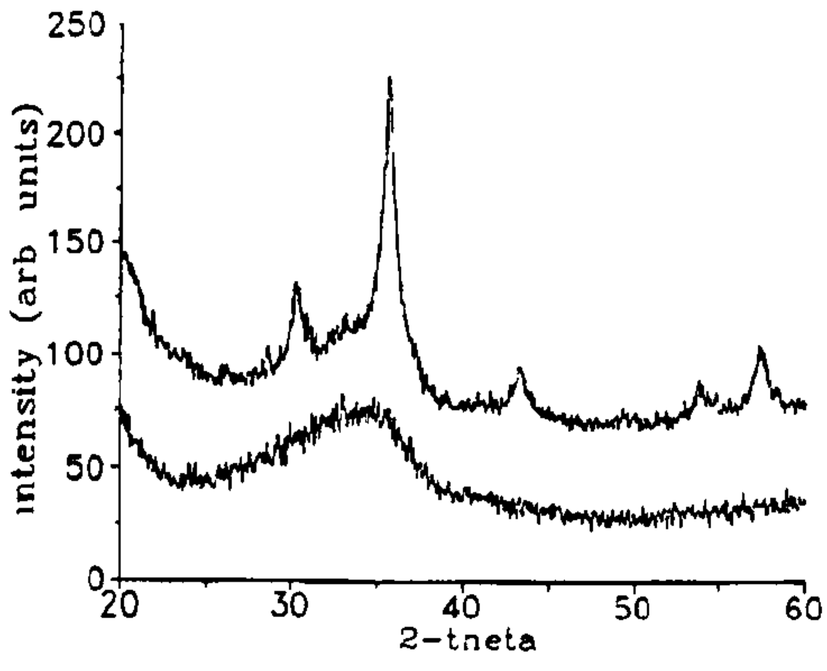

The lower curve corresponds to amorphous Fe_2O_3 from a microemulsion with ω_0=30;
The upper curve represents γ-Fe_2O_3 from a microemulsion with ω_0=40.

Figure 2.5-6 XRD of the Fe_2O_3 particles produced via the microemulsion followed by calcination at 225°C [139].

Table 2.5-4 Crystallographic phases of Fe_2O_3 obtained at different calcination temperature for different values of ω_0.

Calcination Temperature [°C]	ω_0			
	30	40	50	60
225	amorphous	γ	γ	γ
250	γ	α+ γ	α+ γ	α+ γ
275	α+ γ	α+ γ	α+ γ	α+ γ
300	α+ γ	α+ γ	α+ γ	α+ γ

α: α-Fe_2O_3; γ: γ- Fe_2O_3

formed when ω_0 varied from 40-60 followed by calcination at 225°C. The amorphous γ-Fe_2O_3 appeared when ω_0=30. When the calcination temperature was increased, the single-phase γ-Fe_2O_3 was only formed when ω_0=30, (which correspond to smaller droplet size) [139]. Other samples consisted of the mixture of γ and α phase **[Table 2.5-4]**.

It was also found that with the increase of ω_0, there is a slight increase in the droplet diameter, D_h. Consequently, the equivalent spherical diameter, D of the corresponding γ-Fe_2O_3 particles synthesised *in* situ increased as well **[Table 2.5-5]**. Hence, it is possible to control the average size of the solid particles by the size of the microemulsion droplets [139] in synthesis via microemulsion system.

Table 2.5-5 Correlation between the droplet diameter of microemulsion and the diameter of product for different ω_0.

Microemulsion phase		Product Fe_2O_3 (calcined at 225°C)
ω_0	D_h /nm	D /nm
30	24	7.5
40	27	7.6
50	30	7.7
60	32	8.2

- **Effect of Surfactant**

According to the investigation of hematite nanoparticles synthesised with and without surfactants by Jing *et al.* [140], different surfactants influenced not only the morphology of particles but also their magnetic properties.

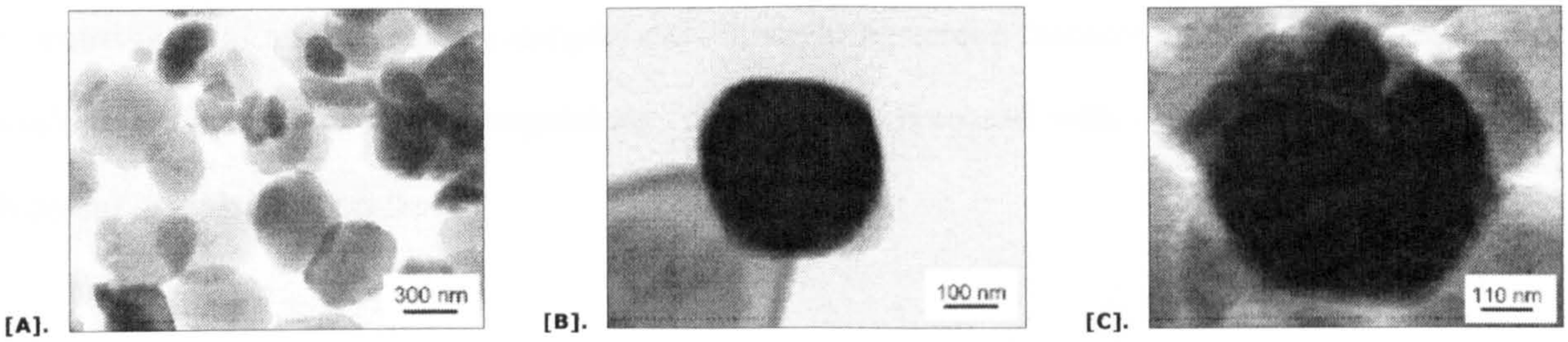

Figure 2.5-7 TEM micrographs of α-Fe_2O_3 prepared with **A.** no surfactant, **B.** DBS, **C.** SDS, **D.** CTAB, **E.** HPC [140].

Sodium dodecylsulphonate (SDS), hexadecyipyridinium chloride (HPC), sodium dodecylebenzene sulphonate (DBS) and cetyltrimethyl ammonium bromide (CTAB) are four surfactants used in the preparation of α-Fe_2O_3. TEM micrographs of α-Fe_2O_3 nanoparticles prepared by microemulsion with different surfactants are shown in **Figure 2.5-7**. The particle size of the sample prepared with surfactant was clearly smaller than particles prepared without surfactant. The TEM micrographs of the particles from α-Fe_2O_3/SDS, α-Fe_2O_3/HPC, α-Fe_2O_3/DBS and α-Fe_2O_3/CTAB shows hexagonal, rhombohedral, sub-round and hexagonal-like morphology, respectively and the corresponding particle size was about 230±10, 150±8, 240±15 and 260±5 nm. Meanwhile the α-Fe_2O_3 prepared without surfactant showed irregular shape with the size around 380±50 nm.

Table 2.5-6 Shape, particles size and magnetic parameters of the samples prepared with and without surfactants

Sample	Shape	Particle size	Coercivity [Oe]	Remnant magnetisation [emu/g]
α-Fe_2O_3	Irregular	380±50	68.00	0.01058
α-Fe_2O_3/SDS	Hexagonal	230±10	19.01	0.00382
α-Fe_2O_3/DBS	Subround	240±15	179.2	0.04189
α-Fe_2O_3/CTAB	Hexagonal-like	660±5	577.8	0.05931
α-Fe_2O_3/HPC	Rhombohedral	150±8	93.29	0.01483

The magnetic parameters of each sample are summarised in **Table 2.5-6**. The magnetisation measurements of all the α-Fe_2O_3 samples exhibit slight hysteretic features, indicating that they are all weak ferromagnetic at room temperature. The α-Fe_2O_3 prepared with different surfactant showed different magnetic properties.

2.5.2 Synthesis of core-shell structured nanocomposites via microemulsion

The water-in-oil microemulsion is a versatile and effective technique for size-specific synthesis of nanoparticles and core/shell structured nanocomposites. Normally, the overall procedure for preparation of magnetic nanocomposites involves the following steps:

- Core formation: synthesis of nano-magnetic particles via w/o microemulsion;
- Coating layer on the nano-magnets in w/o microemulsion:
  - Encapsulate the nano-magnetic core in polymer spherical shell
  - Magnetic nanoparticles coated with ceramic by hydrolysis reaction of alkoxide.

The first stage, core formation, has been discussed in **2.5.1.3: Mechanism of magnetic nanoparticles formation in w/o microemulsions**. Hence, the synthesis of core-shell structured nanocomposites will only include polymer and ceramic coating via microemulsion systems.

2.5.2.1 Polymerisation in microemulsion

Polymerisation reactions in microemulsion (also called microemulsion polymerisation) can be used to produce very small polymer spheres. The stable microemulsion polymerisations usually produce nearly spherical nanoparticles with sizes below approximately 100 nm [141].

W/O microemulsion polymerisation involves the dispersion of an aqueous monomer solution in a continuous oil phase under continuous agitation. Surfactants are added into the organic oil phase to

make the overall hydrophilic-lipohilic balance (HLB) of system between 3 and 8 [142]. Since the w/o microemulsion system is thermodynamically stable. It avoids the need for periodic mixing which is required during the long-term storage of macro-emulsions [143]. Furthermore, the polymerisation in w/o microemulsions often leads to very high-molecular weight products with good rheological properties such as high fluidity even at large volume fractions [144].

The mechanism of polymerisations in the w/o microemulsion system includes droplet collisions or migration of monomer through the interface into the droplets. The final product is composed of one single highly collapsed polymer chain per latex [143].

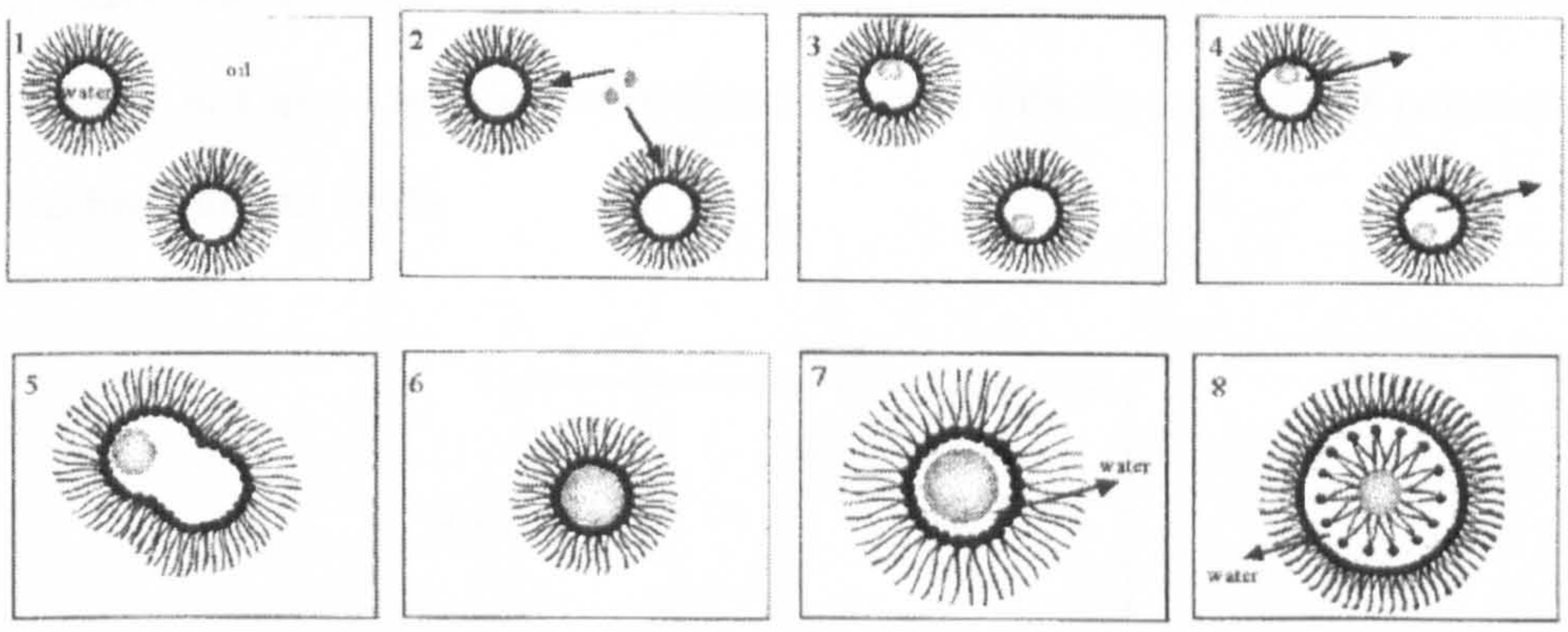

Figure 2.5-8 Schematics of the formation of polymer nano-spheres in w/o microemulsion systems.

The formation of polymer nanospheres in microemulsion is consisted of several stages. The schematic of step-by-step polymerisation in w/o microemulsion systems is shown in **Figure 2.5-8** [145]:

❶: The aqueous cores are surrounded by the surfactant and disperse in the oil phase to form w/o microemulsion system.

❷: The water-soluble monomer dissolved in the appropriate aqueous solution is added drop-wise into the w/o microemulsion. The solution goes to the aqueous cores by diffusion and penetrates inside by crossing the surfactant layers. The aqueous solution plays a role in the transport of the water-soluble organic molecule into the aqueous cores [145].

❸: The polymer nano-sphere forms in the aqueous cores.

❹❺: The reactants exchange between the aqueous cores as a result of collisions between droplets and the formed nuclei can grow [145].

❻❼❽: The formed nanospheres are stabilised by surfactant molecules.

The parameters which could affect the result of the reaction of polymerisation in microemulsion are summarised in following for pure polymer nanospheres and core-shell structured nanocomposites.

- **Effect of time**

The conversion-time plots of replicate polymerisations are shown in **Figure 2.5-9** from the research work of Hernández-Barajas *et al.* [146], which indicate the dependence of polymerisation conversion (%) on time. As shown in **Figure 2.5-9**, the conversion increased with the increase of polymerisation time and finally reached close to 100%.

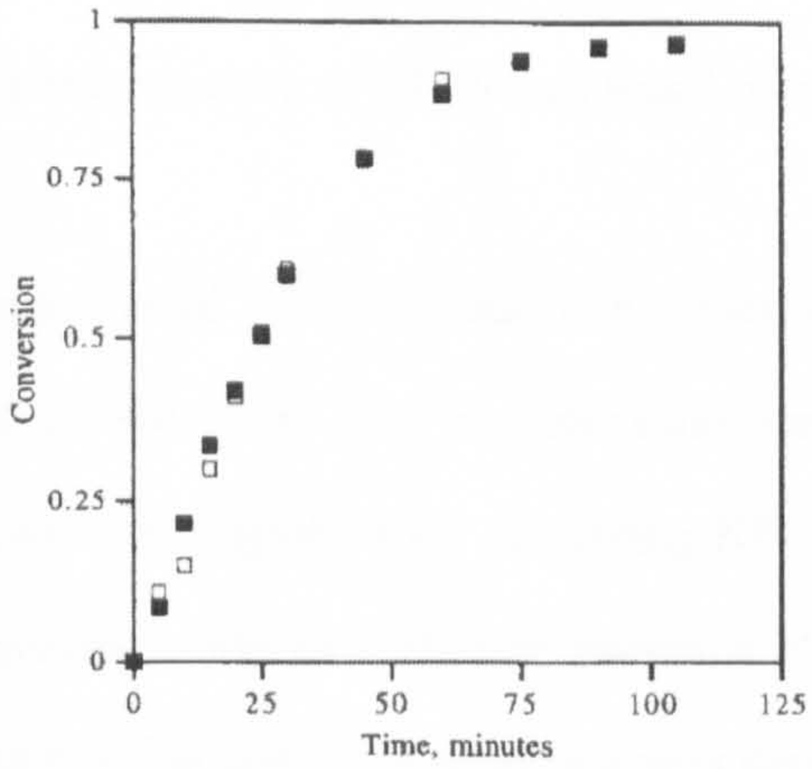

Figure 2.5-9 W/O microemulsion polymerisation of acrylamide using V-70 as initiator [146].
A. ME6 (■) and ME7 (□) are two samples with same experimental conditions.

- **Effect of Monomer and Initiator Concentration**

Candau *et al.* [147] investigated the effect of monomer and initiator concentration on the polymerisation of acrylamide (AM) in w/o microemulsions stabilised by Aerosol OT (AOT) and initiated with azobisisobutyronitrile (AIBN) or potassium persulphate (KPS).

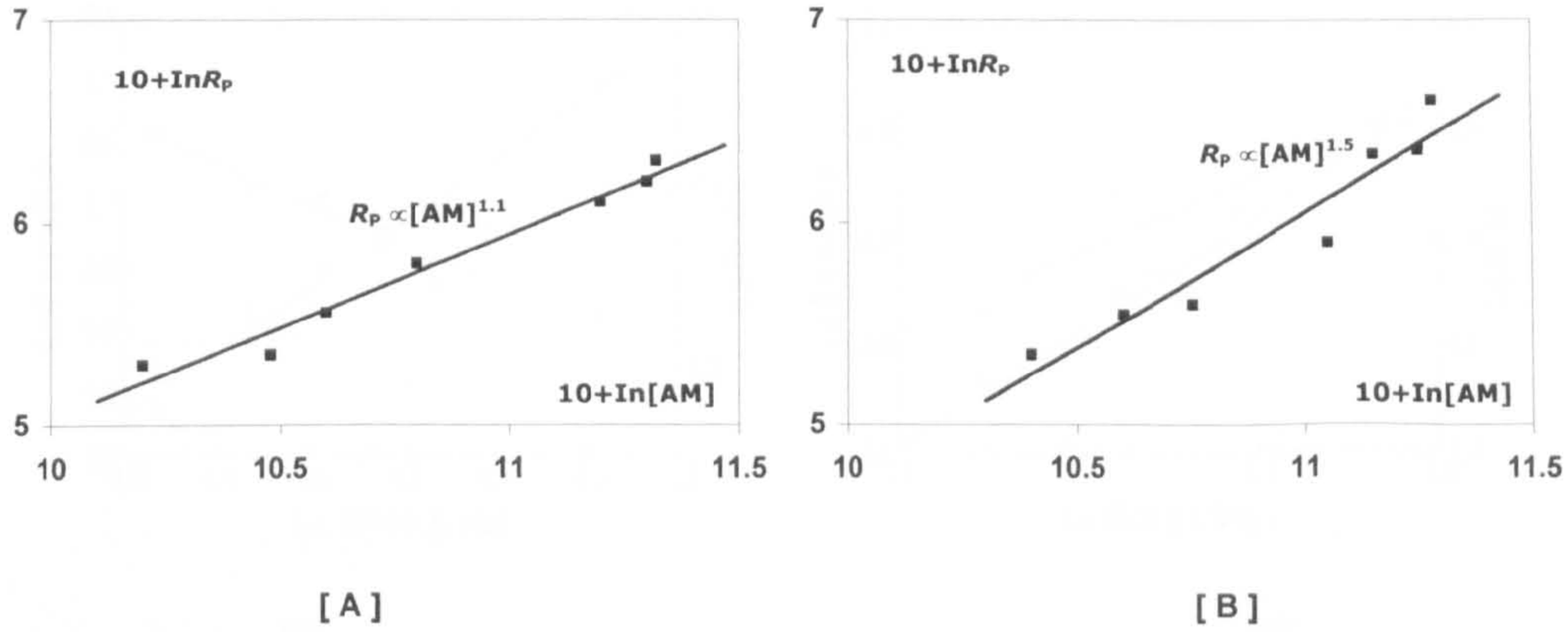

Figure 2.5-10 Dependence of the rate of polymerisation on monomer concentration in the presence of A. AIBN, B. KPS [147].

Since KPS is a water soluble initiator and acrylamide is a water soluble monomer, both of them will be located in the dispersed water phase. In the AM polymerisation initiated by KPS, the initiators do not need to migrate through the interface, which is on contrary to the reaction initiated by AIBN, an oil-soluble initiator. As shown in **Figure 2.5-10**, the rate of polymerisation, R_p increased with the increase of monomer concentration in both polymerisation processes. R_p was first order with respect to initial monomer concentration in the presence of AIBN and was 1.5 orders with KPS [147].

According to the result of Candau *et al.* [147], the rate of polymerisation seems independent of the initiator concentration, except in the very low concentration range. The molecular weight of polyacrylamide (PAM) decreases very slightly with increasing KPS concentration. However, in the study of the microemulsion polymerisation of AM with presence of sodium bisulphite, $NaHSO_3$ as initiator, Hao *et al.* [148] reported that the polymerisation rate was dependent on the square root of the initiator concentrations. This dependence has been confirmed for many different monomer-initiator combinations over ranges of monomer and initiator concentrations [149]. Therefore, in some cases, the concentration of initiator could affect the polymerisation rate.

In the investigation of microemulsion polymerisation of methyl methacrylate (MMA) initiated by benzoyl peroxide (BPO), Xu *at el.* [150] found that the polymerisation rate R_p increased almost linearly with the increase of initiator concentration, meanwhile the polymer molecular weight, $\overline{M_n}$ decreased

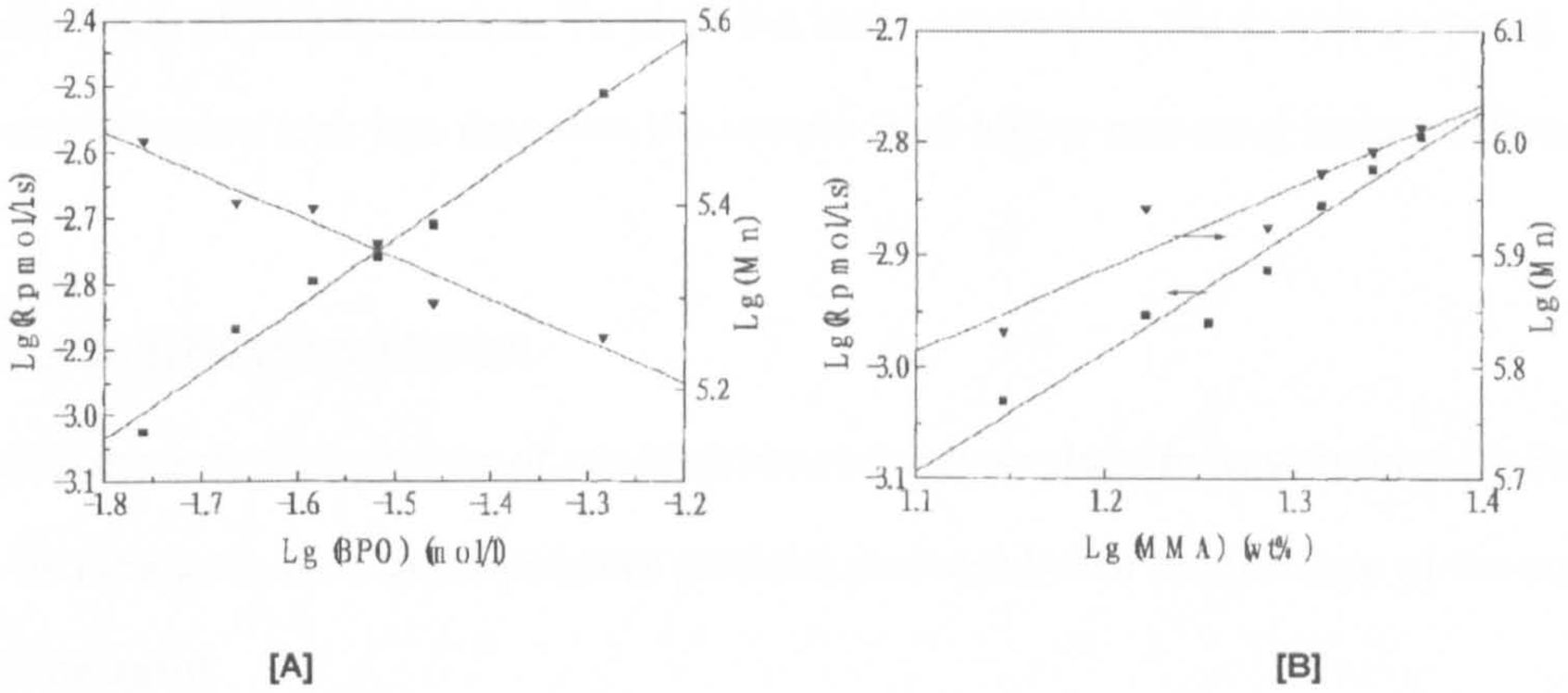

Figure 2.5-11 Effect of BPO and monomer concentration on polymerisation of MMA at 60°C [150]. **[A]** Effect of BPO concentration on polymerisation. 20%MMA, 68% H_2O; **[B]** Effect of monomer concentration on polymerisation. 30.8×10^{-3} BPO

[**Figure 2.5-11 A**]. R_p was first order with respect to BPO concentration and the molecular weight of poly-(methyl methacrylate) (PMMA) was negative 0.45 orders to initiator concentration. However, as shown in **Figure 2.5-11 B**, the polymerisation rate and polymer molecular weight both increased with the increase of monomer concentration: $R_p \propto [MMA]^{1.07}$; $\overline{M_n} \propto [MMA]^{0.75}$.

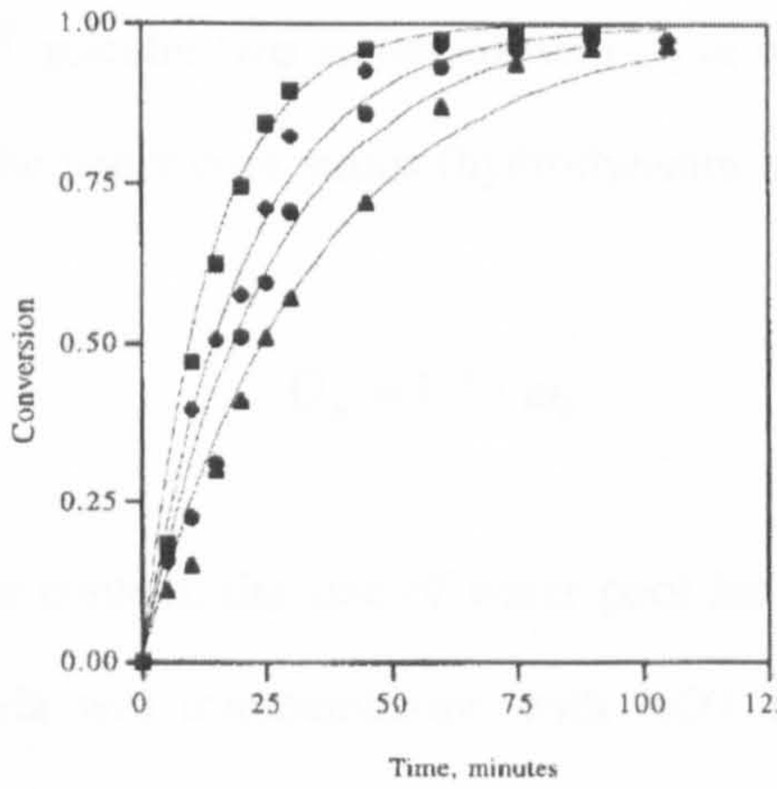

Figure 2.5-12 W/O microemulsion polymerisation of acrylamide using V-70 as initiator [146] with various molar initiator concentrations: 2.43 mmol/L (■), 1.62 mmol/L (◆), 1.29 mmol/L (●), 0.972 mmol/L (▲)

The effect of monomer concentration on polymerisation in w/o microemulsion was also investigated by Hernández-Barajas *et al.*[146]. As shown in **Figure 2.5-12**, the conversion of monomer increased with

the increase of polymerisation time. The reaction with different monomer concentration showed different efficiency of polymerisation. To yield the same conversion, the sample prepared from lower monomer concentration took less time than the sample from higher monomer concentration.

- **Effect of crosslinking concentration**

A two-stage polymerisation process of micro-structured polyacrylamide was reported by Puig *et al.* [151]. As shown in **Table 2.5-7**, the size of polymer particles increased with the increase of the concentration of crosslinking agent.

Table 2.5-7 Particle size for the w/o microemulsion polymerisation of acrylamide in the presence of various concentrations of crosslinking agent [151]

$m_{crosslinking\ agent}/m_{AM}$ [g/g]	D^a [nm]	D^b [nm]
0.01	53	41
0.02	58	45
0.05	62	48

[a]: Particle size in final latex; [b]: Estimated dry particle size

- **Effect of molar ratio of water to surfactant ω_0**

As reported in the literature [152], micelle size increased with ω_0 in w/o microemulsion with AOT [153] and a direct correlation of D_h, the water core radius (hydrodynamic radius) with ω_0 is given as below, and D_h is in nm:

$$D_h = 1.15\,\omega_0 \qquad \textbf{(2-4)}$$

Therefore with increasing water content, the size of water pool increases. The TEM micrographs of PAM nano-spheres prepared via w/o microemulsion with AOT is shown in **Figure 2.5-13**. In the presence of water, the polymer particles swell, and the internal density of PAM particles decreased with the increase of ω_0, but resulted in larger polymer micro spheres. It is also observed that, with $\omega_0 \geq 30$, over 70% of the particles have a somewhat hollow interior structure [154], probably due to the tendency of the incorporated water to segregate from the bulk aliphatic hydrocarbon solvent into the polymer matrix [154].

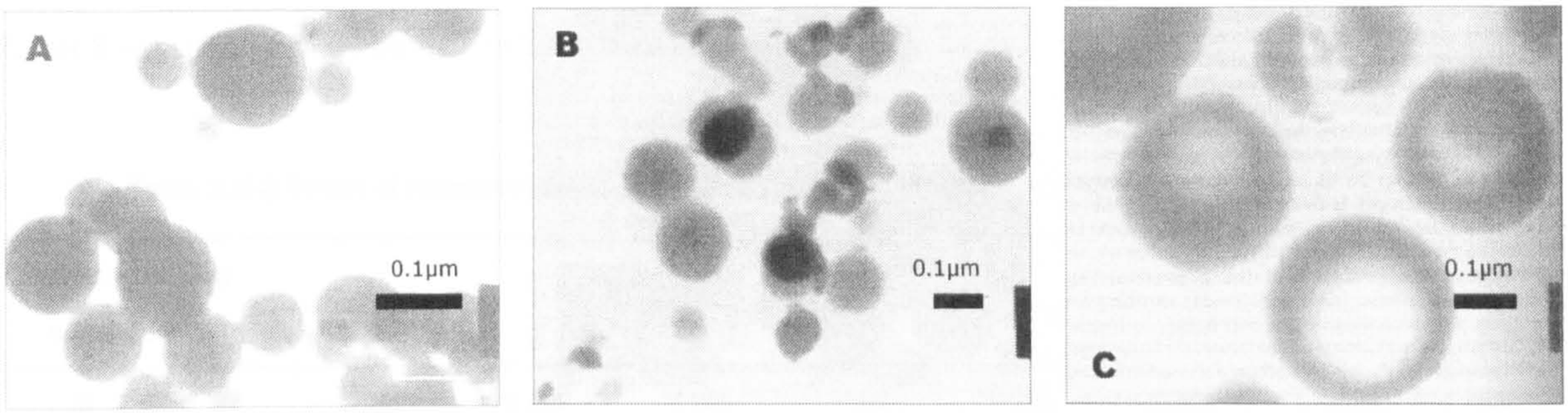

Figure 2.5-13 Transmission electron micrographs of the polymer precipitated in AOT/isooctane w/o microemulsions micelles when **[A].** $\omega_0 = 0$, **[B].** $\omega_0 = 20$, **[C].** $\omega_0 = 35$ [154]

The same dependence of polymer particles on ω_0 was reported by Dresco *et al.* [155]. According to his results, the radius of polymeric particles increased with the increase of ω_0. The size of polymer particles was about 1.5 order to the molar ratio of water to surfactant **[Figure 2.5-14]**.

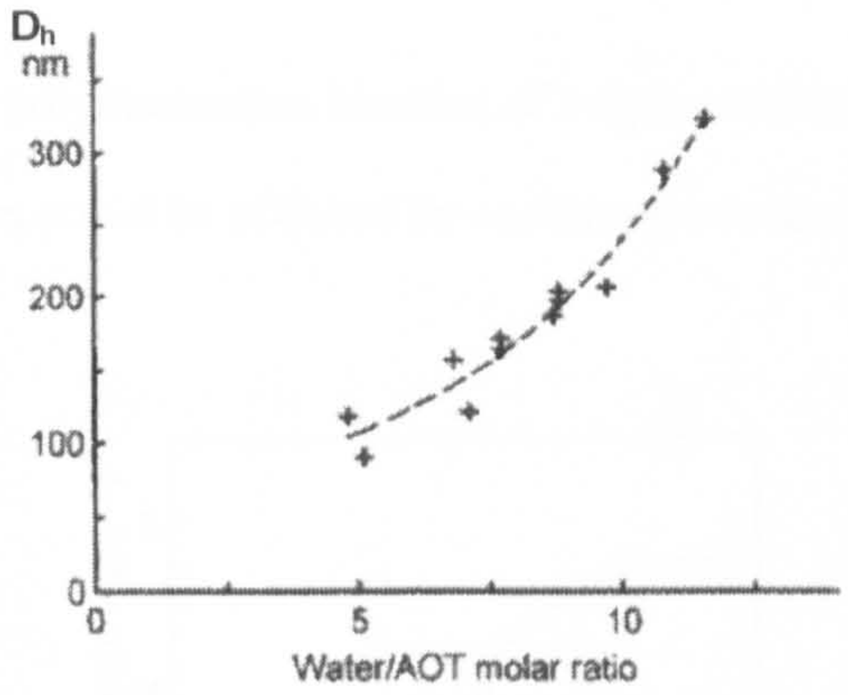

Figure 2.5-14 Variation of hydrodynamic radius D_h with water to AOT molar ratio. The dotted line is given as a trend line [155].

In fact, the interior structure of microemulsion system would change consequently with the changing of ω_0. Hao *et al.* [148] investigated the effect of microemulsion structure on polymerisation of acrylamide. As shown in **Table 2.5-8**, the microemulsion composition for 1, 2, 3 and 4 were w/o microemulsion systems with the weight ratio of $Surfactant : Oil : Water = 9:2:9$ and the contents of co-surfactant (n-butanol) decreased in proper order. The composition for 5, 6 and 7 were bi-continuous (BC) microemulsion system with the weight ratio of $Surfactant : Oil : Co-surfactant = 9:2:9$ and

the contents of water increased in proper order. The component content for 8 was the same as 5, 6 and 7, but 8 was prepared as an o/w microemulsion system.

Table 2.5-8 Effect of microemulsion structures on polyacrylamide molecular weights at 30 °C [148].

Microemulsion composition	W/O				BC			O/W
	1	2	3	4	5	6	7	8
$M \times 10^{-5}$	6.58	9.65	9.58	7.34	5.75	3.68	2.92	5.60

The molecular weights of PAM shown in **Table 2.5-8** were different in different microemulsion. The highest molecular weights are obtained in W/O microemulsion system because water-soluble monomer, acrylamide is solubilised mostly in the water-pool. The lowest molecular weight was obtained in BC because the polymerisation might be stopped [168] by the free-radical reaction

- **Effect of Surfactant**

Hao *et al.* [148] investigated the polymerisation kinetics of acrylamide in the w/o microemulsion system and found that the reaction rates could be affected by surfactant concentrations.

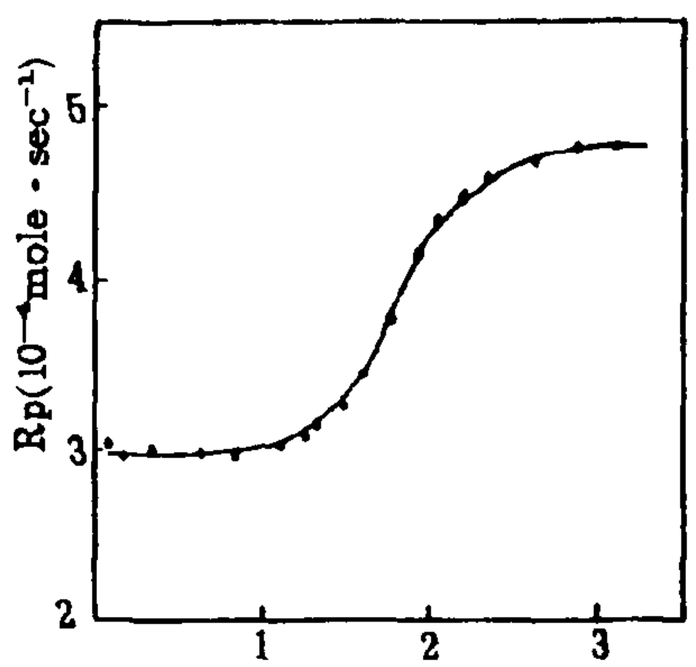

Figure 2.5-15 Plot of the initial rate of polymerisation, R_p *vs.* the logarithm of CTAB concentration.

As shown in **Figure 2.5-15**, at concentrations of cetyl-tri-methyl-tetrammonium bromide (CTAB) below the critical micelle concentration, CMC, the polymerisation rate R_P was nearly the same as that in the

aqueous solution. The increase of R_P was modest small in the CMC region but there is a remarkable rise of R_P when [CTAB]=8.0×10^{-3} M, the second CMC, which is the transition concentration of the structure of microemulsion system from spherical to rod-like micelles. With further increase of CTAB concentration, the polymerisation rate approached an unchanged value [148]. The high R_P occurring in the concentration of the second CMC of CTAB indicated that the reaction rates were sensitive to the change in microemulsion structure [148]. The different concentration of surfactant could result in different arrangement of micelles. And the latter would probably affect inter- and intra- micelle exchange of the reactant, which result in different kinetics of polymerisation.

Capek [156] investigated the effect of surfactant on polymerisation by the synthesis of polyacrylamide via microemulsion system with Tween 85 as surfactant. The effect of Tween 85 concentration on the AIBN-initiated microemulsion polymerisation of AM is summarised in **Figure 2.5-16**. The polymerisation was very fast and the final conversion (close to 100%) was reached in 10 minutes. It could be observed that to yield the same conversion, the sample prepared from lower initiator concentration took less time than the sample from higher initiator concentration, which presumably due to the increased size of surfactant aggregates decreased the entry rate efficiency of oil-soluble initiator AIBN and consequently decreased the AM polymerisation rate in w/o microemulsion. That

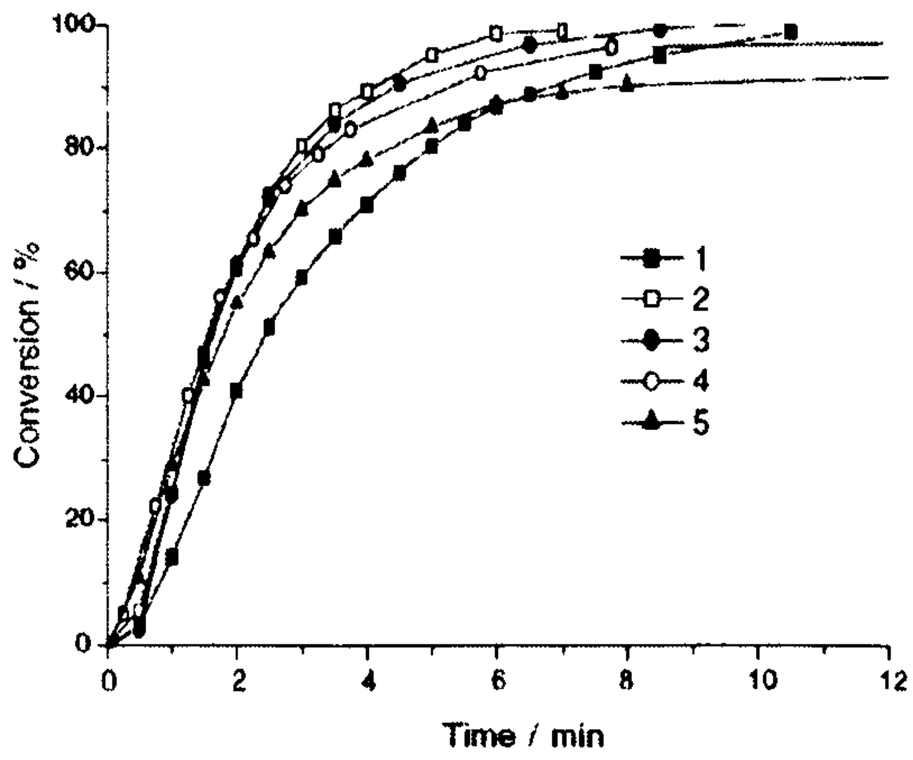

Figure 2.5-16 Variation of the monomer conversion in the w/o microemulsion polymerisation of AM, with different Tween 85 concentration and the reaction time at 60°C [156].

Tween 85 concentration /mol·dm^{-3} $\times10^{2}$: **[1].** 2.72, **[2].** 5.44, **[3].** 8.16, **[4].** 10.88; **[5].** 13.6.

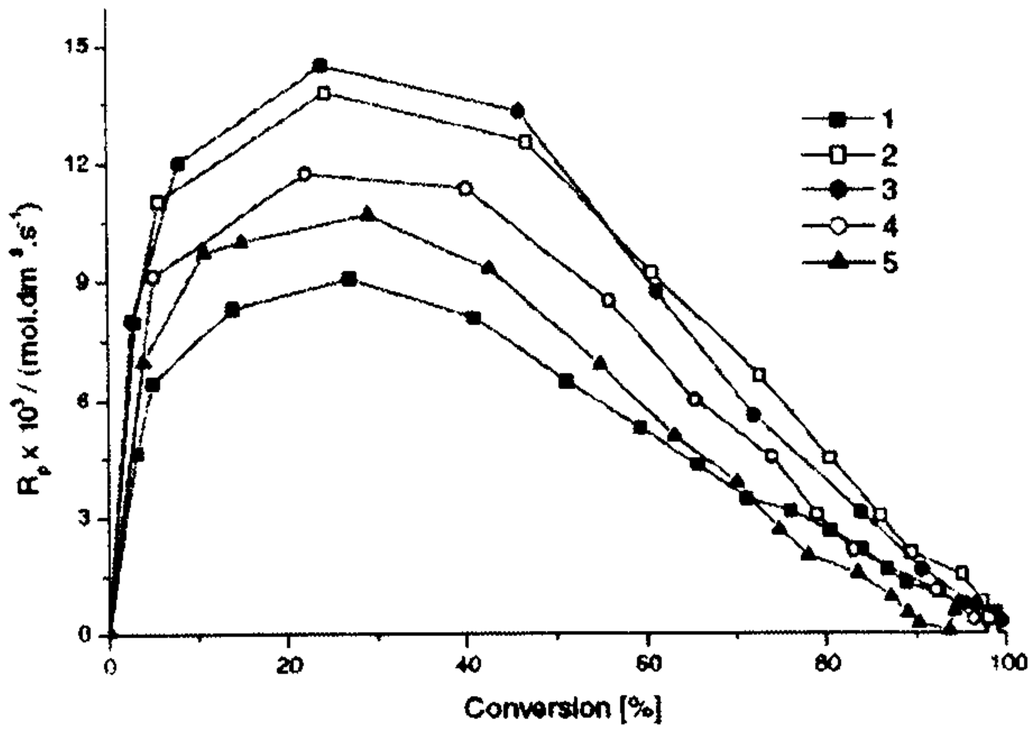

Figure 2.5-17 Variation of the rate of polymerisation in w/o microemulsion polymerisation of AM, with different Tween 85 concentration and the reaction time at 60°C [156].

Tween 85 concentration /mol·dm^{-3} $\times 10^2$: **[1]**. 2.72, **[2]**. 5.44, **[3]**. 8.16, **[4]**. 10.88; **[5]**. 13.6.

was supported by the results of the effect of surfactant concentration on rate of polymerisation and its conversion shown in **Figure 2.5-17**. The rate of polymerisation R_p of all samples rapid firstly increased to the maximum value (stage I), then kept a constant value where the conversion was up to 50% (stage II), and finally decreased until the end of reaction (stage III), where the conversion was close to 100%. The increase in the initial rate of polymerisation probably results from the particle nucleation. In stage I, it is same as the previous investigation that the higher surfactant concentration resulted in the higher polymerisation rate. However, in stage III the higher concentration of surfactant resulted in the lower polymerisation rate **[Figure 2.5-17, the curves 1, 2 and 3]** [156].

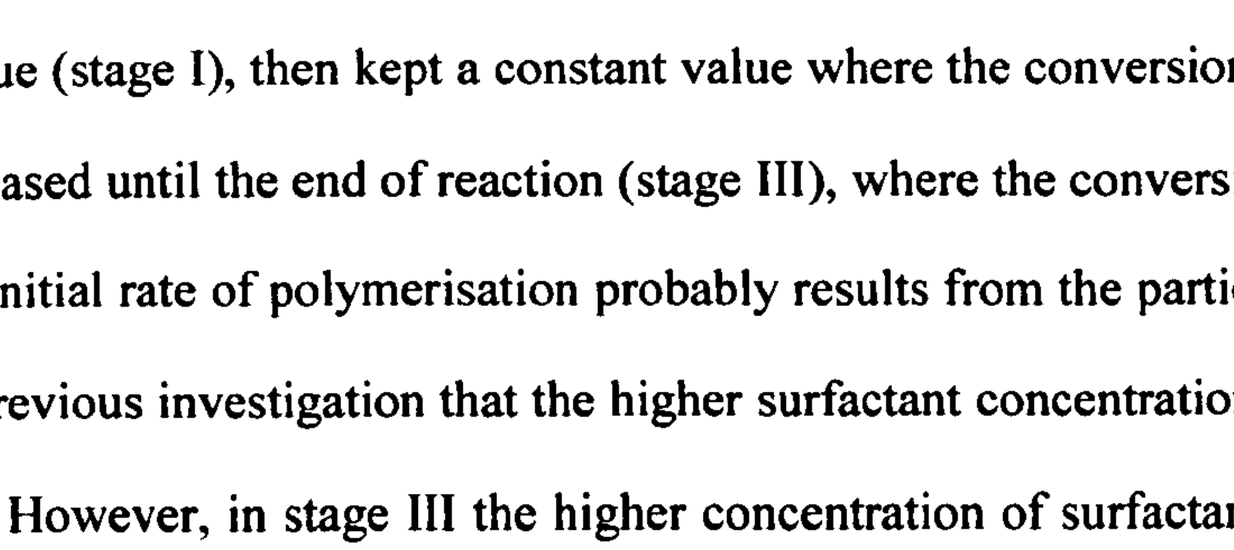

Figure 2.5-18 Variation of the rate of polymerisation in the w/o microemulsion polymerisation of acrylamide (AM), with the Tw85 concentration. 100g cyclohexane, 35g water, 5g AM, 0.104g AIBN, 60°C [156].

The dependence of the maximal rate of AIBN-initiated polymerisation *vs*. Tween 85 concentration is described by a curve as shown in **Figure 2.5-18**. The decrease in the polymerisation rate appeared at the higher surfactant concentration, which is possibly attributed to the decreased radical concentration in the polymer particle. Hence the dilution of monomer concentration could result in the reduction of the polymerisation rate.

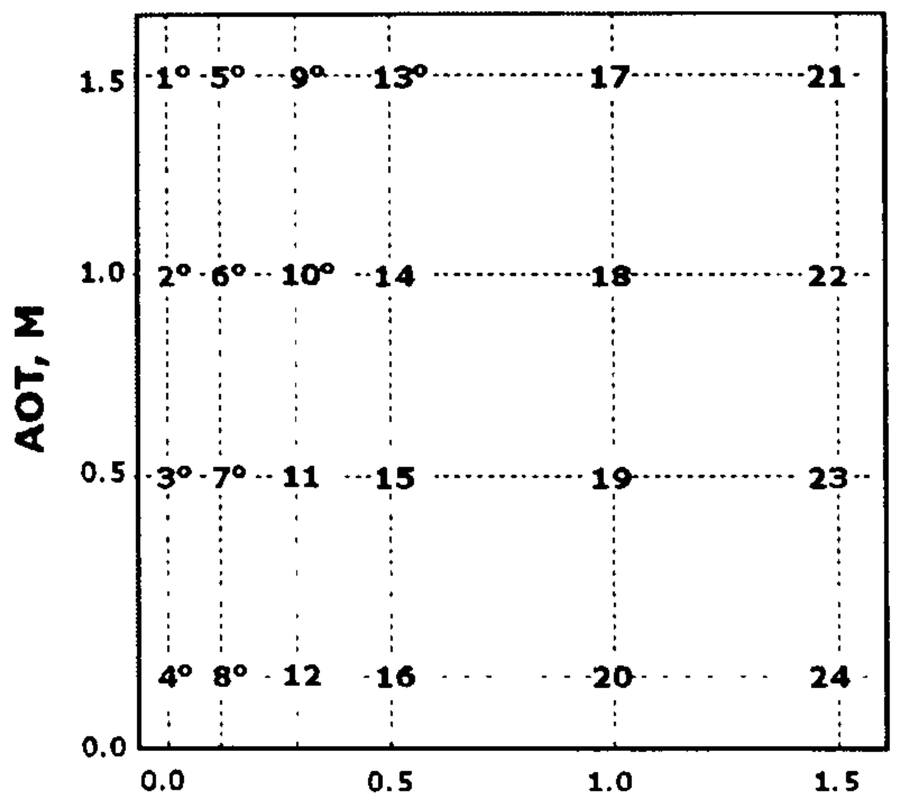

Figure 2.5-19 AOT and p-ethylphenol compositions corresponding to synthesis experiments The numbers with superscripted circles indicate compositions where the synthesised polymer has spherical morphologies [167].

The ratio of surfactant to monomer in polymerisation significantly affects the morphology of final products. Karatyigitoglu et al. [157] found that clear and well-defined spherical morphologies are not always obtained. The spherical morphology can be produced only at specific phase compositions dictated by the surfactant to monomer ratio. In **Figure 2.5-19**, the points with the superscripted O (1, 2, 3, 4, 5, 6, 7, 8, 9, 10, 13) correspond to phase compositions where spherical polymer particles are generated. Generally, the polymer spheres appeared when the monomer concentration was low. With the increase of monomer concentration, the spherical polymer particles appeared at the high concentration of AOT. As a conservative estimate, the molar ratio of AOT to monomer had to be maintained as 3:1 for the generation of spherical morphology.

2.5.2.2 Synthesis of Ceramics via microemulsion

The mechanism of the alkoxide hydrolysis process involves both hydrolysis and condensation reactions. The question of bound or free water in the polar domain of the fluid medium is relevant to the formation of particles in W/O microemulsion systems, since the hydrolysis reaction is expected to be facilitated when free water is present [158]. Hence, the rate of hydrolysis is affected by the percentage of the surfactant and the water phase in microemulsion system, which is attributed to both steric effects and hydrogen bonding.

Silicon oxide is a good example of the hydrolysis process. In the hydrolysis of silica alkoxide, particle formation can be analyzed in terms of nucleation and growth models [159-160]. The particle size depends on the relative rates of the hydrolysis (producing silanol groups) and condensation (forming silicon-oxygen-silicon bonds) reactions, which can be represented as follows [49]:

Hydrolysis:
$$M-OR + H_2O \Leftrightarrow \equiv M-OH + ROH$$

Condensation:
$$\equiv M-OH + \equiv M-OR \Leftrightarrow \equiv M-O-M \equiv + ROH$$
$$\equiv M-OH + \equiv M-OH \Leftrightarrow \equiv M-O-M \equiv + H_2O$$

As for the synthesis of silica nanospheres via w/o microemulsion system, the reactions in the water-droplets are the same as the reactions mentioned above. The microemulsion mediated hydrolysis of metal alkoxides also provides an effective method for the synthesis of mono-disperse ceramic nanospheres (typically less than 100 nm) [161]. The effect of time, pH value and reactant concentration on hydrolysis reaction in microemulsion would be discussed as following.

- **Effect of time**

Figure 2.5-20 shows the change in average particle size with the change of reaction time in tetra-ethyl-ortho-silicate (TEOS) hydrolysis via w/o microemulsion. The size of SiO_2 particles increased with the increase of reaction time and levelled off after 200 minutes.

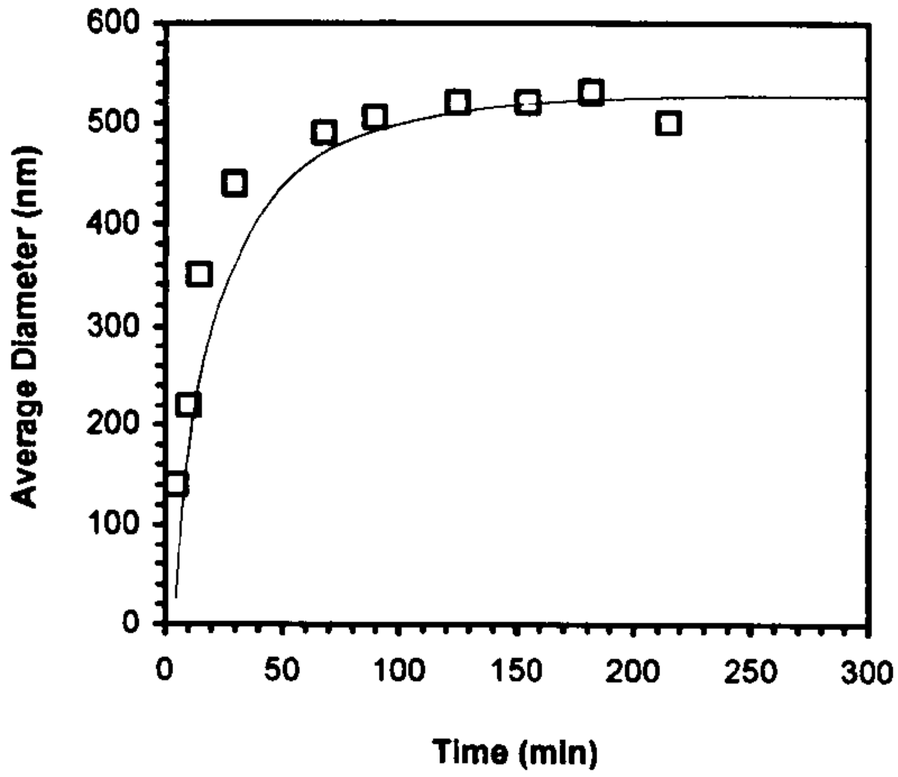

Figure 2.5-20 Average particle size as a function of reaction time at 25°C.

- **Effect of pH Value**

The reactions about hydrolysis and condensation of metal alkoxides are highly pH dependent. As reported by the early work by Stöber *et al.* [162] under basic conditions TEOS undergoes hydrolysis and poly-condensation reactions which result in the formation of nano-disperse spherical particles of amorphous silica. A three-dimensional gel network was formed at low pH values, and at discrete particles were produced high pH values [163].

Arriagada *et al.* [164] found that the morphology of silica particles prepared in w/o microemulsion became more irregular as the ammonia concentration decreased [**Figure 2.5-21 A-D and Figure 2.5-21 E-F**]. However, the effect appeared more significant at high ω_0 value when comparing the **Figure 2.5-21 D** and **Figure 2.5-21 H**. It seemed that the high ammonia concentrations (i.e., relatively strong alkaline conditions) were required in morphological control in the w/o microemulsion system.

The observed morphology dependence on ammonia concentration may be related to the ability of the OH^- ion (generated by the hydrolysis of ammonia) to catalyze both hydrolysis and condensation reactions and the tendency for siloxane bonds to break in highly alkaline solutions [164].

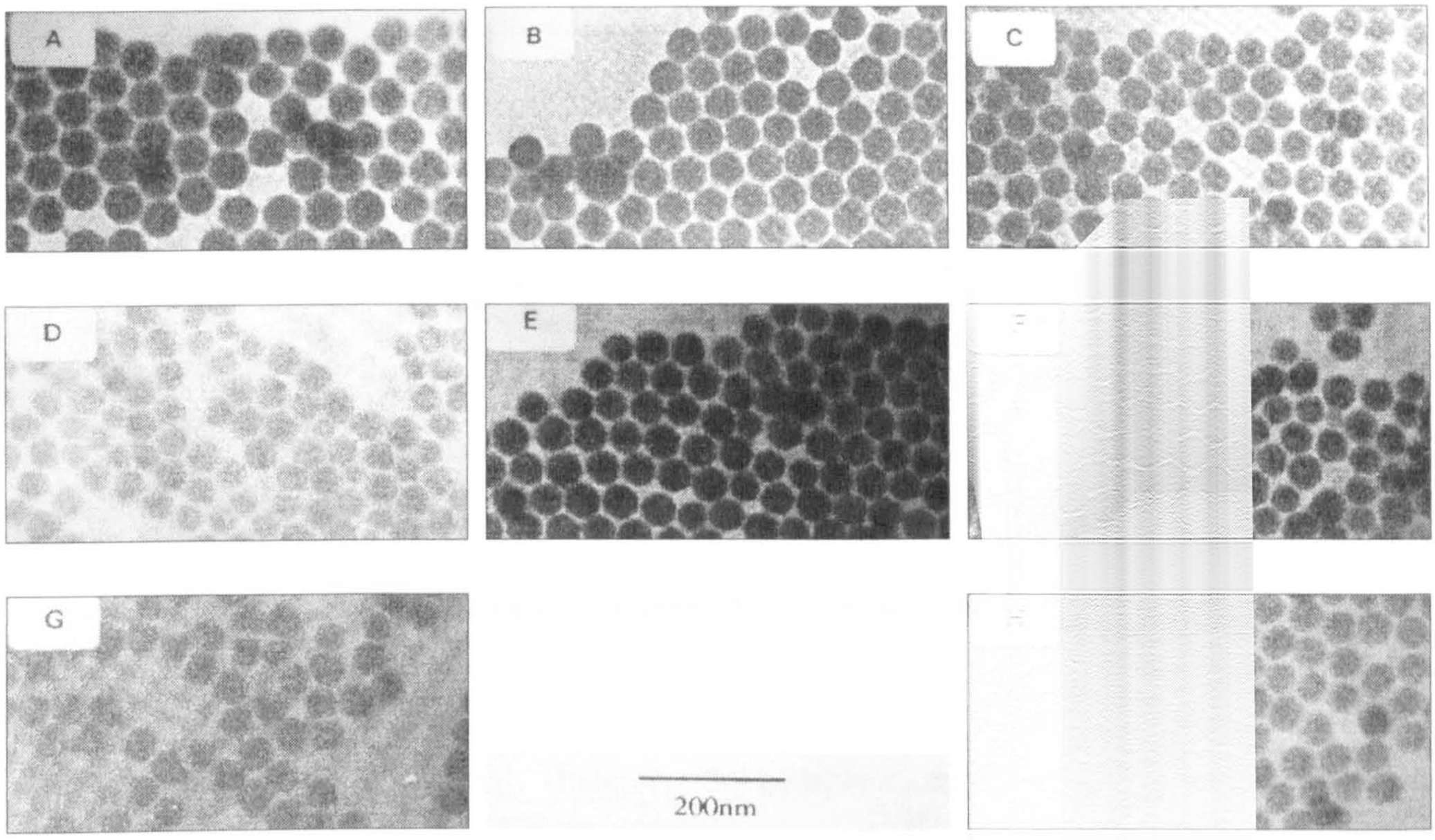

Figure 2.5-21 Effect of ammonia concentration (wt% NH_3) on the morphology of SiO_2 particles [164].

[A-D]: *R* = 4.5, E-H: R = 1.7, **[A.E]:** 29.6 %, **[B.F]:** 14.6 %, **[C.G]:** 6.3 %, **[D.H]:** 1.6 %

- **Effect of molar ratio of water to surfactant ω_0**

The size distribution of SiO_2 particles shows a complex dependence on the water to surfactant molar ratio ω_0. The particle size was controlled by varying water to surfactant molar ratio.

Arriagada *et al.* [164] prepared a series of samples from different water-to-surfactant molar ratios and various constant ammonium hydroxide concentrations in the solubilised aqueous phase. The particle diameter is shown in **Figure 2.5-22**. It can be seen that as ω_0, water to surfactant ratio, increased, the particle size decreased initially, after reached a minimum at an ω_0 value of about 1.8, the size increased again. The effect of pH value on hydrolysis has been discussed before, here it could also be found that in the most dilute ammonia solution utilised in this work (1.6 % NH_3), no minimum is observed within the ω_0 range investigated, and the particle size decreases continuously [164].

The effect of ω_0 on particle size in the synthesis of silica nanospheres via microemulsion could be explained by "free-water". When ω_0 is low, water is mostly bound to the surfactant molecules, and the

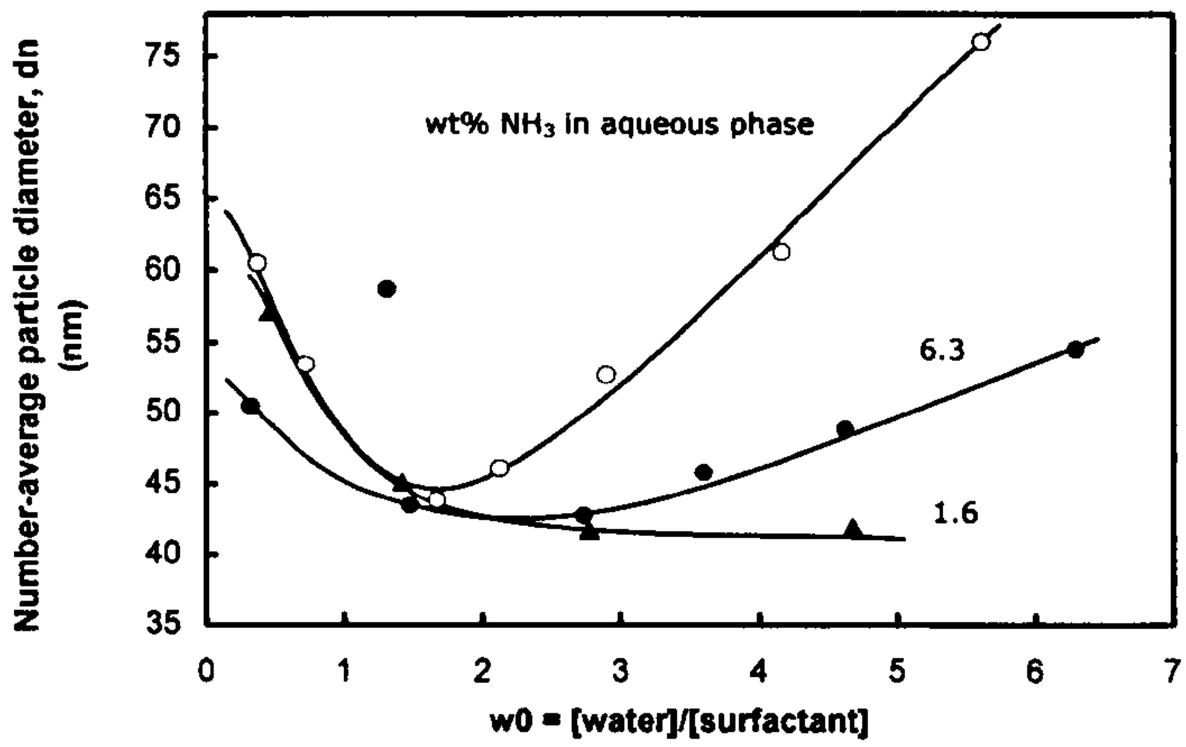

Figure 2.5-22 Effect of the ω_0 on the mean diameter of SiO_2 particles at different ammonia concentrations;

mobility of the OH^- ions is reduced. Therefore, the hydrolysis and the nucleation reactions are not favoured in a given w/o microemulsion system. Furthermore, there are few TEOS monomers per aggregate, so that intra-micelle nucleation is less promising. On the contrary at high ω_0 values, water molecules are mostly "free" from surfactant bonding. A larger number of hydrolysed TEOS species are expected to present in water-droplets. The nucleation in the aggregates containing few monomers may depend heavily on inter-micellar collisions, while in contrast each reverse micelle would be able to produce a nucleus at high ω_0 values. Therefore, if nucleation occurs in the w/o microemulsion system over a limited period of time as suggested above, then the final particle size would decrease continuously as ω_0 increases [164].

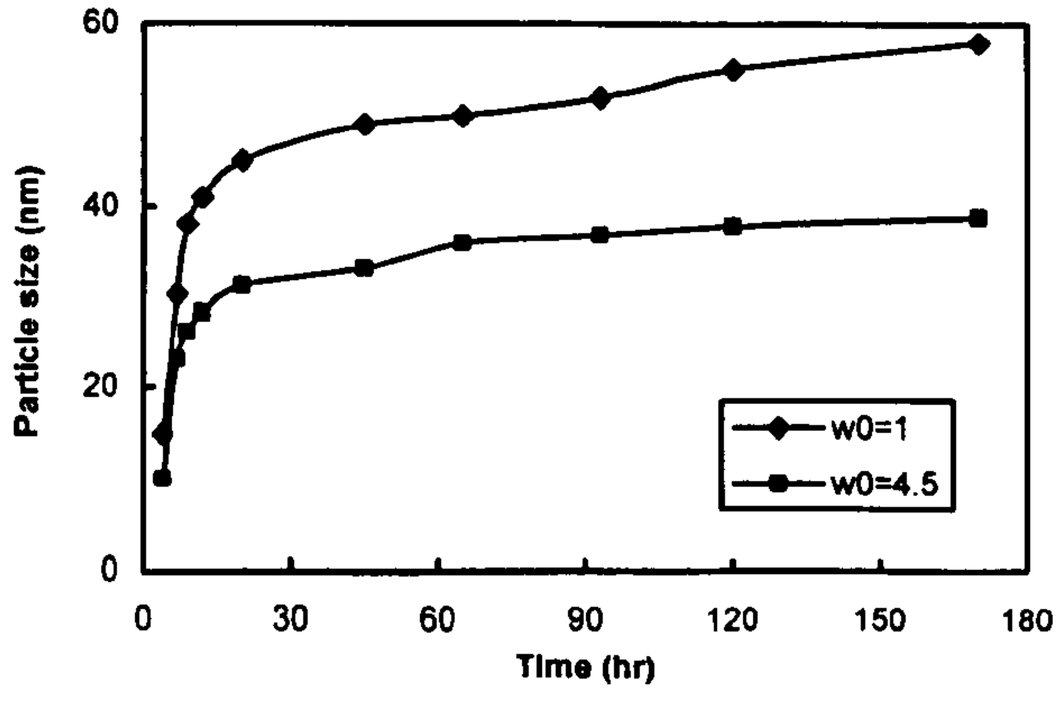

Figure 2.5-23 Silica particle growth kinetics measured by DLS at different values of ω_0 =[H_2O] / [Surfactant Tx-45] [62].

However, this ω_0-dependent particle size conforms to the experimental data only for the samples prepared with the lowest ammonia concentration (1.6 wt% NH_3). At higher ammonia concentrations, a minimum in particle size is observed as ω_0 is increased. The minimum in particle size can be rationalised by effects of inter-micellar interactions on the particle formation process [164].

When the molar ratio of water to TEOS is constant as 7.8, Fu *et al.* [52] found that a decrease in water content (smaller ω_0) resulted in larger particle size [**Figure 2.5-23**].

- **Effect of surfactant**

In synthesis of silica nanoparticles via w/o microemulsion, according to the research of Santra *et al.*[23], different non-ionic surfactants could result in the different particle size [**Table 2.5-9**]. Compared to Igepal CO-520 and Triton X-100, Brij 97 surfactant has a longer hydrophobic chain. Therefore, the interaction between hydrophobic groups attached to adjacent nanoparticles will be stronger. More ordered fashion in particle aggregation in the case of Brij 97 was obtained [23] as a result.

Table 2.5-9 Data of silica-coated iron oxide nanoparticles prepared via different w/o microemulsion systems [23].

Surfactant	Sample	Particle size [nm]
Brij 97	NH_4OH coated	3 ± 1
	NH_4OH uncoated	2 ± 1
Igepal 520	NH_4OH coated	9 ± 4
	NH_4OH uncoated	4 ± 2
Triton x-100	NH_4OH coated	6 ± 1
	NH_4OH uncoated	4 ± 1

2.5.2.3 Mechanism of coating nano-magnets with polymer/ceramic

The property of magnetic nanoparticles could be modified by applying coating materials with polymer or ceramics. For example, in the drug delivery technology, the nanoparticles binding drugs are localised by magnetic forces at a particular part of body. But the body's reticuloendothelial system usually take up the nanoparticles due to the hydrophobic surface then probably delays them off the

target tissue. Surface coverage by amphiphilic polymer derivatives over the nanoparticles significantly increases the blood circulation time by minimizing or eliminating the off-target adsorption to the nanoparticles [165]. The advantage of core-shell structured nanocomposites has been discussed in earlier sections. The synthesis of magnetic nanocomposites coated by polymer or ceramics would be included in following.

- **Mechanism of polymer coating**

In the case of coating magnetic oxide particles with polymer, generally, these magnetic polymeric particles could be fabricated by coating the magnetic particles with performed natural or synthetic polymers [167]. That is a simple and classic method to produce polymer-magnetic composites and has been widely applied.

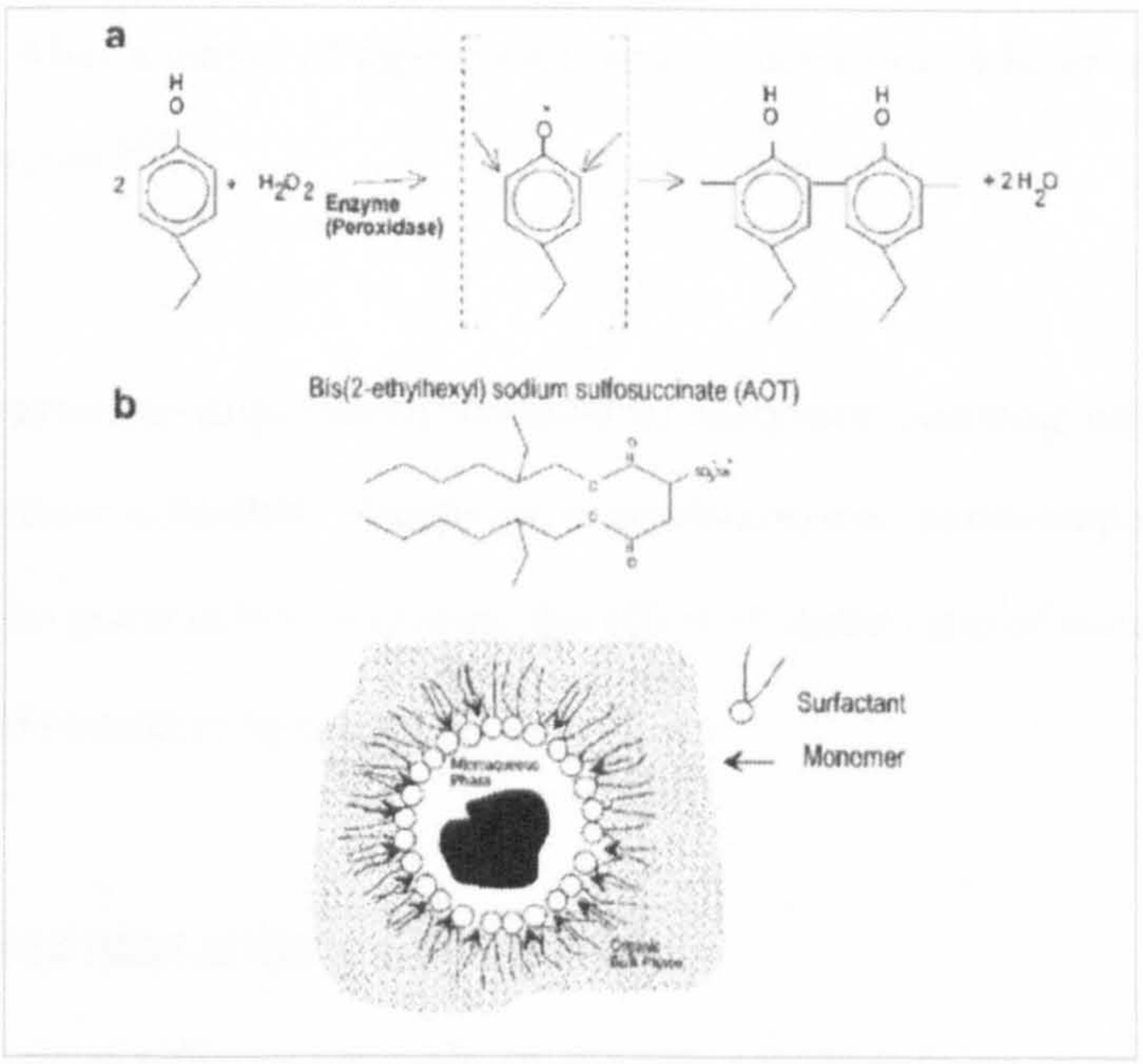

Figure 2.5-24 Schematic of the enzyme-catalyzed polymerisation reaction in w/o microemulsion systems **[a]** Simplified mechanism; **[b]** The enzyme is resident in the water core of the w/o microemulsion. The monomer is surface active and partitions to the water/oil interface [166].

The development of emulsion polymerisation, especially microemulsion polymerisation, led to new approaches to synthesise magnets/polymer core-shell structured nanocomposite. An example of

coating polymer on the magnetic nanoparticles in w/o microemulsion system is shown in **Figure 2.5-24** [166]. The water pools of the system are capable of solubilising bio-molecules such as enzymes, which retain catalytic activity in water environment [166]. The monomer partitions to the oil-water interface directed to the water core as shown in the **Figure 2.5-24b**. Consequently, an oxidative enzyme encapsulated in the micelles could polymerise the monomer very efficiently to produce polymer. The polymer particle size normally is significantly larger than the micelle size. Their morphological details indicate that they are not always independent spherical particles, but often exist as interconnected spheres [29].

- **Mechanism of ceramic coating**

As for ceramics coating, alkoxide is added drop wise to w/o microemulsion with preformed particles in water pools. When the hydrolysis starts, freshly formed ceramic nuclei precipitated onto the surface of magnetic cores [44]. After a period of aggregation and condensation, a layer of ceramic shell formed on preformed nanoparticles [23].

2.5.2.4 Parameter-dependent studies of polymer coating nanocomposites

The parameter-dependence core-shell structured magnets/polymer nanocomposites prepared in w/o microemulsion would be given below, including the effect of molar ratio of water to surfactant and the effect of weight ratio of monomer to magnetic core.

- **Effect of Molar ratio of water phase to surfactant ω_0**

As discussed in synthesis of polymer nanospheres via w/o microemulsion system, the size of polymer nanospheres increased with increasing ω_0. The same tendency was found in the synthesis of the polymeric nanocomposites **[Table 2.5-10]**. Dresco *et al.* [155] reported that, the nanospheres obtained through microemulsion polymerisation had size values ranging from 220 to 320 nm, depending on the water/surfactant molar ratio. The size of polymeric nanocomposites increased with the increase of molar ration of water to surfactant.

Table 2.5-10 Sizes of polymeric magnetite particles synthesised with hydrophilic initiator

Water [wt %]	Monomers [wt%]	ω_0	Size [nm]
7	1	8.9	320
6	2	7.5	316
6	2	7.5	311
6	2	7.5	270
5	3	6.4	220

Table 2.5-11 Relative amount of polymer bound to magnetite, coating thickness.

Initial monomer/magnetite weight ratio	Relative weight of coating polymer	Coating thickness [nm]
2:4	0.183 ± 0.001	40 ± 20
3:4	0.193 ± 0.001	50 ± 30
1:1	0.1236 ± 0.0009	90 ± 50
4:3	0.602 ± 0.001	46 ± 19
4:2	1.418 ± 0.003	62 ± 15

- **Effect of monomer to magnets weight ratio**

The synthesis of poly(ethyl-2-cyanoacrylate) nanoparticles with a magnetic core was reported by Arias *et al.* [168]. The amount of polymer (PE-2-CA) incorporated to the particles increased consistently when the increase of monomer/magnetite weight ratio. Meanwhile the thickness of the polymer coating was not necessarily increased with an excess of initially added monomer [168] **[Table 2.5-11]**.

2.5.2.5 Synthesis of magnetic nanocomposites vs. magnetic properties

All the above discussions are concentrated on the change of size and morphology of nanoparticles prepared via w/o microemulsion system. In this section, the factors in preparation which could affect the magnetic properties of nanomaterials synthesised in w/o microemulsion will be investigated.

The molar ratio of water to surfactant could probably affect the magnet content in magnetic nanocomposites. In the research of Kommareddi *et al.* [166], the weight percent of iron contained in ferrite-PEP composites decrease when the ω_0 became smaller. For ferrite particles synthesised at ω_0 = 5 micelles, the composite ferrite content was 4.03 %, synthesis in ω_0 = 10 micelles resulted in a composite ferrite content of 4.48 %, and synthesis in ω_0 = 15 micelles led to a composite ferrite content of 5.34 %. A similar result was reported by Dresco *et al.* [155] that the encapsulation of magnetite particles was found to be low when the water/AOT ratio became lower that 4.5.

Table 2.5-12 Summary of key parameters from magnetic measurements.

ω_0	wt% Fe in composite	(dM/dH) H=0 emu/g G	Dmag nm	Tb, K
5	4.03	4.9×10^{-5}	0.51	12
10	4.48	1.4×10^{-4}	1.05	20
15	5.34	1.06×10^{-3}	1.42	27

The lower ω_0 resulted in lower content of encapsulated magnets in nanocomposites and consequently the ω_0 value also could affect the blocking temperature of the magnetic material. Sunderland *et al.* reported that the blocking temperature increased with the increase of the concentration of the magnetic nanoparticles in the nanocomposites. This behaviour is consistent with an increase of magnetic dipolar interactions due to the diminishing of average inter-crystal distance as the concentration of the magnetic nano-phase increases [169].The similar results has been reported by Kommareddi *et al.* [166] as summarised in **Table 2.5-12.**

3 EXPERIMENTAL DETAILS

3.1 MATERIALS

All the chemicals were purchased from Sigma-Aldrich Company Ltd. (Gillingham, United Kingdom) or Fisher Scientific UK (Loughborough, United Kingdom) in analytical grade purity. The chemicals involved in the inorganic chemistry experiment were used as received. In the polymerisation experiment most of chemicals needed to be purified before being used in the reaction. Methacrylic acid (MAA) was vacuum distilled at 60°C just prior to the reaction. Acrylamide (AM) and N,N-(methylene bis acrylamide) (MBA) was re-crystallised from chloroform and acetone respectively as recommended [170]. Potassium persulphate (KPS) was used as the initiator without further purifying treatment.

Table 3.1-1 List of all chemicals used in this project.

Surfactant	Solvent	Chemicals
AOT	Cyclohexane	Iron Chloride (II) Tetrahydrate 99%
Tween 85	Isooctane	Iron Chloride (III) Hexahydrate 98%
Tween 80	Petroleum Ether	Ammonia Solution 35%
Triton X-100	Toluene	Tetraethylorthosilicate
Triton X-114	Acetone	Acrylamide
Igepal CO-520	Ethanol	Methacrylic Acid
Igepal CO-720	Chloroform	Potassium Persulphate
Brij 97		N,N'-Methylene-Bis-Acrylamide
		Azobisisobutyronitrile
		Azobiscyclohexane-1-carbonitrile

De-ionised water was used throughout the experiment. In the synthesis of iron oxide nanoparticles, the iron salt solution was always prepared freshly in order to prevent the possibility of hydrolysis of the iron salt to form the iron hydroxide. In the polymerisation, the monomer water solution and the initiator water solution were also prepared just before the reaction to avoid "self-initiated-polymerisation" (monomers polymerise without initiator). **Table 3.1-1** lists all the chemicals used, more information in details is given in Appendices.

3.2 INVESTIGATION OF W/O MICROEMULSIONS

In the preparation of the water-in-oil (w/o) microemulsion system, first, the surfactant was mixed with the oil phase to form surfactant/oil solution; then a certain amount of aqueous phase was added, drop wise. The mixture was kept stirring by using a magnetic stirrer until it transferred from turbid to clear. Then a three-component (oil, surfactant and water), microemulsion system was formed as a result. A loading test was normally employed in the investigation of the maximum solubilisation of aqueous phase of a microemulsion system. The aqueous phase was added drop wise into surfactant/oil mixture continuously until the mixture could not turn clear and kept in turbid. In that case, the phase separation would happen short after.

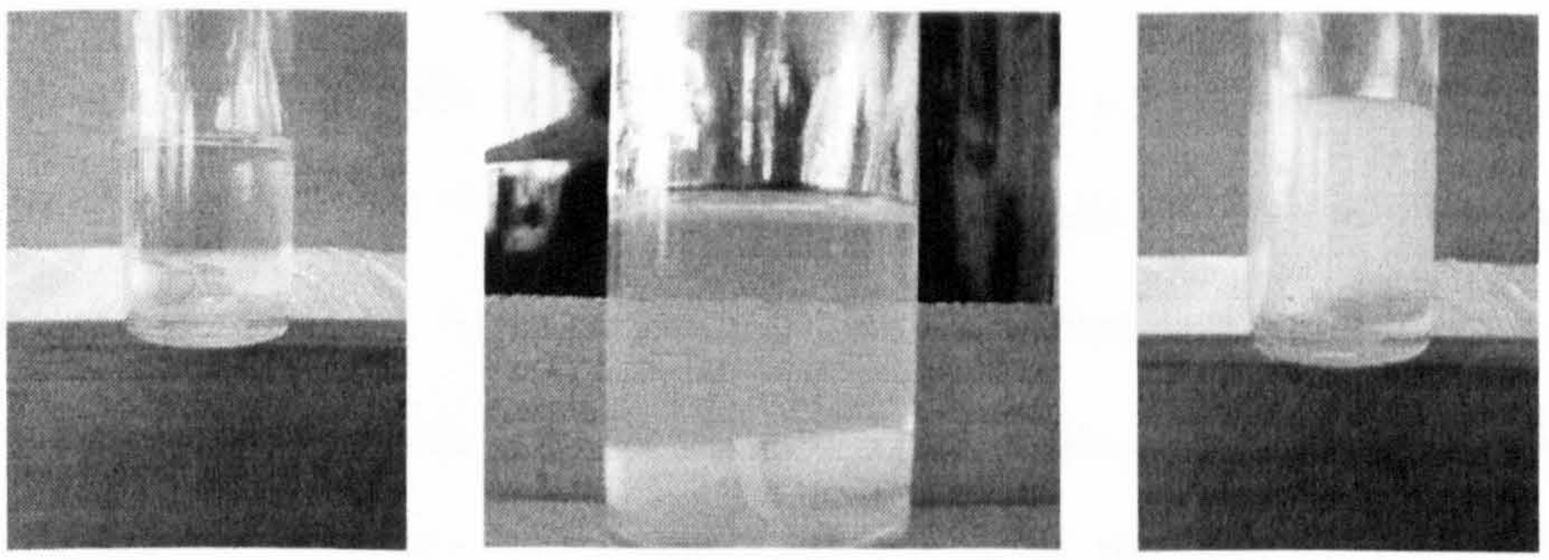

[A]. Clear **[B].** Translucent **[C].** Opaque

Figure 3.2-1 Photos of w/o microemulsion systems with the different loading of the aqueous phase

The transparency of the system was judged by visualizing. **Figure 3.2-1** shows the photos of

microemulsion systems under different loading of the aqueous phase. The clear sample [**Figure 3.2-1 A**] was a w/o microemulsion system. The translucent appearance [**Figure 3.2-1 B**] was normally viewed as the ending signal for the addition of the aqueous phase in our loading tests. Over-loaded systems, which could not be called as microemulsion, looked opaque as shown in **Figure 3.2-1 C**.

The investigations were carried out at room temperature which was around 25°C. An overall loading amount is defined as the percent ratio of the weight of the aqueous phase to the total weight of the microemulsion:

$$Loading\ Amount\ of\ Aqueous\ Phase = \frac{[Aqueous\ Phase]_{Weight}}{[Surfactant + Oil\ Phase + Aqueous\ Phase]_{Weight}} \cdot 100\% \quad \textbf{(3-1)}$$

The power of solubilisation of the aqueous phase in a microemulsion system was evaluated by its maximum solubilisation value at a particular temperature. In loading tests, the continuous blending time was generally less than 5 min. When the mixture remained turbid after stirring for more than 15 minutes, it was viewed as the system having reached the maximum solubilisation point.

- **Phase diagram**

A water-in-oil microemulsion system normally is formed by the solubilisation of the aqueous phase (water) into oil/surfactant mixture. With the increase of the amount of the solubilised aqueous phase, the size of water pools increases. A transition from microemulsion to non-microemulsion, which is emulsion or bi-continuous structure, will happen when the loading of the aqueous phase reaches a critical value. Before the transition point, the conductivity of the w/o microemulsion system is dominated by the continuous oil phase, which generally appears non-conductive. As the transition happens, the bulk phase is the mixture of oil and some water (aqueous phase), then the conductivity of the system is supposed to slightly increase due to the existence of the conductive matter, water.

Therefore, the difference of the conductivity of the system could be utilised to resolve the transition from microemulsion to non-microemulsion.

The phase diagram of the ternary system consisting of cyclohexane, Igepal CO-520 and water, was determined at 25°C by the measurement of conductivity. The system consisting of cyclohexane, Brij 97 and the aqueous phase and the system consisting of cyclohexane, Triton X-114 and methacrylic acid aqueous solution, were determined at 60°C. The surfactant was first dissolved in the oil in a cylinder flask fitted with a magnetic stirrer and a probe of conductivity meter (HANNA Instruments, model HI 8633). Then the flask was immersed in a water bath at a set temperature. After stirring for 30 min, the aqueous phase was added drop wise into to the oil phase while keep stirring. The next drop was not added until the system returned to transparent. Meanwhile, the conductivity of the system was recorded at intervals. When the composition was close to the microemulsion-emulsion boundary, the system returned to transparent very slowly. If the system could not come back to transparent after 30 min, this point was taken as the microemulsion-emulsion boundary. The transparency of the system was also judged by visual observation.

3.3 SYNTHESIS OF NANOMATERIALS VIA W/O MICROEMULSIONS

The synthesis of iron oxide nanoparticles, silica nano-spheres and silica/iron oxide nanocomposites was carried out in the Igepal CO-520/cyclohexane w/o microemulsion system. The synthesis of polymer nano-spheres and polymer/iron oxide nanocomposites was carried out in Brij 97/cyclohexane and Triton X-114/cyclohexane w/o microemulsion systems respectively. For any of above reactions, the system was always kept stirring by a magnetic stirrer during the ripening period. At the end of reaction, acetone was added immediately to precipitate the product synthesised in the water pool of the microemulsion. The w/o microemulsion system was then broken into a suspension. A centrifuge (Heraeus, Bofuge Primo) was used to accelerate the precipitation of particles from the suspension. Different washing procedures and post-treatments were carried out according to different products.

3.3.1 Synthesis of iron oxide nanoparticles

Pre-calculated amounts of the iron salt solution were firstly added into the mixture of Igepal CO-520 and cyclohexane to form a w/o microemulsion system. The ammonia solution was then added drop wise into the system by a plastic micro-syringe to react with the iron salt. The system was continuously purged with argon during the reaction. Products were precipitated by centrifugation after adding acetone to break up the system. Iron oxide samples were washed thoroughly with acetone and de-ionised water to remove the oil, surfactant and any remained reactants. Normally, samples were washed by four times with acetone followed by two times with de-ionised water and finally with acetone again. The whole procedure of the synthesis of iron oxide via the w/o microemulsion system is shown in **Figure 3.3-1**.

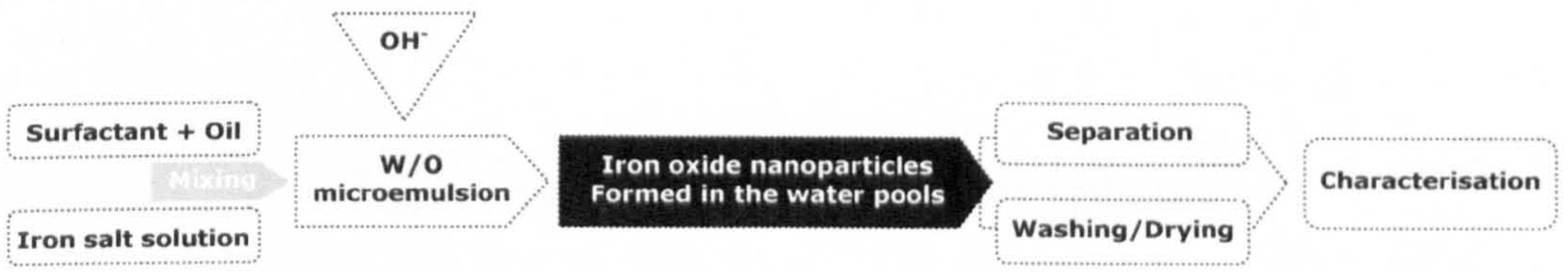

Figure 3.3-1 Flow chart of the synthesis of iron oxide via w/o microemulsion system.

3.3.2 Synthesis of polymer nano-spheres

AM and MAA were the monomers employed in the experiment. They were both prepared into solutions of the required concentration with the small amount of N,N'-methylen-bisacrylamide. The

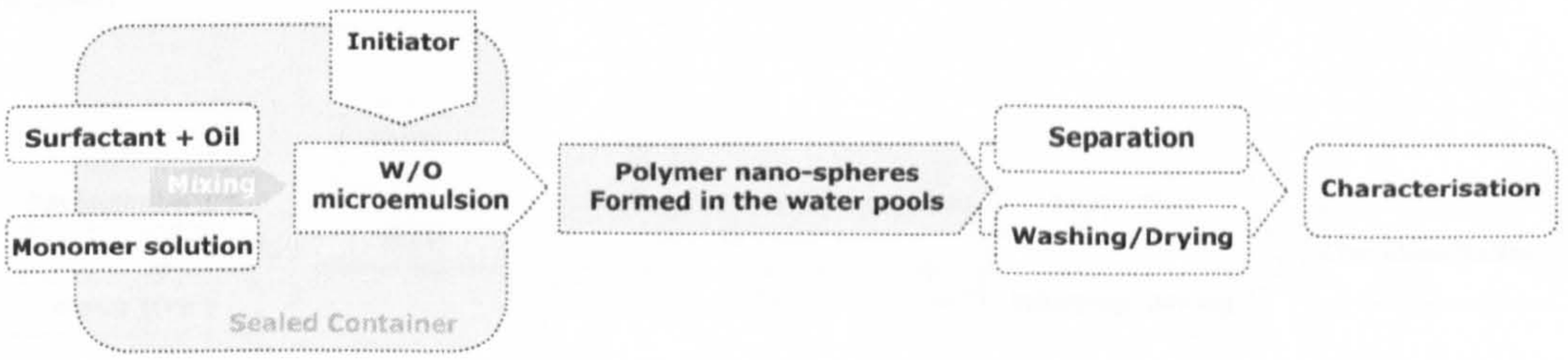

Figure 3.3-2 Flow chart of the synthesis of polymer nano-spheres via w/o microemulsion system.

microemulsion system was formed when the monomer solution and the heat initiator solution were added into surfactant and oil mixture. Argon was bubbled at room temperature through the microemulsion for the first 30 min to eliminate oxygen. The polymerisation was initiated when the temperature was increased by using an oil bath. The whole procedure of the synthesis of polymer nano-spheres via w/o microemulsion was similar as the synthesis of iron oxide **[Figure 3.3-2]**.

$$Conversion = \frac{(m_{polymerisation\ product} - m_{monomer})}{m_{monomer}} \cdot 100\% \qquad \textbf{(3-2)}$$

The conversion in polymerisation was taken to evaluate the polymerisation result with different conditions. The conversion was calculated by the polymerisation product after washing and drying. Any loss in washing could be neglected. The equation is given as **Equation 3-2**.

3.3.3 Synthesis of silica nano-spheres

Silica nano-spheres were prepared by the hydrolysis of tetra-ethyl-ortho-silicate (TEOS) in Igepal CO-520/cyclohexane w/o microemulsion. De-ionised water and ammonia solution were solubilised in Igepal CO-520/cyclohexane solution with the certain molar ratio of H_2O to TEOS and NH_3 to TEOS. TEOS was injected into the microemulsion with a micro-syringe. The hydrolysis took place at room temperature (~25°C) for 24 hours. Acetone was also used to precipitate the product. After that, samples were separated by centrifugation and washed thoroughly with acetone by four times to remove the oil and the surfactant followed by 2 times with de-ionised water to remove the remained ammonia. The whole procedure of the synthesis of silica via the w/o microemulsion system is shown in **Figure 3.3-3**.

Figure 3.3-3 Flow chart of the synthesis of silica nano-spheres via w/o microemulsion system.

3.3.4 Synthesis of nanocomposites of iron oxide with ceramics/polymer

- **Silica/iron oxide**

Nanocomposites of iron oxide/silica were prepared by two steps: iron oxide nanoparticles were first

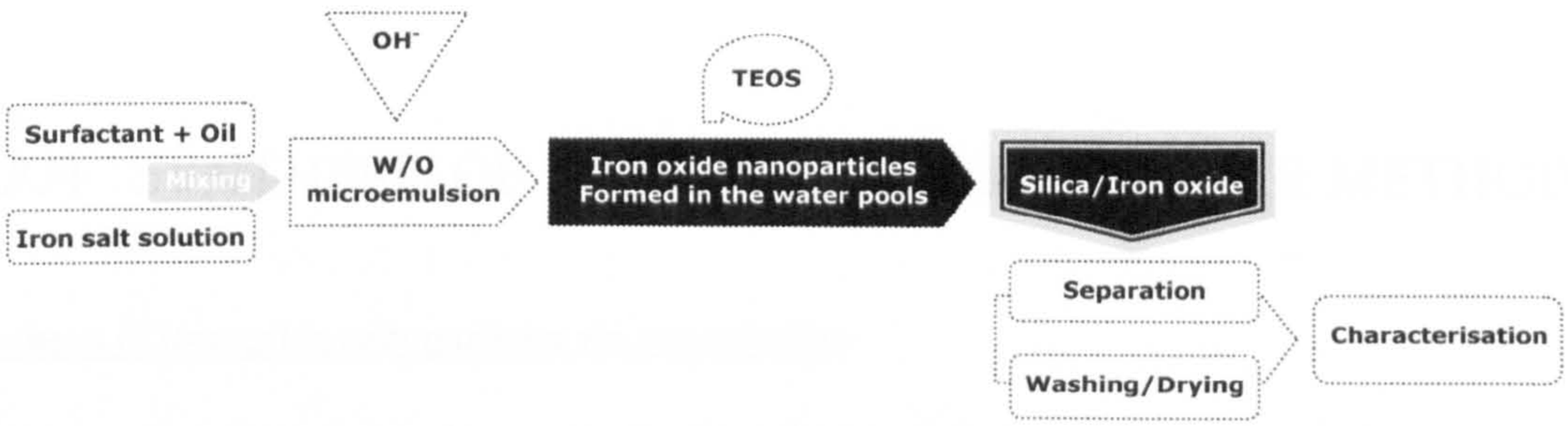

Figure 3.3-4 Flow chart of the synthesis of silica/iron oxide nano-composites via w/o microemulsion system.

synthesised as described in ***3.3.1***, then pre-calculated TEOS was added into the microemulsion system containing preformed iron oxide nanoparticles. The hydrolysis reaction of TEOS at room temperature (~25°C) was carried out for 24 hours. Products were treated by the same procedure as the pure silica. The flowchart of the silica/iron oxide nano-composites synthesis is illustrated in **Figure 3.3-4**.

- **Poly-acrylamide/iron oxide nano-composites**

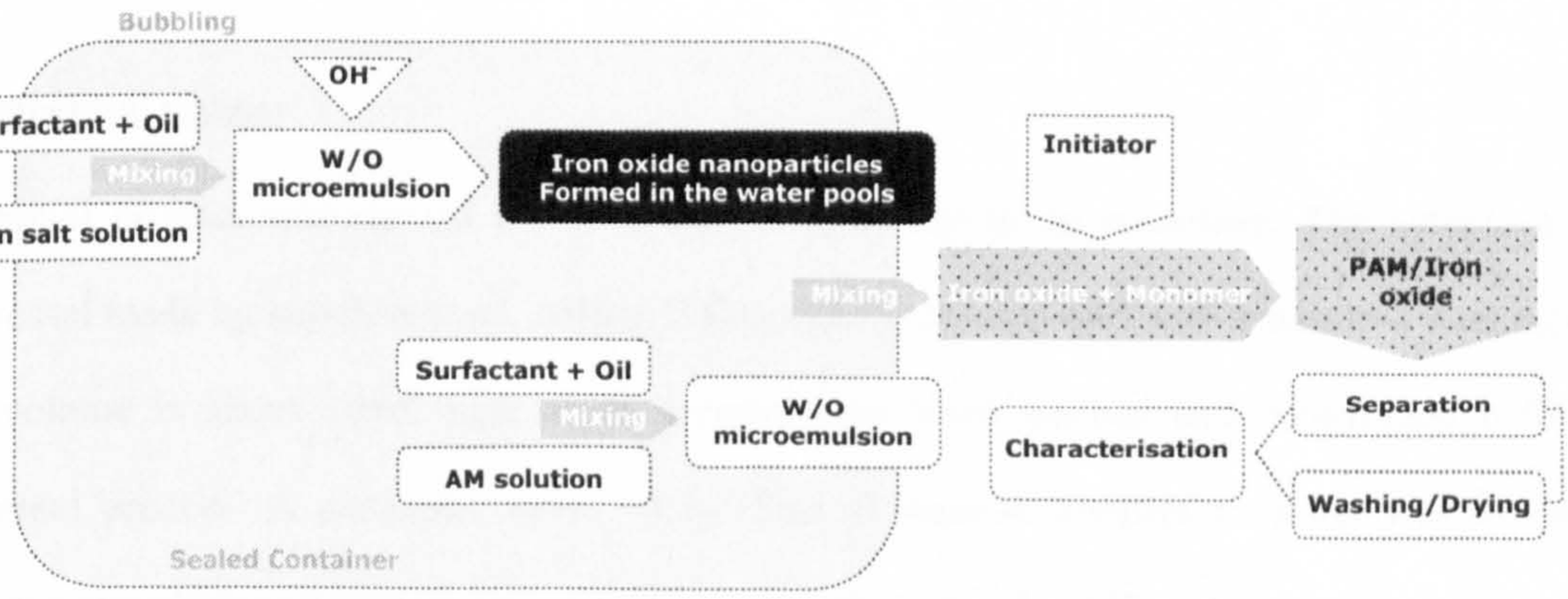

Figure 3.3-5 Flow chart of synthesis of PAM-iron oxide nanocomposites via microemulsion.

Iron oxide nanoparticles were synthesised via Brij 97/cyclohexane system at 60°C. Then this "parent"

microemulsion system containing magnetic nanoparticles was added into another microemulsion system with the monomer, initiator and cross linking agent as the aqueous phase. Encapsulation process was carried out under the same condition as the polymerisation of monomer initiated by heat initiator. The whole procedure of polymer coating is shown in **Figure 3.3-5**.

3.4 SYNTHESIS OF NANOPARTICLES BY OTHER METHODS

- **Synthesis of iron oxide nanoparticles via precipitation**

Iron oxide nanoparticles were also synthesised by the precipitation of iron salt solution with ammonia solution, then washed by de-ionised water till the PH value was around 7. The effects of different starting materials, ripening time and ripening temperature on the formation of iron oxide nanoparticles were investigated as shown in **Table 3.4-1**.

Table 3.4-1 Investigation of iron oxide nanoparticles prepared by precipitation.

Starting materials $[Fe]^{3+}$:$[Fe]^{2+}$	$[Fe]^{3+}$	9:1	3:2	2:1									1:1	1:2	1:9	$[Fe]^{2+}$
Ripening temperature [°C]	25			25			40	60			90			25		
Ripening time [H]	2			2	12	24	2	2	12	24	2	12	24	2		

- **Hydrothermal process**

Hydrothermal process was carried out at a high temperature in an autoclave. The autoclave is an airtight vessel made by stainless steel, with a Teflon container with a lid, and a stainless steel cap. The internal volume is about 30ml. Iron oxide nanoparticles were washed and centrifuged before the hydrothermal process. A particular ratio, ~0.7g/15ml of washed samples to water was mixed and sealed in the autoclave and kept in a temperature-controlled oven for different aging times.

- **Calcination**

Calcination of iron oxide nanoparticles were carried out in a tube furnace. Samples were wrapped in a

piece of foil and placed in the middle of the tube. The heating programme was started at 2°C/min heating rate, followed by 120-minute holding at the set temperature then cooled down to 30°C at 2°C/min.

3.5 CHARACTERISATIONS

- **Molecular weight**

The molecular weight of polymer products was calculated by **Dilute Solution Viscosity Measurements**. The viscosity of a polymer in a solution is normally directly related to its molecular weight. Since the measurement of the solution viscosity does not require any complex equipment and generally gives good agreement between laboratories, so it is a valuable technique related to the measurement of the molecular weight.

The viscosity average molecular weight is calculated from the intrinsic viscosity [η] by applying the Mark-Houwink equation [171]:

$$[\eta] = K \cdot \overline{M}_v{}^{\alpha} \qquad \textbf{(3-3)}$$

'K' and 'α' are parameters determined for polymers where absolute molecular weight data is available. There are a large number of literature values. The molecular weight dependence of intrinsic viscosity as reference in our experiment is given by [172]:

Acrylamide: $$[\eta] = 6.31\times10^{-3} \cdot \overline{M}_v{}^{0.80} \qquad \textbf{(3-4)}$$

Methacrylic acid: $$[\eta] = 66\times10^{-3} \cdot \overline{M}_v{}^{0.5} \qquad \textbf{(3-5)}$$

An Ostwald viscometer [**Figure 3.4-1**] was employed in viscosity measurement of prepared polymer solution. Solution was measured with a graduated reservoir and de-ionised water was used as solvent. The liquid was injected into viscometer by a titrator. A bulb was used to pull the liquid level up then let it down through the capillary freely.

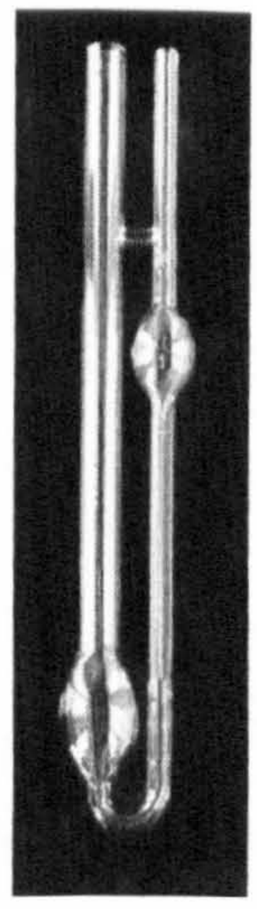

Figure 3.4-1
Ostwald viscometer

An electronic stopwatch was applied to record the time of travelling through the two standard marks on capillary for the polymer solution with a specified concentration. The original polymer solution was diluted into several different concentrations; that is as half as the previous value each time. Then a series of travelling time against different concentration was achieved. Since the flow time is proportional to the viscosity, a relative viscosity could be defined as a simple time ratio:

$$\eta_{rel} = t_{solution} / t_{solvent} \tag{3-6}$$

We also define a specific viscosity to be the fractional change in viscosity upon addition of polymer:

$$\eta_{sp} = \frac{t_{solution} - t_{solvent}}{t_{solvent}} \tag{3-7}$$

The reduced viscosity is the fluid viscosity increase per unit of polymer solute concentration, c:

$$\eta_{\text{red}} = \eta_{sp} / c \tag{3-8}$$

The intrinsic viscosity, [η] is the limit of the reduced viscosity, as the polymer solute concentration approaches zero. The intrinsic viscosity is also the limit of the inherent viscosity, $\ln(\eta_{rel})$, as the solution polymer concentration approaches zero:

$$[\eta] = \lim \frac{\eta_{red}}{c} = \lim \frac{\ln(\eta_{rel})}{c} \tag{3-9}$$

Plot $\ln(\eta_{rel})$ vs. c and η_{red} vs. c. Both plots have the same intercept, which is called the intrinsic viscosity, [η]. Finally, calculate the molecular weight of the synthesised polymer from the Mark-Houwink equation and the intrinsic viscosity of the unknown.

- **X-Ray Diffractometry**

The structure of the powder samples was measured using a Bruker D8 X-ray with a quarter-circle eulerian cradle. The X-ray diffraction patterns were taken from 10° to 70° (2θ value). Samples to be

characterized using XRD would preferably be dried and grinded into fine powders. The X-ray radiation source can be CoKα or FeKα.

- **Transmission Electron Microscope**

A transmission electron microscope, TEM (JEM 100CX, JEOL, Japan) was used to examine the size and shape distribution, crystallinity and morphology of nanoparticles and core-shell structures. The nanoparticles were firstly diluted with acetone. The solvent was allowed to evaporate at room temperature. A specimen substrate, copper grid coated with carbon film, was then covered with a hemispherical drop of the diluted suspension. The prepared sample was finally placed in the specimen chamber of the TEM.

- **Fourier Transform Infrared**

Fourier transform infrared (FTIR) spectra were obtained using Mattson 300 FTIR spectrometer (Unicam Ltd., United Kingdom). The spectra were recorded from 400 to 4000 wave numbers at 4 cm^{-1} resolution averaging 64 scans. The FTIR spectrums were measured at room temperature and compared with standard reference, matching fingerprint region (additional information).

The samples for FTIR measurement were dried in a oven or a vacuum oven at 40°C. Fully dried samples (about 1 vol%) would be milled with potassium bromide to form a very fine powder. This powder is then compressed into a thin pellet which can be analysed.

- **Superconducting quantum interference device (SQUID) magnetomery**

Magnetisation of nano-sized iron oxide and magnetic nano-composites prepared via w/o microemulsion system and precipitation processing had been investigated by superconducting quantum interference device (SQUID) magnetomery. Measurements were carried out at 5K and 300K with a full hysteresis curve in addition to a scan at a constant field of 0.1 Tesla (1000 Gauss) between 5K and 300K.

4 APPROPRIATE W/O MICROEMULSIONS

4.1 INVESTIGATION OF W/O MICROEMULSIONS

Finding appropriate water-in-oil (w/o) microemulsion systems are the fundamental work for the synthesis of different nanoparticles. It should be noticed that during the reactions, the introduction of reactants and the precipitation of products both could probably de-stabilise the system; the particular temperature required by the reaction might disturb the thermodynamic balance of microemulsions and result in the phase separation. Hence, it is necessary to study the behaviours of microemulsions under different circumstances in order to find proper systems which could endure any change in reaction conditions and keep its thermodynamic stability simultaneously.

4.1.1 Studies on different surfactants

Ionic surfactants, AOT, and some non-ionic surfactants: Tween 85, Igepal CO-520, Triton X-114, Triton X-100, Brij 97 etc, were involved in this investigation.

4.1.1.1 The miscibility of surfactant in oil

The miscibility of different surfactants in different oil phases at room 25°C and 60°C was investigated and the results are given in **Table 4.1-1, 4.1-2**, respectively. At 25°C, the ionic surfactant AOT and the non-ionic surfactant Tween 85, were miscible with all three oil phases (isooctane, petroleum ether and isooctane), while Tween 80, Triton X-100, Igepal CO-720 and Brij 97 did not dissolve in any selected oil phase. Non-ionic surfactants Triton X-114 and Igepal CO-520 dissolved in petroleum ether (PE) and cyclohexane but not in isooctane.

Table 4.1-1 The miscibility of different surfactants in different oil phases at 25°C.
(Please not that, ☑ means the surfactant could dissolve in that oil and ☒ means not.)

	Isooctane	Petroleum Ether	Cyclohexane
AOT	✓	✓	✓
Tween 85	✓	✓	✓
Tween 80	☒	☒	☒
Triton X-100	☒	☒	☒
Triton X-114	☒	✓	✓
Igepal CO-520	☒	✓	✓
Igepal CO-720	☒	☒	☒
Brij 97	☒	☒	☒

Table 4.1-2 The miscibility of different surfactants in different oil phases at 60°C.
(Please not that, ☑ means the surfactant could dissolve in that oil and ☒ means not.)

	Isooctane	Petroleum Ether	Cyclohexane
AOT	✓	✓	✓
Tween 85	✓	✓	✓
Tween 80	☒	☒	☒
Triton X-100	☒	☒	☒
Triton X-114	☒	✓	✓
Igepal CO-520	☒	✓	✓
Igepal CO-720	☒	☒	☒
Brij 97	☒	☒	✓

When the temperature was increased to 60°C, as shown in **Table 4.1-2** Brij 97 became miscible with cyclohexane but maintained non-miscibility with isooctane and PE. There were no changes observed in miscibility for other surfactants with the change of temperature from ambient to 60°C.

4.1.1.2 Behaviour of non-ionic surfactant in w/o microemulsions

The behaviour of different non-ionic surfactants with different oil phases in w/o microemulsion systems was investigated through the loading test by titrating water into the mixtures of surfactant and oil to determine the power of solubilisation of water phase in the w/o microemulsion system. The

maximum solubilisation of water, S-w_{max} was mainly used to evaluate test results. The definitions and calculations of the loading and maximum solubilisation of aqueous phase were given in **Chapter 3**.

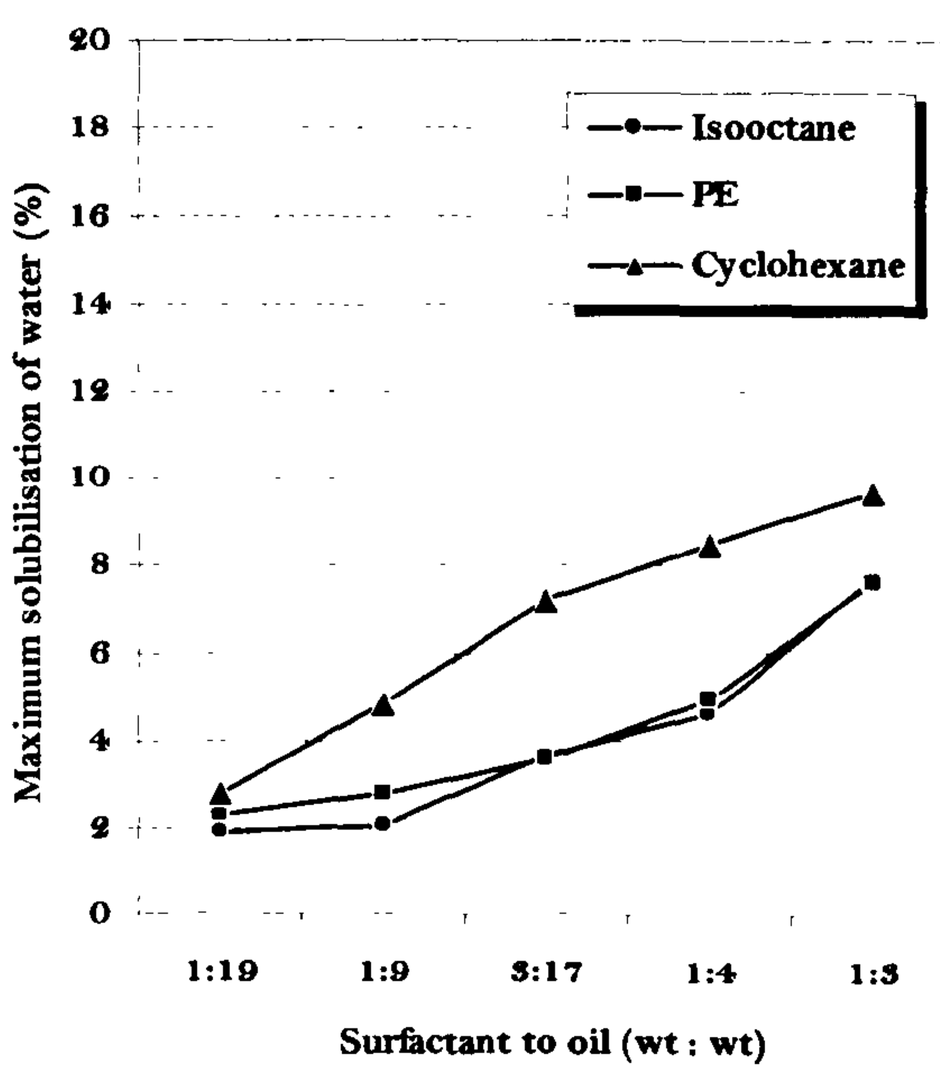

Figure 4.1-1 Maximum solubilisation of water in Tween 85 systems at 25°C.

Figure 4.1-1 shows the maximum solubilisation of water, S-w_{max}, in the systems consisted of Tween 85 with different oil phases at 25°C. Basically, S-w_{max} increased with the increase of weight ratio of surfactant to oil, from 1.9%, 2.3% and 2.8% at surfactant/oil of 1:19 to 7.7%, 7.6% and 9.7% at 1:3, for Tween 85/isooctane system, PE system and cyclohexane system respectively. Tween 85/cyclohexane system showed the highest S-w_{max} at every weight ratio of surfactant to oil.

The maximum water solubilisation in the w/o microemulsion increased with the increase of the weight ratio of surfactant to oil was also observed in Igepal CO-520/cyclohexane system **[Figure 4.1-2]** and Triton X-114/cyclohexane system **[Figure 4.1-3]**. S-w_{max} increased steadily from 7.4% and 1.1% at 1:19 to 16.9% and 7.3% at 1:3 for these two systems respectively. A different result was observed in the Igepal CO-520/PE system **[Figure 4.1-2]**, where there was a rapid increase of S-w_{max} from 2.2% to 23.4% when the ratio was increased from 1:9 to 3:17. However, those Igepal CO-520/PE systems with

extreme high *S*-w_{max} values were not stable. They first looked like a transparent gel, then separated after 12 hours. Therefore, dotted lines were applied for Igepal CO-520/PE system at the ratio of 3:17, 1:4 and 1:3, because those values could not simply mark the boundary between w/o microemulsion and non-w/o microemulsion.

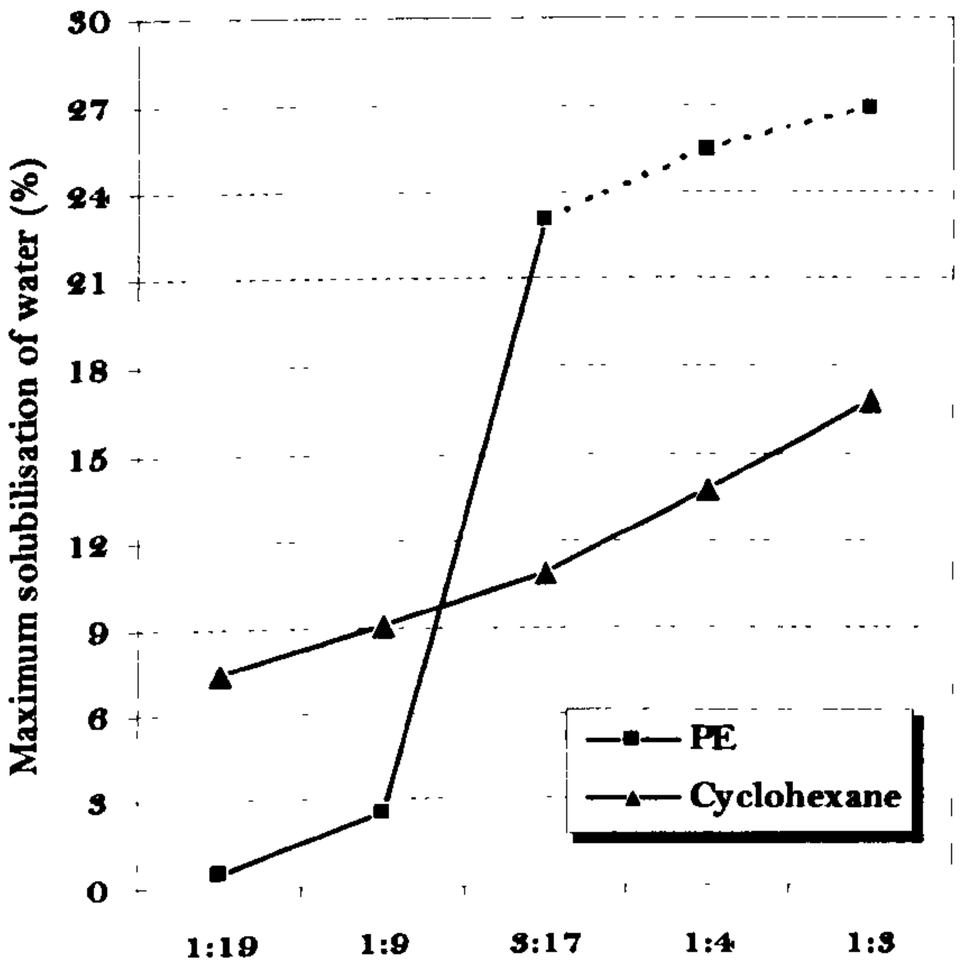

Figure 4.1-2 Maximum solubilisation of water in Igepal CO-520 systems at 25°C.

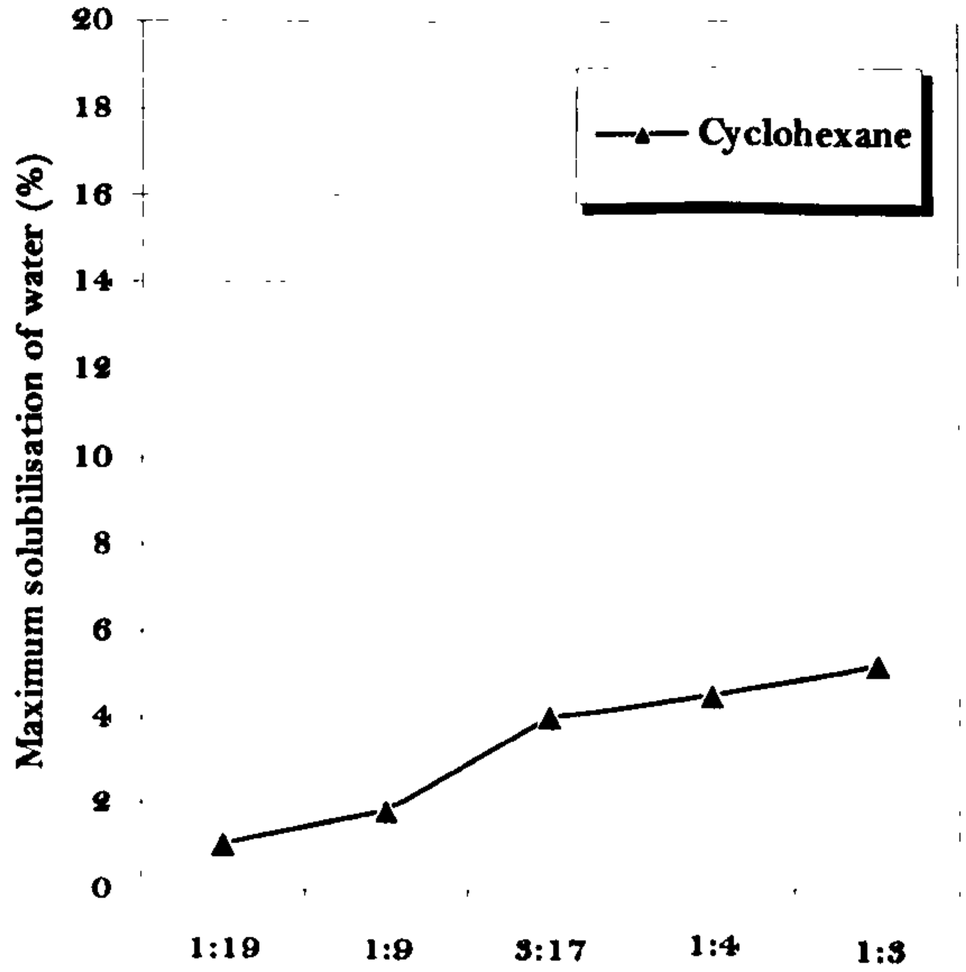

Figure 4.1-3 Maximum solubilisation of water in Triton X-114/cyclohexane system at 25°C.

4.1.1.3 Behaviour of ionic surfactant in w/o microemulsion systems

AOT was the only ionic surfactant investigated in the experiment. The maximum solubilisation of water in systems with AOT and different oil phases (isooctane, cyclohexane and toluene) are given in **Figure 4.1-4**. AOT system showed the similar trend as above non-ionic surfactant systems, i.e. the maximum water solubilisation increased with the increase of weight ratio of AOT to the oil phase. AOT/isooctane system exhibited more power of water solubilisation than others. For example, the maximum solubilisation of water in AOT/isooctane system at 1:9 was about 22%, which was twice higher than 7.4% of cyclohexane system, and nearly triple times higher than 5.0% of toluene system at the same ratio.

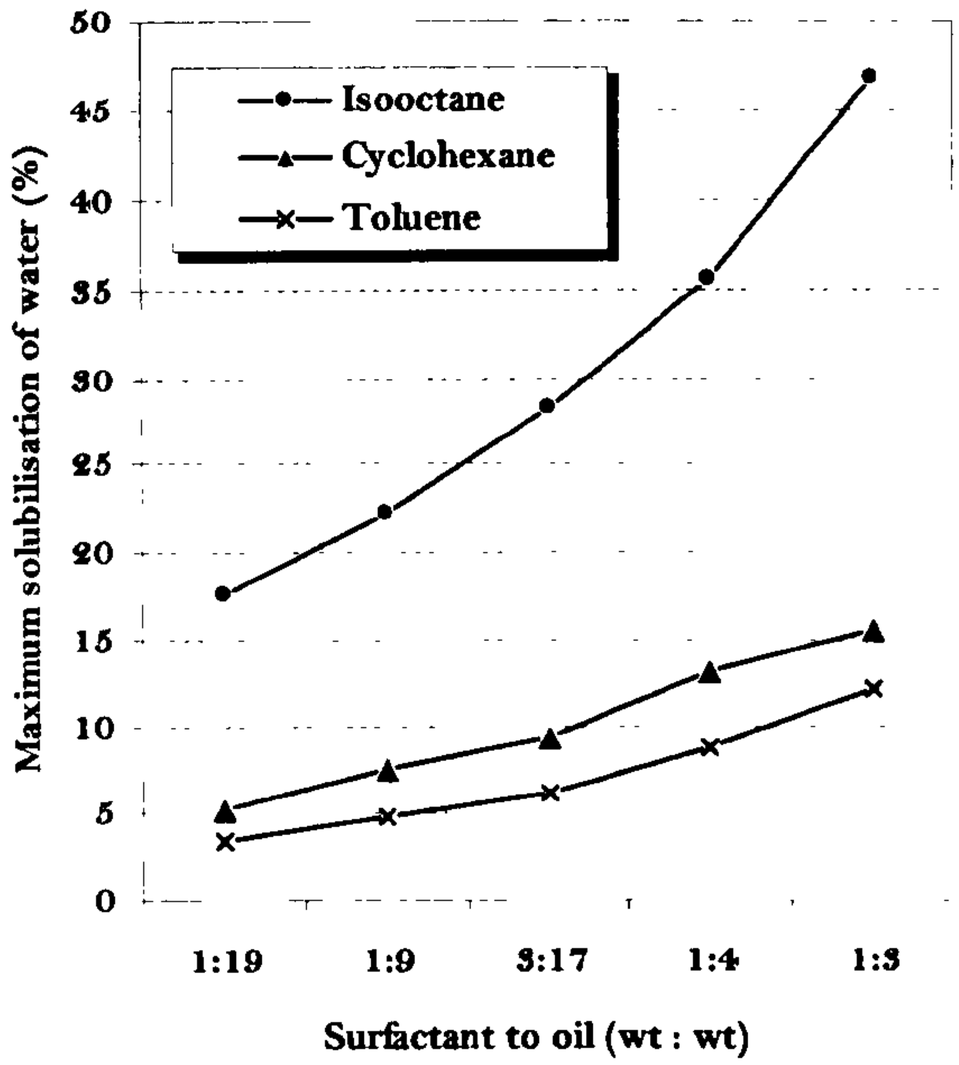

Figure 4.1-4 Maximum solubilisation of water in AOT systems at 25°C.

Table 4.1-3 Maximum water solubilisation (%) in w/o microemulsion systems at 25°C.

Microemulsion system	Weight ratio of surfactant to oil (wt/wt)				
	1:19	1:9	3:17	1:4	1:3
Tween 85/cyclohexane	2.8	4.9	7.2	8.5	9.7
Igepal CO-520/cyclohexane	7.4	9.1	11.0	13.8	16.9
Triton X-114/cyclohexane	1.1	1.9	4.1	4.5	5.3
AOT/Isooctane	17.6	22.3	28.4	35.6	46.7

In summary, for systems with either ionic surfactant, AOT or non-ionic surfactants, the maximum water solubilisation was all observed at the weight ratio of surfactant to oil of 1:3, which was the highest percentage of surfactant applied in experiments. Furthermore the AOT w/o microemulsion system with exhibited much higher S-w_{max} than most non-ionic systems **[Table 4.1-3]**.

4.1.2 Studies on addition of co-surfactants

As given in **Table 4.1-1** and **Table 4.1-2**, Triton X-100 cannot dissolve in cyclohexane at either room temperature (25°C) or higher temperature (60°C). However, with the presence of co-surfactant,

hexanol, Triton X-100 dissolved in it. The mixture of cyclohexane, Triton X-100, hexanol and the added water can form a four-component w/o microemulsion system. **Figure 4.1-5** gives the maximum solubilisation of water in Triton X-100/hexanol/cyclohexane system. The weight ratio of hexanol to Triton X-100 was kept constant as 1:5. *S*-w_{max} increased with the increase of weight ratio of surfactant mixture (surfactant and co-surfactant) to oil, from 1.5% at 1:19 to 10.5% at 1:3.

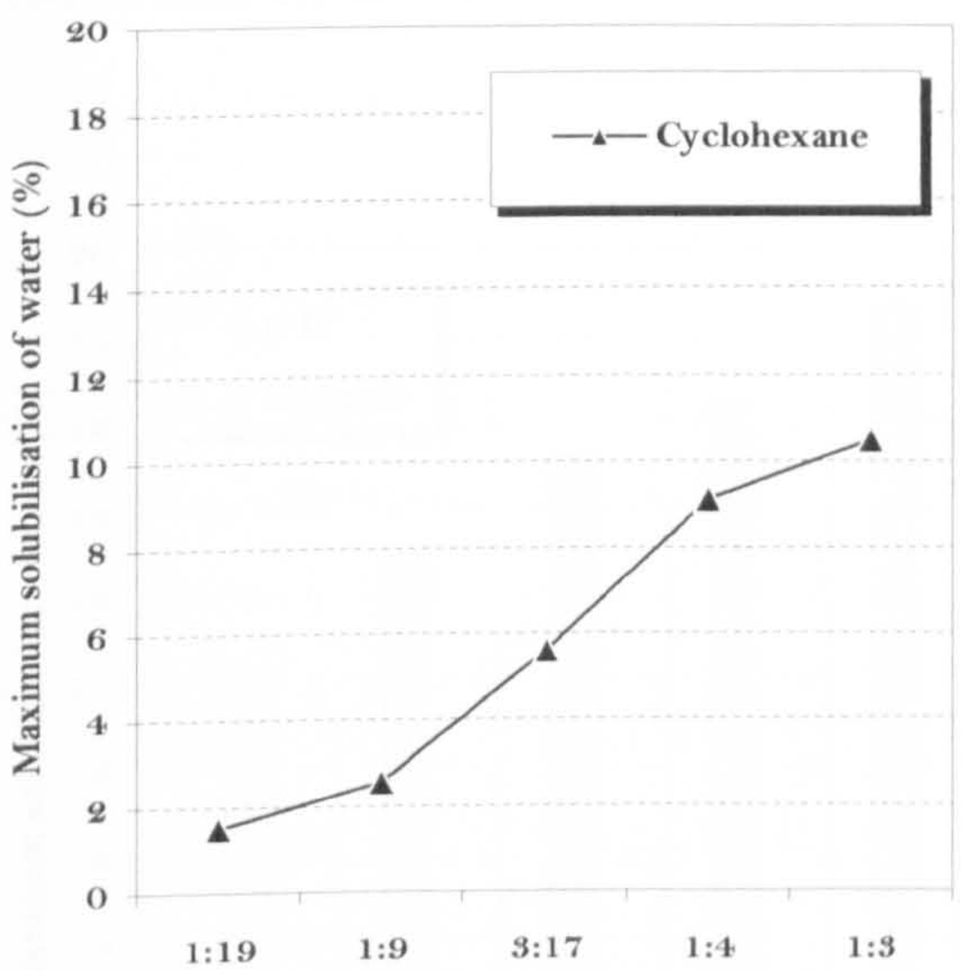

Figure 4.1-5 Maximum solubilisation of water in Triton X-100/Hexanol/cyclohexane system at 25°C.

Hexanol : Triton X-100 = 1:5 (wt:wt).

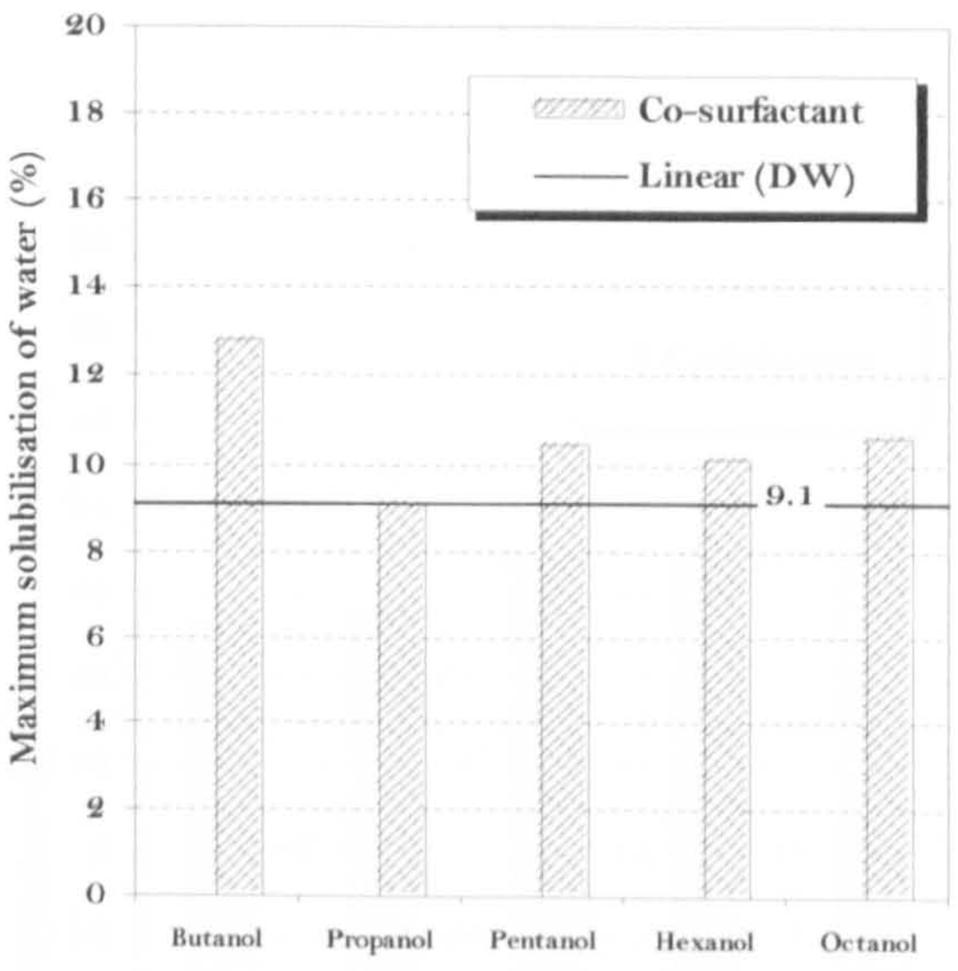

Figure 4.1-6 Maximum solubilisation of water in Igepal CO-520/cyclohexane system with different co-surfactant applied at 25°C.

Surfactant mixture : oil = 1:9 (wt:wt).
Co-surfactant : Igepal CO-520 = 1:5 (wt:wt).

The capability of co-surfactants on the improvement of the maximum water solubilisation was also investigated in the Igepal CO-520/co-surfactant/cyclohexane/water microemulsion systems [**Figure 4.1-6**]. *S*-w_{max} of the system without co-surfactant was 9.1% at the weight ratio of surfactant to oil was 1:9. With the addition of different co-surfactants (butanol, propanol, pentanol, hexanol or octanol), all the systems showed increased *S*-w_{max} and the *S*-w_{max} value of the microemulsion with butanol showed the most significant increase. Therefore, the system with butanol was further investigated with different surfactant to oil weight ratio was shown in **Figure 4.1-7**. *S*-w_{max} of the system with the butanol was

higher than the system without co-surfactant. It also could be observed that the rate of change of maximum solubilisation levelled off when the ratio was larger than 1:9.

The effect of the percentage of co-surfactant in the surfactant mixture on the maximum water solubilisation of Igepal CO520/cyclohexane /butanol system is shown in **Figure 4.1-8**. It can be seen that S-w_{max} slightly increased from 11.2% to 14.1% with the increase of weight ratio of butanol to Igepal CO-520 from 1:8 to 1:3.

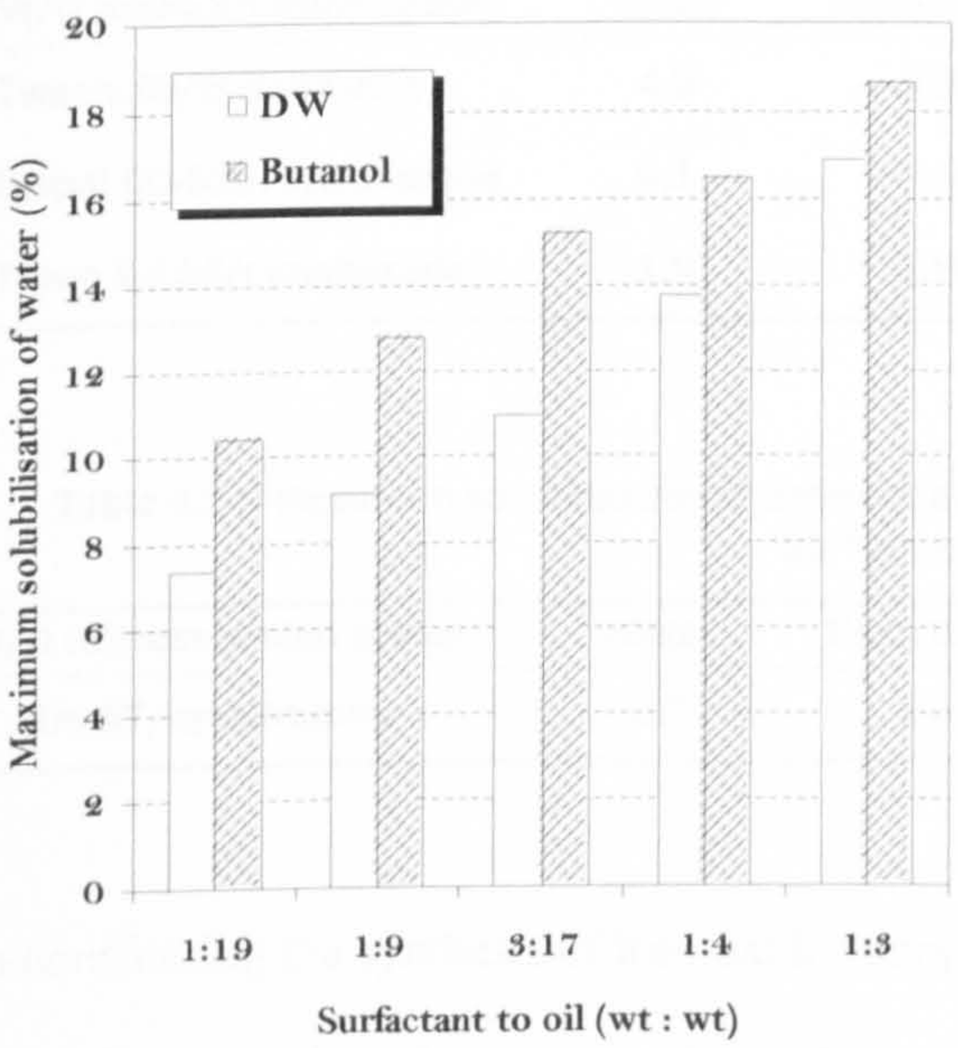

Figure 4.1-7 Maximum solubilisation of water in Igepal CO-520/cyclohexane system with butanol applied as co-surfactant at 25°C.

Surfactant mixture : oil = 1:9 (wt:wt).
Butanol : Igepal CO-520 = 1:5 (wt:wt).

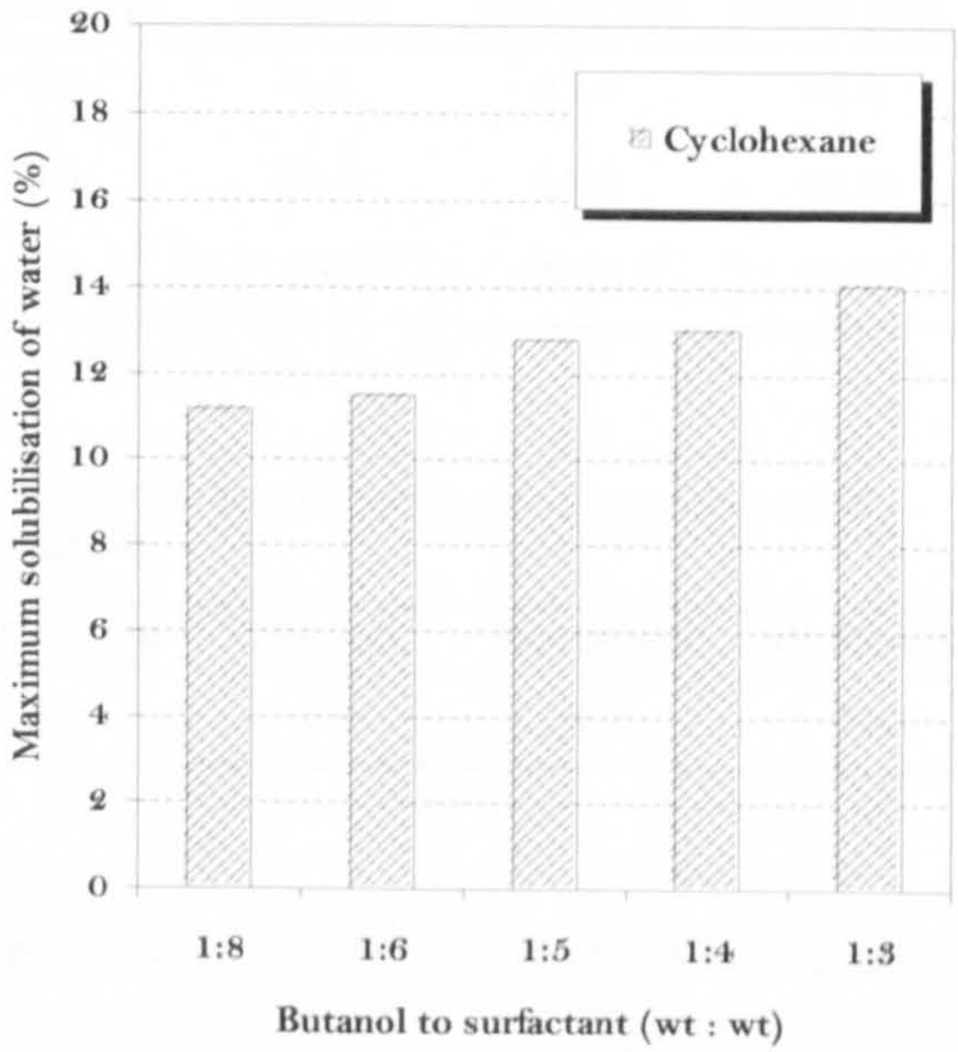

Figure 4.1-8 Maximum solubilisation of water in Igepal CO-520/butanol/cyclohexane system at 25°C.

Surfactant mixture : oil =1:9 (wt:wt).

4.1.3 Studies on aqueous phases

The capability of solubilisation of microemulsion system could be varied with the different aqueous phases. The loading tests were carried out again to evaluate the influence of the aqueous phase on the solubilisation of microemulsion systems and water, iron salt water solution, ammonia solution and monomer water solution were used as different aqueous phases in the study.

Table 4.1-4 showed the maximum solubilisation of different aqueous phases in Tween 85/cyclohexane system, Igepal CO-520/cyclohexane system and Triton X-114/cyclohexane system respectively at 25°C. The monomer solution (methacrylic acid, MAA and acrylamide, AM) showed the highest S_{max} value (>10%) in all three systems, compared with the solubilisation of the water, the iron salt water solution and the ammonia solution (2%-10%). The similar phenomenon was also observed in Brij 97/cyclohexane system at 60°C **[Table 4.1-5]**.

Table 4.1-4 Maximum solubilisation of different aqueous phases (%) in different w/o microemulsion systems at 25°C. Surfactant : oil = 1:9 (wt:wt).

W/O microemulsion system	Water	Fe(II) 0.1M	Fe(III) 0.1M	NH_3-H_2O	MAA 25 wt%	AM 50 wt%
Tween 85/cyclohexane	4.9	3.8	3.6	4.4	11.5	15.0
Igepal CO-520/cyclohexane	9.1	7.6	8.9	10.4	11.7	16.9
Triton X-114/cyclohexane	1.9	1.9	2.0	2.6	13.2	11.8

Table 4.1-5 Maximum solubilisation of different aqueous phases (%) in Brij 97/cyclohexane system at 60°C. Surfactant : oil = 1:9 (wt:wt).

W/O microemulsion system	Water	Fe(II) 0.1M	Fe(III) 0.1M	NH_3-H_2O	MAA 25 wt%	AM 50 wt%
Brij 97/cyclohexane	2.3	1.0	1.2	1.8	5.7	7.4

In considering the synthesis of iron oxide nanoparticles in w/o microemulsion system in the next stage, the influence of mole concentration of iron salt water solution was investigated in Igepal CO-520/cyclohexane system.

As shown in **Figure 4.1-9**, the system with low mole concentration (0.1M) of the $[Fe]^{2+}$ water solution showed higher S_{max} values than the system with higher concentration (0.5M) solution. However, when the aqueous phase was $[Fe]^{3+}$ water solution, the system with higher mole concentration did not always exhibit the higher maximum solubilisation values **[Figure 4.1-10]**. As the weight ratio of surfactant to oil was 1:19 and 1:9, the S_{max} values of the 0.1M $[Fe]^{3+}$ water solution were similar to 0.5M aqueous solution. When the ratio was increased,, the maximum solubilisation of 0.1M solution was continuously increased, meanwhile the S_{max} value of 0.5M solution showed no much difference.

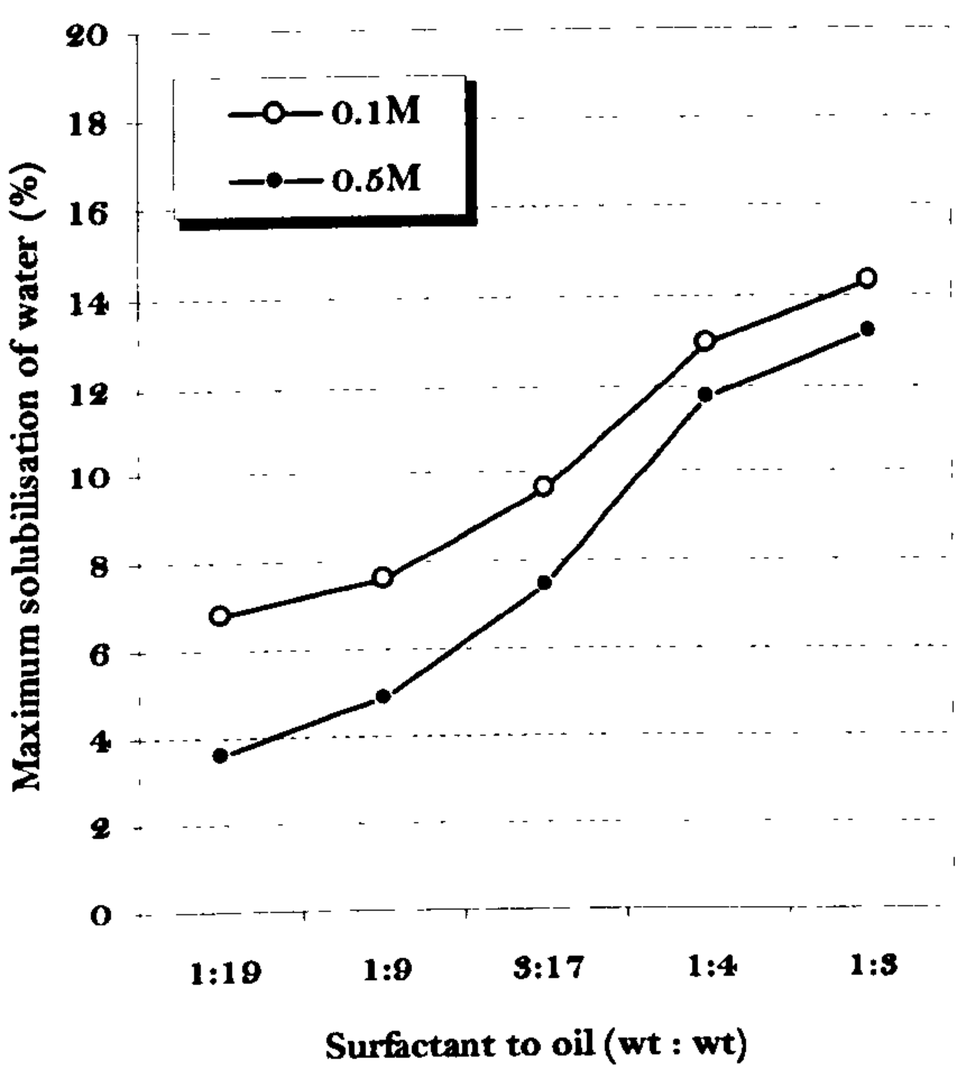

Figure 4.1-9 Maximum solubilisation of iron (II) salt water solution with different molar concentrations in Igepal CO-520 / cyclohexane system at 25°C.

Surfactant : oil = 1:9

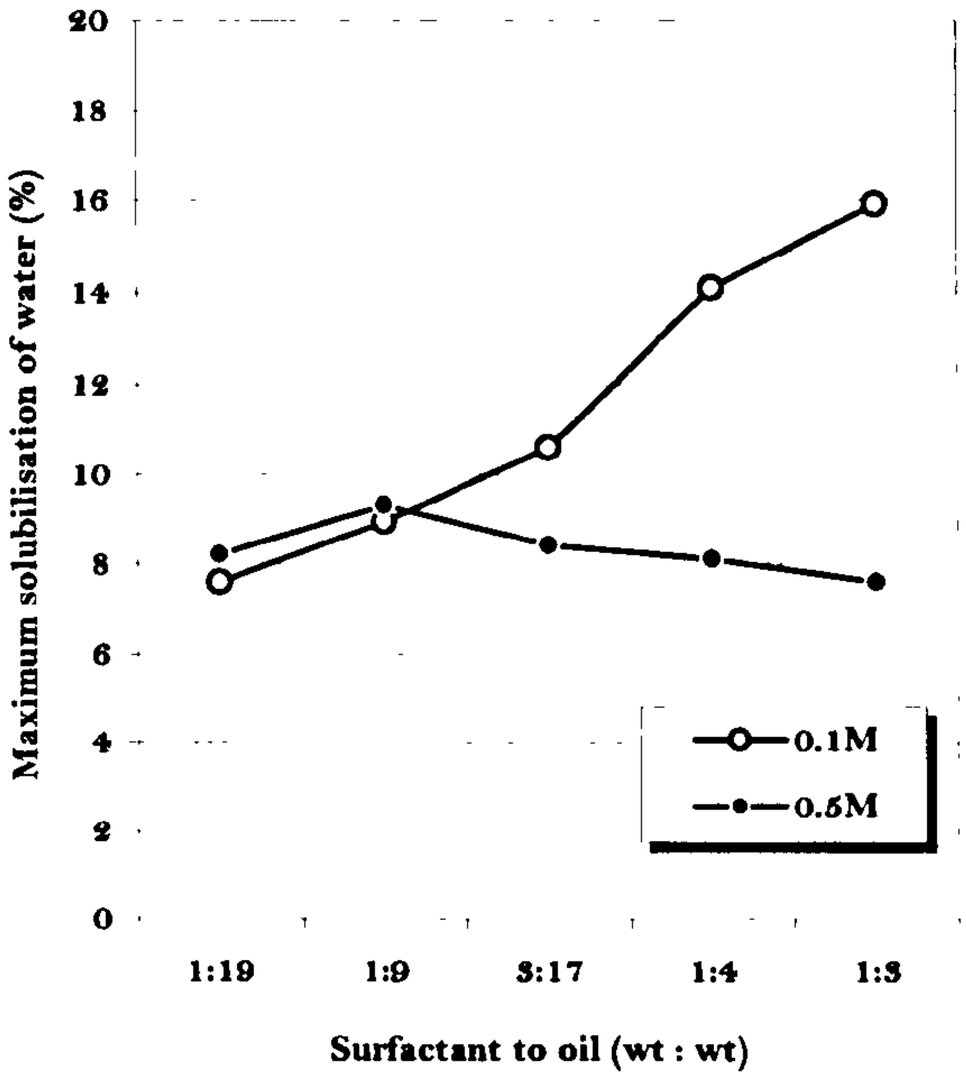

Figure 4.1-10 Maximum solubilisation of iron (III) salt water solution with different molar concentrations in Igepal CO-520 / cyclohexane system 25°C.

Surfactant : oil = 1:9.

4.1.4 Studies on temperature

The investigation of temperature effect on w/o microemulsion systems is very important particularly for the synthesis of polymer at elevated temperature. In this part of experiments, temperature was varied from room temperature (~25°C) to 70°C, which covers the general range of reaction temperatures in the later synthesis. It can be seen from **Figures 4.1-11, 12** and **13**, that the maximum solubilisation of water in microemulsion systems with non-ionic surfactants (Tween 85, Igepal CO-520 and Triton X-114) significantly decreased with the increase of temperature. Particularly for Igepal CO-520/cyclohexane system, $S\text{-}w_{max}$ decreased from 8.9% at 25°C to 0.4% at 60°C.

A different tendency of maximum solubilisation changing with temperature was observed in Brij 97/cyclohexane system **[Figure 4.1-14]**. $S\text{-}w_{max}$ increased from 3.6% to 9.1% as the temperature increased from 40°C to 70°C. When the aqueous phase was AM water solution, S_{max} increased from 8.93% at 40°C to 12.6% at 70°C.

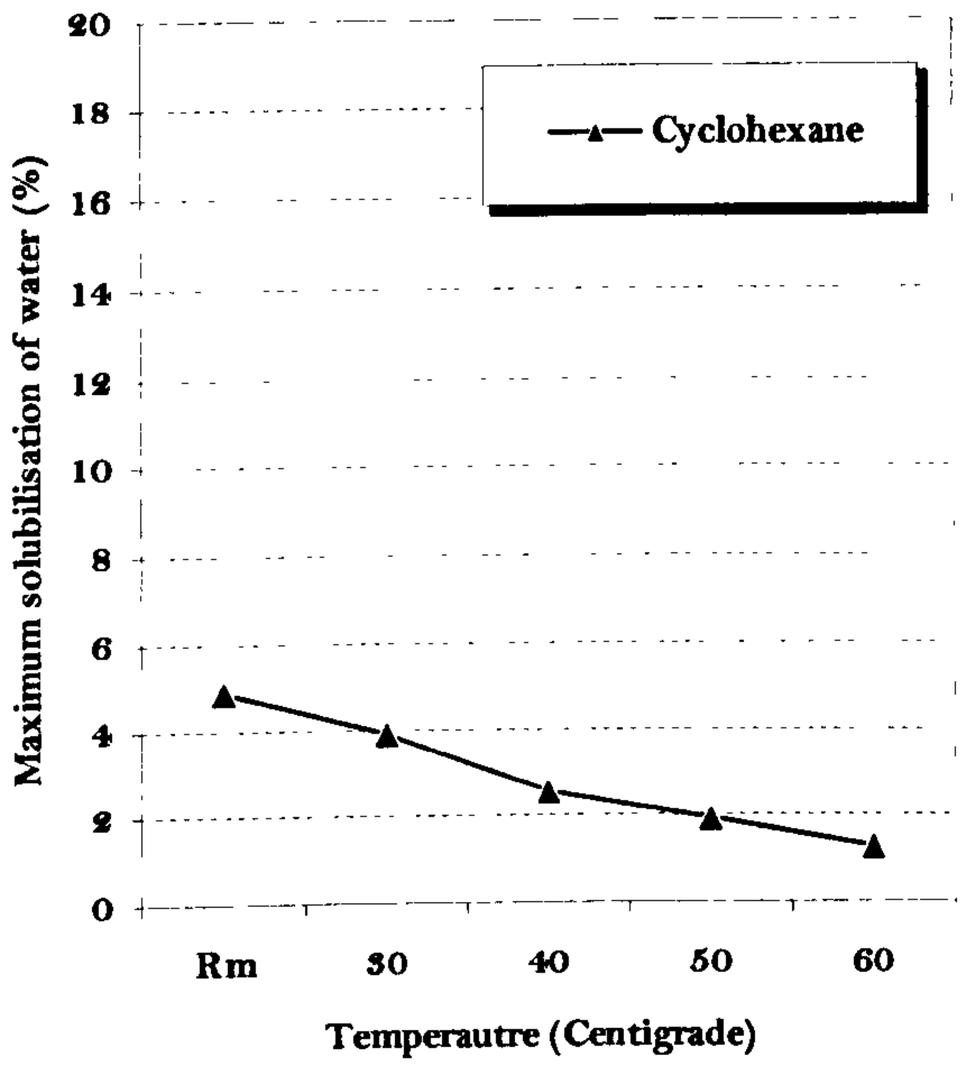

Figure 4.1-11 Maximum solubilisation of water in Tween 85 / cyclohexane system at different temperatures.

Surfactant : oil = 1:9.

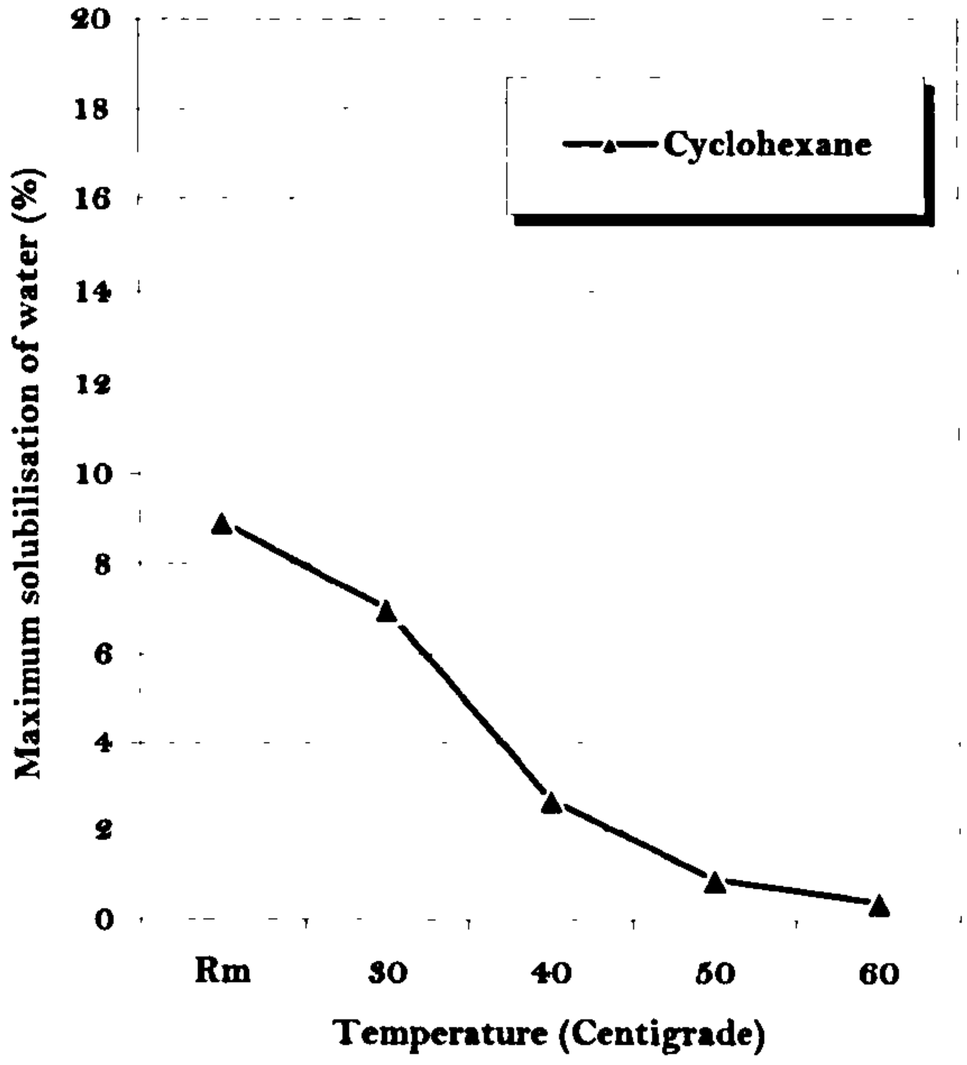

Figure 4.1-12 Maximum solubilisation of water in Igepal CO-520 / cyclohexane system at different temperatures.

Surfactant : oil = 1:9.

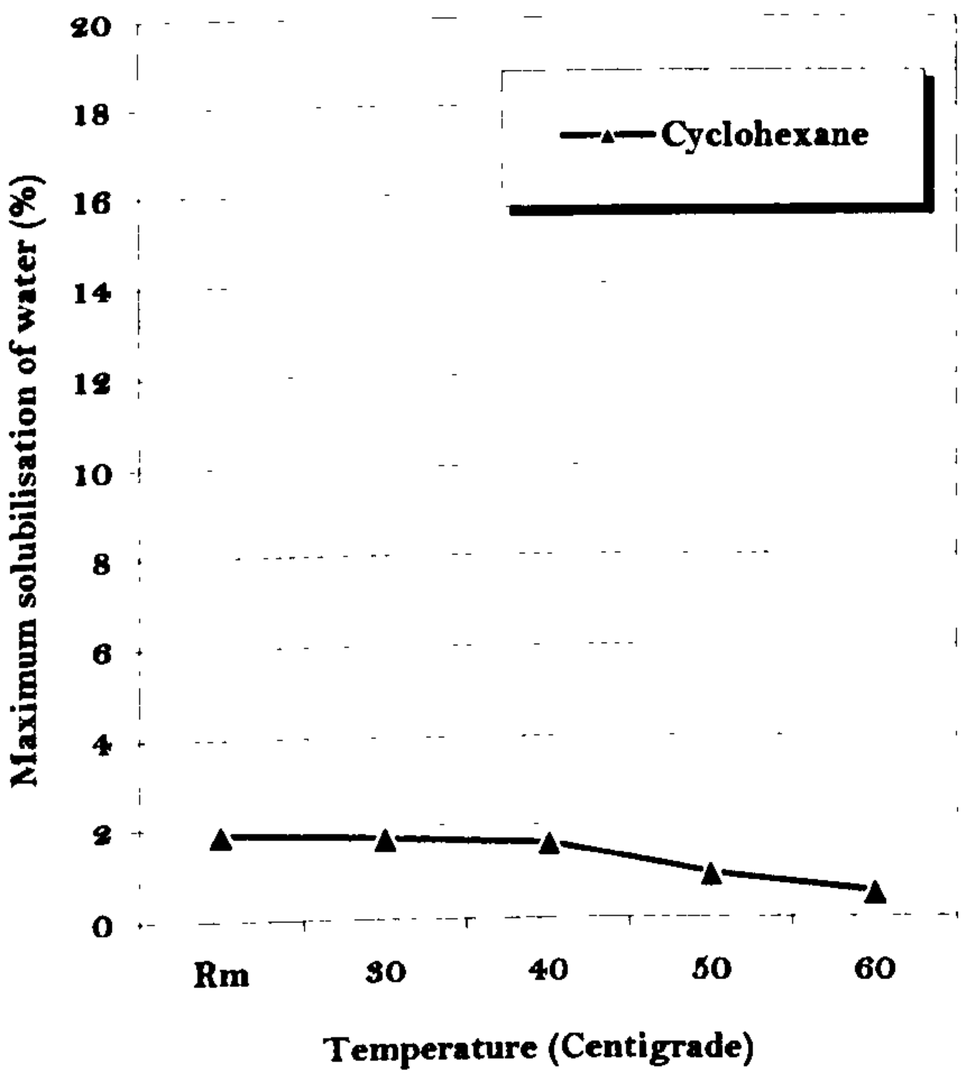

Figure 4.1-13 Maximum solubilisation of water in Triton X-114 / cyclohexane system at different temperatures.

Surfactant : oil = 1:9.

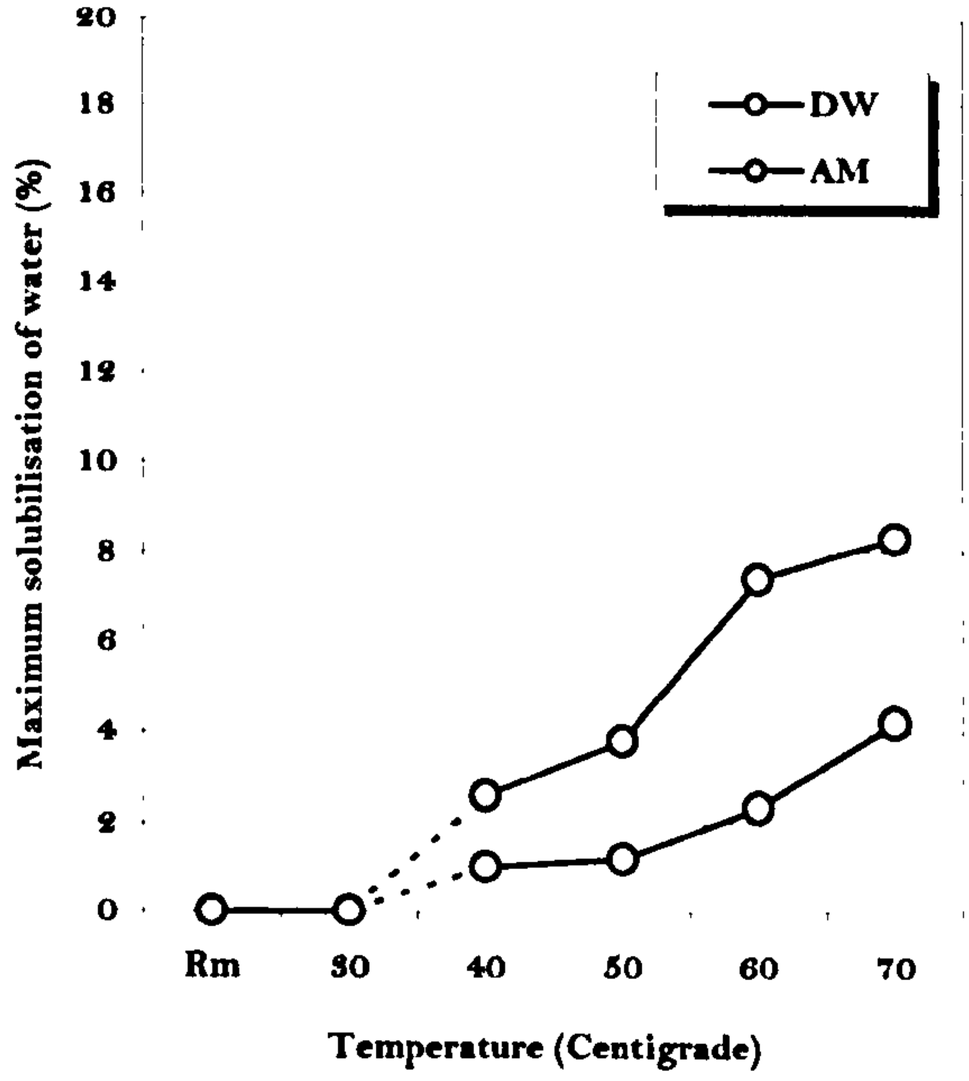

Figure 4.1-14 Maximum solubilisation of water in Brij 97/Cyclohexane system at different temperatures.

Surfactant : oil = 1:9.

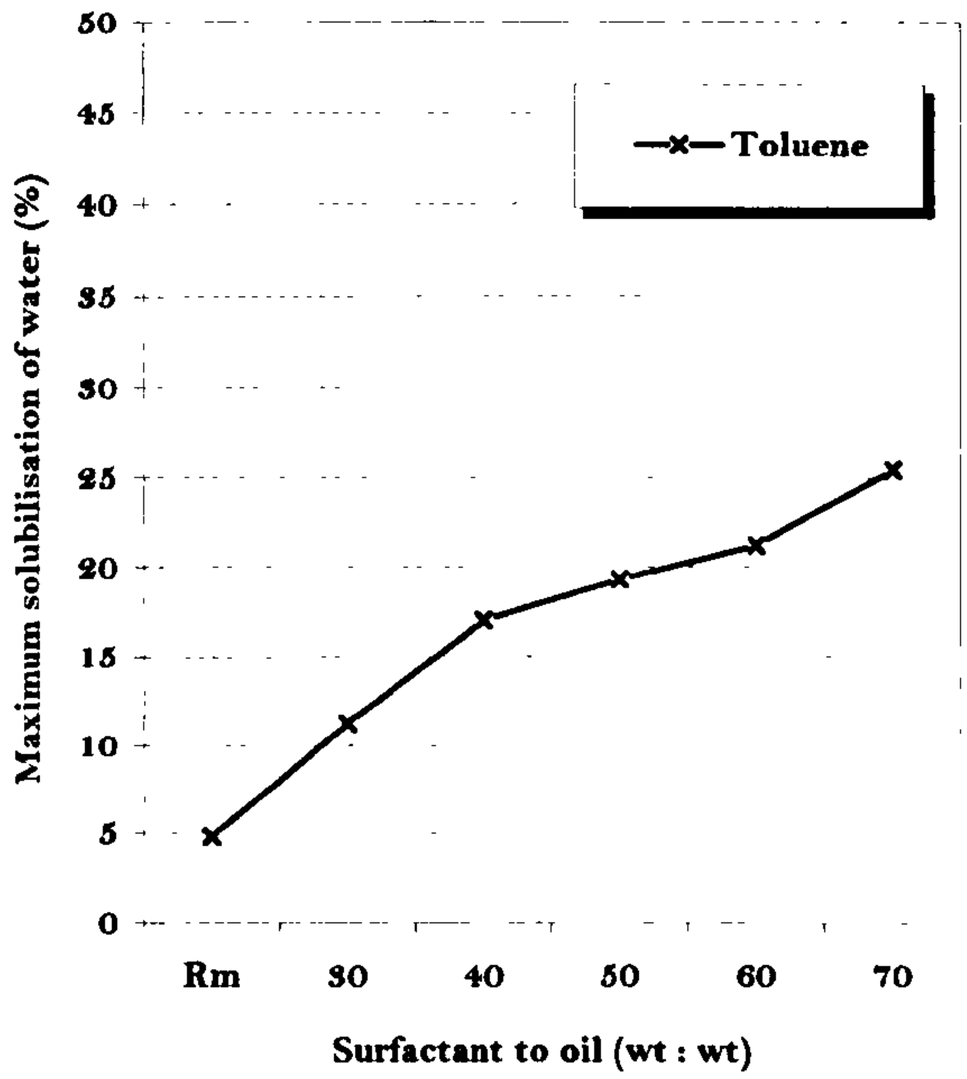

Figure 4.1-15 Maximum solubilisation of water in AOT/Toluene system at different temperatures. Surfactant : oil = 1:9.

The ionic surfactant AOT exhibited the similar relationship between temperature and the maximum solubilisation of aqueous phase in toluene as Brij 97 in cyclohexane. As shown in **Figure 4.1-15**, with increasing temperature, the loading of water increased in the AOT / toluene system.

4.2 DISCUSSIONS

A w/o microemulsion is a transparent solution consisting of water droplets stabilised by the surfactant, (and in some cases co-surfactant) and dispersed in continuous oil phase. According to the theoretical Winsor model, the interior structure of microemulsion system can be varied by changing the percentage of each component. The stability of w/o microemulsion could be affected by different

surfactants, oils, addition of co-surfactants, the nature of dispersed phase and the temperature, arising from the change of interactions between each component.

4.2.1 Effect of surfactant (co-surfactant) and oil

The stability of w/o microemulsion system is strongly dependent on the type of the surfactant and the oil phase. The function of surfactant is to reduce the interfacial tension between the pair of immiscible liquids, enabling them to be dispersed between each other and promotes the formation of microemulsions. The oil phase also plays a important role. The interaction between the surfactant and the oil phase affects the behaviour of w/o microemulsion system formed.

4.2.1.1 Compatibility between surfactant and oil

Although the mechanism of solubility of a surfactant in oil is complicated, there is a common principle which can be used to approximately determine the miscibility of a surfactant and an oil – the structure similarity, i.e. the better miscibility more likely exists between two phases with the more similar structures. For example, linear structured Triton X-100 can not dissolve in cyclohexane which has a cyclic structure, but can dissolve in isooctane which is a linear chain.

The comparison of structure similarity gives us a basic idea, but it is still far from satisfying. For example, Tween 85, Triton X-100, Triton X-114, Igepal CO-520 and Igepal CO-720 all have a cyclic chain within each of their structures, but not all of them dissolved in cyclohexane; this indicates that a structure similarity is not sufficient in this interpretation. With respect to the different behaviours of surfactants, their HLB (Hydrophile-Lipophile Balance) values provide a more practical solution.

Figure 4.2-1 shows the HLB values of all the surfactants used in this project, which are placed in HLB axial by sequence of their HLB values. The higher HLB value means the stronger hydrophilic of the surfactant. Therefore having a higher HLB value, Tween 80, Igepal CO-720, Triton X-100 are more difficult to dissolve in the non-aqueous oil phase. However, AOT is a different case. Although having

the highest HLB value comparing with other non-ionic surfactants, AOT can easily dissolve in all selected oil phases as AOT is an ionic surfactant and could ionise in oil phases. Hence the HLB principle is more appropriate when applied to non-ionic surfactants.

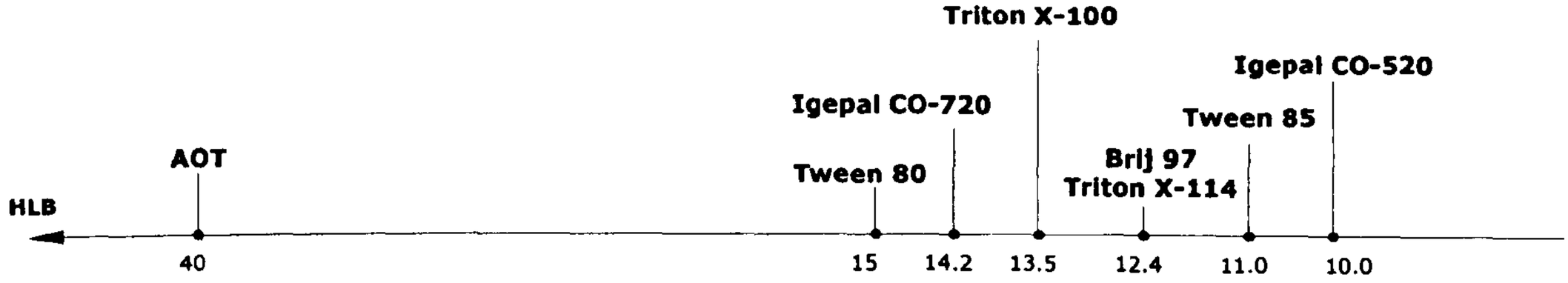

Figure 4.2-1 Schematic of HLB value of all surfactants used in this project

Brij 97 appears non-soluble in cyclohexane at 25°C but became soluble in the same oil phase at 60°C. The determinative factor is the melting point of surfactant itself. Brij 97 turns into liquid at 30°C, while having a paste-like appearance at 25°C. Precisely speaking, Brij 97 is soluble with haze in cyclohexane at 25°C.

4.2.1.2 Effect of different non-ionic surfactants

Non-ionic surfactants are usually composed of ethylene oxide (EO) units, such as **IGEPAL CO** series and **Triton X** series (polyoxyethylenated alkylphenols), **BRIJ** series (polyoxyethylenated fatty acids) and **TWEEN** series (polyoxyethylenated polyols). The hydrophilic properties of the non-ionic surfactant depend on the number of EO units in the compound. The addition of EO units enables the manufacturer to produce a series of products in a broad spectrum of solubility and performance characteristic [173]. At the same time, the addition of the EO units could also determine the solubility of the compound in organic solvents.

In the solution of the non-ionic surfactant with the oil, surfactant molecules could aggregate by the intermolecular hydrogen-bonding [76-77] to form surfactant clusters known as micelles, which can

solubilise the aqueous phase by the interaction with the EO of the polyoxyethylenated (POE) chain [174]. A three-component (surfactant, oil and water) w/o microemulsion system is formed as a result.

Different oil phases result in different extent of solubilisation of the aqueous phase in the microemulsion system. In our investigation, cyclohexane seemed the best oil phase for all soluble surfactants in terms of the power of the water solubilisation than isooctane and PE. In fact, the extent to which a substance can be solubilised into a micelle in the microemulsion depends upon the size of the micelle that is the locus of the solubilisation [174]. The amount of solubilised aqueous phase generally increases with the increase of the size of micelles. The determination of the size of the micelle could be further interpreted by another important measurement, *aggregation number*, which is the number of surfactant units making up the micelle. If the molecular weight of the surfactant unit making up the micelle is known, the aggregation number can be calculated as:

$$n = M_m / M_0 \qquad \textbf{(5-1)}$$

where n is the aggregation number, M_m the micelle weight, and M_0 the molecular weight of the individual surfactant molecule [174]. According to the **Equation 5-1**, the increase of aggregation number means the increase of micellar size and the better capability of solubilisation. Hence, the better capability of the system with cyclohexane suggests that it may have the larger size of micelles with the larger aggregation number comparing with the isooctane and the PE systems, which is presumably attributed to the different miscibility between the different oil phases and surfactants.

All the surfactants used, i.e. Tween 85, Igepal CO-520 and Triton X-114, have cyclic structures similar to cyclohexane, but isooctane and PE have the straight chains. On the basis of the previous discussion, cyclohexane may have better miscibility with non-ionic surfactants employed. The hydrophobic groups of the surfactant might extend towards the oil phase, i.e. cyclohexane, rather than coiling together in the interface. Such arrangement of surfactant molecules in the interface decreased the cross-sectional area of the hydrophobic group. From the geometric consideration, the decrease of the cross-sectional area would probably result in the increase of the number of surfactant molecules

surrounding a micelle. Therefore, cyclohexane, due to its better miscibility, leads to the larger aggregation number comparing with other two oil phases, which consequently favours the higher solubilisation of water into the w/o microemulsion system.

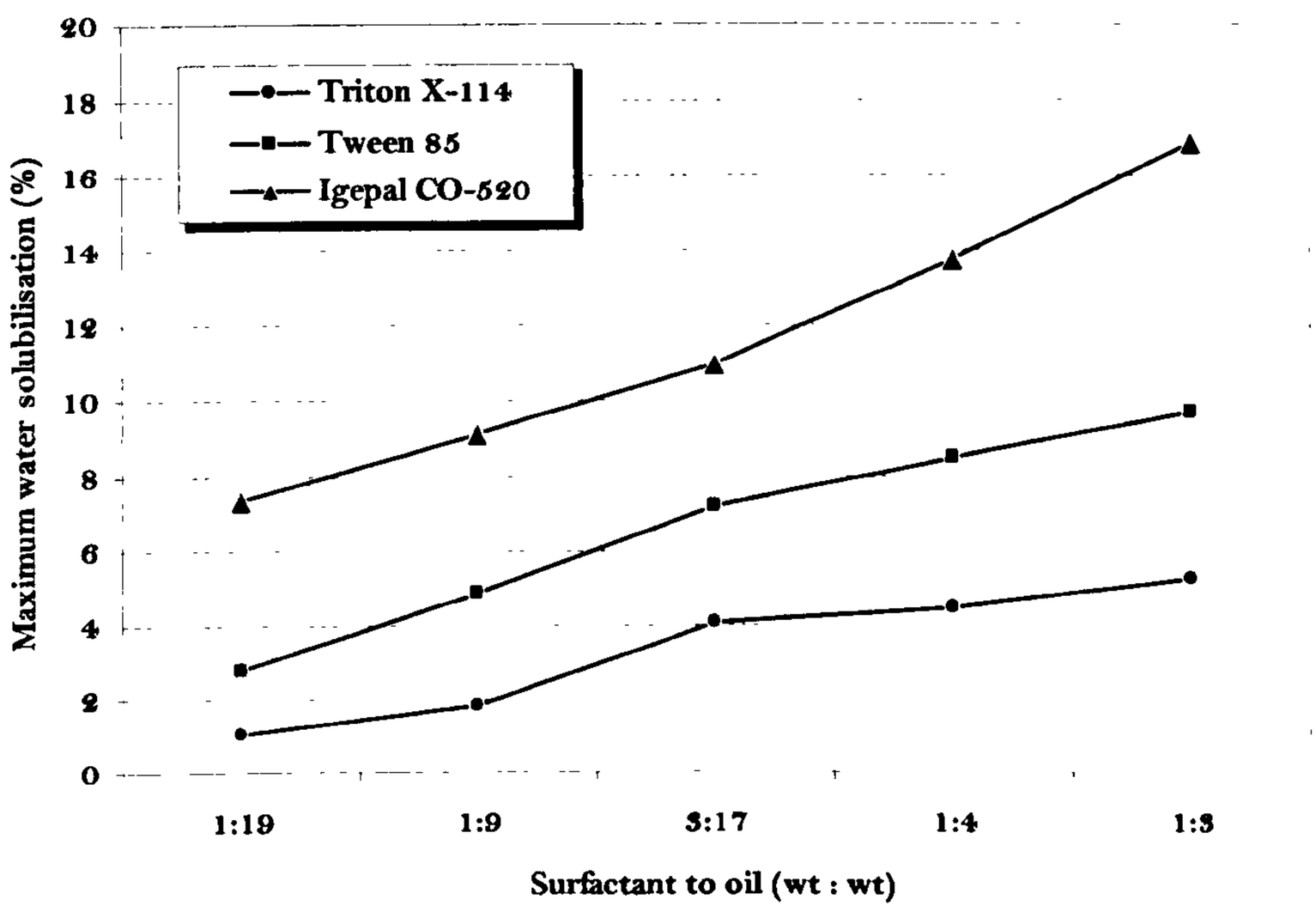

Figure 4.2-2 Effect of different surfactants on the maximum water solubilisation in w/o microemulsion systems with cyclohexane as the oil phase at 25°C.

As for the systems with the same oil phase, the nature of non-ionic surfactant is another determinative factor affecting the solubilisation power of the aqueous phase. The amount of the aqueous phase solubilised into the oil phase by POE non-ionic surfactants appears to increase with the increase of the surfactant concentration and the length of the POE chain [173]. The experimental results of the water solubilisation in w/o microemulsions with Tween 85, Igepal CO-520 and Triton X-114, respectively, were all in agreement with the surfactant influence mentioned above, i.e. the increase of surfactant concentration lead to the increase of the maximum water solubilisation. Additionally, Igepal CO-520 was found to exhibit better water solubilisation than Tween 85 and Triton X-114 **[Figure 4.2-2]** in cyclohexane presumably because the different length of POE chains. The length of POE chain in Tween 85, Igepal CO-520 and Triton X-114 is 20, 5 and 8 respectively. As shown in **Figure 4.2-3**, POE chain lies flat on the surface of the water phase [173]. For the surfactant with multiple EO units, the

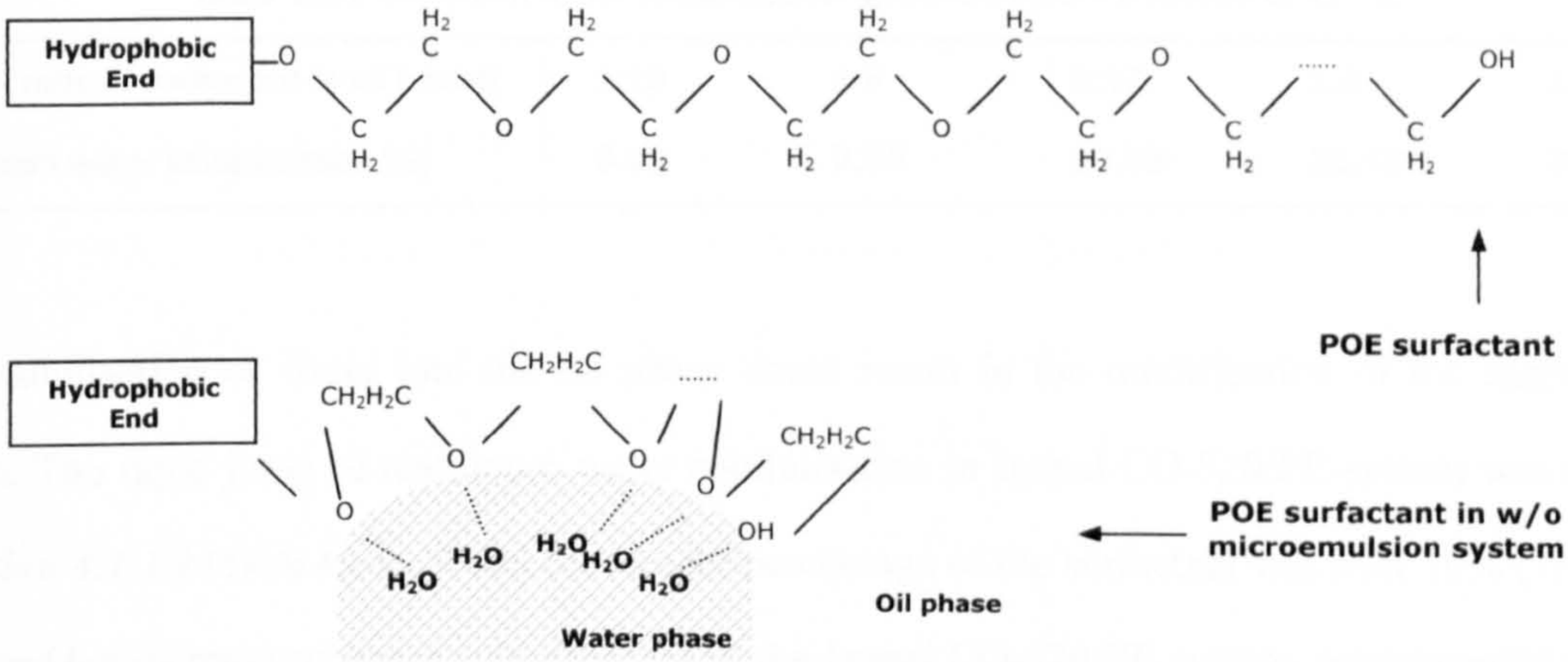

Figure 4.2-3 Schematics of the POE surfactant in w/o microemulsion.

portion of the molecule between the two hydrophilic groups tends to lie flat in the interface [174]. An increase in the POE chain length appears to be associated with an increase of cross-sectional area and so a consequent decrease in the aggregation number. Hence, as having the shortest POE chain, Igepal CO-520 apparently has the largest aggregation number and then the better solubilisation of water in emulsifying cyclohexane. In another words, the aggregation number could be affected by the change of cross-sectional area due to the different packing situation of hydrophilic groups of different surfactants.

On the other hand, the aggregation number could also be affected by the HLB value of the non-ionic surfactant. The higher HLB value means the higher hydrophilicity of the surfactant, which would be far more repelled by the oil phase. Hence, surfactant molecules with the higher HLB value would tend to aggregate into micelles even at lower concentration in the oil phase. In this case the aggregation number was comparably smaller than the surfactant with the lower HLB value [120]. As shown in **Figure 4.2-1**, the HLB values of Tween 85, Igepal CO-520 and Triton X-114 are 11.0, 10.0 and 12.4 respectively. Therefore the corresponding capability of water solubilisation of these three surfactants would be expected to be as Igepal CO-520 > Tween 85 > Triton X-114, which is in agreement with our investigation results.

Table 4.2-1 Maximum water solubilisation Igepal CO-520/PE system at 25°C.

Weight ratio of surfactant to oil [wt:wt]	1:19	1:9	3:17	1:4	1:3
Maximum water solubilisation [%]	0.43	2.53	**23.03**	**25.43**	**26.83**

The solubilisation of water into the oil phase could result in the modification of the shape of the micelle. The rapid jump of maximum water solubilisation in Igepal CO-520/PE system was reported in ***Section 4.1.1.2*** **[Table 4.2-1]**. When the weight percentage of the surfactant was over 10% (1:9), there was a sudden increase of water solubilisation in the Igepal CO-520/PE system, accompanied with the large increase of viscosity of microemulsion system, which perhaps suggested the formation of a hexagonal liquid crystalline phase.

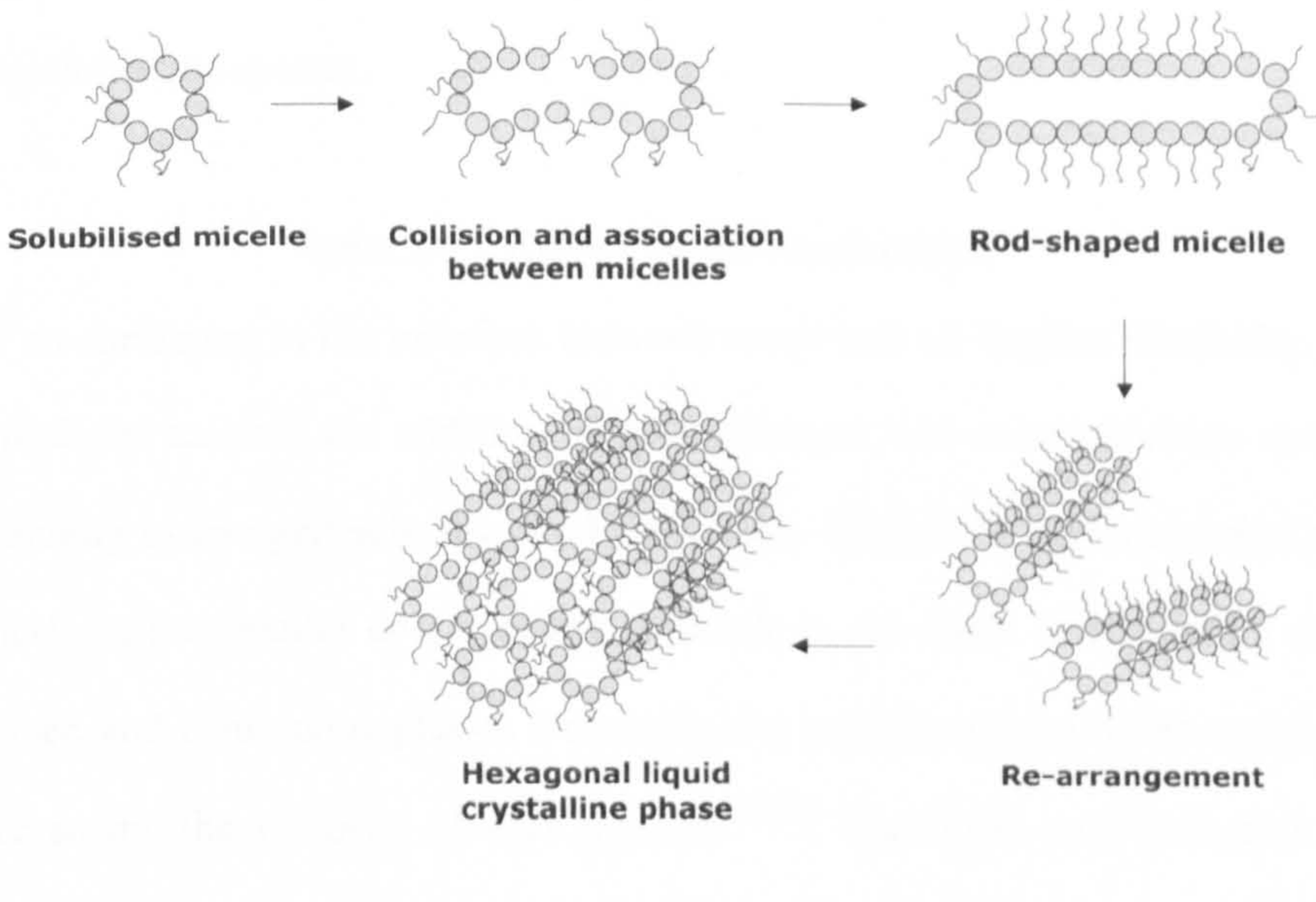

Figure 4.2-4 Transition of the arrangement of micelles in the w/o microemulsion with the increase of the loading amount of the aqueous phase.

The hexagonal liquid crystalline phase is a high viscosity fluid phase composed of a close-packed array of cylindrical assemblies of surfactant molecules **[Figure 4.2-4]**. The arrangement of solubilised micelles changes with the addition of the aqueous phase. At the beginning, since the aqueous phase is little, micelles are in a relatively small size and could move somewhat freely in the bulk phase, (dilute

micelle solution). With the increase of the amount of the aqueous phase, micelles swell and by the inter-micellar collision and association, they turn from the original spherical shaped micelles into cylindrical micelles in order to solubilise larger amount of aqueous phase. If the addition of aqueous phase is continuously increased, the space was almost fully occupied and the micelles have to change into a more compacted packing model for the stability and the lowest surface tension. Then hexagonal packing of rod-shaped micelles is formed. The presence of hexagonal liquid crystalline phase results in the sudden increase of viscosity of the system.

Hence the different phenomena observed in prepared Igepal CO-520/PE system was probably attributed to the formation of the hexagonal liquid crystalline phase. However, due to the lyotropic property of surfactant liquid crystalline phase, characteristics of the system are highly dependent on the nature of solvent [80]. That maybe the reason why there was no similar phenomenon observed in the Igepal CO-520/cyclohexane system.

4.2.1.3 Effect of co-surfactant

The presence of co-surfactant in the interface between water and oil imparts flexibility. In addition to lowering the interfacial tension, the addition of co-surfactants into microemulsion system results in easier surface bending to energetically favoured dispersion. Unlike the surfactant that resides only at the water/oil interface, the smaller co-surfactant molecule is not static. It constantly migrates in and out of the dispersed and continuous phases increasing the mobility of the mono-molecular interface, consequently decreasing the viscosity of such systems [176]. Therefore, a co-surfactant mixed with a surfactant in a certain proportion is a convenient method to improve the solubilisation of aqueous phase in the w/o microemulsions system. Alknaols with 4-8 carbon chains, i.e. butanol, pentanol and hexanol, and amines (like butylamine, hexylamine) are generally employed for this purpose.

By introducing co-surfactant into the system, some of the non-soluble surfactants can be dissolved in a particular oil phase, for example, Triton X-100. Compared with Triton X-114, Triton X-100 has the similar structure but the lager number of EO units and consequently the poor oil solubility. Hence,

Triton X-100 was shown to be insoluble in cyclohexane, either at room temperature (25°C) or 60°C. However, with the addition of hexanol as the co-surfactant, Triton X-100 became to be dissolved in the cyclohexane, presumably because the added alkanol molecules enlarged the distance between two adjacent surfactant molecules and turned the micelle into a loose packing state. The flexibility of interface was consequently improved, which was of benefits to help the system changing into more homogeneous state.

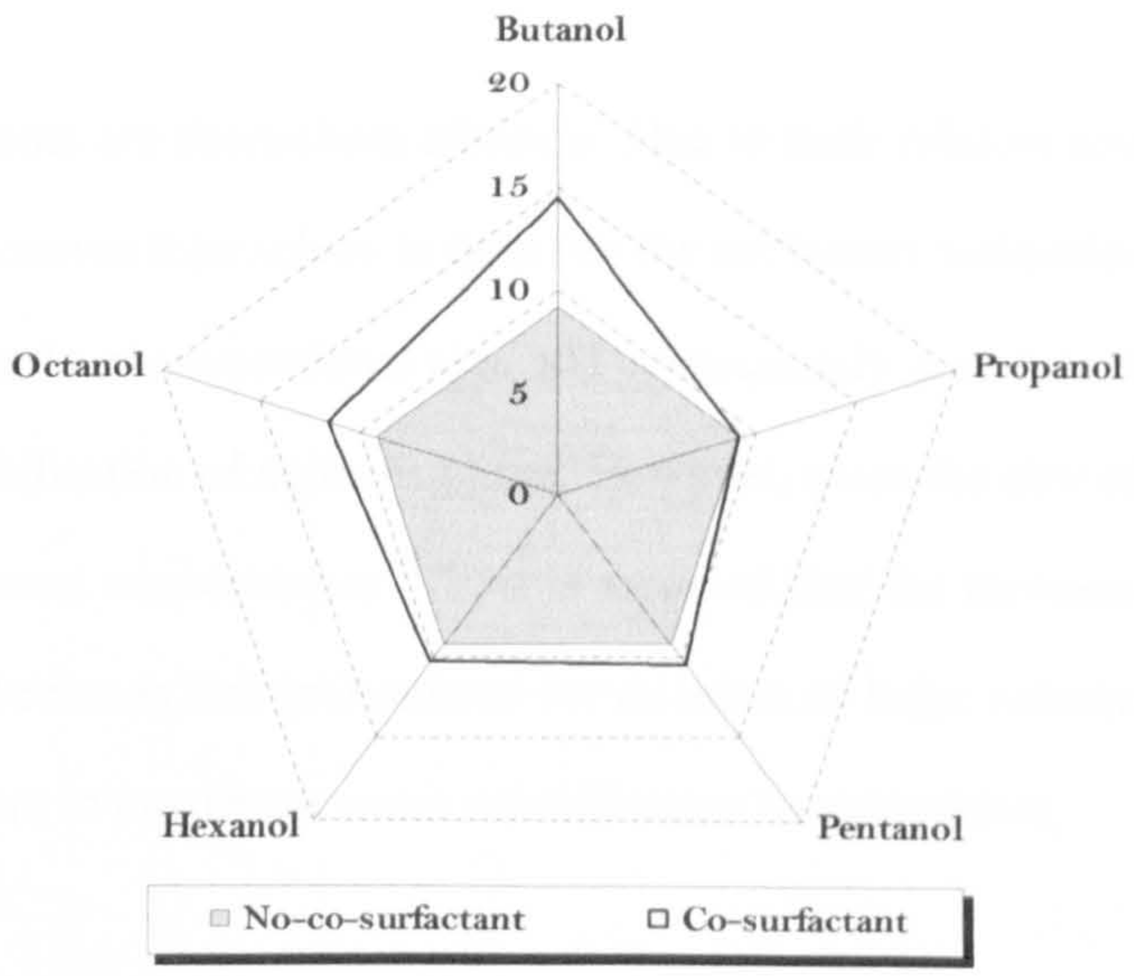

Figure 4.2-5 Maximum water solubilisation in Igepal CO-520/cyclohexane system with different co-surfactants applied at 25°C. Surfactant mixture: oil =1:9 (wt:wt). Co-surfactant: Igepal CO-520 = 1:5 (wt:wt).

In addition to making insoluble surfactants soluble in oil phases, the presence of co-surfactant also increased the extent of solubilisation of the aqueous phase in w/o microemulsions. The effect of different co-surfactants was examined in our experiment. For Igepal CO-520/cyclhexane system [**Figure 4.2-5**], the highest water solubilisation appeared when the co-surfactant was butanol, probably because butanol as of the shortest length of the chain could migrate more easily in/out the surfactant layer which could greatly increase the flexibility and the solubilisation capability.

Table 4.2-2 shows the difference of maximum water solubilisation in Igepal CO-520/cyclohexane system with and without the co-surfactant, butanol. In this four-component system, $S_{w\text{-}max}$ increased

with the increase of the concentration of the surfactant mixture, i.e. surfactant + co-surfactant, in which the weight ratio of co-surfactant to surfactant was kept in constant as 1:5.

Table 4.2-2 Maximum water solubilisation (%) in Igepal CO-520/cyclohexane system with butanol applied as co-surfactant at 25°C. Butanol: Igepal CO-520 = 1:5 (weight ratio).

Surfactant : Oil [wt : wt]	1:19	1:9	3:17	1:4	1:3
No co-surfactant	7.4	9.1	11.0	13.8	16.9
Butanol	9.4	14.6	15.7	18.3	18.9

In general the co-surfactants are short-chain alkanols. Due to their relative smaller size, co-surfactant molecules normally manoeuvre themselves in between the surfactant molecules. Hence the addition of the co-surfactant enlarges the cross-sectional area and consequently increases the capacity of micelles, which improves the solubilisation of aqueous phase. However, since the size of micelle increases with the increase of the surfactant concentration [174], it is assumed that the increase of cross-sectional area by adding co-surfactant becomes less pronounced for micelles of large volume than small. Therefore, the accompanied increment in maximum water solubilisation seems modest.

Table 4.2-3 Maximum water solubilisation in Igepal CO-520/butanol/cyclohexane system at 25°C.

Co-surfactant : Surfactant [wt : wt]	1:8	1:6	1:4	1:3
Maximum water solubilisation [%]	2.13	2.2	2.62	2.87

On the other hand, with the same amount of the surfactant added, the decrease of co-surfactant concentration in surfactant mixture might result in the decrease of solubilisation of water phase in w/o microemulsion system, apparently because of the decrease in cross-sectional area and the aggregation number [**Table 4.2-3**].

4.2.2 Effect of aqueous phase

A fundamental characteristic of surfactants is their tendency to adsorb at interface in an oriented fashion [174]. In the w/o microemulsion with the non-ionic surfactant, surfactant molecules adsorb at

the interface of oil and water; the hydrophobic groups orient towards the oil phase and POE chains immerse in the inner core of micelle with aqueous phase. The interfacial tension is determined by the competition results of the interactions between surfactant/oil and surfactant/water.

Therefore, for a particular w/o microemulsion system, different aqueous phases could result in different interactions between the surfactant and the solubilised aqueous phase. The absorption of surfactant molecules on interface can be altered due to the different interfacial tension. Then, the aggregation number, which is related to the absorption of the surfactant at interface, might be affected. Consequently, the extent of solubilisation of the aqueous phase in the w/o microemulsion system would be changed.

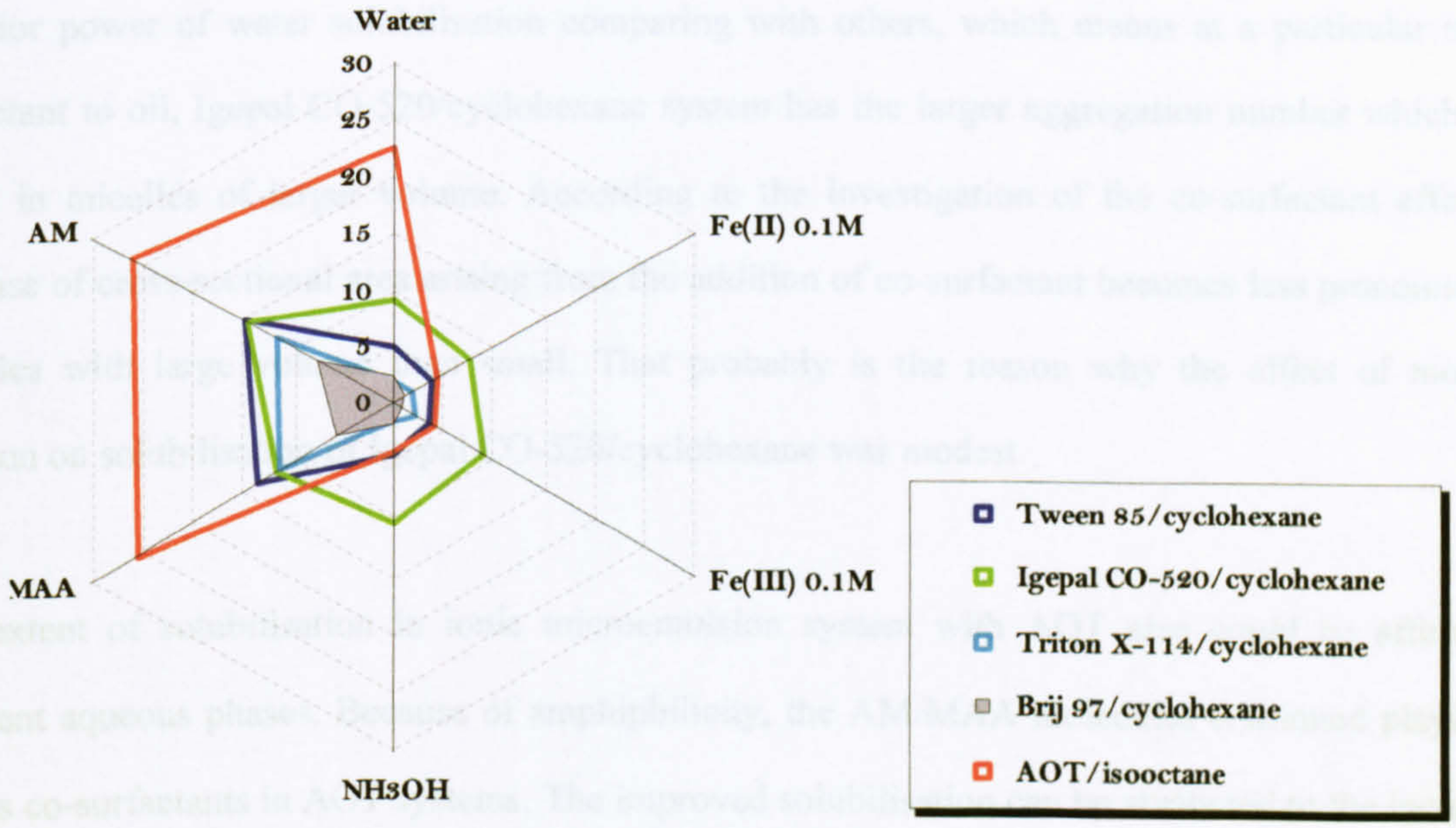

Figure 4.2-6 Effect of different aqueous phases on the maximum water solubilisation in different w/o microemulsion systems. Surfactant : oil = 1:9.

Figure 4.2-6 shows the effect of different aqueous phases on the maximum water solubilisation in different microemulsion systems. For most of the investigated systems, S_{max} of monomer water solution (AM and MAA) was higher than other aqueous solutions or water. As is known, AM and MAA are amphiphilic materials. Although as solubilisate, the AM/MAA molecules do not entirely

stay in the inner core of micelles in w/o microemulsion system. Due to their amphiphilic property, some of the AM/MAA molecules prefers to reside in the interface of oil-water phases and act like co-surfactants, which result in significantly improved solubilisation of the aqueous phase.

However, the effect of AM/MAA molecules on the capability of solubilisation was varied with the different w/o microemulsion systems. For Tween 85/cyclohexane, Triton X-114/cyclohexane and Brij 97/cyclohexane systems, the maximum solubilisation of monomer solution was much higher than other aqueous phase. For Igepal CO-520/cyclohexane system, the maximum solubilisation values of five different aqueous phases were relatively close to each other. In another word, the influence of monomer molecules on the solubilisation in Igepal CO-520/cyclohexane system was not as significant as they acted in other systems. As found at 25°C, Igepal CO-520/cyclohexane system exhibited superior power of water solubilisation comparing with others, which means at a particular ratio of surfactant to oil, Igepal CO-520/cyclohexane system has the larger aggregation number which could result in micelles of larger volume. According to the investigation of the co-surfactant effect, the increase of cross-sectional area arising from the addition of co-surfactant becomes less pronounced for micelles with large volume than small. That probably is the reason why the effect of monomer solution on solubilisation of Igepal CO-520/cyclohexane was modest.

The extent of solubilisation in ionic microemulsion system with AOT also could be affected by different aqueous phases. Because of amphiphilicity, the AM/MAA molecules continued playing the role as co-surfactants in AOT systems. The improved solubilisation can be attributed to the increase of cross-sectional area due to the existence of AM/MAA molecules in the interface. It should be noticed that, in AOT/isooctane system, except the significantly higher solubilisation of MAA solution, the extent of solubilisation of water was the second higher value much more than iron salt solution and ammonia solution, which was different from what we found in non-ionic systems, which will be discussed in **4.2.5 non-ionic and ionic surfactants.**

4.2.3 Effect of temperature

The hydrophilicity of non-ionic surfactant basically depends on the number of EO units in the surfactant structure. Consequently, a rise in temperature usually results in the dehydration of POE group, which could affect the over-all solubility of these materials [173]. In the water solution of non-ionic surfactants, raising temperature normally leads to the precipitation of non-ionic surfactants from water even below the critical micelle concentration (CMC). In a word, the POE non-ionic surfactants show inverse temperature-solubility.

The dehydration of EO units with increased temperature may change the interfacial tension of surfactant-water phases [175] and the aggregation number in consequence. It was reported that the average aggregation number decreases with the increase of temperature [177], which would result in the reduction of the capacity of micelles. Since the smaller size of micelle yields the lower extent of solubilisation of aqueous phase, the increase of temperature generally leads to the decrease of the extent of solubilisation of the aqueous phase in non-ionic w/o microemulsion systems.

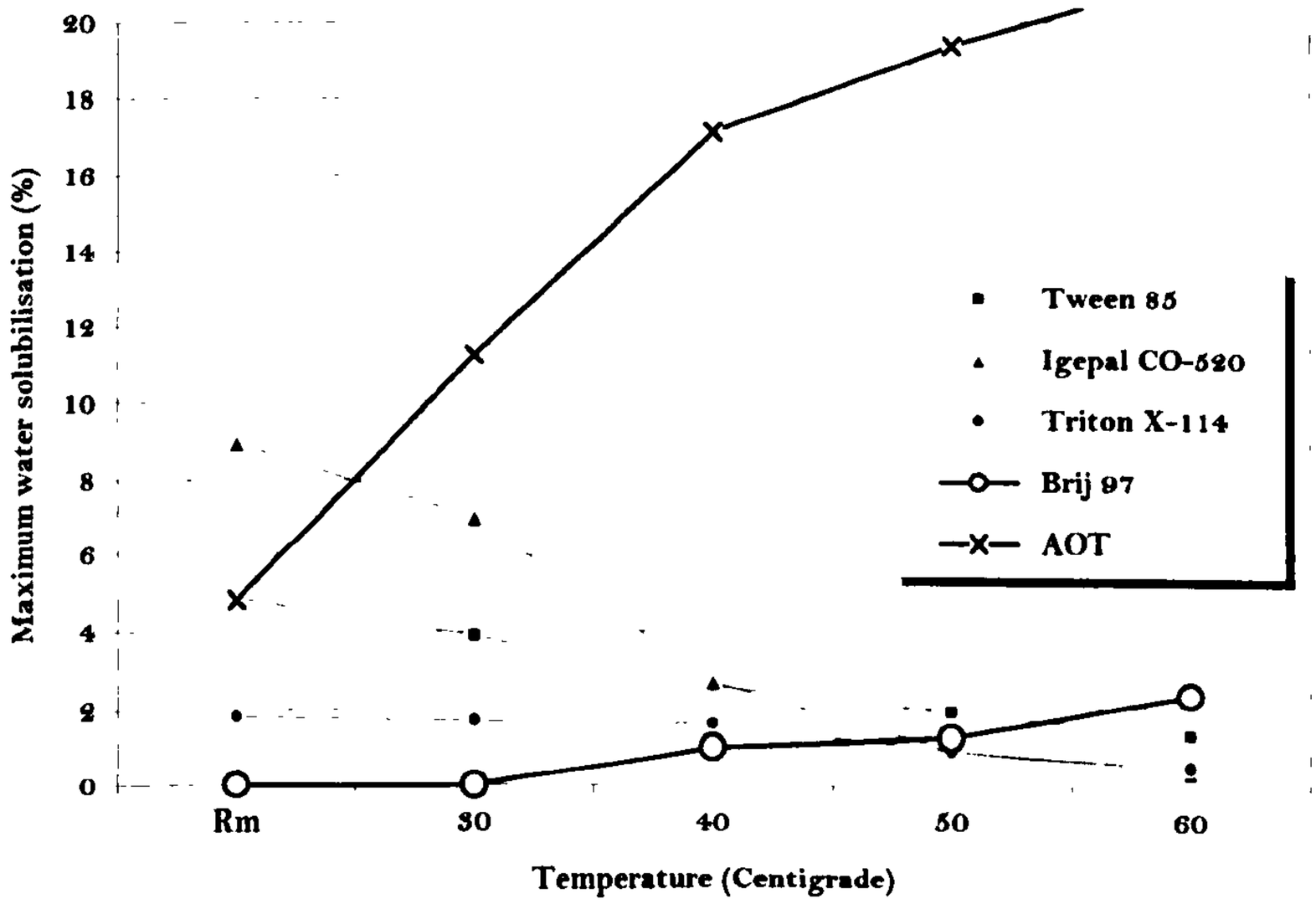

Figure 4.2-7 The changing of maximum water solubilisation in different w/o microemulsion systems with the increase of temperature. Surfactant . oil = 1:9 (wt:wt)

For example, the w/o microemulsion system with Tween 85, Igepal CO-520 and Triton X-114 showed decreased solubilisation of the aqueous phase with the increase of temperature. **Figure 4.2-7** shows that the maximum solubilisation of these three non-ionic systems, exhibited negative results with the increased temperature. The comparably abrupt slope of the line referring to Igepal CO-520/cyclohexane system suggests that Igepal CO-520 is more sensitive to the changing of temperature than Tween 85 and Triton X-114. Normally, non-ionic surfactants with longer POE chains show a higher cloud point by virtue of a greater capacity to hydrate [173]. In comparison to Tween 85 (x=20) and Triton X-114 (x=8), Igepal CO-520 (x=5) has the shortest POE chains. Therefore the solubilisation of aqueous phase in the system with Igepal CO-520, might be more significantly influenced by the dehydration of EO units with the increased temperature.

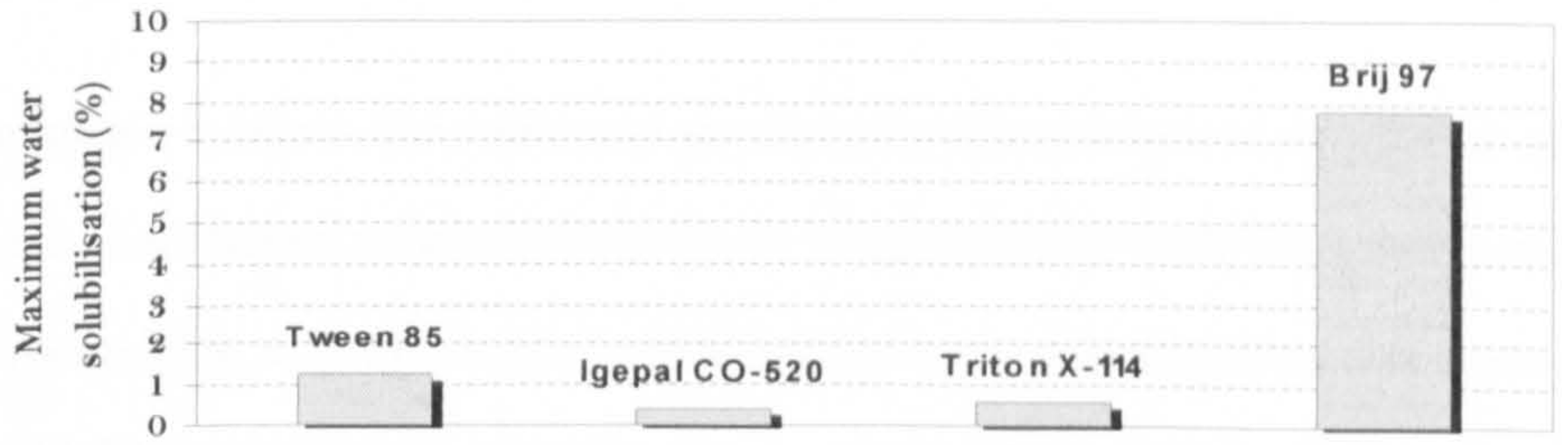

Figure 4.2-8 Maximum water solubilisation in individual surfactant/oil system at 60°C. Surfactant : oil = 1 :3 (wt:wt).

However, a positive result of solubilisation *vs.* temperature was observed in the Brij 97/cyclohexane non-ionic microemulsion system [**Figure 4.2-7**]. The extent of solubilisation increased with the increase of temperature above 30°C. The similar result was also found by Elworthy *et al.* [178] in $CH_3(CH_2)_{15}(OE)_7OH$ non-ionic surfactant, which showed a positive effect of temperature on solubilisation by the results from light-scattering, viscosity and vapour-pressure techniques. The apparent discrepancy seems ascribable to the fact that the water trapped in POE chain may increase with rising temperature [173]. **Figure 4.2-8** summarises the extent of water solubilisation in w/o microemulsion systems with different non-ionic surfactants at 60°C. Brij 97/cycohexane system exhibited the relatively higher value of maximum solubilisation at higher temperature, meanwhile, the capability of solubilisation in the other three systems were not satisfactory. This comparison indicates that, in consideration of the preparation of nanoparticles, Brij 97/cyclohexane w/o microemulsion

system would be more appropriate as a synthesis medium capable of performing under the high reaction/ripening temperature, especially for the polymerisation.

4.2.4 Non-ionic and ionic surfactants

The different behaviours of non-ionic surfactants and ionic surfactants, are attributed to the mechanism of hydrophilicity. POE non-ionic surfactants show hydrophilic behaviour by introducing the EO unit to compounds. The water molecules are affixed to the EO units through hydrogen bonding. As for the ionic surfactant (e.g. AOT), the surface-active portion of molecule bears a negative/positive charge in water. The mechanism of hydrophilicity involves ion-dipole interactions between the solubilised water and the counter-ions of the surfactant presenting in the interior of the micelle [173].

In w/o microemulsion systems, the maximum amount of water solubilised into the oil phase increases with the increase of surfactant concentration, which is applicable in both ionic and non-ionic systems. AOT w/o microemulsion systems showed much higher water solubilisation than non-ionic systems, particularly at higher temperature, partially due to the different effect of the temperature on the hydrophilicity of ionic and non-ionic surfactants respectively. As we know, the increased temperature leads to the dehydration of EO groups of non-ionic surfactants, which consequently weakens the capability of water solubilisation in corresponding microemulsion systems, i.e. the inverse-temperature maximum water solubilisation in Tween 85/cyclohexane, Igepal CO-520/cyclohexane and Triton X-114/cyclohexane systems was observed. On the contrary, for ionic surfactants an increase in temperature generally results in an increase in the extent of solubilisation for water phase, presumably due to increased thermal agitation increases the space available for solubilisation in micelles [174].

It has been discussed in above that the aqueous phase solubilised may affect the power of solubilisation in systems with ionic surfactants. The different aqueous phases exhibited the different maximum solubilisation values in AOT/isooctane system, which was the same as non-ionic surfactants. Furthermore, there were two considerably higher maximum loadings were observed in solublising the

monomer solution and the de-ionised water in AOT/isooctane w/o microemulsion system, which was different from what was found in the investigation of non-ionic surfactants. The former could be explained by the co-surfactant effect of amphiphilic monomer molecules; the latter indicated the effect of the pH value on the solubilisation of systems, as the pH values of iron salt solution are ammonia solution are 12.0 and 14.0, respectively, while the water is neutral. It should be mentioned that, the extent of water solubilisation into hydrocarbon solvents by POE non-ionic surfactants could also be affected by the pH value of aqueous phases, but not as much as for ionic surfactants.

SUMMARY

The main purpose of the investigation of w/o microemulsion systems is to find out appropriate systems for the synthesis of nanoparticles. The major concern is the extent of solubilisation of aqueous phase. The higher solubilisation of aqueous phase gives the more freedom in changing reaction parameters to produce different products.

At 25°C, since the w/o microemulsion system with **Igepal CO-520**/cyclohexane showed the highest maximum water solubilisation value mainly attributed to the lower HLB value (10.0) of Igepal CO-520 and the shortest length of POE chains in its structure, so it will be used in the synthesis of iron oxide nanoparticles and silica nano-spheres at 25°C. Although the addition of co-surfactant 1-butanol improved the extent of water solubilisation in microemulsion systems, in regard to the possible effect of co-surfactant (alkanols) on the hydrolysis of metal alkoxides and the polymerisation, the synthesis of nanoparticles and nanocomposites would be carried out in the system without co-surfactant.

The heat initiated polymerisation in w/o microemulsions need to endure the temperatures up to 60°C. The system employed in this part should have the better stability at higher temperature accompanied by the relatively higher solubilisation value of water phase. In this point of view, **Brij 97/cyclohexane** system is the better choice. It was thereby selected for use in the synthesis of nanoparticles at higher temperature, the microemulsion polymerisation and the synthesis of polymer/magnets nanocomposites.

5 SYNTHESIS OF NANO-MAGNETS

5.1 PREPARATION OF IRON OXIDE NANOPARTICLES

Iron oxide nanoparticles were synthesised via precipitation method and w/o microemulsion. The studies on different starting materials, different ripening time and temperature, and different post-heat-treatments were presented in this section.

Some characteristic values of standard XRD peak values of magnetite (Fe_3O_4), maghemite (γ-Fe_2O_3) and hematite (α-Fe_2O_3) are given in **Table 5.1-1**. The identification of crystal phases in iron oxide nanoparticles synthesised will base on these reference data. The characteristic values of all samples can be found in **Appendix III**.

Table 5.1-1 Standard XRD peaks for different forms of iron oxide.

Magnetite [Fe_3O_4]		Hematite [α-Fe_2O_3]	
D spacing	Intensity	D spacing	Intensity
2.532	999*	2.700	100
1.484	367	2.519	70
2.969	293	1.694	45
1.616	277	1.840	40
2.099	202	3.684	30

Maghemite [γ-Fe_2O_3]			
D spacing	Intensity	D spacing	Intensity
2.517	100	2.51	100
2.953	35	1.47	40
1.475	34	2.95	30
1.607	24	1.60	20
2.088	16	2.08	15

5.1.1 Preparation by precipitation method

The investigation of reaction parameters including different starting materials, ripening temperature and ripening time were carried out in the synthesis via the precipitation method. Since the reaction in the precipitation method is the same as what occurred in the water pool of microemulsions, it was thought the results from this part of work would give a good indication for the synthesis of iron oxide nanoparticles via w/o microemulsion system.

5.1.1.1 Studies on different molar ratio of $[Fe]^{3+}$ to $[Fe]^{2+}$ in starting materials

Figure 5.1-1 shows the X-ray diffractograms of iron oxides prepared from different starting materials, i.e. iron salt solutions, with different molar ratio of ferric ions to ferrous ions. The reaction with pure ferric ion solution produced an amorphous product [Figure 5.1-1 H] and the similar amorphous pattern

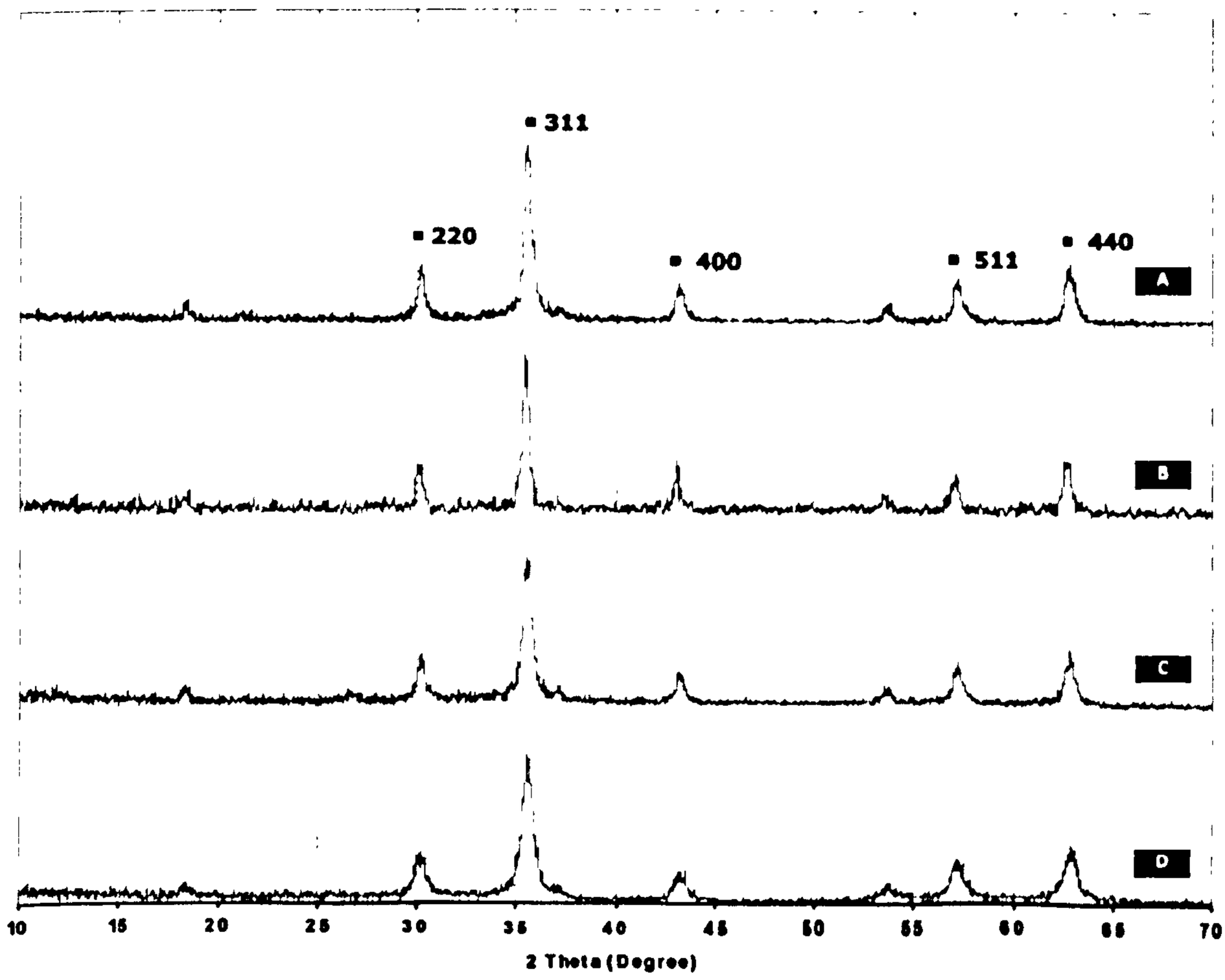

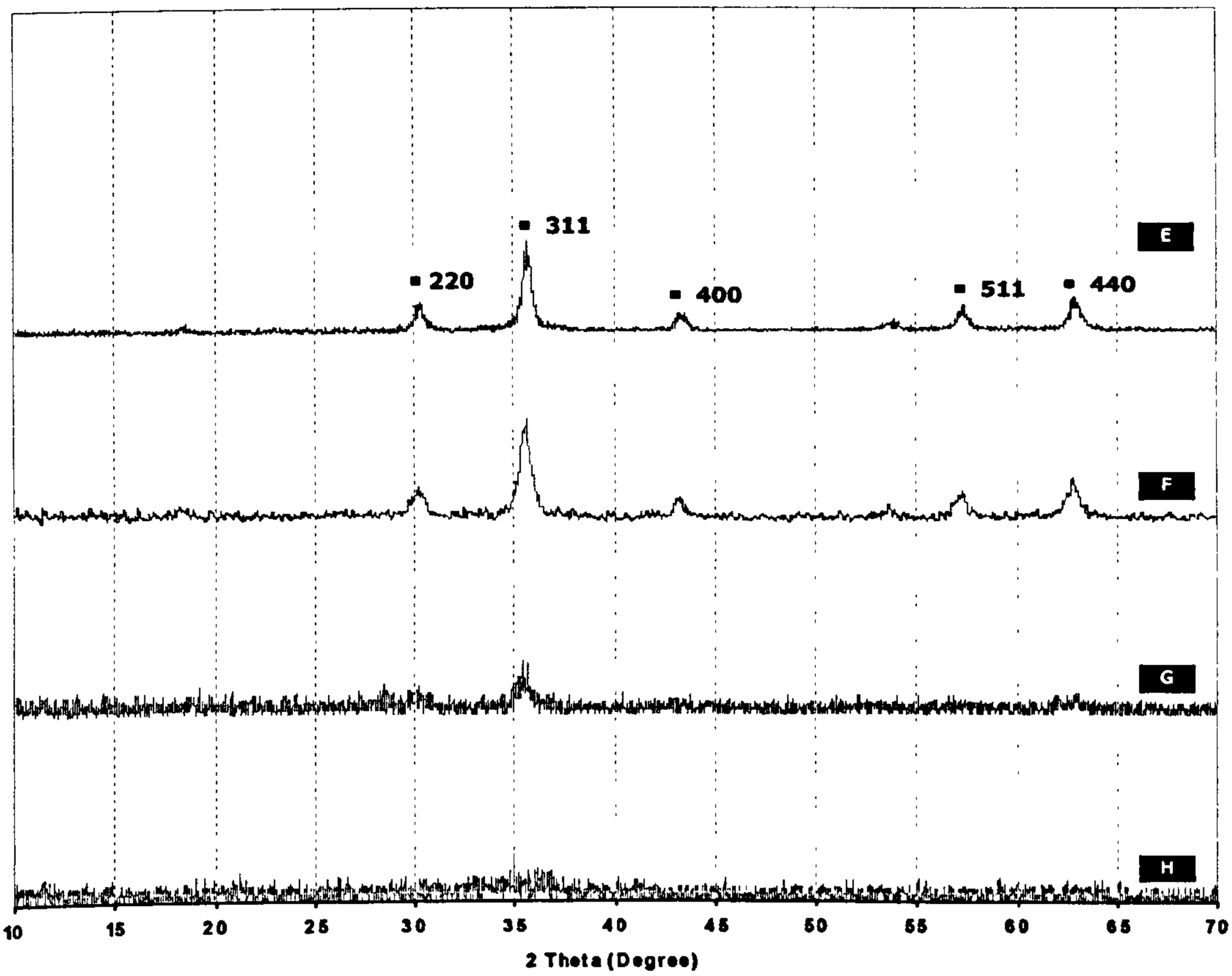

Figure 5.1-1 X-Ray diffractogram of iron oxide samples prepared from different starting materials with different ratio of $[Fe]^{3+}$ to $[Fe]^{2+}$. Temperature was 25°C.

[A]. $[Fe]^{2+}$, [B]. $[Fe]^{3+}$:$[Fe]^{2+}$=1:9, [C]. [Fe]3+:[Fe]2+=1:2, [D]. [Fe]3+:[Fe]2+=1:1,
[E]. $[Fe]^{3+}$:$[Fe]^{2+}$=2:1, [F]. $[Fe]^{3+}$:$[Fe]^{2+}$=3:2, [G]. $[Fe]^{3+}$:$[Fe]^{2+}$=9:1, [H]. $[Fe]^{3+}$

was observed in the sample prepared from the starting material with the molar ratio of 9:1 [**Figure 5.1-1** G]. The characteristic peaks were clearly observed until the content of ferrous ion $[Fe]^{3+}$ reached to 60% (3:2). The intensity of the main characteristic peak (311) increased and became sharper with the increase of the concentration of ferrous ions $[Fe]^{2+}$ in the starting iron salt solution. All the recognised iron oxide samples were identified as magnetite.

5.1.1.2 Studies on ripening temperature

Figure 5.1-2 shows the X-ray diffractograms of the iron oxide samples prepared at different ripening temperatures for 2 hours. It was found that all samples showed similar XRD patterns. However, with

an increase of ripening temperature from 25°C to 90°C, the intensity of the main characteristic peak (311) of samples increased. There was no phase transition observed in samples prepared at different temperatures, varied from 25°C to 90°C for 2 hours. The samples were all identified as magnetite.

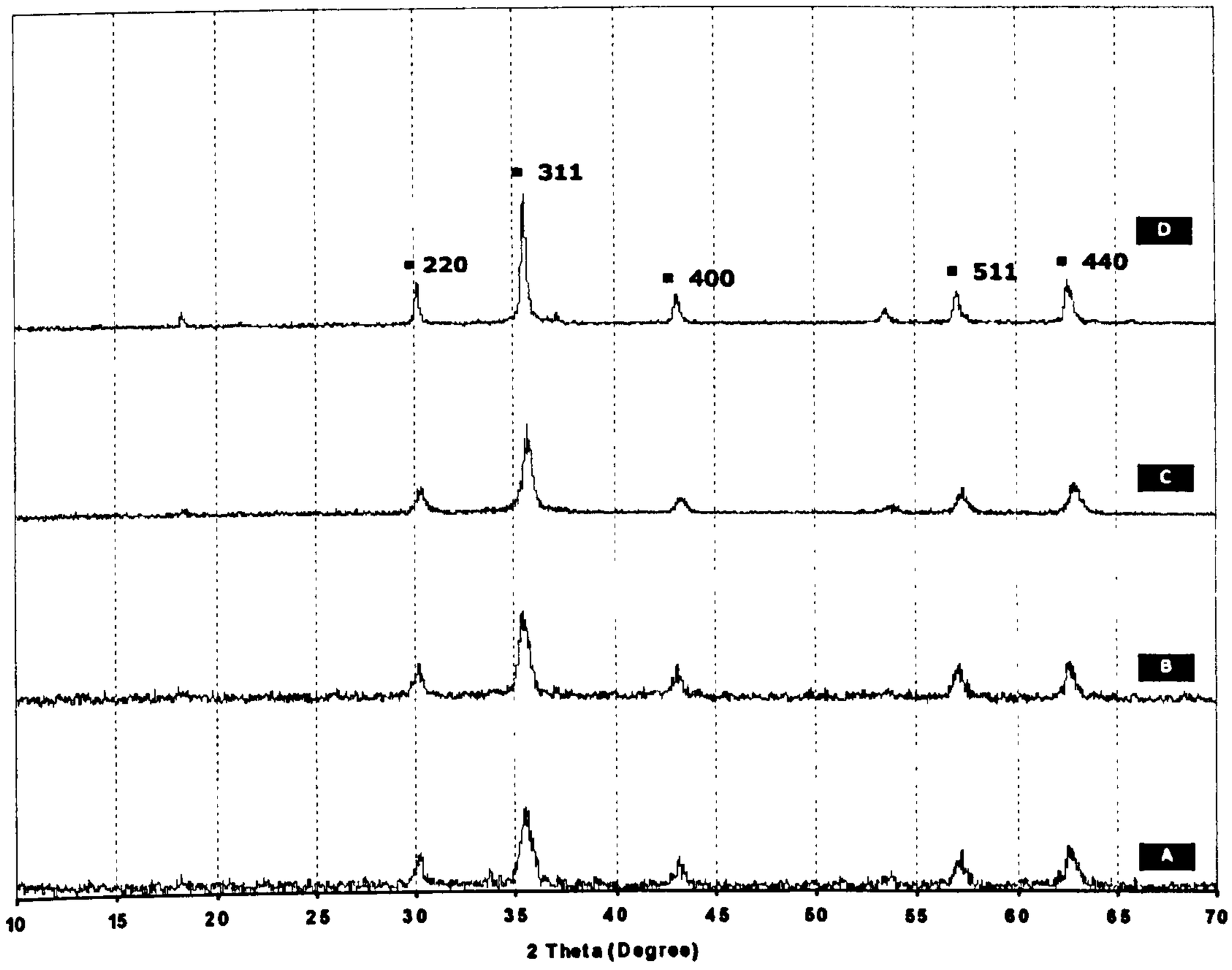

Figure 5.1-2 X-Ray diffractogram of iron oxide samples prepared in different ripening temperatures for 2 hours.

[A]. 25°C, [B]. 40°C, [C]. 60°C, [D]. 90°C

TEM micrographs of iron oxide nanoparticles prepared by precipitation at different temperatures (i.e. 25°C and 90°C), and their diffraction patterns are shown in **Figure 5.1-3**. The size of nanoparticles in different samples was all about 20 nm. The increase of the ripening temperature from 25°C to 90°C did not result in the significant difference of size and shape of iron oxide nanoparticles produced.

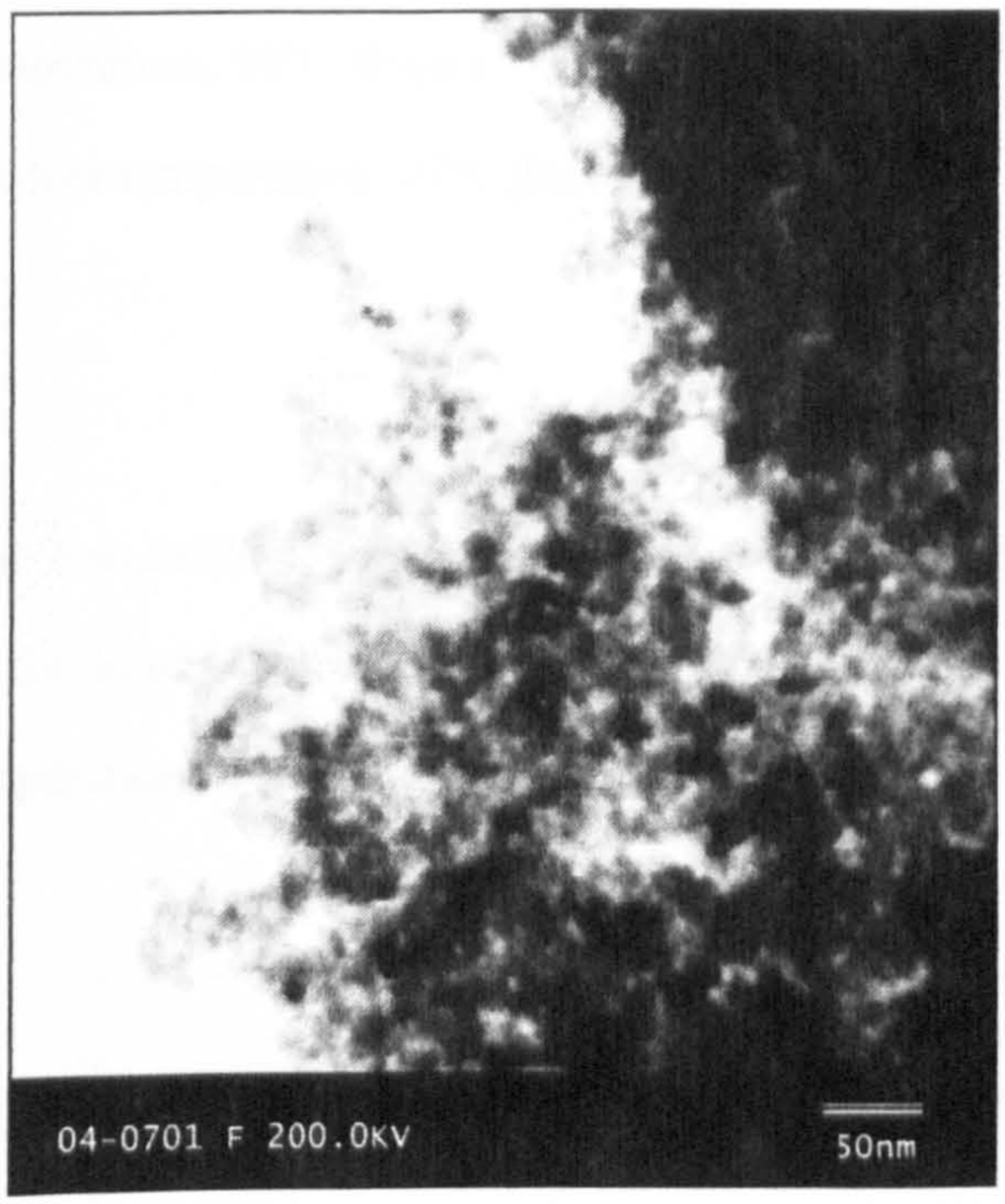

[A]. 25°C

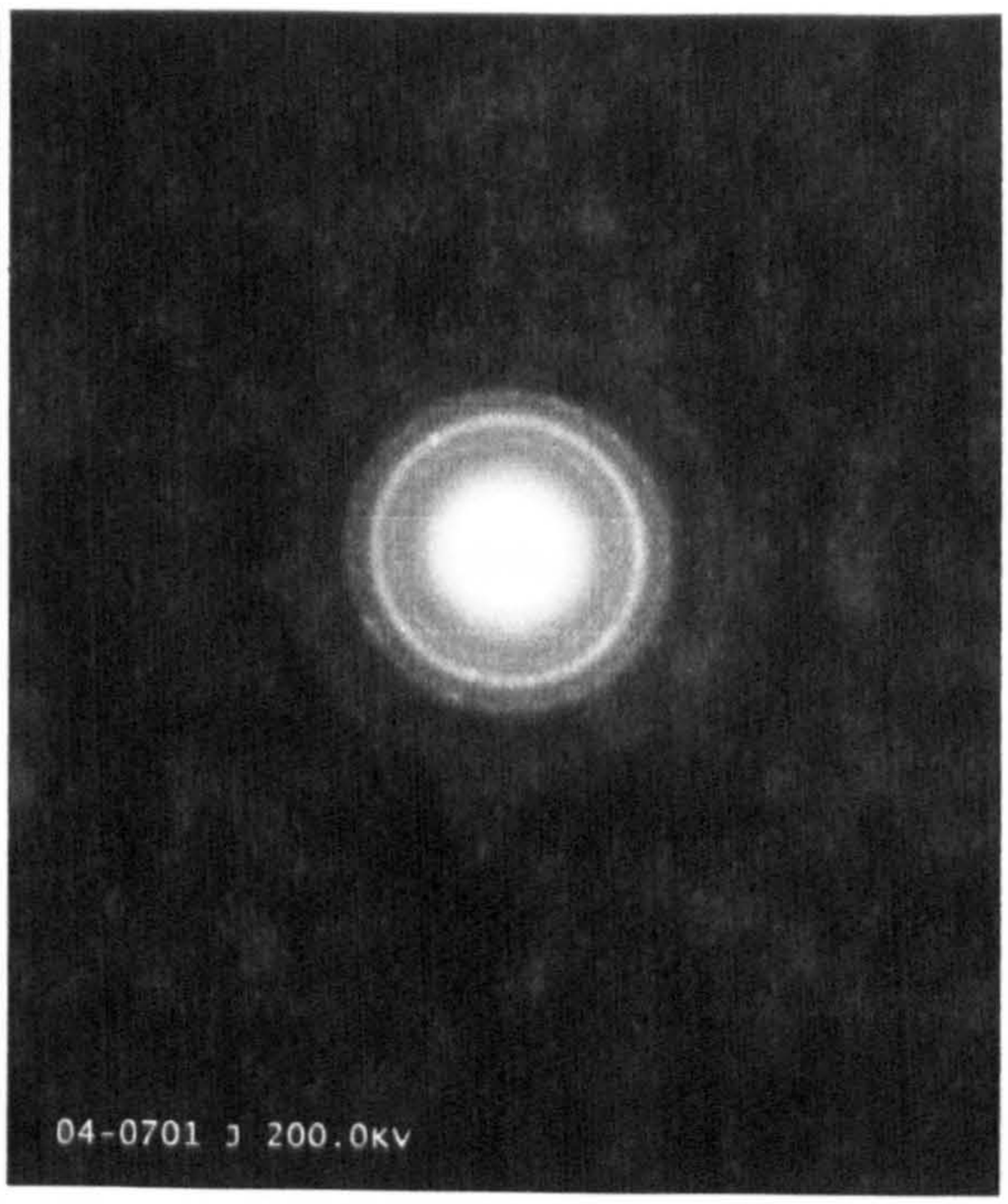

[A.DF]

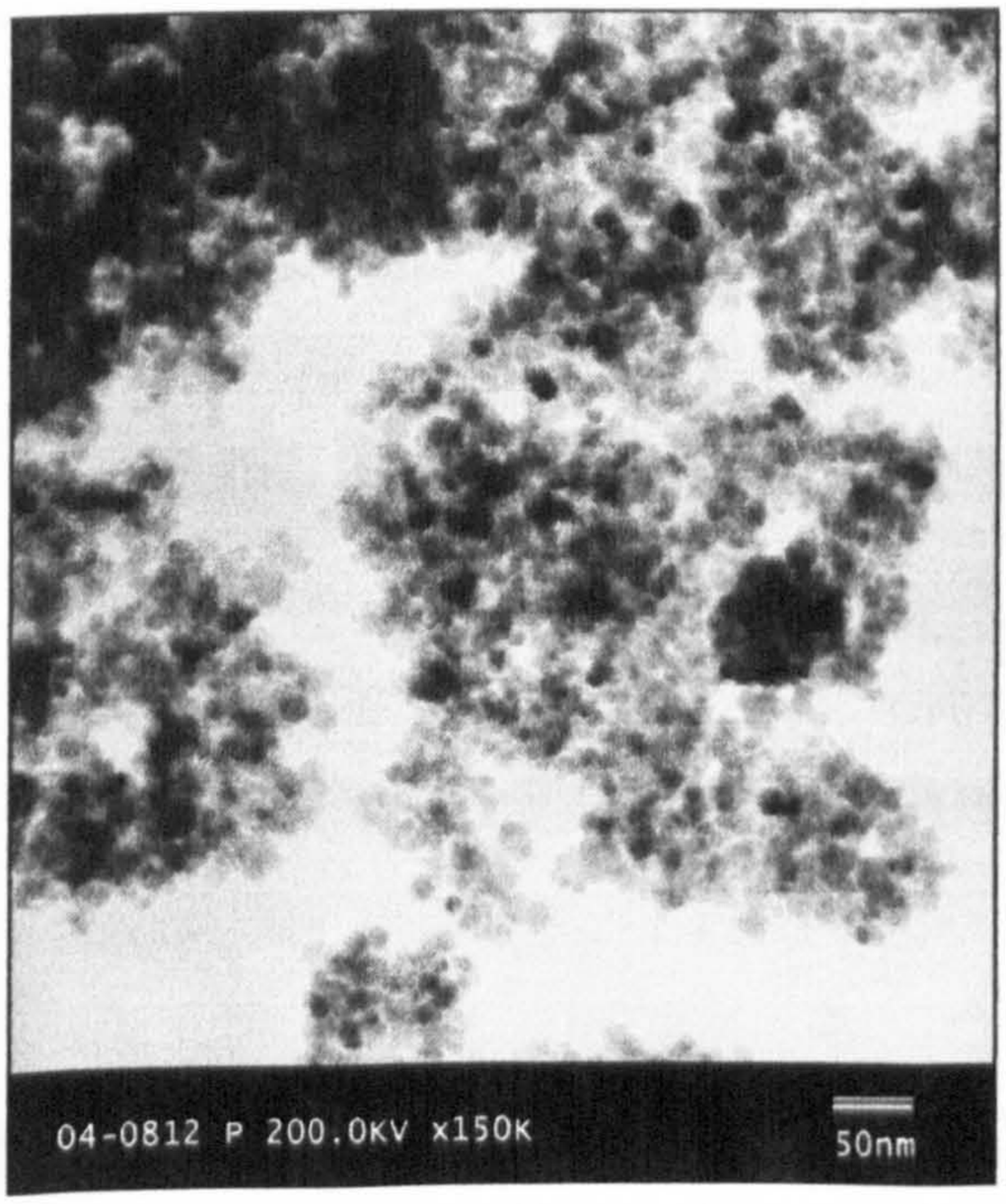

[B]. 90°C

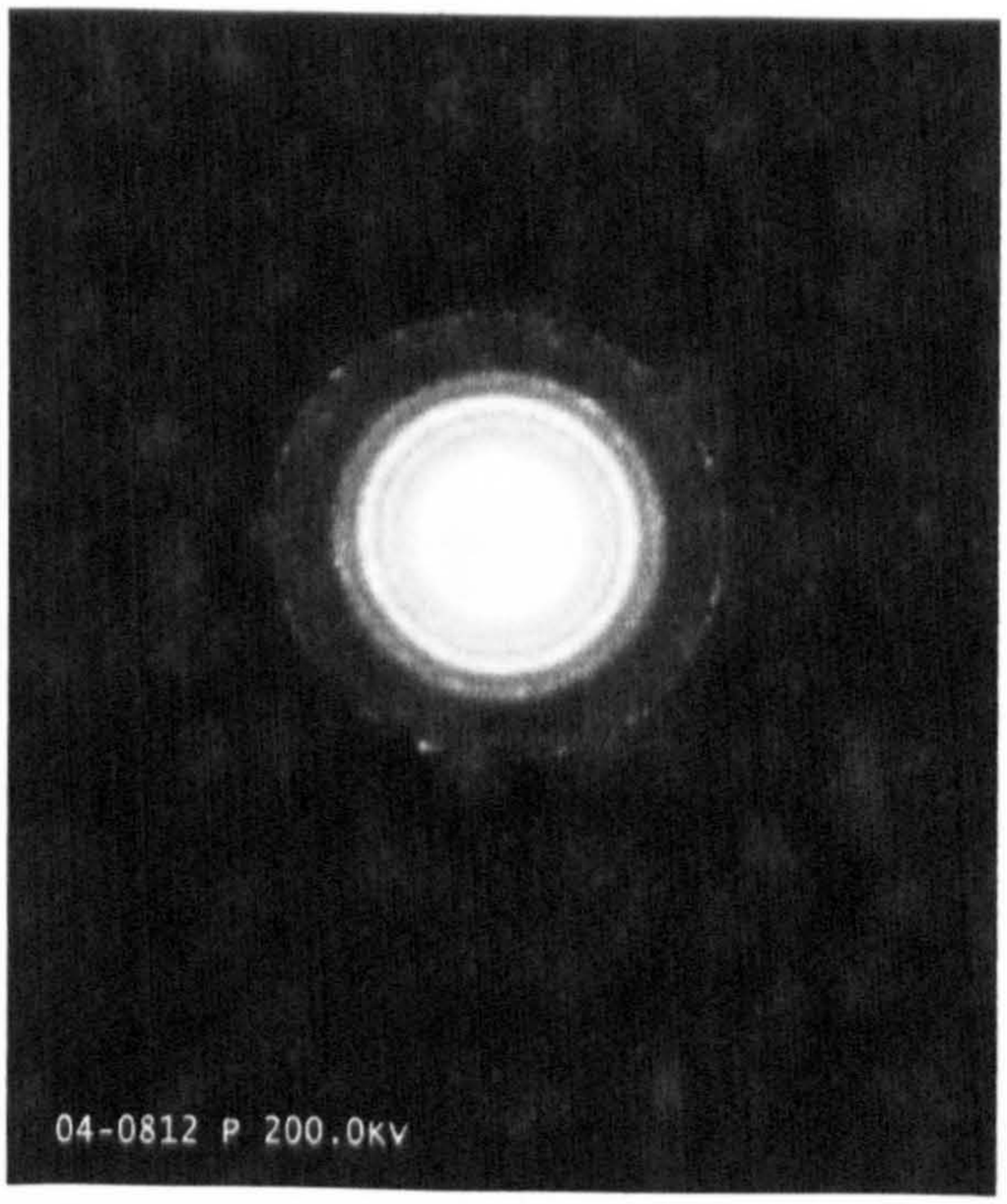

[B.DF]

Figure 5.1-3 TEM micrographs of iron oxide nanoparticles and their diffraction patterns prepared via precipitation method at different temperatures.

However, the crystallinity observed from the diffraction pattern of iron oxide prepared at the high temperature, 90°C **[Figure 5.1-3 B.DF]** seemed stronger than the crystallinity of the sample prepared at the low temperature, 25°C **[Figure 5.1-2 A.DF]**.

5.1.1.3 Studies on ripening time

The iron oxide nanoparticles were prepared for different ripening times varied from 2 hours, 12 hours to 24 hours, with three different ripening temperatures, 25°C, 60°C and 90°C, to carry out the preparation of samples.

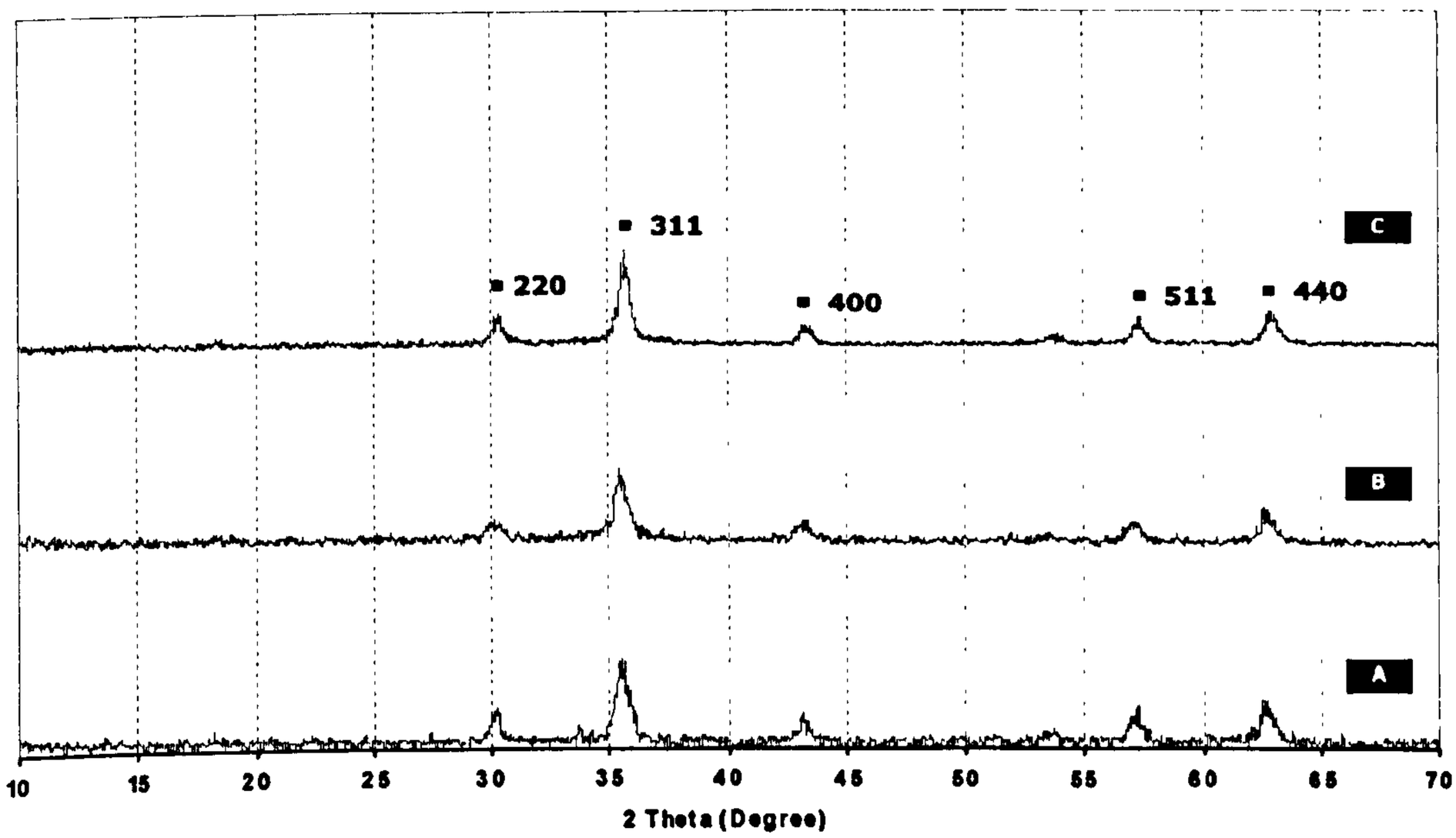

Figure 5.1-4 X-Ray diffractogram of iron oxide samples prepared in different ripening times at 25°C.

[A]. 2 hours, [B]. 12 hours, [C]. 24 hours

Figure 5.1-4 shows the X-ray diffractogram of iron oxide samples prepared at 25°C with different ripening times. The iron oxide samples were all identified as magnetite. There was no phase transition observed with the increased ripening time. However, the slightly increased intensity of main characteristic peak (311) observed in X-ray diffractograms indicated the increase of crystallinity of iron oxide nanoparticles prepared with the increase of the ripening time.

The X-ray diffractograms of the iron oxide synthesised at 60°C, shown in **Figure 5.1-5**, also show an increase of the intensity of main characteristic peak **(311)** with the increase of ripening time. The iron oxide samples were identified as magnetite after being ripened at 60°C for 2 hours and 12 hours respectively. There was a phase transition from magnetite to maghemite observed when the ripening time was 24 hours.

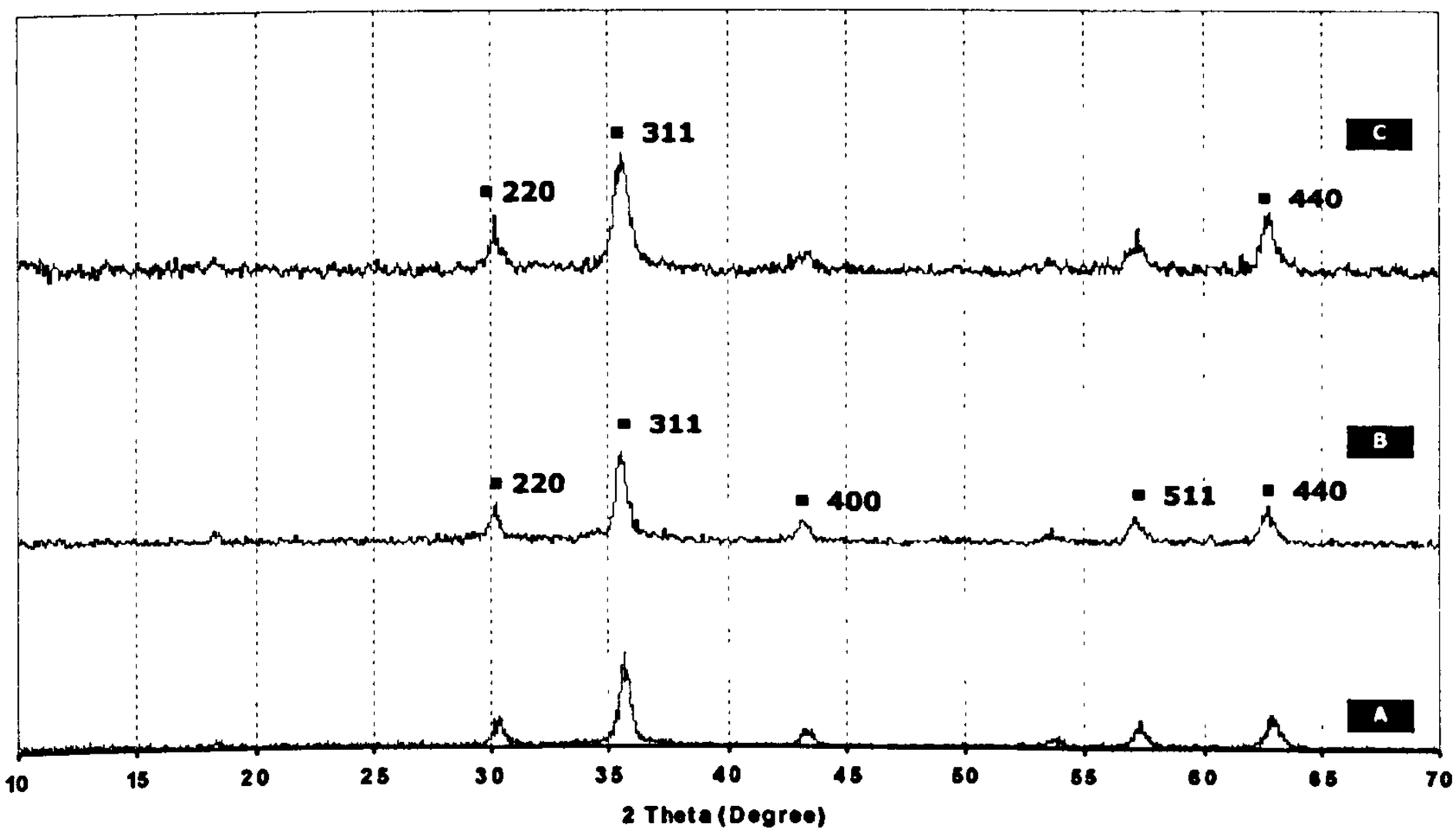

Figure 5.1-5 X-Ray diffractogram of iron oxide samples prepared in different ripening times at 60°C

[A]. 2 hours, [B]. 12 hours, [C]. 24 hours

As mentioned above, magnetite iron oxide nanoparticles were synthesised by the precipitation method at 90°C with 2-hour ripening. When the ripening time was increased to 12 hours, magnetite transformed into maghemite. There was no further phase transition observed, when the time was progressively increased to 24 hours. Additionally, the increase of the intensity of the main characteristic peak **(311)** of the samples was also observed with the increase of ripening time **[Figure 5.1-6]**.

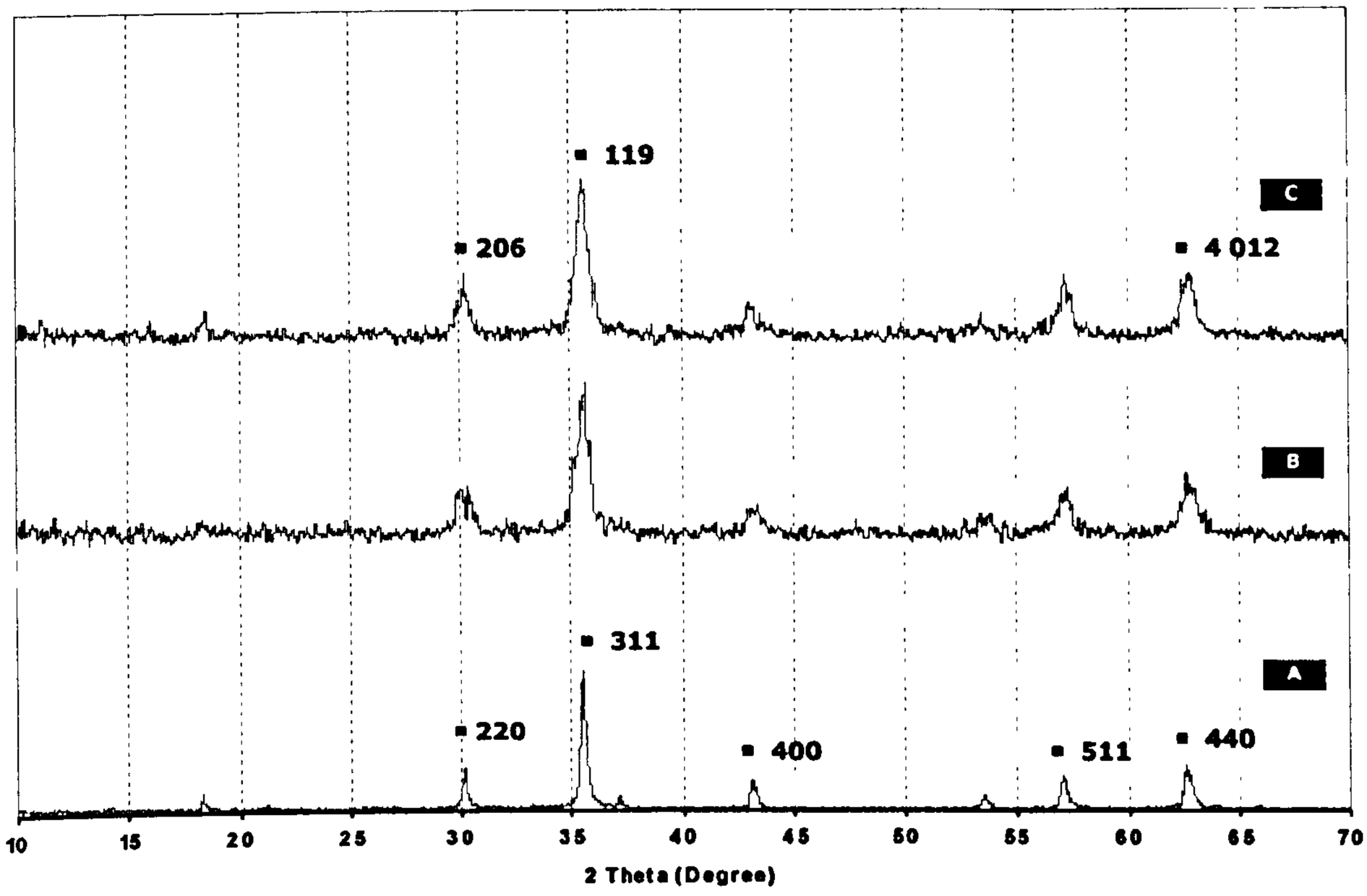

Figure 5.1-6 X-Ray diffractogram of iron oxide samples prepared in different ripening times at 90°C
[A]. 24 hours, [B]. 12 hours, [C]. 2 hours

To summarise, magnetite nanoparticles were prepared by the precipitation method at 25°C, when the ripening time ranged from 2 hours to 24 hours. A phase transition from magnetite to maghemite took place when the iron oxide was prepared at 60°C, with the ripening time up to 24 hours. With the synthesis of iron oxide nanoparticles by precipitation at 90°C, such transition appeared after 12-hour ripening.

5.1.2 Preparation by w/o microemulsion

Igepal CO-520/cyclohexane was selected as the w/o microemulsion system to prepare iron oxide nanoparticles at room temperature (~25°C). Brij 97/cyclohexane was selected to form another w/o microemulsion system to synthesis iron oxide nanoparticles at 60°C. The latter was mainly employed for the microemulsion polymerisation and the synthesis of the iron oxide/polymer nanocomposites.

5.1.2.1 Phase diagrams of two employed W/O microemulsion systems

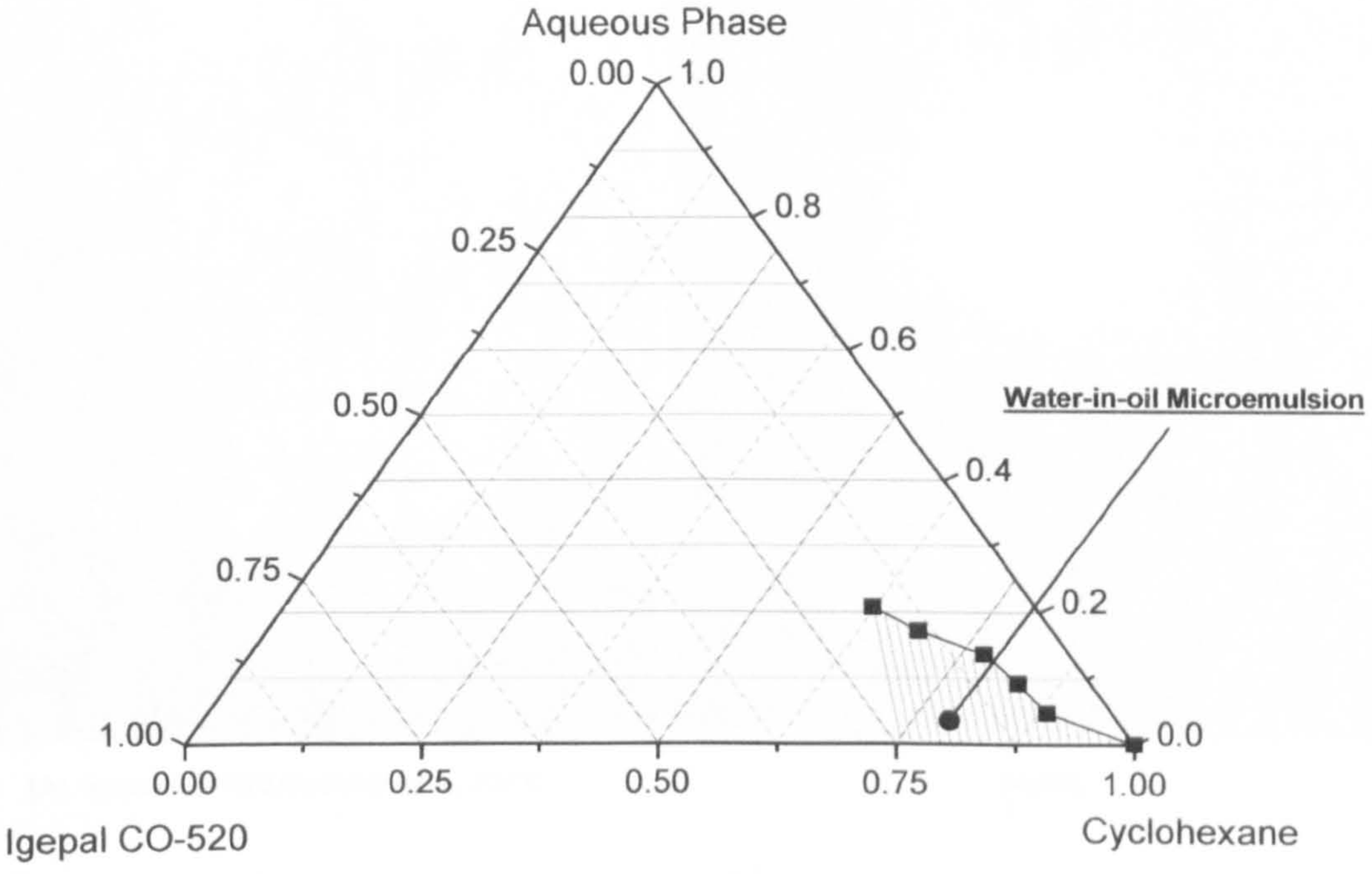

Figure 5.1-7 Phase diagram of w/o microemulsion system: Igepal CO-520/cyclohexane/aqueous phase at 25°C.

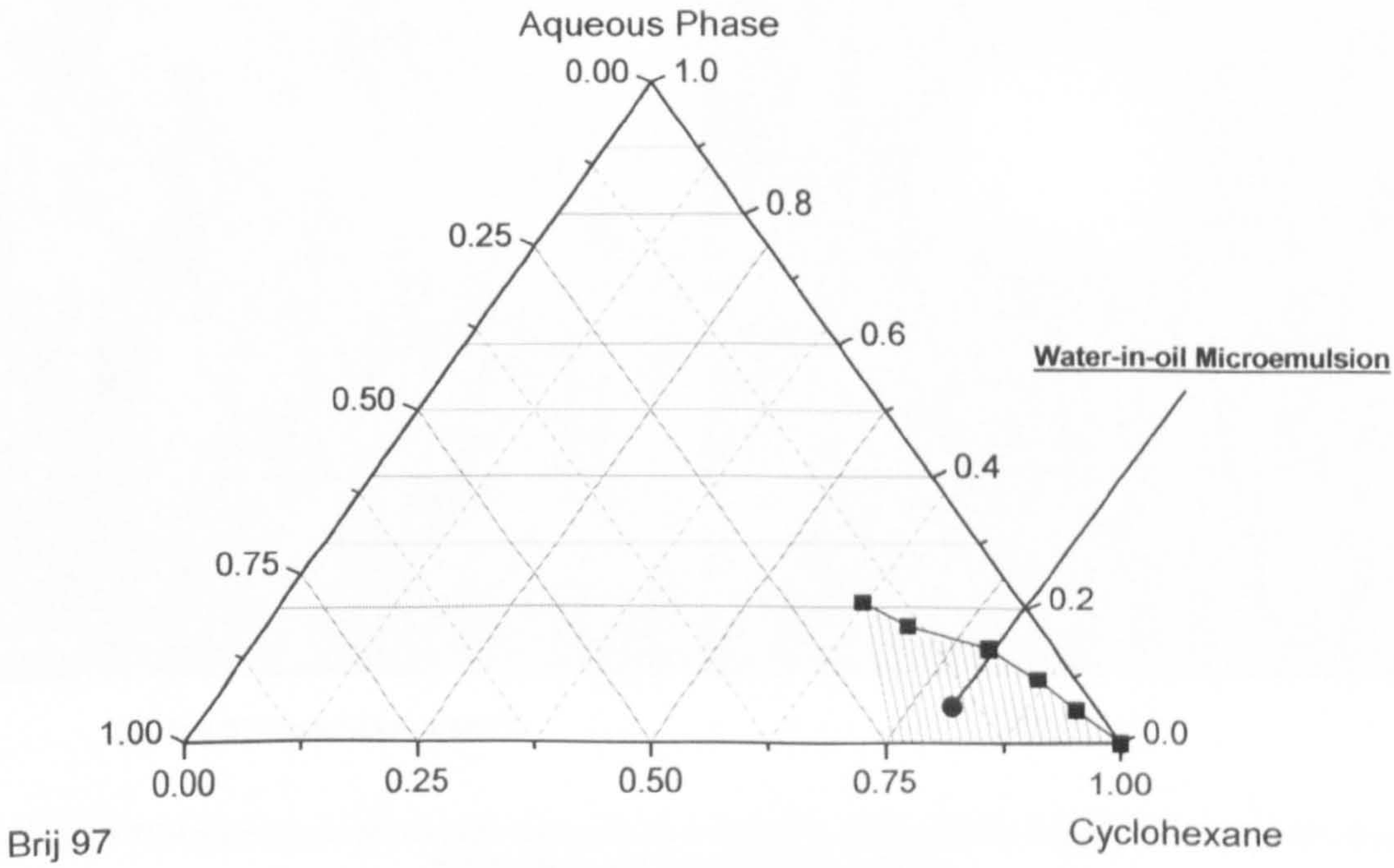

Figure 5.1-8 Phase diagram of w/o microemulsion system: Brij 97/cyclohexane/aqueous phase at 60°C.

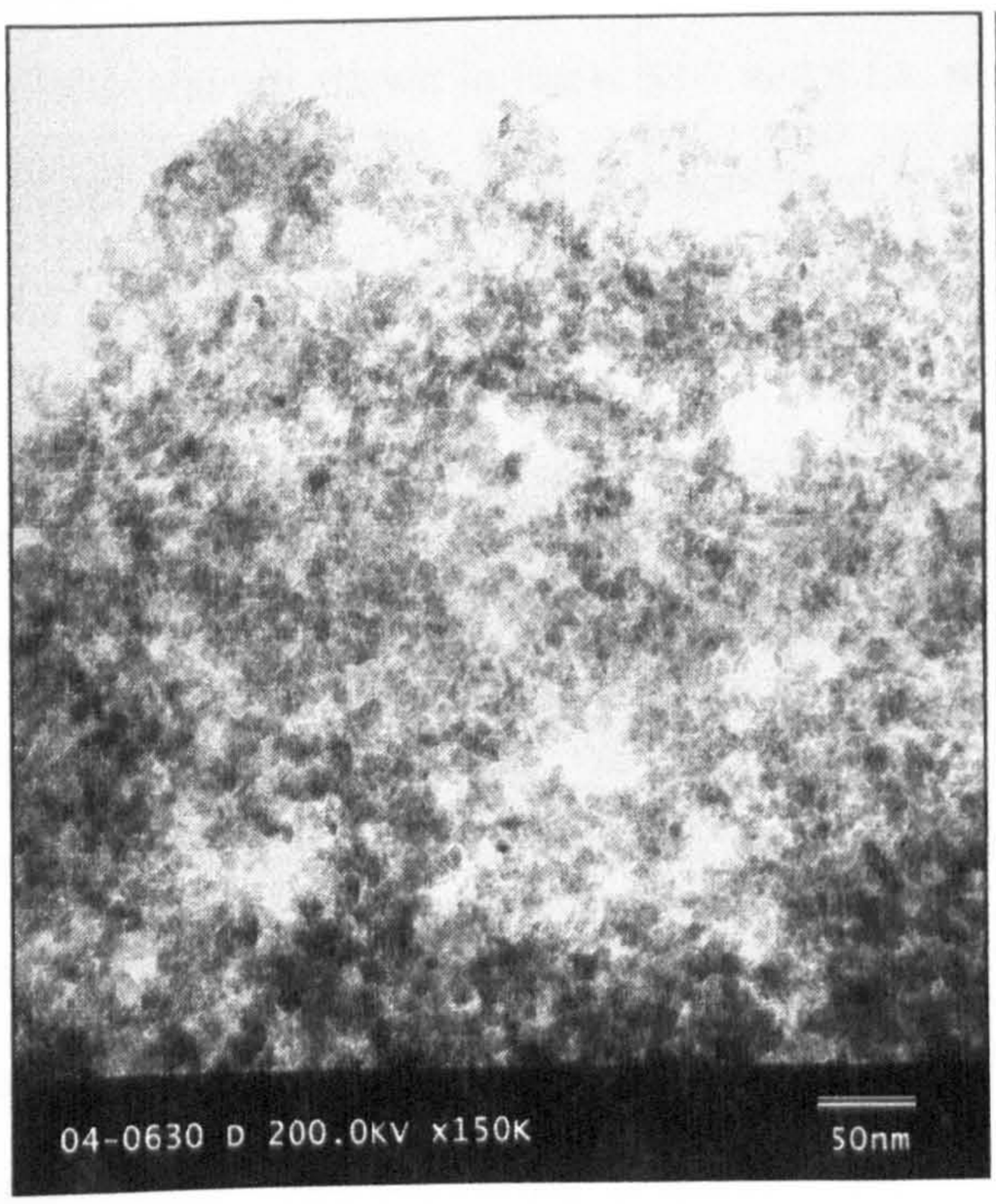

[A]. Igepal CO-520/cyclohexane, 25°C

[A.DF]

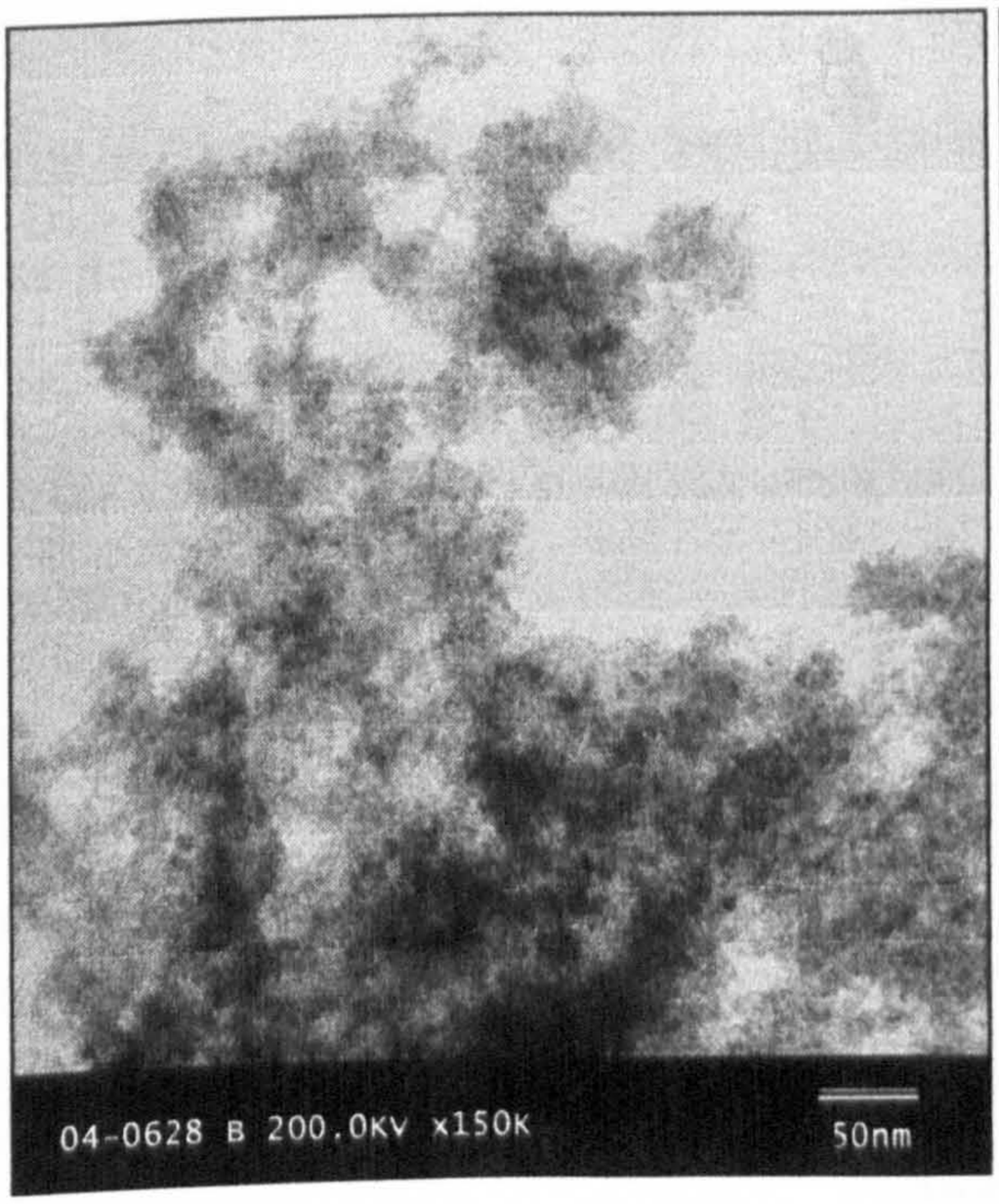

[B]. Brij 97/cyclohexane, 60°C

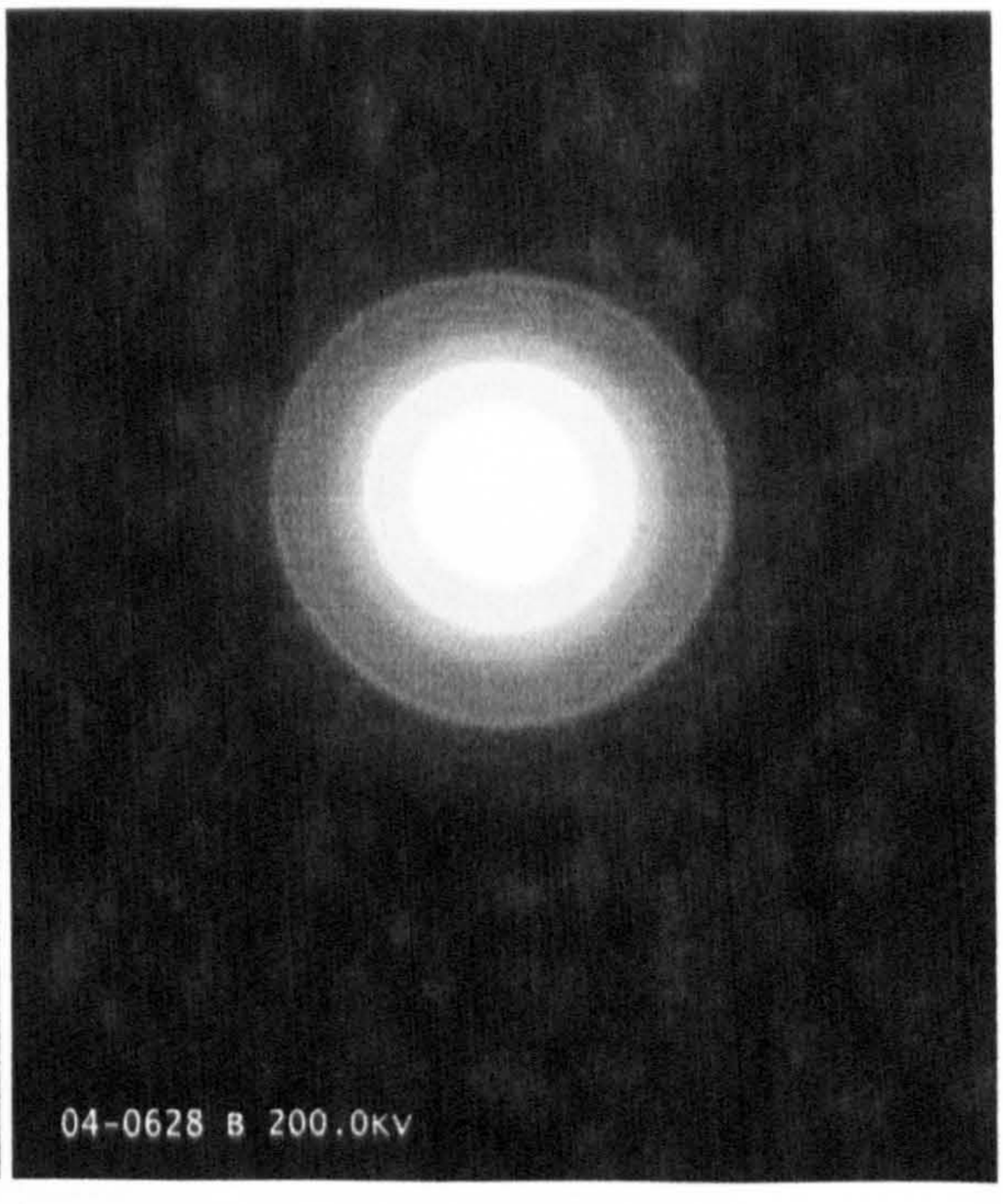

[B.DF]

Figure 5.1-9 TEM micrographs of iron oxide nanoparticles prepared via different w/o microemulsion system at different temperatures and their diffraction patterns.

The phase diagrams of w/o microemulsion systems: Igepal CO-520/cyclhexane and Brij 97 /cyclohexane are shown in **Figure 5.1-7** and **5.1-8**, respectively. The ratchet area marks the ratio of each component in the microemulsion systems and no microemulsion was formed with the component ratio at the points beyond this area.

Figure 5.1-9 shows the TEM micrographs of iron oxide nanoparticles prepared at different temperatures via the above two w/o microemulsion systems. The synthesis of iron oxide in Igepal CO-520/cyclohexane system was carried out at 25°C, while the Brij 97/cyclohexane system was carried out at 60°C. The size of iron oxide nanoparticles produced was around 5 nm. The iron oxide nanoparticles prepared from microemulsion had the smaller dimension and narrower size-distribution than the sample prepared by precipitation. Moreover, the latter were more aggregated. The diffraction patterns shows that the sample prepared at 60°C **[Figure 5.1-9 B.DF]**, exhibited better crystallinity than the sample prepared at 25°C **[Figure 5.1-9 A.DF]**. The X-Ray diffractograms of iron oxide nanoparticles prepared via Igepal CO-520/cyclohexane at 25°C and Brij 97/cyclohexane at 60°C respectively are shown in **Figure 5.1-10**. The main characteristic peak **(311)** was still observed from both samples.

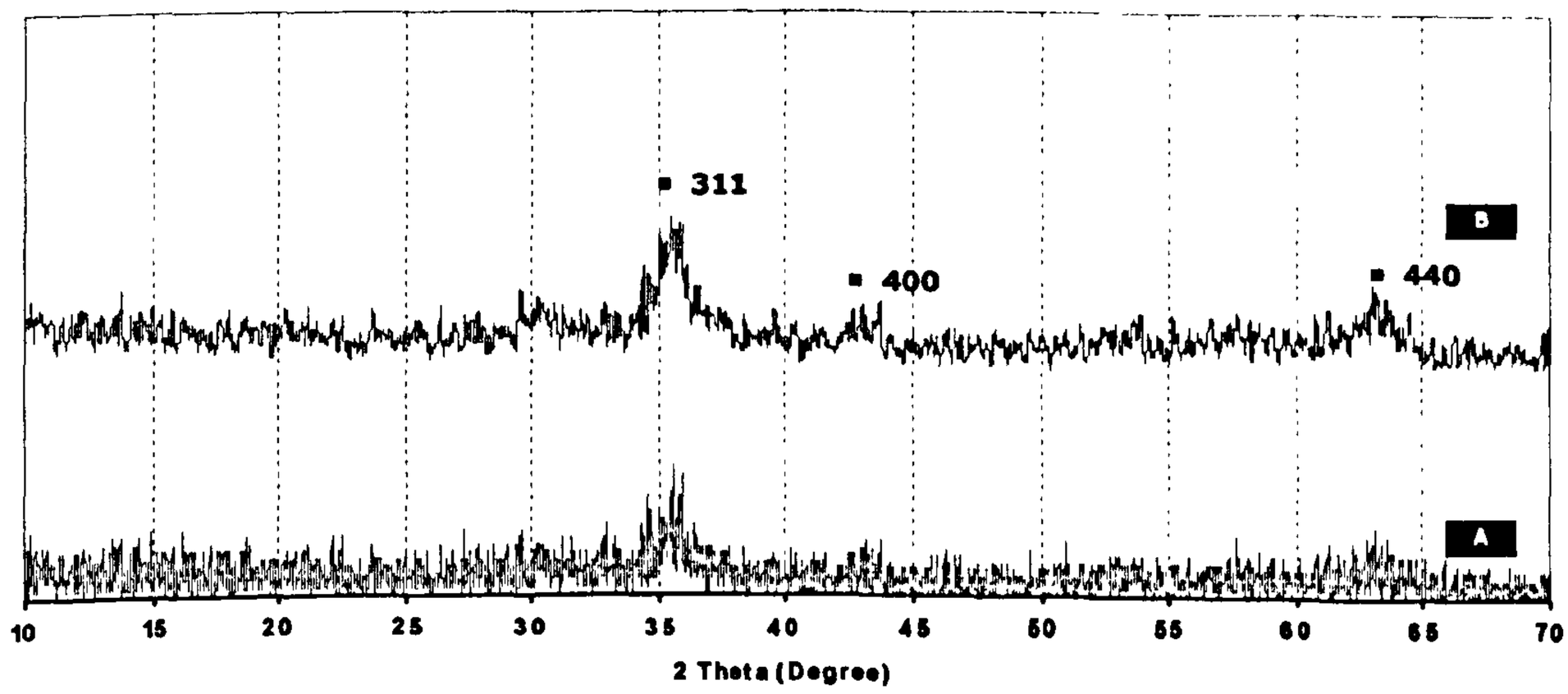

Figure 5.1-10 X-Ray diffractogram of iron oxide samples prepared via different w/o microemulsion system at different temperatures. **[A]**. Igepal CO-520/Cyclohexane, 25°C, **[B]**. Brij 97/Cyclohexane, 60°C.

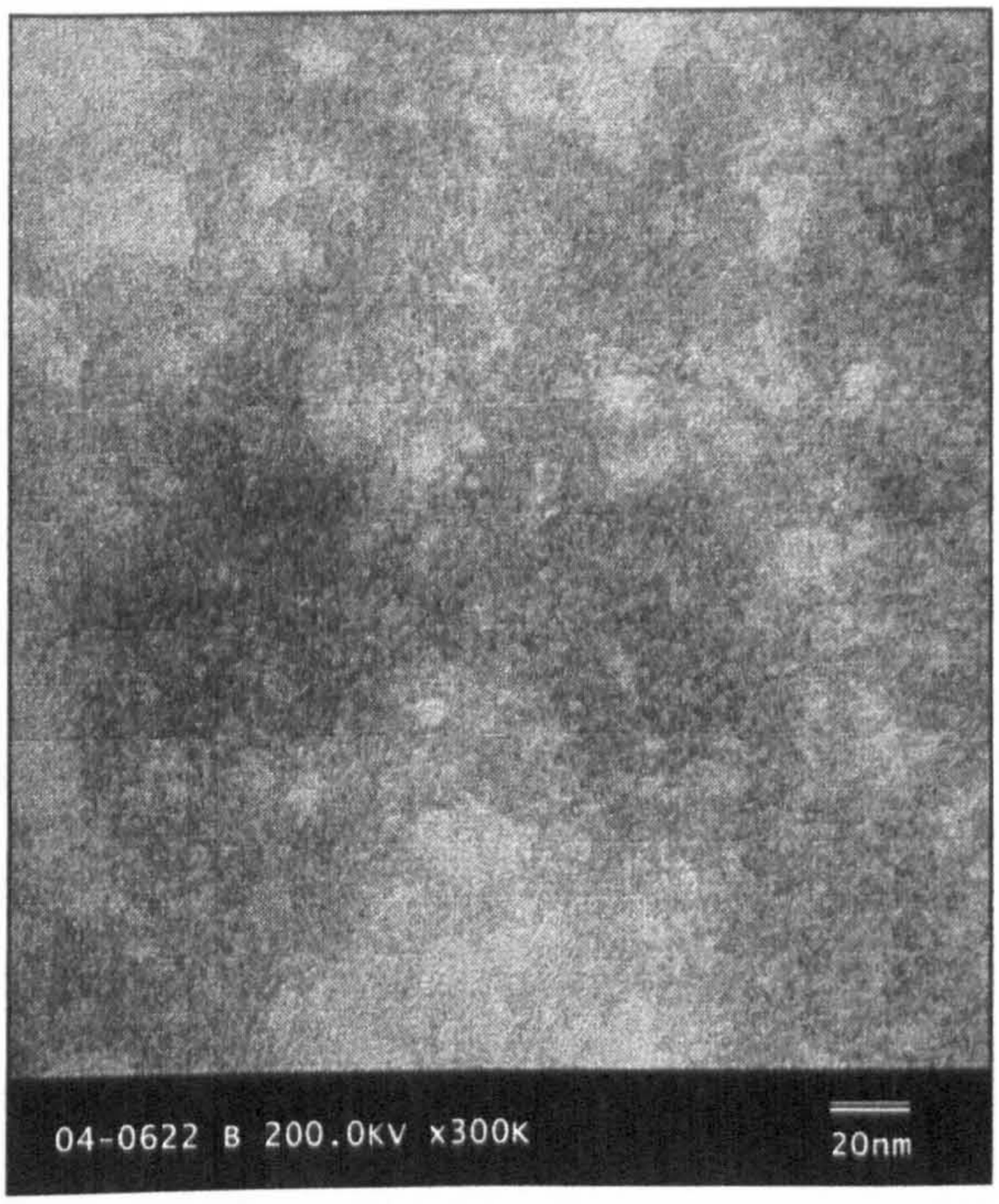

[A]. 1%

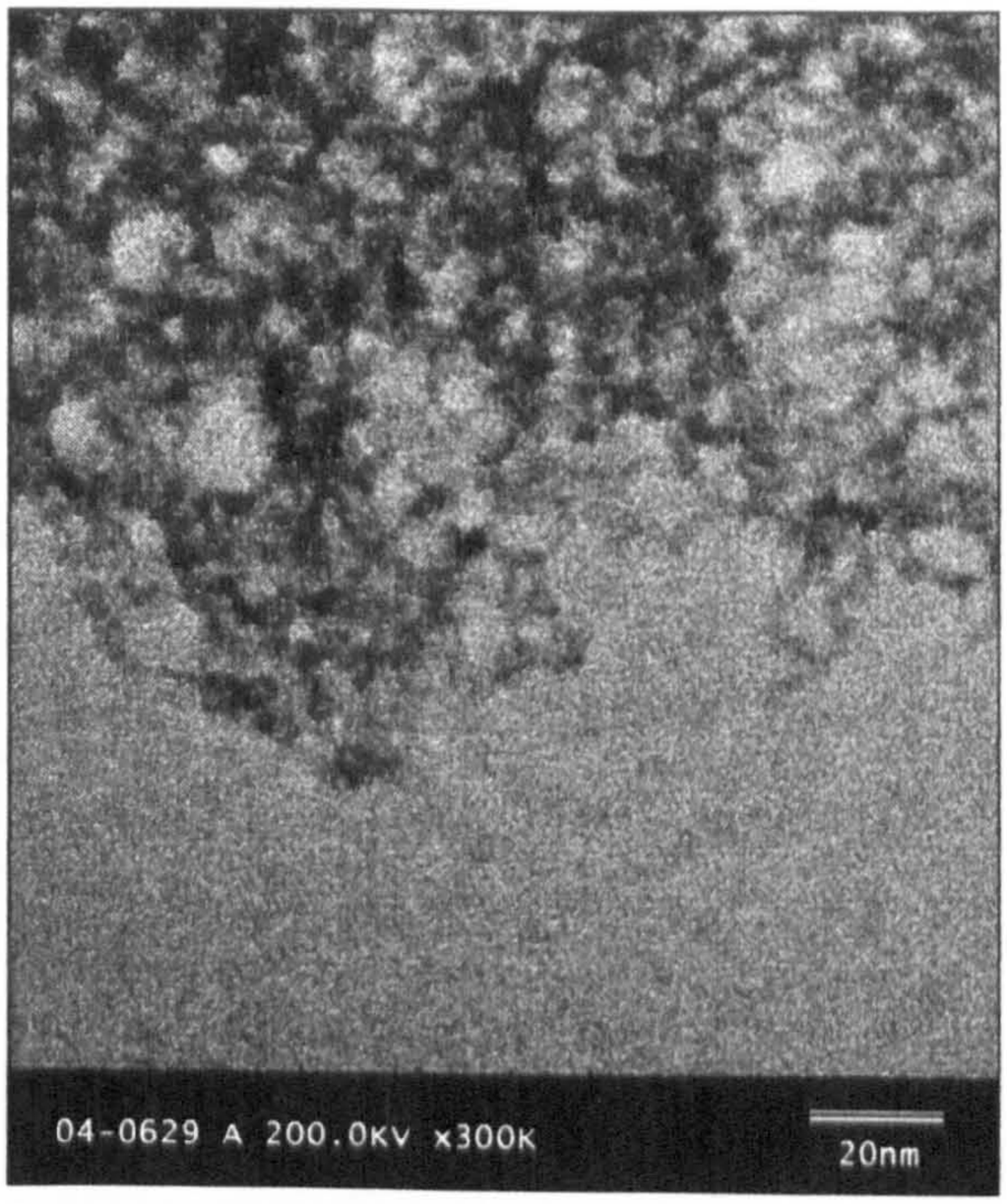

[B]. 2%

[C]. 8%

[D]. 10%

Figure 5.1-11 TEM Micrographs of iron oxide nanoparticles prepared via different w/o microemulsion system with different loading of aqueous phase.

5.1.2.2 Studies on different loading of aqueous phase

Iron oxide nanoparticles were synthesised in the w/o microemulsion system (Igepal CO-520/cyclohexane) with different loading of aqueous phase. The loading amount was varied from 1%, 2%, 6%, 8% to 10%. The TEM micrograph of 6% sample has been shown in **Figure 5.1-9 A** and others are shown in **Figure 5.1-11**. Comparing the micrographs, it was found that the iron oxide nanoparticles produced with 10% and 8% were bigger than samples prepared with 2% and 1%. As shown above, the size of nanoparticles with 6% was around 5 nm. The size of particles with 10% **[Figure 5.1-11 D]** and 8% **[Figure 5.1-11 C]** looked bigger than that and the size of 2% iron oxide particles in **Figure 5.1-11 B** was less than 5 nm, especially the particles shown in **Figure 5.1-11 A**, obviously about 1 nm.

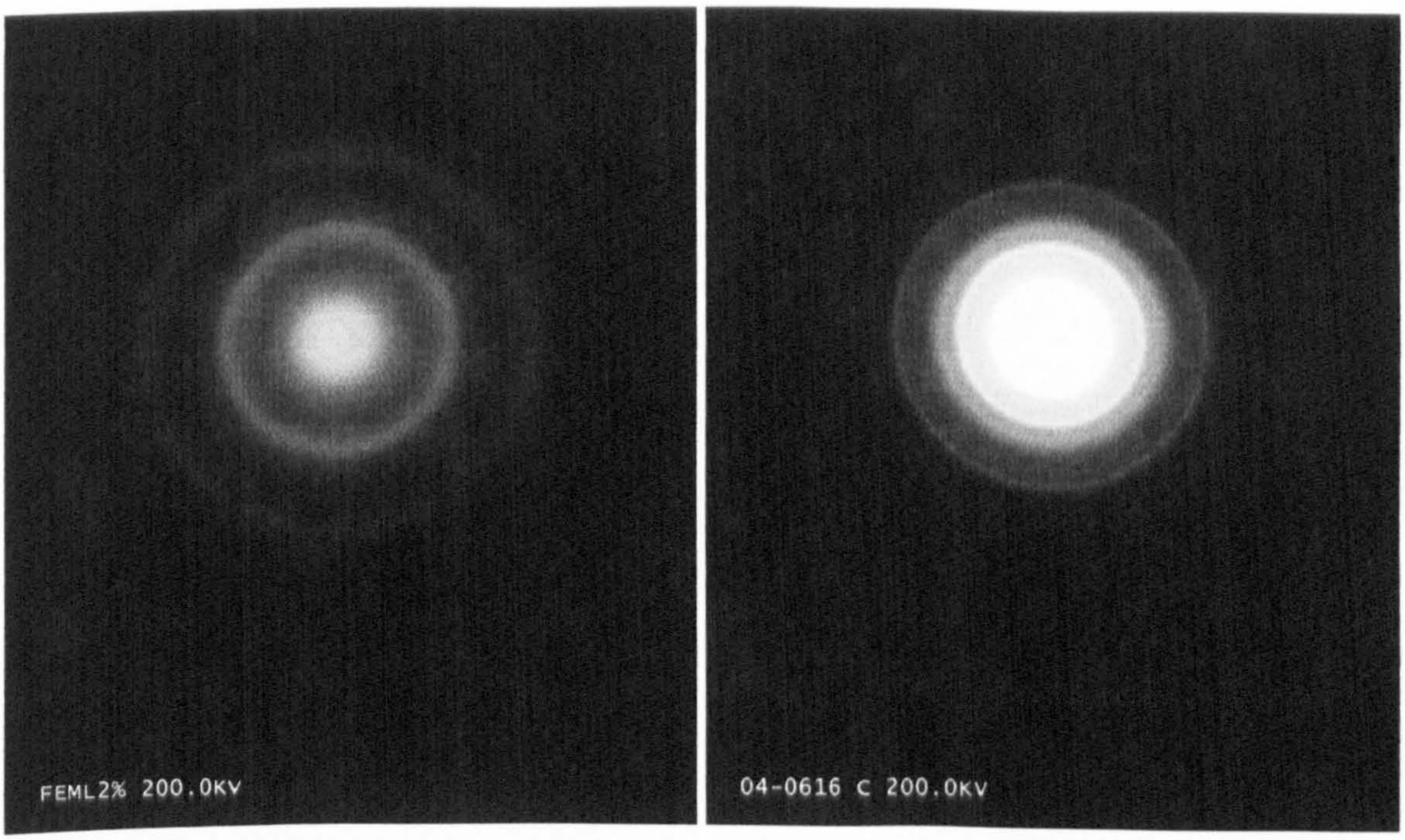

[A.DF]. 2% **[B.DF]. 10%**

Figure 5.1-12 TEM Micrographs of diffraction patterns of iron oxide nanoparticles prepared via different w/o microemulsion system with different loading of aqueous phase.

Hence, the size of iron oxide nanoparticles slightly increased with the increase of aqueous phase loading of the Igepal CO-520/cyclhexane microemulsion system. The micrographs of diffraction patterns of iron oxide samples prepared with different loading are shown in **Figure 5.1-12**. The

crystallinity of 10% sample looked better than 2%, which indicated the loading of aqueous phase in microemulsion could also affect the crystallinity of iron oxide nanoparticles prepared.

5.1.3 Studies on post-heat treatment

In order to investigate the crystallinity of the iron oxide nanoparticles, the samples prepared in experiments were heat-treated by either hydrothermal process or calcinations.

5.1.3.1 Hydrothermal process

- **Studies on different aging temperature**

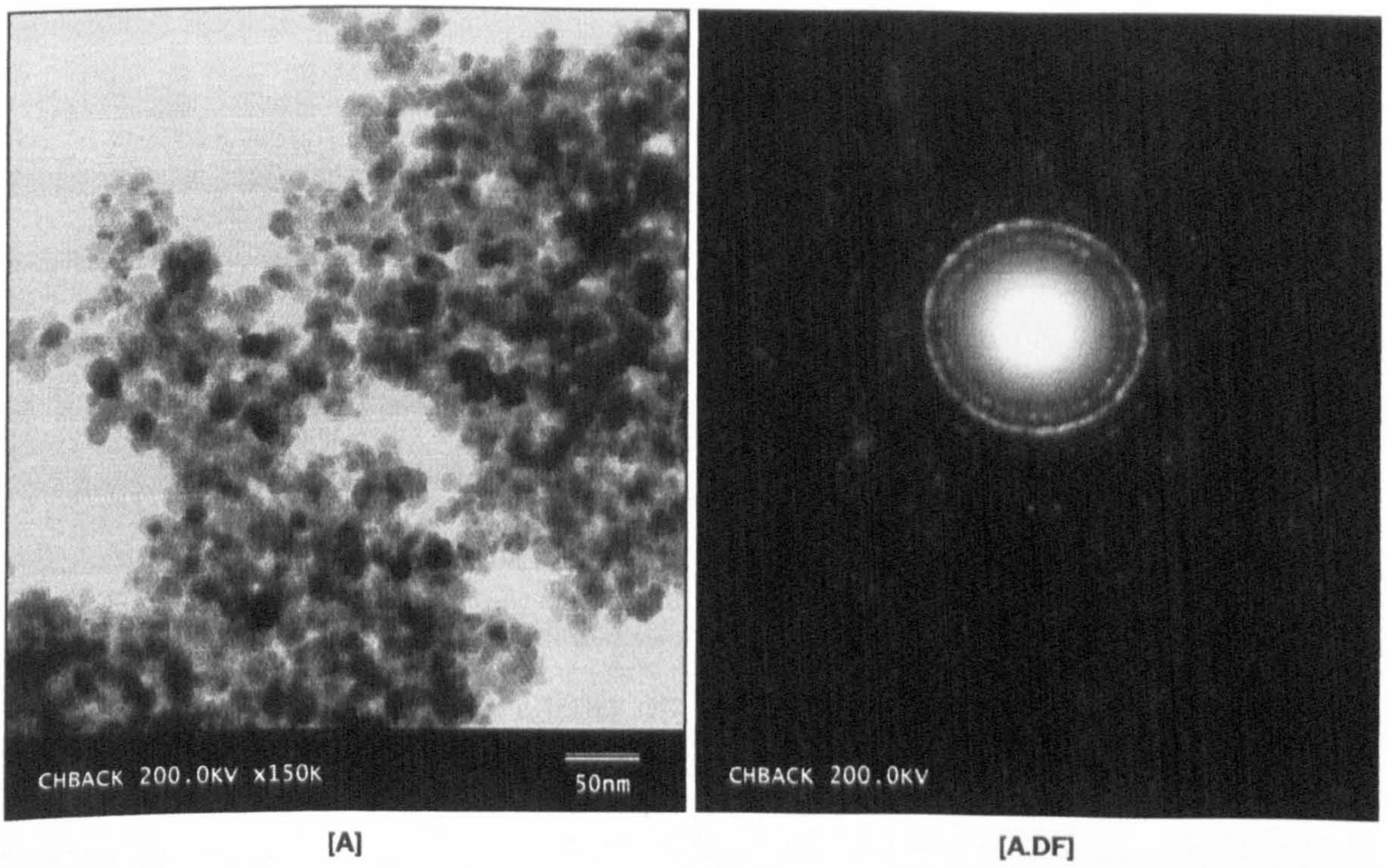

Figure 5.1-13 TEM micrographs of diffraction pattern of iron oxide nanoparticles prepared by precipitation at 25°C.

The investigation of different aging temperatures in hydrothermal process was carried out for the iron oxide nanoparticles prepared by precipitation. The initial particle size before the hydrothermal

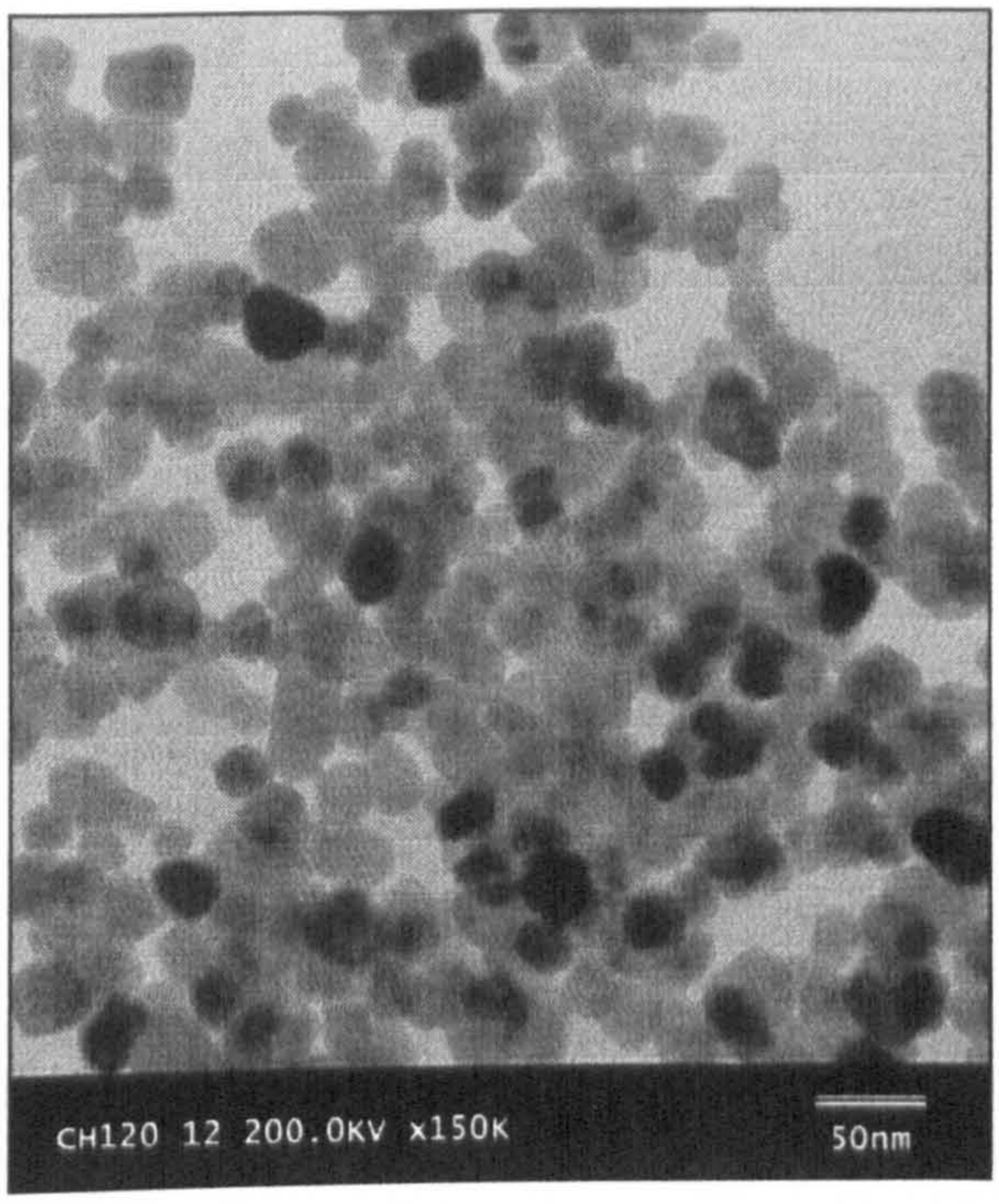

[A]. 120°C

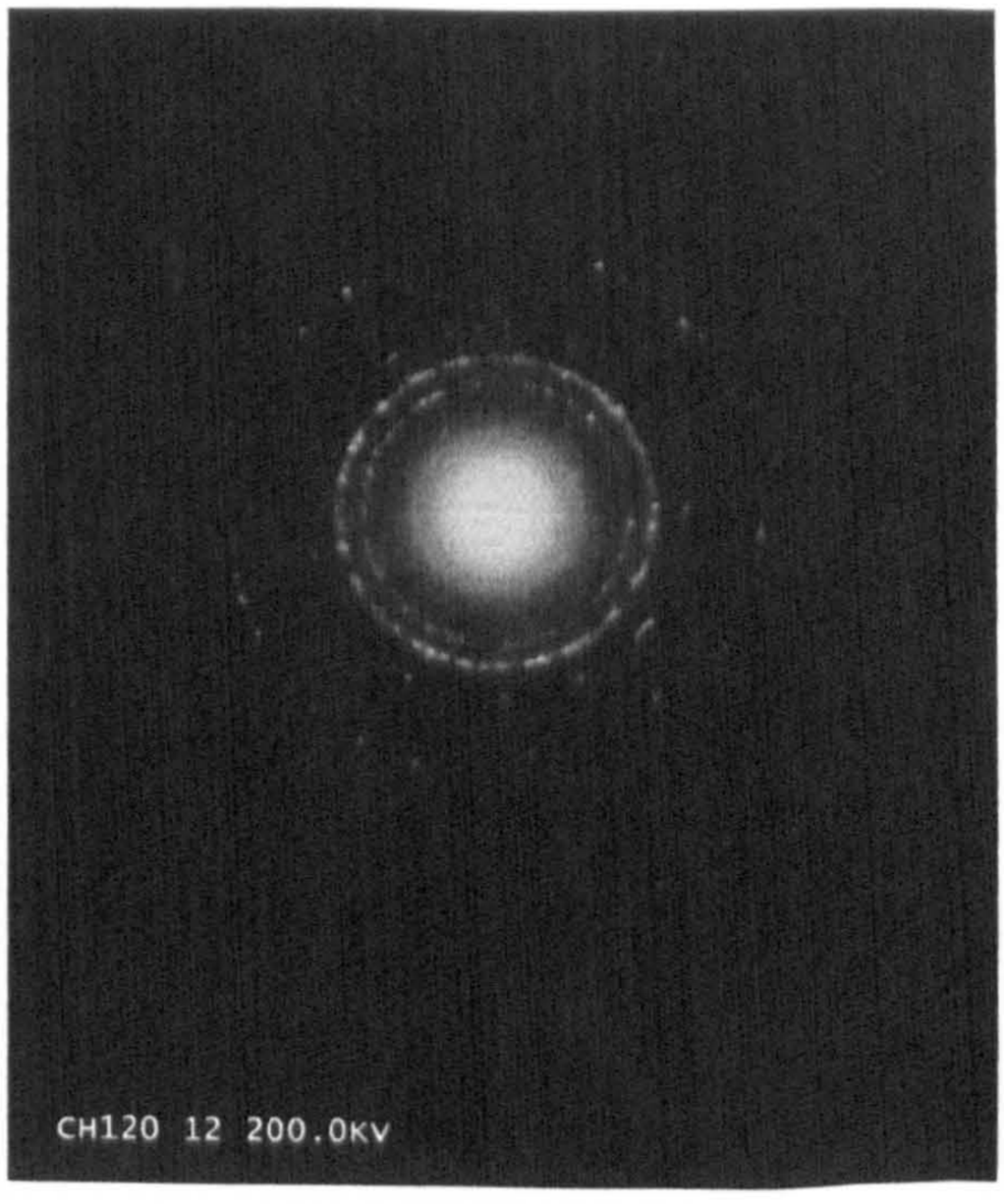

[A.DF]

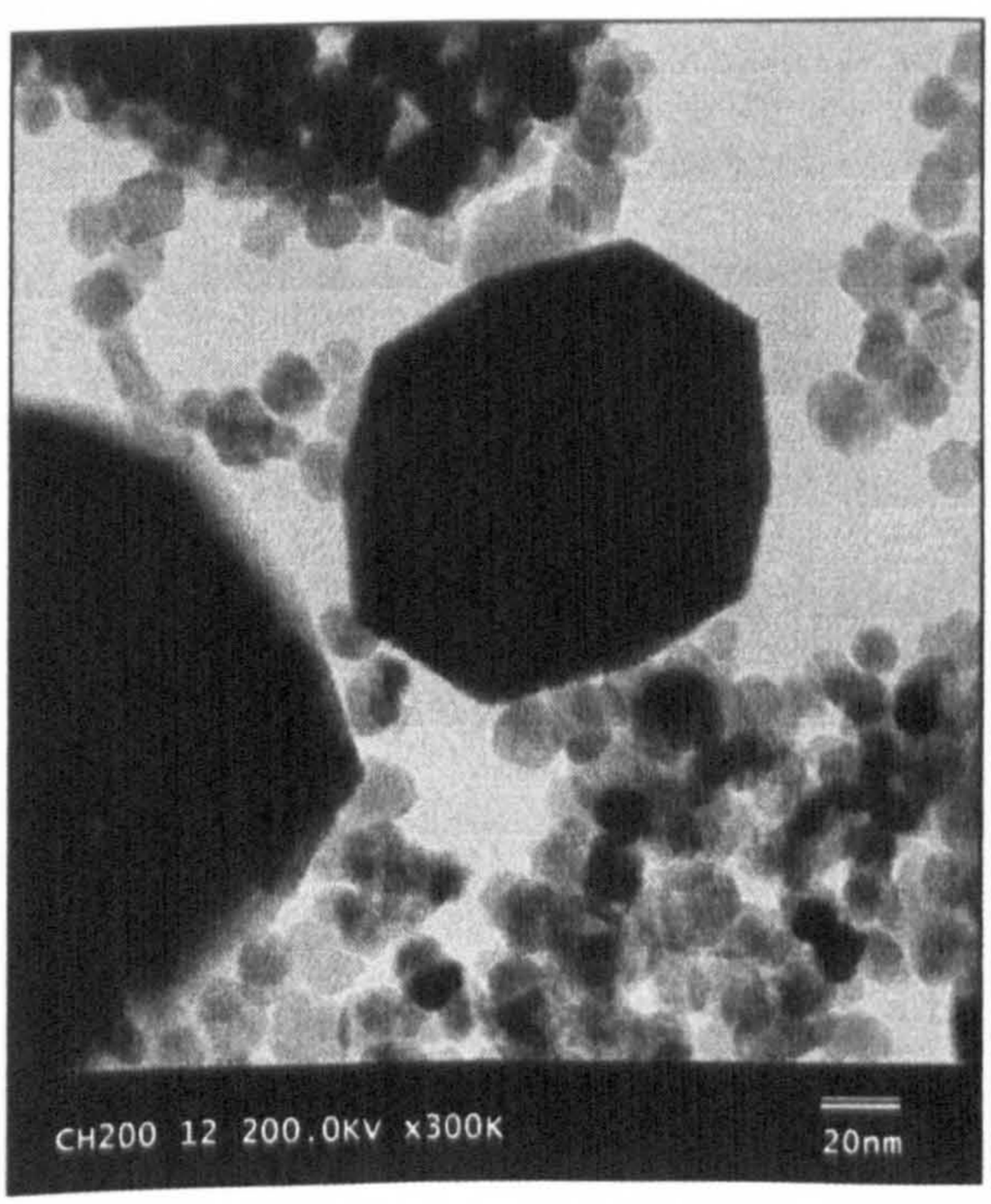

[B]. 200°C

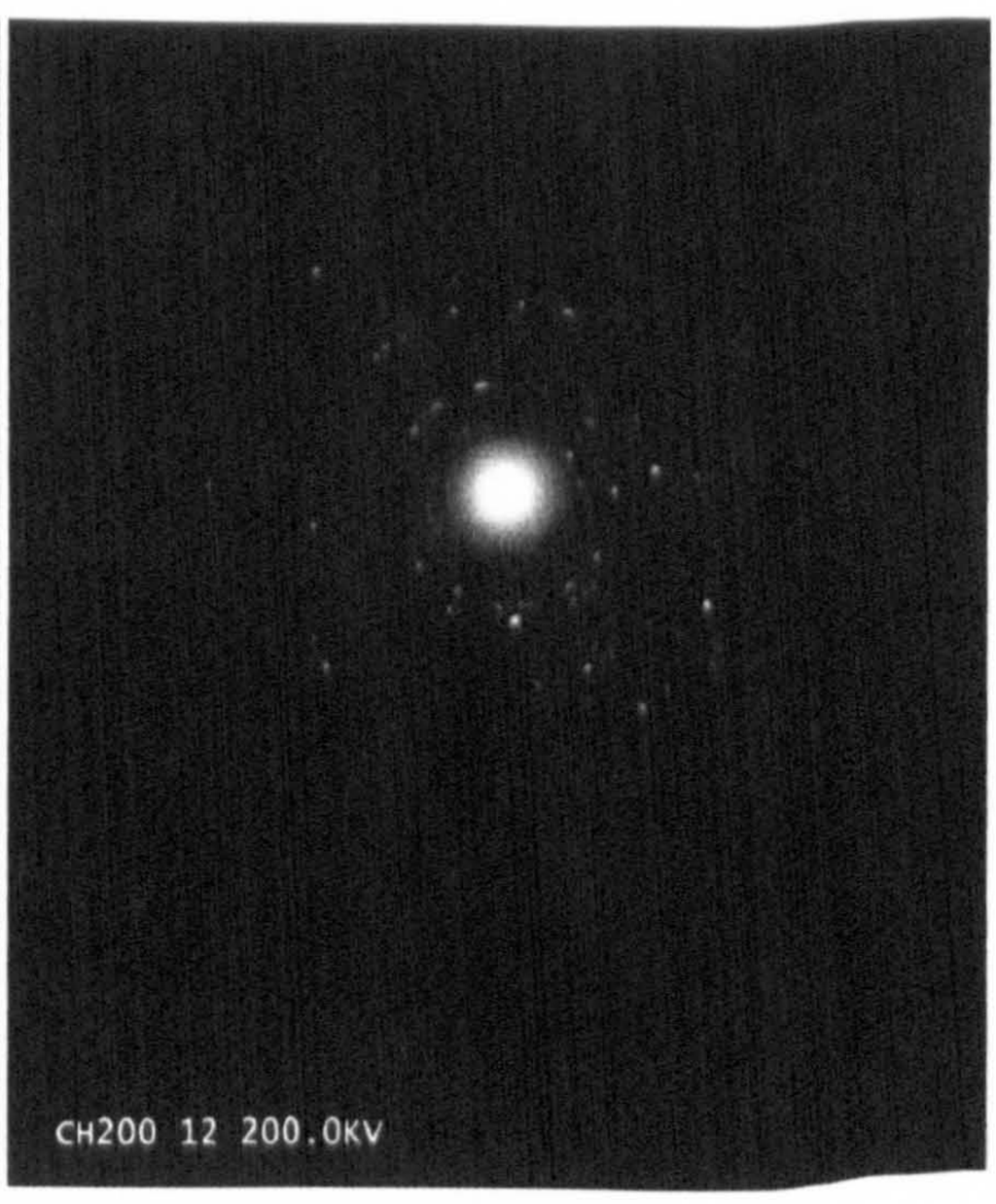

[B.DF]

Figure 5.1-14 TEM micrographs of iron oxide nanoparticles prepared by precipitation after hydrothermal at different temperatures for 12 hours, accompanied with their diffraction patterns.

process was about 5-20 nm [**Figure 5.1-13 A**]. The TEM micrograph of the diffraction pattern of these iron oxide nanoparticles is shown in **Figure 5.1-13 A.DF.**

The iron oxide samples prepared by precipitation underwent hydrothermal treatment at different temperatures, ranged from 120°C to 200°C. The TEM micrographs of samples treated at 120°C and 200°C are shown in **Figure 5.1-14 A, B** respectively. The growth of the particle size after hydrothermal process can be clearly observed. The average particle size of 120°C sample [**Figure 5.1-14 A**] was about 20-30 nm. When the aging temperature was increased to 200°C, the size of iron oxide

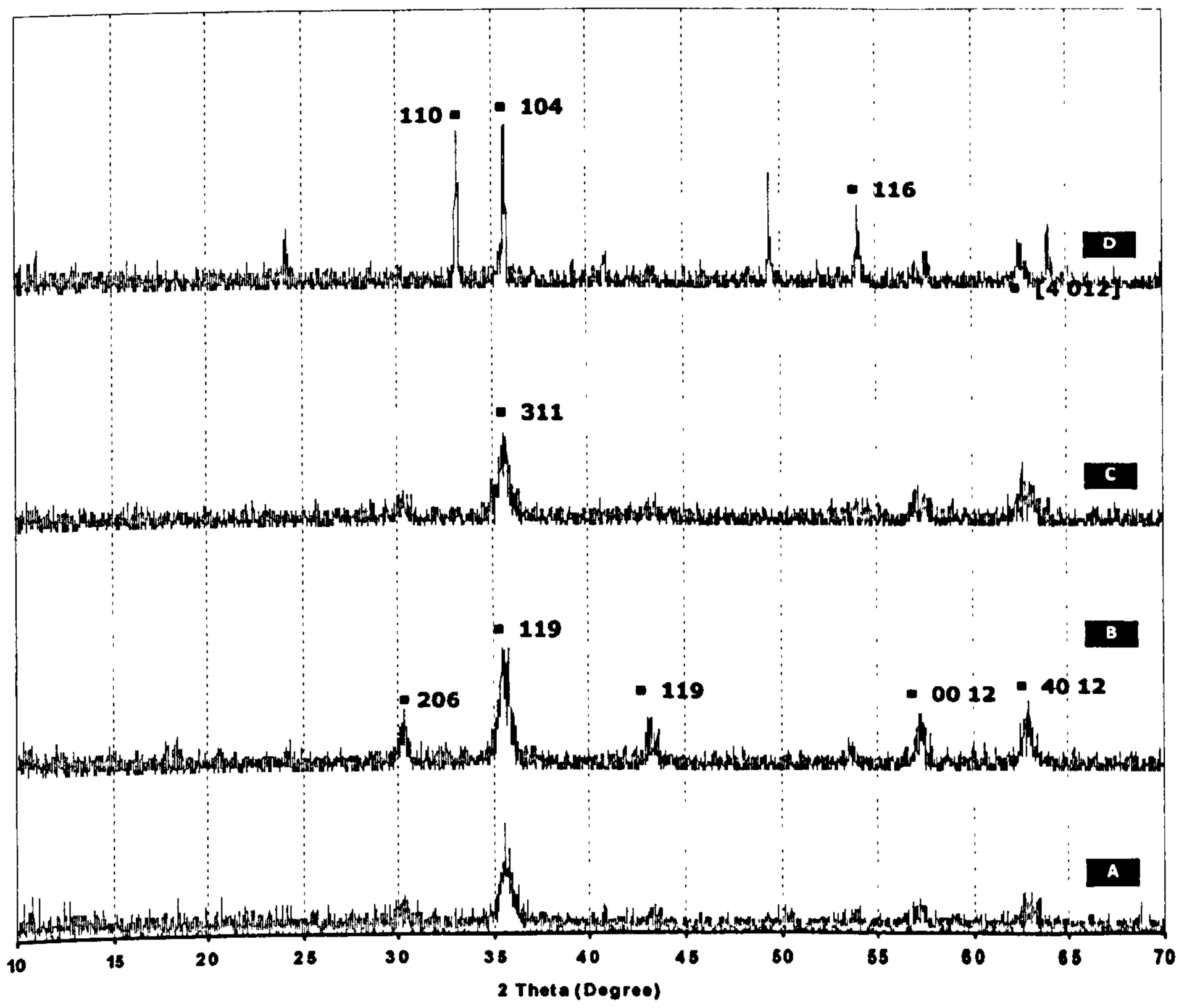

Figure 5.1-15 X-Ray diffractogram of iron oxide nanoparticles prepared by precipitation after hydrothermal at different temperatures.

[A]. 120°C, [B]. 140°C, [C]. 160°C, [D]. 200°C

nanoparticles ranged from 20-180 nm [Figure 5.1-14 B]. The TEM micrographs of the diffraction patterns [Figure 5.1-14 A.DF, B.DF] showed that the crystallinity of iron oxide treated-samples increased with the increase of aging temperature.

The X-ray diffractograms of iron oxide samples prepared by precipitation followed by hydrothermal process at different aging temperatures are shown in Figure 5.1-15. The most remarkable change of iron oxide samples with hydrothermal temperature was the phase transition. They were identified as magnetite when prepared at 25°C and transformed into maghemite when treated by the hydrothermal process at 120°C for 12 hours. Hematite phases were clearly observed when the aging temperature was 200°C.

The investigation of aging temperature in hydrothermal process was also carried out for the iron oxide samples prepared via the w/o microemulsion system. The original particle size was around 5 nm [Figure 5.1-9 A]. After the hydrothermal at 120°C for 12 hours, the iron oxide nanoparticles grew up with the size about 10-20 nm [Figure 5.1-16 A]. When the aging temperature was increased to 200°C, the size of iron oxide samples was increased into about 60 nm accompanied with narrow size distribution [Figure 5.1-16 B]. At the same time, the crystallinity was improved with the increase of hydrothermal temperature [Figure 5.1-16 A.DF, B.DF].

Figure 5.1-17 shows the diffractograms of iron oxide samples prepared by w/o microemulsion system followed by hydrothermal at different aging temperatures. The samples were identified as magnetite as prepared at 25°C. A phase transition from magnetite to maghemite happened after the hydrothermal at 120°C for 12 hours. A further transition from maghemite to hematite was observed when the aging temperature was increased to 140°C, which was lower than the transition temperature of the iron oxide samples prepared by precipitation.

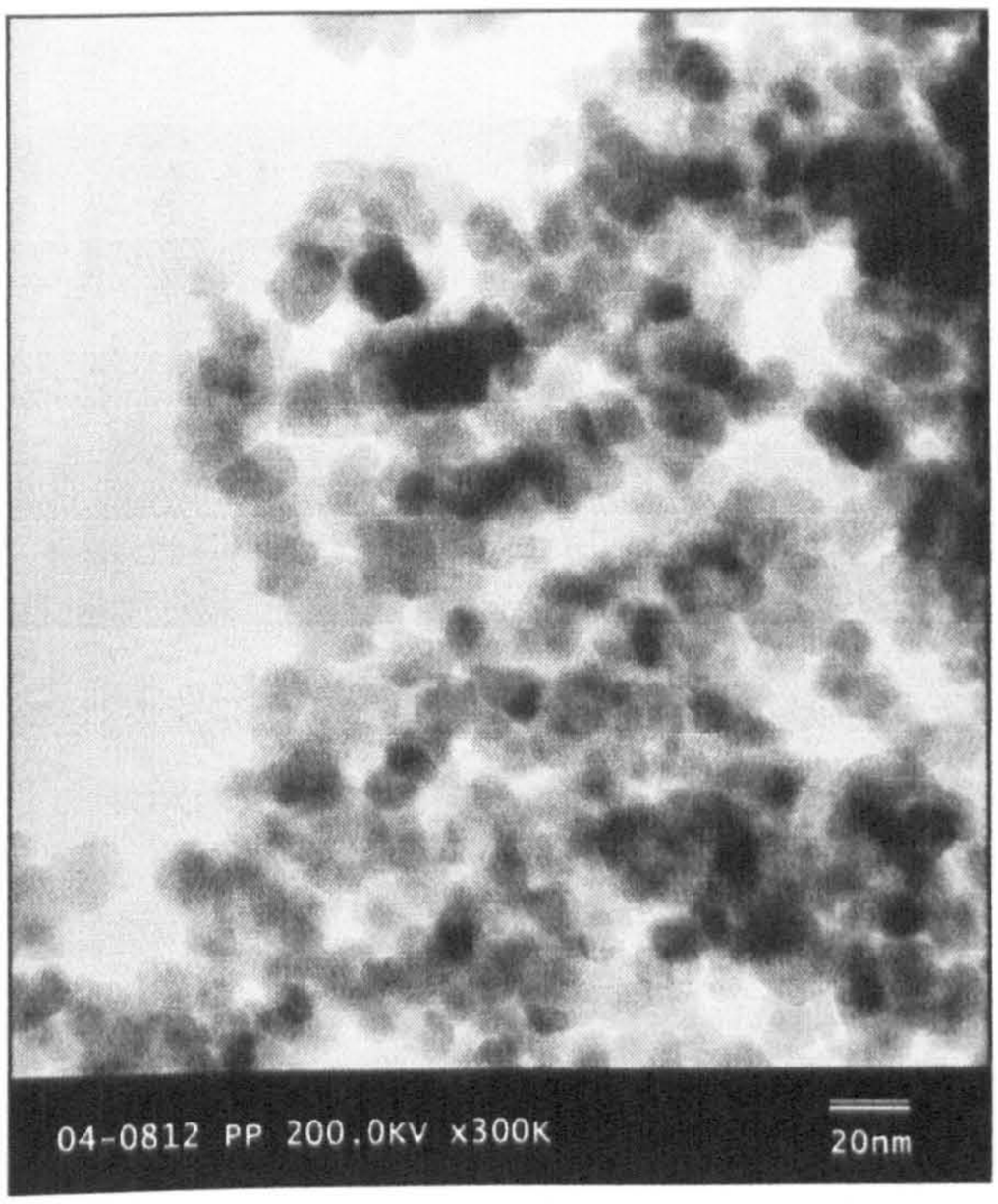

[A]. 120°C

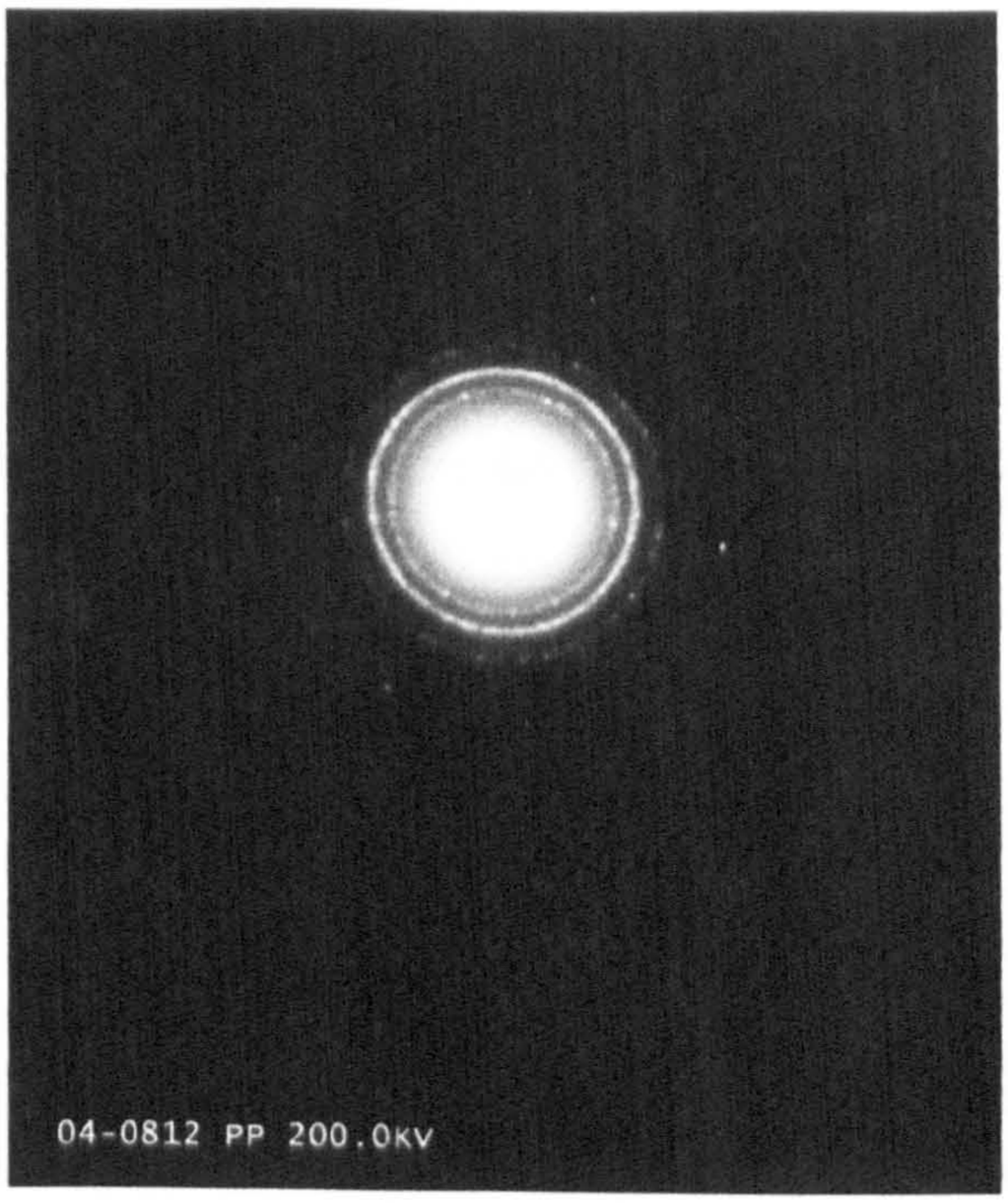

[A.DF]

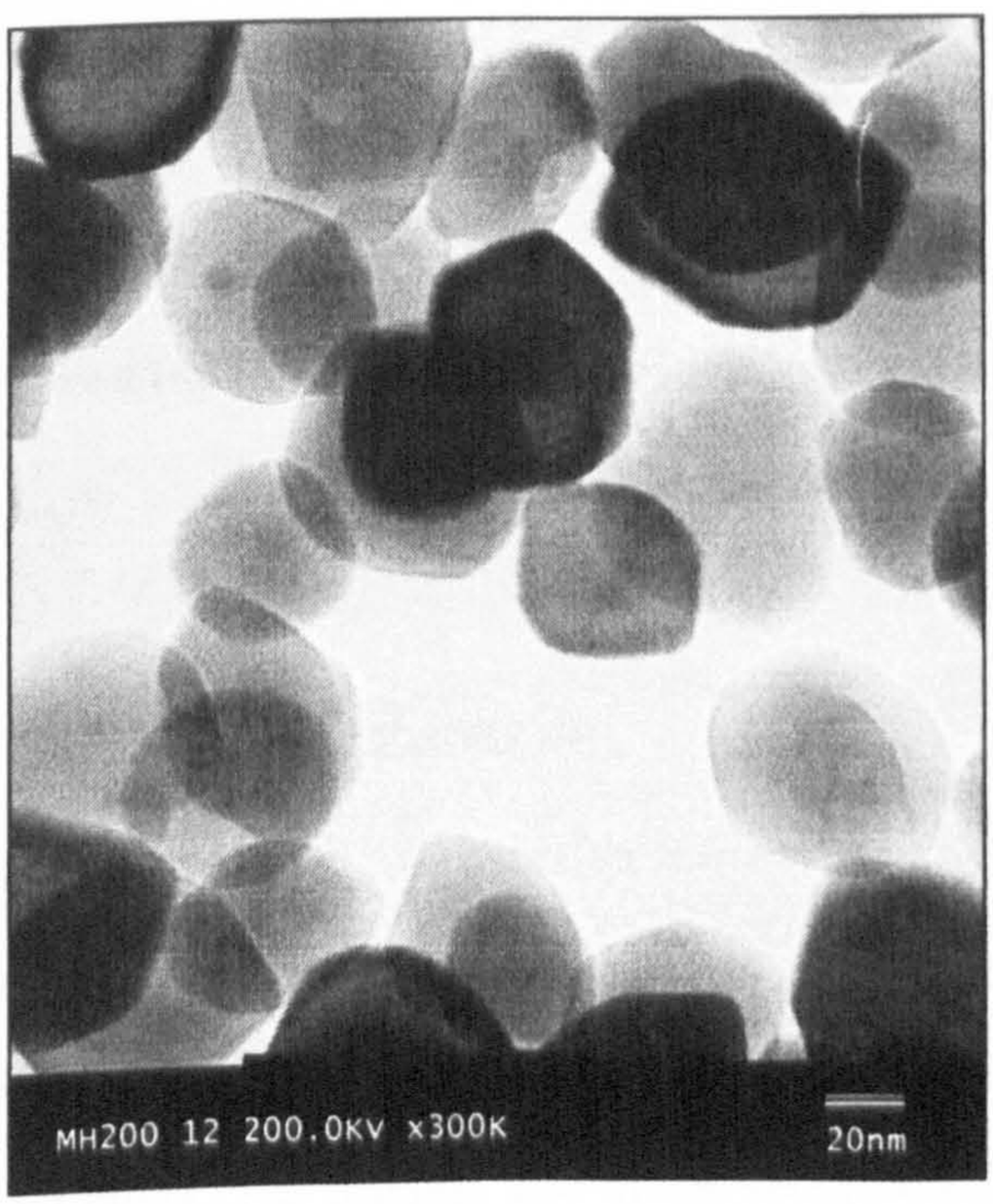

[B]. 200°C

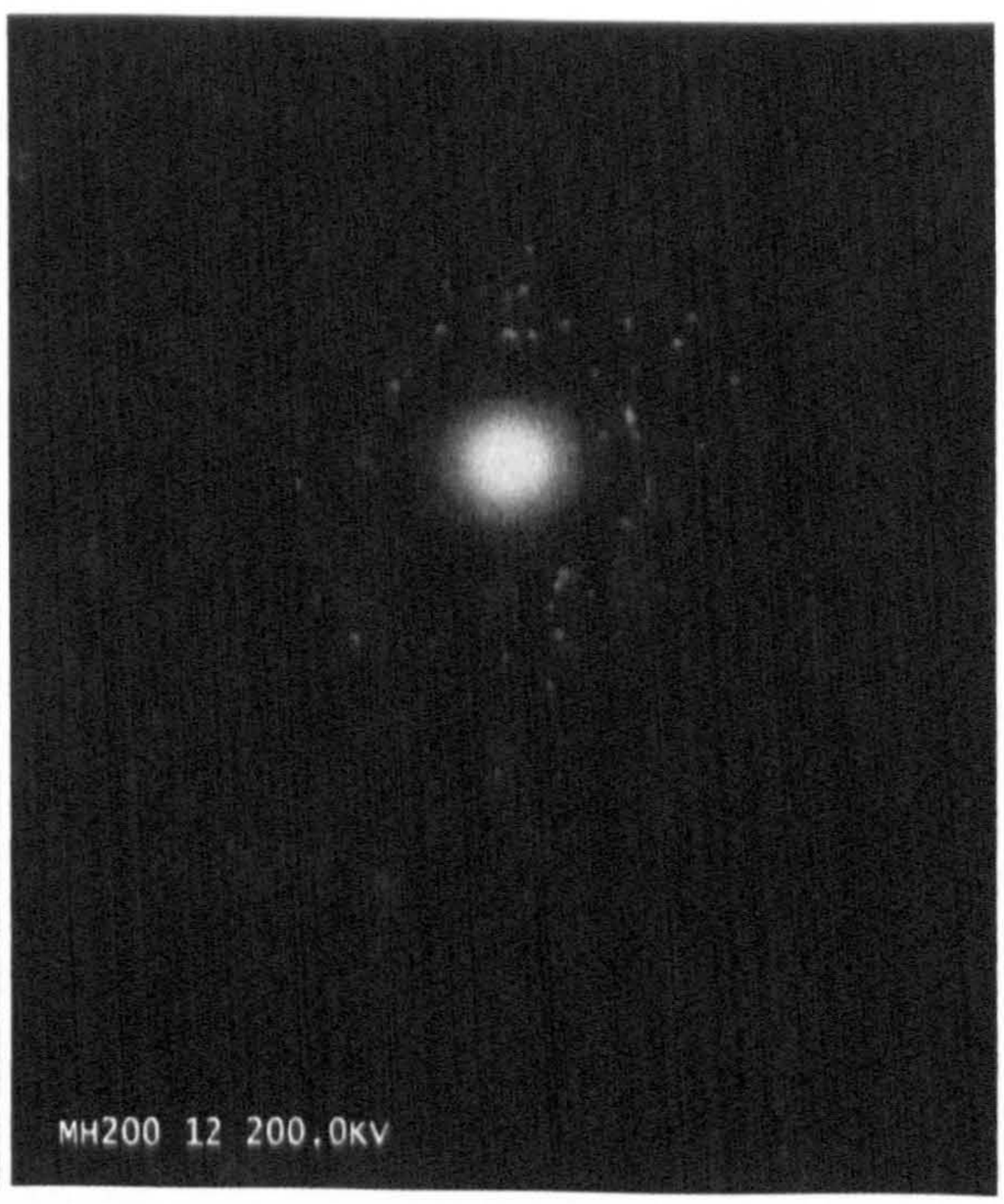

[B.DF]

Figure 5.1-16 TEM micrographs of iron oxide nanoparticles prepared by W/O microemulsion after hydrothermal at different temperatures for 12 hours, accompanied with their diffraction patterns.

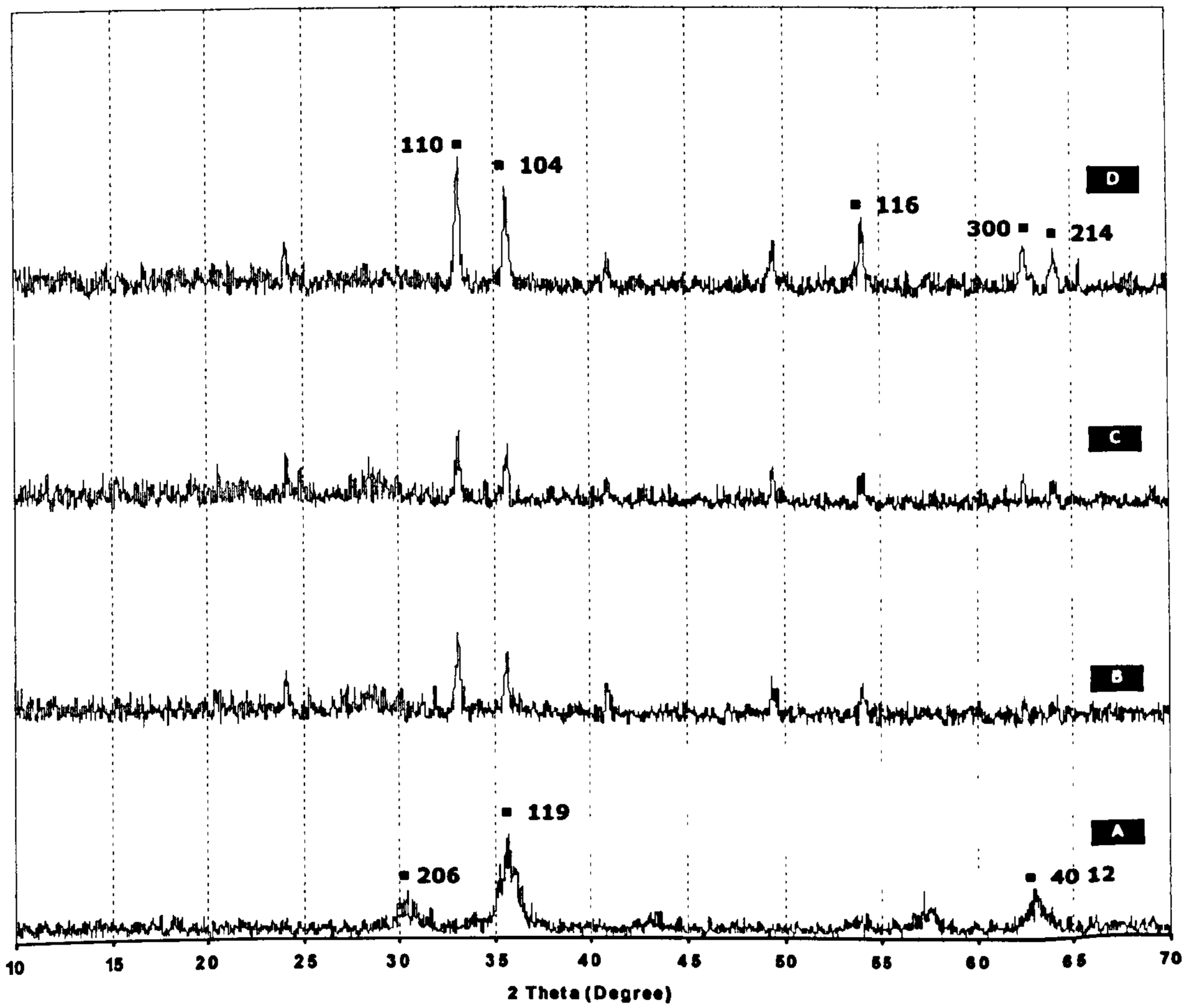

Figure 5.1-17 X-Ray diffractogram of iron oxide nanoparticles prepared via w/o microemulsion system after hydrothermal at 120°C with different temperatures.

[A]. 120°C, [B]. 140°C, [C]. 160°C, [D]. 200°C

- **Studies on different aging time**

With the iron oxide nanoparticles prepared by precipitation, no phase transition was observed with the hydrothermal temperature at 120°C, so further studies of different aging time were carried out. As shown in **Figure 5.1-18,** the size of nanoparticles increased with the increase of aging time, from 2 hours to 96 hours. The original size of the samples before the treatment was 5-20 nm **[Figure 5.1-13]**. The average size of nanoparticles increased to 20 nm **[Figure 5.1-18 A]** after the hydrothermal process at 120°C for 2 hours. The particles continuously grew from an average size of 20 nm to 30 nm **[Figure 5.1-18 D]** as the aging time was increased progressively to 96 hours. At the same time, the mono-dispersity of the particles seemed to improve as well. The TEM micrographs of diffraction patterns of these post-

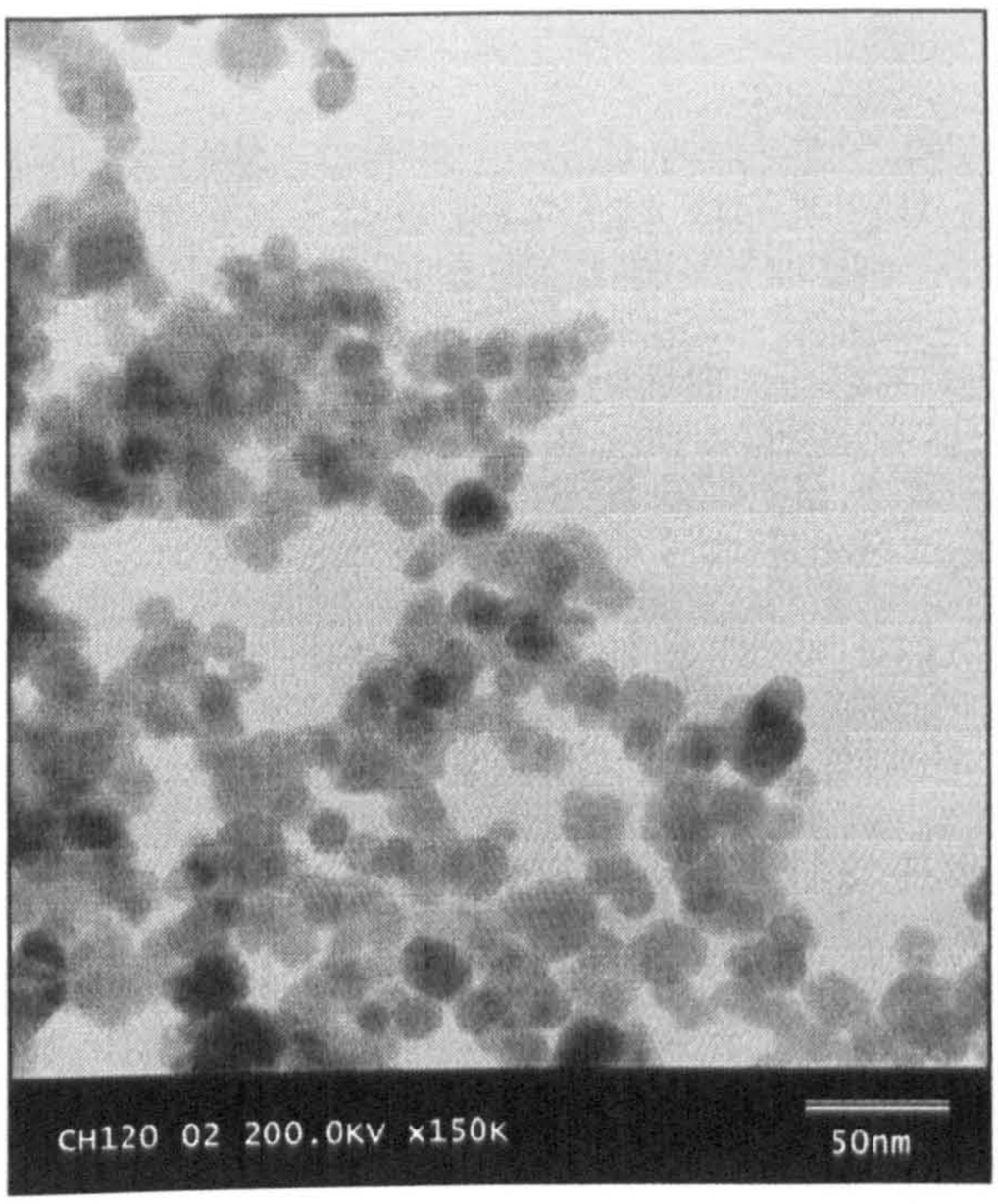

[A]. 2 Hours

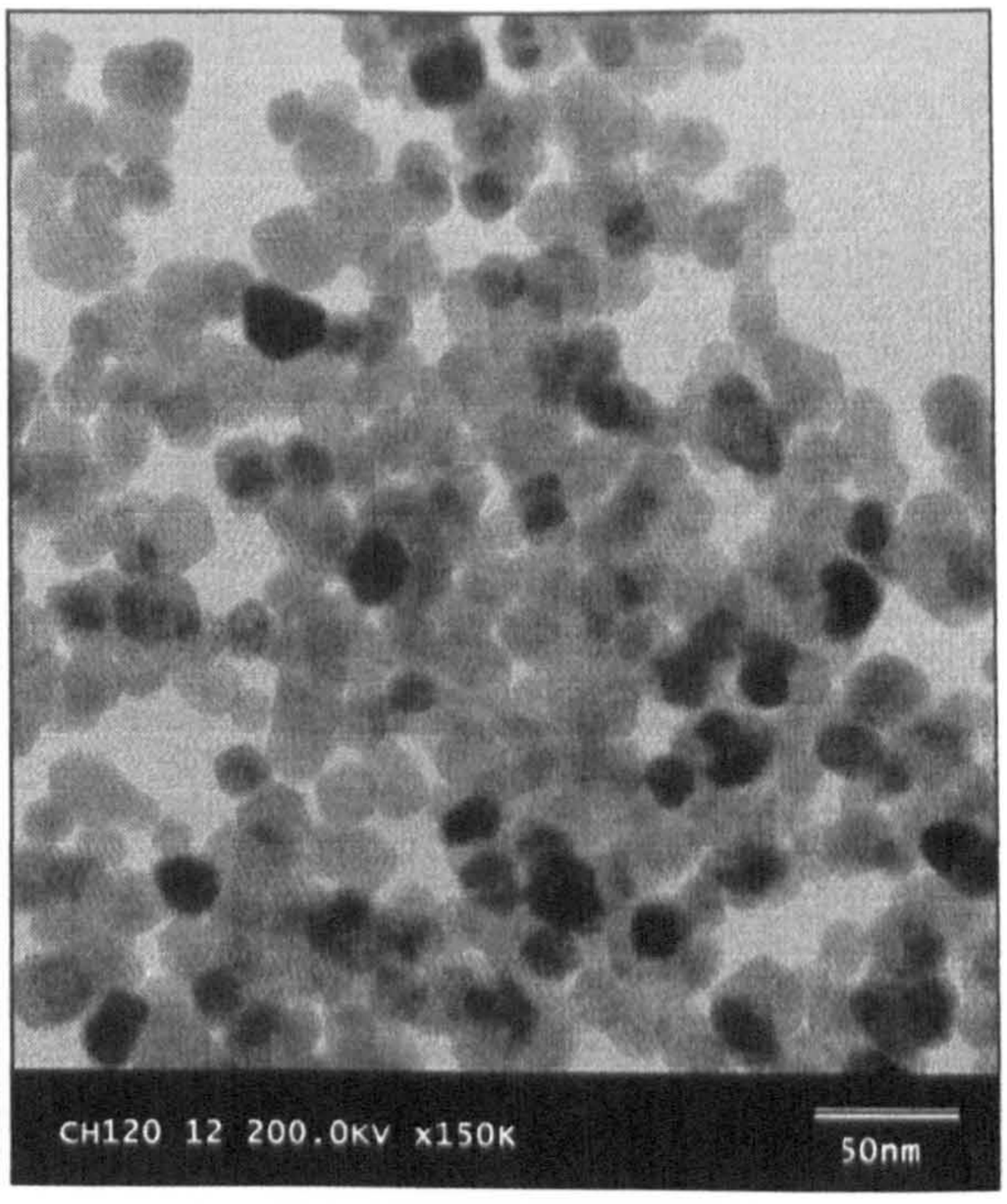

[B]. 12 Hours

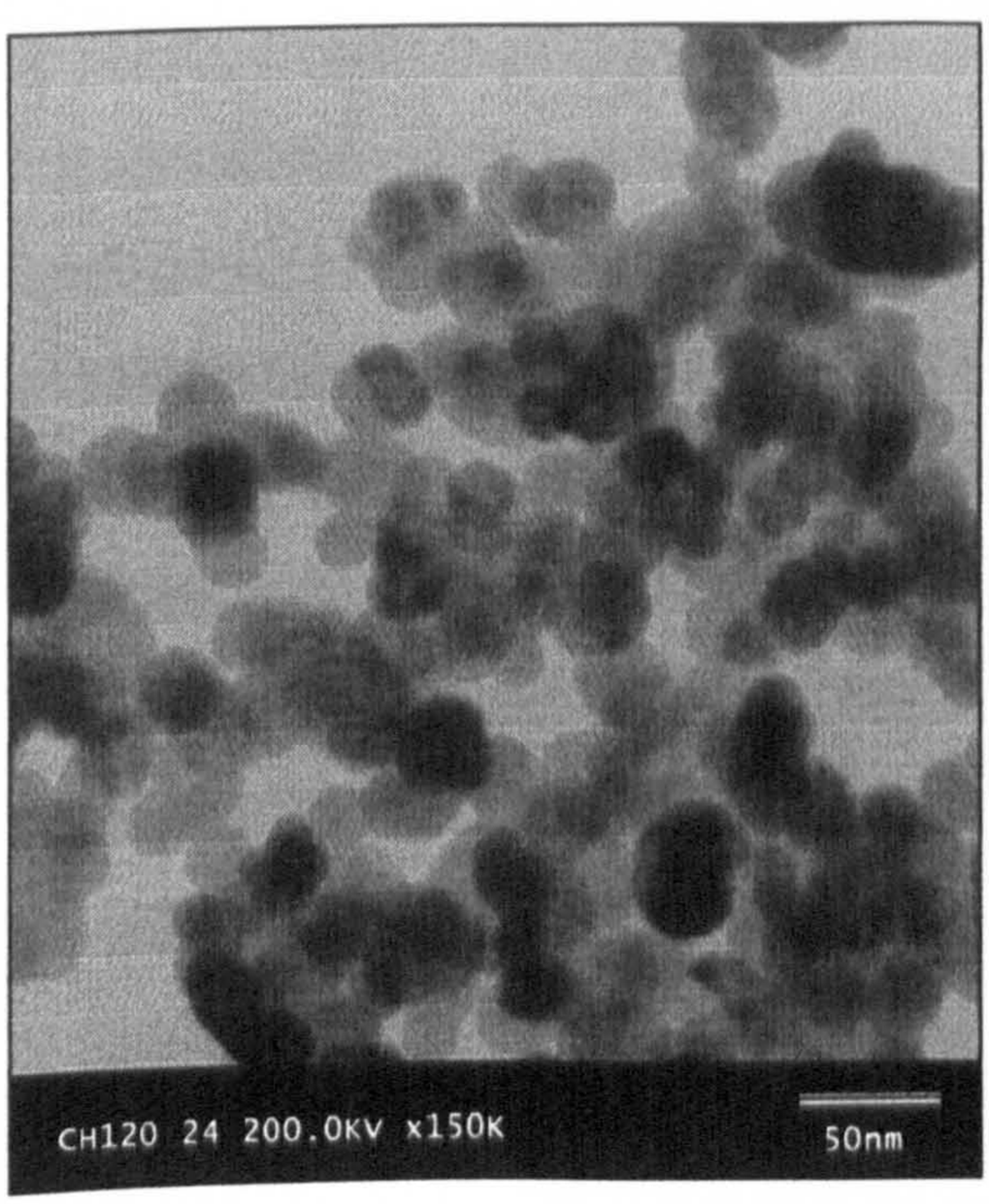

[C]. 24 Hours

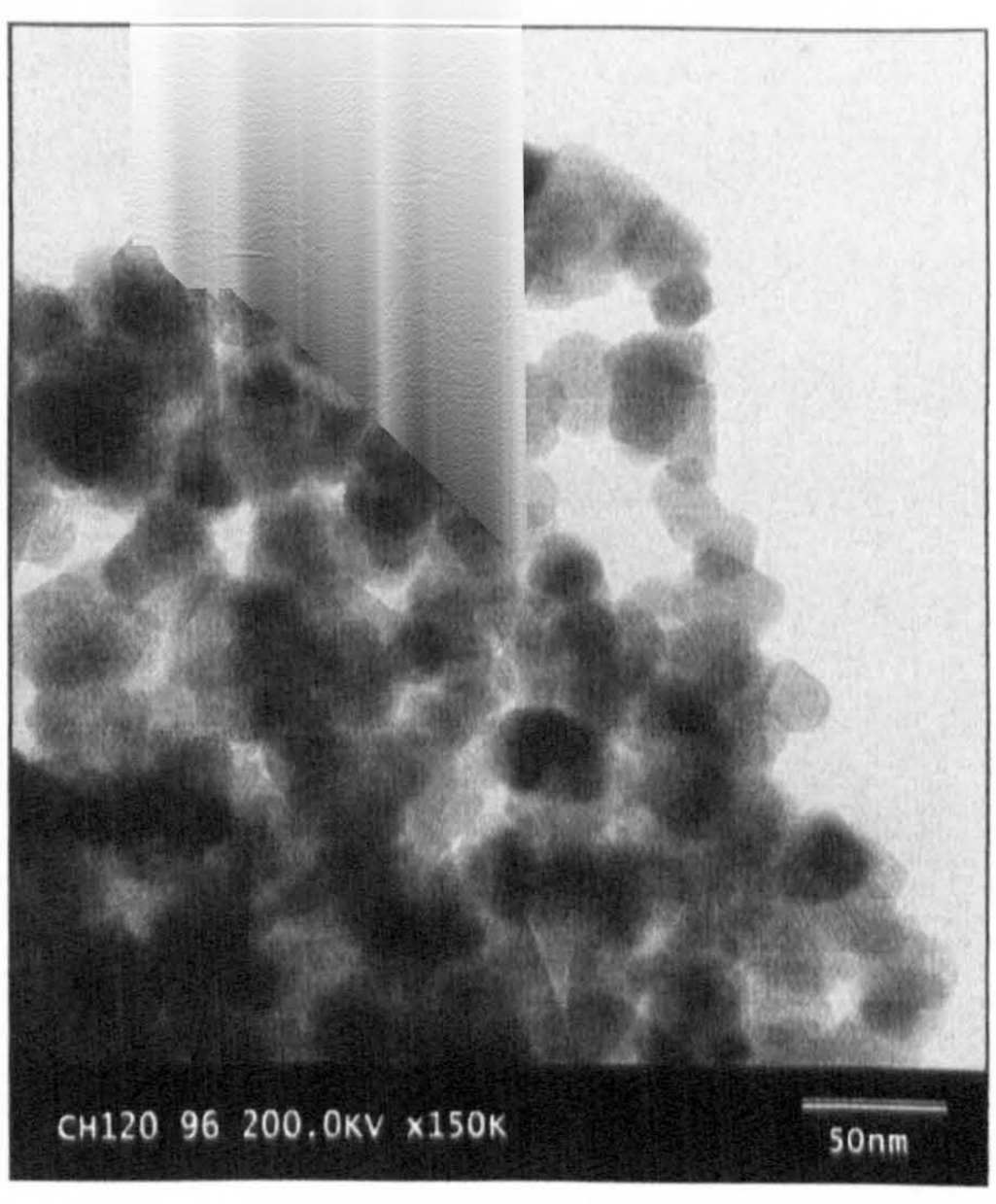

[D]. 96 Hours

Figure 5.1-18 TEM micrographs of iron oxide nanoparticles prepared by precipitation after hydrothermal process at 120°C with different aging times.

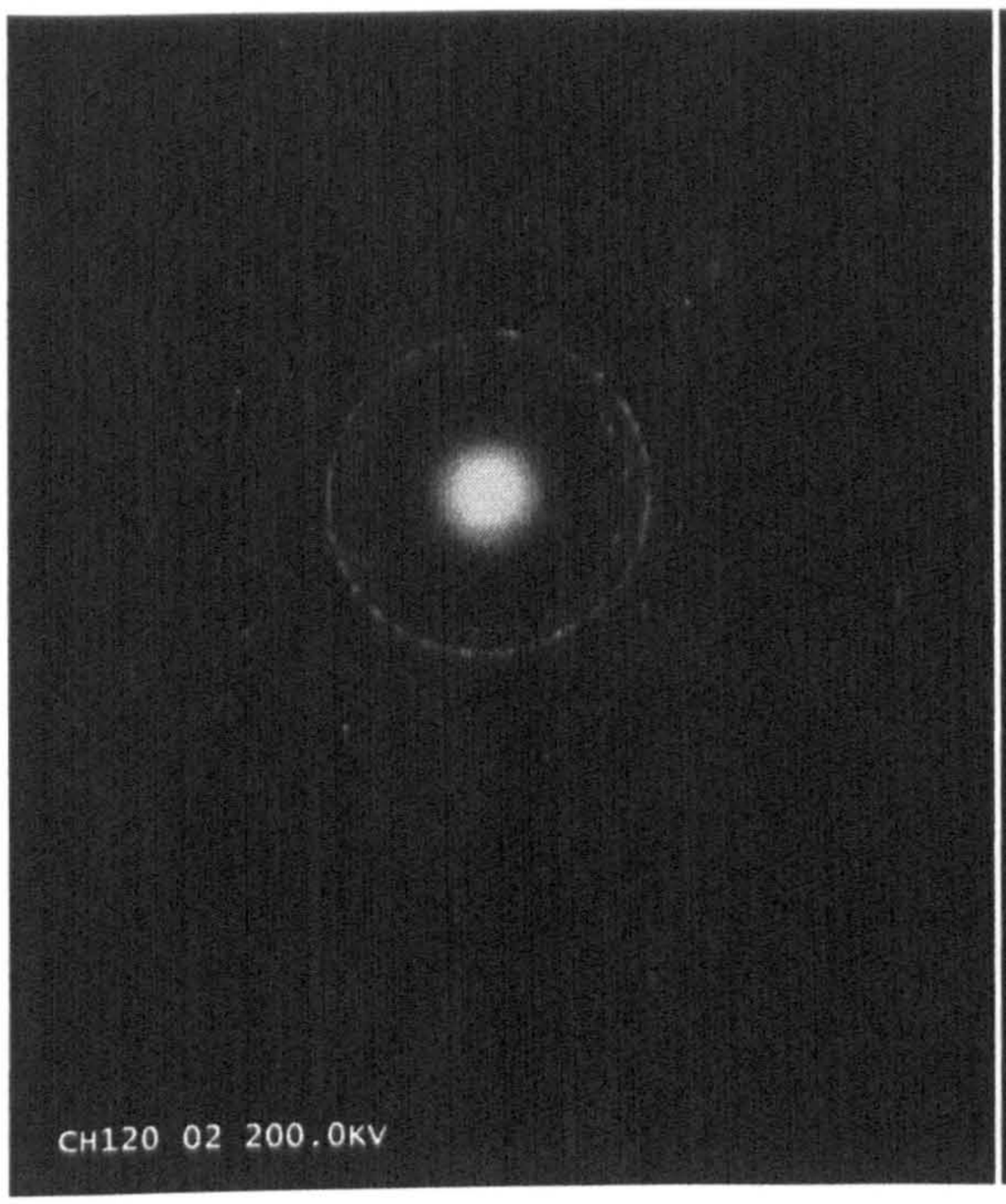

[A.DF]. 2 Hours

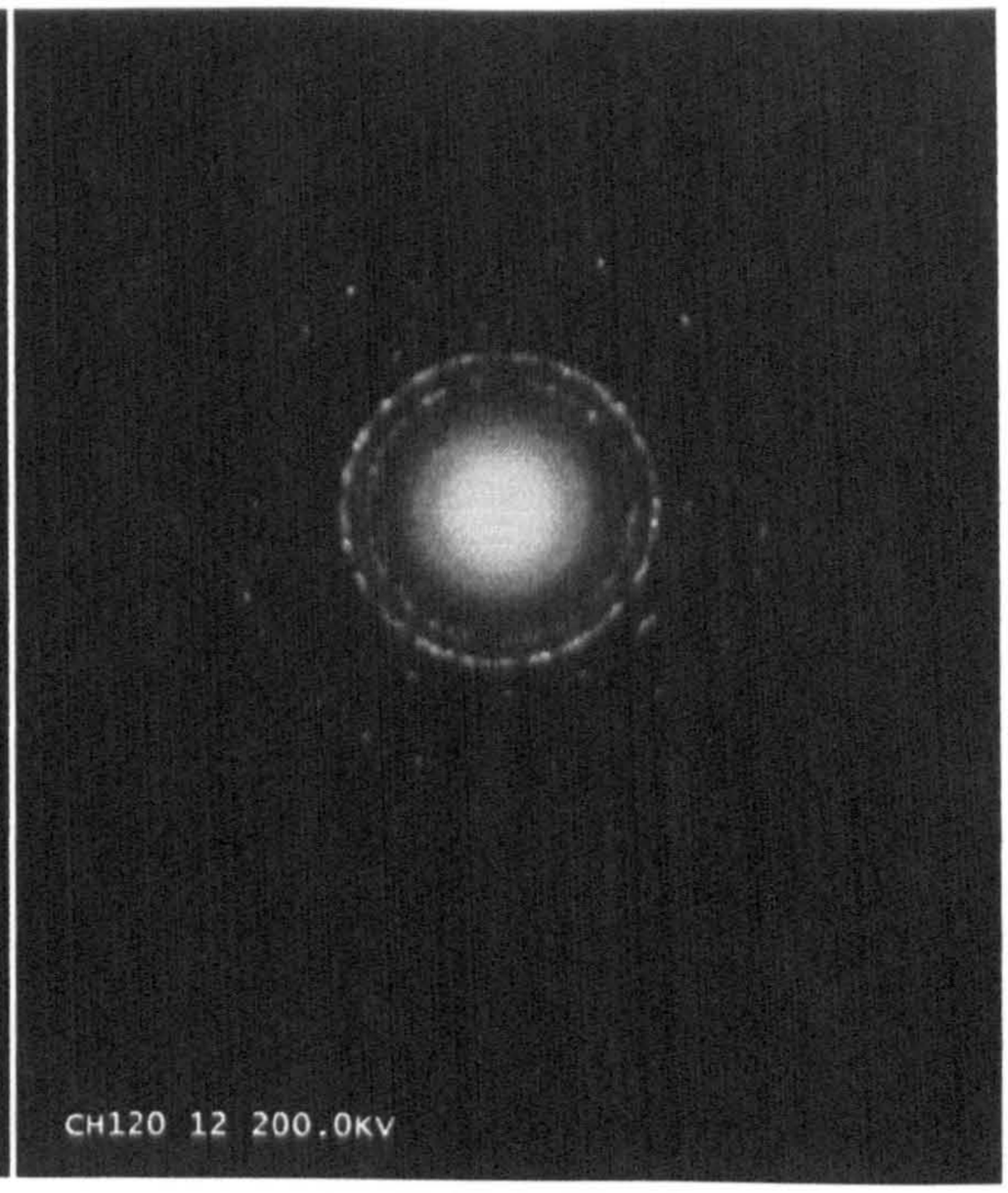

[B.DF]. 12 Hours

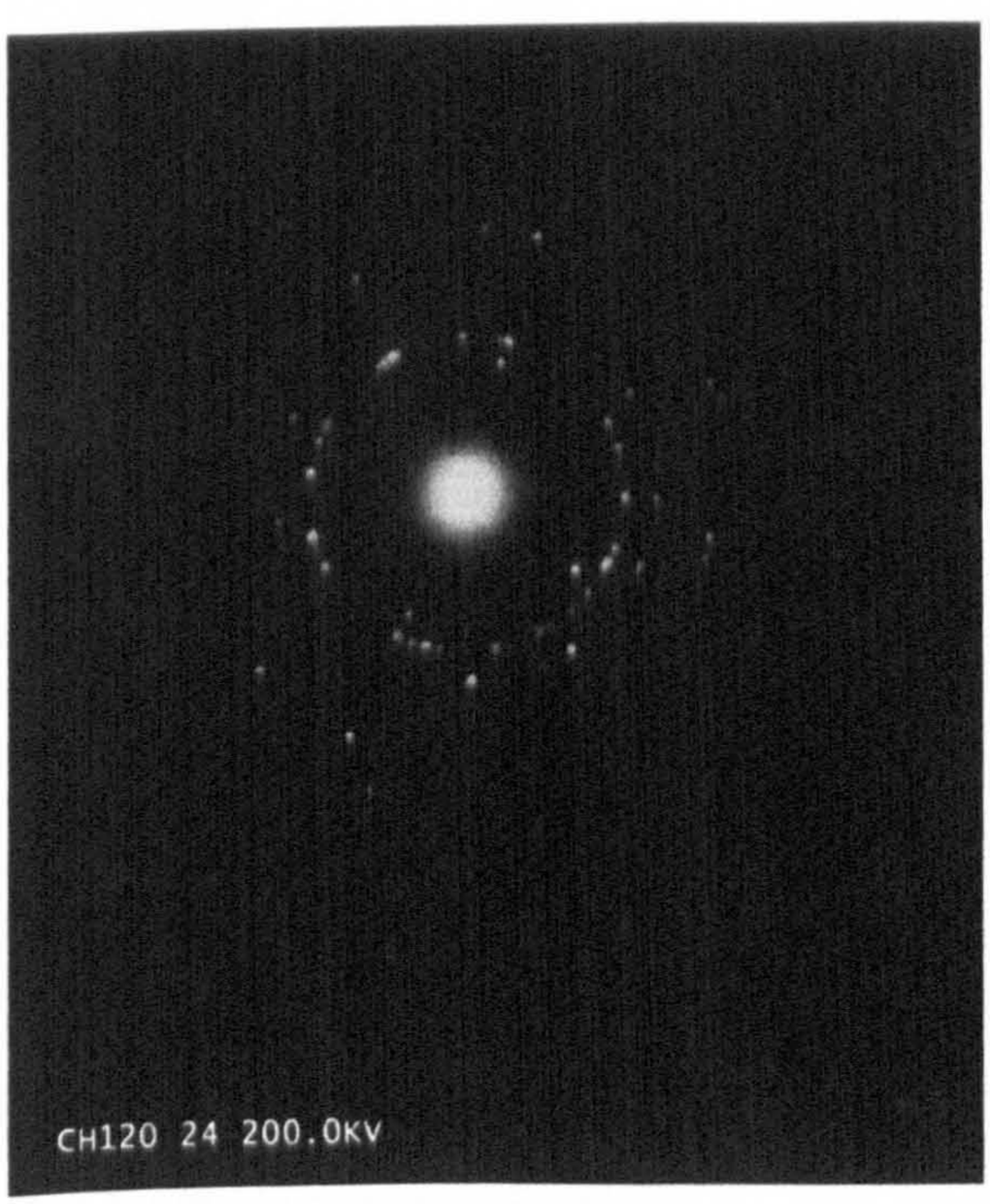

[C.DF]. 24 Hours

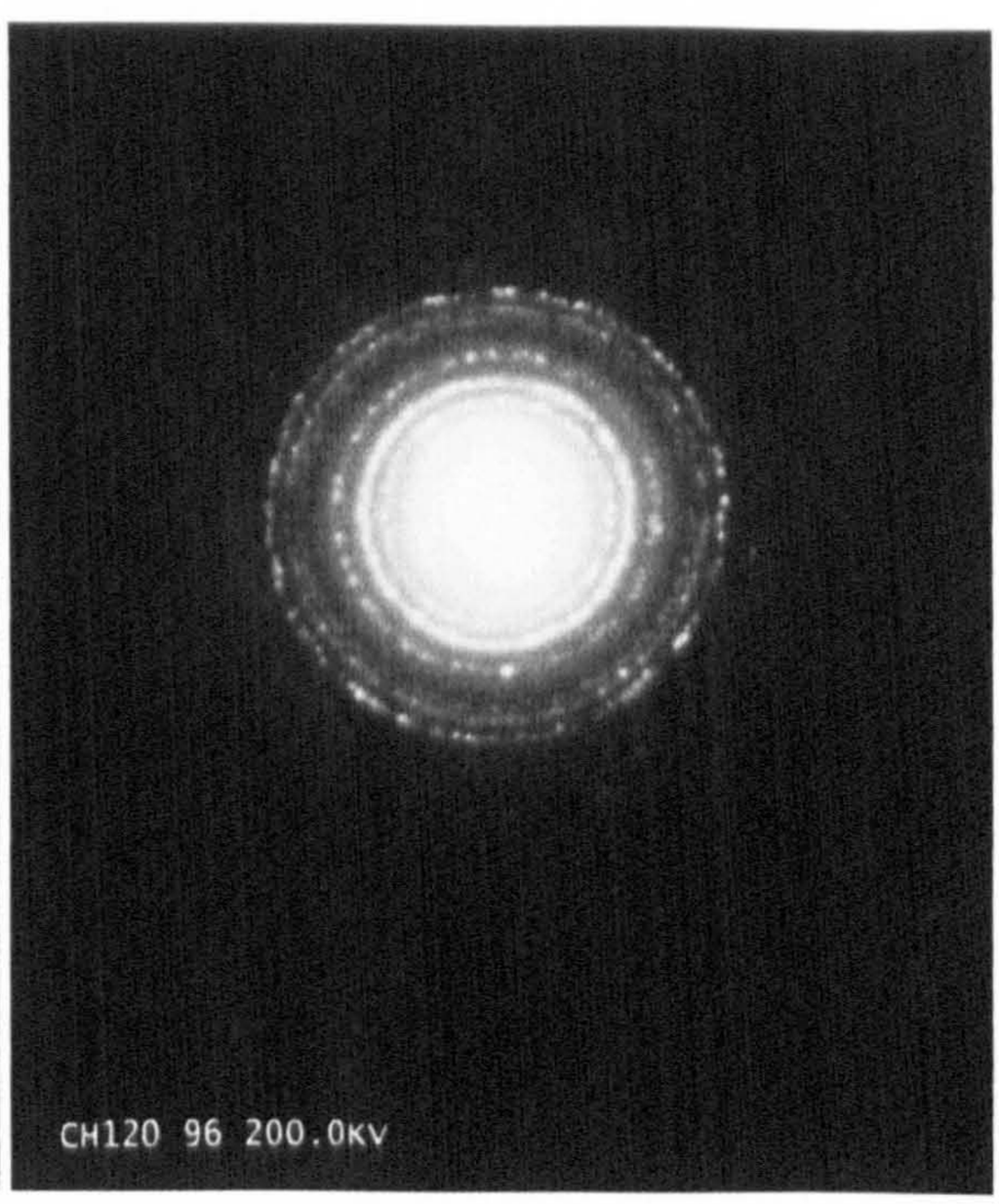

[D.DF]. 96 Hours

Figure 5.1-19 TEM micrographs of diffraction pattern of iron oxide nanoparticles prepared by precipitation after hydrothermal process at 120°C with different aging times.

treated iron oxide nanoparticles shows that the increase of aging time in hydrothermal process increased the crystallinity of iron oxide nanoparticles produced.

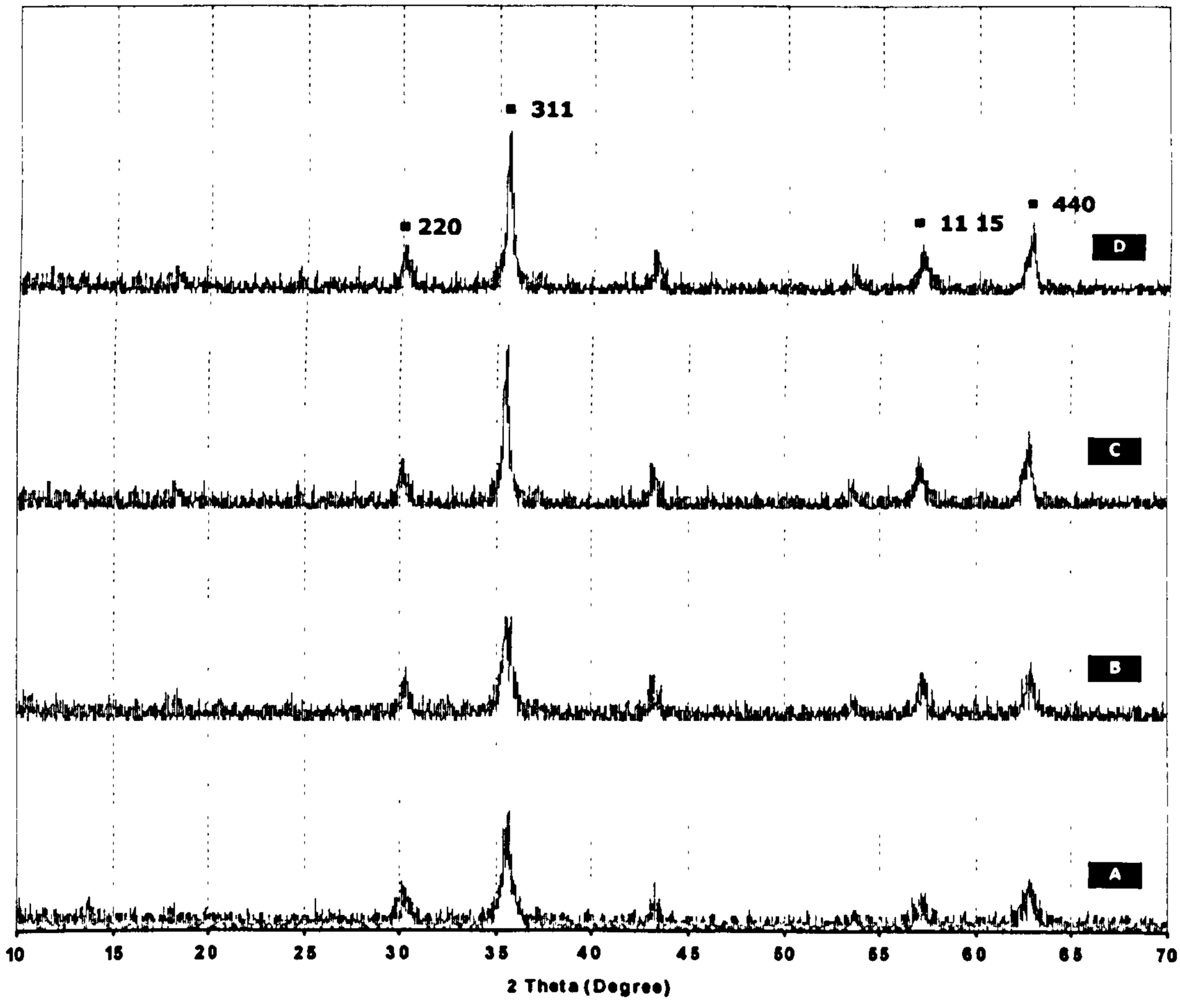

Figure 5.1-20 XRD diffractogram of iron oxide samples prepared by precipitation after hydrothermal at 120°C with different aging times.

[A]. 2 Hours, [B]. 12 Hours, [C]. 24 Hours, [D]. 96 Hours

The increase of crystallisation intensity with the increase of aging time in the hydrothermal process was also observed in the diffractogram of these iron oxide samples prepared by precipitation, post-treated by the hydrothermal process at 120°C, shown in **Figure 5.1-20**. With the aging time increased from 2 hours to 96 hours, the intensity of the main characteristic peak **(311)** also increased; there was no phase transition observed. Iron oxide samples were identified as maghemite after the hydrothermal process at 120°C with the aging time from 2 hours to 96 hours.

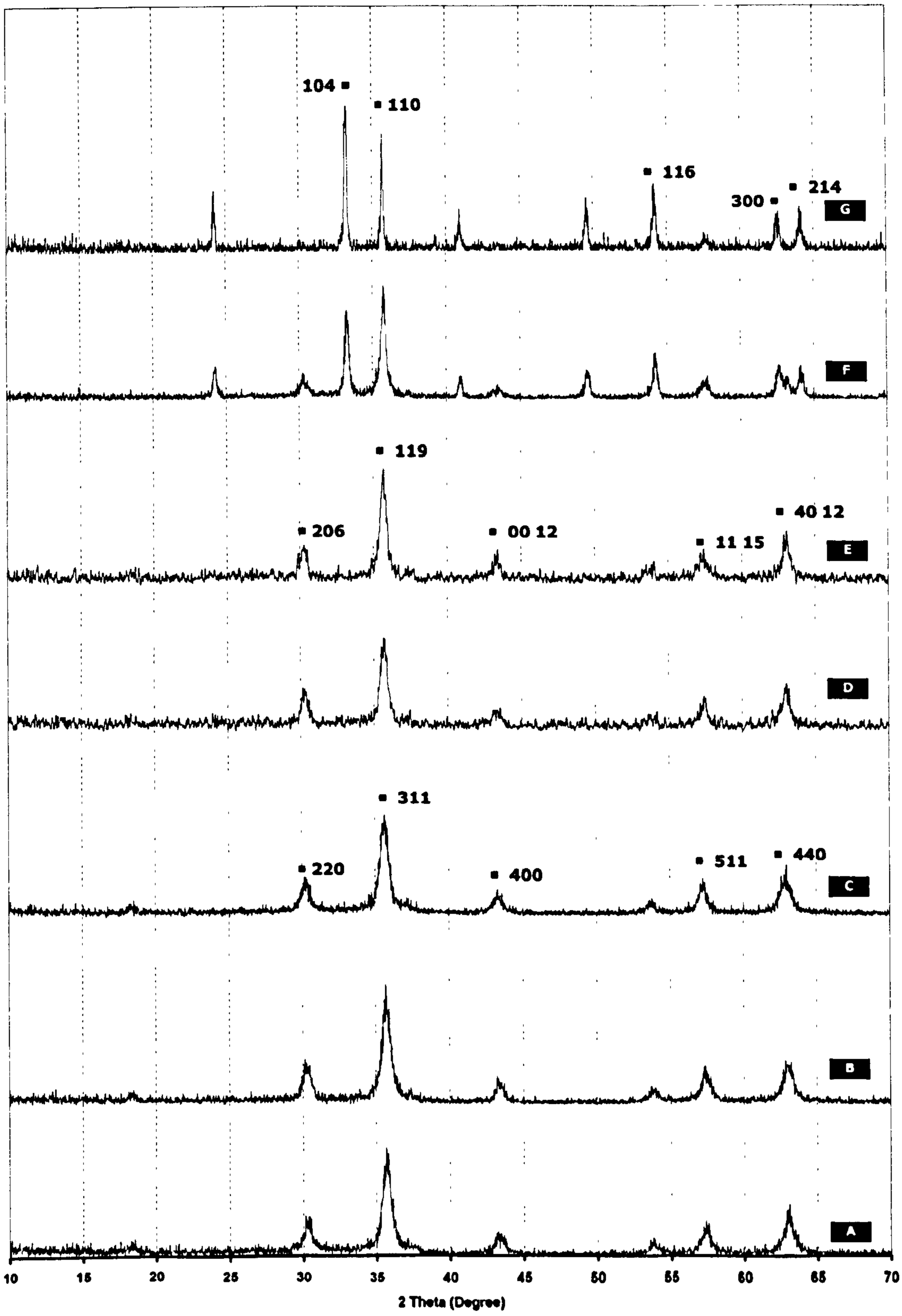

Figure 5.1-21 X-Ray diffractogram of iron oxide samples prepared by precipitation at different calcination temperatures:

[A]. 140°C, [B]. 200°C, [C]. 250°C, [D]. 300°C, [E]. 400°C, [F]. 450°C, [G]. 500°C

5.1.3.2 Calcination

- **Studies on different calcination temperature**

The iron oxide samples prepared by precipitation at 25°C, were calcined at different temperatures ranged from 140°C to 500°C for 2 hours. The diffractograms of these samples are shown in **Figure 5.1-21**. The original iron oxide sample prepared by precipitation, was identified as magnetite. There was no phase transition observed with a calcination temperature of 200°C. The iron oxide samples transformed from magnetite into maghemite with the calcination at 250°C. For calcination temperature of 250°C to 400°C, samples were all identified as maghemite. Hematite phase was observed when the calcination temperature was above 450°.

- **Studies on different starting materials in preparation of iron oxide via precipitation**

The calcination treatment was also carried out at 300°C for 2 hours on iron oxide samples prepared by precipitation, with different starting materials, (i.e. different molar ratio of ferric ion to ferrous ion in iron salt solution). Whatever the starting materials was, the products prepared by precipitation at 25°C were all identified as magnetite.

After calcination at 300°C, the samples prepared from $[Fe]^{2+}$ transformed into maghemite. The maghemite phase was also observed from the sample prepared from the iron salt solution with the molar ratio of $[Fe]^{3+}$ to $[Fe]^{2+}$ as 2:1. The iron oxide particles prepared from the ratio as 1:2 transformed into hematite after calcinations at 300°C for 2 hours. The sample prepared from the starting materials with the ratio as 1:1 did not undergo any phase transition during the calcination, i.e. the final products were still magnetite.

As mentioned in **5.1.1.1**, the sample prepared from pure ferric ion showed an amorphous XRD pattern. However, after 300°C calcination, it transformed into hematite and the characteristic peaks could be clearly identified. The X-ray diffractograms of these samples are shown in **Figure 5.1-22.**

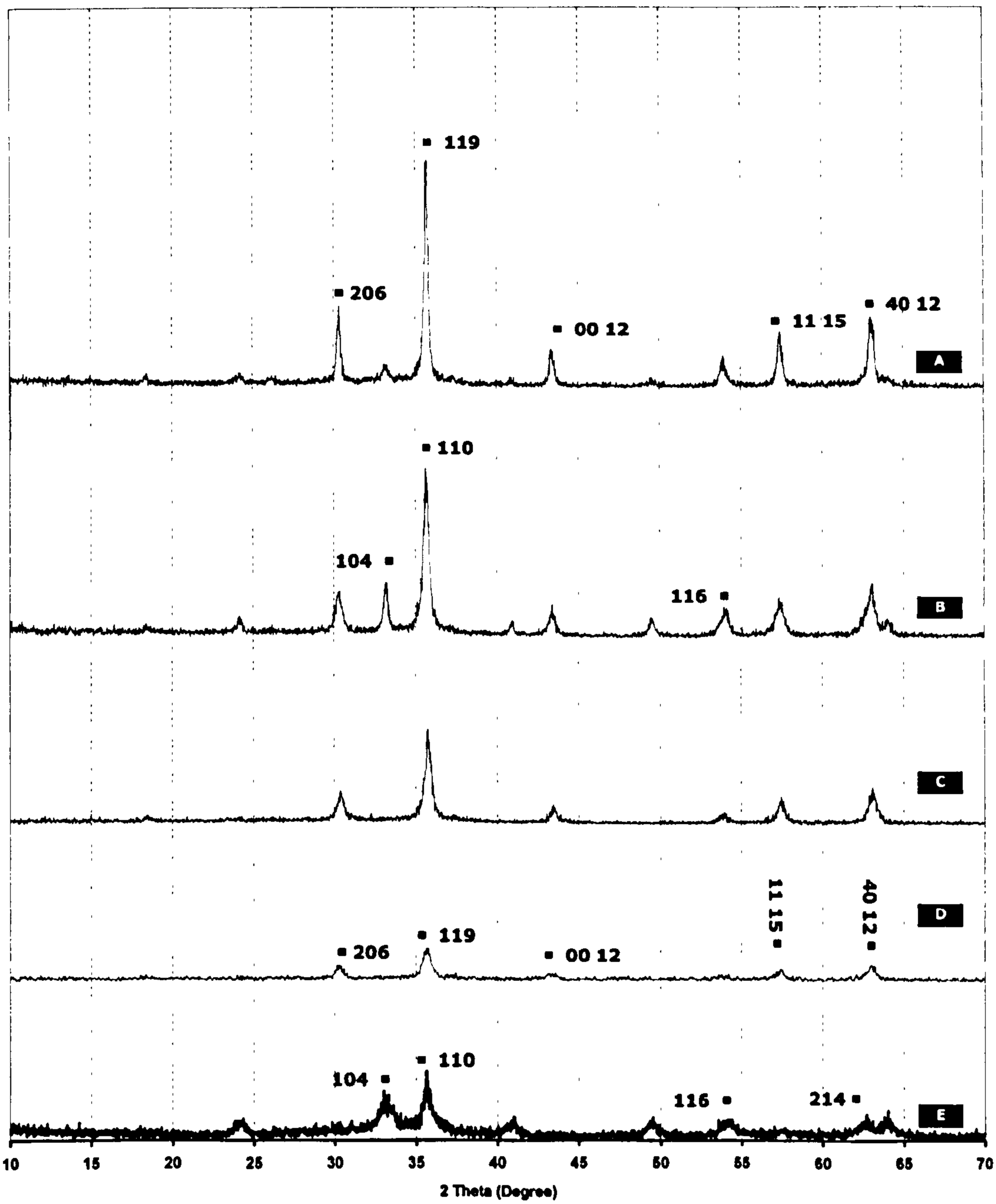

Figure 5.1-22 XRD diffractogram of iron oxide samples prepared by precipitation with different starting materials calcined at 300°C for 2 hours.

A. $[Fe]^{2+}$, B. $[Fe]^{3+}$:$[Fe]^{2+}$=1:2, C. $[Fe]^{3+}$:$[Fe]^{2+}$=1:1, D. $[Fe]^{3+}$:$[Fe]^{2+}$=2:1, E. $[Fe]^{3+}$

5.1.4 Magnetism characterisation

Magnetic characterisation of the microemulsion-derived iron oxide nanoparticles was carried out using a SQUID (Quantum design) magnetometer. Hysteresis measurements were made with a field scan of ±5.5 kOe. Representative room temperature (300K) and 5K data for the sample prepared via w/o microemulsion is shown in **Figure 5.1-23**.

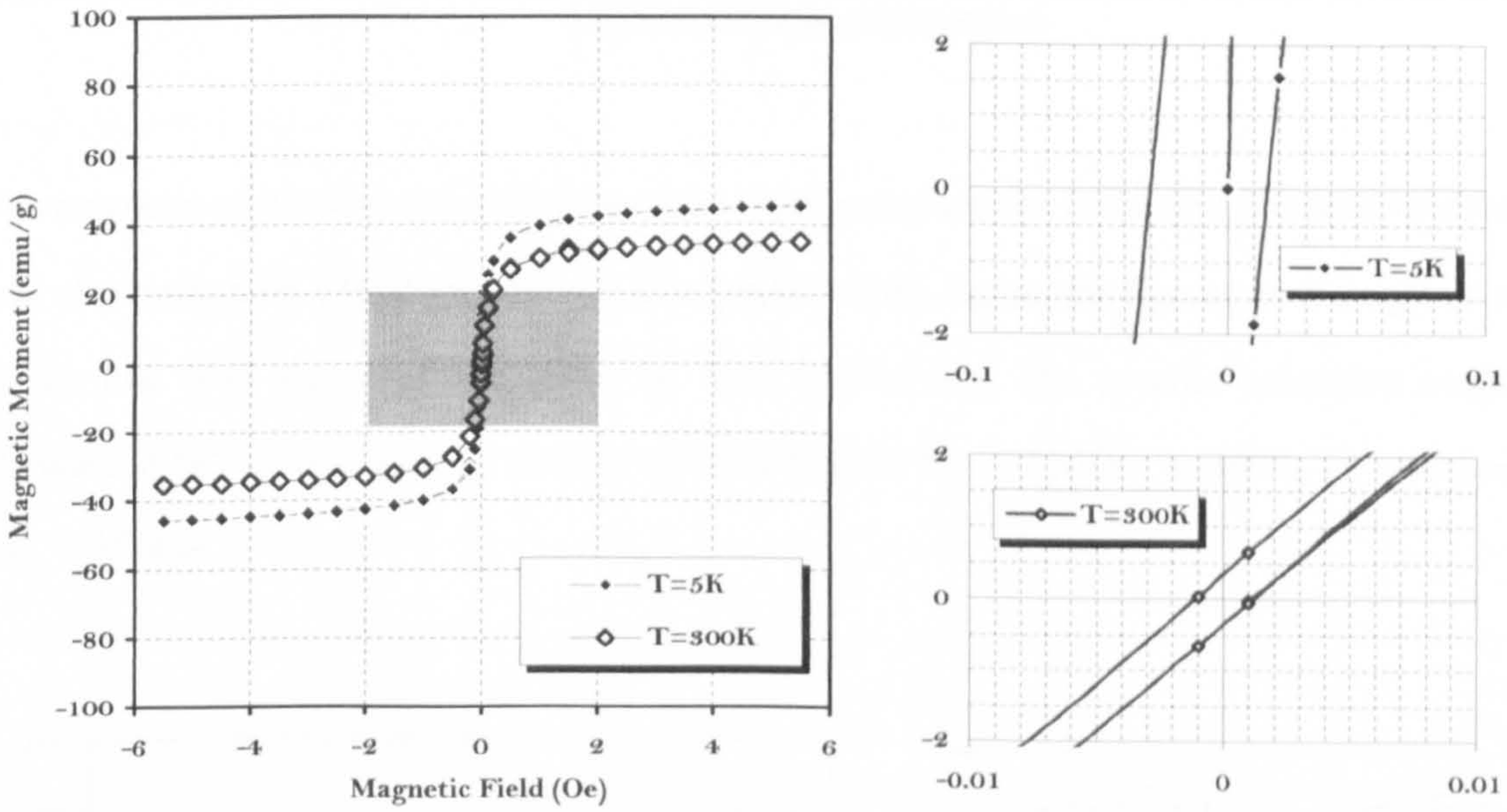

Figure 5.1-23 Magnetisation curve for iron oxide nanoparticles prepared via w/o microemulsion at different temperatures.

The figure on the left shows the full hysteresis curve between fields of -5.5 to +5.5 kOe. The figures on the right show details of the low field region of 300K and 5K data respectively. For this collection of iron oxide nanoparticles with an equivalent spherical diameter of 5 nm, the specific saturation magnetisation obtained at 5K, $\sigma_s = 45\, emu/g$ and the coercive field is $H_c = 400\text{Oe}$; at 300K, $\sigma_s = 35\, emu/g$ and $H_c = 20\text{Oe}$. **Figure 5.1-24** shows the temperature dependence of the saturation magnetisation below room temperature. The saturation magnetisation decreased smoothly with increasing temperature. The transition temperature is well above 350K, the maximum temperature employed in this experiments.

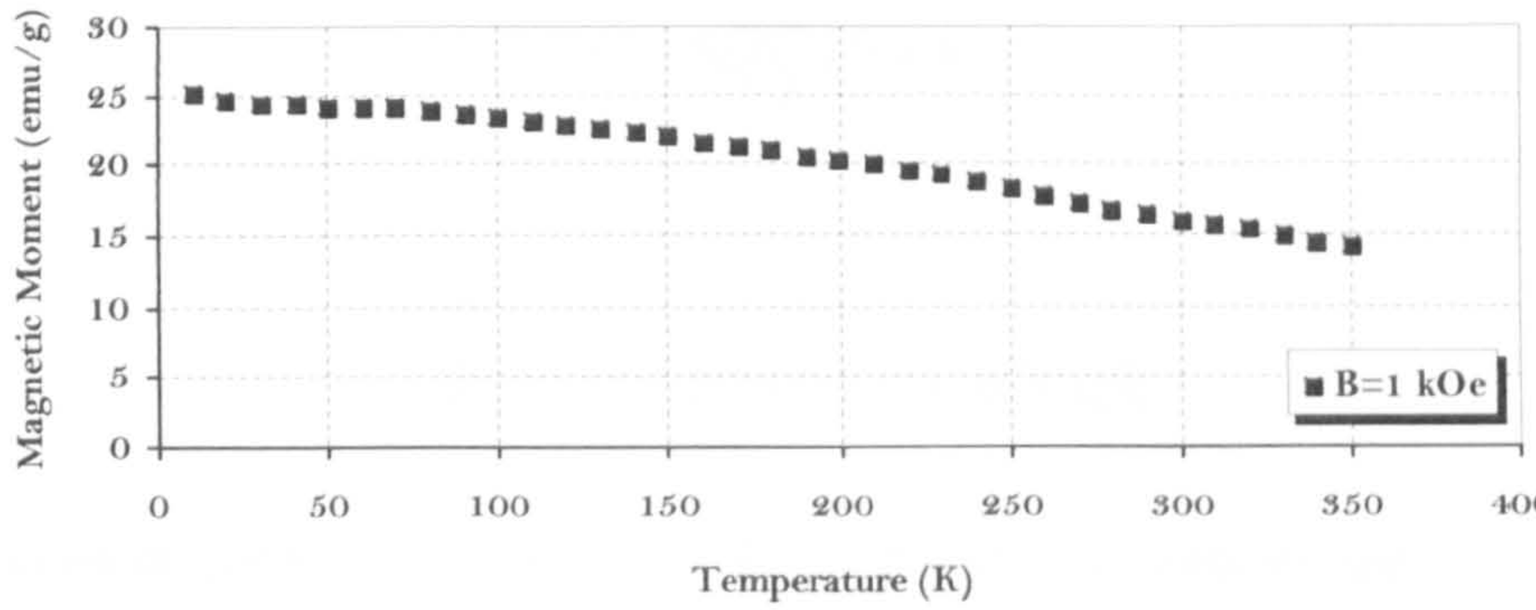

Figure 5.1-24 Field-cooled effect of the temperature variation of magnetisation measured at 1 kOe for iron oxide nanoparticles prepared via the w/o microemulsion.

The magnetic measurement for the larger iron oxide nanoparticles (5-20 nm) prepared by precipitation, was also made with a field scan of ±5.5 kOe **[Figure 5.1-25]**. Again, the figures on the right show details of the low field region of 300K and 5K data respectively. The specific saturation magnetisation obtained at 5K, $\sigma_s = 87\ emu/g$ and the coercive field is $H_c = 720\text{Oe}$; at 300K, $\sigma_s = 78\ emu/g$ and $H_c = 250\text{Oe}$.

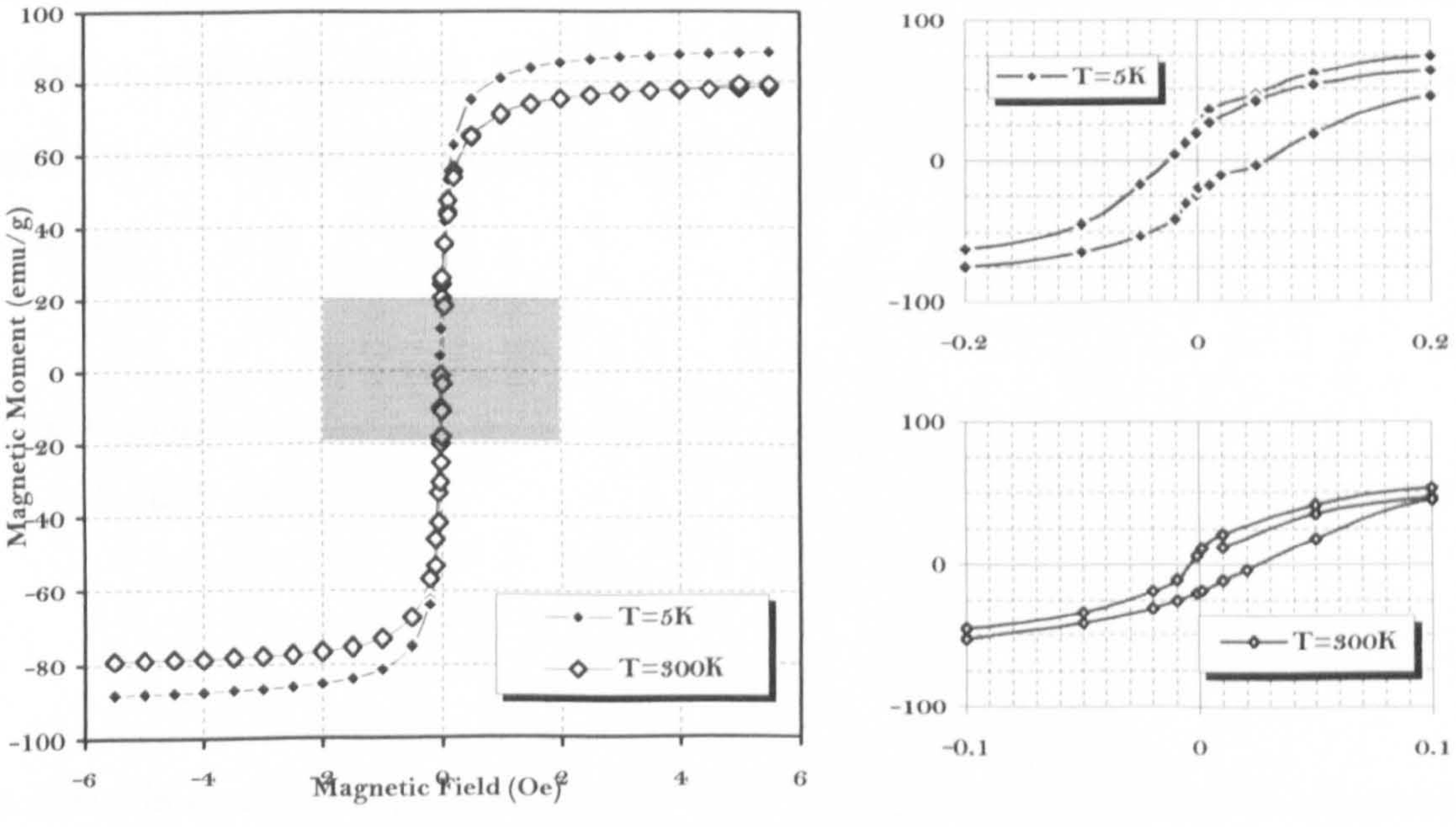

Figure 5.1-25 Magnetisation curve for iron oxide nanoparticles prepared by precipitation at different temperatures.

5.2 DISCUSSIONS

Nano-sized iron oxide particles were synthesised by precipitation methods and w/o microemulsion systems (Igepal CO-520/cyclohexane, Brij 97/cyclohexane). The samples prepared by two different methods exhibited the different morphologies and the different activities under the same heat-treatment conditions.

5.2.1 Investigation of reaction parameters by precipitation

The precipitation method was applied to prepare iron oxide nanoparticles, mainly because the reaction is the same as the reaction taking place in water pools in microemulsions. Compared to microemulsion synthesis, precipitation is simple and economical for characterisations. Therefore a large number of synthesis experiments were carried out using the precipitation method, in order to find out the effects of reaction parameters, such as the starting materials, ripening temperature and ripening time on the properties of iron oxide nanoparticles prepared. The basic reactions preparing iron oxide samples are as follows:

$$\left.\begin{array}{l} Fe^{2+} + OH^- \rightarrow Fe(OH)_2 \downarrow \rightarrow Fe(OH)_2 \downarrow + Fe(OH)_3 \downarrow \\ Fe^{3+} + OH^- \rightarrow Fe(OH)_3 \downarrow \end{array}\right\} \Rightarrow Fe(OH)_2 \downarrow + Fe(OH)_3 \downarrow$$
$$\Downarrow \qquad (5\text{-}1)$$
$$Fe_xO_y \cdot nH_2O$$

As shown in **Equation 5-1**, iron hydroxide is firstly precipitated from aqueous iron salt solutions then dehydrates into iron oxide. Although the precipitate is written as $Fe_xO_y \cdot nH_2O$, FeO(OH) might be a component sometimes [114]. As the different degree of oxidation, the final product is probably a

mixture of different iron oxides. For example, if the oxidising potential is insufficient to form higher oxidation products as hematite (α-Fe_2O_3) or maghemite (γ-Fe_2O_3), the reaction will produce magnetite (Fe_3O_4) which is a mixed oxide, $Fe^{2+}Fe^{3+}O_4$.

5.2.1.1 Effect of different starting materials

The effect of different starting materials on iron oxide nanoparticles was investigated through the different ratio of ferric ion $[Fe]^{3+}$ to ferrous ion $[Fe]^{2+}$ in starting iron salt solution. With the increase of the percentage of $[Fe]^{3+}$ in starting materials, the crystallinity of iron oxide samples synthesised was found to be depressed and the intensity of the major characteristic peak (311) decreased.

The mechanism existed in the reaction including $[Fe]^{3+}$ is different from the reaction without $[Fe]^{3+}$. One of the most conspicuous features of $[Fe]^{3+}$ in the aqueous solution is its tendency to hydrolyse forming complexes such as the hydrated ion $[Fe(H_2O)_6]^{3+}$. Even at pH 2-3, the extent of hydrolysis is significant [114], governed in its initial stages by the following equilibrium equations:

$$[Fe(H_2O)_6]^{3+} = [Fe(H_2O)_5(OH)]^{2+} + H^+ \quad \textbf{(5-2)}$$

$$[Fe(H_2O)_5(OH)]^{2+} = [Fe(H_2O)_4(OH)_2]^{+} + H^+ \quad \textbf{(5-3)}$$

$$2[Fe(H_2O)_6]^{3+} = [Fe(H_2O)_4(OH)_2 Fe(H_2O)_4]^{4+} + 2H^+ \quad \textbf{(5-4)}$$

At pH 4-5 the hydroxide species forms a dimer [179]:

$$2[Fe(H_2O)_5 \cdot OH]^{2+} \rightarrow \left[\begin{array}{ccc} & H & \\ & O & \\ \cdot^{\cdot^{\cdot}} & & \ddots \\ (H_2O)_4 \cdot Fe & & Fe \cdot (H_2O)_4 \\ \ddots & & \cdot^{\cdot^{\cdot}} \\ & O & \\ & H & \end{array}\right]^{4+} \quad \textbf{(5-5)}$$

The formation of the dimer above, with two OH groups, has been accepted for a long time. However, following the work of Knudsen [180], a linear Fe-O-Fe bridge seems more likely to be formed in the structure. As the pH is increased above 2-3, more highly condensed species than the di-nuclear one are formed, attainment of equilibrium becomes sluggish, and so colloidal gels are formed; ultimately, hydrous ferric oxide is precipitated out as a red-brown gelatinous mass [114].

According to the work of Matijevionć *et al.* [5], in addition to amorphous ferric hydroxides generated, the hydrous oxides also tend to crystallise either into α-FeOOH or into α-Fe_2O_3, depending on the ripening temperature. In this part of work, the reaction/ripening temperature employed was just 25°C, with 2-hour ripening. It seemed the temperature (25°C) was too low for ferric hydrous oxides to be transformed into the crystallised phase, therefore the sample prepared from pure ferric ion solution did not show any characteristic peaks in its X-Ray diffractogram.

If changing the percentage of ferric ion in starting materials, the content of amorphous hydroxide in final product would be changed. So, the presence of amorphous hydroxide might introduce a disturbance into the diffractogram of the whole sample. Hence, it was observed that the crystallinity of the iron oxide samples prepared by precipitation at 25°C, was improved with the decrease of the ferric ion content in the starting iron salt solution. However, the ripening time and temperature also played an important role in phase transition. Since the reactions were all carried out at 25°C for 2 hours, different starting materials did not result in any different phases in the iron oxide nanoparticles prepared by precipitation. Whatever starting materials were used, the final products were all magnetite.

5.2.1.2 Effect of ripening temperature

The formation of crystals is based on producing a super-saturated solution. There are different stages of the precipitation in solutions. Since each of the crystallisation stages is governed by several factors, the kinetics of the whole process is a function of these variables.

Generally, the time dependence of the concentration of the crystallising substance can be illustrated as

Figure 5.2-1 [181]. There are three stages involved: nucleation (ab), growth (bc) and re-crystallisation (cd). The concentration of the solution during the nucleation period remains practically constant. During period bc (a time interval τ_c-τ_b) the growth of crystals takes place. Finally, the third part of the curve, denoted by cd, represents slow re-crystallisation.

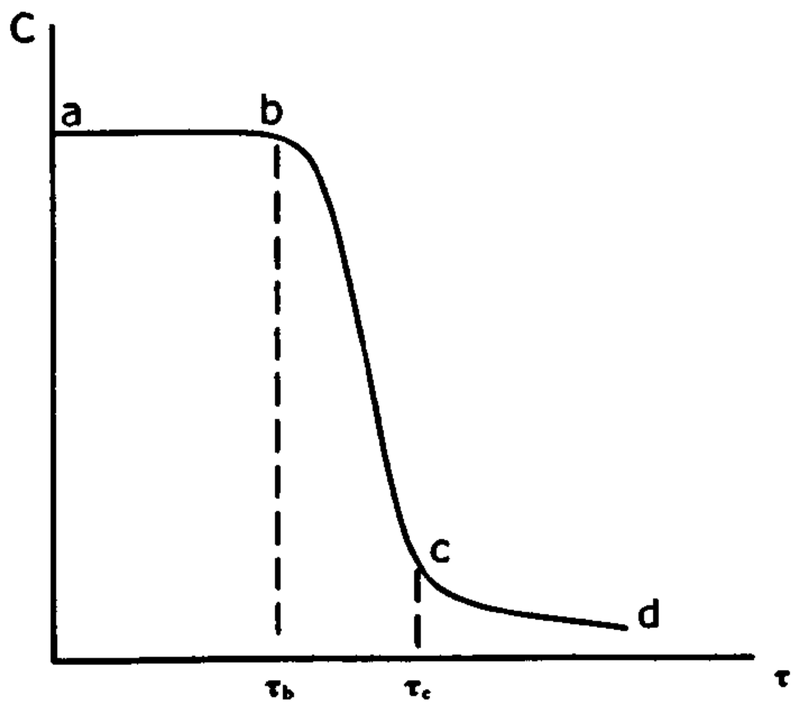

Figure 5.2-1 Dependence of the concentration of the crystallising substance on time.

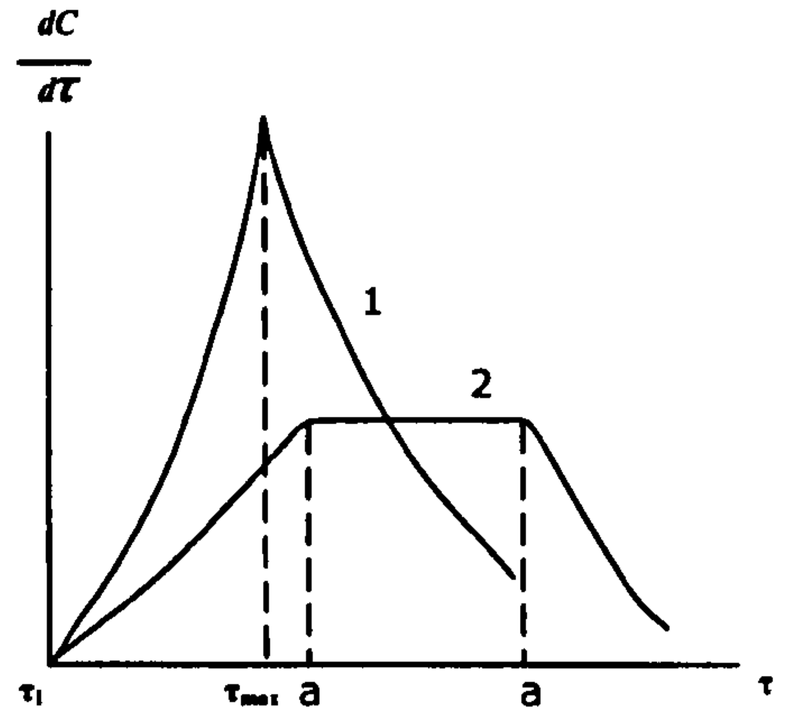

Figure 5.2-2 Dependence of the crystallisation rate on time:
[1]. at relatively high super-saturation;
[2]. at low super-saturation.

The duration of the nucleation period depends on the degree of super-saturation of a solution, the nature of the solute and the solvent, the vigour of stirring the solution, the presence of impurities [182]. Within the second period (b-c), the crystallisation rate may vary with the degree of super-saturation. **Figure 5.2-2** shows two types of curves which represent the dependence of the crystallisation rate on time. At low super-saturations the curve has a plateau where the crystallisation rate reaches its maximum value. At high super-saturations the rate has a maximum. When there is no residual super-saturation, the final stage of re-crystallisation of the precipitate takes place, which includes dissolution and crystallisation. Re-crystallisation of precipitates in saturated solutions, takes place due to the dynamic nature of the equilibrium between the liquid and solid phases [182]. The dissolution or re-deposition of crystals in saturated solution introduces a variable concentration layer near the surfaces of such crystals. Then diffusion of matter in solution will be promoted by the presence of such concentration gradient. Increasing the temperature will affect Brownian movement in solution and

consequently affect the rate of diffusion. According to the observation by Belopol'skii and Margolis [183], when the temperature is increased, not only does the crystallisation rate increase, but the value of $v_{c\text{-}max}$ (i.e. the maximum crystallisation rate), increases as well, and the time needed to reach this value decreased. Therefore, the particles grow up during bc; grow larger and homogenous during cd. The increase of temperature will reduce the duration of re-crystallisation period. The extent of super-saturation of the solution could affect the growth of particle size before the stage cd.

In our experiment, since the precipitation took place rapidly in 1~2 minutes after the addition of ammonia hydroxide, the first two stages of the crystallisation, (i.e. nucleation and growth), might be finished before the ripening treatment, and consequently the influence of ripening time and temperature on the crystallinity of the particles would be mainly controlled by the re-crystallisation stage. If the ripening time was restricted as 2 hours, the higher temperature applied could result in the further extent of re-crystallisation.

Hence, the increase of crystallinity of iron oxide nanoparticles with the increase of reaction/ripening temperature varied from 25°C to 90°C, was observed by the sharpening of the diffraction peaks. Although, there was no much difference in the particle size (~20 nm) observed in the TEM micrographs when being prepared with the different temperatures, the peak broadening of X-ray diffraction can be used to estimate the crystallite size in a direction perpendicular to the crystallographic plane, based on Scherrer's formula as follows [184]:

$$X_s = 0.9\lambda/(FWHM * \cos\theta) \qquad \textbf{(5-6)}$$

where X_s is the crystallite size (nm); λ the wavelength of monochromatic X-ray beam (nm) (λ=0.15406nm for CuKα radiation); FWHM the full width at half maximum for the diffraction peak under consideration (rad); and (°). The diffraction peak at 2θ = 35.4° (311) was chosen for calculation of the crystallite size since it is sharper . The calculated Xs for the iron oxide nanoparticles synthesised at different temperatures based on this diffraction peak using Scherrer's formula, are listed in **Table 5.2-1.**

Table 5.2-1 Effect of ripening temperature on the crystallite size and phase transition of iron oxide nanoparticles.

Ripening temperature	Crystallite size Xs [nm]	Identification
25°C	10.0	Magnetite
40°C	12.5	Magnetite
60°C	17.7	Magnetite
90°C	25.0	Magnetite

As shown in **Table 5.2-1**, the crystallite size increased with the increase of reaction/ripening temperature and the reaction at 90°C for 2 hours was insufficient with respect to oxidising potential to produce maghemite.

The reason for not increasing the reaction/ripening temperature any higher was in consideration in considering of the effect of such temperatures on the stability of a microemulsion system. The main purpose of using the precipitation method in the preparation of iron oxide nanoparticles, was to study the basic reaction parameters and make comparison between it and the microemulsion method, i.e. comparison of the traditional *vs*. novel. Therefore the reaction conditions for the precipitation method were restricted to these which could be applicable in the synthesis via a w/o microemulsion.

5.2.1.3 Effect of ripening time

The preparation of iron oxide nanoparticles was also investigated with different ripening times. Since by having the same starting materials and reaction conditions, but with the exception of the ripening time, the same kinetics in first two stages of crystallisation would be expected. The possible difference in the crystallisation at different ripening time was mainly attributed to the third stage, re-crystallisation.

The increase of crystallinity with the increase of the ripening time, was observed clearly from the sharpening and increased intensity of the diffraction peaks of the iron oxide samples. The phase transition from magnetite to maghemite, (i.e. higher oxidation status), appeared when the sample was prepared/ripened at 60°C followed by 24-hour aging, or prepared/ripened at 90°C with 12-hour aging.

It was found that the temperature seems a more determinative factor in terms of the phase transition, than the ripening time, i.e. it took the sample less time at higher temperature ripening (90°C) to complete the phase transition than at lower temperature ripening (60°C).

The tendency for a phase transition to overcome the energy required and reach equilibrium is driven by the Gibb's free energy, G. The Gibb's free energy comes from the enthalpy, *H* and entropy, *S* of reaction in the system, and ΔG has been defined in terms of enthalpy and entropy changes, ΔH and ΔS, and temperature T as:

$$\Delta G = \Delta H - T \cdot \Delta S \qquad \textbf{(5-7)}$$

From **Equation 5-7**, if ΔG is positive, the forward transition is blocked while the reverse transition is spontaneous; when ΔG is negative, the forward transition is promoted. Gibb's free energy, enthalpy, and entropy are state functions in thermodynamics and they are all the function of temperature. In considering the phase transition, increasing the temperature can result in the increase of entropy against the enthalpy of transition and consequently the decrease of ΔG, which would push the phase transition forward. Certainly, it takes time for the system to reach the new thermodynamic equilibrium driven by the Gibb's free energy. That is why we found in these experiments that, the increase of ripening time sometimes could result in a phase transition, for example, increasing the time of 60°C-ripening from 12 hours to 24 hours lead to the phase transition from magnetite to maghemite. If the temperature is too low, then the enthalpy of transition ΔH cannot be overcome, which would lead to a positive value of ΔG for the system. In this case, no phase transition will be observed. Therefore, when the temperature was as low as 25°C, there was no phase transition even with the ripening time increased from 2 hours to 24 hours

Table 5.2-2 Effect of reaction/ripening time on the crystallite size and phase transition of iron oxide nanoparticles.

Ripening time (h)	Crystallite size Xs [nm]			Identification		
	25°C	60°C	90°C	25°C	60°C	90°C
2	10.0	17.7	25.0	Magnetite	Magnetite	Magnetite
12	11.4	19.6	15.3	Magnetite	Magnetite	Maghemite
24	13.9	14.1	18.6	Magnetite	Maghemite	Maghemite

The crystallite sizes calculated from **Equation 5-7** as a function of ripening time are given in **Table 5.2-2**. The crystallite size generally increased with an increase of ripening time. The shaded size values refer to the different phase as maghemite. The crystalline behaviour as a function of ripening time can be explained by the mechanism of crystal growth in solution. Generally, re-crystallisation produced larger crystals because small particles were dissolved and re-deposited on the surfaces of larger crystals. This process of particle coarsening was called "Ostwald ripening" [185-186]. So increasing the ripening time could result in the growth of crystals.

5.2.2 Synthesis of nano-magnets via w/o microemulsions

Igepal CO-520/cyclohexane and Brij 97/cyclohexane were selected to form two different w/o microemulsion systems for the synthesis of iron oxide nanoparticles. The latter was mainly employed for higher temperature (60°C) reactions. According to the research of Santra *et al.* [23], although there was no major difference in particle morphology observed by using strong base or mild base, the total ionic strength of the water pool increased in the presence of a large amount of strong base, which will have introduced instability of the microemulsion system [23]. That is one of the reasons why a mild base, $NH_3 \cdot H_2O$, was chosen to prepare iron oxide rather than other alkaline-based hydroxides. The other reason is the nature of the by-product formed, NH_4Cl, which could be simply removed by washing with de-ionised water.

Regarding the application in synthesis, w/o microemulsion systems are featured by the water pools, which are spherical in shape. The surfactant molecules constructing a wall surround these nano-sized water-droplets. These walls act as cages for the growing particles and thereby reduce the average size of the particles during the collision and aggregation. That is why the microemulsion method has become a powerful tool to produce sub-micro particles, especially nanoparticles, in recent years.

As shown in **Figure 5.2-3**, the reaction was initiated by adding of the ammonia solution into the microemulsion system; after the second aqueous phase, $NH_3 \cdot H_2O$ passing through the surfactant wall,

reagents rapidly mixed followed by a precipitation reaction.

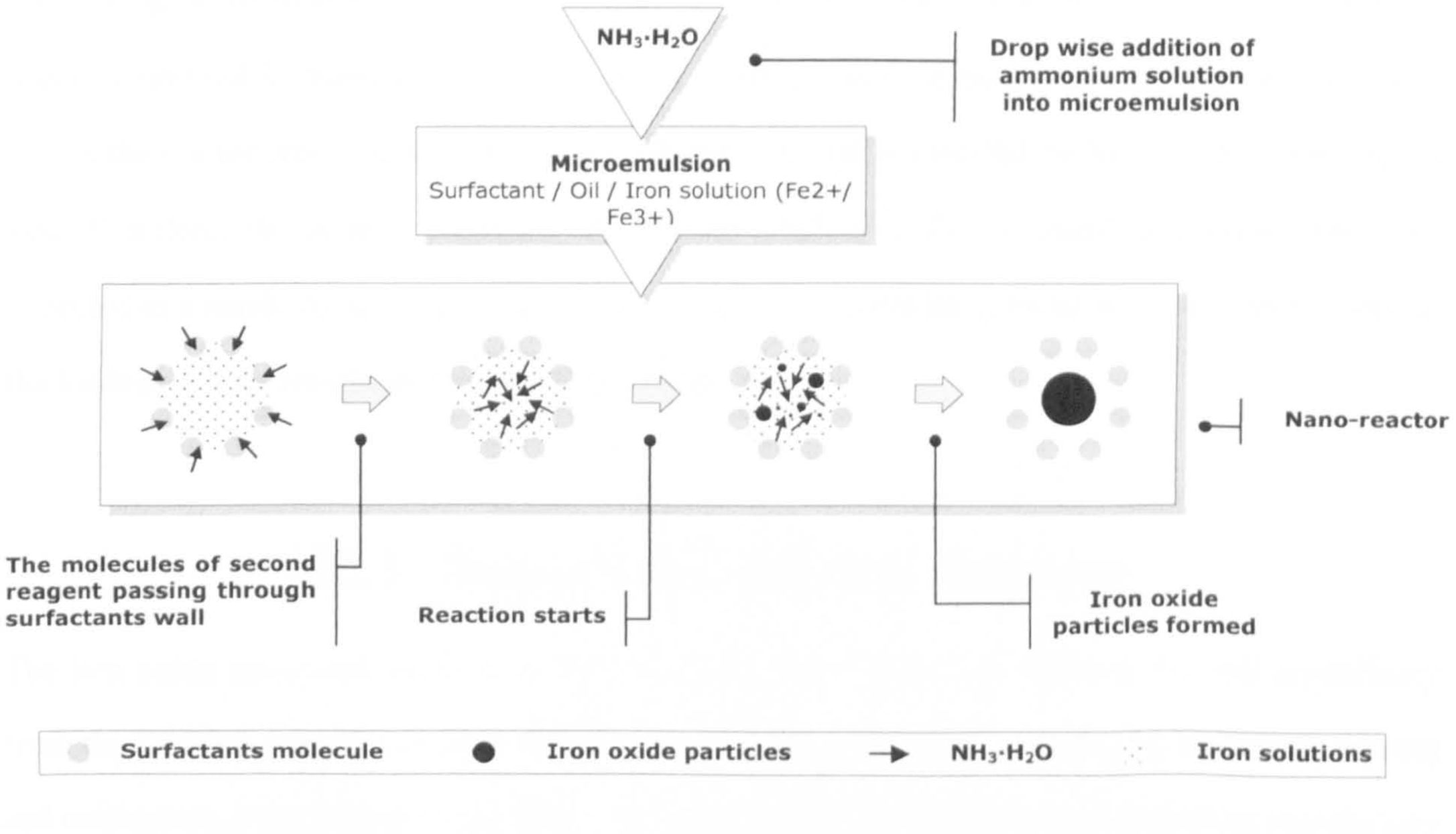

Figure 5.2-3 Schematics of procedure in synthesis of iron oxide nanoparticles via w/o microemulsions.

The reaction in the microemulsion is the same mechanism as in the precipitation method. Only one difference is that the reaction via w/o microemulsions, takes place in individual water pools rather than in a bulk phase. The advantage of the restricted environment in microemulsion is that, the iron oxide nanoparticles prepared from w/o microemulsion could be smaller than those by precipitation. That was in agreement with the results here, i.e. the size of particles prepared from microemulsion was about 5 nm, smaller than the size of particles prepared by precipitation, i.e. 20 nm. Moreover, the latter showed poly-dispersity in size distribution but the former were all mono-dispersed nanoparticles. However, the crystallinity of microemulsion-derived iron oxide nanoparticles was not as good as precipitation-derived samples, although the characteristic peaks **(311)**, **(440)** were still identified. The noisy XRD pattern of microemulsion sample is probably due both to poor crystallised materials and ultra small crystalline materials, where diffraction peaks cannot be well resolved.

The micrographs of diffraction pattern showed that the crystallinity of microemulsion-derived iron oxide nanoparticles increased with the increase of reaction/ripening temperature and the increase of the loading of the aqueous phase. As discussed in previous section **5.2**, the increase of the aqueous phase solubilised in microemulsion could result in the increase of the capacity of water pools, which means the reactor grows larger, hence there will be more space provided for the growth of particles *in situ*. Therefore, the increased particle size accompanied with the increased crystallinity could be expected as a result. In our experiment, the iron oxide nanoparticles grew from 1 nm to over 5 nm, as the loading of aqueous phase increased from 2% to 10%.

5.2.3 Investigations of post-heat-treatments

The iron oxide nanoparticles prepared via w/o microemulsion showed different size and crystallinity from the particles prepared by precipitation. The post-heat-treatment, including hydrothermal process and calcination, were employed for further investigation of the effect of heat-treatment on morphology and crystallinity or iron oxide nanoparticles. Especially in the studies of hydrothermal process, the difference between iron oxide samples prepared by different methods was amplified, which suggested the size-dependent properties of nanoparticles.

5.2.3.1 Hydrothermal process

Hydrothermal process is using aqueous solvents under high pressure and relative low temperature, (compared to the melting point of the material), to dissolve and re-crystallise materials which are relatively difficult to grow under ordinary conditions [53]. The high pressure and relatively high temperature attributed to the hydrothermal process result in rapid convection and very efficient solute exchange, which encourage comparatively rapid growth of larger, purer and dislocation free crystals. Hence, when the hydrothermal system reaches its saturated point, fine particles, e.g. iron oxide, start to dissolve in the solvent (i.e. de-ionised water) and form a saturated solution. This saturated solution then moves to the upper region due to convection currents induced by the temperature gradient. In the upper region the nanoparticles grow by the deposition of the material as the solubility in the upper

region is lower due to low temperature conditions. Thus, the gradient of temperature and solute concentration in whole system results in a loop current and promotes the particle growth [53].

The discussion included the effect of hydrothermal temperature and aging time on the crystallinity of the iron oxide nanoparticles. However, the aging time does not affect the crystallisation rate, but is an important factor whose change leads to different crystallisation states [182].

- **Effect of aging temperature**

Different aging temperatures affect both the rates of solute of dissolving and aggregating in autoclave. Consequently it affects the crystallinity and morphology of the final product. From the TEM micrographs, it could be seen that iron oxide nanoparticles prepared by both microemulsion and precipitation were shown to be growing in size after hydrothermal process at different aging temperatures for 12 hours. The higher aging temperature could result in the larger particle size. The precipitation-derived particles grew from the original 5-20 nm to 20-30 nm after 120°C aging, and then to 20-180 nm after 200°C aging. Although, the homogeneity of particles from precipitation increased with the particle growth after the hydrothermal process, some huge particles (180 nm), appeared as well as the small ones (20 nm), when the aging temperature was 200°C. As for microemulsion-derived particles with the original size of 5 nm, increased to 5-10 nm after 120°C aging and to 60 nm after 200°C aging. Comparing with the precipitation samples, the homogeneity of microemulsion samples were maintained, whatever the aging temperature was.

Since the use of a closed system increasing the hydrothermal temperature, basically leads to the increase of pressure inside and the super-saturation of the solution, resulting in the growth of particles. The difference in the temperature effect on the particle size, for samples derived from different methods could be explained by the mechanism of Ostwald ripening, which is based on the fact that the equilibrium solute concentration with a particle of radius r, increases as r decreases in agreement with the Thompson Freundlich equation:

$$C_s(r) = C_s \exp\frac{2\gamma V_m}{RTr} \quad \textbf{(5-8)}$$

where γ is the surface tension of solid-solvent and V_m is the molar volume of the solute molecules in the solid. As shown in **Figure 5.2-4**, when a solution comprises a distribution of particles with different sizes, a small particle of radius r_s has a higher equilibrium solute concentration C_s than a larger particle with radius $r_l > r_s$. A solute gradient concentration establishes in the liquid so that this solute undertakes a diffusion flow from the smaller towards the larger particles. This process keeps going on as long as the dissolution kinetics of the smaller remaining particles is significant. Due to the poly-dispersed size distribution in iron oxide nanoparticles prepared by precipitation method, some big particles might exist in the original samples accompanied with some ultra small ones. After the hydrothermal process, the ultra small particles were "eaten" by the bigger particles. In addition to the medium-sized particles growth and grow homogeneity, some big particles will grow even larger. However, since the microemulsion-derived particles has the narrow size-distribution, so there was no size-variation observed in the after-hydrothermal samples.

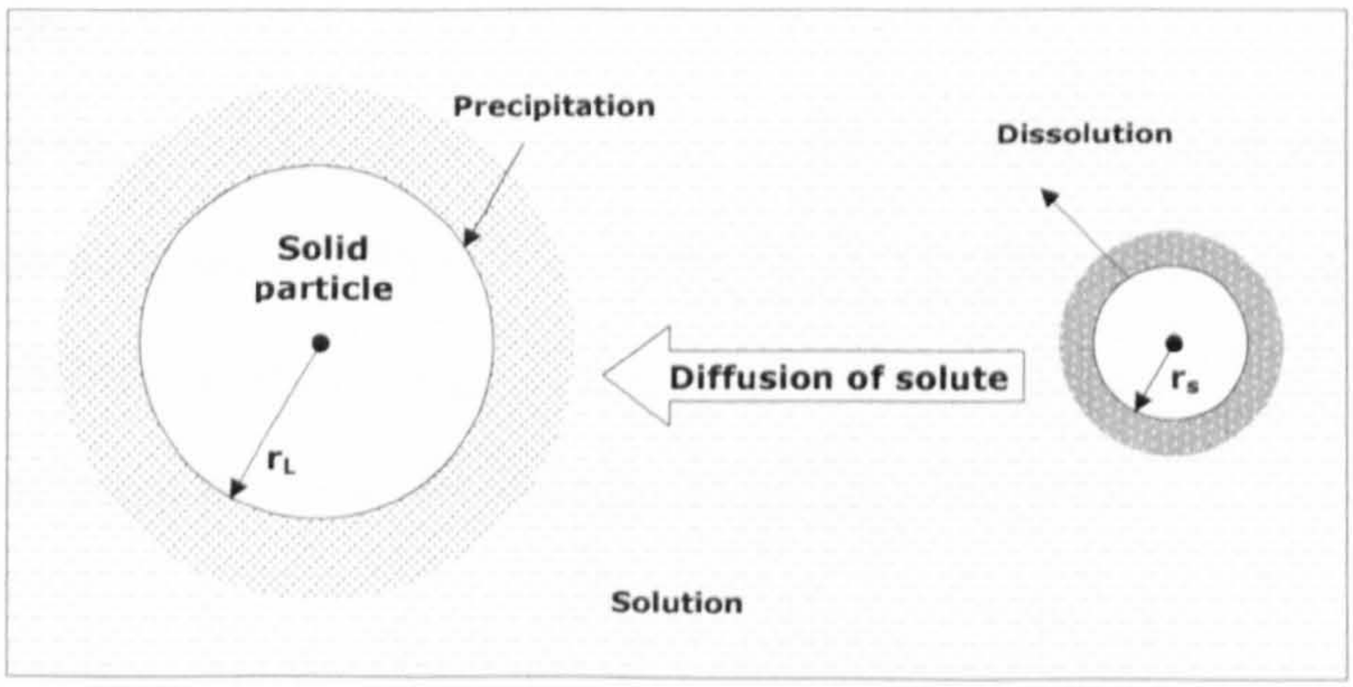

Figure 5.2-4 Schematics of the mechanism of Ostwald ripening

The crystallite size calculated by **Equation 5-7** and the phase transition as a function of hydrothermal temperature, are given in **Table 5.2-3**. The size of crystallite also increased with the increase of aging temperature. Both the precipitation particles and the microemulsion particles transformed into

Table 5.2-3 Effect of hydrothermal temperature on the crystallite size and phase transition of iron oxide nanoparticles.

Temperature	Precipitation-derived particles		Microemulsion-derived particles	
	Crystallite Size X_s [nm]	Identification	Crystallite Size X_s [nm]	Identification
Before	10.0	Magnetite	/	Magnetite
120°C	12.0	Maghemite	10.4	Maghemite
140°C	15.0	Maghemite	14.4	Hematite
160°C	14.6	Maghemite + Hematite	18.1	Hematite
200°C	26.9	Hematite	21.7	Hematite

the complete oxidation phase, hematite, after 200°C hydrothermal process with 12 hours. However, this transition took place with microemulsion-derived particles at a lower temperature (140°C), than with the precipitation-derived particles, i.e. at 200°C, presumably because the particles synthesised by microemulsion have smaller particle size and so larger surface area, resulting in increased chemical reactivity [27]. It should be mentioned that, the size-gap observed from precipitation sample was a temporary phenomenon. If the aging time could be prolonged, the particles would be expected grow to mono-size finally.

- **Effect of aging time**

The effect of aging time was investigated for iron oxide nanoparticles prepared by precipitation followed by hydrothermal process at 120°C for different periods. Both the micrographs of diffraction patterns and X-ray diffractograms show an increase in crystallinity of particles, with increase of aging time. The intensity of the main characteristic peak (311) increased as well.

In terms of the morphology, TEM micrographs showed that the particles grew homogeneous with increase of aging time. Although there was no much growth in particle size as the time varied from 2 hour to 96 hours, the average size increased from 5 nm to 30 nm. Hence, the major effect of increasing aging temperature, probably is to encourage the particles growth and the major effect of increasing aging time, probably is to render the particles into mono-size.

Table 5.2-3 Effect of hydrothermal time at 120°C on the crystallite size and phase transition of iron oxide nanoparticles prepared by precipitation.

Time [Hour]	Precipitation-derived particles	
	Crystallite Size X_s [nm]	Identification
Before	10.0	Magnetite
2	8.03	Maghemite
12	12.0	Maghemite
24	14.5	Maghemite
96	24.1	Maghemite

Table 5.2-3 gives the effect of aging time on the crystallite size and phase transition of iron oxide nanoparticles prepared by precipitation. The increase of aging time led to the growth of crystals. The hydrothermal process not only affects the morphology of nanoparticles, but also, in some cases, encourages the oxidation of compounds by attracting oxygen into solutions. As shown in **Table 5.2-3**, the nanoparticles transformed from magnetite into maghemite after the heat-treatment, but there was no further phase transition happened as the aging time varied from 2 hours to 96 hours, i.e. the prolonged time at 120°C aging did not change the degree of oxidation transforming ferrous ions completely into ferric ions. The oxidising potential was possibly insufficient as the time varied from 2 to 96 hours.

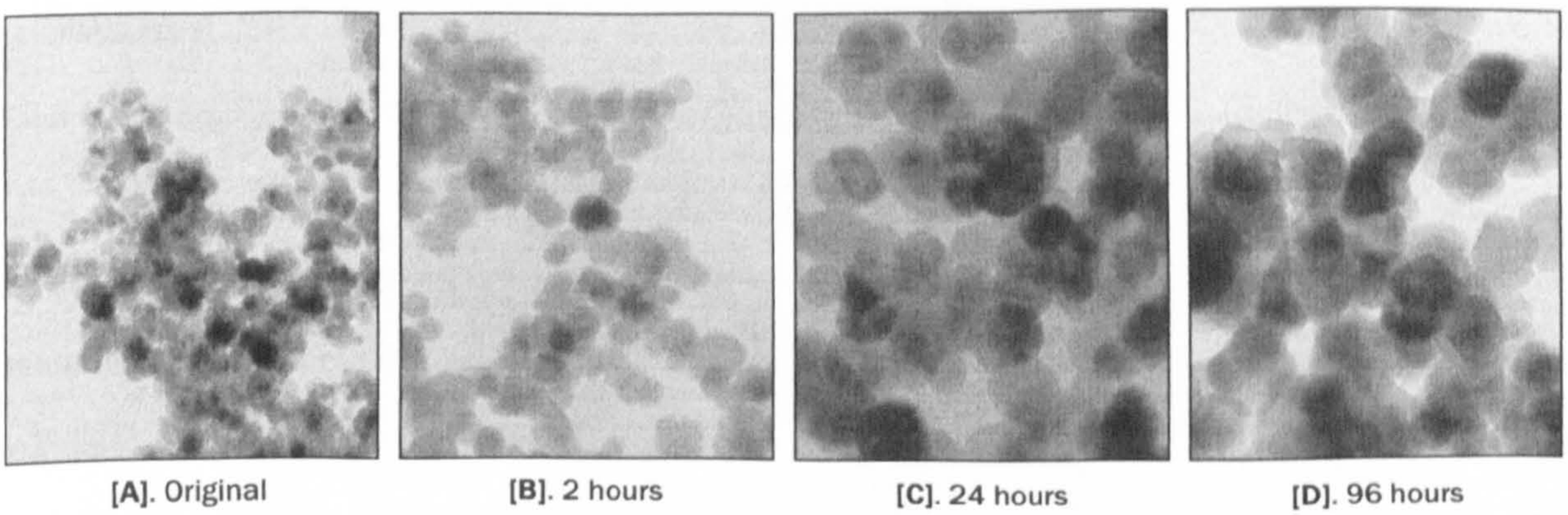

[A]. Original **[B]**. 2 hours **[C]**. 24 hours **[D]**. 96 hours

Figure 5.2-5 TEM micrographs of iron oxide nanoparticles prepared by precipitation after hydrothermal at 120°C with different aging times.

Despite of the change in particle's dimension and size-distribution, the shape of iron oxide nanoparticles underwent a significant change as well. As shown in **Figure 5.2-5**, before the hydrothermal process, particles were spherical. After 2 hours, some rectangular particle formed. When aged for 24 hours, the particles were more like hexagon. Finally they turned into diamond shape with 96 hours.

The shape change of crystals indicated the dependence of the growth rate on the crystallographic direction. There appears to be structural reasons for facilitating growth in a certain preferred direction [128]. When these tendencies are present, rapid growth appears to accentuate the differences between the preferred and other directions. It needs a relative long period to have the difference between growth rate in different directions to take effect. The phenomenon was observed are a rather long investigation time period. The same anisotropic growth could happen in the synthesis of nanoparticles via microemulsion. That is because the preferential surfactant adsorption restricts the side-ways interconnection of the particles and allows a further aggregation process in an ordered fashion [36].

5.2.3.2 Calcination

Calcination was applied in experiment to study the crystallinity and phase transition of iron oxide nanoparticles. It was found that the extent of oxidation of samples was improved with the increase of calcination temperature, i.e. the iron oxide transformed from magnetite to maghemite after calcinations at 250°C for 2 hours and to hematite after calcinations at 450°C for 2 hours. As shown in **Table 5.2-4**, the crystallite size also grew with the increase of temperature.

As discussed at the beginning of **5.2**, different starting materials could affect the crystallinity of iron oxide nanoparticles prepared by precipitation at 25°C. The decrease content of $[Fe]^{3+}$ in the starting solutions lead to the increased crystallinity of the final products. **Table 5.2-5** gives the calculated crystallite size of iron oxide nanoparticles prepared with different starting materials, before and after calcination at 300°C and accompanied phase transition details. It was found that the treatment by calcination resulted in the growth of crystal in all the iron oxide samples. Iron oxide nanoparticles

transformed into different phases after calcination at 300°C, presumably due to the effect of the choice of starting materials. Although they were all identified as magnetite as prepared, except amorphous products from pure ferric ion, it is assumed that the content of ferric ions and ferrous ions in the solid would be different, which was attributed to the starting stage. As a result, the oxidising potential needed to accomplish the phase transition to a higher oxidation state could be perhaps different for individual samples. Therefore, 300°C calcination resulted in different iron oxide phases, samples prepared from different starting materials.

Table 5.2-4 Effect of calcination temperature on the crystallite size and phase transition of iron oxide nanoparticles prepared by precipitation at 25°C for 2 hours.

Temperature [°C]	Crystallite Size X_s [nm]	Identification
Before	10.0	Magnetite
140	10.8	Magnetite
200	12.0	Magnetite
250	13.6	Maghemite
300	15.5	Maghemite
400	19.7	Maghemite
450	31.0	Hematite
500	43.4	Hematite

Table 5.2-5 Effect of 300°C calcination on the crystallite size and phase transition of iron oxide nanoparticles prepared by precipitation with different starting materials at 25°C.

$[Fe]^{3+}$: $[Fe]^{2+}$ [mol/mol]	Crystallite size X_s [nm]		Identification	
	Before	After	Before	After
$[Fe]^{2+}$	18.7	50.0	Magnetite	Maghemite
1:2	15.4	48.7	Magnetite	Hematite
1:1	12.5	17.7	Magnetite	Magnetite
2:1	10.0	15.5	Magnetite	Maghemite
$[Fe]^{3+}$	/	6.2	Amorphous	Hematite

SUMMARY

The precipitation method was employed accompanied with w/o microemulsion to investigate the synthesis of iron oxide nanoparticles. It was found that: different molar ratio of ferric ion to ferrous ion in starting iron salt solution could result in magnetite products, but having with different crystallinity. As the reaction/ripening was temperature varied from 25°C to 90°C, the products were all found to be magnetite for a 2-hour reaction. The increase of time and temperature both could introduce the phase transition from magnetite to maghemite. The higher temperature applied, the shorter ripening time needed to produce maghemite nanoparticles.

The size of iron oxide particles obtained by the w/o microemulsion method was smaller (1-5nm) than that prepared by precipitation (~20nm). After the hydrothermal process, the nanoparticles from both methods grew larger, meanwhile the microemulsion-derived particles maintained homogeneity. The increase of hydrothermal temperature improved the oxidation of iron oxide samples. The transition temperature from maghemite to hematite of samples prepared by w/o microemulsion (140°C), was lower than samples by precipitation (200°C). Different calcination temperature resulted in different phase of iron oxide. When being calcined at 300°C, the magnetite samples prepared from different starting materials transformed into different iron oxide phase.

Due to the smaller size and narrower size-distribution, microemulsion-derived iron oxide nanoparticles exhibited lower saturation magnetisation and coercivity compared with precipitation-derived samples.

6 POLYMERISATION IN W/O MICROEMULSIONS

6.1 PREPARATION OF POLYMER NANO-SPHERES

The heat-initiated polymerisation of acrylamide (AM) and methacrylicacid (MAA) were carried out in Brij 97/cyclohexane and Triton X-114/cyclohexane w/o microemulsion systems, respectively. The investigation of microemulsion polymerisation included the influence of different reaction conditions, different concentrations of reagents (i.e. KPS, crosslinking agent, monomers), and the microemulsion-dependent factors (i.e. ω_0, surfactant concentration).

6.1.1 Acrylamide partitioning in oil and water

The partitioning of AM in oil and water was investigated at room temperature (25°C). As shown in **Table 6.1-1**, 95.5% of AM was soluble in de-ionised water (i.e. water phase), and only 4.5% of AM was soluble in cyclohexane (i.e. oil phase). The solubility values indicated that, AM monomers preferred to "stay" in the water phase rather than in the oil phase of the w/o microemulsion system at 25°C. However, because of its amphiphilic property (soluble in both oil and water), most of AM monomers would be located near the interface of oil/water but not the core of micelles.

Table 6.1-1 Partitioning of AM in oil and de-ionised water at 25°C

Solubility in cyclohexane [wt%]	Solubility in de-ionised water [wt%]
4.5	95.5

6.1.2 Studies on different surfactants

According to the investigation of w/o microemulsions, the Brij 97/cyclohexane system exhibited the higher extent of water solubilisation and the better stability when the reaction temperature was above 30°C, so it could be an appropriate system to undergo the AM polymerisation. In order to find out the suitable w/o system, it is still necessary to compare the different surfactants in terms of the microemulsion polymerisation of AM. As shown in **Table 6.1-2**, the conversion of AM polymerisation was affected by different surfactants. A nearly 100% conversion was obtained in Brij 97 system and Tween 85 system. However, the conversion of AM polymerisation in Igepal CO-520/cyclohexane system and Triton X-114/cyclohexane system were about 86.5% and 80.2%, respectively.

Table 6.1-2 The molecular weight of PAM prepared via w/o microemulsion system

Surfactant used in system	Brij 97	Tween 85	Igepal CO-520	Triton X-114
Conversion [%]	99.4	98.6	86.5	80.2
Molecular weight [x10^5 g/mol]	4.20	3.86	3.74	2.40

The molecular weight *vs.* surfactant exhibited the similar trend as conversion *vs.* surfactant **[Table 6.1-2]**. The molecular weight of polyacrylamide (PAM) synthesised from Triton X-114/cyclohexane system was 2.40×10^5 g/mol, which was the lowest value compared with others. The comparably highest molecular weight of PAM, 4.20×10^5 g/mol, was obtained from the polymerisation via Brij 97/cyclohexane w/o microemulsion system.

Figure 6.1-1 shows TEM micrographs of PAM prepared via microemulsion with different surfactants. The spherical morphology of PAM particles was clearly observed in the sample prepared from Brij 97 system. The size was 80-100 nm **[Figure 6.1-1 A]**. The morphology observed in the samples prepared from Tween 85/cyclohexane system and Igepal system looked more like the swelling results from small PAM particles **[Figure 6.1-1 B, C]**. Some huge PAM spheres (> 1 μm) were observed in the sample prepared in Triton X-114/cyclohexane system **[Figure 6.1-1 D]**. Hence, Brij 97/cyclohexane seemed the

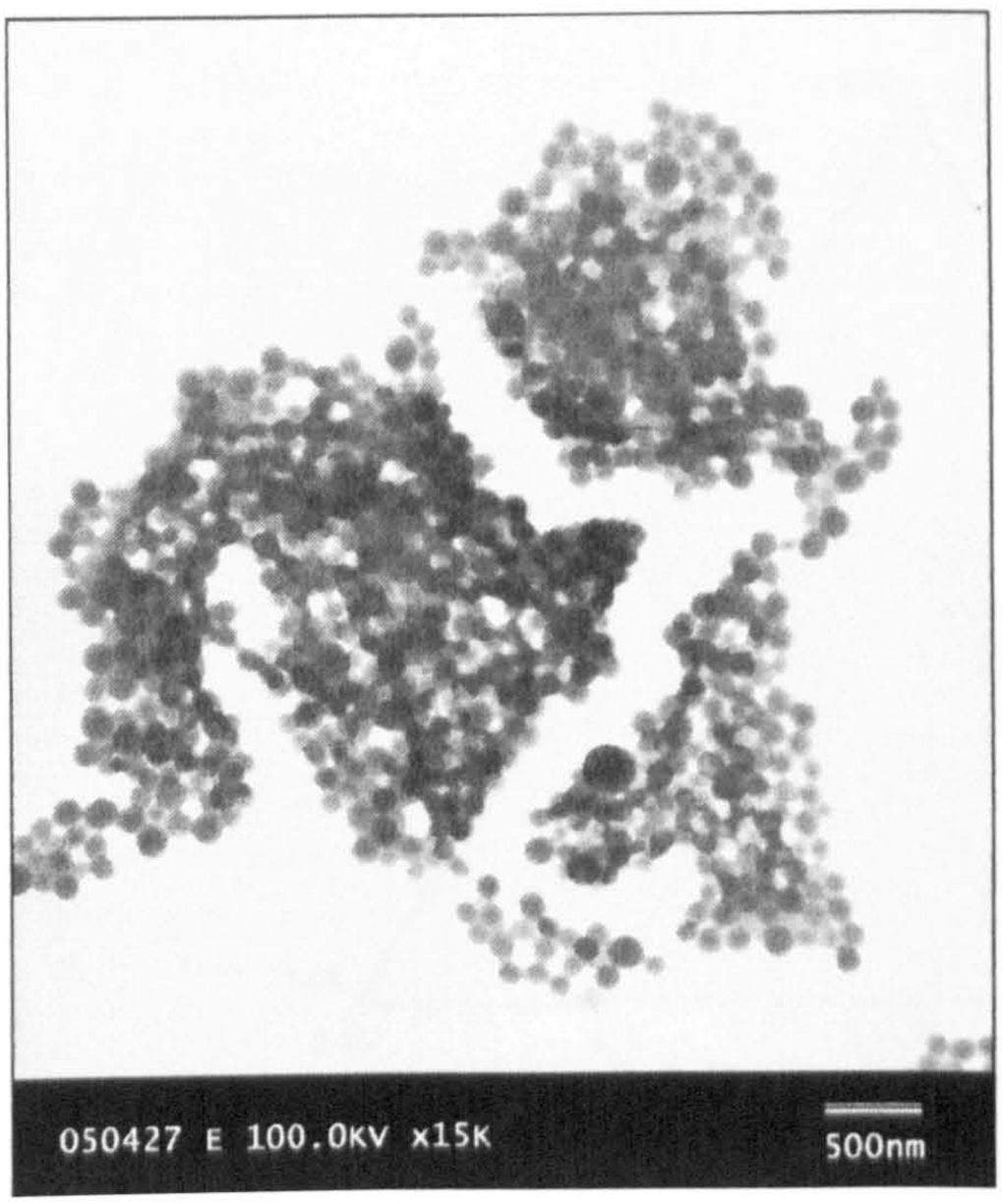

[A] Brij 97

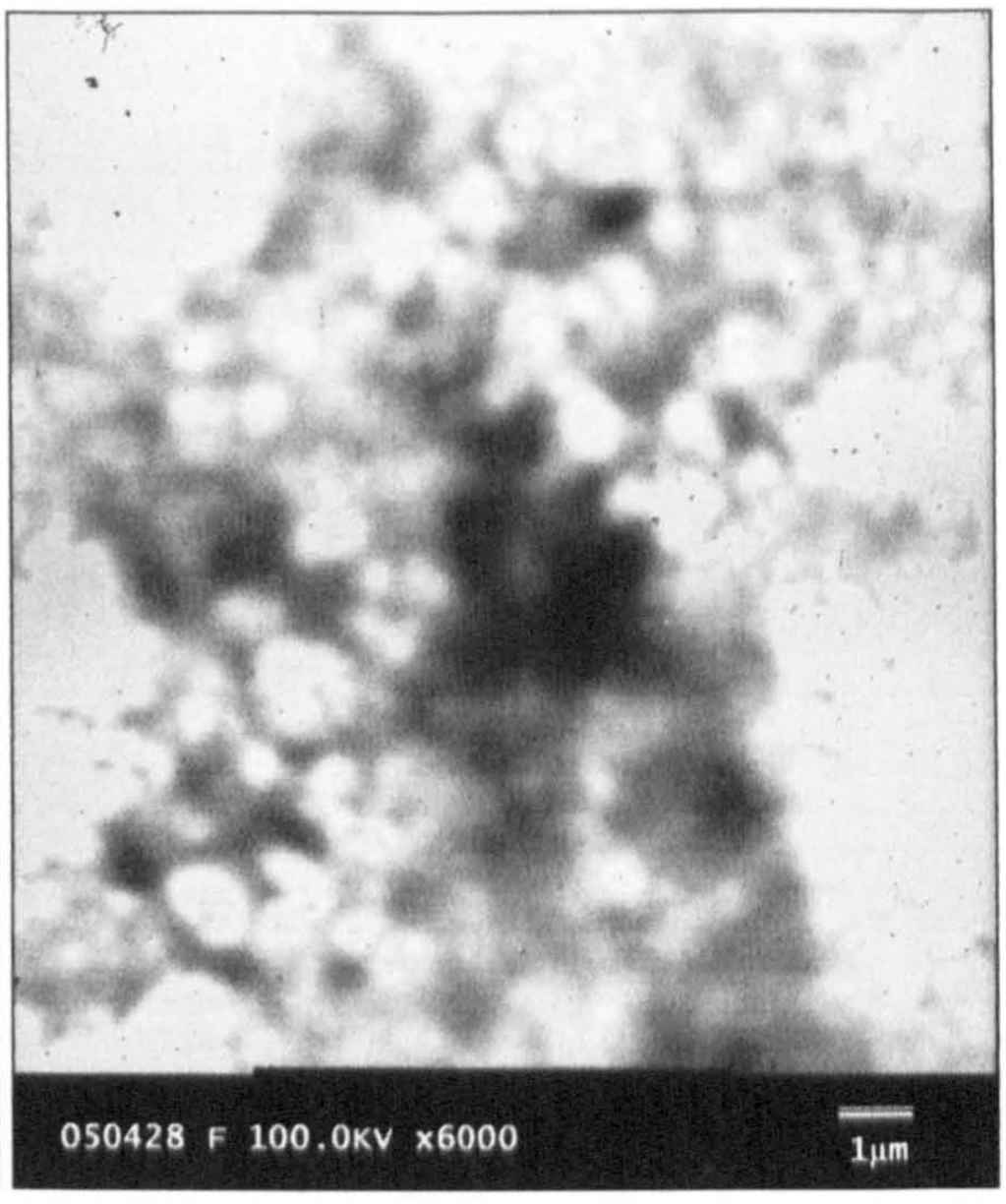

[B] Tween 85

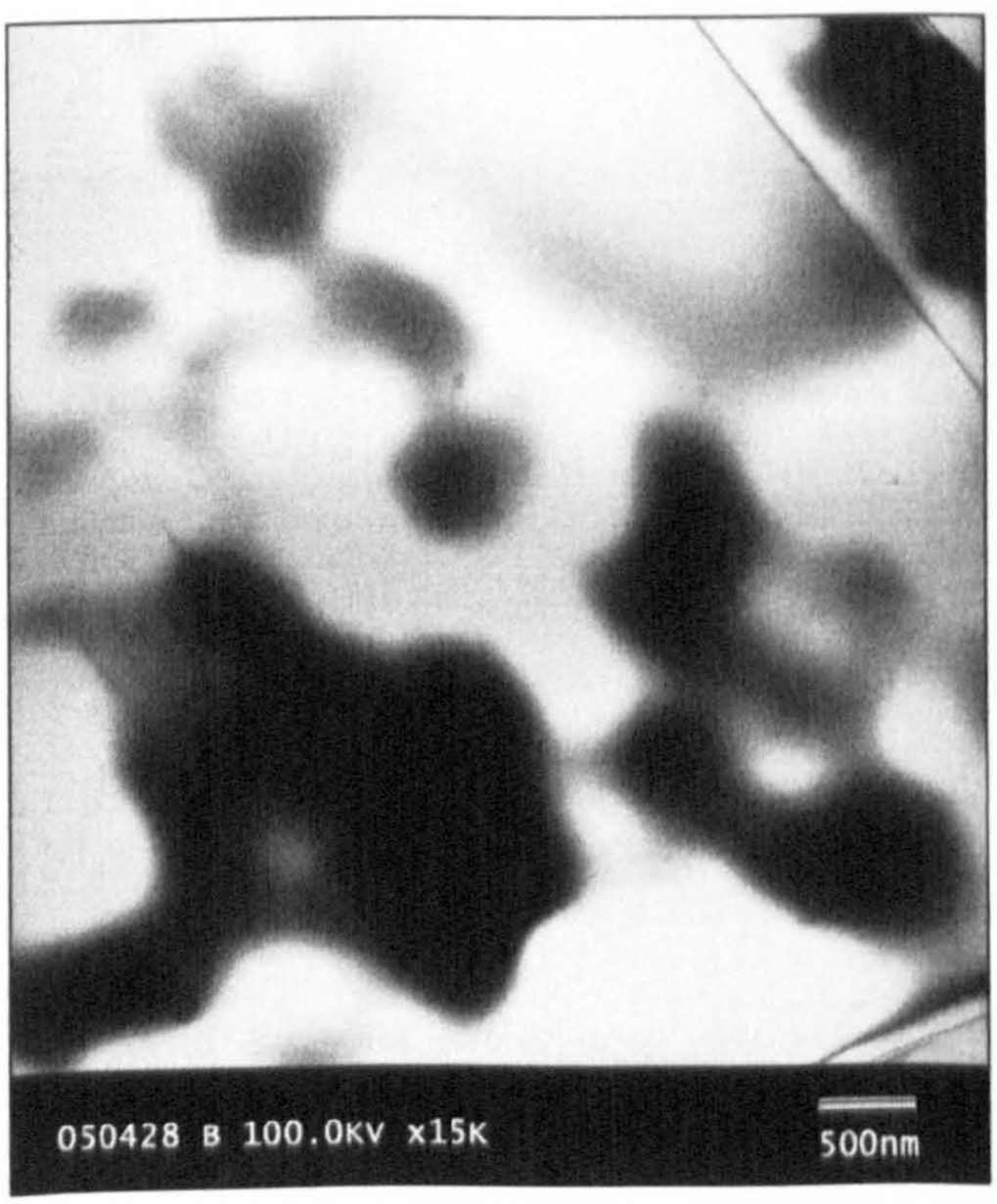

[C] Igepal CO-520

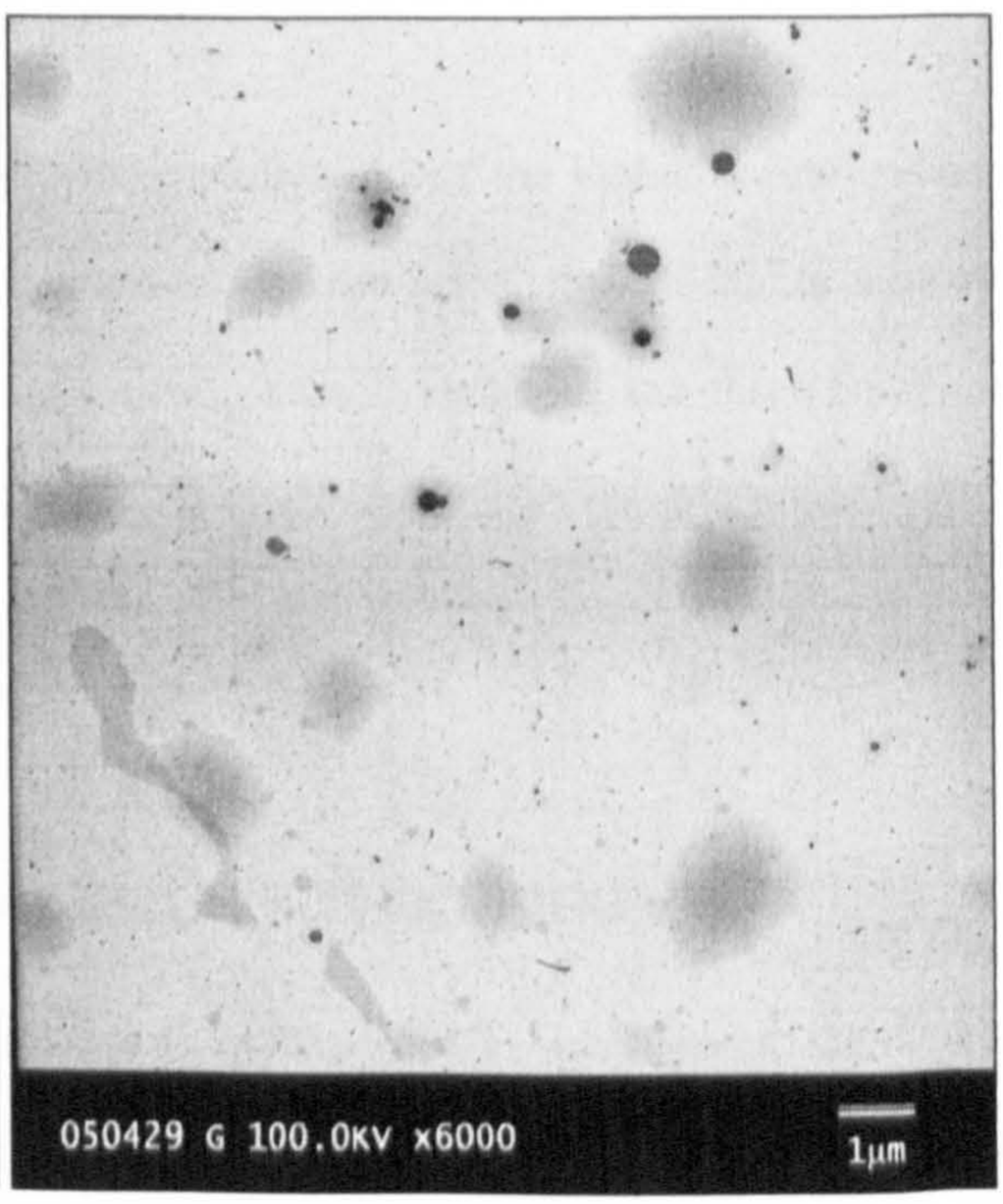

[D] Triton X-114

Figure 6.1-1 TEM micrographs of PAM nano-spheres polymerised via different w/o microemulsion systems at 60°C for 6 hours.

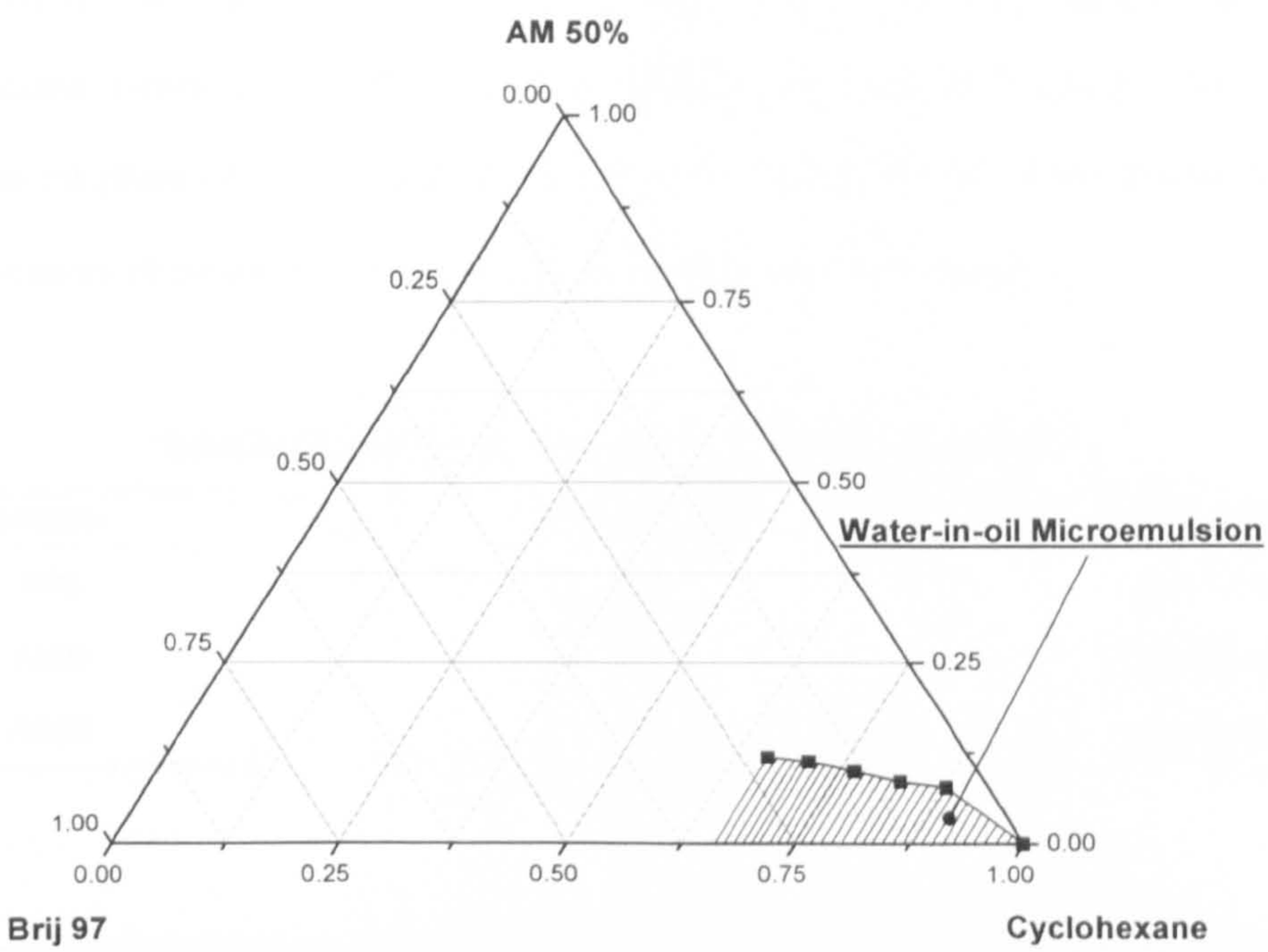

Figure 6.1-2 Phase diagram of w/o microemulsion system: Brij 97/cyclohexane/AM solution at 60°C.

better system to prepare PAM nano-spheres not only in consideration of the higher solubilisation of the aqueous phase at high temperature, but also the formation of the polymer with higher molecular weight and the spherical morphology. **Figure 6.1-2** gives the phase diagram of the three-component system with Brij 97/cyclohexane/AM aqueous solution. The slash area marks the component ratio to form the w/o microemulsion system.

6.1.3 Studies on initiator in AM polymerisation

The effect of different initiators on AM polymerisation was investigated in two aspects: the different kinds of initiator and the concentration of water soluble initiator (KPS) employed in the microemulsion polymerisation reactions.

Table 6.1-3 listed all the initiators used in our experiment and the conversion value of the monomers after polymerisation at 60°C for 6 hours. KPS, due to its hydrophilicity, would mostly present in the

water phase of the w/o microemulsion. On the other hand, azobis-iso-butyronitrile (AIBN) and azobiscyclohexane-1-carbonitrile (ABCN), due to their hydrophobicity would be likely to present in the continuous oil phase of the w/o microemulsions. The AM polymerisation initiated by any one of these three initiators obtained the comparably high conversion of monomers.

Table 6.1-3 Initiators employed in microemulsion polymerisation.

Initiator	Conversion [%]	Property
KPS	97.4	Hydrophilic
AIBN	96.2	Hydrophobic
ABCN	96.1	Hydrophobic

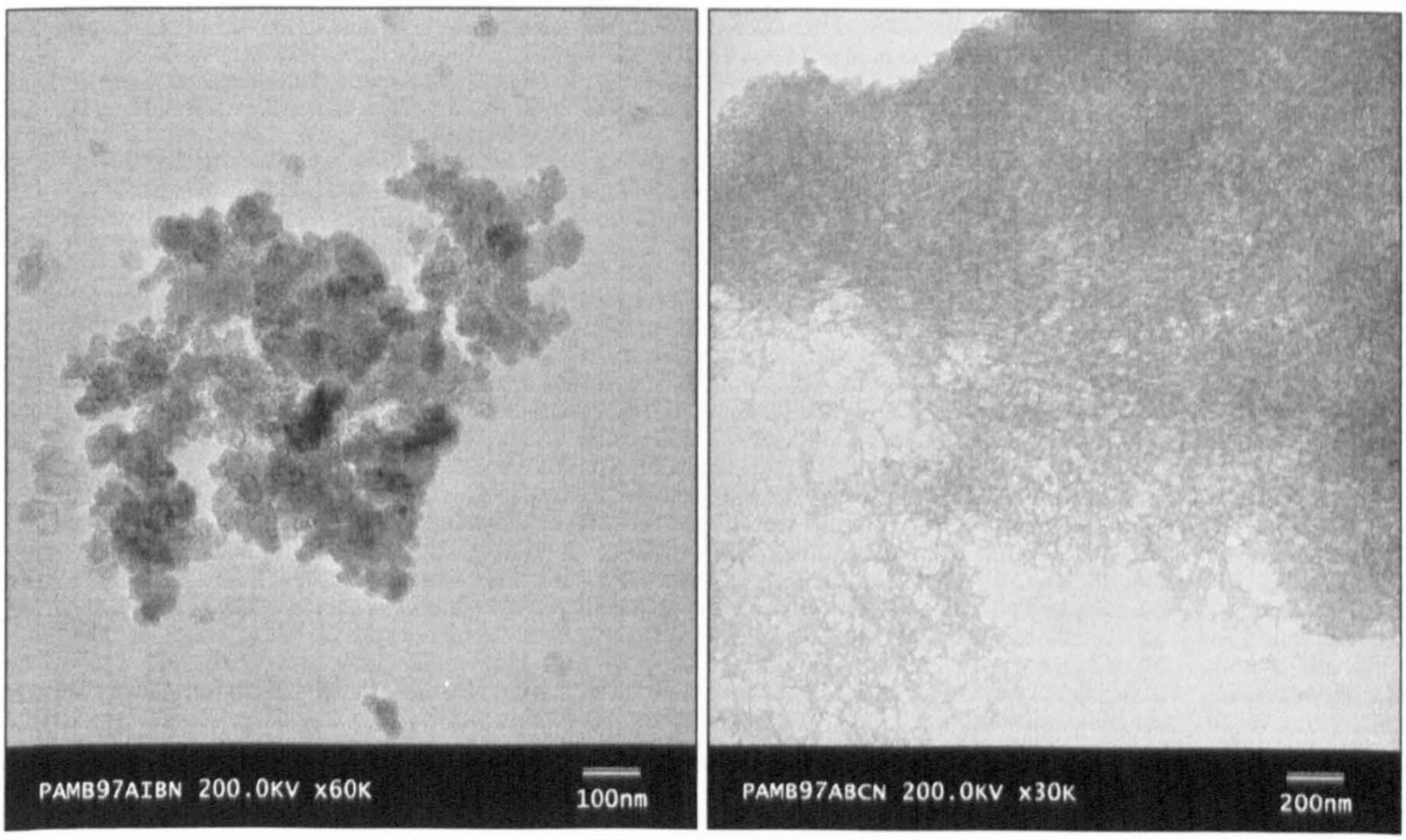

[A]. AIBN **[B]. ABCN**

Figure 6.1-3 TEM micrographs of PAM prepared via Brij 97/cyclohexane initiated by different initiators at 60°C

The TEM micrographs of PAM product prepared via w/o microemulsion system with KPS has been shown in **Figure 6.1-1 A**. The micrographs of PAM samples prepared with other two different initiators are shown in **Figure 6.1-3**. The spherical morphology was observed from the PAM sample prepared by KPS [**Figure 6.1-1 A**] with the size of 80-100 nm. However, under exactly the same reaction conditions,

no obvious nano-spheres were found in the samples prepared using AIBN or ABCN [Figure 6.1-3]. In Figure 6.1-3 A, it was difficult to identify the individual particles which were heavily aggregated. Therefore, KPS was used as the initiator in the further investigation of microemulsion polymerisation of AM.

Table 6.1-4 Molecular weight of PAM prepared via w/o microemulsion system at 60°C for 6 hours.

[KPS] / water [$x10^{-2}$ M]	Conversion [%]	Molecular weight [$x10^5$]
2.0	93.8	4.81
2.8	95.1	4.46
5.3	99.6	4.20
6.7	96.1	3.92
8.0	100	4.05

The influence of the concentration of heat initiator KPS on AM polymerisation via w/o microemulsion was evaluated by conversion value and the molecular weight of PAM. As listed in Table 6.1-4, generally speaking, an increase of KPS concentration resulted in a slightly decrease in molecular weight of PAM, but a slightly increase in conversion value.

6.1.4 Studies on reaction temperature and time of AM polymerisation

Temperature is always an important factor in a heat-initiated polymerisation. Figure 6.1-4 shows the dependence of conversion of AM monomers *vs.* polymerisation temperature. The conversion value increased as the temperature increased. TEM micrographs of PAM [Figure 6.1-5] shows that the PAM nanoparticles synthesized at either 40°C or 60°C for 6 hours were spherical and about 80 nm. It seemed that the change of polymerisation temperature did not significantly affect the shape and size of PAM synthesized.

The investigation of the AM polymerisation at different reaction times [Figure 6.1-6] shows that, the conversion of AM increased with the increase of reaction time. At 40°C, 95% conversion was achieved when the time was longer than 5 hours. At 60°C, the polymerisation time as short as 2 hours

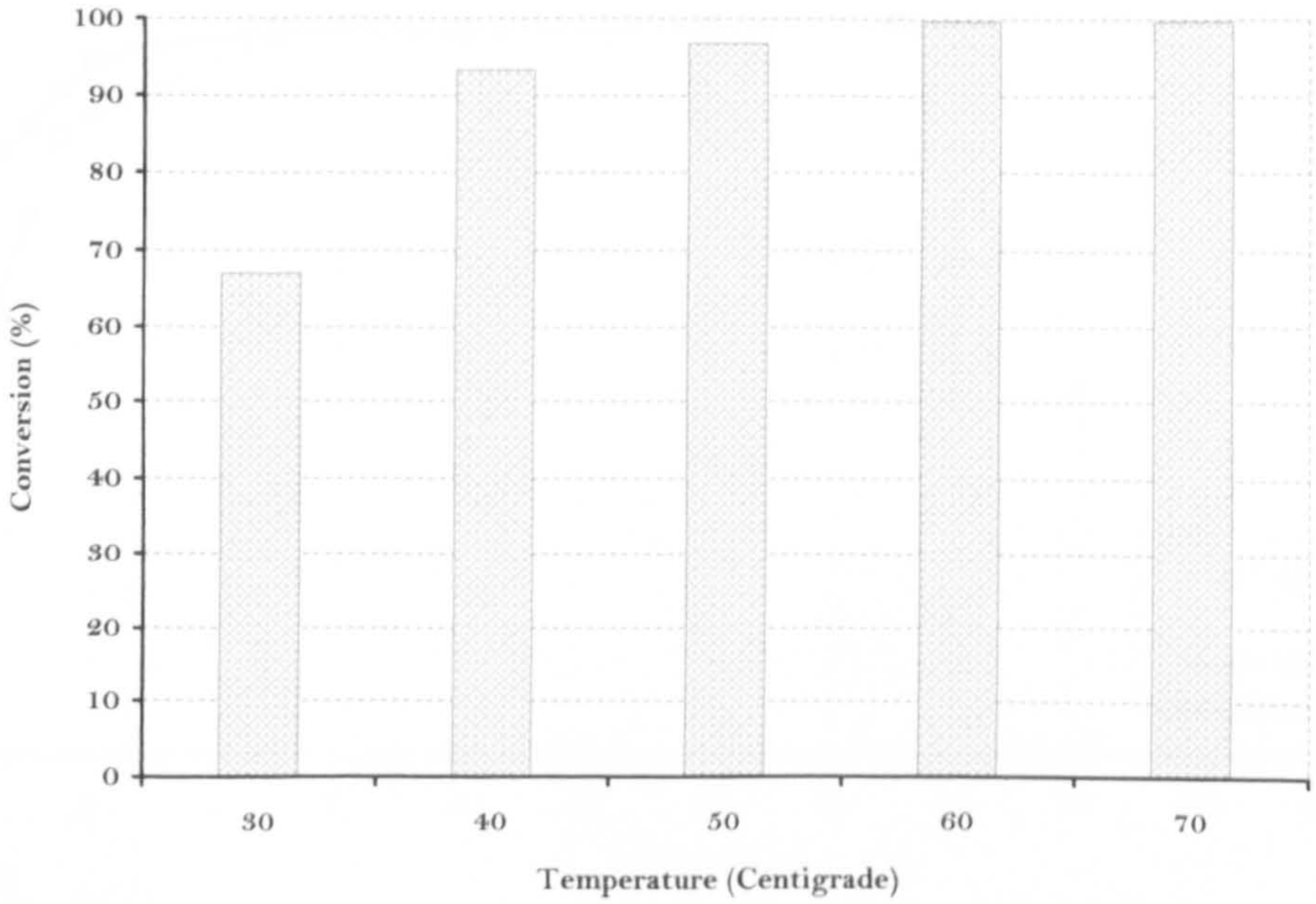

Figure 6.1-4 The conversion of AM polymerisation in Brij 97/cyclohexane at different temperatures for 6 hours

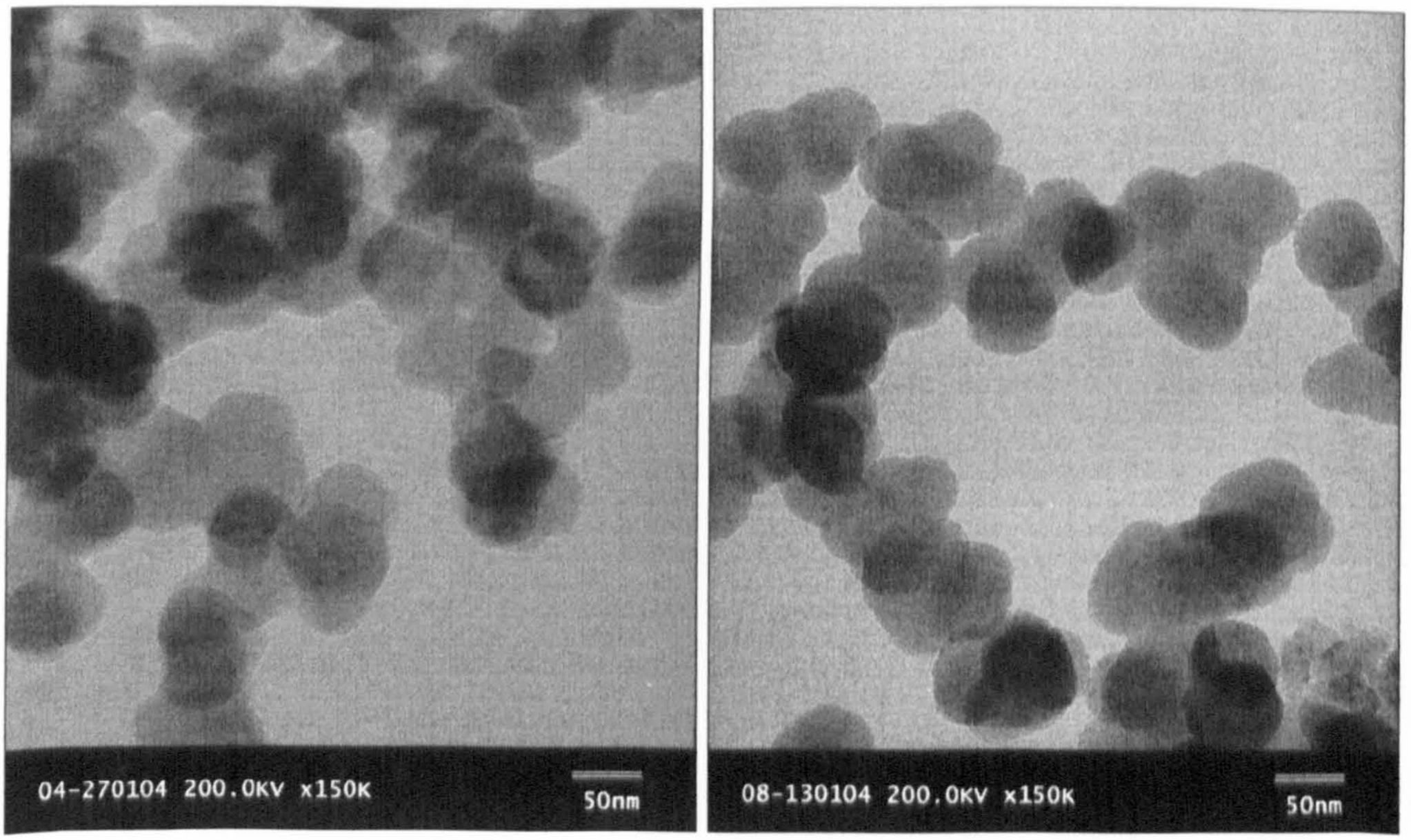

[A]. 40 °C **[B].** 60 °C

Figure 6.1-5 TEM micrographs of PAM nano-spheres polymerised via Brij 97/cyclohexane at different temperatures for 6 hours.

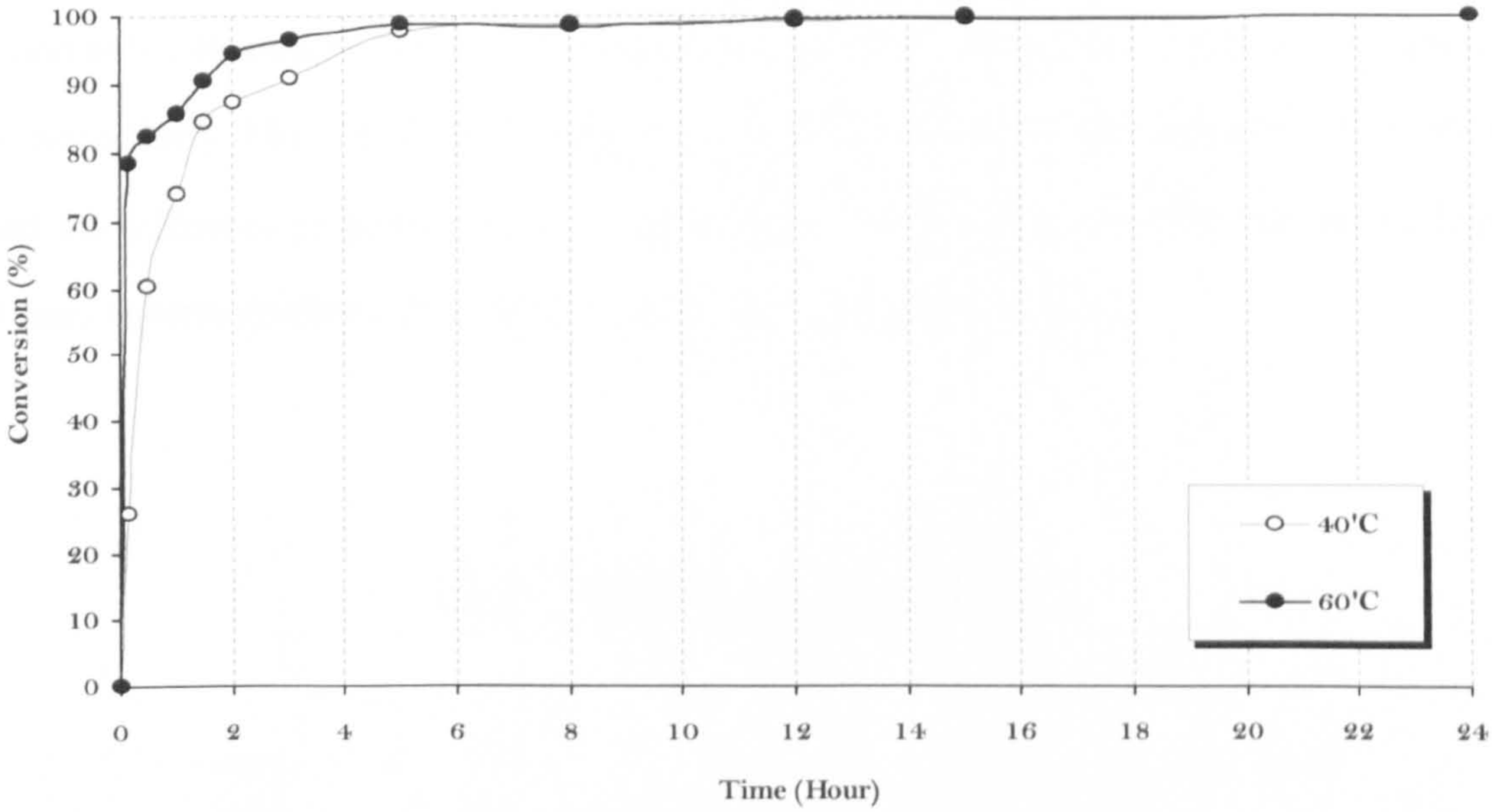

Figure 6.1-6 Conversion of AM polymerisation in Brij 97/cyclohexane with different reaction times at 40°C and 60°C.

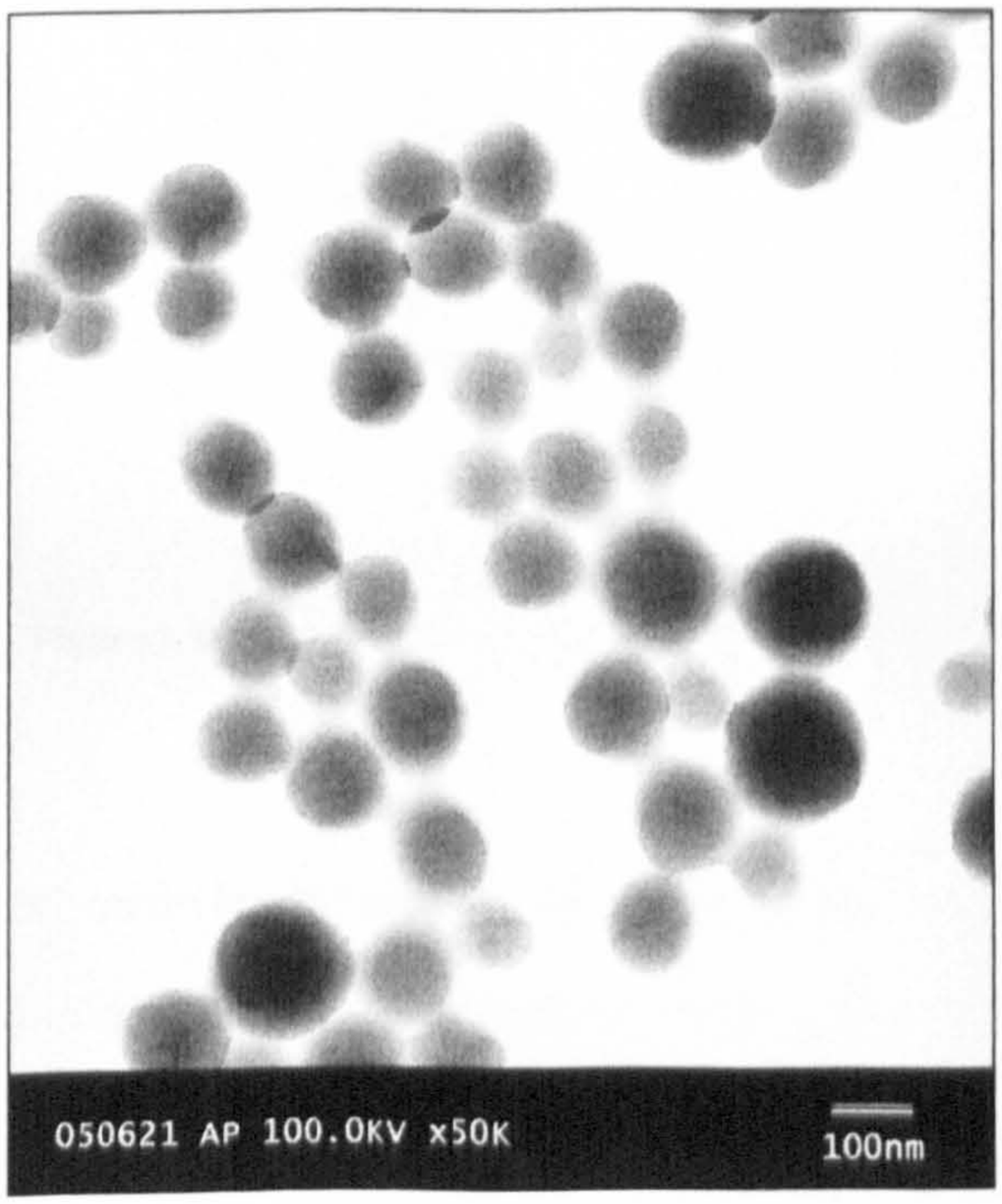

[A]. 6 Hours

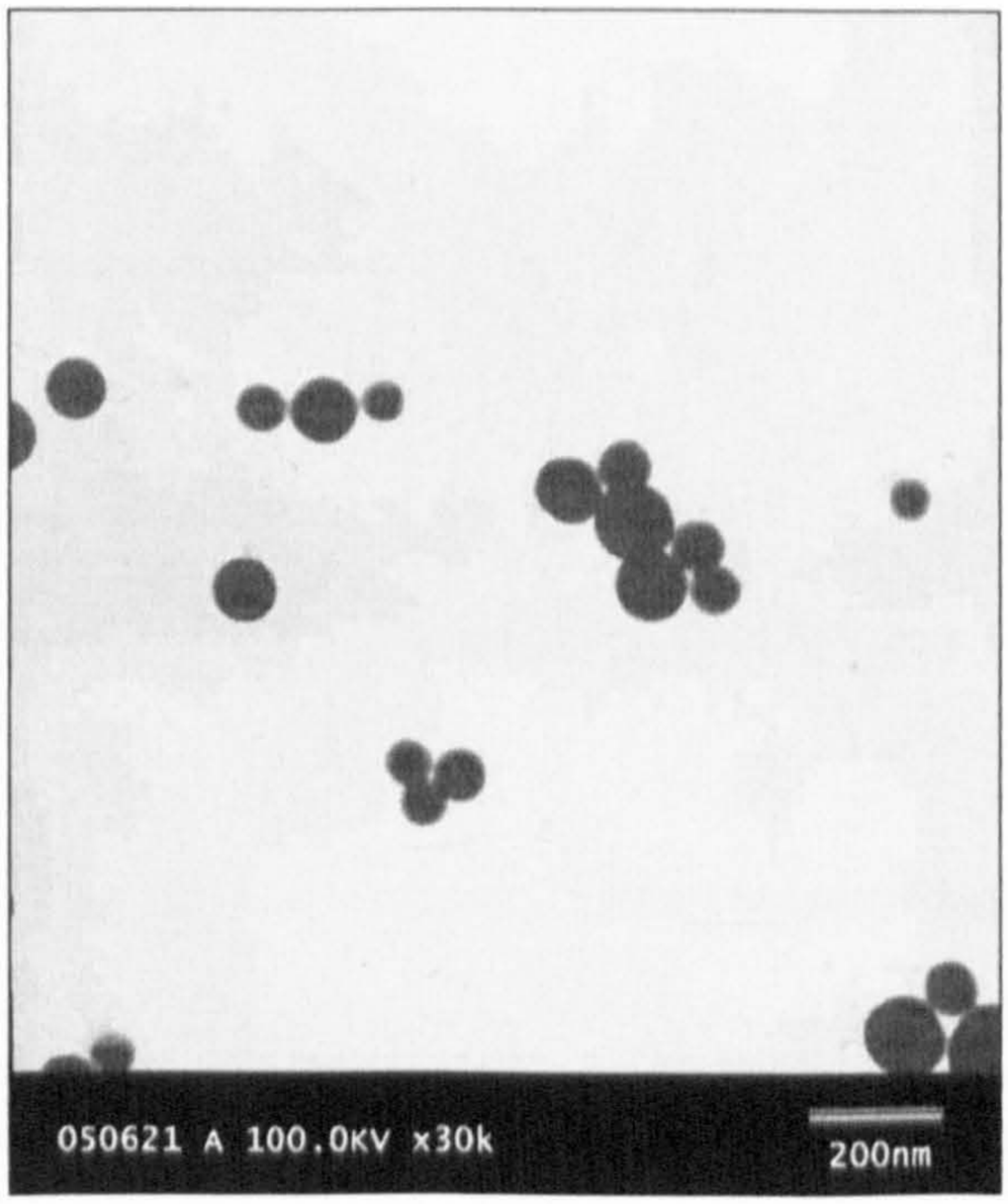

[B]. 3 Hours

Figure 6.1-7 TEM micrographs of PAM nano-spheres polymerised in Brij 97/cyclohexane at 60°C for different times.

was sufficient to yield 95% AM conversion. 100% conversion was achieved after 6 hours for both 40°C and 60°C. **Figure 6.1-7** shows TEM micrographs of PAM synthesised at 60°C for 3 hours and 6 hours, respectively. The size of both samples was 80-100 nm, spherical with mono-size-distribution. It seemed the difference in polymerisation temperature did not significantly affect the morphology of PAM nano-spheres synthesised via Brij 97/cyclohexane w/o microemulsion.

6.1.5 Studies on crosslinking

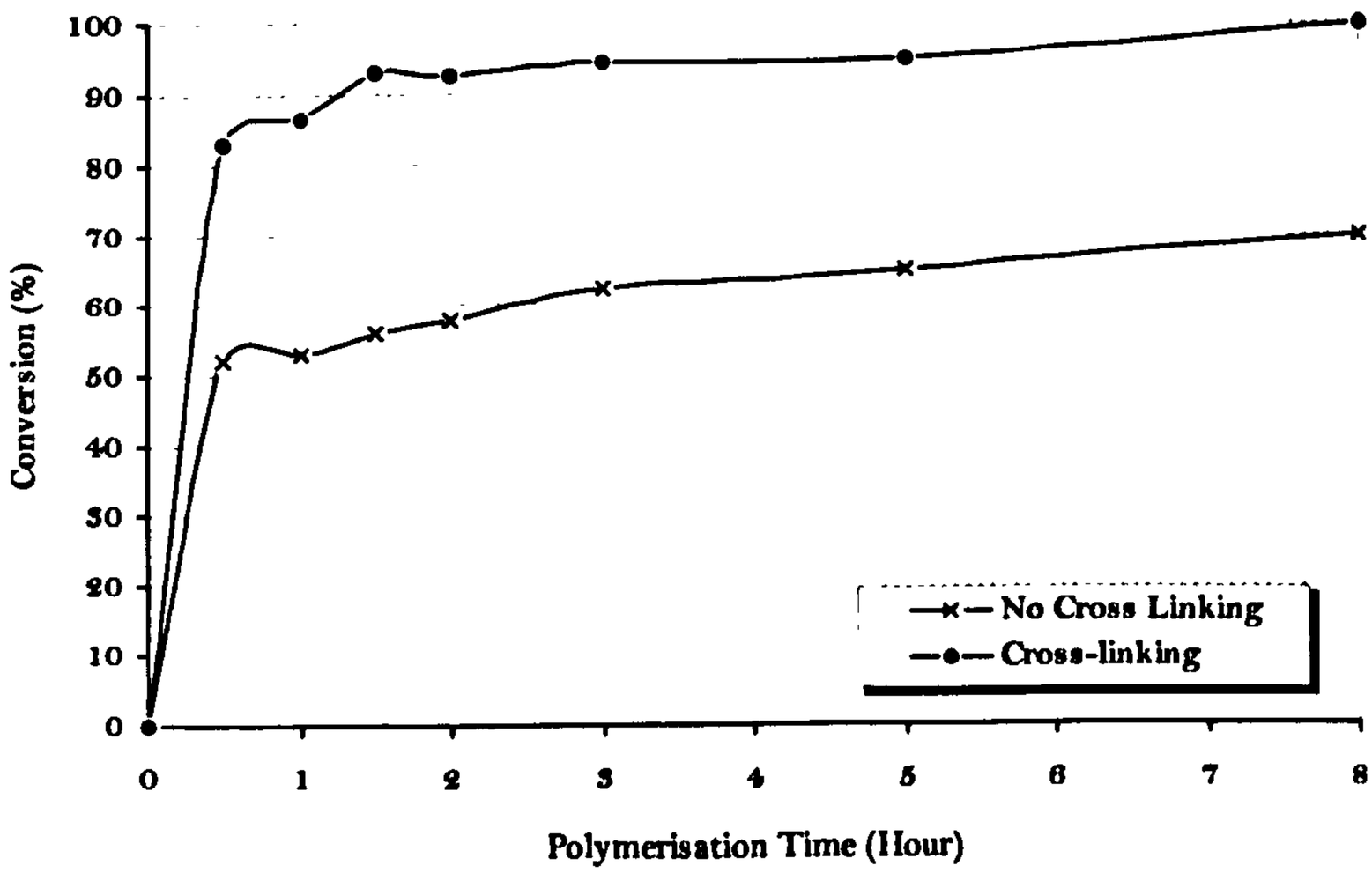

Figure 6.1-8 Conversion of AM polymerisation via w/o microemulsion with or without cross-linking at 60°C for 6 hours.

N, N'-methylen-bisacrylamide (MBA) was the crosslinking agent used in AM polymerisation via the w/o microemulsion. Conversion values of polymerisation with and without the crosslinking with the different reaction time are shown in **Figure 6.1-8**. It was found that, with or without the crosslinking, the conversion of polymerisation increased with the increase of reaction time. However, nearly 30% higher conversion was obtained for the polymerisation with crosslinking agent compared with the reaction without crosslinking agent.

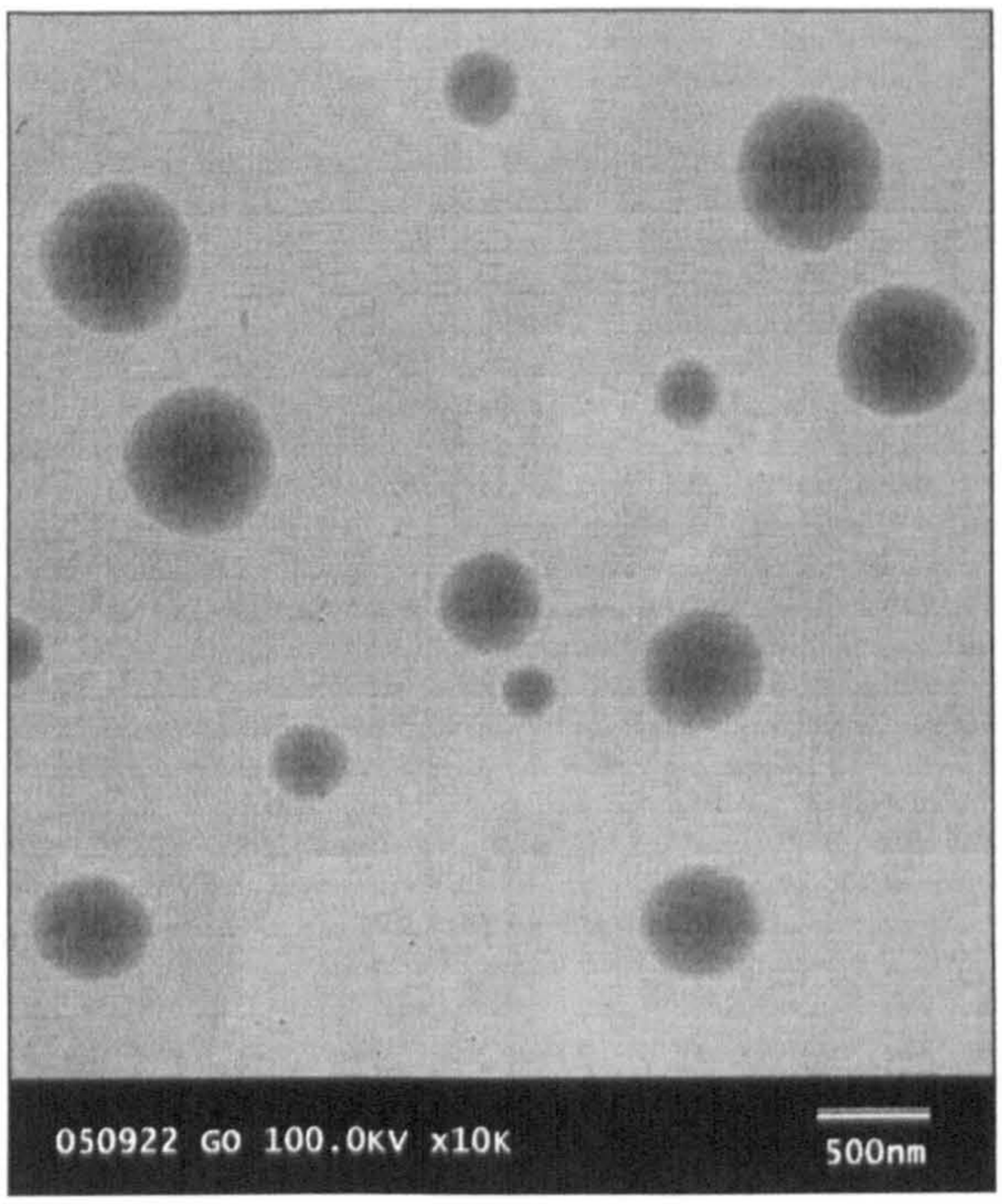

[A] 0.27 x 10^{-2} M

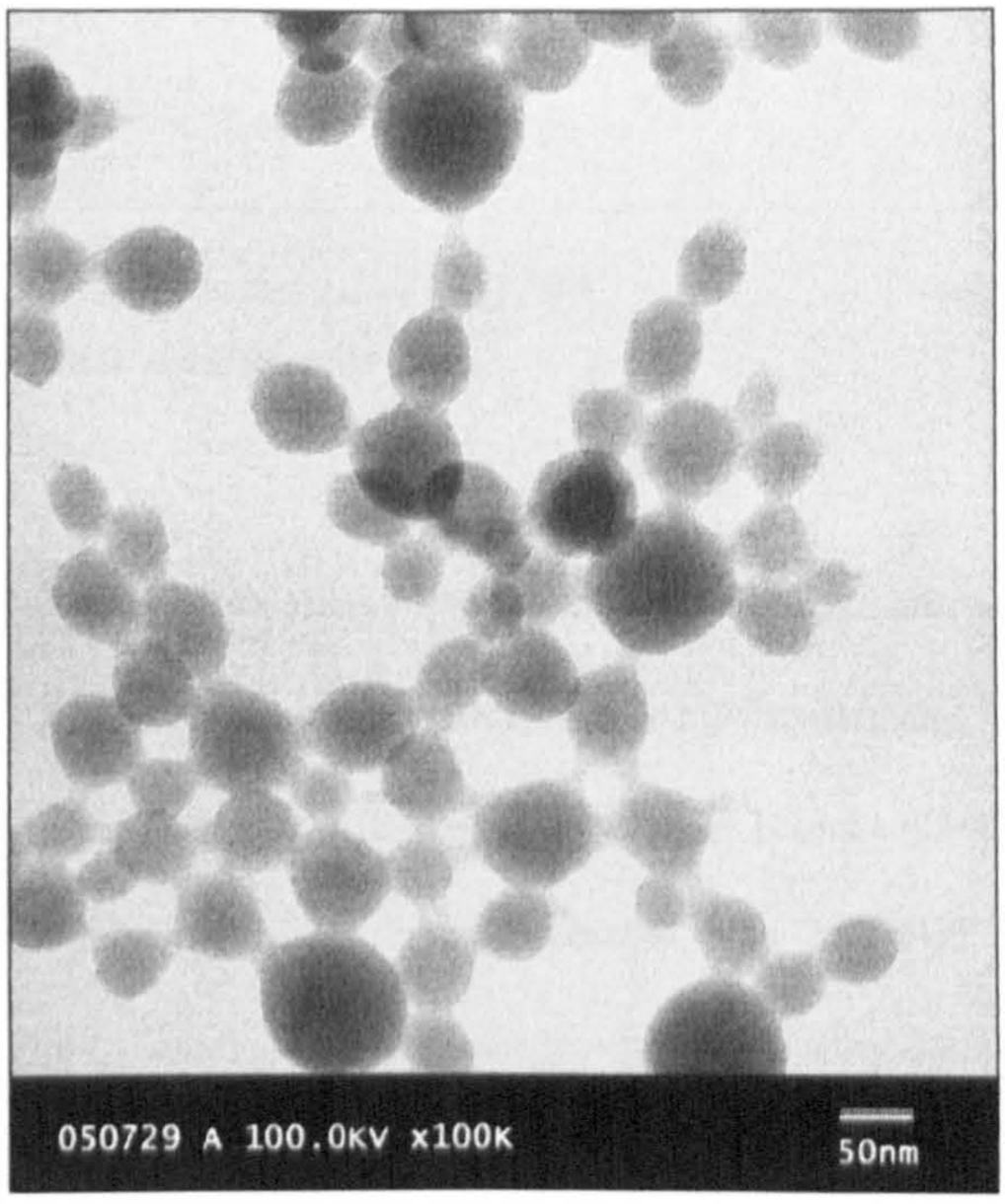

[B] 6.6 x 10^{-2} M

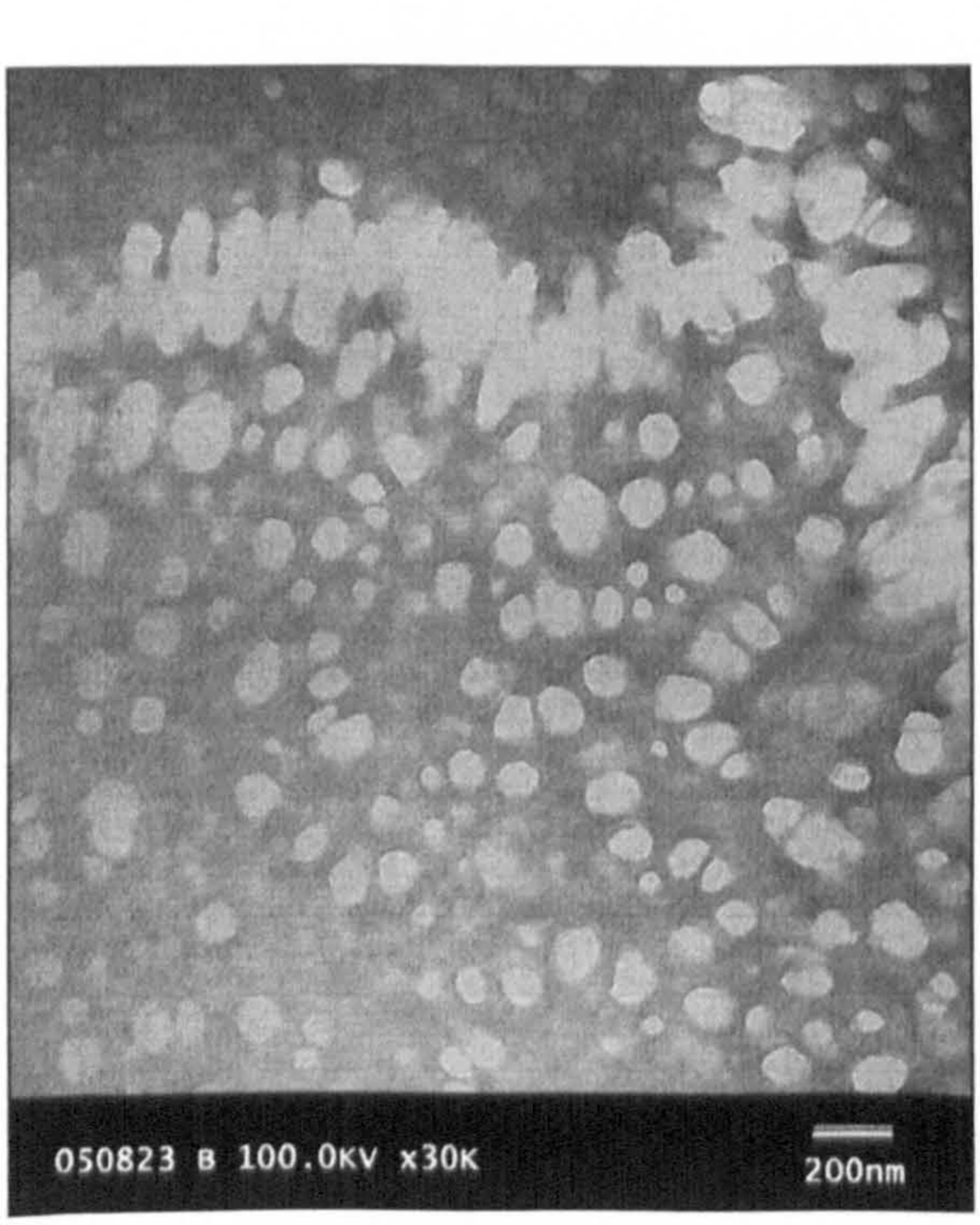

[C] 10.6 x 10^{-2} M

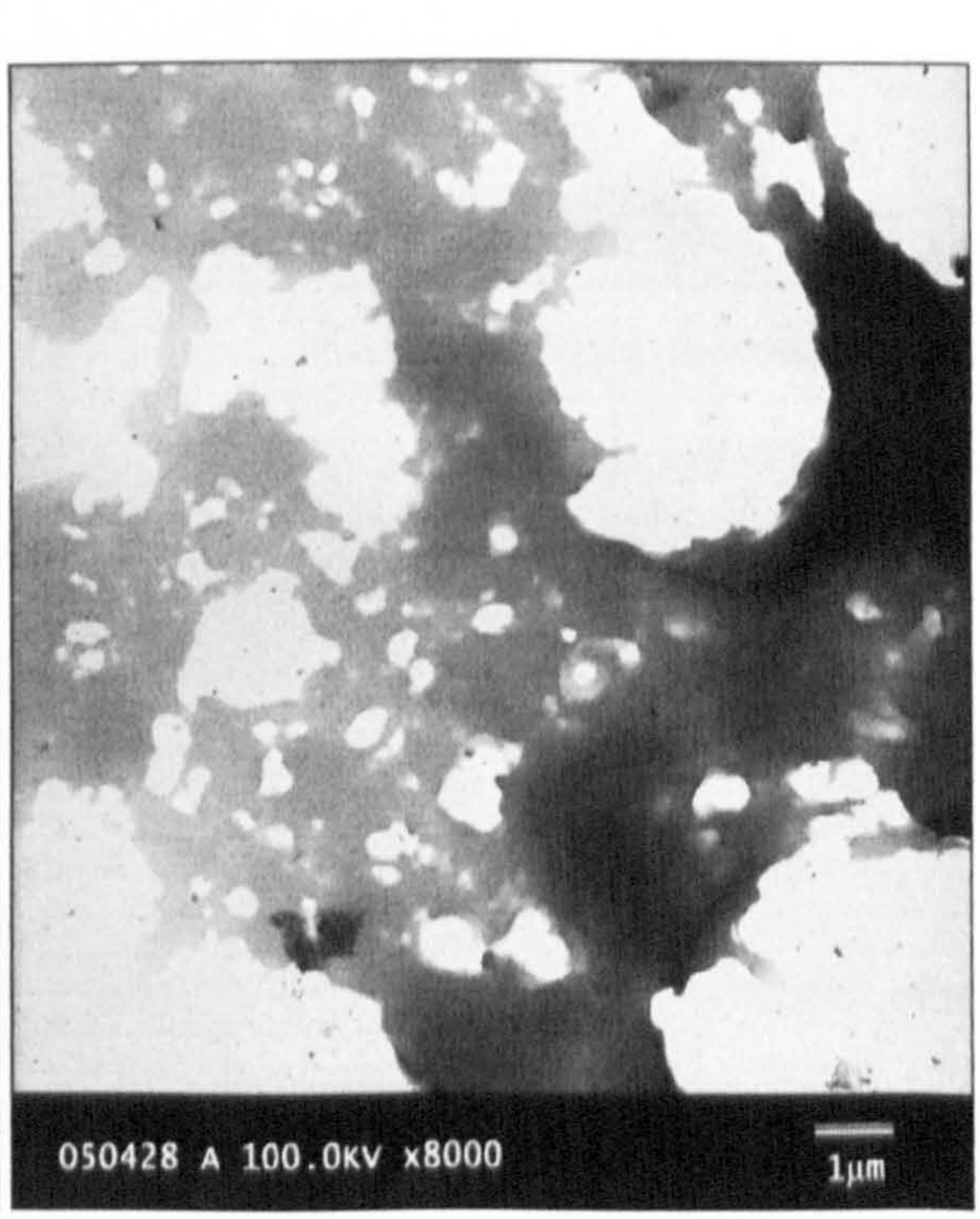

[D] 26.5 x 10^{-2} M

Figure 6.1-9 TEM micrographs of PAM nano-spheres prepared via Brij 97/cyclohexane microemulsion system with different concentrations of cross-linking agent at 60°C for 6 hours.

The molar concentration of MBA, (based on the total mass of MBA and AM in water solution), was calculated, as below:

$$Concentration\ of\ MBA = \frac{m_{MBA}}{V_{water\ solution\ of\ AM\ and\ MBA}}\ (mol/L) \qquad \textbf{(6-1)}$$

The TEM micrographs of PAM samples prepared with different cross-linking molar concentrations is shown in **Figure 6.1-9**. Spherical PAM nanoparticles were obtained at lower MBA concentration. For example, when $[MBA] = 6.6 \times 10^{-2}$ M, the size of PAM nano-spheres was 80-100 nm **[Figure 6.1-9.B]**; when the concentration decreased to 2.7×10^{-3} M, the size of PAM nano-spheres was 300-400 nm **[Figure 6.1-9.A]**. However, the PAM nano-spheres could not be clearly identified when the concentration was increased to 10.6×10^{-2} M **[Figure 6.1-9.C]**. When the concentration was continuously increased to 26.5×10^{-2} M, only film or strip-like product was observed in TEM micrographs **[Figure 6.1-9.D]**.

6.1.6 Studies on AM concentration in polymerisation

The effect of monomer concentration on the conversion of w/o microemulsion polymerisation of AM and the molecular weight was given in **Table 6.1-5**. The calculation of monomer concentration was based on the total mass of the disperse phase:

$$Monomer\ Concentration = \frac{m_{monomer}}{V_{monomer\ solution}}\ (mol/L) \qquad \textbf{(6-2)}$$

Table 6.1-5 shows that the conversion of AM polymerisation increased from 81.3% to 99.8% with an increase of initial monomer concentration from 0.58M to 5.75M. The molecular weight of PAM nano-spheres also increased from 2.26×10^5 g/mol to 4.20×10^5 g/mol with the increase of initial AM concentration from 2.30M to 5.75M. On the other hand, as shown in the TEM micrographs of PAM samples **[Figure 6.1-10]**, the particle size of PAM nano-spheres increased with the increase of the monomer concentration. Some comparably large PAM spheres, about 300-500 nm diameter, were

Table 6.1-5 Molecular weight of PAM prepared via Brij 97/cyclohexane microemulsion system at 60 °C for 6 hours.

Monomer concentration [M]	Conversion [%]	Molecular weight [x10^5 g/mol]
0.58	81.3	/
1.15	84.1	/
2.30	88.2	2.26
3.45	89.9	3.60
4.60	98.7	3.93
5.75	99.8	4.20

observed in the PAM samples with the AM solution as $[AM]=1.15M$. But when the initial AM concentration was increased to 2.30M, it became difficult to clearly identify the individual PAM particles. As shown in **Figure 6.1-10 B**, it looked like the aggregate of small particles. As the concentration was continuously increased to 3.45M, the size of PAM nano-spheres was about 40 nm **[Figure 6.1-10 C]**. When the initial AM concentration was increased to 4.60M, the size of spherical PAM particles was increased to about 50-80 nm **[Figure 6.1-10 D]**. PAM nano-spheres with the size of 80-100 nm was observed in the sample prepared from monomer solution with $[AM]=5.75M$ **[Figure 6.1-10 E]**.

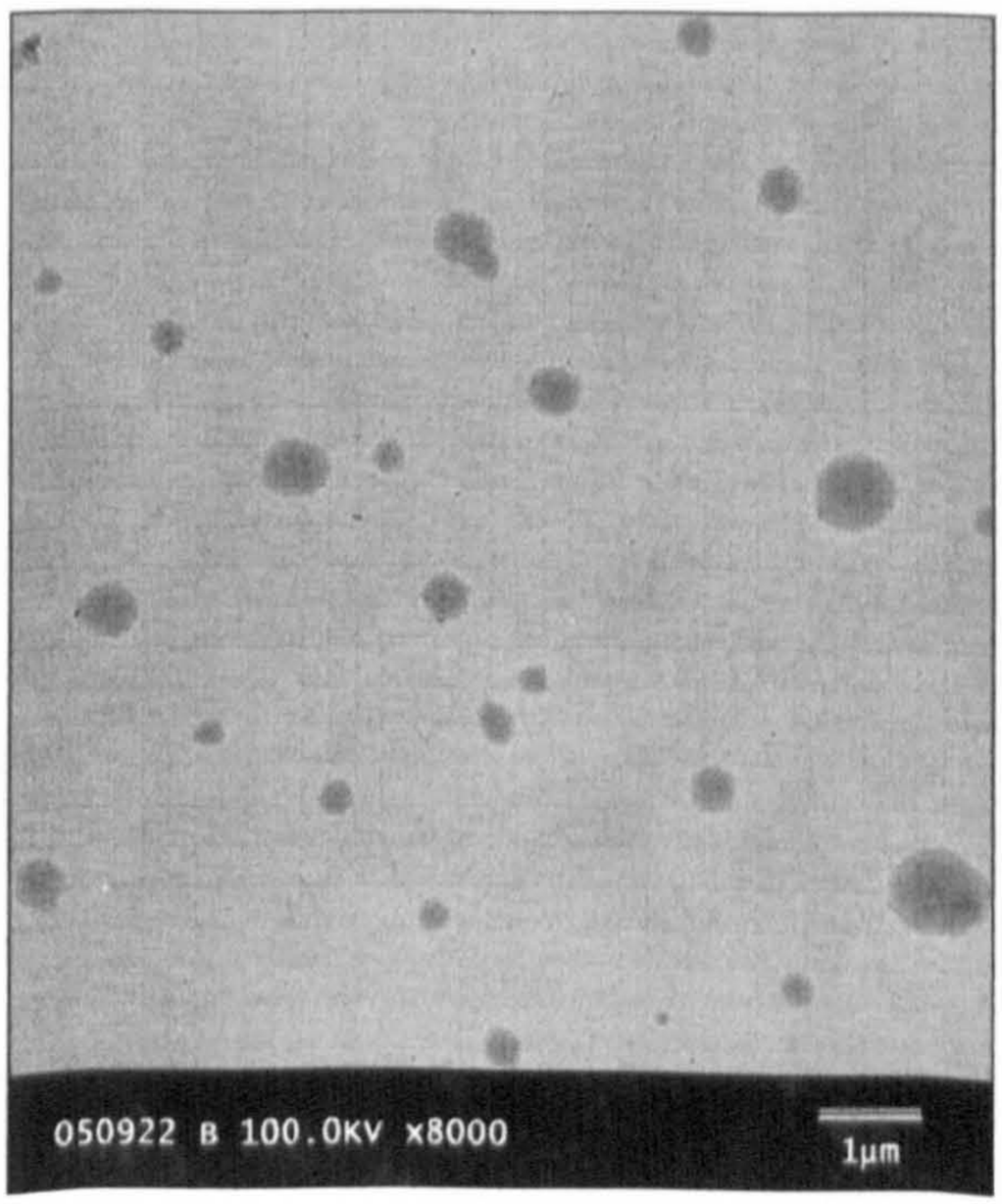

[A]. 1.15M

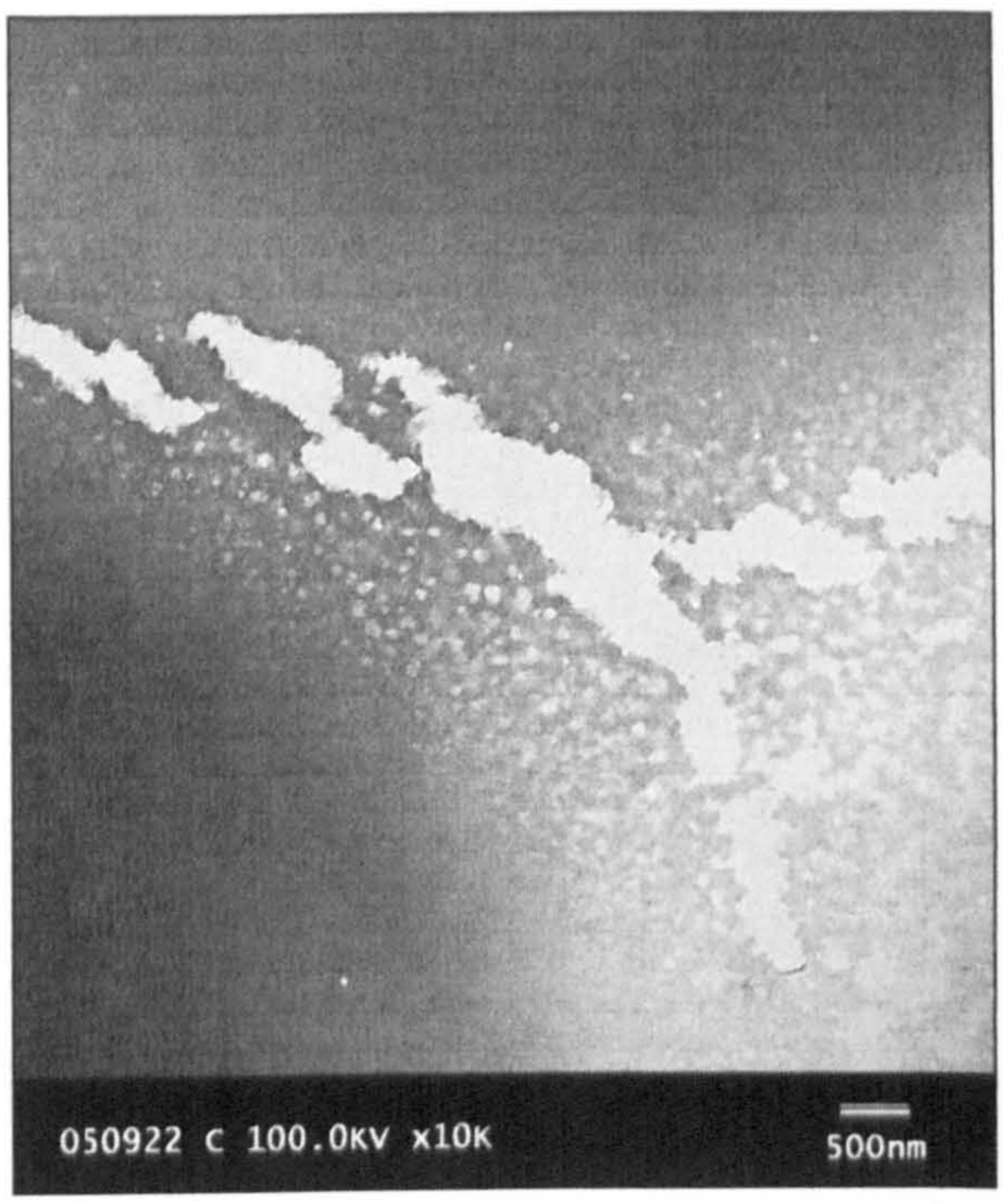

[B]. 2.30M

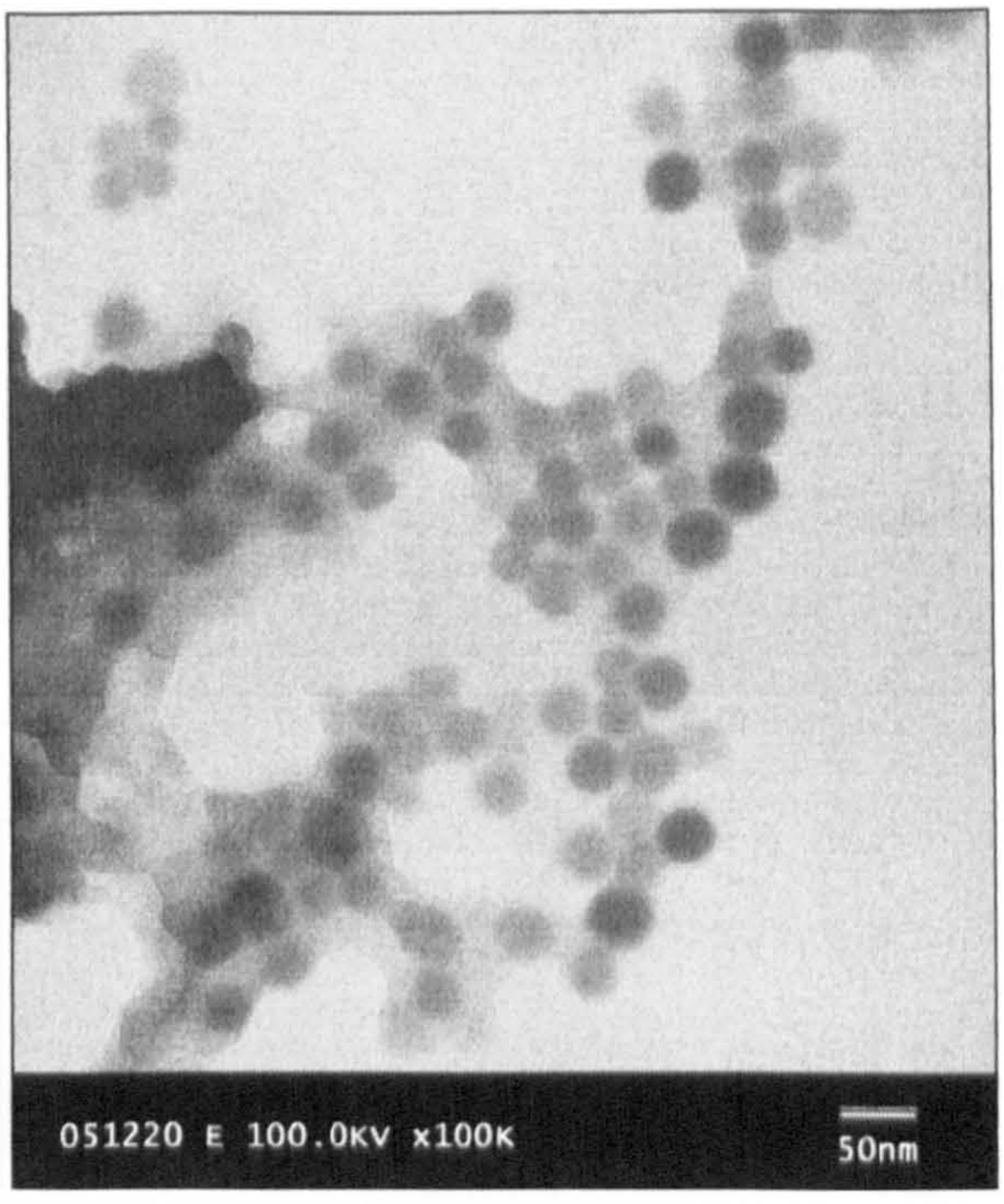

[C]. 3.45M

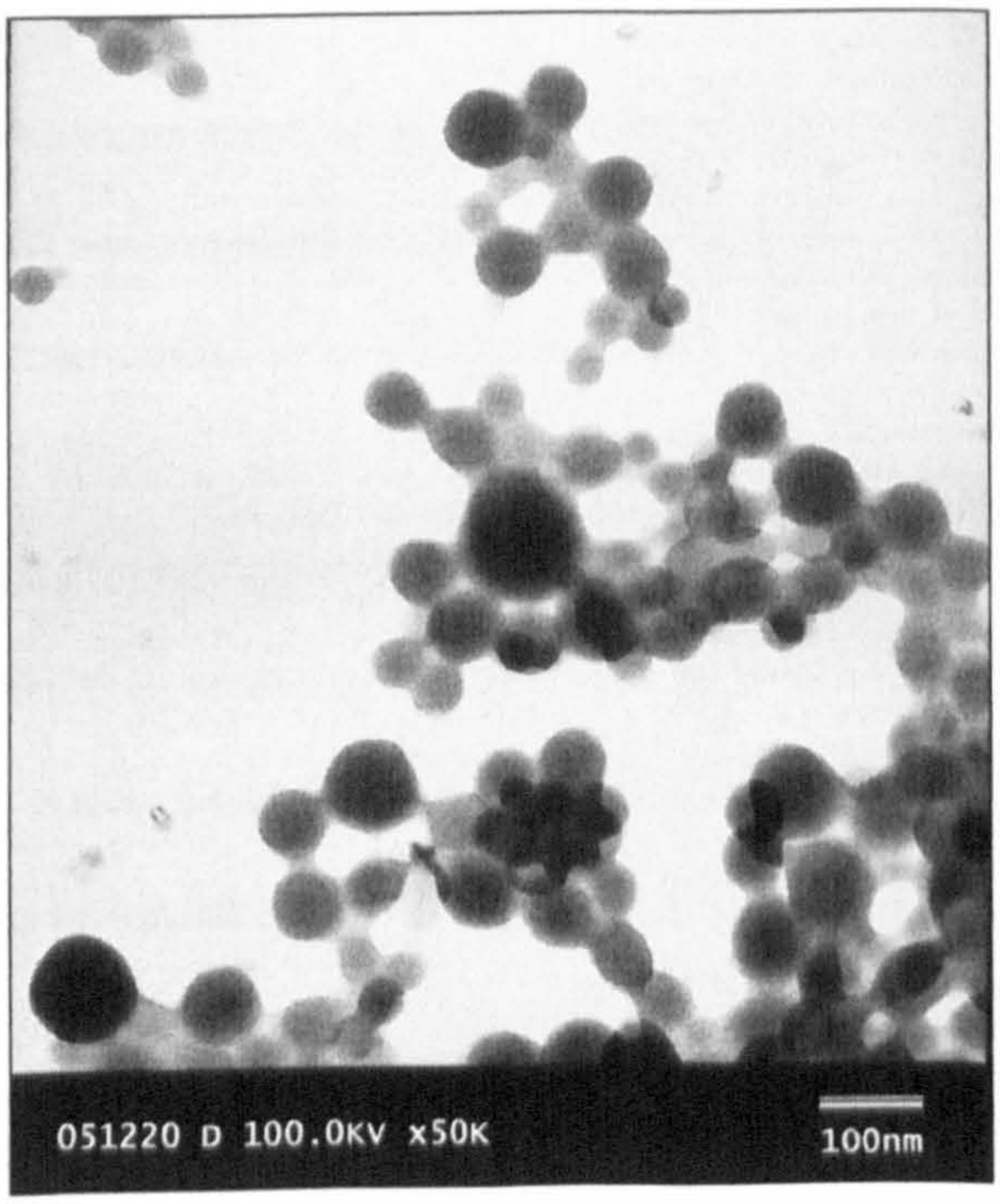

[D]. 4.60M

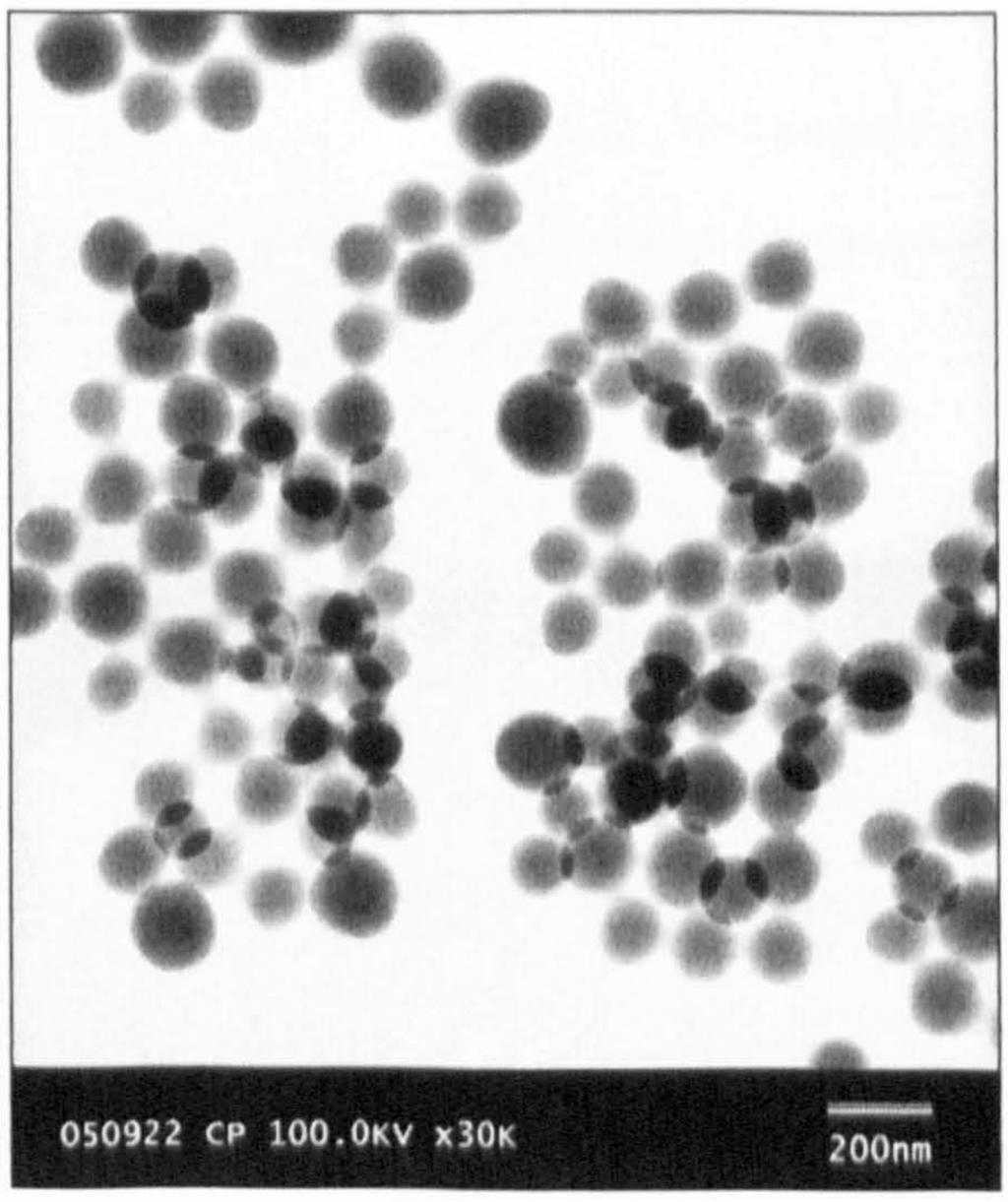

[E]. 5.75M

Figure 6.1-10 TEM micrographs of PAM nano-spheres polymerised via Brij 97/cyclohexane w/o microemulsion with different monomer concentrations at 60°C for 6 hours,

6.1.7 Studies on microemulsion system control

The system factors, such as surfactant, percentage of surfactant/oil and the loading of water phase could affect the polymerisation results. We call the possible dependence between system factors and microemulsion polymerisation results as ***system control***. The investigation of different surfactants has been reported in ***Section 6.1.2*** and the investigation of other system-dependent factors will be included in the following sections.

6.1.7.1 Studies on concentration of surfactant

The effect of surfactant on AM polymerisation in Brij 97/cyclohexane microemulsion system was investigated by its weight concentration, (based on the total mass of surfactant, oil and water phase):

$$Concentration = \frac{m_{surfactant}}{m_{surfactant} + m_{oil} + m_{water\ phase}} \cdot 100\% \qquad \textbf{(6-3)}$$

In the experiment, as the concentration of Brij 97 was varied from 14.5% to 28.9%, the morphology of PAM nano-spheres changed as a consequence. The TEM micrographs of PAM samples prepared from microemulsion systems with different surfactant concentrations are shown in **Figure 6.1-11**.

It was found that the size of PAM nano-spheres increased with the increase of surfactant concentration. When the percentage of surfactant in the system was 19.3%, the size of PAM nano- spheres was 50-80 nm **[Figure 6.1-11 B]**. With the increase of surfactant concentration from 19.3% to 24.1%, the spheres' size increased to 80-100 nm **[Figure 6.1-11 C]**. The size of PAM nano-spheres reached 150-200 nm as the surfactant concentration was increased to 28.9% **[Figure 6.1-11 D]**. However, when the surfactant concentration was 14.5%, no PAM nano-spheres could be clearly identified by TEM **[Figure 6.1-11 A]**.

6.1.7.2 Studies on different loading of aqueous phase

The system control of microemulsion polymerisation of AM was also investigated in terms of different loading amount of the aqueous phase. **Figure 6.1-12** shows the TEM micrographs of PAM samples

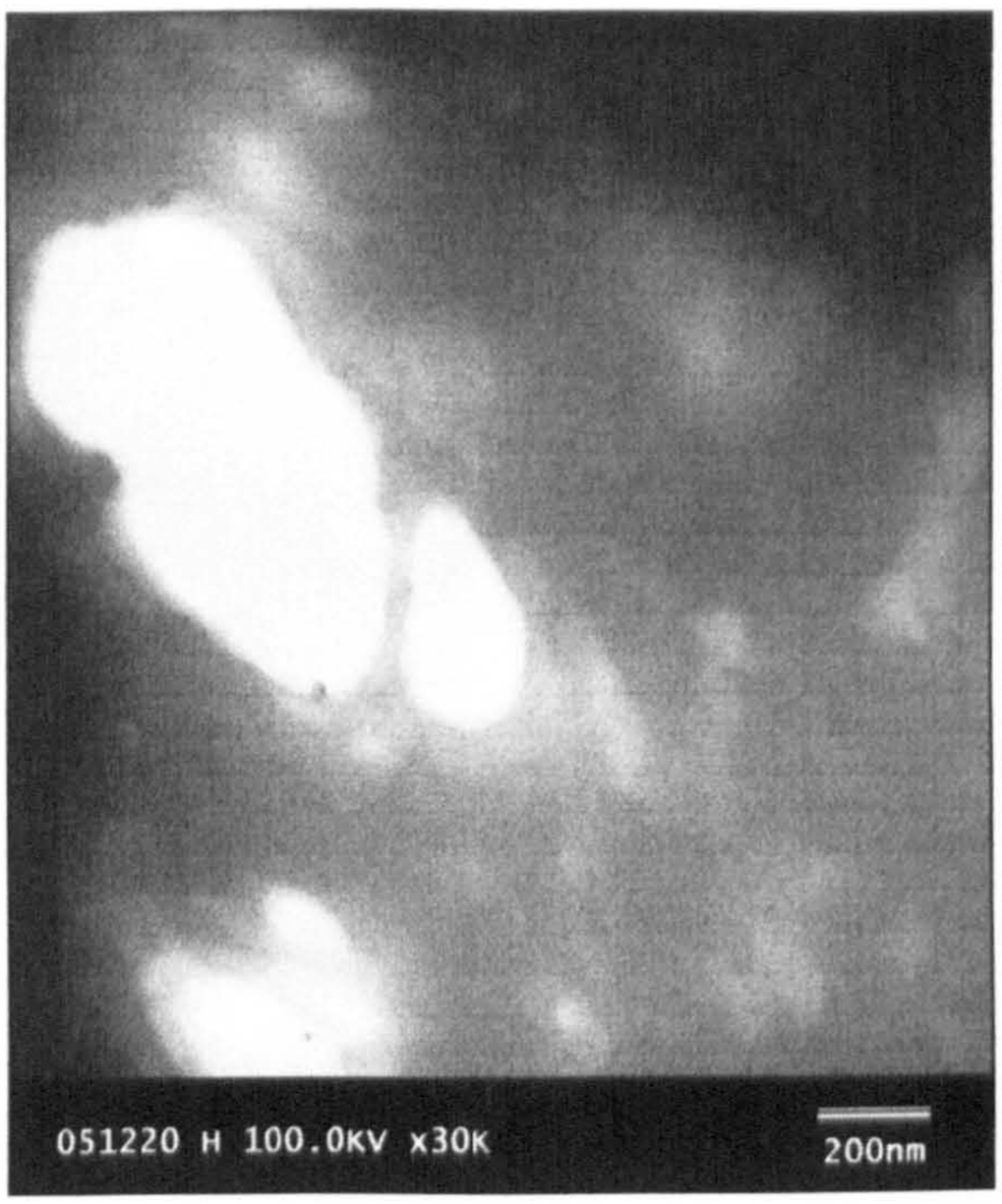

[A]. 14.5%

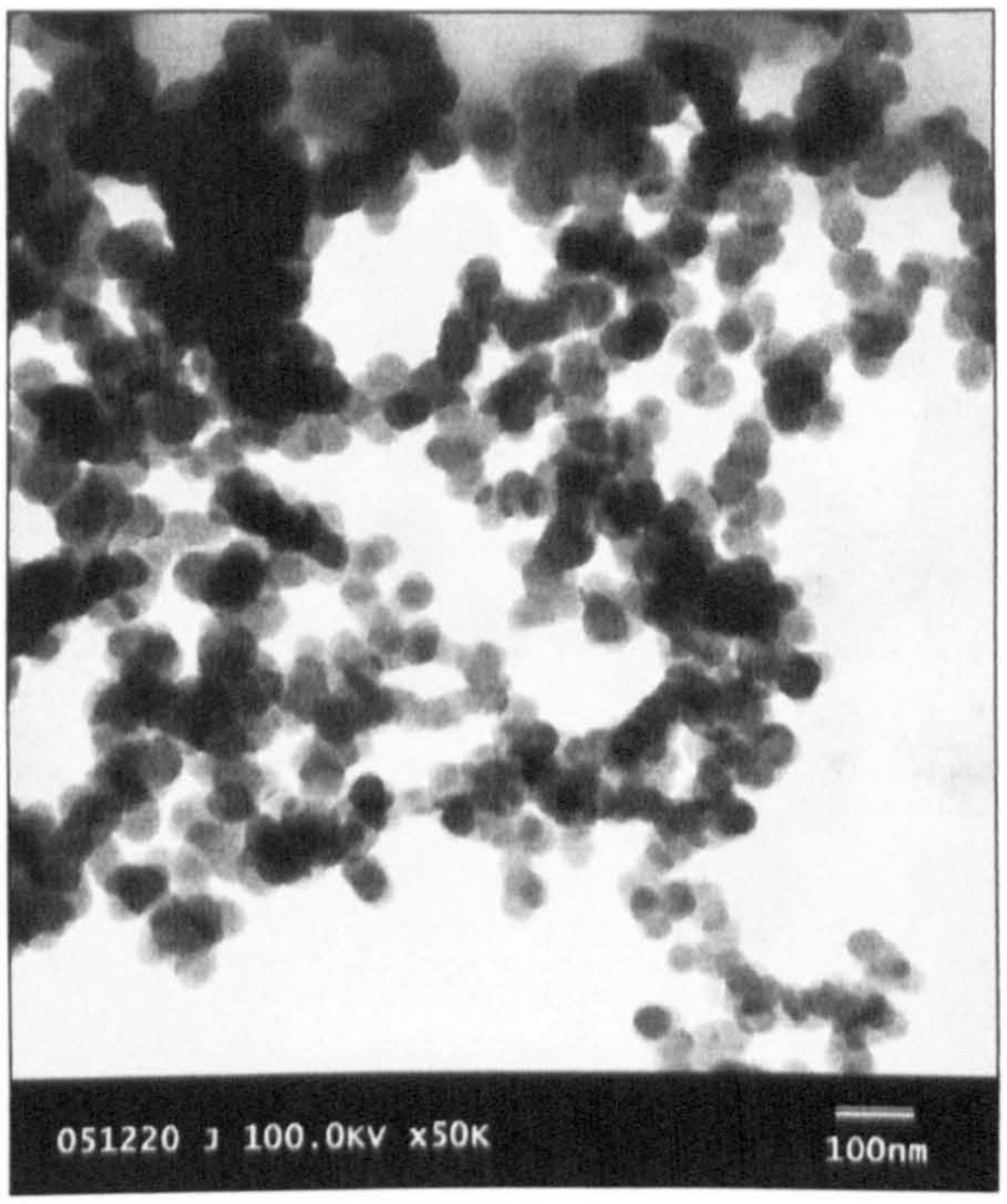

[B]. 19.3%

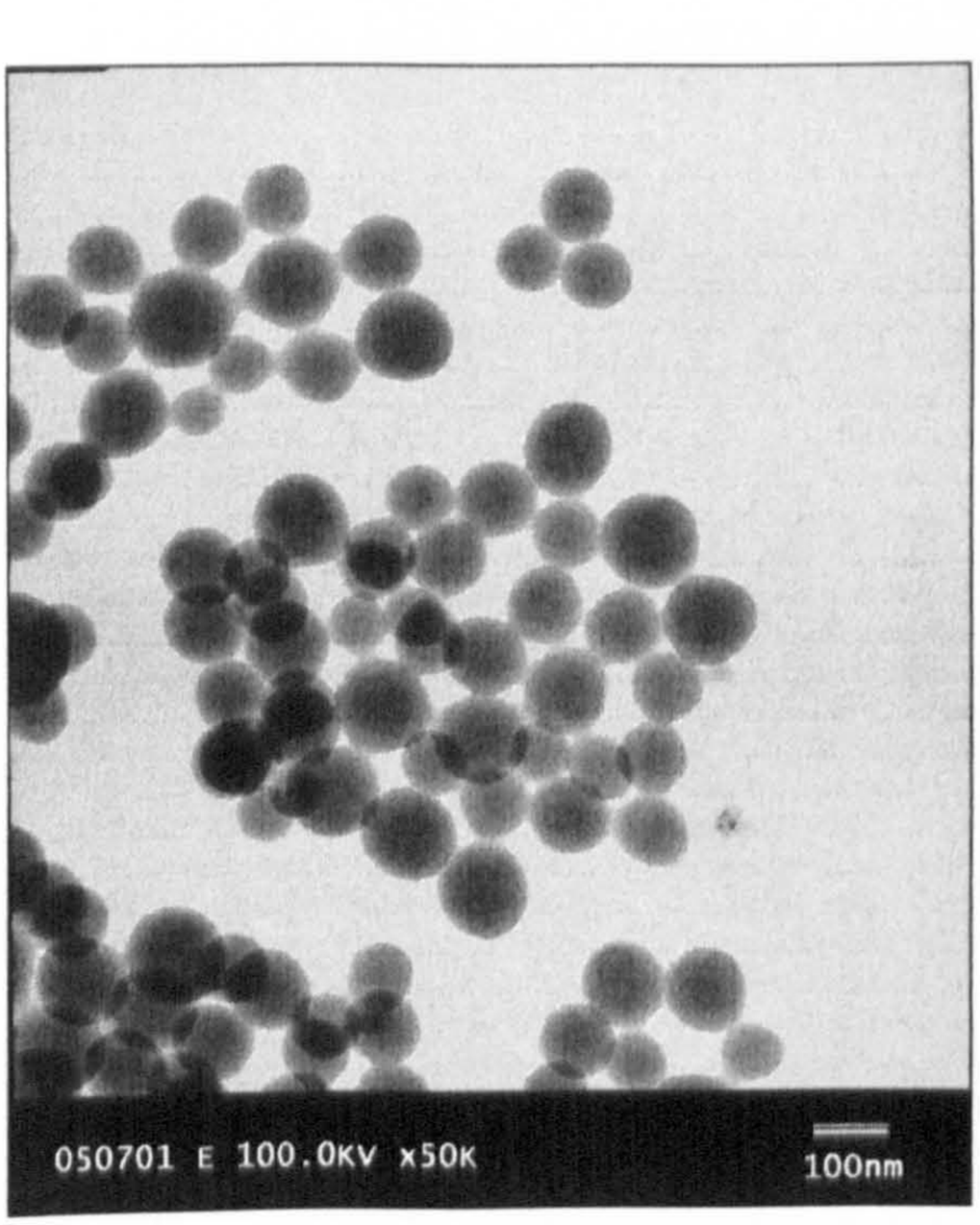

[C]. 24.1%

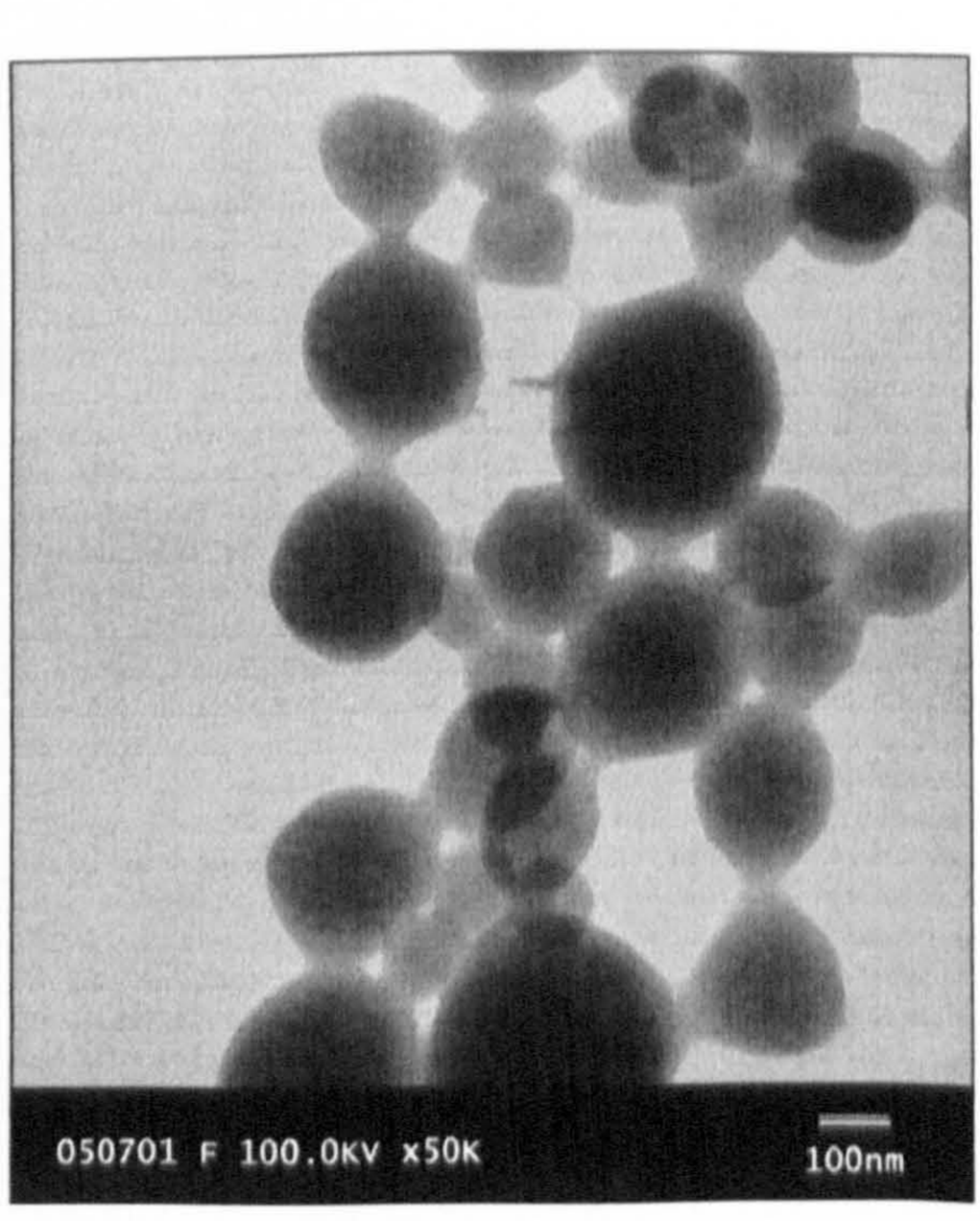

[D]. 28.9%

Figure 6.1-11 TEM micrographs of PAM nano-spheres polymerised via Brij 97/cyclohexane at 60°C for 6 hours, with different surfactant concentration.

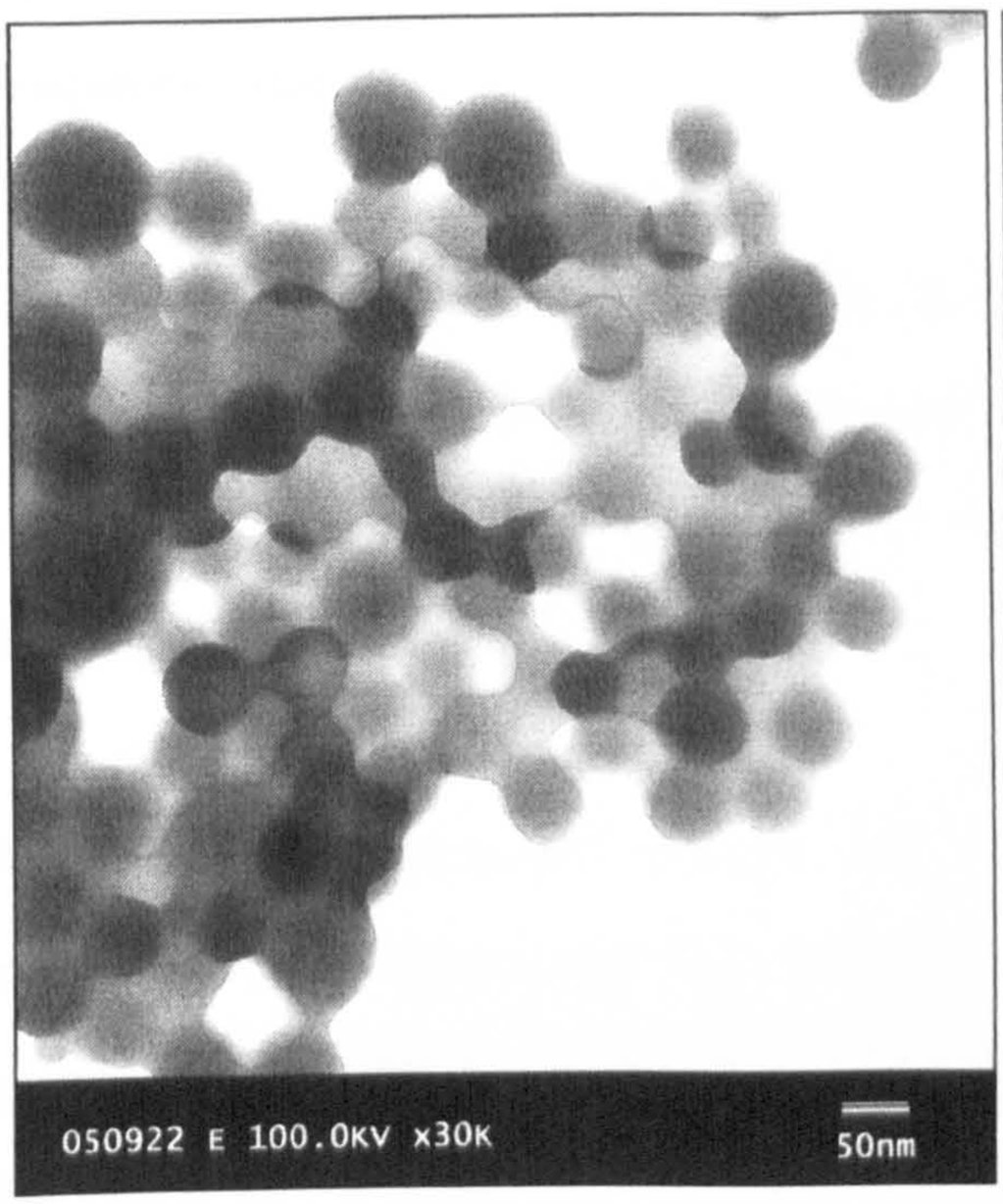

[A]. 2.4%

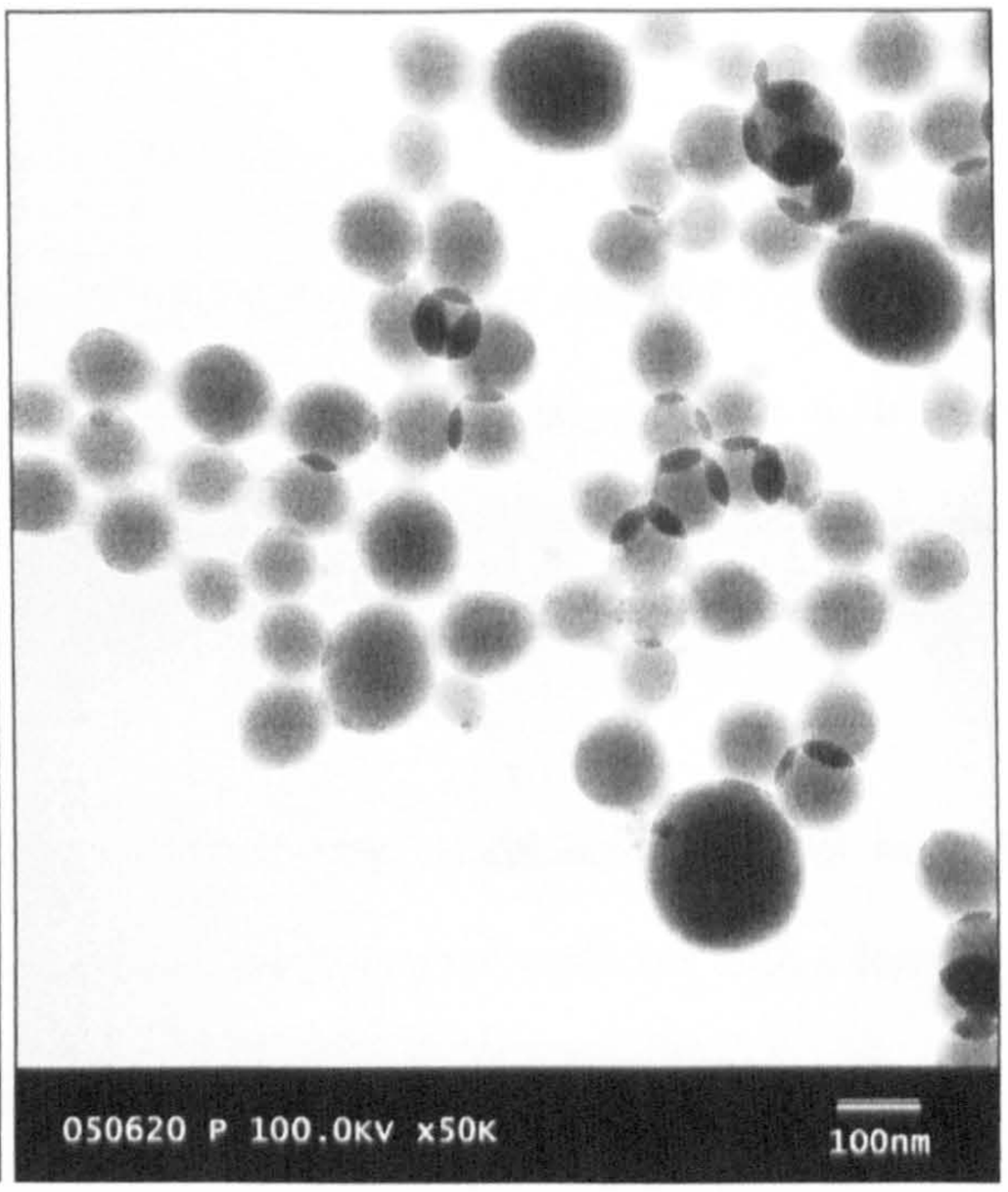

[B]. 3.5%

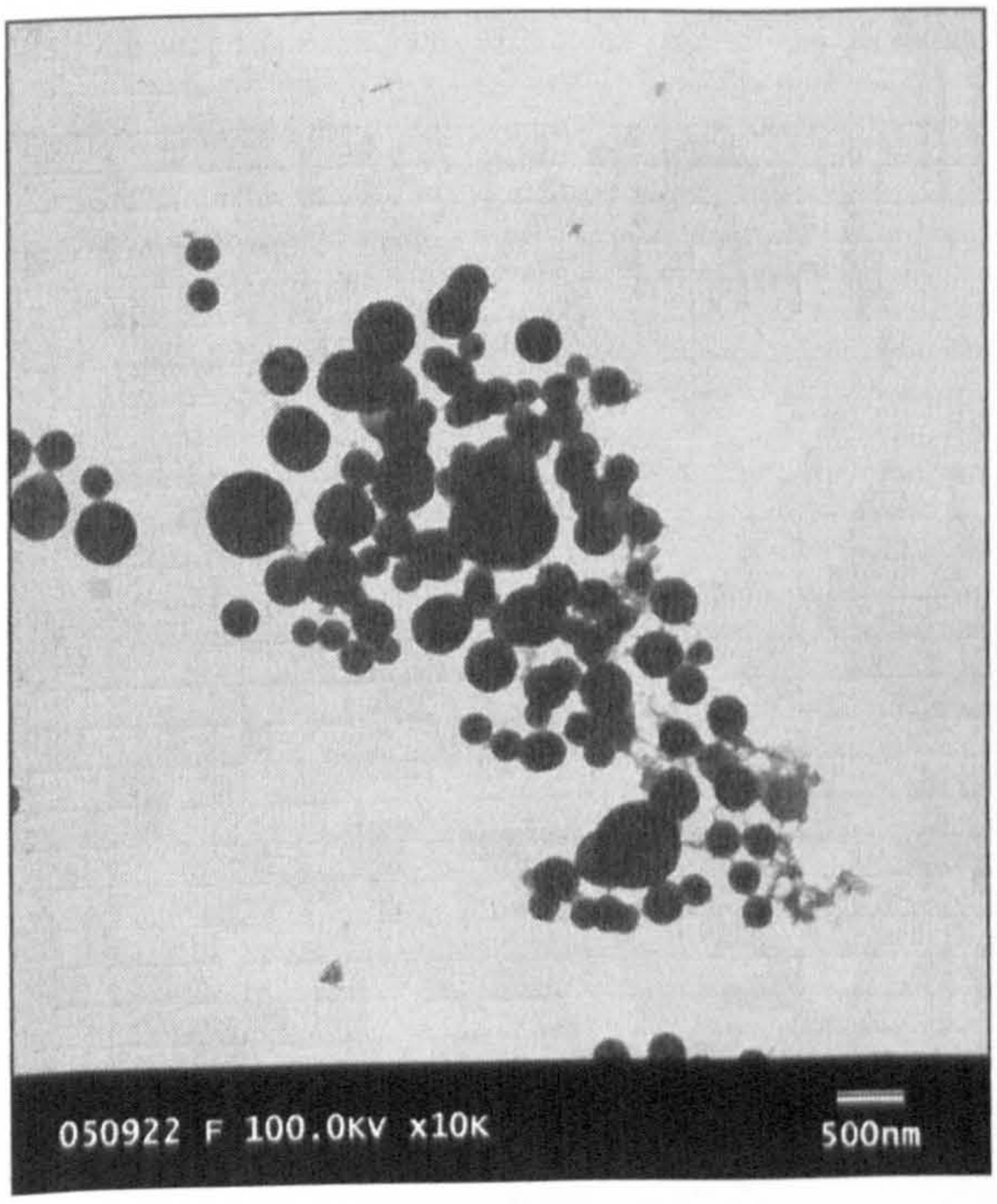

[C]. 4.2%

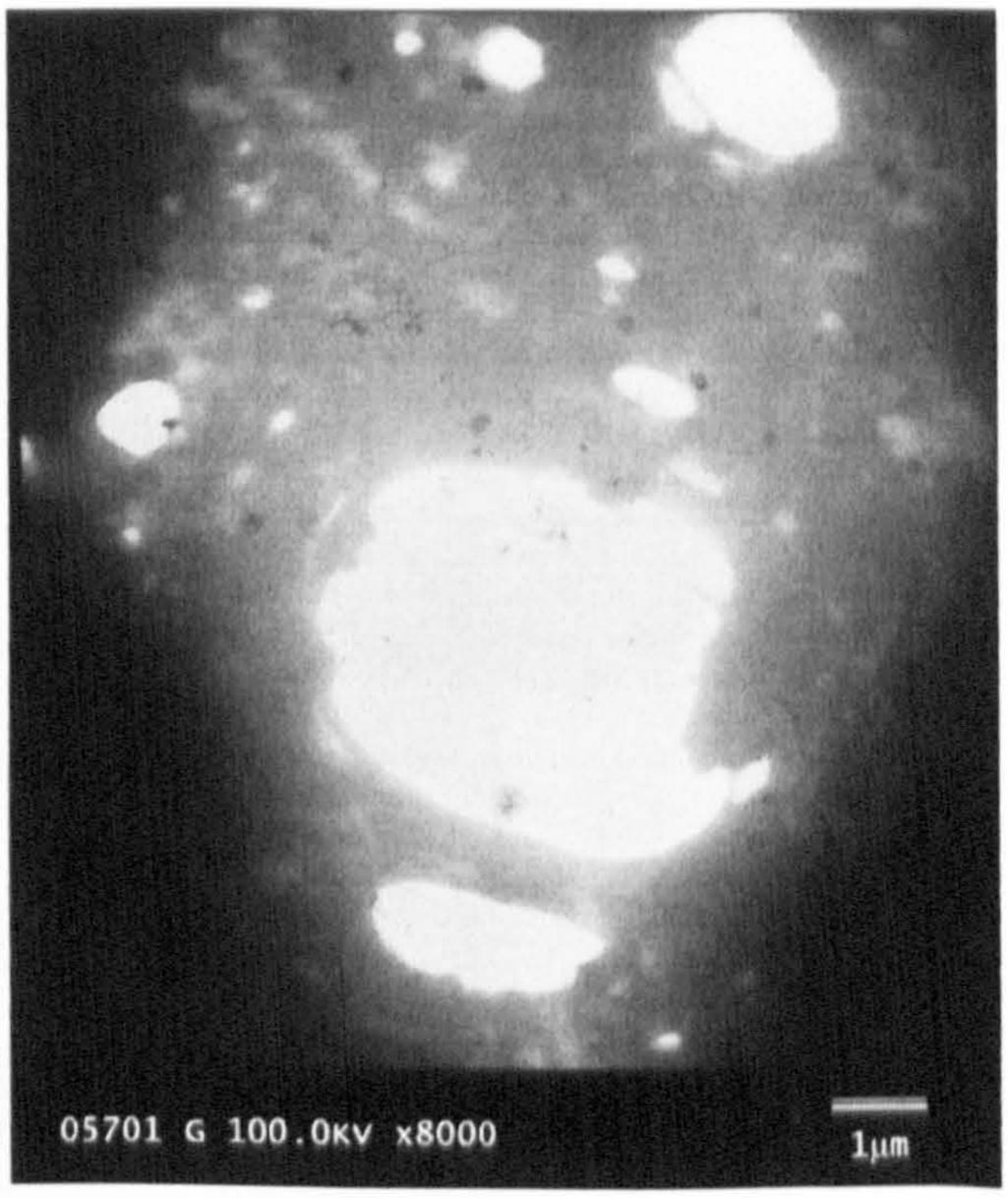

[D]. 5.8%

Figure 6.1-12 TEM micrographs of PAM nano-spheres polymerised via Brij 97/cyclohexane w/o microemulsion at 60°C for 6 hours, with different loadings of aqueous phase.

prepared via Brij 97/cyclohexane microemulsion system at 60°C for 6 hours with different loadings of the aqueous phase.

As for the PAM samples prepared with the loading of aqueous phase less than 5.8% (4.2%, 3.5%, 2.4%), the spherical morphology was observed from TEM micrographs **[Figure 6.1-12 A, B and C]**. However, when the loading of aqueous phase was 5.8%, there were no PAM nano-spheres found in TEM **[Figure 6.1-12 D]**.

The size of PAM nano-spheres changed with the change in loading of aqueous phase as well. The smallest PAM nano-spheres with the size of 50 nm **[Figure 6.1-12 A]**, were obtained with a loading of aqueous phase of 2.4%. When the loading was increased to 3.5%, the size was increased to 80-100 nm **[Figure 6.1-12 B]**. The much larger polymer spheres with the size of 250-500 nm **[Figure 6.1-12 C]** were observed as the loading was further increased to 4.2%.

The AM polymerisation, via Brij 97/cyclohexane w/o microemulsion system, was also carried out with the loading of aqueous phase at 1.6%. A phase separation was observed after the reaction **[Figure 6.1-13]**. The precipitation was so hard that it could not dissolve in the solvent to prepare the TEM specimen.

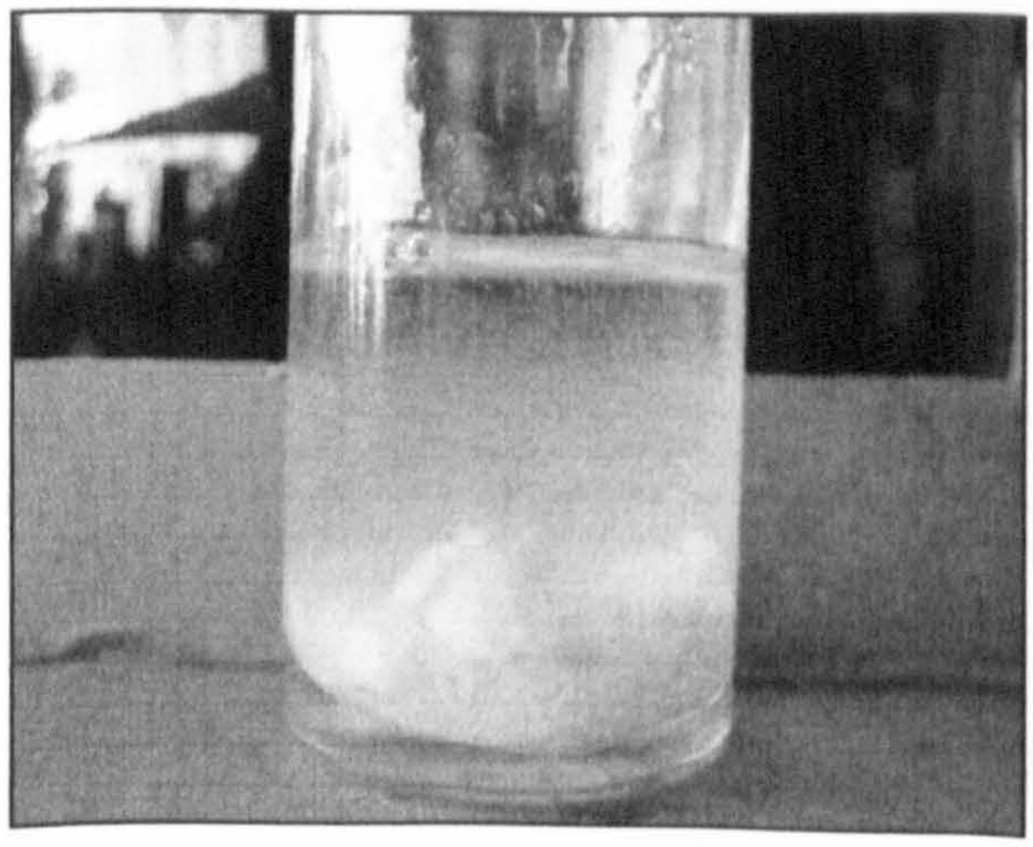

Figure 6.1-13 The photo of Brij 97/cyclohexane microemulsion system after polymerisation at 60°C for 6 hours, with the loading of aqueous phase of 1.6%.

6.1.8 Preparation of PMAA nano-spheres

The polymerisation of methacrylic acid (MAA) is also briefly investigated in this section. The partitioning of MAA in cyclohexane (oil phase) and de-ionised water (water phase) was investigated. As shown in **Table 6.1-6**, it was found that 86% of MAA was soluble in cyclohexane and the remainer in the de-ionised water, i.e. the majority of the MAA monomer had been partitioned into the oil phase. However, due to its amphiphilic property, similar to AM, the monomer molecules of MAA will have mostly located near the interface of oil/water phases.

Table 6.1-6 Partitioning of MAA in oil and de-ionised water at room temperature.

Solubility in cyclohexane [wt%]	Solubility in de-ionised water [wt%]
86	14

From the investigation of the w/o microemulsion systems, it appeared that Brij97/cyclohexane was the better system for the polymerisation at higher temperatures. So it was used in microemulsion polymerisation of AM. However, the preparation of MAA in microemulsion was a different case. **Table 6.1-7** gives the maximum solubilisation values of MAA aqueous solution in different microemulsions and the conversion of monomers polymerised in different systems.

Table 6.1-7 Maximum solubilisation of MAA aqueous solution (25 wt%) in different microemulsions and the conversion of monomers polymerised in different systems at 60°C for 6 hours. Surfactant : oil = 3:7 (wt:wt).

Microemulsion systems	Maximum solubilisation [%]	Conversion [%]
Tween 85/cyclohexane	7.2	92.2
Igepal CO-520/cyclohexane	8.1	94.0
Triton X-114/cyclohexane	13.9	100
Brij 97/cyclohexane	16.1	53.4

Triton X-114/cyclohexane showed the highest maximum solubilisation value of the monomer aqueous solution at 60°C and 100% conversion after 6-hour reaction. On the other hand, a relatively low conversion value of 53.4% was achieved from the polymerisation in Brij 97/cyclohexane system.

Therefore, in comparison to Triton X-114/cyclohexane, Brij 97/cyclohexane may not be an appropriate system for MAA polymerisation although its capability of solubilisation looked good. As for the other two systems listed in **Table 6.1-7**, they were again unsuitable due to the lower solubilisation at higher temperature. Hence, Triton X-114/cyclohexane was chosen as surfactant/oil phase for the preparation of poly-(methacrylic acid) (PMAA) via w/o microemulsion.

- **Studies on reaction time and temperature**

The polymerisations of MAA via w/o microemulsion were carried out at 60°C, and KPS was used as the initiator. **Figure 6.1-14** shows the results of the time and temperature effects on MAA polymerisation. The reaction at 70°C yielded a bit higher conversion, than the reaction at 60°C, although both reactions achieved 100% conversion. It should be mentioned that no polymer was precipitated out in the reaction at 50°C. As shown in **Figure 6.1-14**, the polymerisation of MAA was slow at the beginning of reaction and over 90% conversion of MAA to PMAA was obtained after 2-hour reaction in Triton X-114/cyclohexane system. After 6 hours, 100% conversion to the polymer was obtained. Hence, further investigations were carried out for 6-hour reaction.

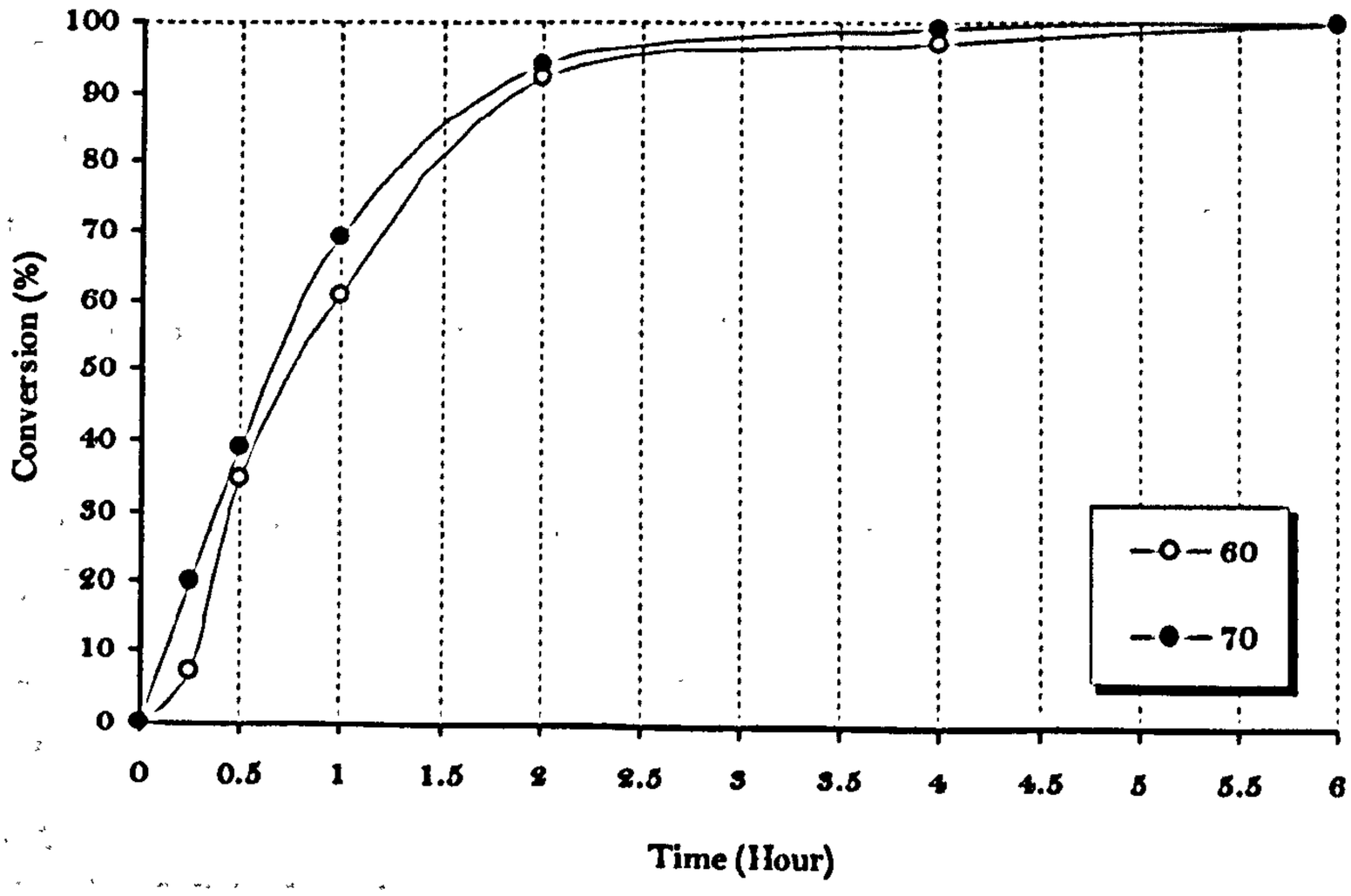

Figure 6.1-14 Conversion of MAA by polymerisation in Triton X-114/cyclohexane w/o microemulsion system with different reaction times and temperatures.

- **Studies on initiator concentration**

The conversion of MAA and molecular weight of the resulting PMAA prepared with different initiator concentrations, are summarised in **Table 6.1-8**. The conversion increased from 22.6% to 100% with an increase of concentration of KPS from 1.75×10^{-3} M to 8.81×10^{-3} M. There was an initial increase in the molecular weight of the polymers, with an increase in the initiator concentration up to 3.38×10^{-3} M and it then decreased with any further increase.

Table 6.1-8 Molecular weight of PMAA prepared via Triton X-114/cyclohexane at 60°C for 6 hours.

[KPS] / water [x10^{-3} M]	Conversion [%]	Molecular weight [x10^{5} g/mol]
1.75	22.6	1.67
3.38	95.9	2.97
6.28	98.9	1.45
8.81	100	1.44

- **Studies on monomer concentration**

The conversion and molecular weight of PMAA produced with different monomer concentrations are given in **Table 6.1-9**. It was found that the conversion value increased with the increase of MAA concentration. However, the molecular weight increased when the concentration increased from 1.30M to 2.61M, then decreased as the concentration reached to 4.17M. **Figure 6.1-15** shows TEM micrographs of the PMAA nano-spheres prepared with different monomer concentrations. The particles with larger size of 80-100 nm were obtained from the higher concentration, 4.17M. When the concentration was decreased to 2.61M, the size of PMAA nano-spheres decreased to 30-50 nm.

Table 6.1-9 Molecular weight of PMAA prepared via Triton X-114/cyclohexane at 60°C for 6 hours.

Monomer concentration [M]	Conversion [%]	Molecular weight [10^{5} g/mol]
1.30	95	0.43
2.61	100	1.45
4.17	100	0.74

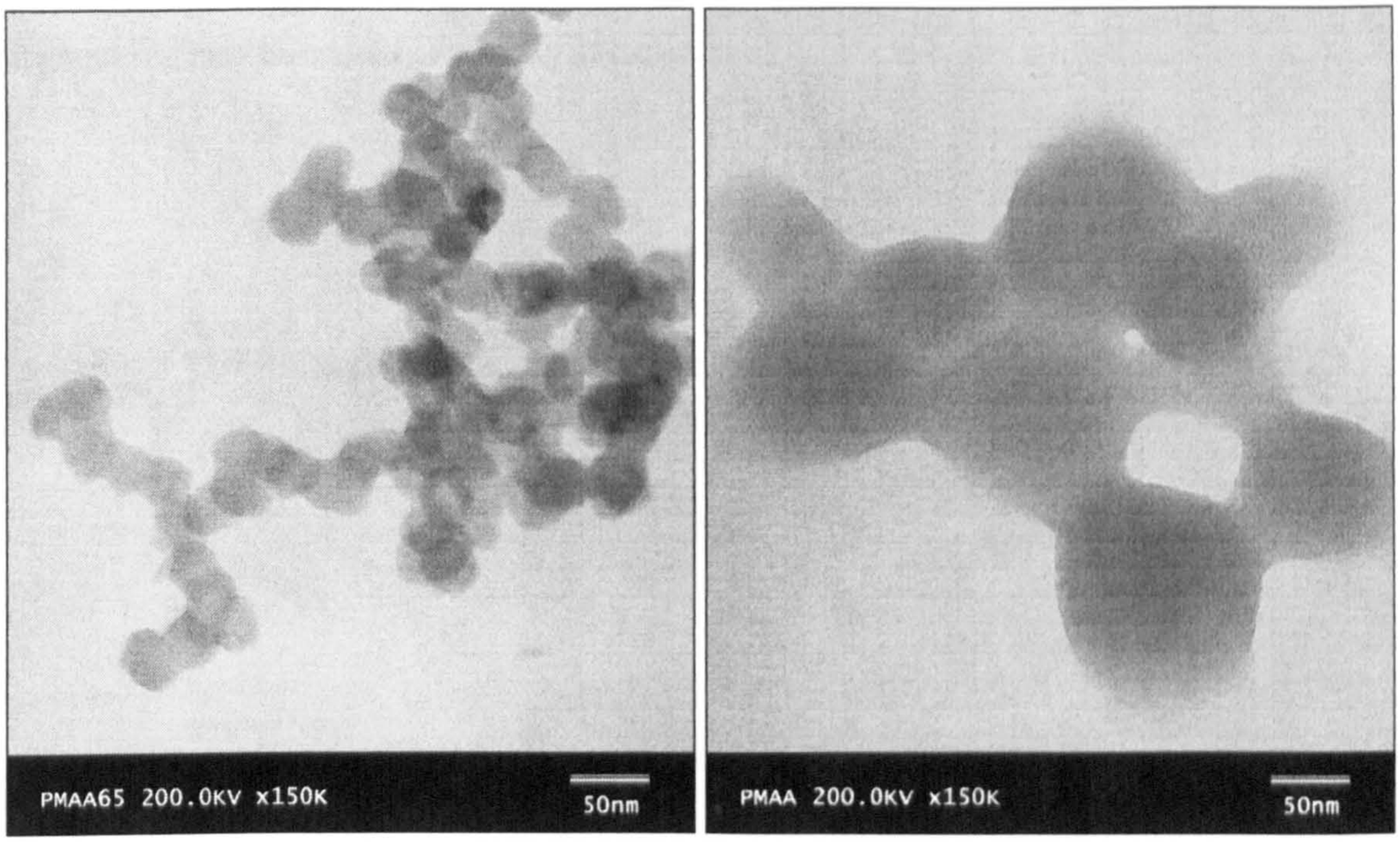

[A] 2.61M

[B] 4.71M

Figure 6.1-15 PMAA nano-spheres prepared via Triton X-114/cyclohexane w/o microemulsion with the different monomer concentrations at 60°C for 6 hours.

6.2 DISCUSSIONS

Polar monomer, acrylamide (AM) polymerised in the Brij 97/cyclohexane w/o microemulsion system with the presence of free-radical initiator KPS at 60°C for 6 hours to form chains of the structure

$$+CH_2\text{-}\underset{\displaystyle CONH_2}{\underset{|}{CH}}+_n$$

, where n is 3, 000 to 7,000.

Solutions of acrylamide in water polymerise at moderate temperatures with the influence of nearly all free-radical initiators, including peroxides, per-sulphates etc. The reaction involves the normal steps of

initiation, propagation, and mutual termination of pairs of growing chains. Reactions are homogeneous throughout and may be carried essentially to completion.

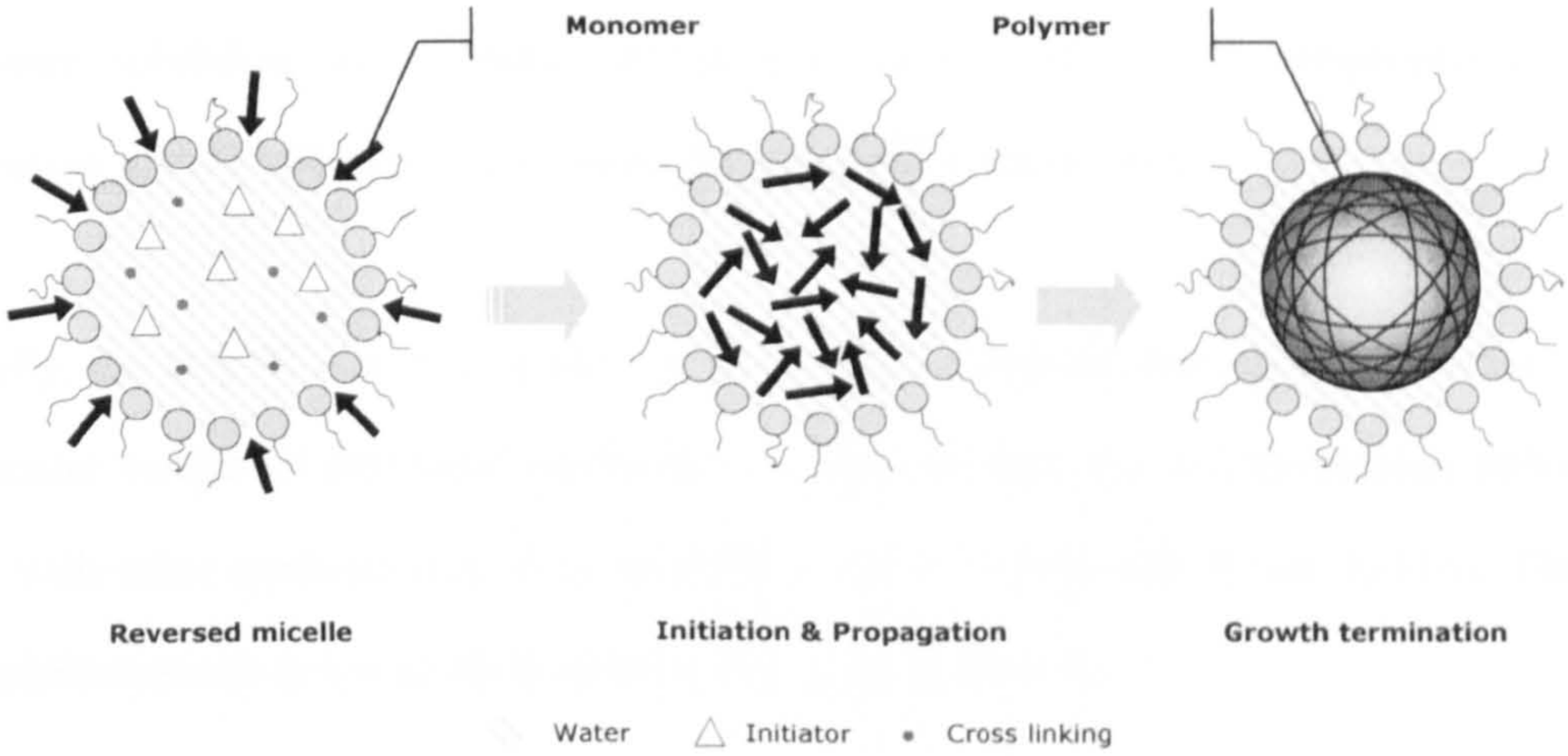

Figure 6.2-1 Schematics of heat initiated polymerisation in a w/o microemulsion system

According to the results of the AM partitioning in oil and water, AM is a highly water soluble monomer (95.5% in water; 4.5% in oil). That means it would prefer stay in the water pool of w/o microemulsion system rather than the continuous oil phase. The reactions occurred in the micro-water-droplets of system are the same as in the monomer water solution. The growth mechanism of AM polymerisation in the w/o microemulsion system is illustrated in **Figure 6.2-1**. The water-soluble initiator is dissolved in the water droplets surrounded by surfactant molecules and disperse in oil to form the w/o microemulsion system containing monomer for polymerisation. Initiator forms free radicals in the water phase and initiates the polymerisation. The reaction is via the normal 3-stage, initiation, propagation and termination. The resultant polymer chains are restricted by surfactant layers and coils in the water-droplets, which form the polymer nano-spheres. The crosslinked polymers will be produced if cross-linking agents are added, the same as the inorganic reactions in the w/o microemulsion, the mechanism includes droplet collision or migration of reactant through the interface into the droplets.

The major problem in the preparation of w/o microemulsion containing monomer as media for a heat initiated polymerisation, is stability. The formation and stability of a w/o microemulsion system are affected by the property of components, the surfactant and the temperature. Therefore, the w/o microemulsion system with Brij 97/cyclohexane, due to its superior stability accompanied with the higher water solubilisation at higher temperature (above 30°C), was employed to study the polymerisation of AM initiated by potassium per-sulphate (KPS) at 60°C.

Additionally, the Brij 97 w/o microemulsion system also exhibited the superiority in the conversion and molecular weight of polymers synthesised, comparing with the microemulsion polymerisation, reactions with other surfactants, (i.e. Tween 85, Igepal CO-520, and Triton X-114). The effect of different surfactants on polymerisation will be discussed in **6.2.5**.

6.2.1 General consideration of AM polymerisation via w/o microemulsions

In free-radical polymerisation, the radical produced by the initiator has an unpaired electron and would like to be paired when possible. The monomer with carbon-carbon double bond has a pair of electrons which could be very easily attacked by the free radicals to form the new chemical bond, between the radical fragment and one of the double bond carbons of the monomer molecule, and leave an unpaired electron to associate itself with the formed radical. Then a new radical unit appears. In this fashion, the monomers can link to each other one by one to form the polymer chains.

The heat is the most widely used mode of generating radicals to initiate polymerisation. The initiators used for thermal initiated polymerisation have different decomposition rate, k_d, at different temperatures. The decomposition rate marks the efficiency of introducing free-radicals of initiators. It is related to half-life, $t_{1/2}$ by the following equation [172]

$$t_{1/2} = 0.693 / k_d \qquad \textbf{(6-4)}$$

According to the **Equation 6-4**, the initiator which has the higher decomposition rate will be more efficient in decomposing and introducing free-radicals, compared with the initiators with lower k_d. The more free radicals decomposing will introduce more monomer molecules to react with them and form new radical units. The rate of monomer being introduced into radicals units can be defined as the polymerisation rate, R_p. So a higher decomposition rate of an initiator will probably result in a higher polymerisation rate of the reaction. Hence, the initiator with a high decomposition rate will initiate the free-radical polymerisation more efficiently.

Table 6.2-1 lists the decomposition rate of KPS in water at different temperatures. It could be found that k_d of KPS increases with the temperature increased from 40°C to 70°C. Hence, ss for our experiment, the rate of AM microemulsion polymerisation at different temperature would be in sequence as: $R_p(70^\circ C) > R_p(60^\circ C) > R_p(50^\circ C) > R_p(40^\circ C)$.

Table 6.2-1 Decomposition rate of potassium persulphate in water at different temperatures [187]

Temperature (°C)	Decomposition rate, k_d (s^{-1})
40	1.65×10^{-2}
50	4.02×10^{-2}
60	5.01×10^{-2}
70	10.08×10^{-2}

The high polymerisation rate indicates that for a particular reaction time, it will result in a higher conversion of monomers, which could explain the results of AM polymerisation *vs.* temperature. The conversion of AM in microemulsion polymerisation increased with the increase of reaction temperature, (ranging from 40°C to 70°C) due to the respective increased decomposing rate of initiator. However, with the increase of reaction time, the conversion of AM will have level off and close to 100%. The polymerisation reaction with the higher polymerisation rate would probably take less time to achieve 100% conversion comparing with the reaction with the lower rate. For example, nearly 80% conversion was obtained from the polymerisation at 60°C for 20 min, but only about 27% conversion

was obtained from the reaction at 40°C after the same time. **Figure 6.2-2** shows the conversion varying with the reaction time of AM microemulsion polymerisation at different temperatures, which is a zoomed-in version of **Figure 6.1-6.**

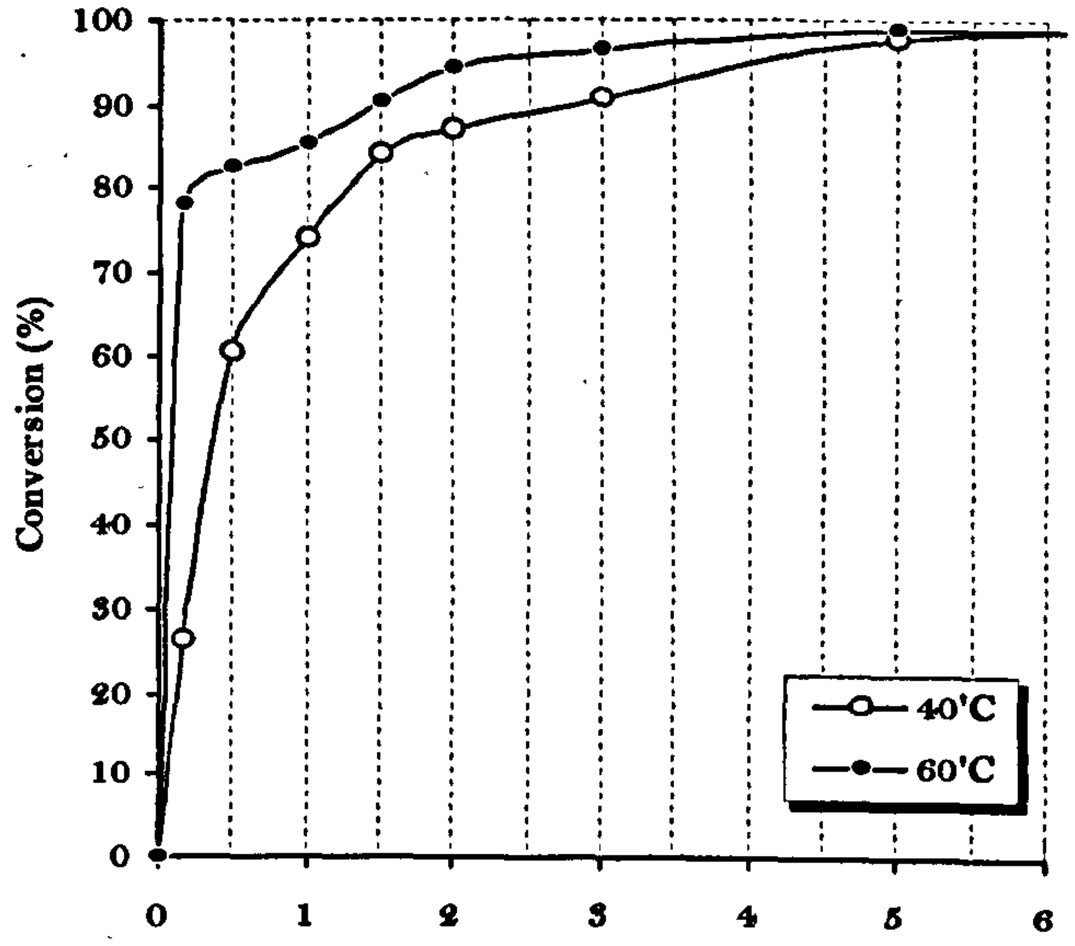

Figure 6.2-2 The conversion of AM polymerisation via Brij 97/cyclohexane w/o microemulsion at different time and temperature.

On the other hand, the free-radical polymerisation of AM initiated by KPS, is a chain polymerisation, where full-sized polymer molecules are produced almost immediately after the start of the reaction. Generally in a chain polymerisation, the polymer size is independent of the conversion [188]. The diameters of the polymer particles remained approximately constant with conversion, while the number of polymer particles grow steadily during the polymerisation [10]. Therefore, it was found that the morphology of PAM nano-spheres produced did not change as the conversion changing with the reaction time. The TEM micrographs of PAM nano-spheres prepared via Brij 97/cyclohexane microemulsion system for 3 hours and 6 hours respectively, showed that polymer produced in both samples was spherical with the size of 80-100 nm.

6.2.2 Effect of initiator

PAM nano-spheres were prepared using different initiators. As hydrophobic initiators, AIBN and ABCN, are present primarily in the continuous oil phase. The monomers will be initiated at the interface by radicals formed from the decomposition of AIBN or ABCN in cyclohexane [147]. If the reaction was initiated by the water-soluble initiator, KPS, which primarily presents in the dispersed water phase, the initiation of AM polymerisation will start mainly in the water-droplets.

Whatever initiator used, (KPS, or AIBN or ABCN), there was no significant difference in conversion value when the reaction finished, however, the morphology of PAM synthesised looked quite different in this case. The spherical polymer particles with the size of 80-100 nm were only obtained from the AM polymerisation initiated by KPS. No PAM nanoparticles could be clearly identified from the TEM micrographs of the samples prepared with AIBN or ABCN, which indicates that for AM polymerisation in Brij 97/cyclohexane system, the site of initiation does not affect the conversion of monomers but probably affects the morphology of the polymer prepared.

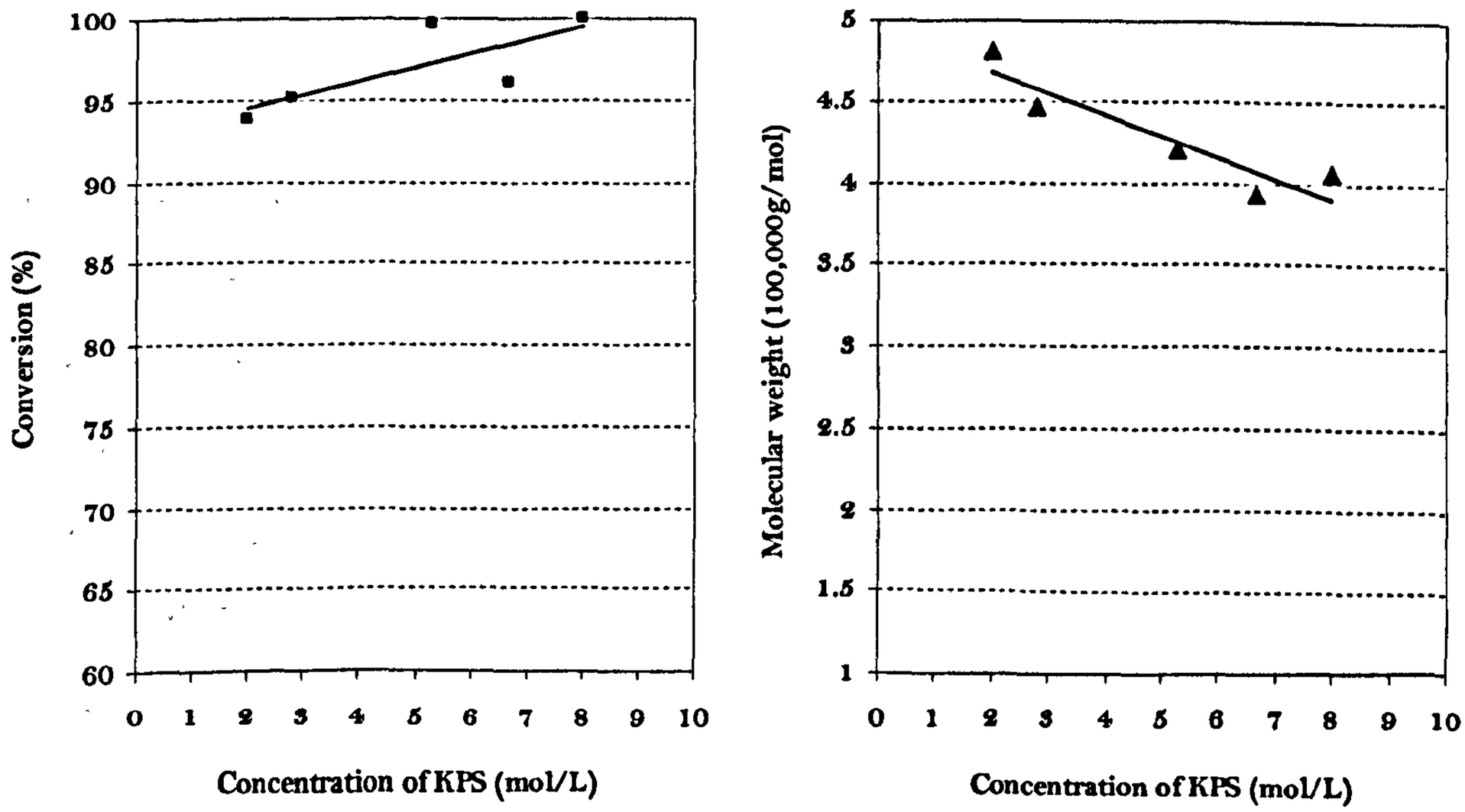

Figure 6.2-3 Effect of the concentration of KPS on the AM conversion and molecular weight of PAM prepared via Brij 97/cyclohexane w/o microemulsion at 60°C for 6 hours.

The effect of initiator concentration was investigated by using KPS in AM polymerisation via w/o microemulsion. As shown in **Figure 6.2-3 A**, for 6-hour reaction, the conversion of AM increased from 93.8% to 100% with an increase of the concentration of KPS. The slight difference between the conversion values was presumably attributed to the different polymerisation rates arising from the different initiator concentrations.

$$R_p = k_p[\mathrm{M}]\left(\frac{fk_d[\mathrm{I}]}{k_t}\right)^{1/2} \qquad \textbf{(6-5)}$$

Equation 6-5 describes the most common case of free radical chain polymerisation [188] where R_p is the polymerisation rate, [M] is the concentration of monomer, [I] is the concentration of initiator, f is the initiator efficiency defined as the fraction of the radicals produced, and k_p, k_t are rate constants of propagation and termination steps respectively. **Equation 6-5** shows that the polymerisation rate is dependent on the square root of the initiator concentration. This dependence has been proved for many different monomer-initiator combinations over wide ranges of monomer and initiator concentrations [189-190].

Since in a particular reaction time, the AM polymerisation with higher polymerisation rate would yield the higher conversion value, therefore increasing the initiator concentration would normally increase the polymerisation rate and result in a higher conversion of monomers.

However, with the increase of the concentration of KPS, the molecular weight of PAM prepared in w/o microemulsion decreased. **Figure 6.2-3 B** shows the dependence of molecular weight on initiator concentration. The slope is about -0.1. An increase of initiator concentration would generally result in an increase of primary radical decomposed. Is has been reported by Deb and Kapoor [191] and Berger *et al.*[192] that, at the high concentration of primary radicals, the termination mode may change from the normal bimolecular termination between propagating radicals to primary termination, which involves propagating radicals reacting with primary radicals:

Bimolecular termination:
$$\mathrm{M}_n\bullet + \mathrm{M}_m\bullet \xrightarrow{k_d} \textit{Dead polymer} : \mathrm{M}_{n+m} \qquad \textbf{(6-6)}$$

Primary termination: $$M_n\bullet + R\bullet \xrightarrow{k_d} Dead\ polymer : M_n - R \qquad \textbf{(6-7)}$$

In this case, the growth of polymer chains could be terminated by the presence of primary radicals. The more primary radicals produced, the more opportunities that the primary termination occurs. Therefore, the increase of the concentration of KPS could interrupt the build-up of molecular weight of PAM and result in comparably lower molecular weight values.

The molecular weight of PAM decreases with increasing KPS concentration was also reported by Candau *et al.* [147], which was synthesised via AOT/toluene w/o microemulsion system. Furthermore, Xu *et al.* [150] found similar results in the preparation of poly-(methyl methacrylate) initiated by benzoyl peroxide via the microemulsion system.

6.2.3 Effect of crosslinking

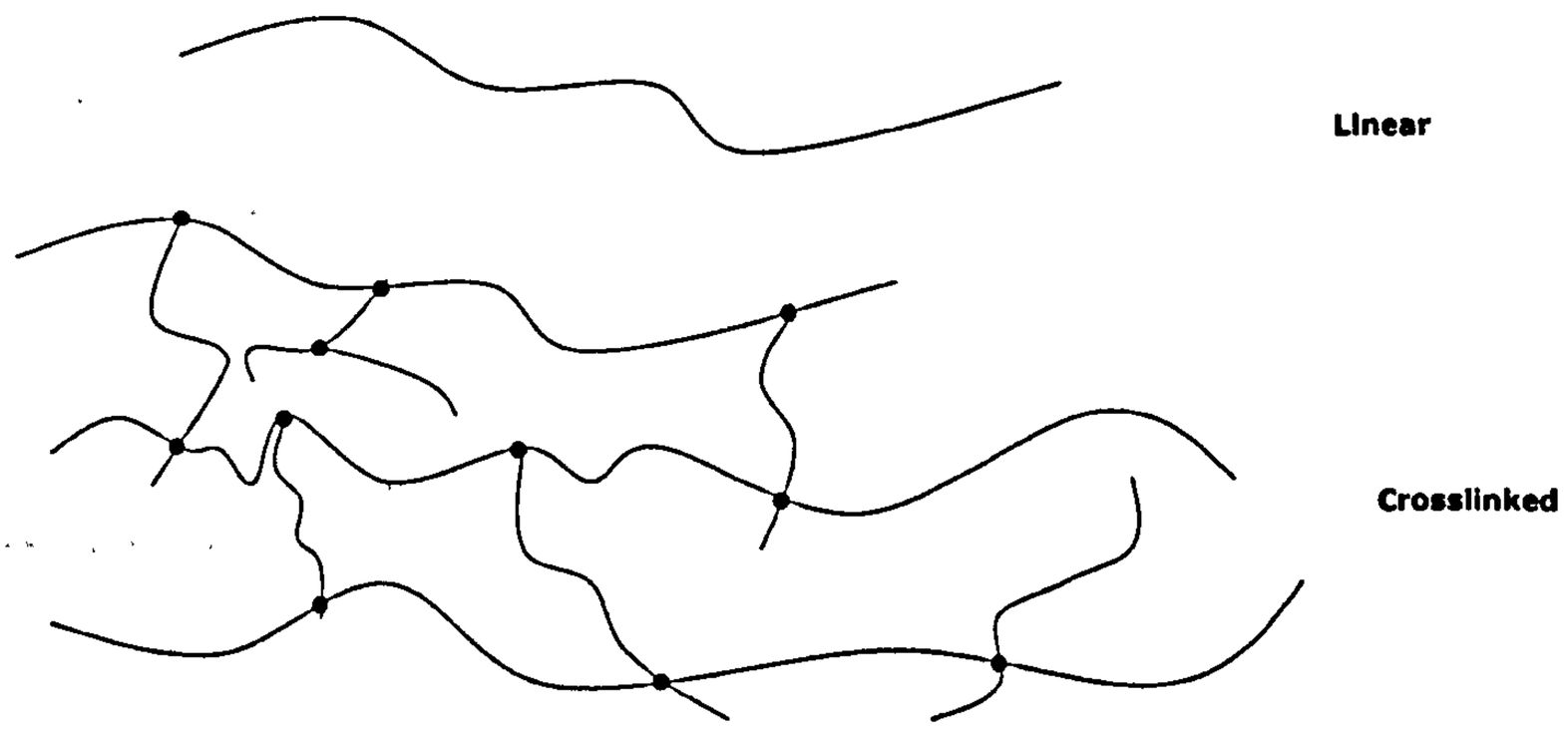

Figure 6.2-4 Structure of linear and crosslinked polymers.

When the polymers are produced in which the polymer molecules are linked to each other, at multi-points other than their ends, the polymers are said to be crosslinked [188] [Figure 6.2-4]. Crosslinking is

important because it turns an assembly of separate chains into a network structure with a resultant change of properties. The polymerisation of acrylamide in the presence of N, N'-methylen-bisacrylamide (MBA), leads to a crosslinked polyacrylamide with a nearly uniform distribution of pendant ethyleneacrylamide groups.

Due to the formation of the network structure, the crosslinking should give the polymers greater solvent resistance. For example, PAM is a water soluble polymer, and it can dissolve in some polar solvents. However, a crosslinked PAM network will only swell in these solvents. That was the reason why in the experiment, the conversion value of AM reacted with crosslinking agent was much higher than the reaction without crosslinking.

Table 6.2-2 Size of PAM nano-spheres prepared in Brij 97/cyclohexane at 60°C for 6 hours with different molar concentrations of MBA.

Concentration of cross-linking $\times 10^{-2}$ [M]	**0.27**	**6.6**	**10.6**	**26.5**
Particle size [nm]	**300-400**	**80-100**	**NA**	**NA**

The addition of a crosslinking agent will affect the morphology of the polymer produced. In the experiment, the PAM nano-nanospheres were only achieved when the concentration of MBA was 6.6×10^{-2} M and 0.27×10^{-2} M, respectively. As shown in **Figure 6.1-9 C**, the sample looked like a network constructed from individual particles linked together when the concentration of crosslinking agent was increased to 10.6×10^{-2} M. When the concentration was increased to 26.5×10^{-2} M, no individual particles were observed **[Figure 6.1-9 D]**. Since the mechanism of microemulsion polymerisation includes the droplet collision or the migration of reactant through the interface into the droplets, a large quantity of MBA in the water phase might not only crosslink the polymer chains in the same water pool, but also probably extend the network structure by inter-micelle exchange during the collision of different droplets. Hence, probably the individual PAM nano-spheres could only be produced when the concentration of crosslinking agent was low.

Table 6.2-2 lists the corresponding particle sizes of different PAM samples prepared with different concentrations of MBA. If was found that when the MBA concentration decreased from 6.6×10^{-2}M to 0.27×10^{-2} M, the particle size of PAM spheres increased from 80-100 nm to 300-400 nm. As mentioned above, it is the crosslinking make the water soluble PAM into network structure and un-dissolved in water or other polar solvents. So when the concentration of crosslinking agent was low, the extent of the swelling of PAM nano-spheres might be promoted and result in the increased size of polymer spheres.

6.2.4 Effect of monomer concentration

From the discussion above, most AM molecules due to their hydrophilicity stay within the interior of water droplets in w/o microemulsion systems. However, the monomers can still part present in the surfactant layers due to their minor lipophilicity. It has been reported in **4.1** that AM monomers are not simply dissolved in the water phase in microemulsion system but some of them will be found in the surfactant layer, most likely playing the role as a co-surfactant, improving the solubilisation of the water phase.

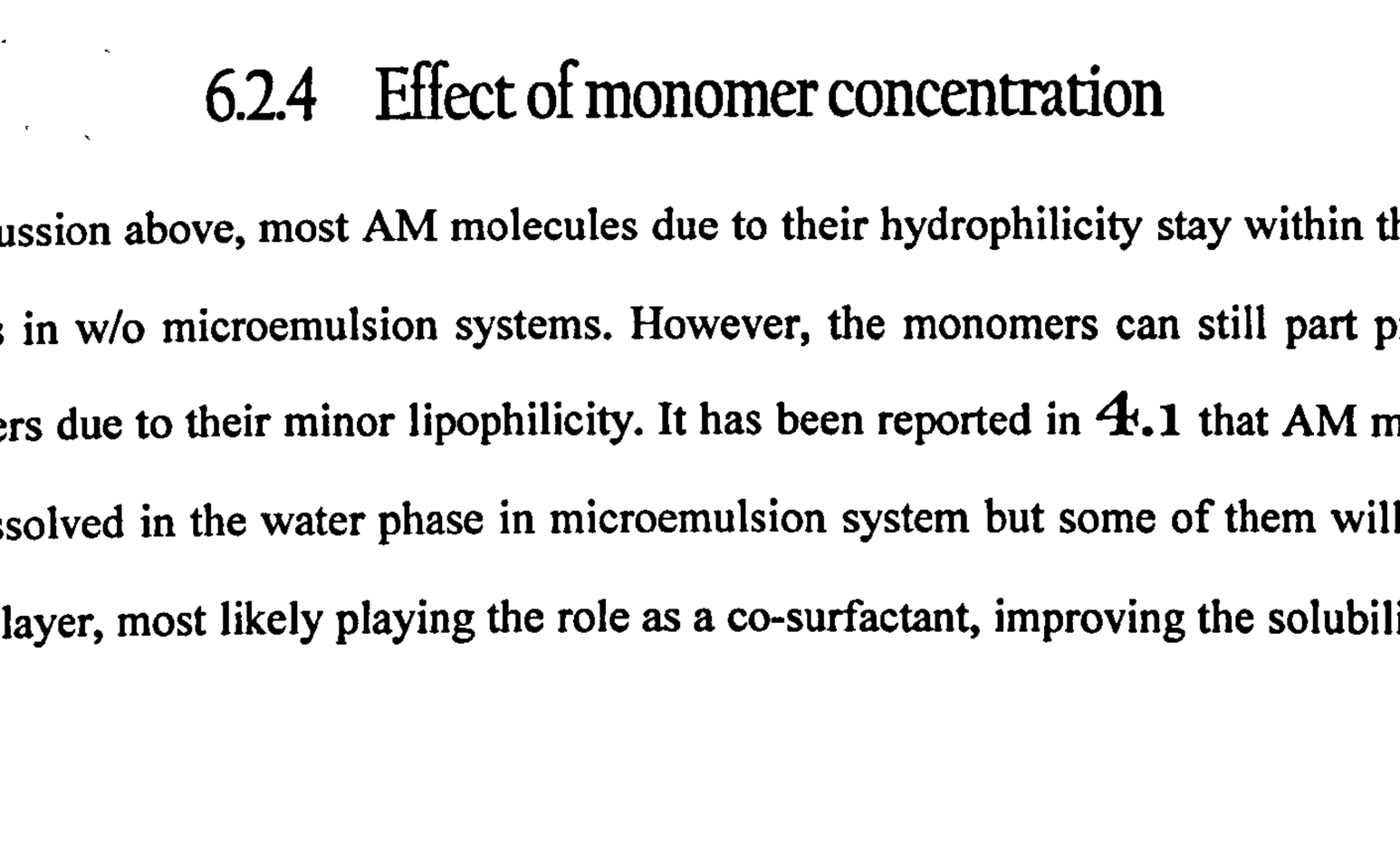

Figure 6.2-5 Maximum solubilisation of AM water solution in Brij 97/cyclohexane w/o microemulsion system with the different weight concentrations at 60°C.

Figure 6.2-5 shows the improvement of maximum solubilisation of the aqueous phase in Brij 97/cyclohexane w/o microemulsion system with the increase of AM concentration in the aqueous phase. From the discussions in **4.2**, the presence of monomers acting as co-surfactants in the interface of water/oil increases the cross-sectional area, which results in the increase of the volume of micelles and consequently the solubilisation of aqueous phase. Hence it was found that with the presence of AM molecules, $S_{w\text{-}max}$ increased from 6.2% for the pure water to 8.68% for 10% AM water solution. However, the improvement of solubilisation will be less pronounced if the AM concentration is increased, presumably because the partitioning of the AM molecules in surfactant layer is saturated and the further increase of AM concentration will most likely result in the increase of AM molecules in the core of the water droplets. This might be the reason why $S_{w\text{-}max}$ seemed to level off when the concentration was above 30%. On the other hand, the increased AM monomers in the water droplets, where the initiation starts, could result in the increase of conversion of microemulsion polymerisation in a particular time **[Figure 6.2-6 A]**.

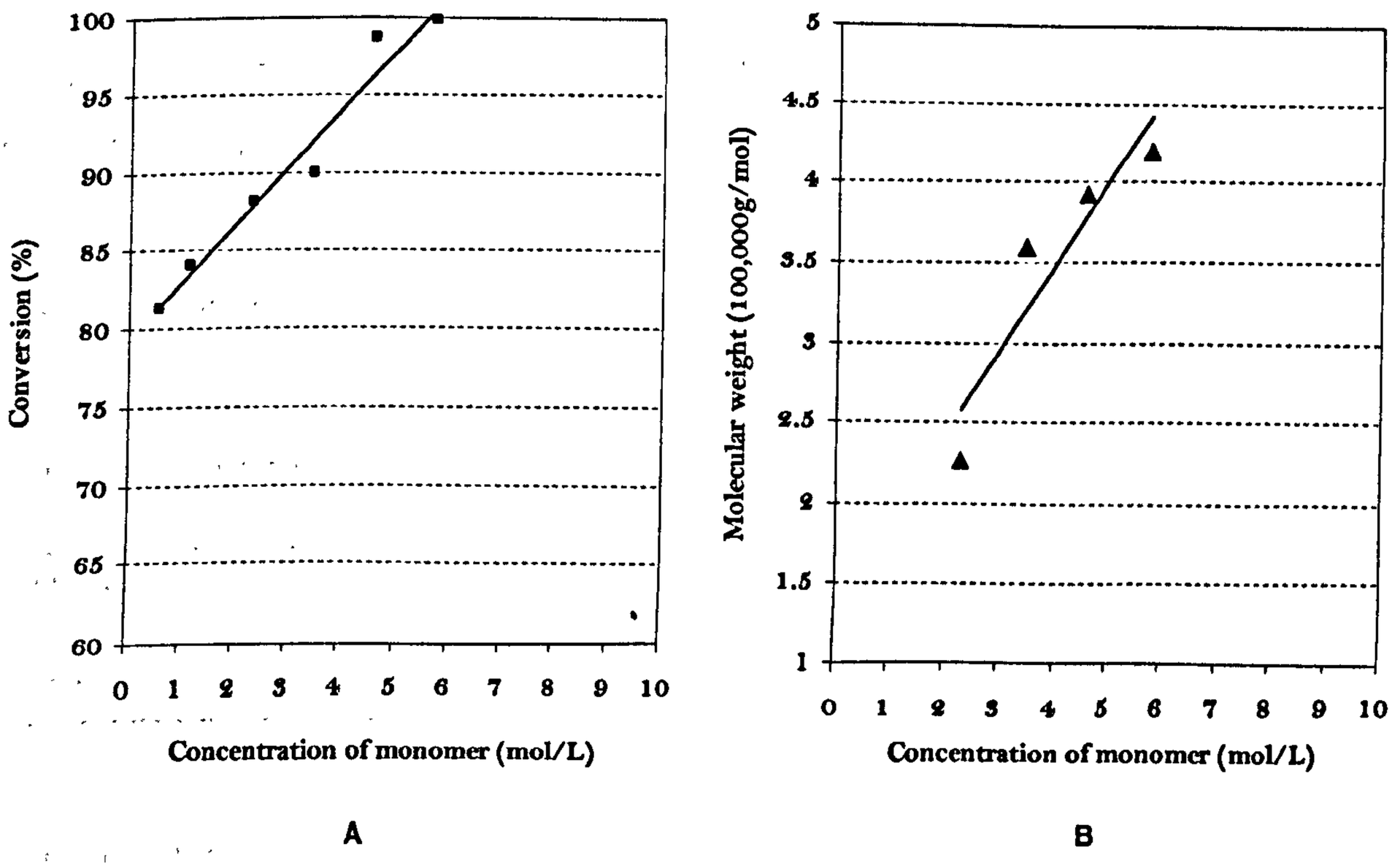

Figure 6.2-6 Effect of the concentration of AM on the conversion and molecular weight of PAM prepared via Brij 97/cyclohexane w/o microemulsion at 60°C for 6 hours.

The different partitioning of AM molecules with the different AM concentrations, is also proposed to account for the resultant difference of molecular weight and the size of PAM prepared. The effect of AM concentration on the molecular weight of PAM prepared, is shown in **Figure 6.2-6 B**. With the increase of AM concentration, the molecular weight of polymer increased, and the slope is about 0.5. Candau *et al.* [147] showed similar results for the synthesis of AM polymerisation in a w/o microemulsion system as $\overline{M_v} \propto [AM]^{0.4}$ without initiator. The free radical polymerisation reaction in the absence of any initiator is usually attributed to the presence of impurities in the medium [193]. The increase of the polymer molecular weight with an increase of monomer content was also found in the synthesis of PMMA in microemulsion systems, as reported by Xu *et al.* [150] that $\overline{M_v} \propto [MMA]^{0.73}$. The increase of AM content would result in the increase of AM molecules reacted with the primary radicals or radical fragments in the water droplets, which probably initiate the propagation reactions and consequently give a rise of k_p. The build-up of molecular weight of polymer could be attributed to the ratio:

$$k_p / k_t^{1/2} \qquad \textbf{(6-8)}$$

being high in an acrylamide free-radical polymerisation [194]. As shown in **Equation 6-8**, with the relatively high rate of propagation, the build-up to high molecular weight can readily be visualised. Therefore, the increase of monomer concentration in AM microemulsion polymerisation would possibly result in the build-up to high molecular weight of PAM.

Table 6.2-3 Size of PAM nano-spheres prepared in Brij 97/cyclohexane w/o microemulsion system at 60°C for 6 hours with the different concentrations of AM.

AM mole concentration $\times 10^{-2}$ [M]	1.15	2.30	3.45	4.6	5.75
Particle size [nm]	300-500	/	40	50-80	80-100

As mentioned above, an increase of AM concentration possibly increases the volume of micelles without disturbing the system stability, which indicates the "micro-reactors" (i.e. water droplets) in microemulsion polymerisation constructed by surfactant molecules, could be larger with the higher

concentration of AM. Therefore, the larger PAM nano-spheres would be expected to be synthesized in the larger micelles. **Table 6.2-3** summarises the effect of monomer concentration on the size of polymer nano-spheres synthesized. As the AM concentration was increased from 3.45M to 5.75M, the size of PAM particles increased from 50 nm to 80-100 nm. No polymer spheres could be observed in the sample prepared with the monomer concentration at 2.30M. However, the TEM micrograph of this sample **[Figure 6.1-9 B]** appears to show the networks consisted of large quantities of small polymer particles, size around 100 nm. For the investigation with the same amount of the solubilisation of aqueous phase, the decrease of monomer concentration means the increase of water content in the system, particularly the water droplets. Water is a solvent for the polymer PAM. So with an increase of water content, the PAM nano-spheres formed in water droplets might be more readily swollen. It is found in **Table 6.2-3** that when the monomer concentration was decreased to 1.15M, the polymer spheres produced became swollen to large spheres, size of 300-500 nm.

6.2.5 Investigation of system-controlled polymerisation

Similar to the synthesis of inorganic nanoparticles via the w/o microemulsion systems, one of the most important considerations in utilising w/o microemulsion to produce polymer nanoparticles, is the possibility of a potential system control, by changing the system parameters such as surfactant percentage or the size of water pool (ω_0), to change the morphology of the polymer nano-spheres produced. The investigation included the effects of different surfactants, different surfactant concentrations and the different sizes of water pools (ω_0).

6.2.5.1 Effect of different surfactants

The Brij 97/cyclohexane w/o microemulsion system was initially selected as the more appropriate system to preparation of PAM nano-spheres, due to its higher water solubilisation at higher temperature. A comparison of the effects on polymerisation with different surfactants, further showed that Brij 97/cyclohexane was a better system also in terms of produced high conversion, molecular weight and the spherical morphology of polymers.

The conversion values and the molecular weight values of PAM prepared in different microemulsion systems with different surfactants are shown in **Figure 6.2-7**. Regarding the morphology, as shown in **Figure 6.1-1**, only the Brij 97 system produced spherical PAM particles. All these different polymerisation results arising from the different surfactants, are presumably attributed to the different partitioning of AM molecules in the different reaction systems.

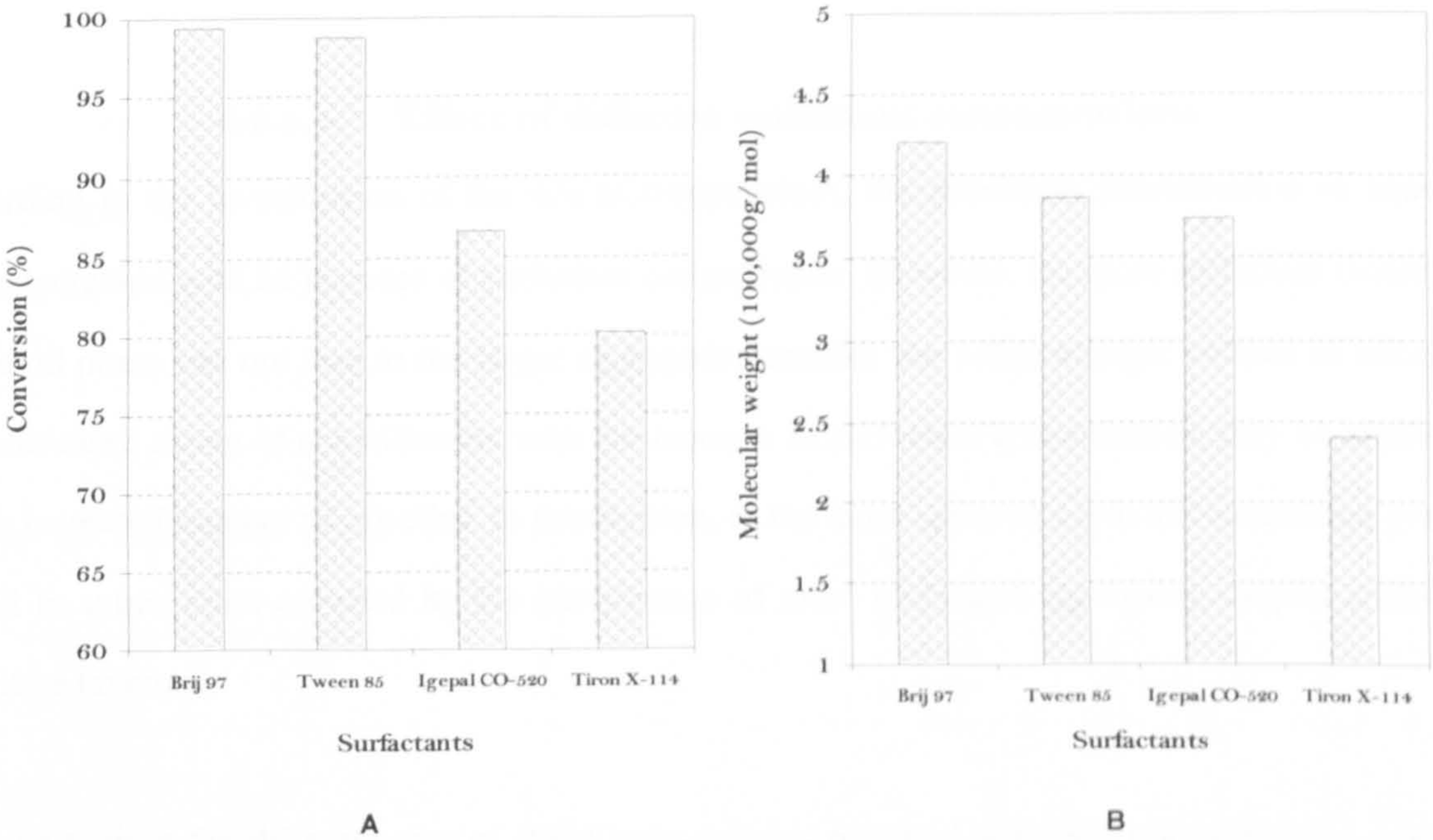

Figure 6.2-7 Effect of the different surfactants on the conversion and molecular weight of PAM prepared via Brij 97/cyclohexane w/o microemulsion at 60°C for 6 hours.

Table 6.2-4 Maximum solubilisation [%] of the aqueous phase in w/o microemulsion systems with different surfactants at 60 °C. Surfactant : oil = 1:3 (wt:wt)

Aqueous phase	water	AM solution (50%)
Brij 97	6.19	11.8
Tween 85	1.4	11.0
Igepal CO-520	0.4	11.9
Triton X-114	0.6	7.4

Table 6.2-4 shows the maximum solubilisation of different aqueous phases in w/o microemulsion systems with different surfactants at 60°C. It was found that in the presence of monomers, the Tween

85, Igepal CO-520 and Triton X-114 systems all exhibited higher solubilisation of aqueous phase and the increase of their $S_{w\text{-}max}$ values of AM solution comparing with water were all larger than Brij 97 system. Hence, to improve the power of solubilisation to such an extent, the AM molecules in these three systems are largely located in the interface to act as co-surfactant. In this case, the propagation will most likely occur near the outer part of water droplets, which would possibly benefit the inter-micellar growth of PAM. Therefore, the formation of individual PAM nano-spheres growing within water droplets would be difficult.

6.2.5.4 Effect of different surfactant concentrations

According to the investigation of the w/o microemulsions, the maximum solubilisation of aqueous phase increased with an increase of surfactant concentration. However, the more surfactant molecules in the oil phase can not lead to the larger aggregation number nor either a larger volume of micelles. The increased extent of solubilisation with the increase of surfactant concentration, may be attributed to the increased number of micelles. In this fashion, as the inner space of a w/o microemulsion system would be much more crowded by the introduction of more surfactant aggregates, droplet collisions would be favoured.

Table 6.2-5 gives the different size of PAM nano-spheres prepared with w/o microemulsion systems with different surfactant concentrations. It was found that the size of polymer spheres increased from 50 nm to 200 nm as the surfactant concentration increased from 19.3% to 28.9%, presumably due to the favoured, further growth of PAM nano-spheres by the mechanism of droplet collision.

Table 6.2-5 Size of PAM nano-spheres prepared in Brij 97/cyclohexane at 60°C for 6 hours with different concentrations of surfactants.

Surfactant concentration [wt%]	14.5	19.3	24.1	28.9
Particle size [nm]	/	50-80	80-100	150-200

6.2.5.3 Effect of different size of water pools (ω_o)

The size of water pools in the w/o microemulsion system increased with the increase of the percentage

of aqueous phase, which means there would be more space for the growth of polymer synthesized. As a result, the larger size of PAM nano-spheres would be expected. **Table 6.2-6** summarises the effect of the size of water pools on the size the PAM synthesised. The water pool size ω_0 is calculated from the molar ratio of water phase to surfactant:

$$\omega_0 = [\text{Water}]/[\text{Surfactant}] \quad (6\text{-}9)$$

It was found that the size of PAM nano-spheres increased from 50 nm to 500 nm as ω_0 increased from 2.43 to 6.08, which indicates the possibility of system-controlled particle growth in the w/o microemulsion system. The similar results have also been reported by Dresco *et al.* [155] that, the polymer nanospheres synthesised by microemulsion polymerisation had size values ranging from 220 to 320 nm, depending on the water/surfactant molar ratio.

Table 6.2-6 Size of PAM nano-spheres prepared in Brij 97/cyclohexane at 60°C for 6 hours with different size of water pools. Surfactant : oil = 1:3 (wt:wt)

Water pool size [mol/mol]	1.60	2.43	3.57	4.32	6.08
Particle size [nm]	/	50	80-100	250-500	/

6.2.6 Investigations of the synthesis of PMAA

In our experiment, PMAA nano-spheres were synthesised via Triton X-114/cyclohexane w/o microemulsion system, at 60°C for 6 hours. The mechanism of MAA polymerisation in microemulsion is different from the polymerisation of AM in microemulsion systems, mainly because MAA monomer is an oil-soluble monomer, which prefers to stay in the continuous oil phase of microemulsion systems. As both reactions were initiated by water-soluble initiator KPS, the initiation of water-soluble monomer AM, would start in the water-droplets but the initiation location of MAA would be probably in the interface of the water/oil. This monomer partitioning also determines the propagation loci of microemulsion polymerisation. As discussed above, since the free radicals are

generated by KPS in the water phase, the build-up of PAM would take place within the water-droplets. However, the propagation of MAA polymerisation seems likely to happen near the interface.

- **Effect of different surfactants**

Tween 85, Igepal CO-520, Triton X-114 and Brij 97 were used in this investigation. It was found that over 90% conversion values of PMAA were obtained by the polymerisation in Tween 85, Igepal CO-520 and Triton X-114 systems, respectively at 60°C for 6 hours, while under the same reaction conditions, the conversion of PMAA in Brij 97 system was only 53.4%.

The different conversion might be attributed to the different arrangement of surfactant molecules in cyclohexane. Since Tween 85, Igepal CO-520 and Triton X-114 all have cyclic chains in their structures, the aggregation of such kind of surfactant molecules in the oil phase would be in a loose packing state [174]. However, Brij 97 due to its straight chain in alkyl group, the packing of Brij 97 molecules in the oil phase would be tight and comparably in-flexible [174], which would probably lead to the lower transfer of the oil-soluble MAA monomers from the oil phase to the water droplets during the microemulsion polymerisation. As a result, the conversion of PMAA was low after the polymerisation in Brij 97/cyclohexane at 60°C for 6 hours. Hence, Brij 97/cyclohexane is not a suitable system in the microemulsion polymerisation of MAA, although it has good capability of the solubilisation of aqueous phase at 60°C. Therefore, Triton X-114/cyclohexane was selected for the w/o microemulsion system to carry out the MAA polymerisation, due to its higher extent of solubilisation of MAA water solution (25wt%) at higher temperature and the higher conversion of the polymer produced.

- **Effect of polymerisation time and temperature**

Due to the partitioning of MAA in the w/o microemulsion systems, most MAA molecules need to penetrate the surfactant layer then react with the free radicals or radical fragments generated in the water phase during the polymerisation. Hence, the initiation efficiency of KPS would probably be depressed, comparing with AM polymerisation in microemulsions. Since the decomposition rate of

KPS in water decreased with the decrease of temperature from 70°C to 40°C, no polymer precipitated out from MAA microemulsion polymerisation after 6 hours with the reaction temperature below 60°C. As for the microemulsion polymerisations of MAA carried out at 60°C and 70°C, respectively, it was found that the polymerisation rate increased with the reaction temperature, presumably due to the increased decomposition rate of KPS at higher temperature.

- **Effect of initiator concentration**

The degree of conversion to PMAA increased from 22.6% to 100% with the increase of KPS concentration from 1.75×10^{-3} M to 8.81×10^{-3} M **[Figure 6.2-8 A]**. The lowest conversion value (22.6%) coming from the lowest KPS concentration, associated with the lower KPS initiation efficiency.

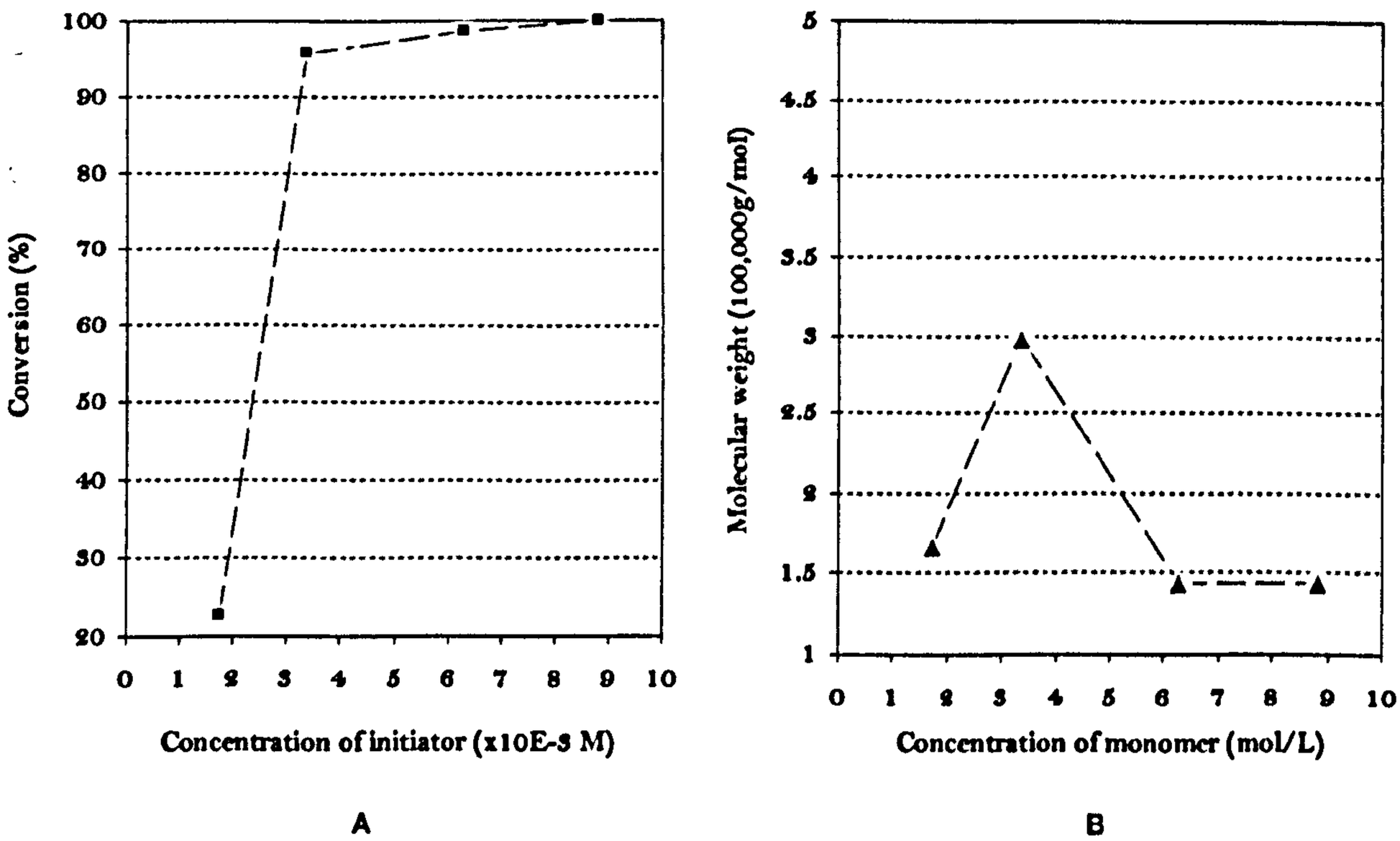

Figure 6.2-8 Effect of the concentration of KPS on the conversion and molecular weight of MAA prepared via Triton X-114/cyclohexane w/o microemulsion at 60°C for 6 hours.

As shown in **Figure 6.2-8 B**, there was an initial increase in the molecular weight of the resulting polymers as the initiator concentration increased up to 3.38×10^{-3}M, and then decreased with a further increase in the KPS concentration. This phenomenon is often the case in conventional inverse

emulsion polymerisations of certain acrylic compounds [195]. When more initiator was used, the more nucleated particles were produced, resulting in a lowering of the molecular weights of the polymers. On the other hand, the lower molecular weight, (e.g. 1.67×10^5 g/mol of PMAA prepared with 1.75×10^{-3} M KPS compared with the sample prepared with 3.38×10^{-3} M) is presumably because of the chain-transfer reactions introduced by the large amount of the surfactant, hence the growing chains would be readily terminate the propagation in the microemulsion systems.

- **Effect of monomer concentration**

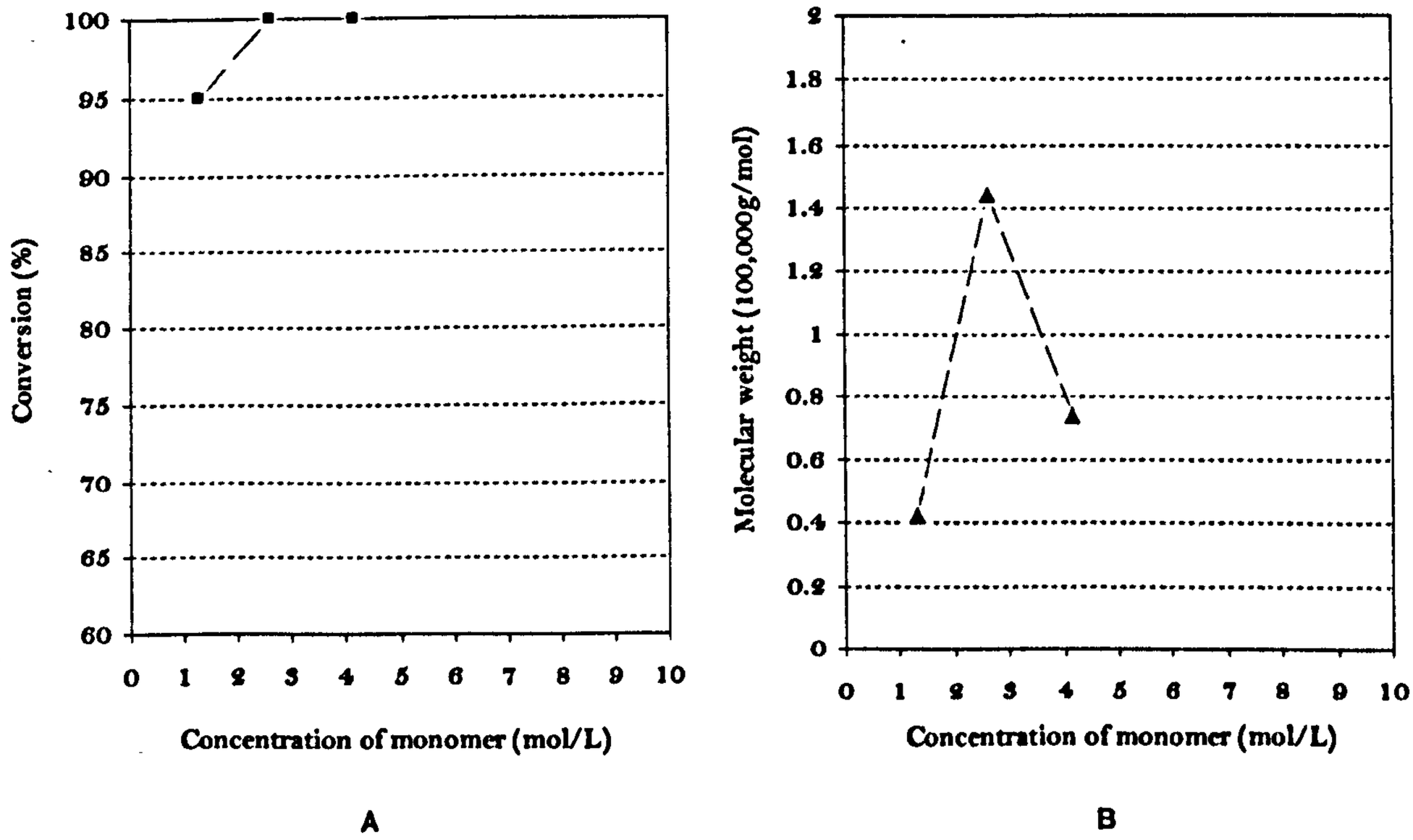

Figure 6.2-9 Effect of the concentration of MAA on the conversion and molecular weight of PMAA prepared via Triton X-114/cyclohexane w/o microemulsion at 60°C for 6 hours.

The increase of MAA concentration generally leads to the increased conversion of PMAA prepared via microemulsion systems [**Figure 6.2-9 A**], due to the increased numbers of monomers captured in the polymerisation. There was an increase in the molecular weight of the PMAA synthesised with an increase in the monomer concentration, as there was more monomer to take part in the propagation reaction [196]. However, the molecular weight of PMAA decreased when the monomer concentration was increased to 4.17×10^{-3} M accompanied with an observed phase separation.

SUMMARY

Polyacrylamide nano-spheres were synthesised in a w/o microemulsion system, at 60°C for 6 hours, initiated by KPS. Brij 97/cyclohexane was shown to be an appropriate system compared with others used in terms of resulting conversion, molecular weight and spherical morphology.

The conversion increased with an increase of reaction time and temperature until 100% complete, while the size of polymer spheres was unchanged. Different concentrations of crosslinking agent produced PAM nano-spheres with a different morphology. The spherical particles were prepared with lower concentration of crosslinking agent ($<10.6\times10^{-2}$M).

The increase of AM concentration from 3.45M to 5.75M could result in the increase of conversion and molecular weight from 3.60×10^5 g/mol to 4.20×10^5 g/mol, as well as the size of polymer nano-spheres increased from 40 nm to 100 nm. The size of PAM spheres also increased with an increase of surfactant concentration and the size of water pools, which indicates the possibility of system-controlled synthesis of PAM nano-spheres.

PMAA nano-spheres were synthesised via w/o microemulsion system, Triton X-114/cyclohexane, at 60°C for 6 hours. The size of PMAA nanospheres increased with the increase of monomer concentration.

7 SYNTHESIS OF NANOCOMPOSITES

7.1 PREPARATION OF SILICA/IRON OXIDE NANOCOMPOSITES

The preparation of silica/iron oxide nanocomposites was carried out in Igepal CO-520/cyclohexane w/o microemulsion system at 25°C. The preparation of silica nano-spheres was also included in the investigation in terms of the different system-dependent parameters, (i.e. loading of the aqueous phase and the surfactant concentration), and the different molar ratio of reactants. The latter was further investigated in the preparation of nanocomposites.

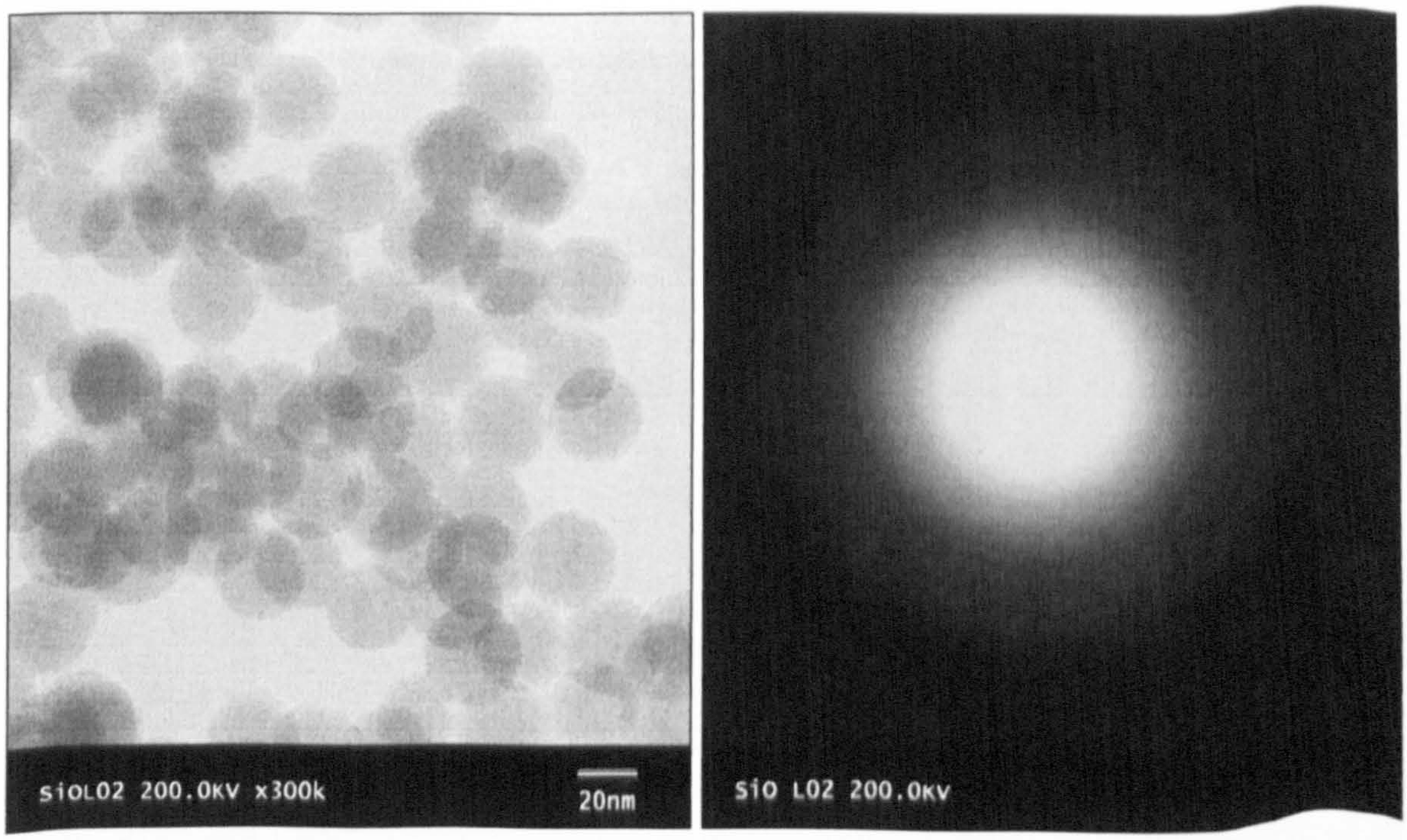

[A]. 2%, 29.1% [A.DF]

Figure 7.1-1 TEM micrographs of silica nano-spheres prepared via Igepal CO-520/cyclohexane w/o microemulsion system at 25°C for 24 hours and their diffraction patterns. Surfactant : oil = 1:4 (wt:wt)

7.1.1 Preparation of silica nano-spheres

The silica (silicon oxide) nano-spheres were prepared by tetra-ethyl-ortho-silicate (TEOS) hydrolysis via a w/o microemulsion system of Igepal CO-520/cyclohexane, at 25°C for 24 hours. The phase diagram of Igepal CO-520/cyclohexane microemulsion system was given in **Chapter 5**. The TEM micrographs of one of the silica samples and its amorphous diffraction pattern are shown in **Figure 7.1-1**. The size of particles in **Figure 7.1-1 A** was about 30 nm and these particles are essentially mono-dispersed and spherical in shape. The following sections of **Chapter 7** include the investigation of the preparation of silica nano-spheres with respect to the molar ratio of H_2O to TEOS, the loading of aqueous phase and the different surfactant concentrations.

7.1.1.1 Studies on the molar ratio of H_2O to TEOS

The silica nano-spheres were prepared in w/o microemulsion at 25°C for 24 hours, with the loading of aqueous phase as 2% and the molar ratio of H_2O to TEOS (RHT) varied between 20 and 60.

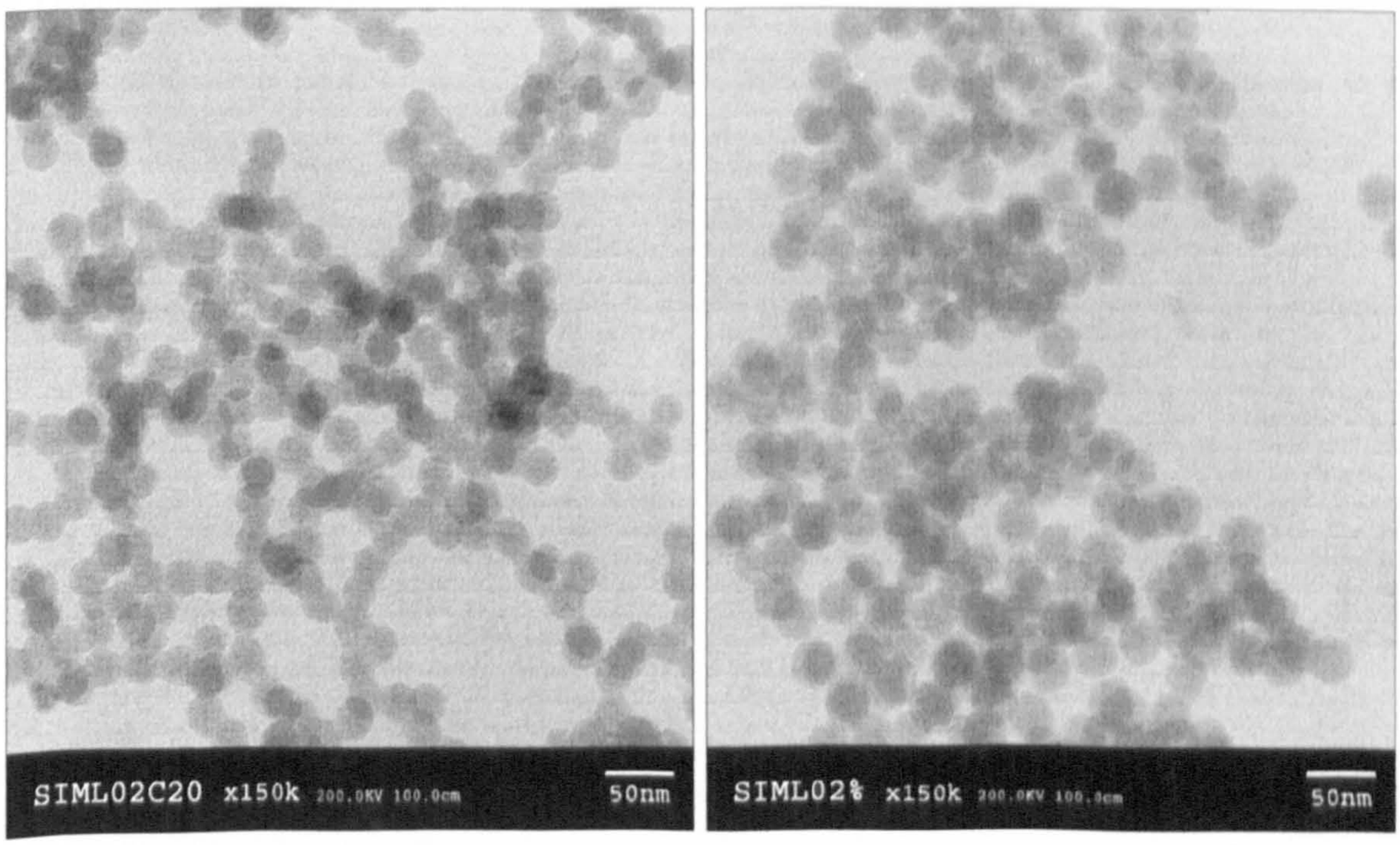

[A]. RHT=20 [B]. RHT=40

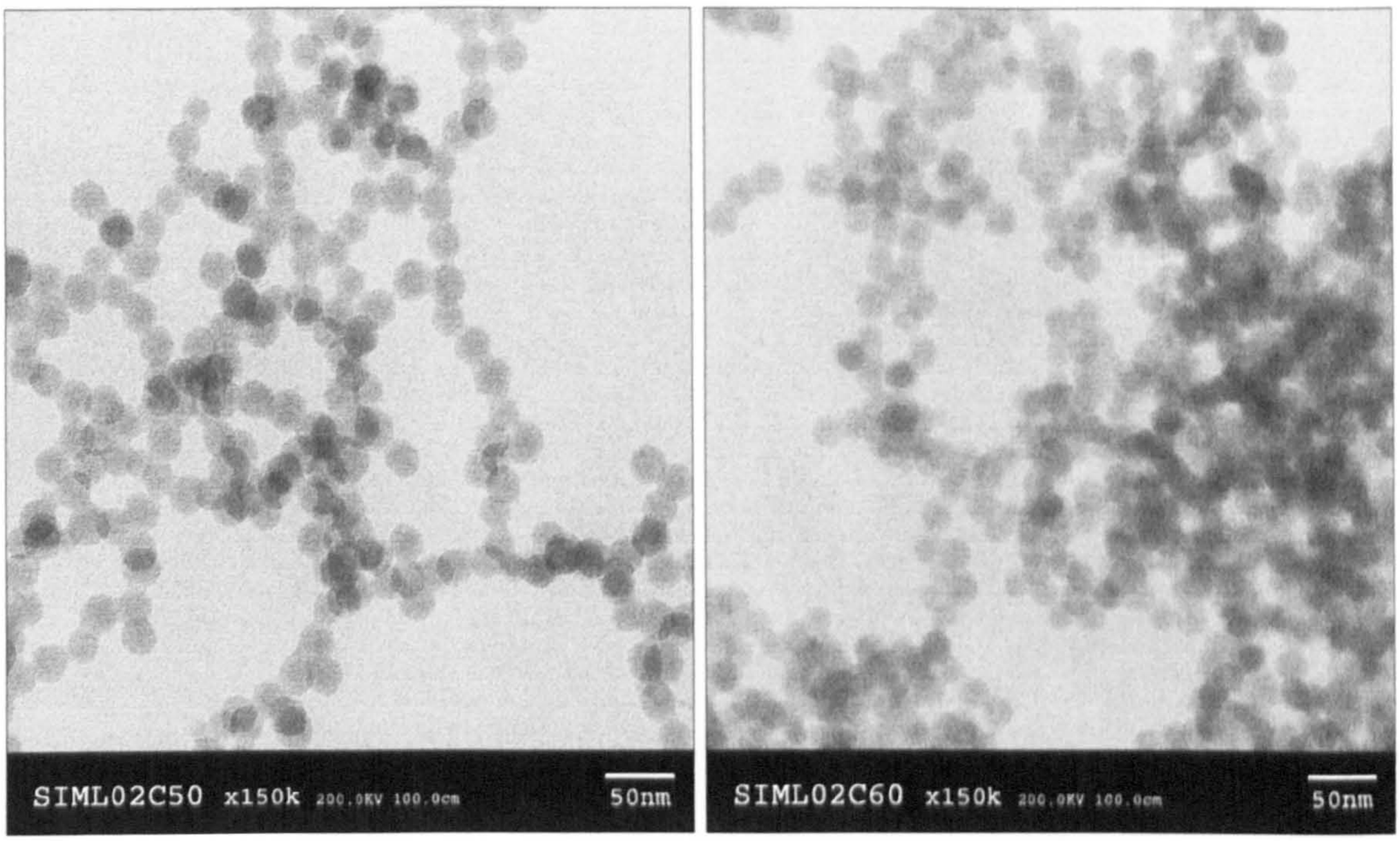

[C]. RHT=50 [D]. RHT=60

Figure 7.1-2 TEM micrographs of silica nano-spheres prepared via Igepal CO-520/cyclohexane w/o microemulsion at 25°C for 24 hours with the different molar ratios (RHT) of water to TEOS. Surfactant : oil = 1:4 (wt:wt)

The TEM micrographs [**Figure 7.1-2**] show that the size of silica nano-spheres produced, increased from 25 nm 35 nm with an increase of RHT from 20 to 40 and then started to decrease with the further increase in the RHT value. For example, when RHT was increased to 50, the size of silica spheres decreased to about 22 nm. When RHT was further increased to 60, the size decreased to 15 nm. The maximum diameter of silica nano-spheres prepared in the w/o microemulsion systems appeared at the RHT of 40 (over a range of 20 to 60).

7.1.1.2 Studies on different loading of the aqueous phase

The size of silica nano-spheres changed with the different loading of the aqueous phase, varied from 2%, 4% to 8% and the RHT of 40. The 2% sample is shown in **Figure 7.1-1 A**, which was 30 nm. As shown in **Figure 7.1-3**, it was be found that the size of silica nano-spheres decreased from 30 nm to 10 nm, as the loading of aqueous phase increased from 2% to 8%.

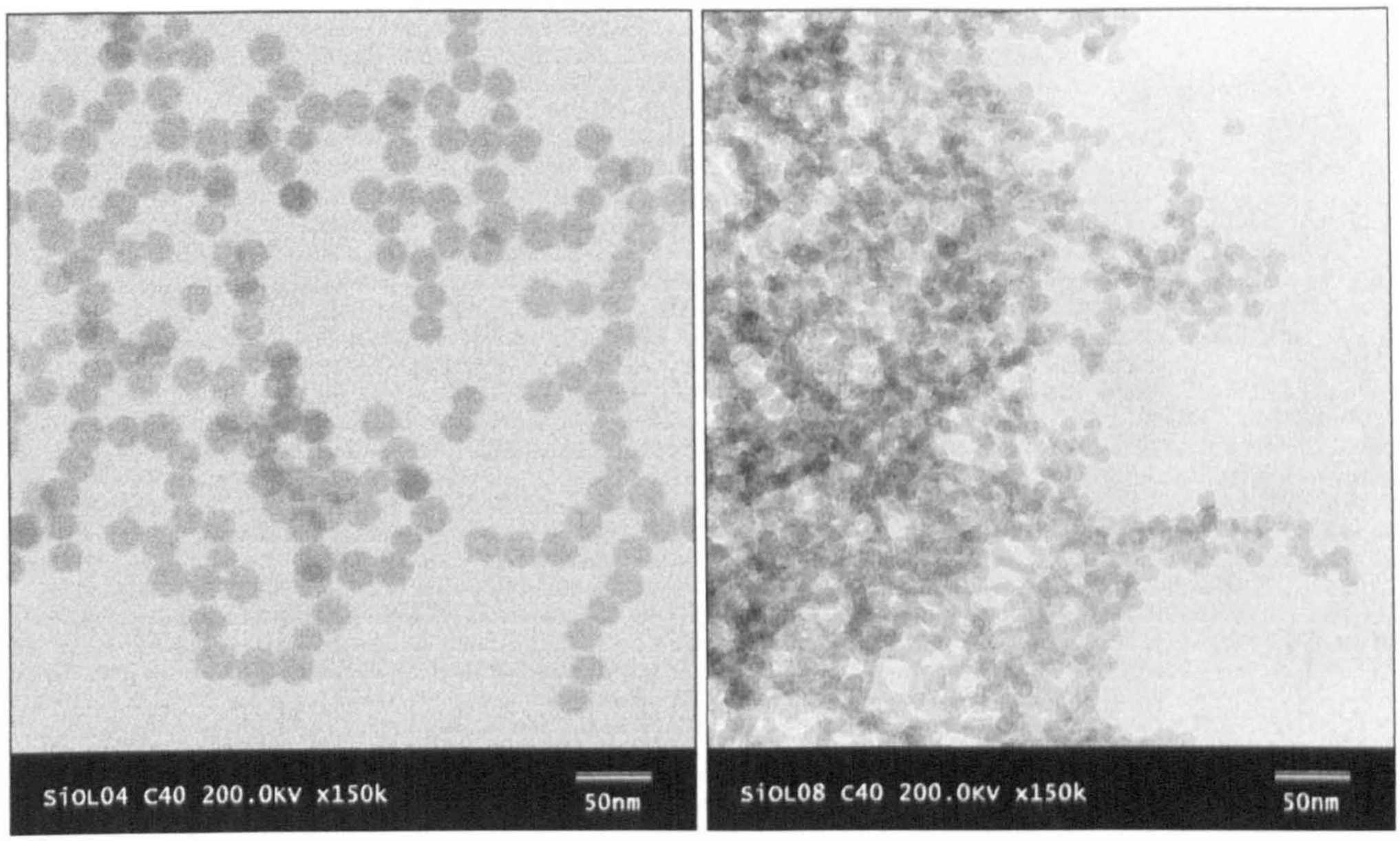

[A]. 4%

[B]. 8%

Figure 7.1-3 TEM micrographs of silica nano-spheres prepared via Igepal CO-520/cyclohexane w/o microemulsion with different loadings of aqueous phase at 25°C for 24 hours. Surfactant : oil = 1:4 (wt:wt).

7.1.1.3 Studies on different concentration of surfactant

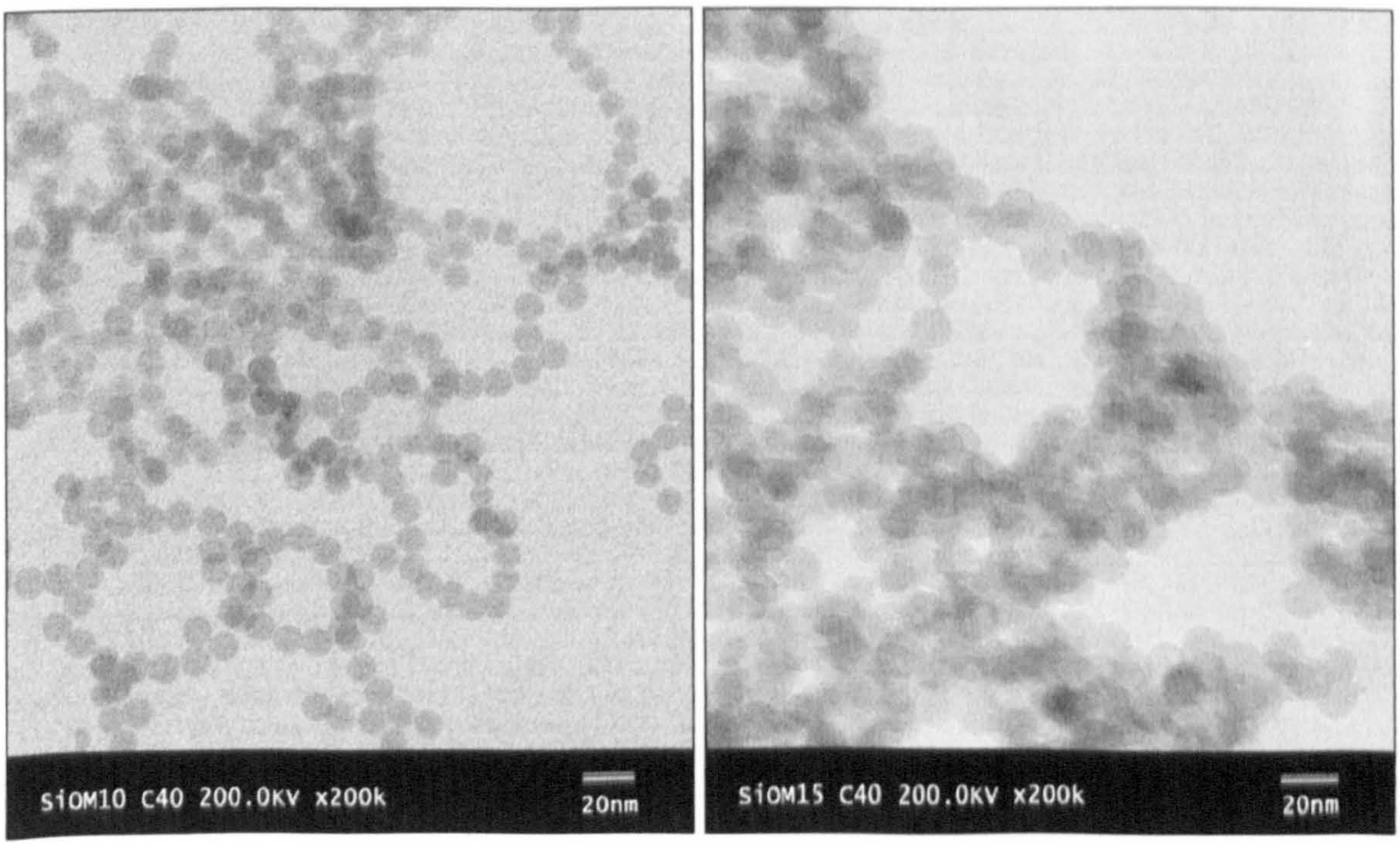

[A]. 14.6%

[B]. 21.8%

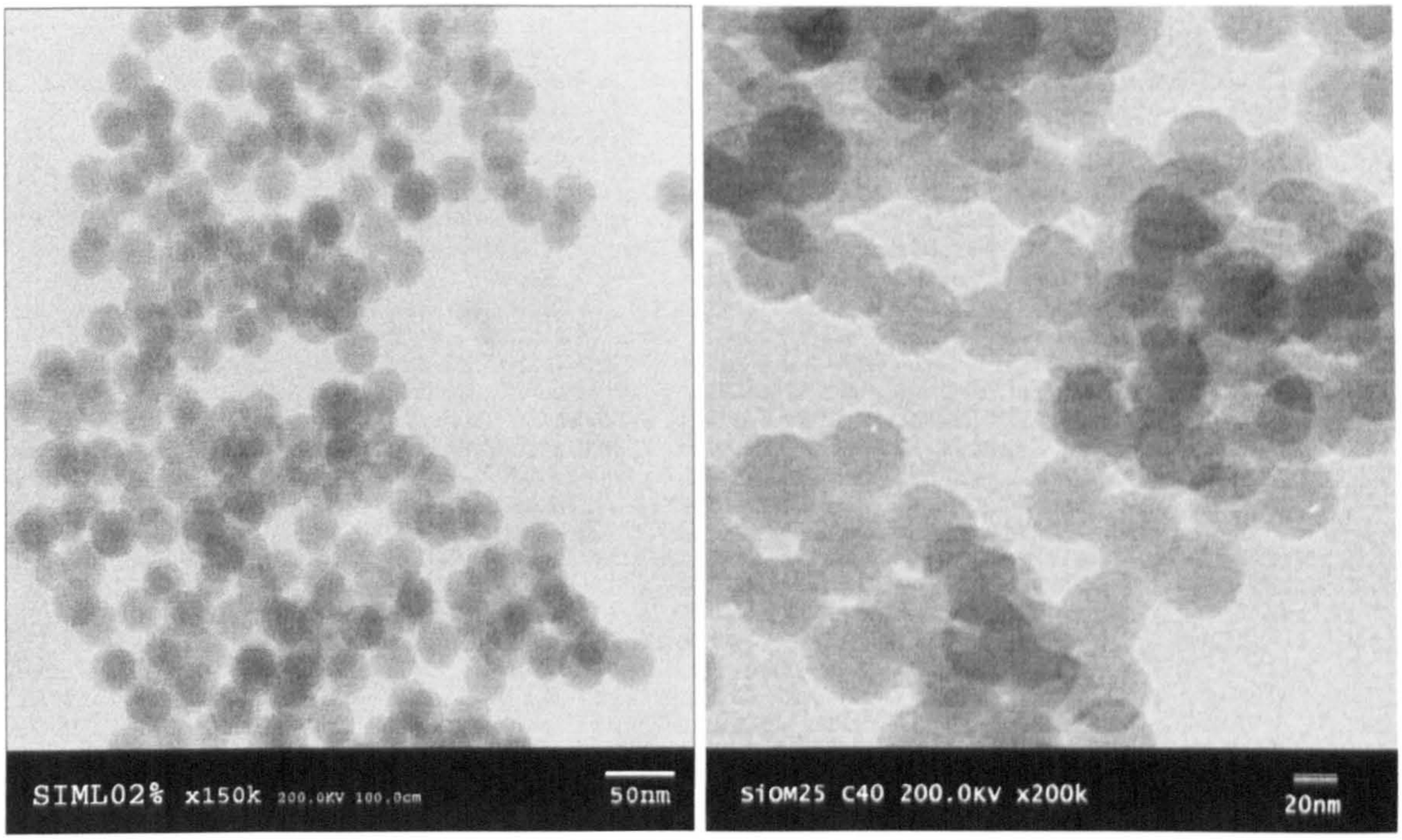

[C]. 29.1% [D]. 36.4%

Figure 7.1-4 TEM micrographs of silica nano-spheres prepared via w/o microemulsion with different concentrations of surfactant at 25°C for 24 hours.

The preparation of silica nano-spheres in w/o microemulsion was also investigated with the different concentration of the surfactant. As shown in **Figure 7.1-4**, the increase of surfactant concentration, (weight concentration based on the total mass of surfactant, oil and aqueous phase in system), from 14.6% to 36.4%, lead to an increase of particle size produced, from 8 nm to 35 nm.

7.1.2 Preparation of silica coated nanocomposites

The preparation of pure iron oxide nanoparticles and silica nano-spheres have been individually discussed in the previous sections. This section deals with the preparation of silica-coated nanocomposites, which was carried out in Igepal CO-520/cyclohexane system at 25°C for 96 hours. The phase diagrams of the w/o microemulsion employed was given in **Figure 5.2-7**.

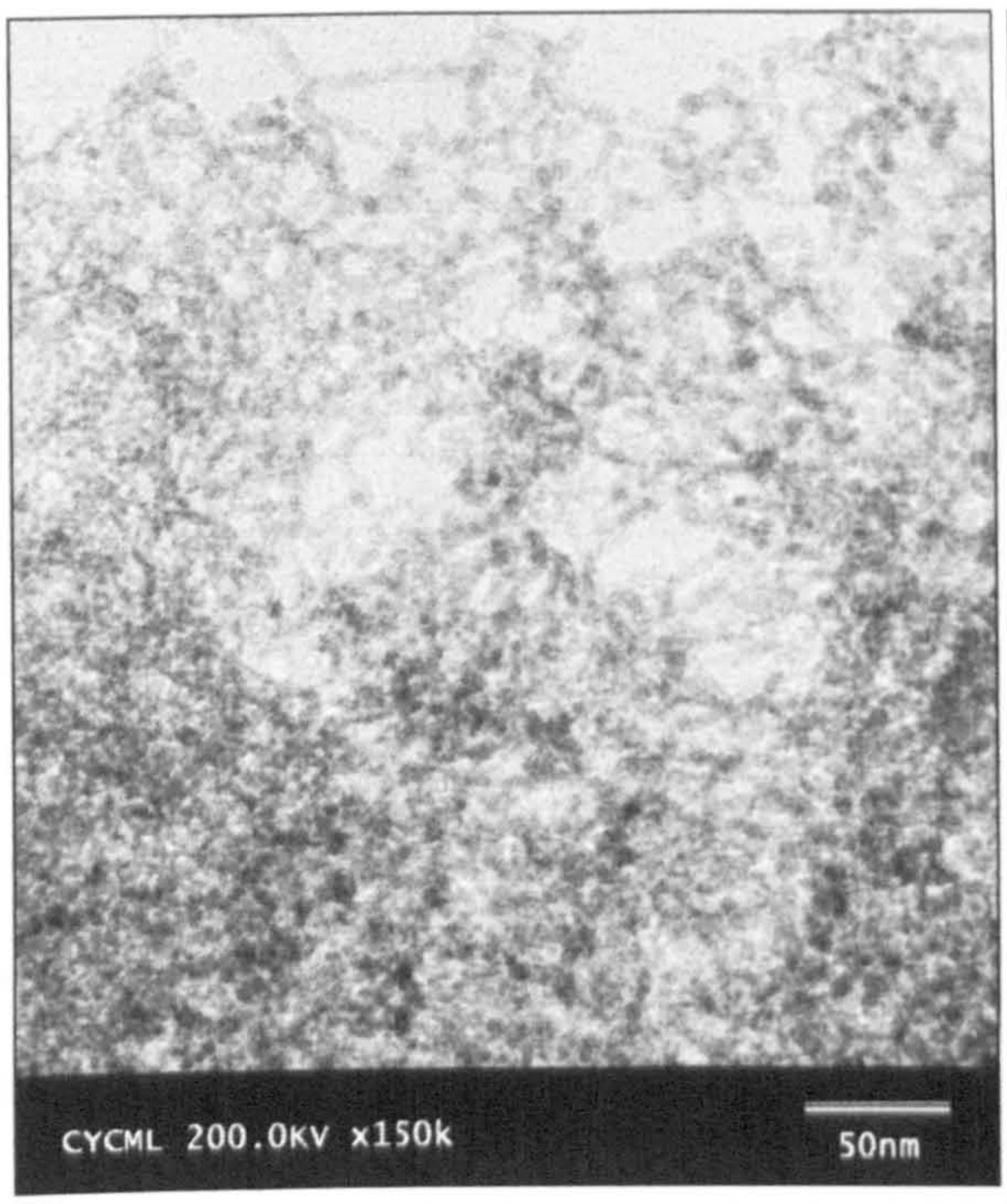

[A] Original iron oxide nanoparticles

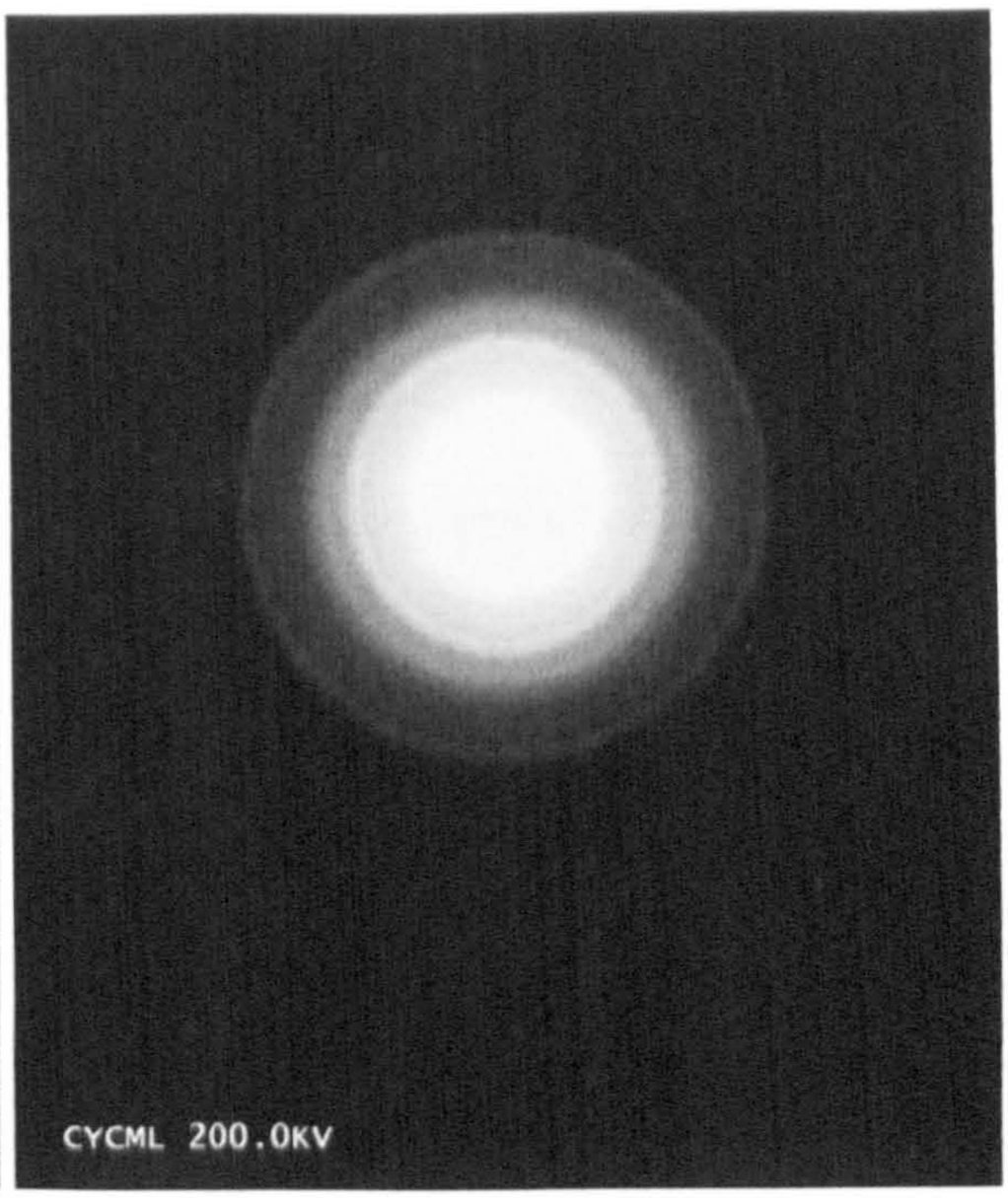

[A.DF]

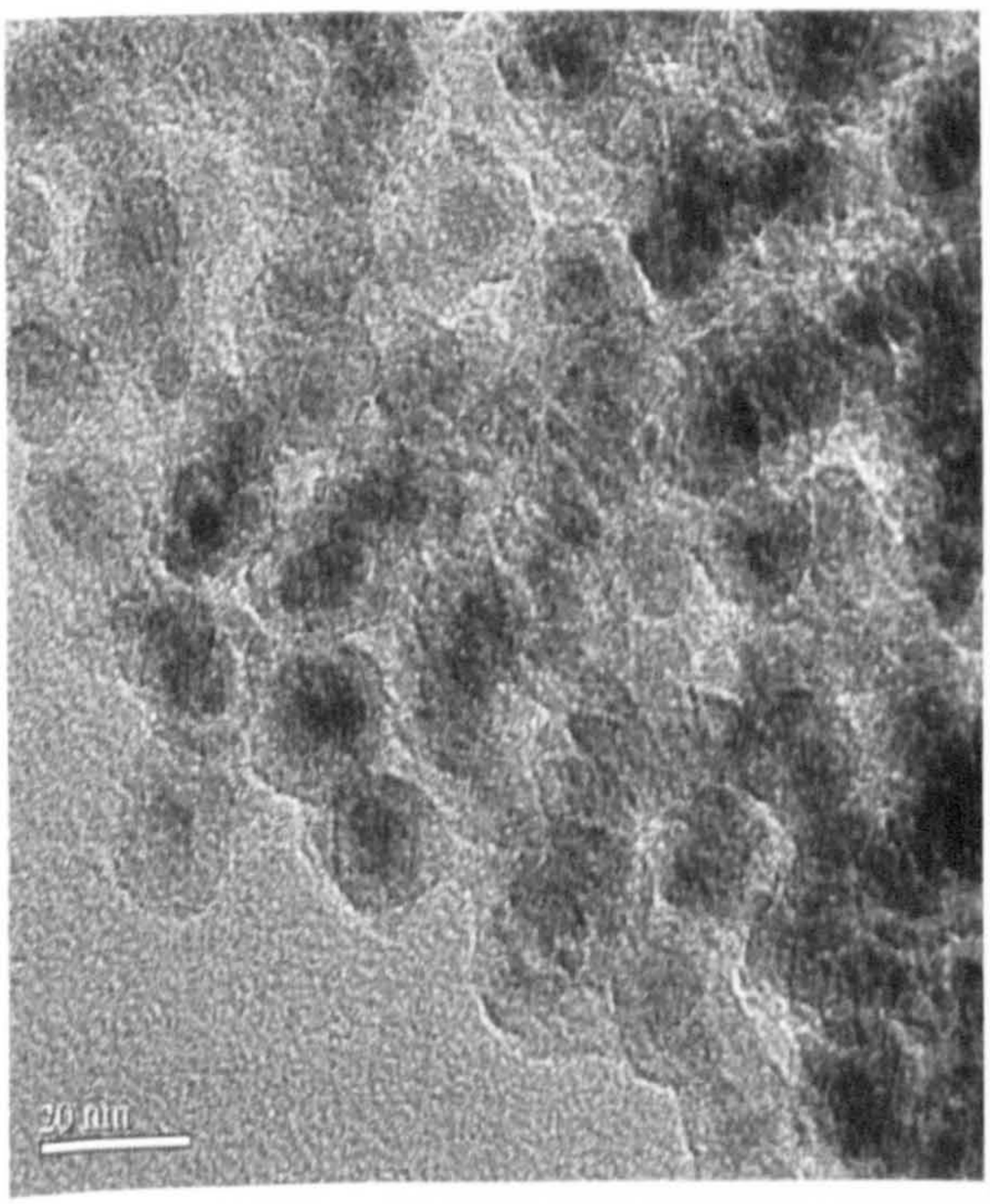

[B]. Silica coated nanocomposites

[B.DF]

Figure 7.1-5 TEM micrographs of iron oxide nanoparticles and silica/iron oxide nanocomposites prepared via Igepal CO-520/cyclohexane w/o microemulsion system at 25°C. Surfactant : oil = 1:4 (wt:wt).

As shown in the TEM micrographs, the size of pure iron oxide nanoparticles prepared by w/o microemulsion system was about 5 nm **[Figure 7.1-5 A]**, and the size of the silica coated magnetic nanocomposites was 15 nm, with the thickness of the ceramic coating layer around 5 nm **[Figure 7.1-5 B]**. The core-shell structure could be observed clearly from the TEM micrographs. The lighter colour silica shell surrounded the darker colour iron-oxide-core evenly. Compared to the pure iron oxide nanoparticles, the silica-coating layer probably prevents iron oxide nanoparticles from aggregating. The micrographs of diffraction patterns of the pure iron oxide nanoparticles and silica coated nanocomposites prepared in microemulsion, are given in **Figure 7.1-5.** The pure iron oxide nanoparticles exhibited a few comparably sharp rings **[Figure 7.1-5 A.DF]**, while the nanocomposites sample exhibited blurred pattern, which probably means the crystallinity of original iron oxide nanoparticles was affected due to the presence of silica coating layer.

X-Ray diffractograms of the nanoparticles with and without coating, are shown in **Figure 7.1-6**, also indicated that the crystallinity of nanocomposites **[Figure 7.1-6 A]** was different from the original iron oxide cores **[Figure 7.1-6 B]**. It was difficult to identify any characteristic peaks from the XRD pattern of silica coated nanocomposites.

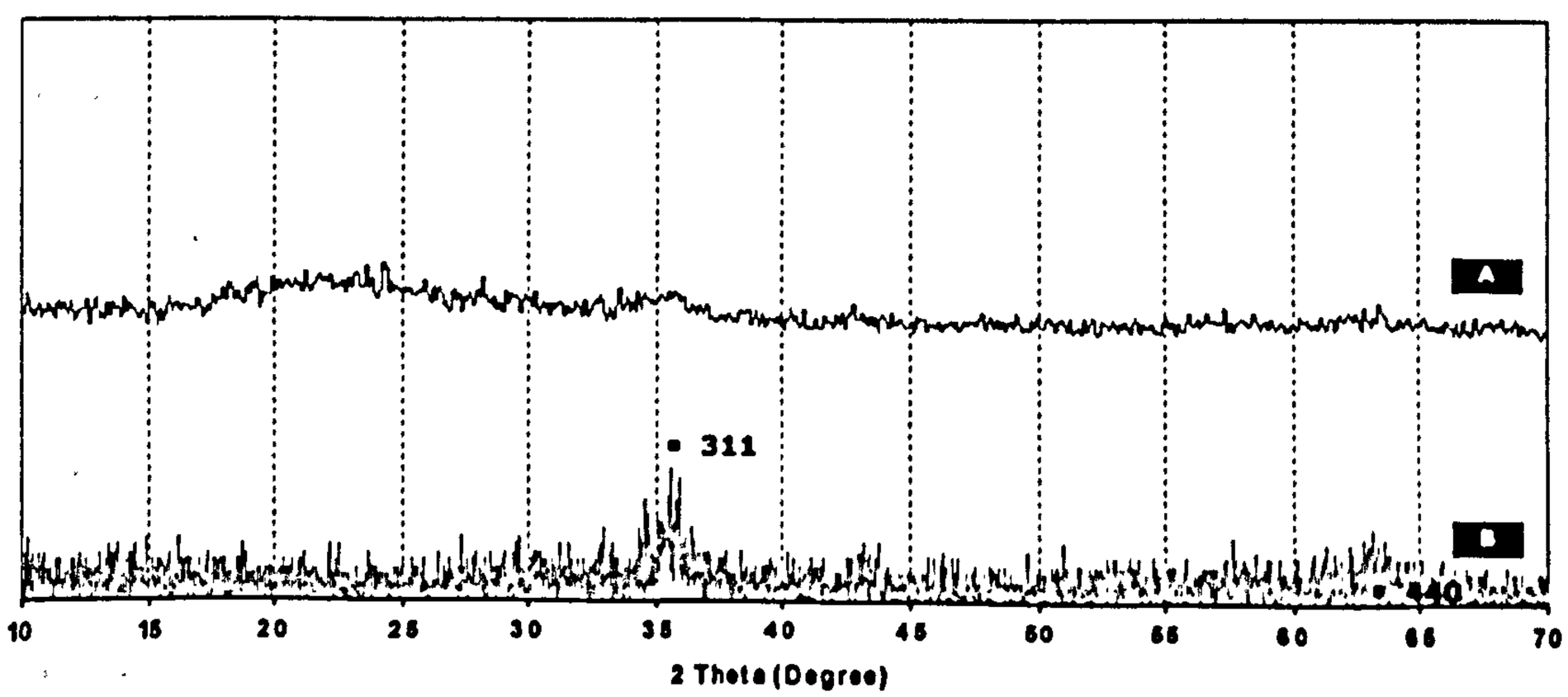

Figure 7.1-6 X-ray diffractograms of iron oxide nanoparticles and silica coated nanocomposites prepared in Igepal CO-520/cyclohexane w/o microemulsion system at 25°C for 96 hours. Surfactant : oil = 1:4.

[A] Silica coated nanocomposites; **[B]** Original iron oxide nanoparticles

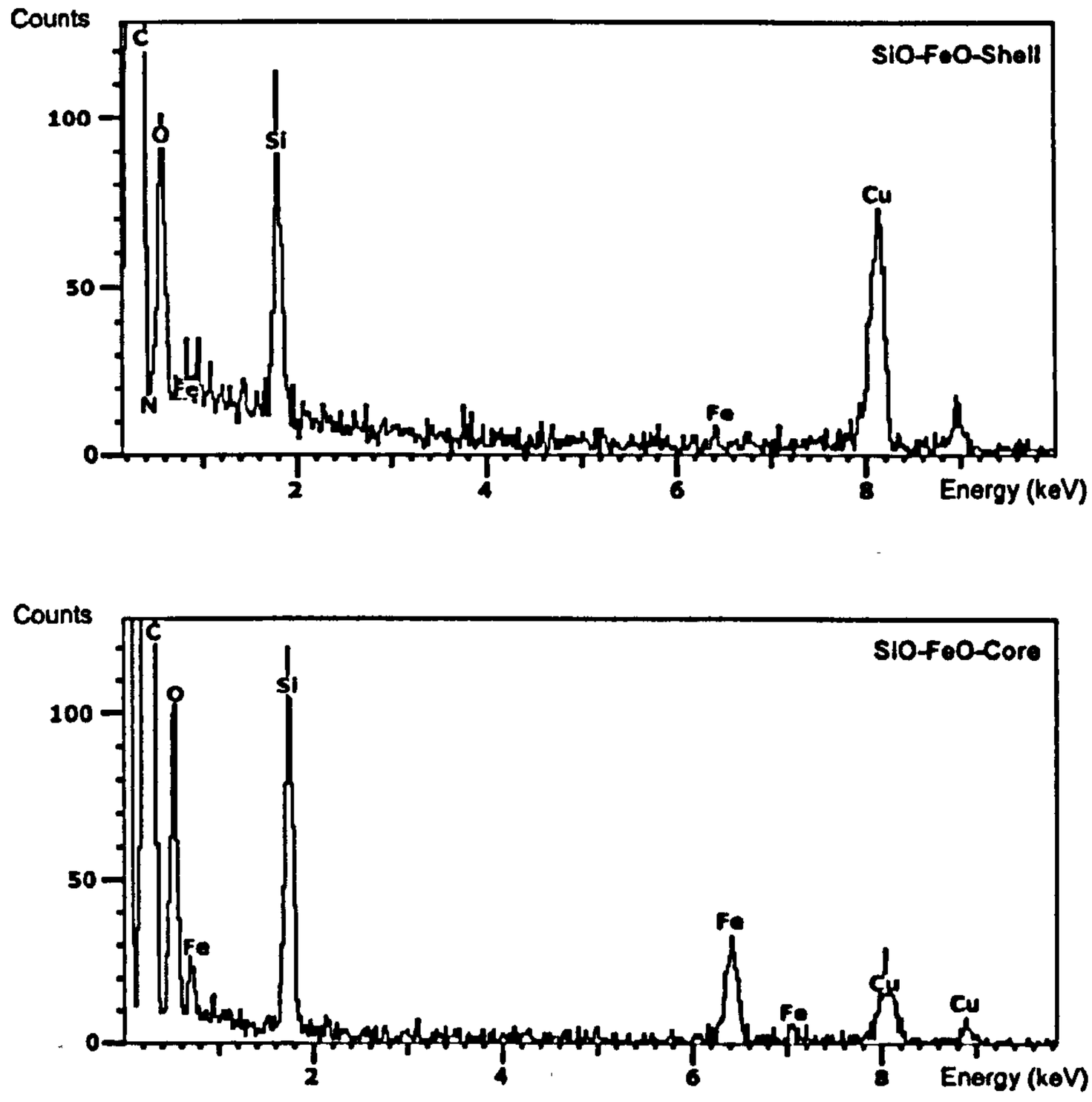

Figure 7.1-7 EDX analysis of [A] outer layer and [B] central part of the silica coated nanocomposites prepared in Igepal CO-520/cyclohexane w/o microemulsion system at 25°C for 96 hours. Surfactant : oil = 1:4.

The evidence of core-shell structure was proved by the **Energy Dispersive X-ray Analysis** as shown in **Figure 7.1-7**. A nano-probe was applied to the outer layer and the central part of the nanocomposites, respectively. There was no elemental iron detected in the outer layer (shell), indicating the iron oxide core being fully encapsulated by the silica shell.

- **Studies on the molar ratio of [H_2O] to [TEOS]**

The effect of molar ratio of [H_2O] to [TEOS] on the morphology was also investigated in the synthesis of silica coated nanocomposites, via the w/o microemulsion system **[Figure 7.1-8]**. According to the TEM micrographs, the thickness of the shell did not change significantly when the ratio was varied from 10 to 50 **[Figure 7.1-8 A, B]**. When the ratio was increased to 60 **[Figure 7.1-8 C]**, the boundary between core and shell looked blurred. The core/shell structure was difficult to observe as the ratio

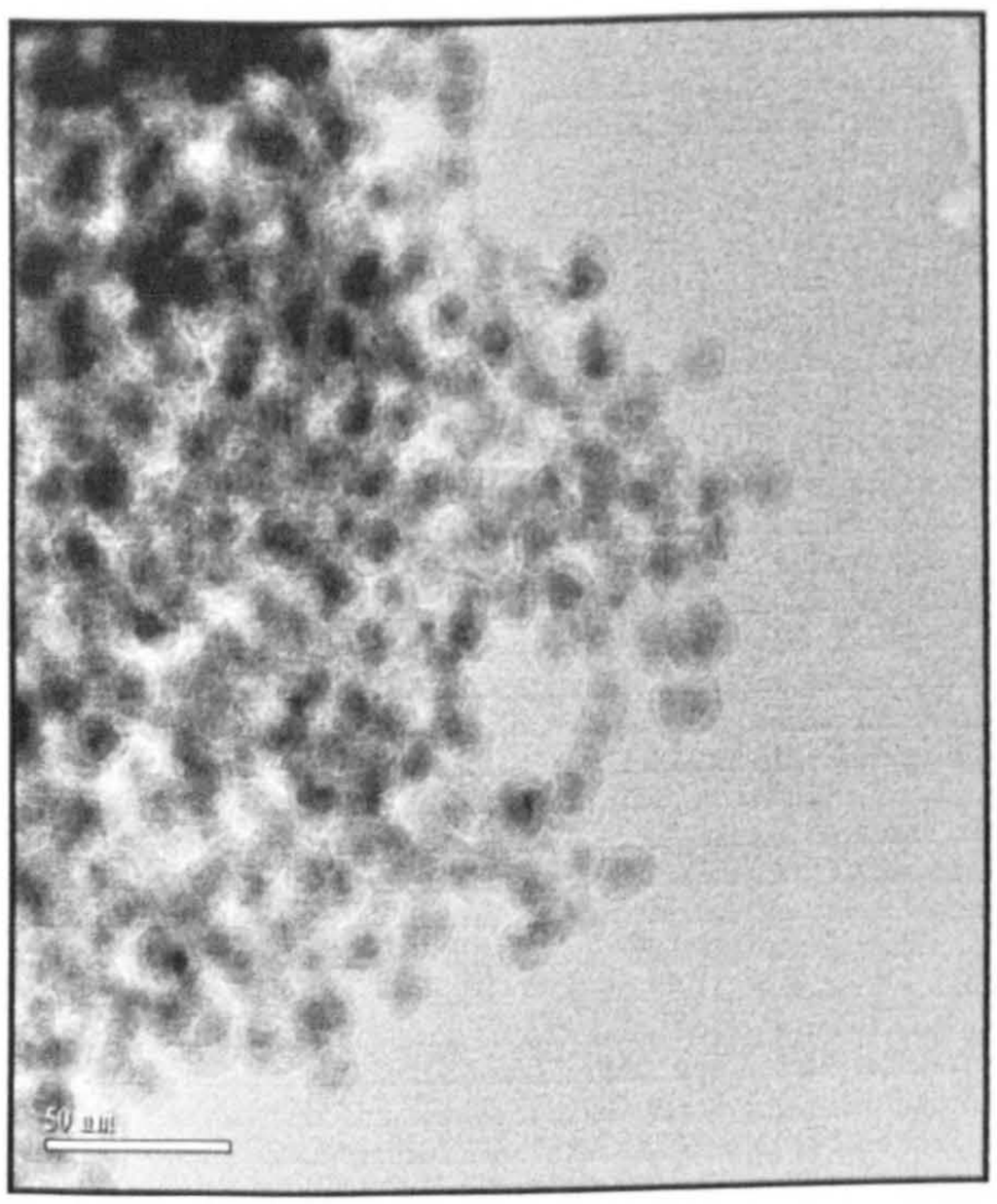

[A]. 10

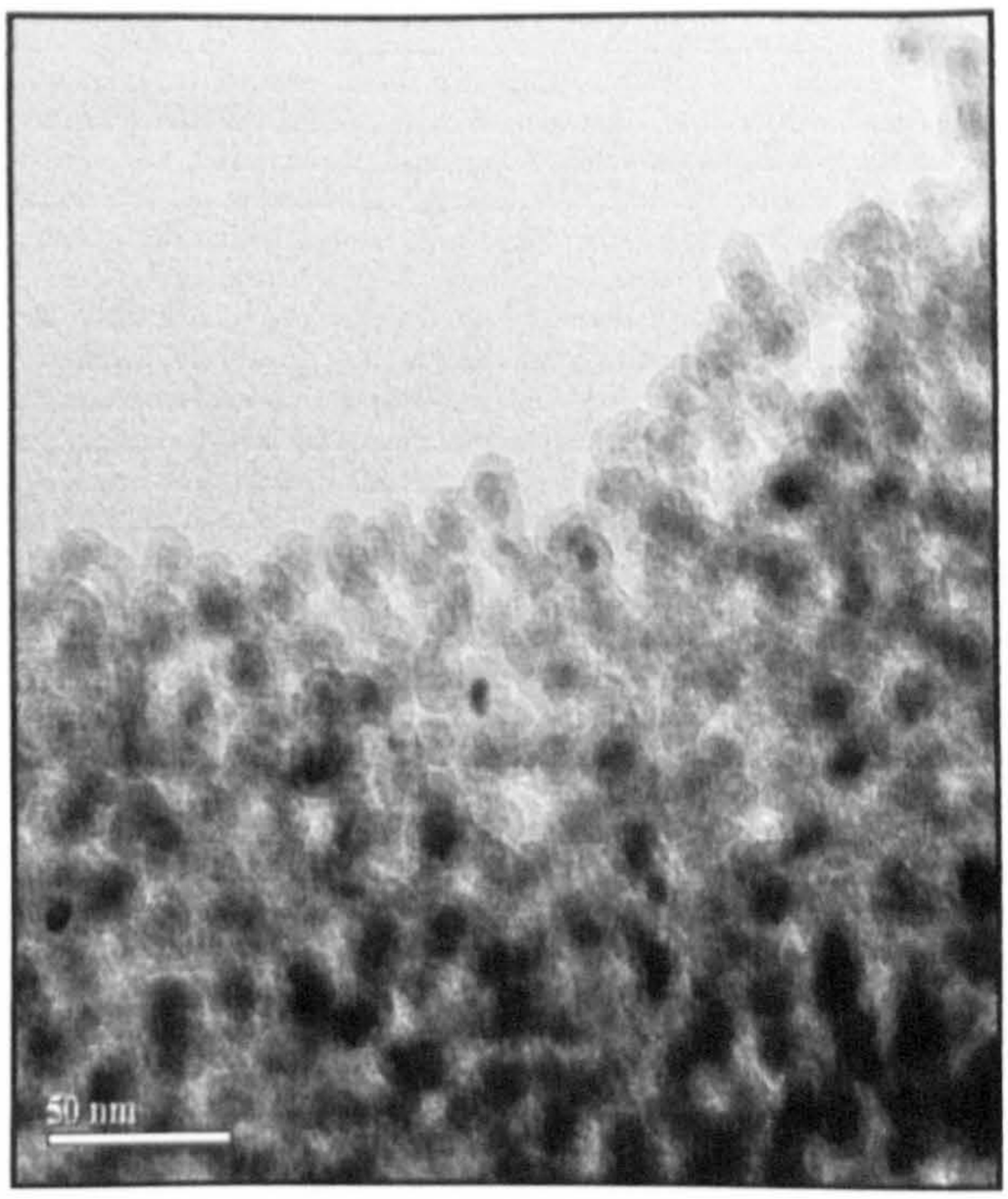

[B]. 50

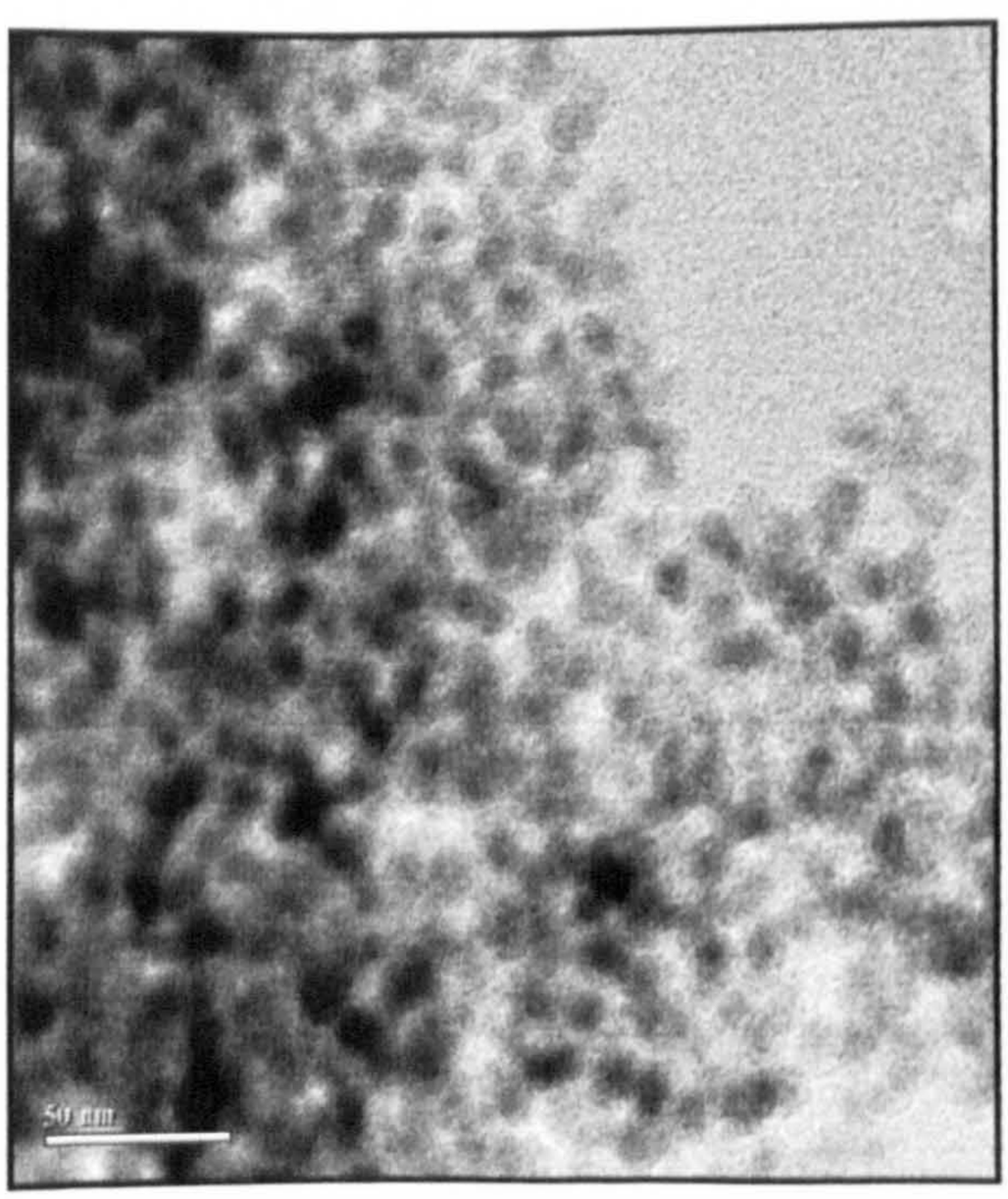

[C]. 60

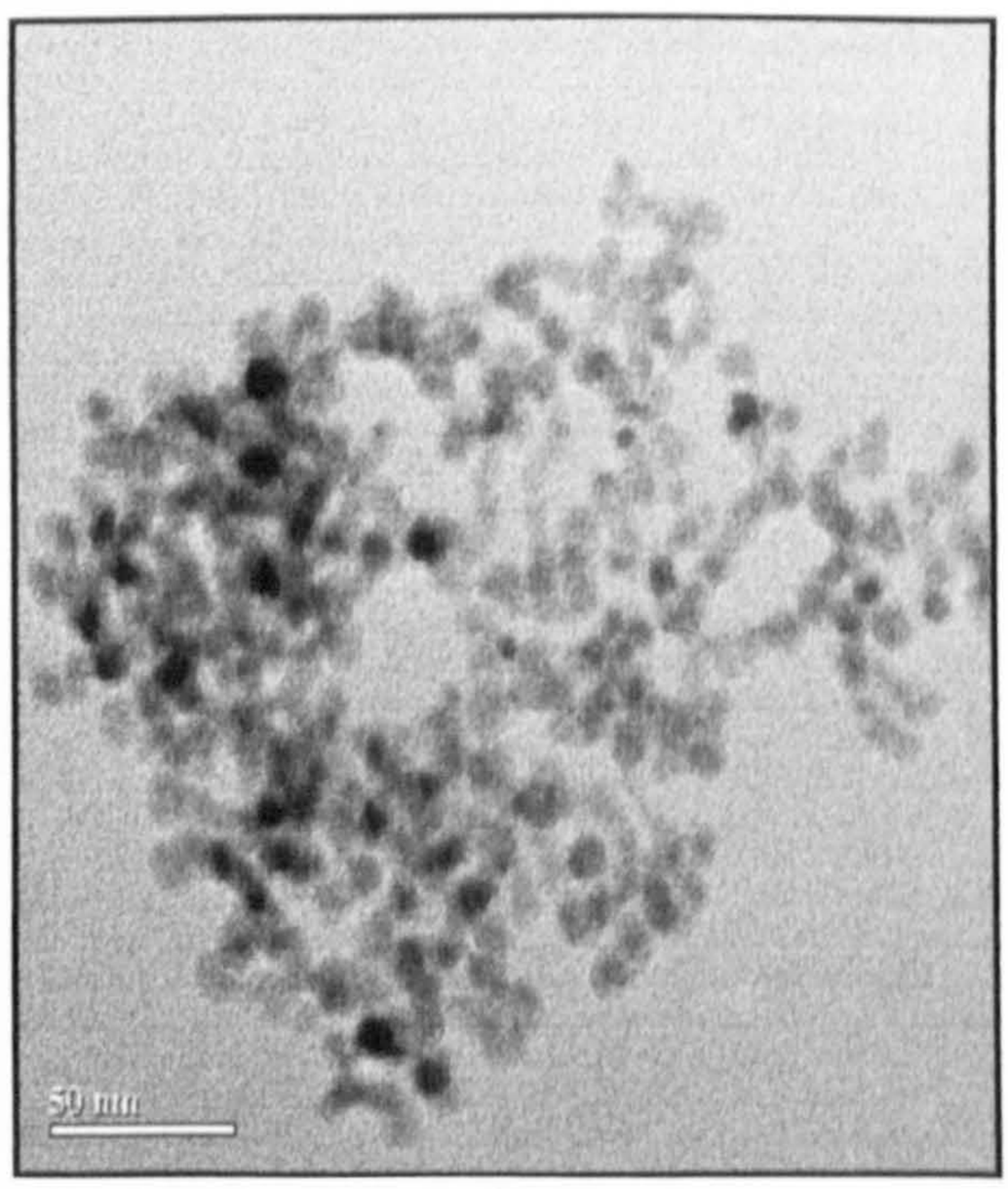

[D]. 100

Figure 7.1-8 TEM micrographs of silica-coated nanocomposites prepared via Igepal CO-520/cyclohexane w/o microemulsion system with the different molar ration of [H_2O] to [TEOS]. Surfactant : oil = 1:4 (wt:wt)

was finally increased to 100, possibly due to a very thin layer of coating. On the other hand, the finely separated particles partially indicate the existence of a coating layer.

7.2 PREPARATION OF PAM/IRON OXIDE NANOCOMPOSITES

PAM/iron oxide nanocomposites were synthesised in Brij 97/cyclohexane w/o microemulsion system at 60°C for 6 hours, initiated by KPS. The original iron oxide nanoparticles were also synthesised in this system at 60°C for 24 hours.

The TEM micrographs of PAM/iron oxide nanocomposites show that those nano-composites were spherical and of narrow size distribution [**Figure 7.2-1**]. It can be seen clearly from the close-up picture, that a large amount of 5 nm iron oxide particles were embedded into PAM nano-spheres,

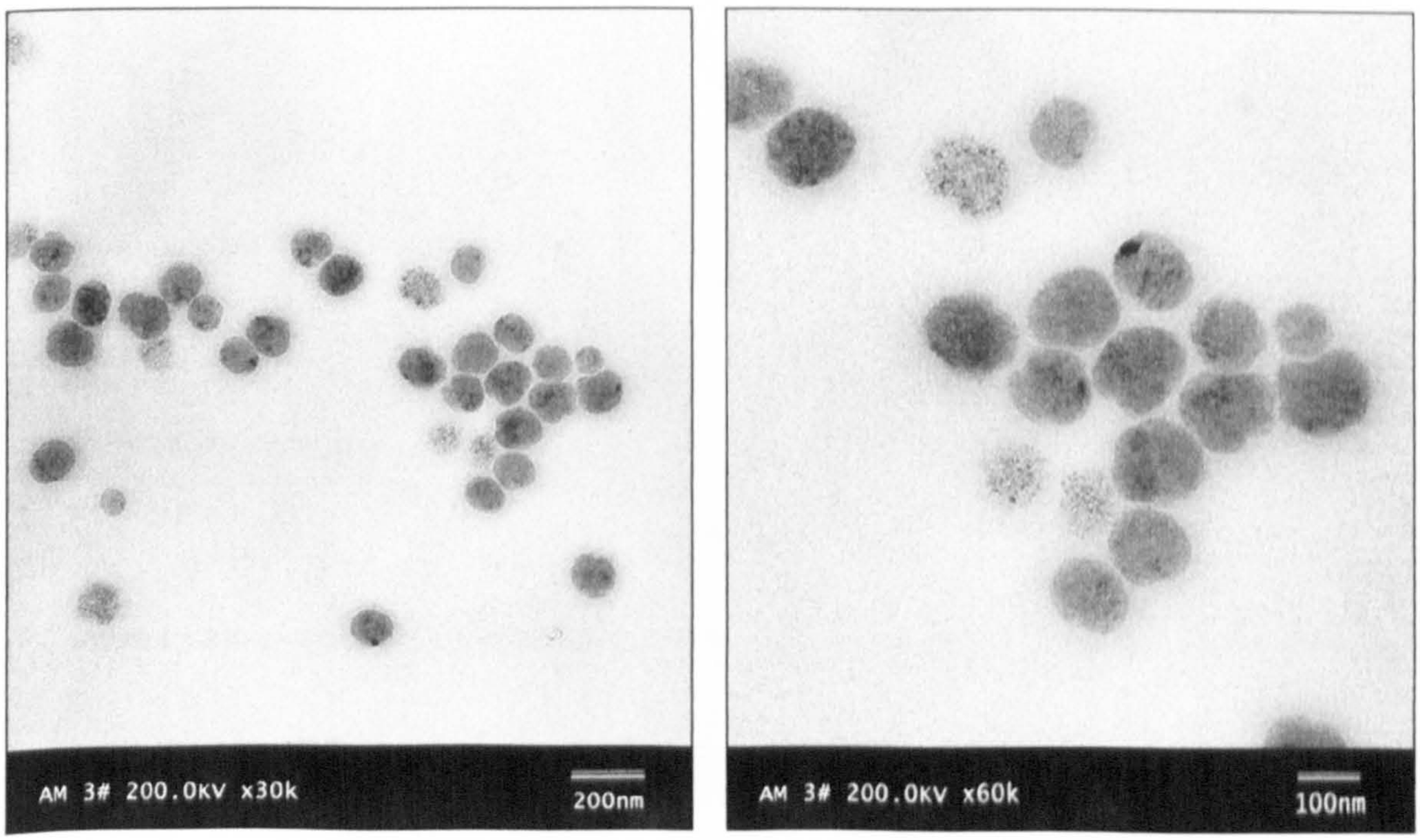

[A] [B]

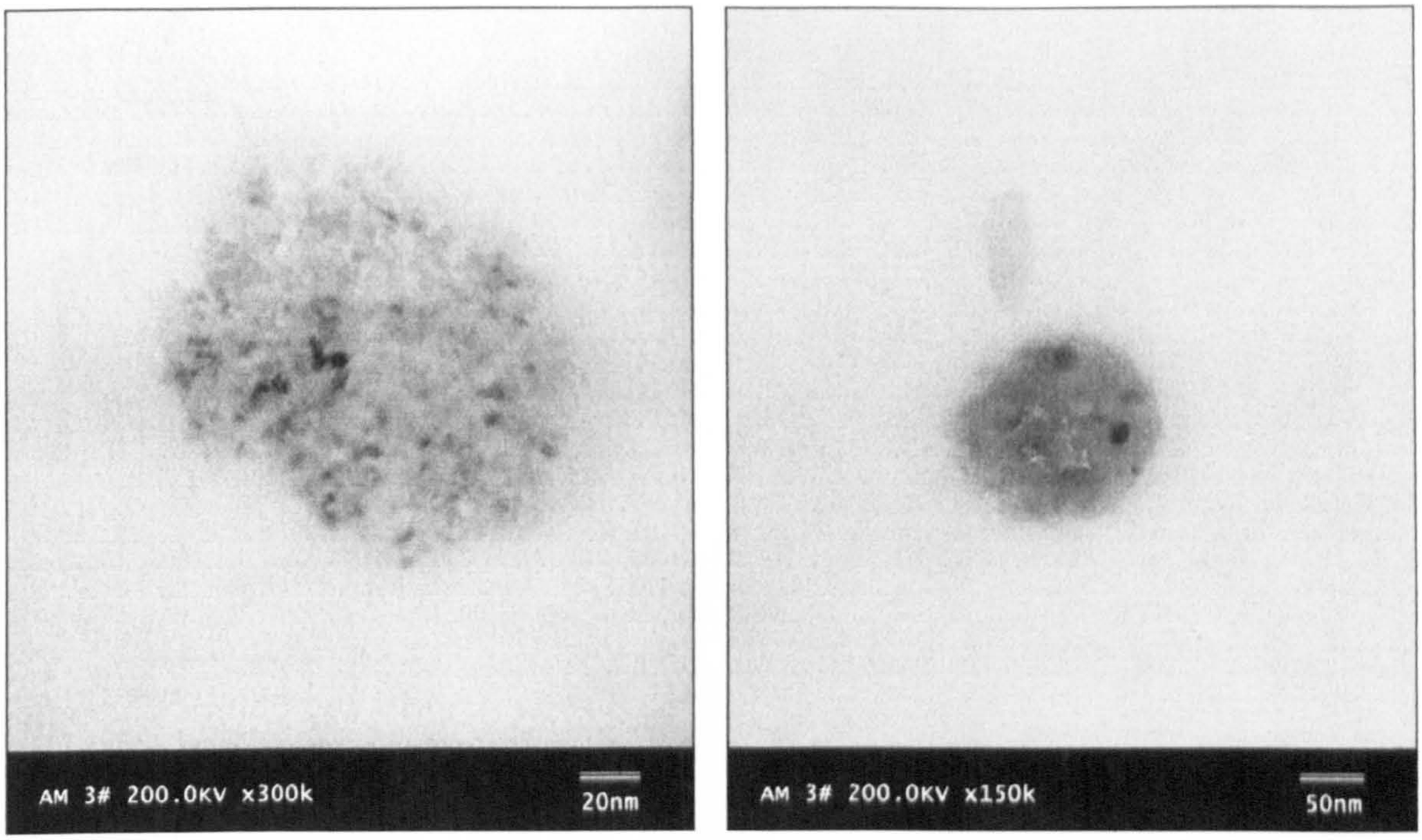

[C] [D]

Figure 7.2-1 TEM micrographs of PAM/iron oxide nanocomposites prepared via Brij 97/cyclohexane w/o microemulsion system at 60°C for 6 hours. Surfactant : oil = 1:3.

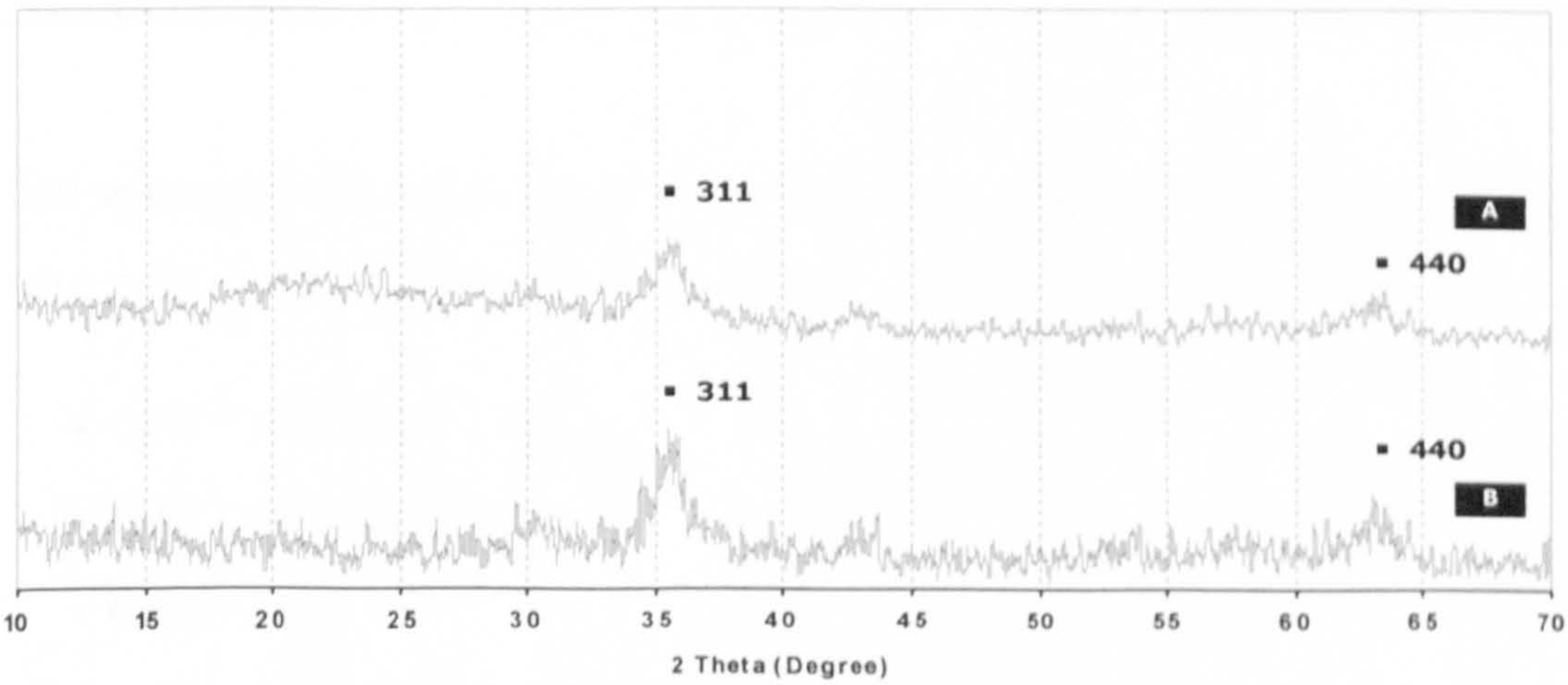

Figure 7.2-2 X-ray diffractograms of **[A]** PAM/iron oxide nanocomposites and **[B]** pure iron oxide nanoparticles.

which was about 120 nm as diameter. Although the original polymer boundary could hardly be seen in the TEM micrographs, the areas marked by bonded iron oxide particles indicates that these

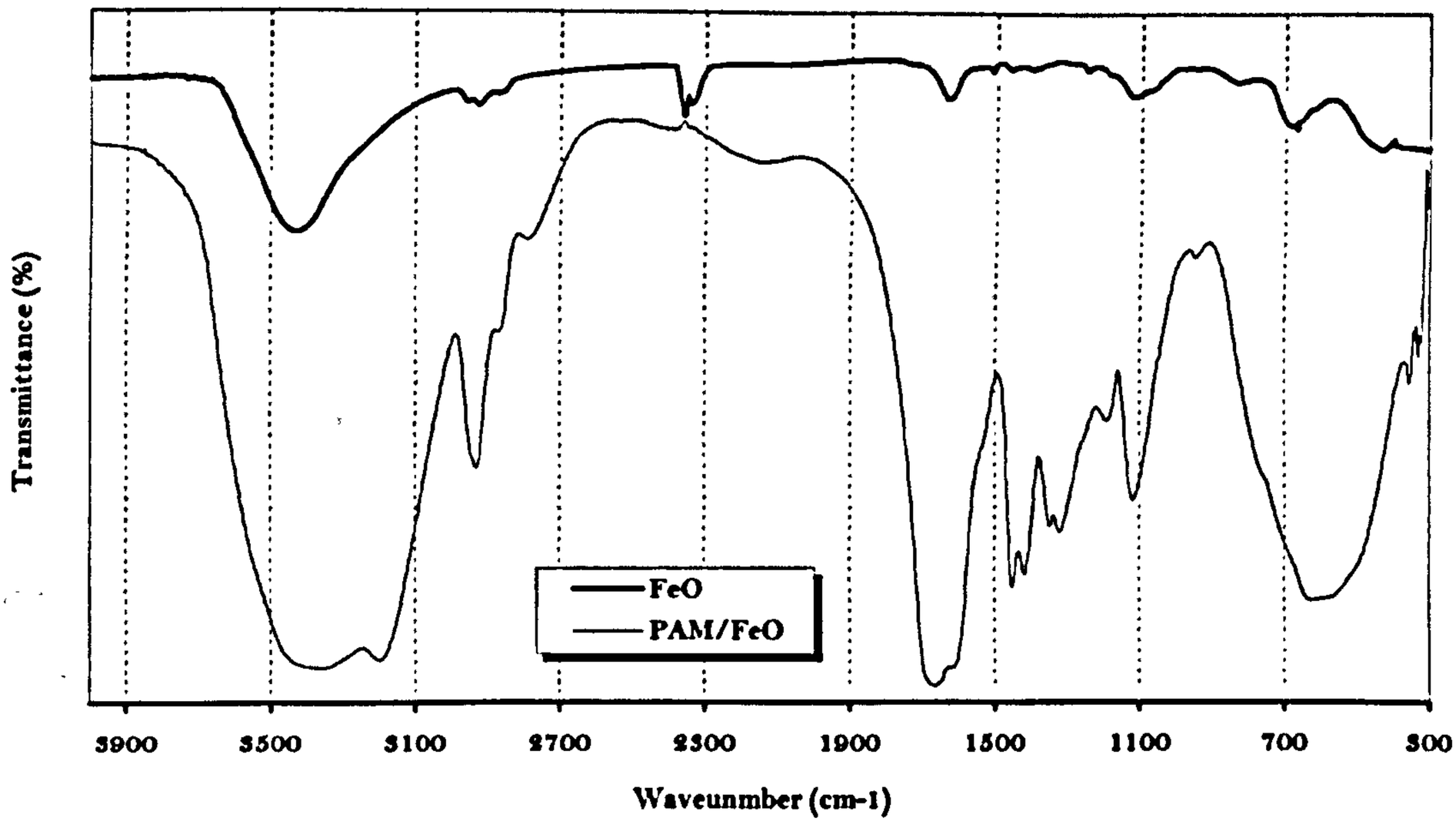

Figure 7.2-3 FT-IR spectra of iron oxide nanoparticles and PAM/iron oxide nanocomposites prepared via Brij 97/cyclohexane w/o microemulsion system at 60°C for 24 hours and 6 hours respectively..

nanocomposites were well isolated. The X-ray diffractograms of iron oxide nanoparticles and PAM/iron oxide nanocomposites prepared via w/o microemulsion system at 60°C, are shown in **Figure 7.2-2.** Characteristic peaks, **(311)** and **(440)** could be identified for both pure and composites samples.

The FT-IR spectra of PAM/iron oxide nanocomposites shows the characteristic absorptions of PAM at 3410, 1618, 1452, 1420, 1325, 1350, 1184 and 1120 cm^{-1}, where are assigned separately as:

- **C-N:** 1325, 1184, 1120;
- **C-H:** 1350, 1420, 1452;
- **C=O:** 1618;
- **N-H:** 3410;

7.3 DISCUSSIONS

Introducing a second material to pure nanoparticles to form core-shell structured nanocomposites or nano-sized host matrices with embedded particles, can effectively avoid the aggregation of pure nanoparticles to be well maintained at the primary nano-scale, while altering the original properties of single nanomaterials.

The synthesis of nanocomposites, based on magnetic nanoparticles (i.e. iron oxide), was carried out in w/o microemulsion systems with silica and PAM, respectively. The following discussion of the synthesis of nanocomposites, will be in regard to the composite morphology and the different mechanisms leading to the formation of ceramic/polymer nanocomposites.

7.3.1 Free-water in synthesis of silica coated nano-composites

W/O microemulsion systems are employed in the synthesis of nanoparticles and nanocomposites, mainly from the consideration of their restricted environments arising from a unique interior structure, which could be expected to give a good control on the morphology of nanomaterials prepared inside. In fact, such a kind of control was partially achieved in the synthesis of silica-coated nanocomposites via Igepal CO-520/cyclohexane w/o microemulsion system at 25°C for 96 hours, by changing the molar ratio of H_2O to TEOS (RHT); this resulted in changing the "free-water".

The term of "free-water" refers to the unbound water molecules in the water droplets in the microemulsions, arising from the little interactions between the polar water phase and hydrophilic groups of the surfactant, and the extent of solubilisation in the microemulsion systems. When the amount of water in the organic oil phase is very low, most of the water molecules are hydrogen

bonded to the surfactant polar groups and they are said to be "bound". With an increase in the water content, unbound or "free water" molecules become increasingly available.

According to the discussion above, free-water is not only a reagent in the hydrolysis reaction of TEOS but also a system-dependent factor. Since TEOS hydrolysis in w/o microemulsion systems can be affected by both steric effects from the surfactant layer and the presence of free-water, hence, the synthesis of silica nano-spheres and silica-coated nanocomposites is expected to be controlled by the w/o microemulsions. From this point of view, the discussion about the free-water in synthesis of pure silica nano-spheres will be given first.

7.3.1.1 Free-water in synthesis of silica nano-spheres

Silica submicron particles have been prepared by the controlled hydrolysis of metal alkoxides in an alcohol and water mixture, [197-198] accompanied with the high poly-dispersity. W/O microemulsion systems provide an effective method of the synthesis of mono-dispersed silica nano-spheres.

The formation of silica nano-spheres in w/o microemulsion systems is given in **Figure 7.3-1** schematically. The synthesis of silica by the alkoxide hydrolysis can be generally described by the reactions [199]:

Hydrolysis:
$$Si(OR)_4 + x \cdot H_2O = Si(OR)_{4-x}(OH)_x + x \cdot ROH \qquad (7\text{-}1)$$

Condensation:
$$-\overset{|}{\underset{|}{Si}}-OR + HO-\overset{|}{\underset{|}{Si}}- = -\overset{|}{\underset{|}{Si}}-O-\overset{|}{\underset{|}{Si}}- + ROH \qquad (7\text{-}2)$$

$$-\overset{|}{\underset{|}{Si}}-OH + HO-\overset{|}{\underset{|}{Si}}- = -\overset{|}{\underset{|}{Si}}-O-\overset{|}{\underset{|}{Si}}- + H_2O \qquad (7\text{-}3)$$

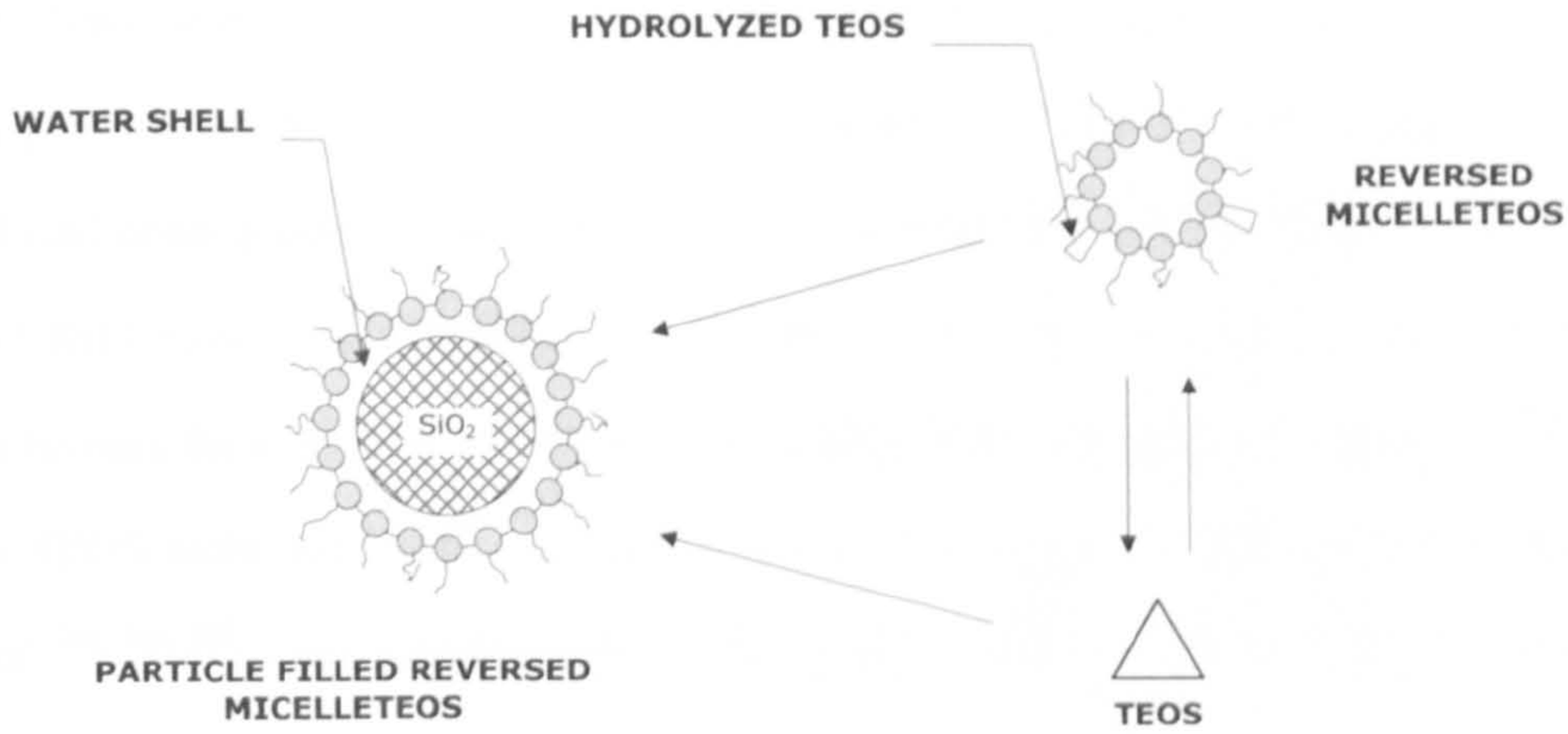

Figure 7.3-1 Growth mechanisms of TEOS nano-spheres in the water-in-oil microemulsion system containing ammonia solution.

The mechanism involves both hydrolysis and condensation reactions. The former reaction results in the formation of nuclei and the latter encourage the addition of monomers to existing particles. The resultant morphology of silica spheres is affected by the effects of the reagent concentration on the relative rates of the hydrolysis and condensation reactions. Once a nucleus is formed in a water droplet, further growth is initially determined mainly by the content of monomers inside. An increase in the rate of hydrolysis **[Equation 7-1]**, will encourage the nucleation of silica "seeds" and result in the small size of ceramic spheres.

The effects of the RHT value, the size of water pools (ω_0) and the surfactant concentration on the size of silica nano-spheres were investigated. It was found that the size of silica nano-spheres increased with an increase of surfactant concentration, but with a decrease of RHT and the size of water pools. The influence of these parameters on the size of silica nano-spheres synthesised in w/o microemulsions, all arise from the influence of different amounts of free-water.

The oxyethylene (EO) units of the non-ionic surfactant interact with water molecules through hydrogen bonding. As the water content increases, self-assembling of surfactant molecules is thermodynamically favoured, and with the increase of water solubilised into systems, free-water

molecules will present in the hydrophilic domain, whose properties approach those of bulk water [53]. According to Guizard *et al.* [200], the rate of hydrolysis clearly increased for larger ω_0 values as the result of the presence of more free-water, with the increased size of water pools, small silica spheres will be produced consequently. From this point of view, the decreased size of particles derived from the increased RHT value, can also be ascribed to the presence of the increased amount of unbound water which favours the hydrolysis reactions and produce small nano-spheres. Selle *et al.* [201] reported the water to TEOS mole ratio (RHT) should be about 50 in order to obtain maximum particle size. Bogush *et al.* [44, 163, 202] have reported a maximum particle size at a ratio of 40. Our results are in agreement with those reported by Bogush *et al.*

The effect of surfactant concentration on the size of particles prepared from TEOS hydrolysis in w/o microemulsions can also be explained by the effect of free-water. As known, with a particular amount of water solubilised in microemulsion systems, the increased concentration of surfactant molecules would result in an increased amount of water bound to the polar groups of the surfactants. In other words, the increase of surfactant concentration leads to an increased amount of bound water and the disappearance of free-water. Hence the hydrolysis rate in this case would be comparably low and the growth of particles would be favoured. Therefore, it was found in our experiment, that the size of silica nano-spheres increased from 8 nm to 35 nm as the surfactant concentration increased from 14.6% to 36.4%.

7.3.1.2 Free-water in synthesis of core-shell structured nanocomposites

The effect of free-water on the formation of silica nano-spheres can be utilised in the synthesis of silica-coated nanocomposites to control the thickness of ceramic shell. **Figure 7.3-2** shows the schematics of the synthesis of silica coated nanocomposites in w/o microemulsion systems. As shown in the picture, the silica monomers are precipitated on the surface of prepared iron oxide nanoparticles in water droplets, by the hydrolysis of TEOS and after the condensation, the core-shell structured nanocomposites are formed.

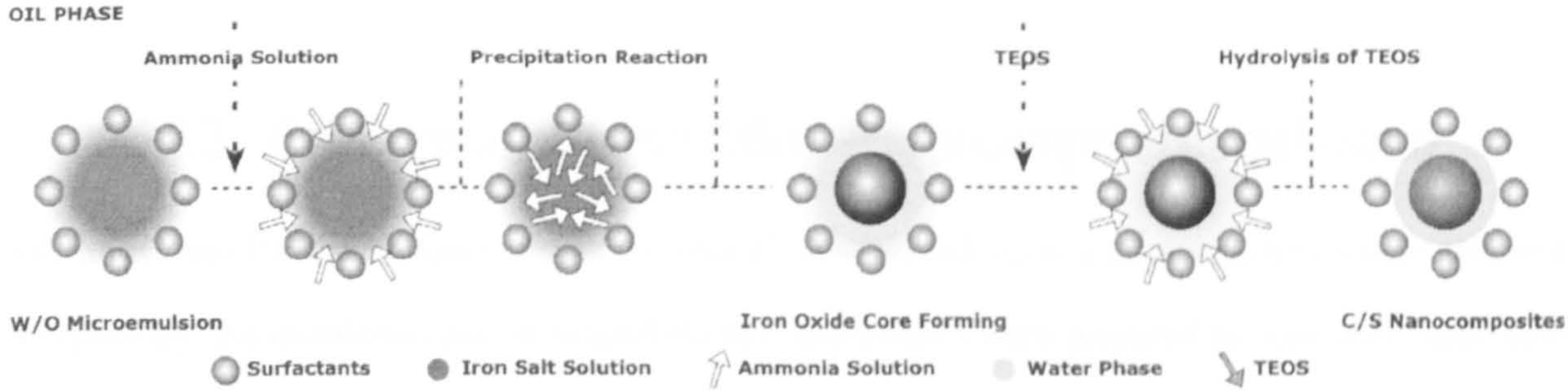

Figure 7.3-2 Schematics of the synthesis of silica coated nanocomposites.

The thickness of silica shell could be affected by free-water effect. As RHT was 10, core-shell structured nanocomposites were shown in TEM micrographs [**Figure 7.1-8**]. When RHT was increased to 60, the resulting shell became difficult to be observed from the TEM micrographs and finally seemed to disappear in the TEM micrographs at a RHT of 100.

According to the discussions about free-water in **7.3.1.1**, the increase of RHT would result in the increase of free-water in water droplets of w/o microemulsions, and the increased of the reaction rate of TEOS hydrolysis. Consequently, the formation of silica nuclei is promoted, in the synthesis of nanocomposites, which probably leads to a thinner shell coating on the iron oxide nanoparticles. As shown in TEM micrographs of the silica coated nanocomposites prepared with RHT of 100 [**Figure 7.2-4 D**], although the existence of the core-shell structure was not clearly observed, the well dispersed composite nanoparticles, with a size of 12 nm, partially indicates one of the advantages of a coating process, preventing aggregations of pure nanoparticles. On the other hand, it was also found that the overall size of the composite nanoparticles decreased from 20 nm to 12 nm, with the increase of RHT from 10 to 100. As the original iron oxide nanoparticles prepared in advance, can not grow during the coating process, one reason to explain the change of composite size, should be the change of the shell.

Therefore, the core-shell structured silica/iron oxide nanocomposites could be synthesised via Igepal CO-520/cyclohexane w/o microemulsion at 25°C for 96 hours. The thickness of the silica shell can be

affected by free-water and consequently controlled by the microemulsion system.

7.3.2 Comparison between different nanocomposites synthesised

Silica/FeO and PAM/FeO nanocomposites were all synthesised via w/o microemulsions with different morphology. As mentioned above, silica/FeO nanocomposites were prepared as core-shell structured nanomaterials with a ceramic shell and the magnet core. PAM/FeO nanocomposites were prepared as a polymer matrix embedded with nano-sized iron oxide particles. The different morphology of these two nanocomposites indicates the different mechanism of composite formation and also resulting in different properties.

In the synthesis of silica/FeO, the prepared iron oxide nanoparticles in water droplets act as nuclei for precipitation of silica monomers. Hence the condensation of silica monomers is generally based on each single magnetic nanoparticle, which probably explains why there was no aggregates of iron oxide nanoparticles encapsulated in silica coating. Additionally, the w/o microemulsion systems also provided a protected environment by surfactant layers for the particle growth.

As for the synthesis of PAM/FeO, the prepared iron oxide nanoparticles are initially mixed with AM monomers. After initiation by KPS at 60°C, the formed polymer chains coil together and trap those magnetic particles, because of the restricted space by surfactants. The addition of the crosslinking agent makes the polymer chains connect to each other and the iron oxide nanoparticles became embedded in the polymer matrices as a result. Due to the amphiphilicity of AM monomers, the surfactant layers in microemulsion polymerisation is assumed to be more flexible and the inter-micellar exchange would be much favoured compared with the silica coating. Generally, the final particle size was significantly greater than the water pool diameters.

The crystallinity of both nanocomposite samples were depressed, compared with original iron oxide nanoparticles. However, the PAM/FeO showed comparably clearer characteristic peaks at (311) and

(440) [Figure 7.2-2], presumably because the interaction between iron oxide nanoparticles and their host matrices was not as strong as those between silica shells and iron oxide cores. In fact, for core-shell structured nanomaterials, there is an intimate close connection in terms of physical and/or chemical interaction existing between the shell and the core, which leads to an interaction between both shell and the core compartments creating synergistic effects [55]. Hence the depression in crystallinity of silica coated nanocomposites, might demonstrate the presence of such a kind of physical/chemical interactions. However, the structure of iron oxide nanoparticles dispersed in polymer matrix may lead to a comparably loose construction of PAM/FeO nanocomposites.

On the other hand, the much stronger crystallinity revealed by the XRD pattern of PAM/FeO nanocomposites, (compared to silica/FeO), might be attributed to the different partitioning of magnetic nanoparticles in the composites. As for the latter, iron oxide nanoparticles were entirely encapsulated in the centre and coated by ceramics. However, apparently much more iron oxide nanoparticles were located on the surface of the PAM/FeO spheres. Hence the crystallinity could be well resolved.

SUMMARY

Core-shell structured silica/iron oxide nanospheres and PAM/iron oxide nanocomposites were synthesised via w/o microemulsions. The thickness of silica shell was partially controlled by the system-dependent factor, free-water. As the RHT was increased from 10 to 100, the size of silica/FeO nanocomposites decreased from 20 nm to 12 nm.

The produced nanocomposites both showed depressed crystallinity compared with original magnetic nanoparticles. However, the characteristic peaks as (300) and (440) could still be recognised from the XRD pattern of PAM/FeO samples.

8 CONCLUSIONS & FUTURE WORKS

Iron oxide nanoparticles, polyacrylamide and poly-(methacrylic acid) nano-spheres, silica/PAM coated nanocomposites with uniform size distribution and controlled morphology, were synthesised in water-in-oil (w/o) microemulsion systems.

Igepal CO-520/cyclohexane was selected to carry out the nano-synthesis at 25°C, due to its higher solubilisation of aqueous phase, which allowed the investigation to be carried out with a broad range of system-dependent parameters, such as loading of aqueous phase and surfactant concentration, without disturbing the thermodynamic stability of systems. From a geometrical point of view, the non-ionic surfactants with the shorter POE chains and the smaller cross-sectional areas, could both result in the increased solubilisation capability of the aqueous phase. Hence, the Igepal CO-520/cyclohexane w/o microemulsion system showed higher extent of water solubilisation at 25°C.

Temperature normally has an inverse-effect on the solubilisation of aqueous phase in w/o microemulsion systems with non-ionic surfactants, due to the dehydration of POE chains with increased temperature. However, the Brij 97/cyclohexane microemulsion system showed an increased solubilisation with the increase of temperature from 40°C to 70°C. Therefore, **Brij 97/cyclohexane** combination because of its better stability at higher temperatures, accompanied with required solubilisation capability, were selected as the high-temperature system (60°C) for the microemulsion polymerisation of acrylamide.

The size of microemulsion-derived magnetic particles increased from 1 nm to over 5 nm with the increase of the size of water pools in the microemulsions. The iron oxide nanoparticles prepared by the

precipitation method were 5-20 nm. The increase of ripening time and temperature, both could result in the increased crystallinity accompanied with the increased crystallite size of the iron oxide particles. The maghemite phase appeared when the sample was prepared at 90°C for 12 hours. Due to the existence of amorphous hydrous ferric oxide, the starting materials with a lower content of ferric ions resulted in the better crystallinity of the nanoparticles.

The complete oxidation phase as hematite was observed from microemulsion-derived samples after 12-hour hydrothermal process at 140°C, while the corresponding transition temperature for precipitation-derived samples was 200°C. The increase of hydrothermal temperature leads to the increase of crystallinity and crystallite size of nanoparticles. As the hydrothermal temperature was increased from 120°C to 200°C, the size of microemulsion-derived particles increased from 10 to 60 nm. Meanwhile, the size of precipitation-derived samples increased from 20~30 nm to 20~180 nm. The broad size distribution of precipitation samples resulted in the size-gap of particles.

Microemulsion-derived iron oxide nanoparticles have the lower saturation magnetisation and the lower coercivity at 5K and 300K, respectively, compared with precipitation-derived particles, due to the smaller particle size which is presumably close to the single domain.

PAM nano-spheres were synthesized via Brij 97/cyclohexane at 60°C for 6 hours, initiated by KPS. The size of polymer spheres increased from 50 nm to 200 nm with an increase of surfactant concentration. The increased size of water pools resulted in the increased size of PAM from 50 nm to 500 nm. KPS was used as the heat initiator in polymerisation of AM. Increasing the concentration of KPS resulted in a slightly increase of conversion and the decrease of molecular weight of the polymer from 4.81×10^5 g/mol to 4.05×10^5 g/mol. The synthesis of PMAA nano-spheres were investigated by polymerisation in a Triton X-114/cyclohexane w/o microemulsion system, at 60°C for 6 hours. Both the KPS and MAA concentrations can affect the molecular weight of polymer produced. The increase of the latter also led to the increase of size of PMAA spheres from 30 nm to 100 nm.

As for the synthesis of core-shell structured nanocomposites, the thickness of the ceramic shell was affected by RHT. The original size of iron oxide core was ~5 nm. The overall size of nanocomposites decreased from 20 to 12 nm with the increase of RHT from 10 to 100, presumably because the increased amount of free-water results in the increased rate of hydrolysis reactions and consequently the decreased size of silica shell. PAM coated nano-magnetic materials have been prepared by a Brij 97/cyclohexane w/o microemulsion system at 60°C for 6 hours. It was seen clearly from the TEM micrographs that many of iron oxide particles, size around 5 nm, were homogeneously embedded in the polymer spheres, size of 120 nm.

FUTURE WORKS

1. The system-controlled synthesis of core-shell structured nanocomposites was partially confirmed, which is still far from completion. The thickness of shell and the content of core are both expected to be nicely controlled by the system parameters, accompanied with required magnetic properties.

2. PAM/FeO nanocomposites was synthesised from Brij 97/cyclohexane w/o microemulsion system in our experiments, in terms of the morphology. For polymer/magnet nanocomposites to be effectively applied in bio-science and technology, not only the magnetic properties of composites need to be further investigated regarding the functionality, but also, other polymers, such as PMAA or some bio-degradable materials, such as poly-ethyl-2-cyanoacrylate, which is very suitable to act as drug carrier, could be introduced in the research and fabrications.

REFERENCES

1. Shafi KVPM, Ulman A, Dyal A, Yan X, Yang N, Estournes C, Fournes L, Wattiaux A, White H, Rafailovich M *Chemistry of Materials* (14) 1778 2002.

2. McMichael RD, Shull RD, Swartzendruber LJ, Bennett LH, Watson RE *Journal of Magnetism and Magnetic Materials* (111) 29 1992.

3. Pope NM, Alsop RC, Chang YA, Sonith AK *Journal of Biomedical Materials Research* (28) 449, 1994.

4. Josephson L, Tsung CH, Moore A, Weissleder R *Bioconjugate Chemistry* (10) 186 1999.

5. Fendler JH *Chemical Reviews* (87) 877 1987.

6. Gobe M, Kon-no K, Kandori K, KitaharaA *Journal of Colloid & Interface Science* (93) 293 1983.

7. Bandow S, Kimura K, Kon-no K, Kitahara A *Japanese Journal of Applied Physics* (26) 713 1987.

8. Chhabra V, Ayyub P, Chattopadhyay S, Maitra AN *Materials Letters* (26) 21 1996.

9. Ayyub P, Multani M, Barma M, Palkar VR, Vijayaraghavan R *Journal of Physics C: Solid Stage Physics* (21) 2229 1988.

10. Carver MT, Hirsch E, Wittmann JC, Fitch RM, Candau F *Journal of Physical Chemistry* (93) 4867 1989.

11. Koch CC [Ed.] *Nanostructured Materials-Processing, Properties and Potential Applications* NOYES P. NY 2002.

12. Karatyigitoglu CF, Kommareddi N, Gonzalez RD, John VT, McPherson GL, Akkara JA, Kaplan DL, *Materials Science and Engineering* (C2) 165 1995.

13. Diandra LL, Reuben DR *Chemistry of Materials* (8) 1770 1996.

14. Eastman J, Siegel RW *Research and Development* (31) 56 1989.

15. Seigel RW *Nanostructured Materials* (3) 1 1993.

16. Suryanarayana C *International Materials Reviews* (40) 41 1995.

17. Shull RD *Report on the First NIST Workshop on Nanostructured Materials National Institute of Standards and Technology* Washington DC 1994.

18. Web Resource: HTTP://WWW.NANOTECH-NOW.COM History of nanotechnology

19. Web Resource: HTTP://WWW.BEGBROKE.OX.AC.UK The basics of nanotechnology

20. Web Resource: HTTP://WWW.IBM.COM IBM Scientists discover nanotech communication

21. Lane R, Craig B, Bakcock W *Materials engineering with nature's building blocks-AMPTIAC*, NY

22. Web Resource: HTTP://WWW.HKC22.COM Helmut kaiser consultancy.

23. Swadeshmukul S, Rovelyn T, Nikoleta T, Jon D, Arthur H, Weihong T *Langmuir* (17) 2900 2001.

24. Elliot SR *Physics of Amorphous Materials* LONGMAN LONDON & NY p350-357 1984.

25. Morup S, Trone E, *Physical Review Letters* (72) 3278 1994.

26. Nieh TG, Wadsworth J *Scripta Metallurgica et Materialia* (25) 955 1991.

27. Tschöpe AS, Ying JY *Nanostructured Materials* (4) 617 1994.

28. Ramon C, Angela H *Nanotechnology* (13) 243 2002.

29. Pascal C, Pascal JL, Favier F, Elidrissi-Moubtassim ML, Payen C *Chemistry of Materials* (11) 141 1999.

30. Ziolo RF, Giannclis EP, Weinstein BA, Horo MPO, Ganguly BN, Mehrotra V,Russell MW,Huffman DR *Science* (257) 219 1992.

31. Kroll E,Winnik FM, Ziolo RF *Chemistry of Materials* (8) 1594 1996.

32. Vollath D, Szabó DV, Tayor RD, Willis JO *Journal of Materials Research* (12) 2175 1997.

33. Taeghwan H, Su SL, Jongnam P, Yunhee C, Hyon BN *Journal of the American Chemical Society* (123) 12798 2001.

34. Egon M, Paul S *Journal of Colloid and Interface Science* (63) 509 1978.

35. Pierre AC *Introduction to Sol-Gel Processing* KLUWER ACADEMIC P. 1998.

36. Hiemenz PC *Principles of Colloid and Surface Chemistry* MARCEL DEKKER P. NY 1977.

37. Sōmiya S, Roy R *Bulletin of Materials Science* (23) 453 2000.

38. Segal D *Chemical Synthesis of Advanced Ceramic Materials* CAMBRIDGE UNIVERSITY PRESS P. Cambridge p182 1989.

39. Dairong C, Ruren X *Journal of Solid State Chemistry* (137) 185 1998.

40. Liu T, Guo L, Tao Y *NanoStructured Materials* (11) 487 1999.

41. Schwuger MJ, Stickdorm K, Schomacker R *Chemical Reviews* (95) 849 1995.

42. Koch C *Nanostructured Materials - Processing, Properties and Potential Applications* NOYES P. NY 2001.

43. Sakai H, Hanawa K, Aoyagi K *IEEE Transactions on Magnetics* (25) 2597 1989.

44. Bogush GH, Tracy MA, Zukoski CF *Journal of Non-Crystalline Solids* (104) 95 1988.

45. Boldú JL, Muñoz E, Bokhimi X, Novaro O, López T, Gómez R *Langmuir* (15) 32 1999.

46. López T, Gómez R, Pecci G, Reyes P, Bokhmi X, Novaro O *Materials Letters* (40) 95 1999.

47. López T, Chimal O, Asomoza M, Gómez R, Bokhimi X, Novaro O, Gonzalez RD *Jouranl of Solid State Chemistry* (144) 349 1999.

48. Pecci G, Reyes P, Orellana F, López T, Gómez R, Fierro JLG, *Journal of Chemical Technology and Biotechnology* (74) 1 1999.

49. Brinker CJ, Scherer GW *Sol-Gel Science* ACADEMIC PRESS PRESS P. San Diego CA 1990.

50. Schneider M, Baider A *Catalysis Reviews - Science and Engineering* (37) 515 1995.

51. Gonzlalez-Carreno T, Morals MP, Gracia M, Serna CJ *Materials Letters* (18) 15 1993.

52. Fu X, Qutubuddin S *Colloids and Surfaces A: Physicochemical and Engineering Aspects* (179) 65 2001.

REFERENCES

53. Osseo-asare K, Arriagada FJ, *Colloids and Surfaces* 321 1990.

54. Sõmiya S *Advanced Materials VI Trans. MRS-Japan frontiers in materials science and engineering* (19B) 1105, 1993.

55. Schneider JJ *Advanced Materials* (13) 529 2001.

56. Mandal TK, Fleming MS, Walt DR *Chemistry of Materials* (12) 3481 2000.

57. Ohmori M, Matijevic E *Journal of Colloid and Interface Science* (160) 288 1993.

58. Goia DV, Matijevic E *New Journal of Chemistry* (22) 1203 1998.

59. Partch R, Brown S, *Journal of Adhesion* (67) 259 1998.

60. Shi J, Gider S, Babcock K, Awschalom DD *Science* (271) 937 1996.

61. Santra S, Tapec R *Langmuir* (17) 2900 2001.

62. Matijevic E *Fine Particle Science and Technology* [Pelizetti E Ed.] KLUWER ACADEMIC P. Netherlands p1-16 1996.

63. Davies R, Schurr GA, Meenan P, Nelson RD, Bergna HE, Brevett CAS, Goldbaum RH *Advanced Materials* (10) 1264 1998.

64. Rembaum A, Dreyer WJ *Science* (208) 364 1980.

65. Li T, Moon J, Morrone AA, Mecholsky JJ, Talham DR, Adair JH *Langmuir* (15) 4328 1999

66. Schulman JH, Stoeckenius W, Prince LM, *Journal of Physical Chemistry* (63) 1677 1959.

67. Friberg SE, Mandell L, Fontell K *Acta Chemica Scandinavica* (23) 1055 1969.

68. Danielsson I, Lindman B *Colloids Surfaces* (3) 391 1981.

69. Stilbs P, Lindman B *Progress in Colloid and Polymer Science* (69) 39 1984.

70. Lindman B, Stilbs P *Microemulsion Sustems* [Rosano H, Clausse M Ed.] MARCEL DEKKER P. NY 1987.

71. Lindman B, Shinoda K, Olsson U, Andersson D, Karlström G, Wennerström H *Colloids Surfaces* (38) 205 1989.

72. Israelachvili JN, Mitchell DJ, Ninham BW *Journal of the Chemical Society: Faraday Transactions* (72) 1525 1976.

73. Mitchell DJ, Ninham BW *Journal of the Chemical Society: Faraday Transactions* (77) 601 1981.

74. Wennerström H *Journal of Colloid Interface Science* (68) 589 1979.

75. Boutonnet M, Kizling J, Stenius P, Marie G *Colloid Surface* (5) 209 1982.

76. Kumar C, Balasubramanian D *Jouranl of Colloid Interface Science* (74) 64 1980.

77. Kumar C, Balasubramanian D *Journal of Physical Chemistry* (84) 1895 1980.

78. Handa T, Sakai M, Nakagaki M *Journal of Physical Chemistry* (90) 3377 1986.

79. Fendler JH *Accounts of Chemical Research* (9) 153 1976.

80. Myers D *Surfactant Science and Technology* VCH P. p235 1988.

81. Griffin WC *Journal of the Society of Cosmetic Chemistry* (5) 249 1954.

REFERENCES

82. Griffin WC *Journal of the Society of Cosmetic Chemistry* (1) 311 1949.

83. Sjoblom J, Lindberg R, Friberg SE *Advanced Colloid Interface Science* (65) 125 1996.

84. Olsson U, Shinoda K, Lindman B *Journal of Physical Chemistry* (90) 4083 1986.

85. Olsson U, Wennerström H *Advanced Colloid Interface Science* (49) 113 1994.

86. Anderson D, Wennerström H, Olsson U *Journal of Physical Chemistry* (93) 4243 1989.

87. Shinoda K, Takeda H *Journal of Colloid Interface Science* (32) 642 1970.

88. Tchikov V, Schutze S, Kronke MK *Journal of Magnetic Materials* (194) 242 1999.

89. Winotomorbach S, Mullerruchholtz W *European Journal of Pharmaceutics and Biopharmaceutics* (41) 55 1995.

90. Babes L, Denizot B, Tanguy G, Le-Jeune JJ, Jallet P *Journal of Colloid Interface Science* (212) 474 1999.

91. Bengele HH, Palmacci S, Rogers J, Jung CW, Crenshaw J, Josephson L *Journal of Magnetic Resonance Imaging* (12) 433 1994.

92. Kiyama M *Bulletin of the Chemical Society of Japan* (47) 1646 1974.

93. Domingo C, Rodriguez-Clemente R, Biesa MA *Solid State Ionics* (59) 78 1993.

94. Kandori K, Fukuoka M, Ishikawa T *Journal of Materials Science* (26) 3313 1991.

95. Concepcion D, Rapael R, Miguel B *Journal of Colloid Interface Science* (165) 244 1994.

96. Truchaud A, Capolaghi B, Yvert JP, Gourmelin Y, Glikmanas G, Bogard M *Pure and Applied Chemistry* (63) 1123 1991.

97. Fukushima T, Sekizawa K, Jin Y, Yamaya M, Sasaki H, Takishima T *American Journal of Physiology* (265) L67 1993.

98. Salata OV *Journal of Nanobiotechnology* (2) 3 2004.

99. Taton TA *Trends of Biotechnology* (20) 277 2002.

100. Tartaj P, Morales M, Veintemillas-Verdaguer S Conzalez-Carreño, Sema CJ, *Journaol of Physics D: Applied Physics* (36) 182 2003.

101. Bang LB *Pure and Applied Chemistry* (68) 1873 1996.

102. Joubert JC *Anales de Quimica International Edition* (93) S70 1997.

103. Häfeli U, Schütt W, Teller J, Zborowski M [Ed.] *Scientific and Clinical Applications of Magnetic Carriers* SPRINGER P. NY 1997.

104. Ai CX, Fei HS, Yang YQ, *Journal of Luminescence* (60-61) 364 1994.

105. López-Quintela MA, Rivas J *Journal of Colloid Interface Science* (158) 446 1993.

106. Ziolo RF XEROX CORP. U.S. Patent 4-474-866 1984.

107. Raineri I, Moroni C, Senn HP *Nucleic Acids Research* (14) 4010 1991.

108. Sharma P, Lonneborg A, Stougaard P *Biotechniques* (15) 610 1993.

109. Winsor A *Transactions of the Faraday Society* (44) 376 1948.

110. Dokoutchaev A, James JT, Shannon CK, Pathak S, Surya-Prakash GK, Thompson ME *Chemistry of Materials* (11) 2389 1999.

111. Homola M, Lorenz MR, Sussner H, Rice SL *Journal of Applied Physics* (61) 3898 1987.

112. Homola M, Rice SL US Patent 4-280-918 1981.

113. López MA *Current Opinion in Colloid and Interface Science* (8) 137 2003.

114. Cotton FA, Wilkinson G *Advanced Inorganic Chemistry* WILEY-INTERSCIENCE P. London 1999.

115. Patton WF, Kim J, Jacobson BS *Biochimica et Biophysica Acta* (816) 83 1985.

116. Kemshead JT, Treleaven JG, Gibson FM, Ugllstad J, Rembaum A, Philip T *Progress in Experimental Tumor Research* (29) 249 1985.

117. Gupta PK, Hung CT *Life Sciences* (44) 175 1989.

118. Tebble RS, Craid DJ *Magnetic Materials* WILEY-INTERSCIENCE P. London 1969.

119. Cornell RM, Schertmann U, *The Iron Oxides: Structure, Properties, Reacctions, Occurrence and Uses* VCH P. Weinheim 1996.

120. Sugimoto T, Yamaguchi T *Journal of Crystal Growth* (34) 253 1976.

121. Tadao S, Egon M *Journal of Colloid and Interface Science* (74) 227 1980.

122. McCurrie RA *Ferromagnetic Materials Structure and Properties* HARCORT BRACE & COMPANY P. London p1 1994.

123. Chatterjee J, Haik Y, Chen C *Journal of Magnetism and Magnetic Materials* (257) 113 2003.

124. Pascal C, Pascal JL, Favier F, Elidrissi-Moubtassim ML, Payen C *Chemistry of Materials* (11) 141 1999.

125. Cornell RM, Schertmann U *Iron Oxides in the Laboratory; Preparation and Characterization* VCH P. Weinheim 1991.

126. Craik DJ [Ed.] *Magnetic Oxides* WILEY-INTERSCIENCE P. London p706 1975.

127. Gonzlalez-Carreno T, Morals MP, Gracia M, Serna CJ *Materials Letters* (18) 15 1993.

128. Janasi SR, Rodrigues D,Landgraf FJG, Emura M *IEEE Transactions on Magnetics* (36) 3327 2000.

129. Kojima H *Ferromagnetic Materials: Fundamental properties of hexagonal ferrites* [Wohlfarth EP Ed.] NORTH-HOLLAND P. NY 1982.

130. Rowlands G *Journal of Physics D: Applied Physics* (9) 1267 1976.

131. Janasi SR, Emura M, Landgraf FJG, Rodrigues D *Journal of Magnetism and Magnetic Materials* (238) 168 2002.

132. Boutonnet M, Kizling J, Stenius P, Maire G *Colloid Surface* (5) 209 1987.

133. Bandow S, Kimura K, Kon-no K, Kitahara A *Japanese Journal of Applied Physics* (26) 713 1987.

134. Ayyub P, Multani M, Barma M, Palkar VR, Vijayaraghavan R *Journal of Physics C: Solid State Physics* (21) 2229 1988.

135. Nagy JB *Handbook of Microemulsion Science and Technology* [Mittal KL Ed.] MARCEL DEKKER P. NY p495 1999.

136. Shiojiri S, Hirai T, Komasawa I *Chemical Communications* (14) 1439 1998.

137. Shah D *Micelles, Microemulsions, and Monolayers-Science and Technology* MARCEL DEKKER P. NY p19 1998.

138. Chang SY, Liu L, Asher SA *Journal of the American Chemical Society* (116) 6739 1994.

139. Chhabra V, Ayyub P, Chattopadhyay S, Maitra AN *Materials Letters* (26) 21 1996.

140. Jing Z, Han D, Wu S *Materials Letters* (59) 804 2005.

141. Candau F, Ottewill RH [Ed.] *Scientific Methods For the Study of Polymer Colloids and Their Applications.*: KLUWER ACADEMIC P. Dordrecht 1990.

142. Graillat C, Lepais M, Pichot C *Journal of Dispersion Science and Technology* (11) 455 1990.

143. Renken A, Hunkeler D *Polymer* (4) 3545 1999.

144. Candau F *Polymer Association Structures: Microemulsions and Liquid Crystals* [EL-Nokaly MA Eds.] AMERICAN CHEMICAL SOCIETY P. Washington DC 1989.

145. Debuigne F, Jeunieau L, Wiame M, Nagy JB *Langmuir* (16) 7605 2000.

146. Hernández-Barajas J, Hunkeler D *Polymer* (38) 5623 1997.

147. Candau F, Leong YS, Fitch RM *Journal of Polymer Science* (23) 193 1985.

148. Hao J, Zheng L, Li G, Wang H, Du Z *Polymer* (37) 3117 1996.

149. Odian G *Principles of Polymerisation* WILEY-INTERSCIENCE NY p218 1991.

150. Xu X, Ge X, Zhang Z, Zhang M, Zuo J, Niu A *European Polymer Journal* (35) 1975 1999.

151. Puig LJ, Sánchez-Díaz JC, Villacampa M, Mendizábal E, Puig JE, Aguiar A, Katime I *Journal of Colloid and Interface Science* (235) 278 2001.

152. Pileni MP, Zemb T, Petit C *Chemical Physics Letters* (118) 4 1985.

153. Zulauf M, Eicke HF *Journal of Physical Chemistry* (83) 480 1979.

154. Banerjee S, John VT, Mcpherson GL, O'Conor CJ, Buisson YSL, Akkara JA, Kaplan DL *Colloid Polymer Science.* (275) 930 1997.

155. Dresco PA, Zaitsev VS, Gambino RJ, Chu B *Langmuir* (15) 1945 1999.

156. Capek I *Polymer Journal* (36) 793 2004.

157. Karatyigitoglu CF, Kommareddi N, Gonzalez RD, John VT, McPherson GL, Akkara JA, Kaplan DL *Materials Science and Engineering C* (2) 165 1995.

158. Pecci C, Reyes P, López, Gómez R *Applied Catalysis A* (17) 1998.

159. Sun XC, Toledo JA, Cui ZL, Zhang ZK *Journal of Nanoparticle Research* (3) 325 2001.

160. Soriano L, Ahonen PP, Kauppinen EI, Gómez-Garcia J, Morant C, Palomares FJ, Sanchez-Agudo M, Bressler PR, Sanz JM *Monatshefte Fur Chemie* (133) 849 2002.

161. Petit C, Lixon P, Pileni MP *Jouranl of Physical Chemistry* (94) 1598 1990.

162. Stöber W, Fink A, Bohn E *Journal of Colloid Interface Science* (26) 62 1968.

163. Look JL, Bogush GH, Zukoski CF *Faraday Discussions of the Chemical Society* (40) 345 1990.

164. Arriagada FJ, Osseo-Asare L *Journal of Colloid Interface Science* (211) 210 1999.

165. Gupta AK, Wells S *IEEE Transactions on Nanobioscience* (3) 66 2004.

166. Kommareddi NS, Tata M, John VT, Mcpherson GL, Herman MF *Chemistry of Materials* (8) 801 1996.

167. Denkbns EB, Kilicay E, Birlkseven C, Ozturk E *Reactive and Functional Polymers* (50) 225 2002.

168. Arias JL, Gallardo V, Gómez-Lopera SA, Plaza RC, Delgado AV *Journal of Controlled Release* (77) 309 2001.

169. Dormann JL, Spinu L, Tronc E, Jolivet JP, Lucari F, D'Orazio F, Fiorani D, *Journal of Magnetism and Magnetic Materials* (183) 255 1998.

170. Leong YS, Candau F *Journal of Physical Chemistry* (86) 2269 1982.

171. Holding SR, Meeham E, *Molecular Weight Characterisation of Synthetic Polymers* CHEMTEC P. Canada 1995.

172. Brandrup J, Immergut EH, Grulke EA [Ed.] *Polymer Handbook* WILEY-INTERSCIENCE P. London 1999.

173. Shick MJ [Ed.] *Surfactant Science Series: Nonionic surfactants* MARCEL DEKKER P. NY 1967.

174. Rosen MJ [Ed.] *Surfactants and Interfacial Phenomena* WILEY-INTERSCIENCE P. New Jersey 2004.

175. Misra DN *Langmuir* (7) 2442 1991.

176. Ruckenstein E, Chi JC *Journal of Chemical Society: Faraday Transactions* (71) 1690 1975.

177. Ruckenstein E, Nagarajan R *Journal of Physical Chemistry* (84) 1349 1980.

178. Elworthy PH, Macfarlane CB, *Journal of the Chemical Society* 311 1964.

179. Lee JD *Concise Inorganic Chemistry BLACKWELLS LTD. P. London 1996.*

180. Knudsen JM *Acta Chemica Scandinavica A* (29) 833 1975.

181. Fabrikanos A, Liceser KH *Zeitchrift Für Physikalische Chemie (Frankfurt)* 34:16, 29 1962.

182. Evgenii V, Khamskii *Crystallization Kinetics IN Crystallization From Solutions* 1967.

183. Belopol'skii AP, Margolis FG *Zh. Prikl. Khim* (20) 331 1947.

184. Jenkins R, Snyder RL *Introduction to X-ray powder diffractometry* WILEY-INTERSCIENCE P. London p90 1996.

185. Liesegang RE *Zeitchrift Für Physikalische Chemie* (75) 1911.

186. Oswald W *Lehrbuch der Algemeinen Chemie* ENGLEMANN P. Leipzig p444 1896.

187. Rasmussen JK, Heilmann SM, Toren PE, Pocius AV, Kotnour TA *Journal of the American Chemical Society* (105) 6845 1983.

188. Odian G [Ed.] *Principles of Polymerisation* NY 1991.

189. Eastmond GC *Comprehensive Chemical Kinetics* [Bamford CH, Tipper CFH Ed.] AMERICAN ELSEVIER P. NY 1976.

190. Kamachi-MSatoh J, Nozakura SI *Journal of Polymer Science* (16) 1789 1978.

191. Deb PC, Kapoor SK *European Journal of Polymer Science* (15) 477 1979.

REFERENCES

192. Berger KC, Deb PC, Meyerhoff G *Macromolecules* (10) 1075 1977.

193. Hasan SM *Journal of Polymer Science* (20) 2969 1982.

194. Sandler SR, Karo W *Polymer Synthesis: Organic Chemistry* [Blomquist AT, Wasserman H Ed.] ACADEMIC PRESS P. NY 1974.

195. Liu Z *Ph. D. Thesis* LOUGHBOROUGH UNIVERSITY 1997.

196. Paleos CM [Ed.] *Polymerisation in Organised Media* CORDON & BREACH P. NY 1992.

197. Matsoukas T, Gulari E *Interfacial Phenomena in Biotechnology and Materials Processing* [Attia YA, Moudgil BM, Chander S Ed.] ELSEVIER P. Amsterdam 1988.

198. Adams J, Baird T, Braterman PS, Cairns JA, Segal DL *Better Ceramics Through Chemistry III* [Brinker CJ, Clark DE, Ulrich DR Ed.] MATERIALS RESEARCH SOCIETY p361 1988.

199. Pecci G, Reyes P, López T, Gómez R *Applied Catalysis A* (17) L7 1998.

200. Guizard C, Stito M *Journal of Physical Chemistry* (104) 149 1988.

201. Selle MH *Colloid and Polymer Science* (273) 951 1995.

202. Bogush GH, Zukoski CFJ *Jouranl of Colloid Interface Science* (142) 1 1991.

APPENDICES

I. Preparation of magnetic nanocomposition via water-in-oil microemulsion

Preparation of nanometer-sized polymethacrylic acid particles in water-in oil microemulsions

II. Structures & properties of materials used in experiments

III. Characteristic values of iron oxide samples

World Journal of Engineering 1 (2004)75 - 81

World Journal of
Engineering

Preparation of magnetic nanocomposition via water-in-oil microemulsion

Xujin Bao, Min Lin, Hwee Zhen Koh and Qiuyu Zhang
Institute of Polymer Technology and Materials Engineering (IPTME), Loughborough University, Loughborough, Leicestershire LE11 3TU, UK. E-mail: x.bao@lboro.ac.uk

(Received 18 March 2004; accepted 12 May 2004)

Abstract

A new water-in-oil (W/O) reverse microemulsion system was developed to prepare silica-coated iron oxide magnetic nanocomposites, where Igepal CO-520 was used as the surfactant and cyclohexane as the oil phase. As a comparison, coprecipitation method was also employed to synthesize the nanomagnets and hydrothermal as a post-treatment to enhance the crystallinity of the iron oxide nanoparticles prepared. The iron oxide nanoparticles prepared via the microemulsion and co-precipitation at ambient temperature are magnetite (Fe_3O_4) and have poor crystallinity with the size of 5-10nm and 10-20nm, respectively. The iron oxide particles via microemulsion grew in size to ~ 60nm after hydrothermal treatment at 200℃ and transformed to hematite (α-Fe_2O_3) at 140℃, while large size distribution (14-180nm) of the nanoparticles was observed for those prepared by coprecipitation after post-hydrothermal treatment at 200℃ and the nanoparticles were in the maghemite ($\tilde{a}$-Fe_2O_3) phase at temperatures 140℃, 160℃ and transformed into the hematite (α-Fe_2O_3) at 200℃. Silicon oxide coated iron oxide nanocomposites were also synthesized in-situ by ammonia-catalyzed tetraethyl orthosilicate (TEOS) hydrolysis and condensation after forming the iron oxide nanoparticles in the microemulsion system. TEM micrograph showed that the iron oxides were coated by a thin layer of silica, which was further supported with EDX analysis.

Key wards : *Microemulsion, Core-shell structure, Nanoparticles, Magnetic.*

1. Introduction

In recent years, there has been considerable interest in the synthesis of nano-sized magnetic particles such as Fe_2O_3 and Fe_3O_4, due to their potential applications as magnetic inks, ferrofluids, magnetic recording, magnetic storage media, and magnetic cell separation and other medical applications (Haik *et al.*, 1999; Safarik and Safarikova, 1999; Tartaj and Serna, 202; Martin *et al.*, 2003). However, pure magnetic particles themselves may not be very useful in practical applications as they tend to form large aggregates and they can undergo rapid biodegradation when they are directly exposed to the biological system (Swadeshmukul *et al.*, 2001). Therefore a coating is very necessary to prevent such problems (Swadeshmukul *et al.*, 2001; Zhong and Maye, 2001; Caruso, 2001; Caruso *et al.*, 2001; Levy *et al.*, 2002). For example, the nanomagnets composite systems with the core/shell structures could result in spin bias exchange at the boundary of the

ISSN: 1708-5284

superparamagnetic particles and, as a consequence of single domain characteristics, lead to enhanced coercivity and apparent ferromagnetic behaviour (Shi *et al.*, 1996). These coated particles would also be very useful for efficient bio molecule separation and for magnetically guided biosensor applications (Swadeshmukul *et al.*, 2001).

A microemulsion is a thermodynamically stable system composed of at least three components: two immiscible components (usually water and oil) and a surfactant (Boutonnet *et al.*, 1982; Shi *et al.*, 1996), which provides a microheterogeneous medium for the generation of nanoparticles. The formation of particles in such systems is controlled by the reactant distribution in the droplets and by the dynamics of interdroplet exchange. The surfactant stabilized micro-cavities provide a cage-like effect that limits particle nucleation, growth and agglomeration. In this report, a new water-in-oil microemulsion system was developed to prepare iron oxide nanoparticles, silicon oxide nanospheres and iron oxide/silicon oxide nanoparticles with core-shell structure. The transmission electron microscope (TEM), X-ray diffractometer (XRD) and Energy dispersion X-ray were employed to study the morphology, particle size and crystallinity of both the uncoated and silica-coated iron oxide particles.

2. Experimental details

2.1. Materials

All chemicals were purchased from Sigma-Aldrich and were used as receive. The surfactant used was Igepal CO-520. The iron chloride (Ⅱ) tetrahydrate 99%, iron chloride (Ⅲ) hexahydrate 98%, tetraethylorthosilicate (TEOS), and ammonium hydroxide 35% were reactants for the iron oxides and silica coated iron oxides. The oil phase was cyclohexane. Distilled water was used throughout the experiment.

2.2. Synthesis of iron oxide, silicon oxide and iron oxide/silicon oxide nanoparticles

The synthesis of the iron oxide nanoparticles was carried out in an Igepal CO-520/cyclohexane (20/80 wt%) reverse microemulsion. Precalculated amounts of iron chloride aqueous solution were added to the microemulsion system with NH_4OH as the base. Nitrogen gas was continuously purged during the mixing. Resultant products were left to react under ambient temperature for 24 hours. Silica nanoparticles were prepared by the hydrolysis of tetraethylorthosilicate (TEOS) (H_2O/TEOS = 40mol/mol) in the same reverse microemulsion as above. Silica coated iron oxide particles were prepared by two steps: iron oxide nanoparticles was first synthesized as described above, then precalculated TEOS was added into the microemulsion. The mixed solution was left to react at ambient temperature for 72 hours. All the nanoparticles synthesised were separated by centrifugation, washed thoroughly with acetone and distilled water to remove any extraneous species (two times with acetone followed by two times with distilled water and finally with acetone again).

2.3. Hydrothermal treatment

The hydrothermal treatment of the nanoparticles synthesised was carried out in an autoclave at the high temperature between 140 and 200℃. The autoclave is an airtight vessel made by stainless steel with a Teflon inner container, and a stainless steel cap. The starting materials had been washed and centrifuged before undergoing the hydrothermal treatment. 1g of nanoparticles and 20g of water was mixed and sealed in the autoclave. The autoclave was kept in a temperature-controlled oven for 5h. Internal pressure depends on the temperature.

2.4. Characterisation

A transmission electron microscope, JEOL 2000FX, was used to examine iron oxide, silica and silica coated iron oxide nanoparticles. Samples were made by placing a drop of the solution on a copper grid. The solvent was allowed to evaporate at room temperature. Particle sizes were estimated from TEM pictures. The silica coated iron oxide particles were further examined using a FEI Tecnai F20 Field Emission Gun Transmission Electron Microscope equipped with thin window Energy Dispersive X-ray Analysis (EDX). The crystallinity of the powder samples was measured using a Bruker D8 X-ray diffractometer with CuK_α radiation $\lambda = 0.15406$nm at 40kv and 30mA. Data were collected over the 2θ ranging 10-70(with a step

size of 0.02° and a count time of 0.5s. Samples to be characterized using XRD were dried and grinded into fine powders before measurement.

3. Results and discussion

Iron oxide particles were synthesized via the microemulsion and coprecipitate methods. The size of the nanoparticles synthesized by microemulsion is in the range of 5-10nm, while the particles prepared by coprecipitation were 10-20nm (Fig. 1). The introduction of microemulsions to produce nanoparticles bound the particle size within smaller nano-range and facilitate the uniform particles. While the co-precipitation method does not hold a micro-cage in "moulding" the particles morphology and thus produces particles with a relative larger particle size and a broader particle size distribution. The X-ray diffraction pattern (XRD) indicated these nanaparticles are magnetite (Fe_3O_4) and have poor crystallinity (Fig. 2).

The investigation of the effect of hydrothermal on the crysatllinity and phase changes of the iron oxide nanoparticles was carried out in a small autoclave at different temperatures ranging from 140℃ to 200℃. It is worthy to note that the growth of iron oxides synthesised via microemulsions was from 10nm to ~ 60nm with rather narrow size distribution after being hydrothermal treatment (Fig. 3a), while irregular size distribution was observed for the iron oxide nanoparticles prepared via pcoprecipitation, sizes ranges from 14-180nm (Fig. 3b). XRD patterns (Fig. 4) showed that the iron oxide prepared via microemulsions was transformed from magnetite to hematite ($\acute{a}$-Fe_2O_3) at hydrothermal temperature above 140℃. In contrast, a maghemite ($\tilde{a}$-Fe_2O_3) phase was observed for the nanoparticles prepared via the coprecipitation when undergoing hydrothermal treatment at temperatures 140℃, 160℃ and transformed into the hematite ($\tilde{a}$-Fe_2O_3) at 200℃ (Fig. 5).

The silicon oxides were also synthesized by the hydrolysis of tetraethylorthosilicate (TEOS) using the same microemulsion at ambient temperature for 72h using NH_4OH as a catalyst. TEM micrographs showed that the silicon oxide particles were in the size around 20 nm with a very uniform particle size distribution (Fig. 6a). Silica coated iron oxide particles were prepared in-situ via microemulsion. TEM micrograph (Fig. 6b) shows that the size of the coated magnetic particles is 15-20nm with the thickness of the coating ~ 2-5nm. X-ray diffraction pattern of the silica coated iron oxide nanoparticles displayed poor crystallinity as compared to the uncoated iron oxide nanoparticles even after hydrothermal treatment at 200℃ for 5h. This may be attributed to the layer of silica coating restricting growth of iron oxide nanoparticles in hydrothermal.

In order to further investigate the core-shell structure of the coated nanopartilces, the sample was examined using a High Resolution Transmission Electron Microscope equipped with a thin window Energy Dispersive X-ray Analysis. A nanoprobe was applied to the outer layer (shell) and the central part (core) of the nanoparticle, respectively. There was no iron element detected in the shell, indicating the iron oxide core being wrapped by a silicon oxide shell (Fig. 7).

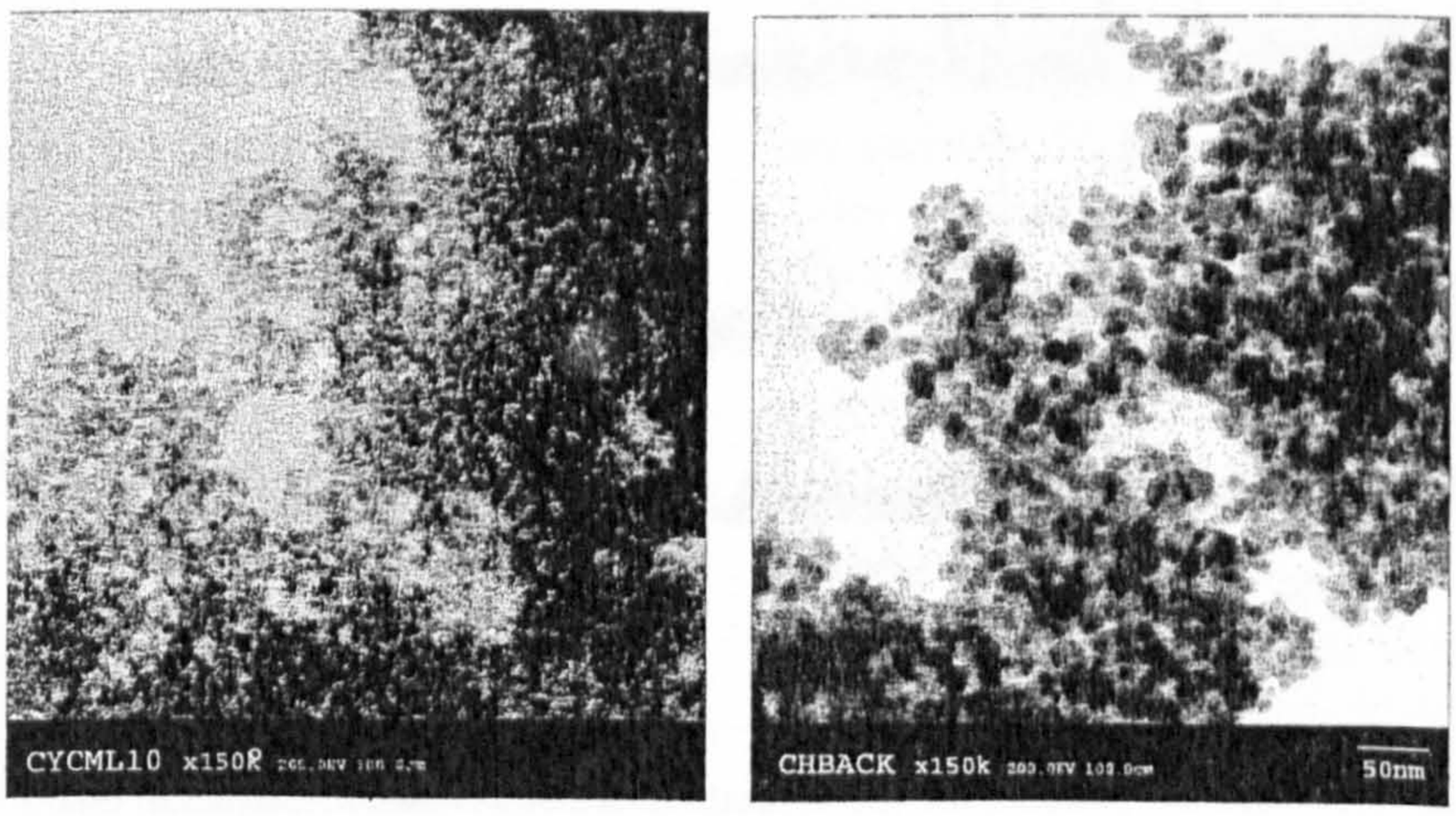

Fig. 1. TEM micrographs of iron oxide nanoparticles prepared by (left) microemulsion and (right) coprecipitated at ambiet temperature.

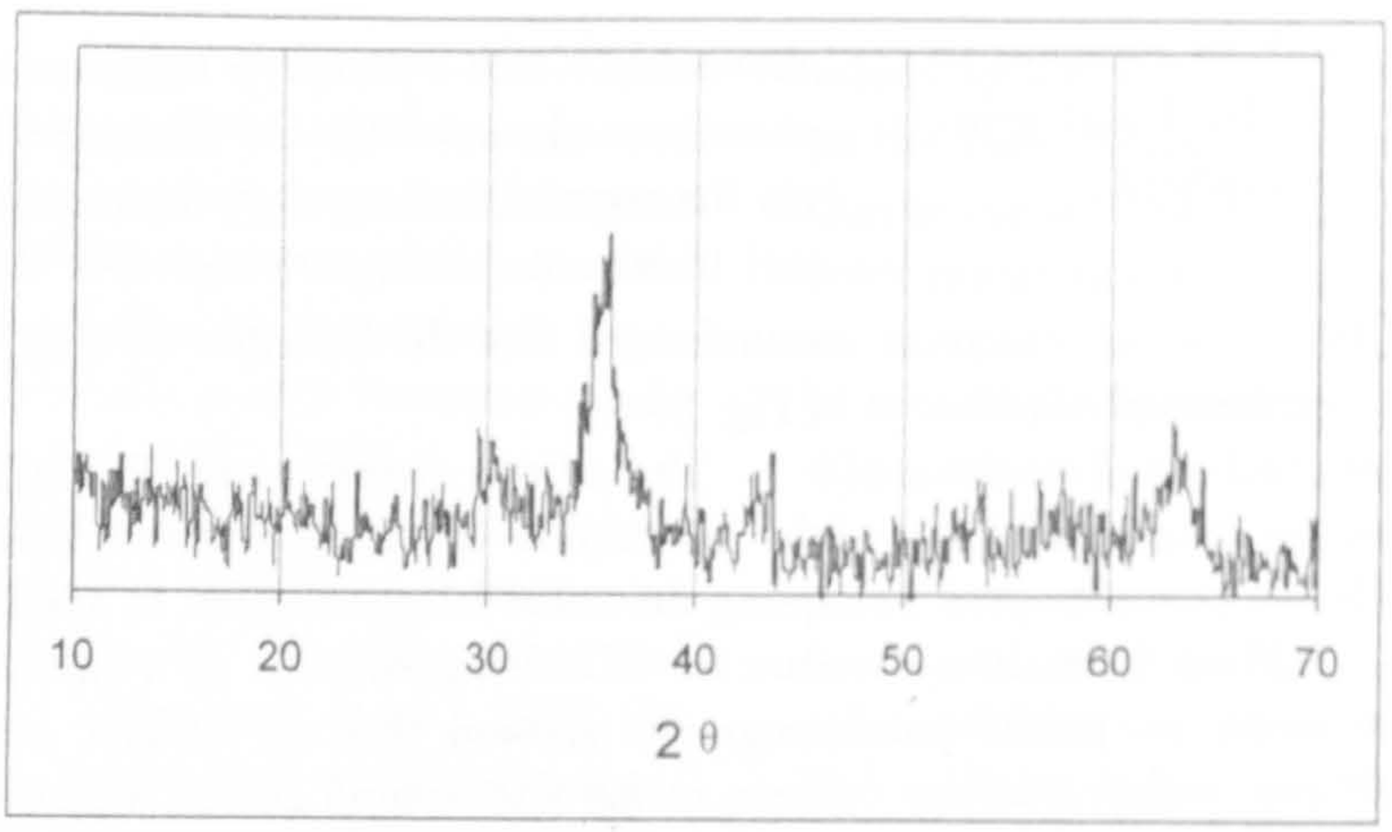

Fig. 2. X-ray diffraction pattern of the iron oxide nanoparticles prepared via microemulsions at ambient temperature.

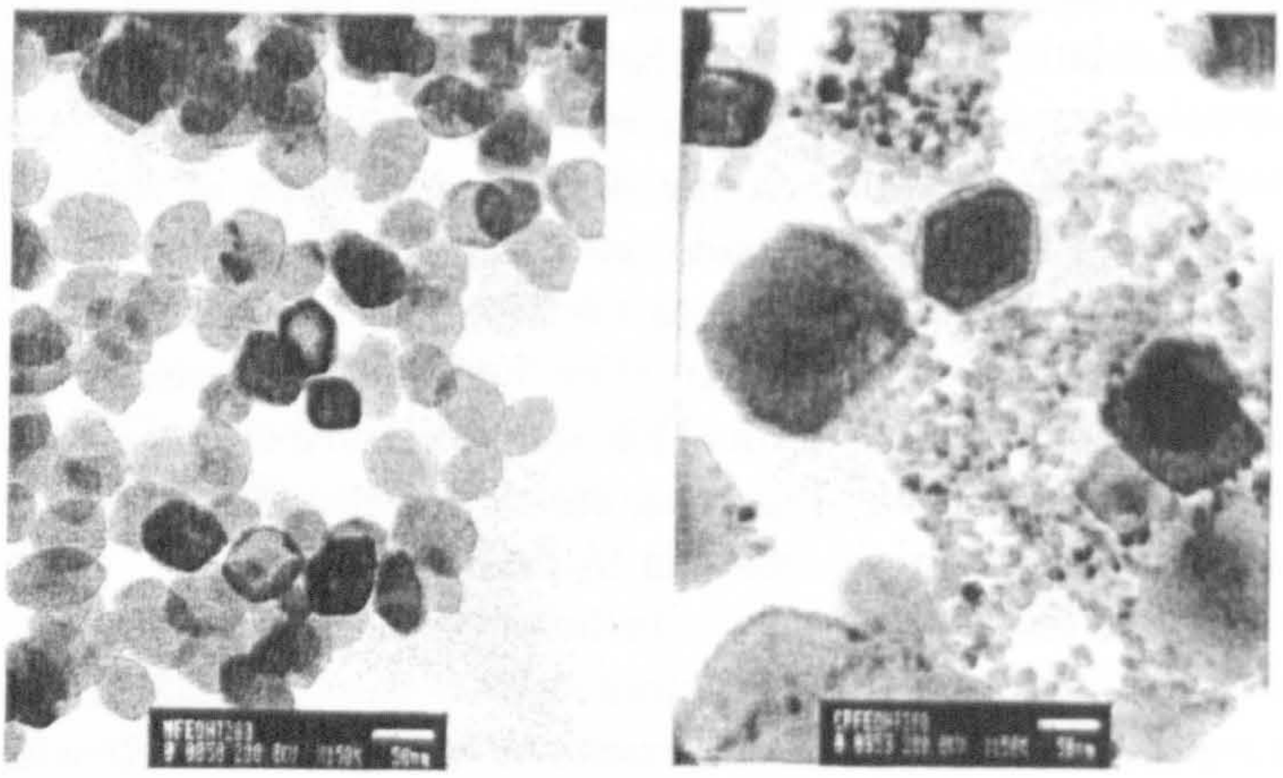

a b

Fig. 3. TEM mirographs of iron oxide nanoparticles prepared by (left) microemulsion and (right) coprecipiation after hydrothermal at temperature 200 ℃.

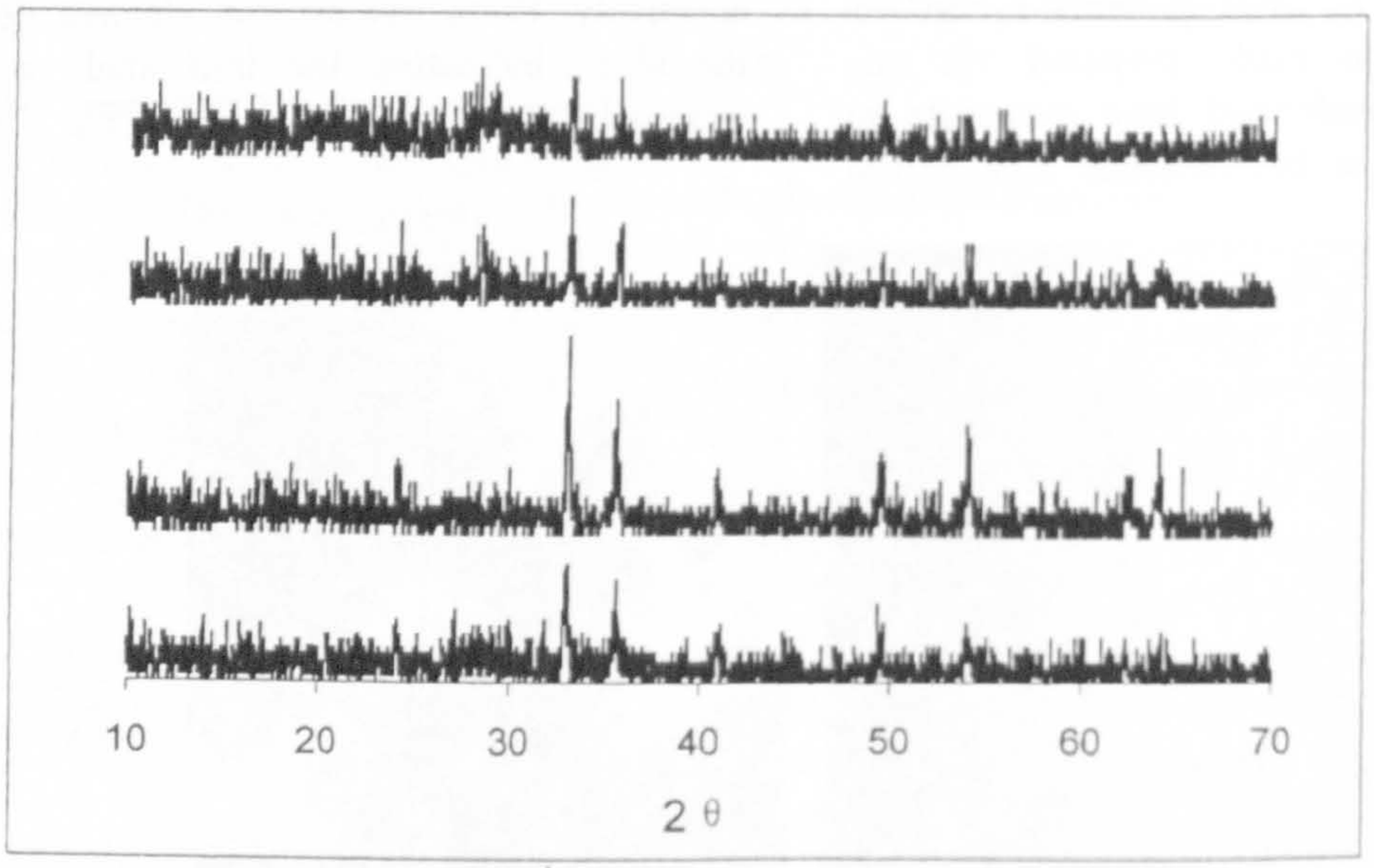

Fig. 4. X-ray diffraction patterns for the hydrothermal microemulsion prepared iron oxide as a function of synthesis temperature as the solution reacted for 5h.

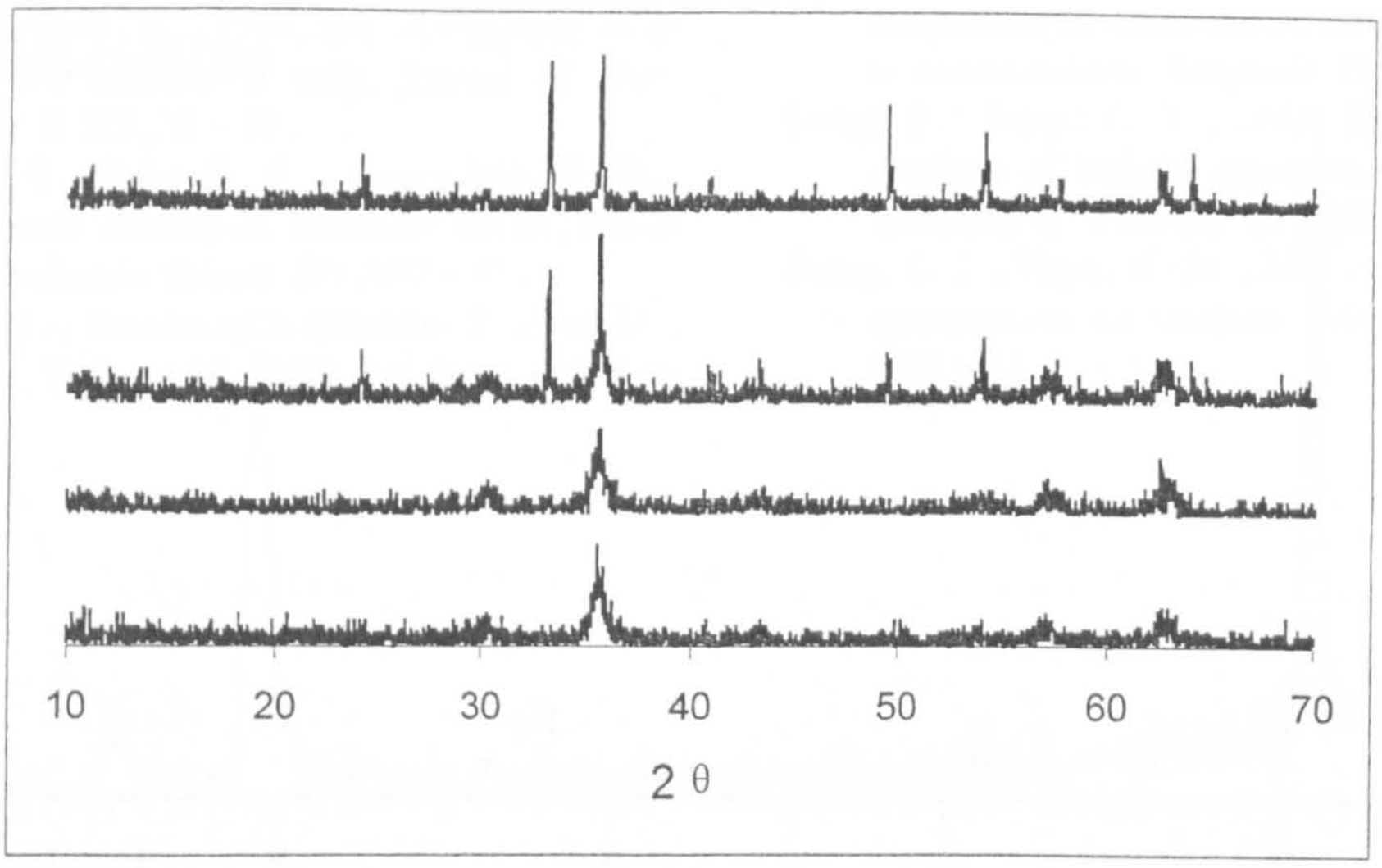

Fig. 5. X-ray diffraction patterns of the nanoparticles prepared via coprecipitation for the hydrothermal as a function of synthesis temperature for 5h.

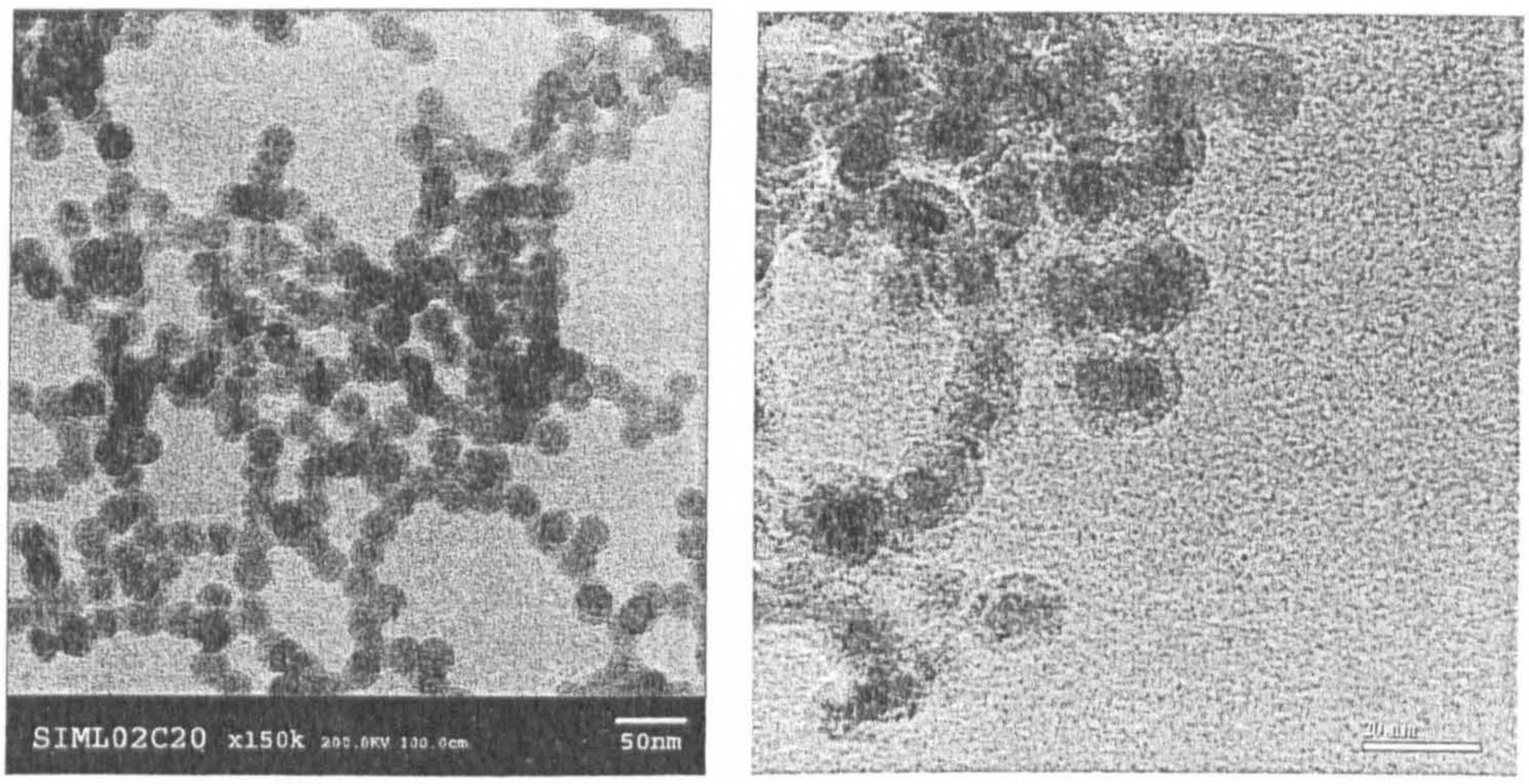

a b

Fig. 6. TEM micrographs showing (left) silica nanoparticles and (right) iron oxide/silica nanopartiles prepared via microemulsions.

4. Conclusions

Both microemulsion and coprecipitation methods were used to synthesize iron oxide nanoparticles. Hydrothermal was also employed as a post-treatment to enhance the crystallinity of the iron oxide nanoparticles. The iron oxide nanoparticles produced via both microemulsion and coprecipitation revealed the increasing in crystallinity after hydrothermal treatment. More stable crystal phase a-Fe_2O_3 was formed for the nanoparticles prepared via microemulsions and a metastable phase $\tilde{a}$-Fe_2O_3 was observed for the nanoparticles prepared via coprecipitation after hydrothermal at 140℃ for 5h. Spherical silica nanoparticles were also synthesized by hydrolysis of TEOS in the microemulsion. TEM micrographs showed that iron oxide nanoparticles were successfully coated by silica via microemulsions: dark spots (iron oxide) being coated by a thin layer of light area (silica), which was further supported with EDX analysis.

Ackknowledgement

The authors would like to thank British Royal Society and Loughborough University for supporting this project.

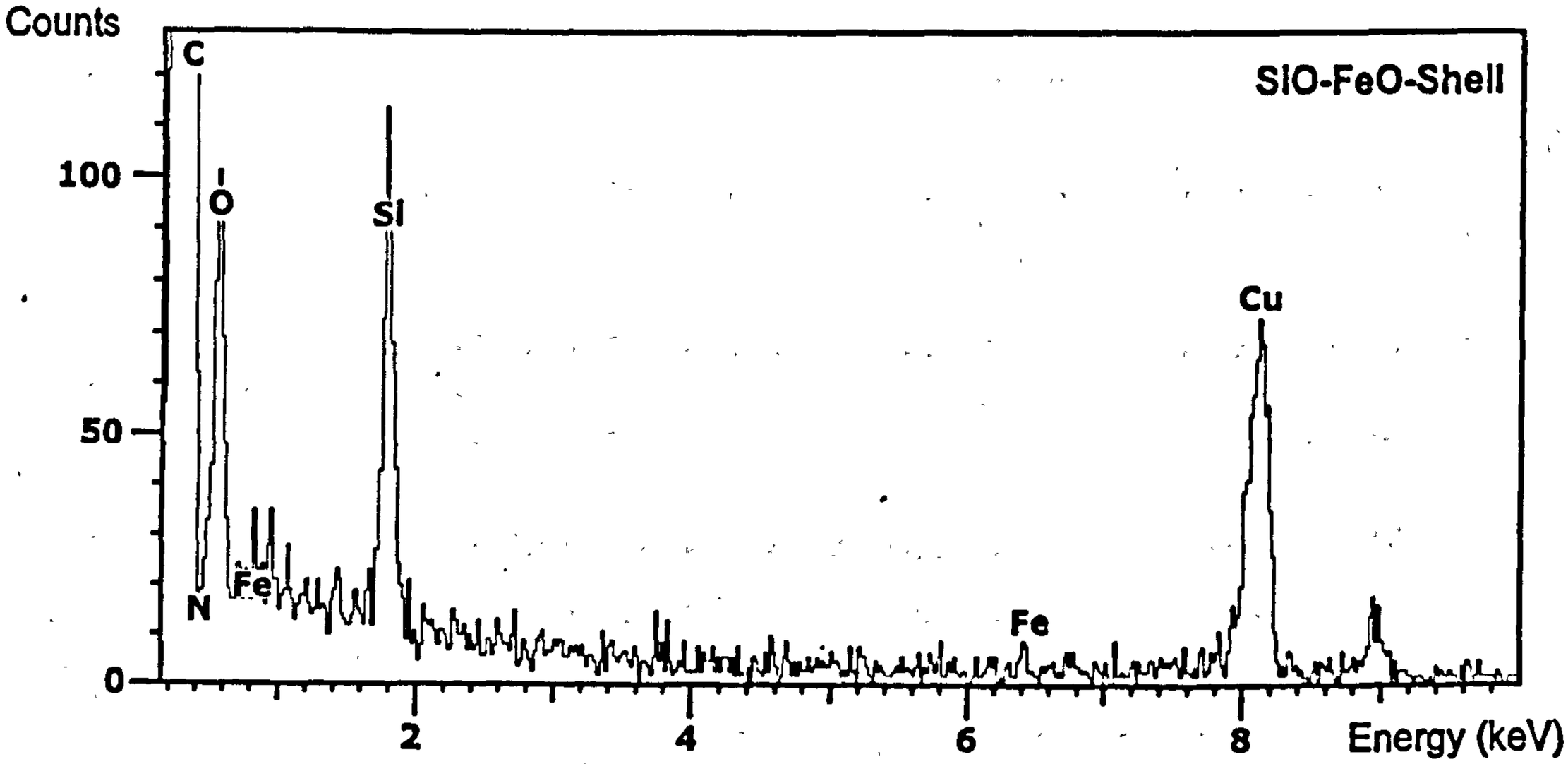

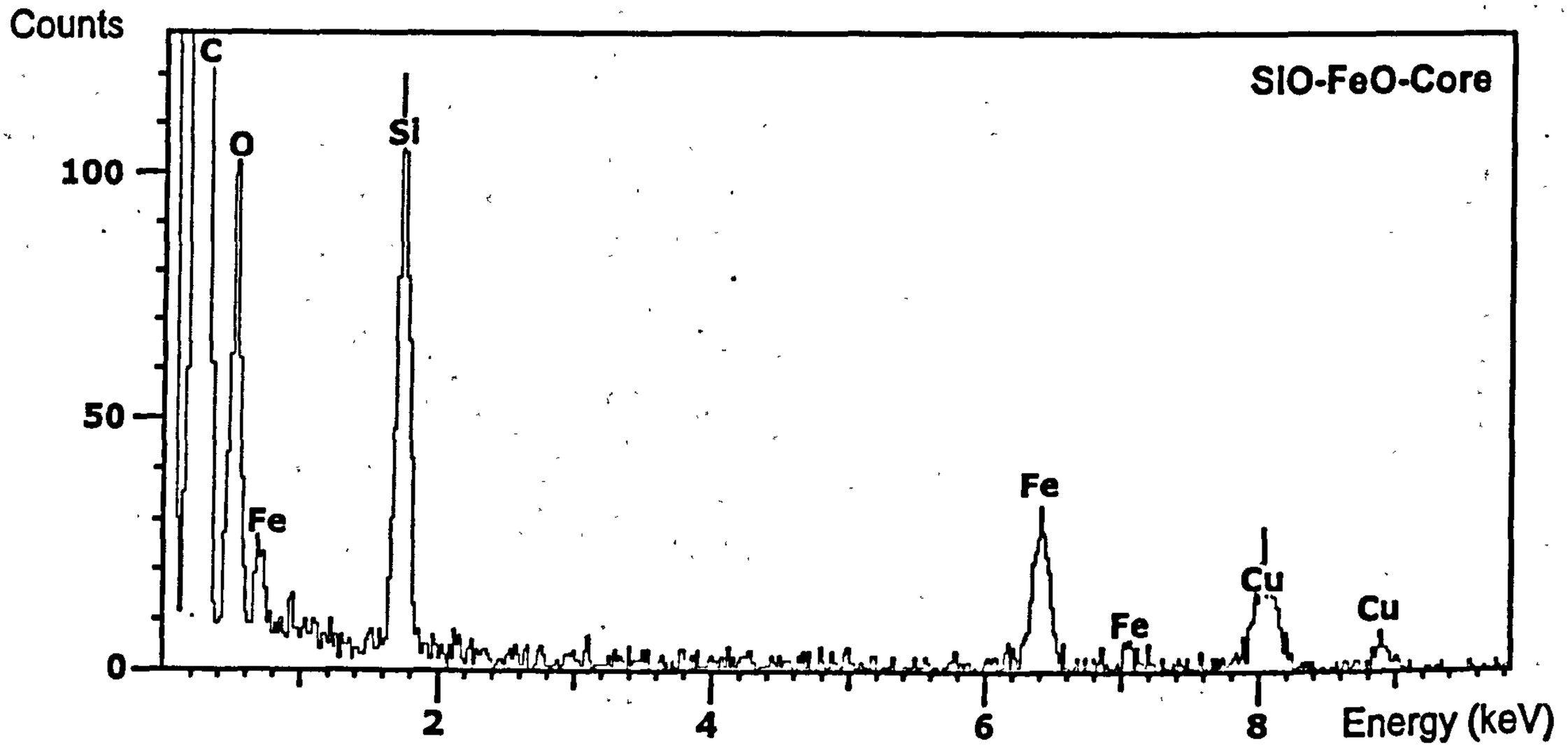

Fig.7. EDX analysis of (top) outer layer and (bottom) central part of the nanoparticle.

References

Boutonnet, M., Kizling, J., Stenius, P., Marie, G., 1982. The preparation of monodisperse colloidal metal particles from microemulsions. *Colloid Surface* 5, 209 - 225.

Caruso, F., 2001. Nanoengineering of particle surfaces. *Advanced Materials* 13, 11 - 22.

Caruso, F., Spasova, M., Susha, A., Giersig, M., Caruso, R. A., 2001. Magnetic nanocomposite particles and hollow spheres constructed by a sequential layering approach. *Chemistry of Materials* 13, 109 - 116.

Haik, Y., Pai, V., Chen, C., 1990. Development of magnetic device for cell separation. *Journal of Magnetism and Magnetic Materials* 194, 254 - 261.

Levy, L., Sahoo, Y., Kim, K. S., Bergey, E. J., Prasad, P. N., 2002. Nanochemistry: synthesis and characterisation of multifunctional nanoclinics for biological applications. *Chemistry of Materials* 14, 3715 - 21.

Martin, J. I., Nogues, J., Liu, K., Vicent, J. L., Schuller, I. K., 2003. Ordered magnetic nanostructures: fabrication and properties. *Journal of Magnetism and Magnetic Materials* 256, 449 - 501.

Safarik, I., Safarikova, M., 1999. Use of magnetic technique for the isolation of cells. *Journal of Chromatography B* **722**, 33 – 53.

Shi, J., Gider, S., Babcock, K., Awschalom, D. D., 1996. Magnetic clusters in molecular beams. *Metals and Semiconductors Science* **271**, 937 – 41.

Swadeshmukul, S., Rovelyn, T., Nikoleta, T., Jon, D., Arthur, H., Weihong, T., 2001. Synthesis and characterization of silica-coated iron oxide nanoparticles in microemulsion. *Langmuir* **17**, 2900 – 2906.

Tartaj, P., Serna, C. J., 2002. Microemulsion-assisted synthesis of tunable superparamagnetic composites. *Chemistry of Materials* **14**, 4396 – 4402.

Zhong, C. J., Maye, M. M., 2001. Core-shell assembled nanoparticles as catalysts. *Advanced Materials* **13**, 1507 – 11.

Preparation of Nanometer-Sized Poly(methacrylic acid) Particles in Water-in-Oil Microemulsions

Qiuyu Zhang,[1] Xujin Bao,[2] Mian Lin,[2] Douglas J. Hourston[2]

[1]Department of Applied Chemistry, Northwestern Polytechnical University, Xian, 710072, China
[2]Institute of Polymer Technology and Materials Engineering, Loughborough University, Loughborough, Leicestershire, LE11 3TU, United Kingdom

Received 9 February 2005; accepted 22 August 2005
DOI 10.1002/app.23619
Published online 17 February 2006 in Wiley InterScience (www.interscience.wiley.com).

ABSTRACT: A water-in-oil microemulsion, water-in-cyclohexane stabilized by poly(ethylene glycol) *tert*-octylphenyl, was developed to prepare poly(methacrylic acid) (PMAA) particles. Up to 100% conversion of the amphiphilic monomer, methacrylic acid (MAA), which could not be converted to the polymer efficiently in a dioctylsulfosuccinate sodium salt/toluene microemulsion, was achieved. The viscosity-average molecular weight of the PMAA prepared was 1.45×10^5 g/mol. The effects of some polymerization parameters, including the reaction temperature and the concentrations of the initiator and the monomer, on the polymerization of MAA were investigated. The results showed that the polymerization rate of MAA was slower than that of acrylamide in the microemulsions reported in the literature. The degree of conversion increased with the initiator concentration, reaction temperature, and monomer concentration. However, the stable microemulsions became turbid during the polymerization when the reaction temperature was at 70°C or at a high monomer concentration (40 wt %) The synthesized PMAA particles were spherical and had diameters in the range of ~50 nm. © 2006 Wiley Periodicals, Inc. J Appl Polym Sci 100: 2497–2503, 2006

Key words: poly(methacrylic acid); microemulsion polymerisation; nanoparticles

INTRODUCTION

A microemulsion may be defined as a thermodynamically stable isotropic dispersion of two immiscible liquids consisting of nanometer-sized domains of one or both liquids in the other, stabilized by an interfacial film of surface-active molecules. They can be classified as oil-in-water and water-in-oil (w/o) according to the dispersed and continuous phases. In both cases, the dispersed phase consists of monodispersed droplets in the size range of 10–100 nm.[1,2]

Recently, w/o (inverse) microemulsions have attracted much more attention as a route for preparing inorganic nanomaterials[3–5] and high-molecular-weight water-soluble polymers.[1,6] This route offers a novel and versatile technique for the synthesis of a wide variety of nanophase materials with the ability to control precisely the size of the particles formed and to yield polymer particles with a narrow particle size distribution and excellent latex stability. It also offers a unique method for controlling the kinetics of particle formation and growth by varying the physicochemical characteristics of the microemulsion system.[4]

Correspondence to: X. Bao (x.bao@lboro.ac.uk).
Contract grant sponsor: Royal Society.
Contract grant sponsor: Loughborough University.

Journal of Applied Polymer Science, Vol. 100, 2497–2503 (2006)

Most studies on the polymerization of water-soluble monomers via inverse microemulsions have mainly focused on acrylamide (AM).[7–11] The use of the microemulsion approach has led to stable and clear microlatices with uniform diameters of about 50 nm. Each of the final latex particles contains only about one high-molecular-weight macromolecule in a collapsed state.[1] More recently, polymerizations in inverse microemulsions of other water-soluble monomers, including 2-methacryloyl oxyethyl trimethyl ammonium chloride, have also been reported.[12–15]

Poly(methacrylic acid) (PMAA) possesses a wide range of physical and chemical properties, such as good variations in the hydrophilicity, hardness, toughness, adhesion, complex formation, a special pH-responsive ability, and electrolyzable properties, and this makes it a good candidate for many applications.[16,17] In some cases, nanometer-sized PMAA particles are preferred, such as controlled drug delivery[18,19] and self-assembly processes.[20] Obviously, the inverse microemulsion route offers a possible way of preparing nanometer-sized PMAA particles as the polymerization is carried out in restricted small droplets in the microemulsion system. However, so far, no results have been reported on the polymerization of methacrylic acid (MAA) with an inverse microemulsion method.

In this work, w/o microemulsion systems were used to prepare nanometer-sized PMAA particles. The effects of the reaction parameters, including the temperature and the initiator and monomer concentrations, on the

polymerization were investigated. The mechanism of the formation of the PMAA nanoparticles is discussed and compared with the ionic surfactant sodium bis(2-ethylhexylsulfosuccinate) (AOT) system.

EXPERIMENTAL

Materials

The surfactants polyoxyethylene(5)nonylphenylether (Igepal-CO-520), poly(ethylene glycol) *tert*-octylphenyl (Triton-114), AOT, and sorbitan trioleate (Tween-85) were purchased from Sigma–Aldrich (Gillingham, United Kingdom), were analytical-grade, and were used without further purification. Toluene, cyclohexane, and 2,2,4-trimethylpentane (analytical-grade) were purchased from Fisher Scientific (Loughborough, United Kingdom) and used as the oil phase. MAA, purchased from Sigma–Aldrich, was vacuum-distilled at 60°C just before the reaction. *N,N*-Methylenebis(acrylamide), purchased from Fisher Scientific, was recrystallized before use. Analytical-grade potassium persulfate (KPS) was used as the initiator without further purifying treatment. Acetone and ethanol were used as supplied. Distilled water was used throughout the experiments.

Loading and partitioning of the monomer solution

The loadings of the monomer and its salt solution in the microemulsions were measured. The monomer, or its ammonium salt solution, was added dropwise into the prepared oil/surfactant solution, which was stirred continuously. The next drop of monomer was not added until the system had turned transparent. If the system did not turn back to the transparent state after 30 min, this point was taken as the loading of the monomer in the microemulsion. The transparency of the system was judged by visual observation, and the experiments were conducted at 20°C.

The partitioning of the monomer solution in the microemulsion systems was measured with the following procedure. The MAA monomer (2 g) was added to a mixture of 10 g of distilled water and 10 g of oil. The resulting mixture was well shaken to allow the monomer to dissolve into the water and oil phases. Then, the mixture was poured into a separating funnel. The funnel was kept still for 4 h to allow the oil and water phases to separate fully. The final weight of MAA in the two phases (water and oil) was determined, and the partitioning percentage of the monomer in the oil and water was calculated. The experiments were carried out at 20°C.

Polymerization

MAA solutions were prepared with, or without, a crosslinking agent, *N,N'*-methylenebisacrylamide (cross-linker/monomer = 0.01 mol %). The monomer solution and the initiator were added to the oil/surfactant solution. The amount of KPS was varied and quoted as the weight percentage of the total weight of the monomer in the microemulsion. Oxygen was removed via the bubbling of nitrogen through the microemulsion reaction medium for about 30 min at the ambient temperature. The polymerizations were carried out at 40–70°C for a certain time. The polymer was precipitated out by the addition of acetone and then washed with acetone 5 five times to remove the surfactant and any monomer residues. The polymers were vacuum-dried at 40°C for 48 h before characterization.

TABLE I
Loadings of MAA Aqueous Solutions in Microeulsion Systems (Surfactant/Oil = 3/7 w/w) at 20°C

Microemulsion system	Loading [aqueous MAA solution/surfactant (g/g)]
AOT/toluene	0.51
Igepal-CO-520/cyclohexane	0.77
Triton-114/cyclohexane	1.54

Characterization

The size and morphology of the polymer particles were investigated with transmission electron microscopy (TEM) (JEM 100CX, JEOL Ltd., Tokyo, Japan). The polymer samples were diluted with acetone. A copper grid coated with carbon film was covered with a hemispherical drop of the aforementioned diluted latex. The molecular weights of PMAA were determined by their relative viscosities in 0.002*M* HCl aqueous solutions with an Ostwald viscometer. The molecular weights of the polymers were calculated with the following equation:[21]

$$[\eta] = 66 \times 10^{-3} M^{0.5} (\mathrm{cm}^3/\mathrm{g}) \quad (1)$$

where $[\eta]$ is the intrinsic viscosity and M is the viscosity average molecular weight.

RESULTS AND DISCUSSION

Selection of the microemulsion systems

It is desirable for selected microemulsion systems to have a high loading of the aqueous monomer solutions and a relatively high stability with temperature, which is particularly important for thermally induced radical polymerization. Based on our previous work in optimizing components of microemulsion systems that have relatively high water loadings, three w/o microemulsion systems—AOT/toluene/aqueous MAA solution, Triton-114/cyclohexane/aqueous MAA solution, and Igepal-CO-520/cyclohexane/aqueous MAA solution—were employed in this research. The loadings of the

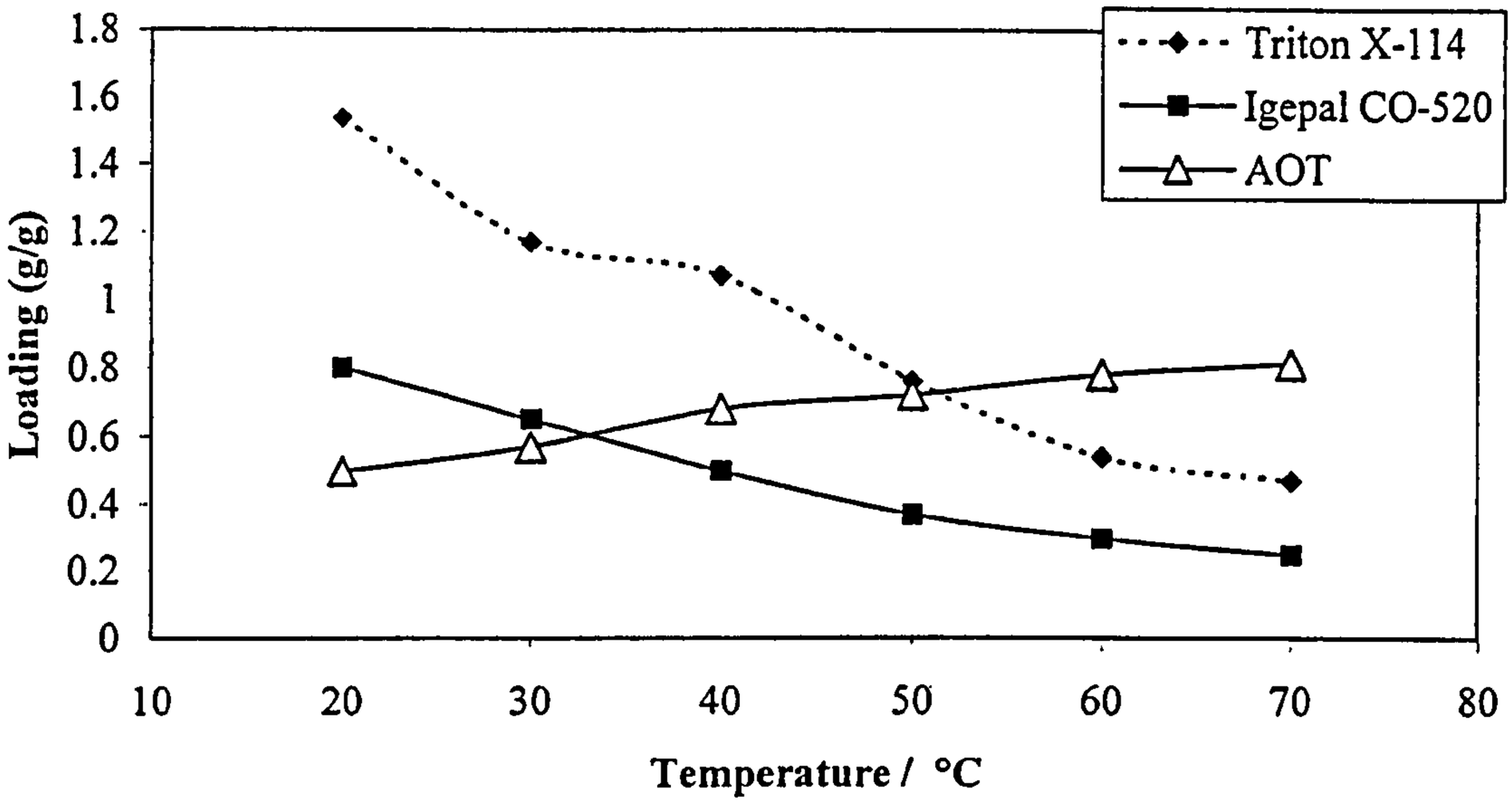

Figure 1 Effect of temperature on the loading of aqueous MAA solutions in microemulsion systems [MAA solution/surfactant (g/g)].

aqueous MAA solution (25 wt %) in these three microemulsion systems at 20°C are listed in Table I. Among the three microemulsion systems, the highest loading of the MAA solution was obtained with the Triton-114 system.

The effect of temperature on the loading of the aqueous MAA solution was also investigated and is shown in Figure 1. Both the Igepal-CO-520 and Triton-114 systems were rather sensitive to changes in the temperature. The loading of the aqueous MAA solution in these two systems decreased with increasing temperature. On the contrary, the AOT system was more stable with a change in the temperature, and the loading even increased with the temperature increasing. As the radical polymerization normally is carried out at a temperature greater than 60°C and the Igepal-CO-520 system had a very low loading at that temperature, the Triton-114 and AOT systems were chosen for the preparation of PMAA.

The polymerizations were carried out at 60°C, and KPS was used as the initiator. The degrees of conversion of MAA in these two microemulsion systems are given in Table II. A very limited conversion of about 3.4% was obtained in the AOT/toluene system. This is quite different from the polymerization of AM in the AOT/toluene/water system, which has been studied extensively,[1,7–9] and 100% conversion of the monomer to the polymer was achieved in a few minutes. A better degree of MAA conversion of nearly 15% was observed in the AOT/cyclohexane system. However, a complete MAA monomer conversion (100%) was achieved in the Triton-114/cyclohexane system.

The low degree of conversion of MAA in the AOT system may be related to the partitioning of the monomer in the water and oil phases. The partitioning of aqueous MAA in water and different oil phases is shown in Table III. The partition of MAA in the water phase was generally very low. Only 0.7% MAA stayed in the water phase in the water/toluene mixture, but 14% MAA dissolved in the water phase in the water/cyclohexane system. Therefore, it can be assumed that the majority of the MAA monomer was partitioned into the oil phase in the AOT/toluene/monomer microemulsion system.

Moreover, the polymerization of MAA generally took place in the water phase in the microemulsion system when the water-soluble initiator, KPS, was used, as the initiating radicals formed in a dispersed water phase and were, at any time, preferentially captured by unnucleated micelles containing MAA monomer.[1] That led to the very low conversion of MAA in the AOT/toluene system, which indicated

TABLE II
Degree of Conversion of MAA Polymerized in Three Microemulsion Systems (Surfactant/Oil = 3/7 wt/wt) at 60°C for 6 h

Microemulsion system	Triton-114/ cyclohexane	AOT/ toluene	AOT/ cyclohexane
Degree of conversion (wt %)	100	3.4	14.9

TABLE III
Percentage of MAA in the Oil and Water Phases (Water/Oil = 50/50 wt/wt)

	Water phase (wt %)	Oil phase (wt %)
Water/cyclohexane	14.0	86.0
Water/toluene	0.7	99.3

TABLE IV
Effect of Temperature and Reaction Time on the Degree of Conversion (wt %) of MAA[a]

Temperature (°C)	Reaction time (h)					
	0.25	0.5	1.0	2.0	4.0	6.0
50	—	—	—	—	—	—
60	7	35	61	92	97	99
70	20	39	69	94	99	100

[a] Monomer solution (4.7 wt % in the 3/7 wt/wt Triton-114/cyclohexane microemulsion.

that the partitioning of the monomer in the water and oil phases played an important role in the conversion of the monomer to the polymer in these w/o microemulsions. This was further supported by the increase in the degree of conversion of MMA to 14.9% in the AOT/cyclohexane/MAA microemulsion due to the greater partitioning of MAA in the water phase.

However, the conversion of MAA to PMAA in the AOT/cyclohexane system was much less than that in the Triton-114/cyclohexane system, although the oil phase was the same in both systems; this implied that the surfactants used in these systems may also play an important role. The anionic surfactant, AOT, had a more hydrophilic head than the nonionic surfactant, Triton-114. Hence, a bigger cagelike effect may have been produced by the strong hydrophilic interactions between the polar head groups of AOT, which could lead to lower transfer of the MAA monomer from the oil phase to the water phase during polymerization in the AOT system. As MAA showed only a small partition in the water phase and the monomer in the water phase was used up rapidly, the propagation of the polymer chains needed more monomer, which was transferred from the monomer-rich oil phase to the water phase through the surfactant layer. The stronger cagelike effect caused by the close packing of the AOT molecules restricted this transfer, resulting in a lower degree of conversion. On the other hand, the barrier formed by the nonionic surfactant, Triton-114, at the oil/water interface was electrically neutral and small, so it had lower steric hindrance to the transfer of the monomer from the oil phase to the water phase during polymerization, leading to a complete conversion of MAA in the Triton-114 system.

Effects of the temperature and reaction time on the polymerization of MAA

As the loading of the MAA aqueous solution in the Triton-114/cyclohexane microemulsion system was sensitive to the temperature (see Fig. 1), a lower temperature was preferred to obtain a higher loading of the aqueous monomer solution in the microemulsion system, which resulted in a higher polymer yield. However, as shown in Table IV, no polymer was precipitated out in the microemulsion systems until the polymerization temperature reached 60°C, and this could be attributed to the low initiation efficiency of KPS at low temperatures in the microemulsion system containing large amounts of the surfactant. It was also observed that the polymerization rate of MAA was not as rapid as that of AM. The latter only needed a few minutes to achieve a total conversion of the monomer to the polymer in a microemulsion.[7] The polymerization of MAA was slow at the beginning of the reaction, and over a 90% conversion of MAA to PMAA was obtained after 2 h of reaction in our systems (Table IV). It was also observed, from Table IV, that the polymerization rate of MAA increased with the reaction temperature. However, the microemulsions were not stable during polymerization at 70°C as they became slightly opaque.

Effects of the concentrations of the initiator and monomer on the polymerization

The effect of the initiator concentration on the degree of conversion of PMAA was investigated, and the results are summarized in Table V. There was only a 23% conversion obtained when the KPS concentration was 0.56 wt % of the monomer. However, nearly complete conversions were reached when the initiator concentration was larger than 1.01 wt %. There was an initial increase in the molecular weight of the polymers with an increase in the initiator concentration up to 1.01 wt %, and it then decreased with a further increase in the KPS concentration. On the basis of the study of the polymerization of the water-soluble monomer AM in an inverse microemulsion,[1] it is believed that the initiation of the water-soluble monomers occurred in the water pools of the inverse micelles by the free radicals generated from the dissolved initiator in these pools. Hence, the higher the initiator concentration was, the more radicals were produced and the higher the polymerization rate and the degree of conversion were.

The phenomenon of a molecular weight decrease with an increase in the initiator concentration is often the case in conventional inverse emulsion polymerizations of certain acrylic compounds.[22] When more initiator was used, more radicals were captured as the

TABLE V
Effects of KPS on the Degree of Conversion and Molecular Weight of PMAA[a]

	KPS/monomer (wt %)			
	0.56	1.01	2.16	3.19
Degree of conversion (wt %)	22.6	95.9	98.9	100
Molecular weight $\times 10^{-5}$ (g/mol)	1.67	2.97	1.45	1.44

[a] MAA (4.7%) aqueous solution reacted at 60°C for 6 h in the 3/7 w/w Triton-114/cyclohexane microemulsion.

TABLE VI
Effect of the Monomer Concentration on the Conversion and Molecular Weight of MAA[a]

	MAA concentration (wt %)		
	12.5	25	40
Degree of conversion (wt%)	95	100	100
Molecular weight $\times 10^{-5}$ (g/mol)	0.43	1.45	0.74

[a] Polymerization at 60°C for 6 h in the 3/7 w/w Triton-114/cyclohexane microemulsion.

amount of the surfactant was greatly augmented with respect to that in conventional emulsions, and more nucleated particles were produced, resulting in a lowering of the molecular weights of the polymers. However, the lower molecular weight of the polymer made with 0.56 wt % KPS compared with that made with 1.01 wt % was probably due to chain-transfer reactions caused by the large amount of the surfactant, so the growing chains had more chance to terminate the propagation reactions in the microemulsion systems.

The effect of the monomer concentration on the polymerization was also investigated in terms of the molecular weights and the degrees of conversion of the polymers formed in the Triton-114/cyclohexane microemulsion system (Table VI). The polymerization rate increased with the monomer concentration (Fig. 2), and a complete conversion of the monomer to the polymer was observed after polymerization for 4 h for a monomer concentration of 25 wt % and for 8 h for a monomer concentration of 12.5%; this was much slower in comparison with the polymerization of AM in the AOT/toluene microemulsion system. There was an increase in the molecular weights of the polymers with an increase in the monomer concentration, as there was more monomer to take part in the propagation reaction.[1] The molecular weights of the polymer decreased when the monomer concentration increased to 40%, and this was accompanied by an observed phase separation.

The molecular weight of PMAA prepared in the Triton-114 system was rather low compared to that of polyacrylamide (PAM) prepared in a microemulsion with AOT as the surfactant [weight-average molecular weight (M_w) > 1.0×10^6 g/mol].[1] The surfactant, Triton-114, probably was the reason for this result. Triton-114 has hydroxyl groups that may act as chain-transfer sites to terminate chain growth, leading to the observed low molecular weights. This assumption was supported by the result obtained when we used another surfactant, Tween-85, in which the molecular weight of the synthesized PMAA was larger than 4.1×10^5 g/mol. Tween-85 does not have hydroxyl groups in its molecular structure.

The low polymerization rate of the PMAA synthesized in our microemulsion systems was probably related to the very low partitioning of the MAA monomer in the water phase, as discussed previously. Most of the MAA monomer dissolved in the oil phase, and the concentration of the monomer in the water phase was low at the beginning of the polymerization. As a water-soluble initiator, KPS was used in the polymerization; the initiation occurred in the water phase. Then, these radicals propagated by the addition of the monomer in the water phase to form oligomers that were water-soluble. Because acetone was used as the solvent to wash the product, these oligomers were able to dissolve in this polar solvent, and so no product was found after washing for the polymers synthesized for short reaction times. Growing (nucleated) inverse micelles, for further propagation, collected the

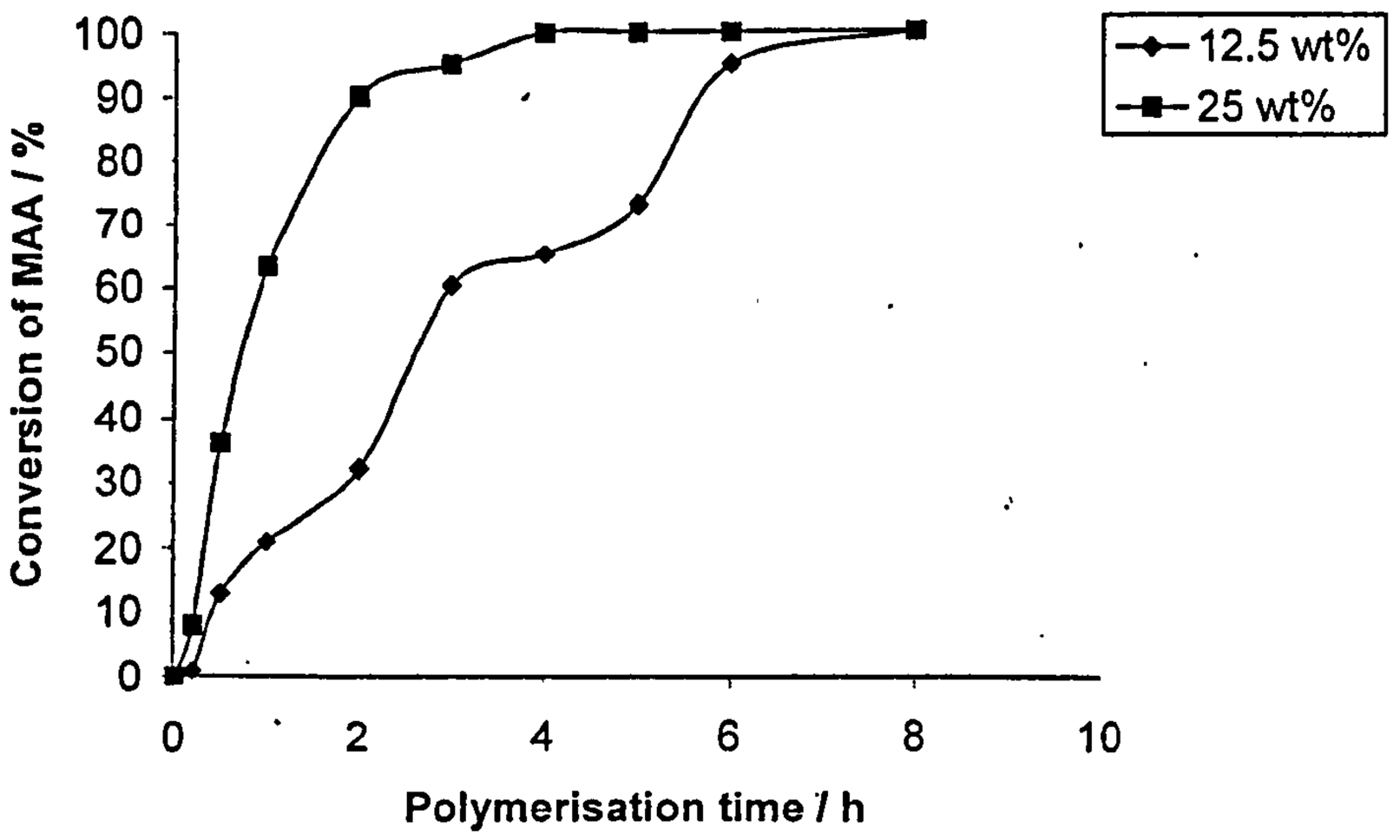

Figure 2 Effect of the monomer concentration on the polymerization rate of MAA in the Triton-114/cyclohexane microemulsion system.

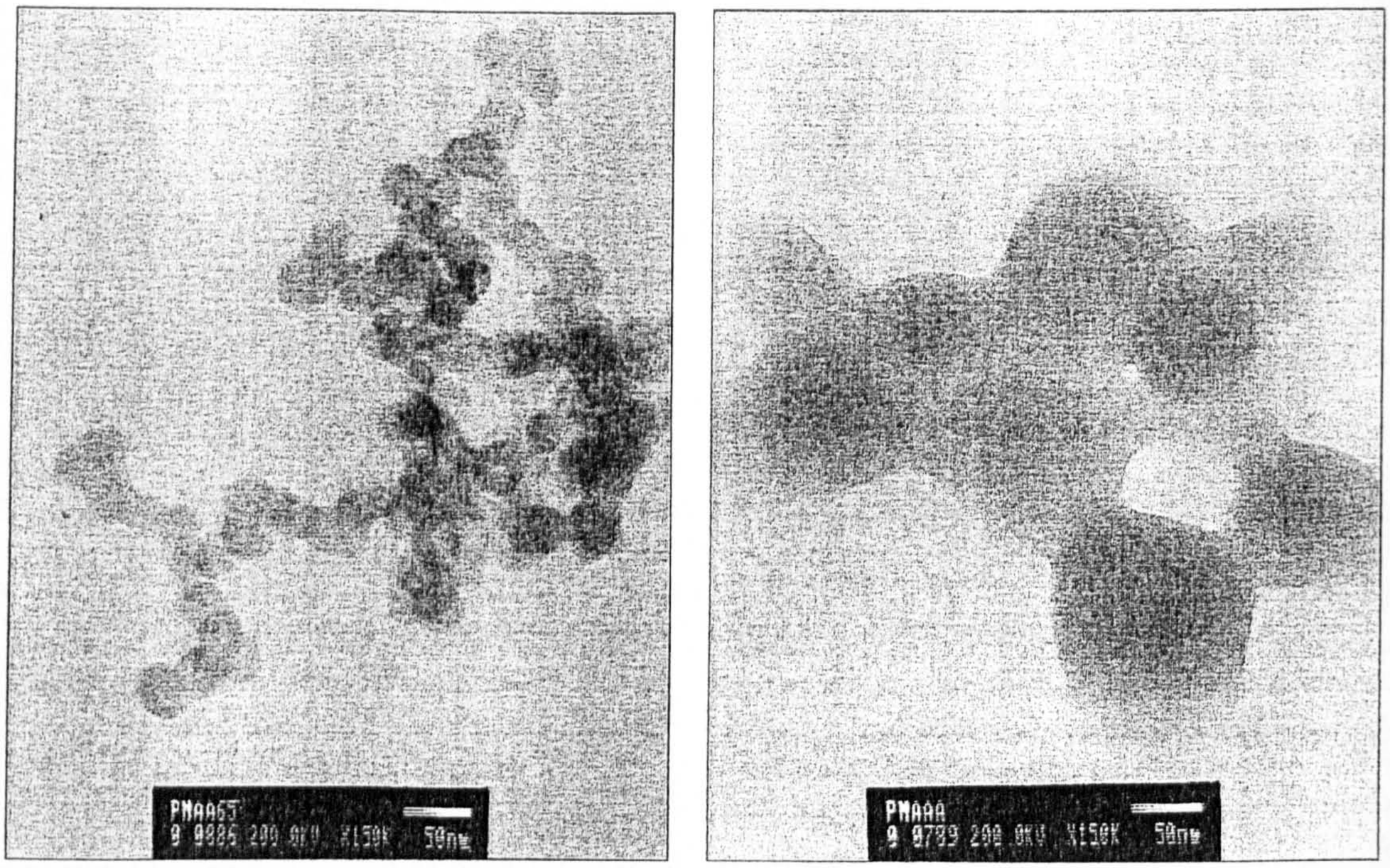

(a) (b)

Figure 3 PMAA nanoparticles prepared via polymerization in the Triton-114/cyclohexane microemulsion with monomer concentrations of (a) 25 and (b) 40 wt %.

monomer from the unnucleated inverse micelles via a micelle collision mechanism or by the diffusion of the monomer through the continuous oil phase to the water phase. However, this monomer feeding rate seemed likely to be slow because of the small partitioning of MAA in the water phase and the cagelike effect of the large amount of the surfactant on the transfer of the monomer. That was why the MAA polymerization rate was lower than that of AM.[7] The dispersability of the monomer from the continuous phase to the disperse phase played a very important role in controlling the polymerization rate.

Morphology of the PMAA particles

Figure 3 shows TEM micrographs of the PMAA synthesized under different reaction conditions. The particles were, in general, spherical and easily aggregated because of the attractions between polar groups. The sizes of the polymer particle were about 30–50 nm [Fig. 3(a)] with a very narrow size distribution when a low monomer concentration (<25 wt %) was used. However, the particle size increased to over 100 nm with a polydisperse size distribution when the polymerization took place at a high monomer concentration [40 wt %; Fig. 3(b)].

CONCLUSIONS

A water-in-cyclohexane microemulsion stabilized by Triton-114 was developed to produce amphiphilic PMAA, which could not be prepared efficiently in an AOT/toluene microemulsion, probably because of a very low partitioning of the MAA monomer in the oil phase and a larger cagelike effect formed by the strong hydrophilic interactions between the polar head groups of AOT. The polymerization rate of the monomer (MAA) in the Triton-114 microemulsion system was slower than that reported[7] for AM in the AOT microemulsion. The polymerization rate and the degree of conversion of the monomer increased with the concentrations of the initiator (KPS) and monomer. The viscosity-average molecular weight of the prepared PMAA was about 1.45×10^5 g/mol, which was rather low compared with that of PAM prepared via an AOT-microemulsion ($M_w > 1.0 \times 10^6$ g/mol). This is probably caused by chain transfer between the surfactant hydroxyl groups and the propagating chains. The PMAA particles were spherical, in general. About 30–50-nm PMAA particles were obtained when low monomer concentrations were used, but the particle sizes increased to over 100 nm at high monomer concentrations.

The authors give special thanks to J. Bates for his help and advice with transmission electron microscopy.

References

1. Polymerization in Organized Media; Paleos, C. M., Ed.; Gordon & Breach: New York, 1992; p 215.

2. Boutonnet, M.; Kizling, J.; Stenius, P.; Marie G. Colloids and Surfaces 1982, 5, 209.
3. Adair, J. H.; Li, T.; Kido, T.; Havey, K.; Moon, J.; Mecholsky, J.; Morrone, A.; Talham, D. R.; Ludwig, M. H.; Wang, L. Mater Sci Eng 1998, 23, 139.
4. Klier, J.; Tucker, C. J.; Kalantar, T. H.; Green, D. P. Adv Mater 2000, 12, 1751.
5. Santra, S.; Tapec, R.; Dobson, N. T.; Hebard, A.; Tan, W. Langmuir 2001, 17, 2900.
6. Barton, J. Prog Polym Sci 1996, 21, 399.
7. Candau, F.; Leong, Y. S. J Polym Sci Polym Chem Ed 1985, 23, 193.
8. Leong, Y. S.; Candau, F. J Phys Chem 1982, 86, 2269.
9. Candau, F.; Leong, Y. S.; Pouyet, G.; Candau, S. J. J Colloid Interface Sci 1984, 101, 167.
10. Carver, M. T.; Dreyer, U.; Knoesel, R.; Candau, F.; Fitch, R. M. J Polym Sci Part A: Polym Chem 1989, 27, 2161.
11. Carver, M. T.; Candau, F.; Fitch, R. M. J Polym Sci Part A: Polym Chem 1989, 27, 2179.
12. Moumen, N.; Pileni, M. P.; Mackay, R. A. Colloids Surf A 1999, 151, 409.
13. Robon, M.; Corpart, J. M.; Selb, J.; Candau, F. J Appl Polym Sci 2002, 84, 1418.
14. Braun, O.; Selb, J.; Candau, F. Polymer 2001, 42, 8499.
15. de Saenz, A.; Buruaga de la Cal, J. C.; Asua, J. M. Polymer 2000, 41, 1260.
16. Glass, J. E. Advances in Chemistry Series 223; American Chemical Society: Washington, DC, 1989; p 113.
17. Meltzer, Y. L. Water-soluble polymers: Developments Since 1978. Noyes Data Corp.: Park Ridge, NJ, 1981; p 41.
18. Victor, S. P.; Sharma, C. P. J Biomater Appl 2002, 17, 125.
19. Lippi, B.; Cerchiara, T.; Bigucci, F.; Orienti, I.; Zecchi, V. Eur J Pharm Biopharm 2003, 55, 199.
20. Schonhoff, M. Curr Opin Colloid Interface Sci 2003, 8, 86.
21. Brandrup, J.; Immergut, E. H.; Grulke, E. A. Abe, A.; Bloch, D. R., Ed.; Polymer Handbook, John Wiley & Sons Inc., New York, 1999.
22. Liu, Z. Ph.D. Thesis, Loughborough University, 1997.

II

STRUCTURES AND PROPERTIES OF SOME CHEMICALS USED

II-1 Surfactants

Name	Structure & Chemical Formula	Properties
AOT	**Dioctyl sulfosuccinate sodium salt** 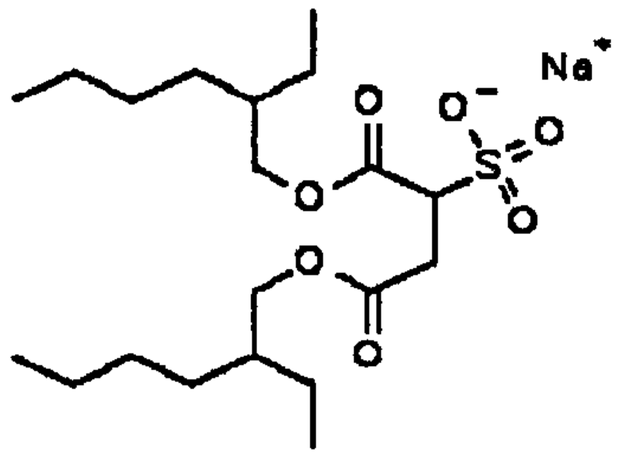	Mol. wt: 444.55 HLB: 40
Tween 85	**Polyoxyethylene (20) sorbitan trioleate** 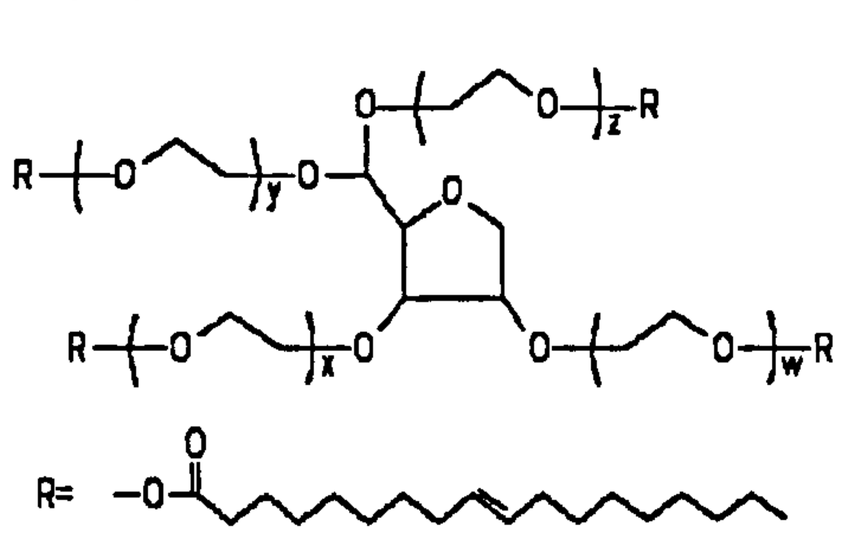	Mol. wt: 1,839 HLB: 11.0
Tween 80	**Polyethylene glycol sorbitan monooleate** 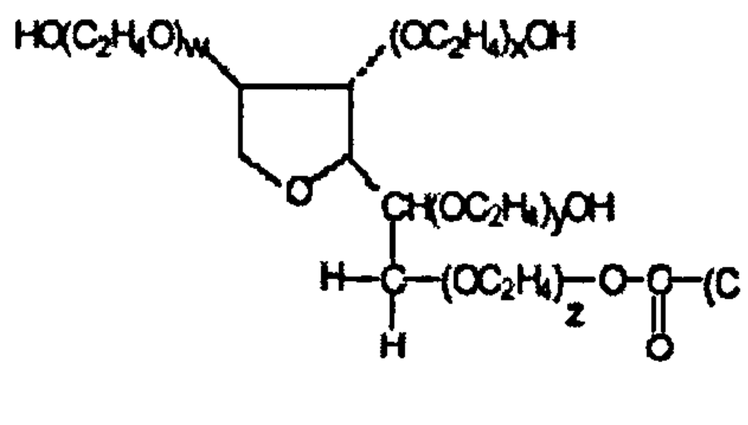 sum of w, x, y, z = 20	Mol. wt: 1,310 HLB: 15.0
Triton X-100	**Polyoxyethylene (10) isooctylphenyl ether** 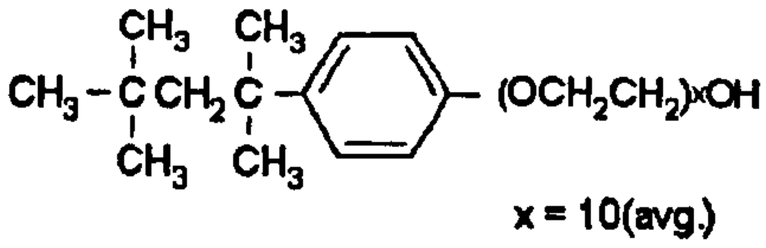 x = 10(avg.)	Mol. wt: 647 HLB: 13.5

Polyethylene (8) glycol tert-octylphenyl ether

Triton X-114

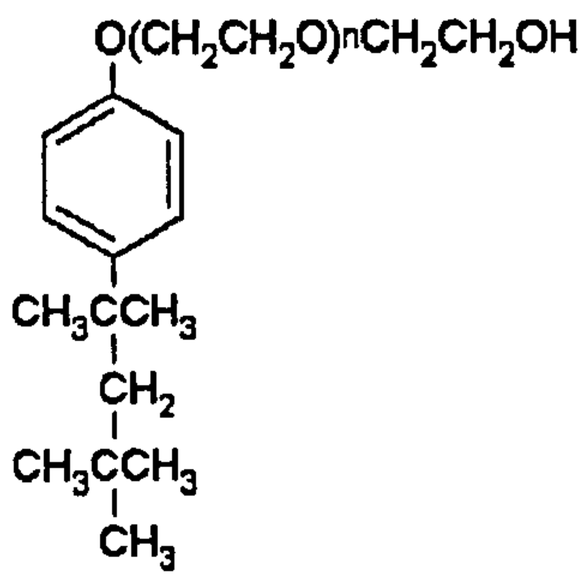

Mol. wt: 637
HLB: 12.4

Polyoxyethylene (5) nonylphenyl ether

Igepal CO-520

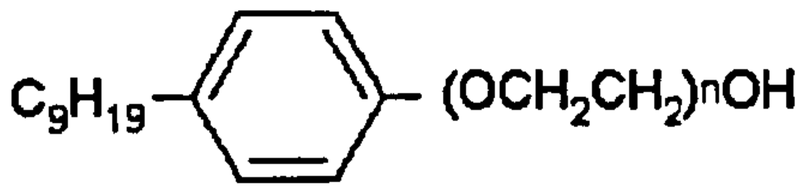

n ~ 5

Mol. wt: 441
HLB: 10.0

Polyoxyethylene (12) nonylphenyl ether

Igepal CO-720

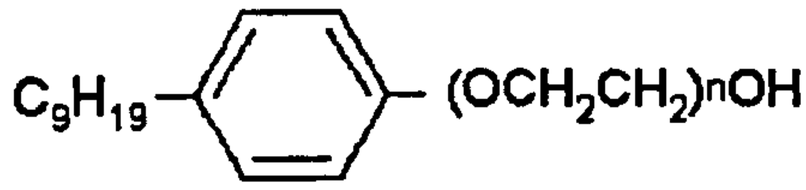

n ~ 12

Mol. wt: 749
HLB: 14.2

Polyoxyethylene (10) oleyl ether

Brij 97

$C_{18}H_{35}(OCH_2CH_2)_nOH$

n ~ 10

Mol. wt: 709
HLB: 12.4

II-2 Co-surfactants

Name	Chemical Formula	Properties
1-Propanol	$CH_3CH_2CH_2OH$	Mol. wt: 60.10 BP: 97°C
1-Butanol	$CH_3CH_2CH_2CH_2OH$	Mol. wt: 74.12 BP: 116-118°C
1-Pentanol	$CH_3(CH_2)_3CH_2OH$	Mol. wt: 88.15 BP: 136-139 °C

2-Pentanol	$CH_3CH_2CH_2CHOHCH_3$	**Mol. wt: 88.15** **BP: 119-121 °C**
1-Hexanol	$CH_3(CH_2)_5OH$	**Mol. wt: 102.18** **BP: 156.5 °C**
1-Octanol	$CH_3(CH_2)_7OH$	**Mol. wt: 130.2** **BP: 193-195 °C**

II-3 Solvents

Name	Structure & Chemical Formula	Properties
Cyclohexane	C_6H_{12} 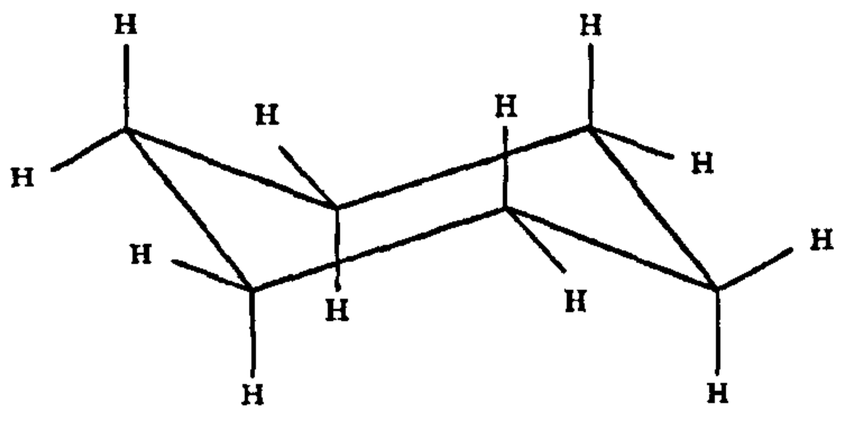	**Mol. wt: 84.16** **BP: 80.7°C**
Isooctane	C_8H_{18} 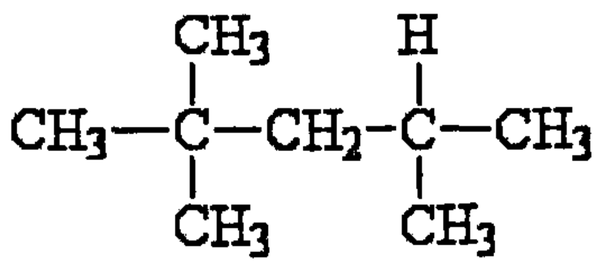	**Mol. wt: 114.23** **BP: 99 °C**
Petroleum Ether	Hydrocarbon	**Mol wt: 87-114** **BP: 20-75 °C**
Toluene	C_7H_8 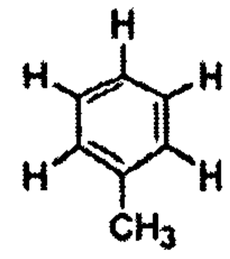	**Mol wt: 92.14** **BP: 110.6 °C**
Acetone	CH_3COCH_3 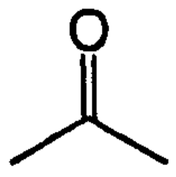	**Mol wt: 58.09** **BP: 56.3 °C**

Ethanol	C_2H_6O 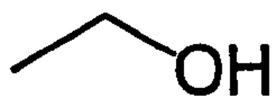	**Mol wt: 46.07** **BP: 78.4 °C**
Chloroform	$CHCl_3$ 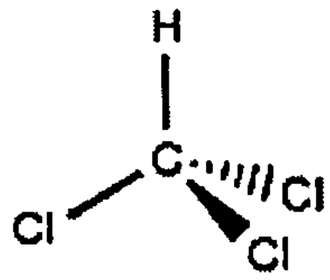	**Mol wt: 119.4** **BP: 62 °C**

II-4 Chemicals

Name	Structure & Chemical Formula	Properties
Tetraethylorthosilicate	$(C_2H_5)_4SiO_4$	**Mol wt: 208.33**
Acrylamide	C_3H_5NO 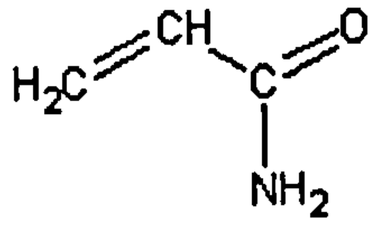	**Mol wt: 71.08**
Methacrylic acid	$C_4H_6O_2$ 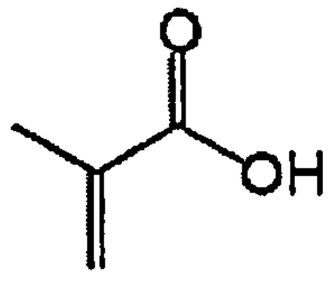	**Mol wt: 86.06**
N, N'-methylene-bis-acrylamide	$(H_2C{=}CHCONH)_2CH_2$	**Mol wt: 154.16** **Slightly soluble in water**
Azobisisobutyronitrile	$C_8H_{12}N_4$ 	**Mol wt: 164.24**
Azobiscycloheane-1-carbonitrile	$C_{14}H_{20}N_4$ 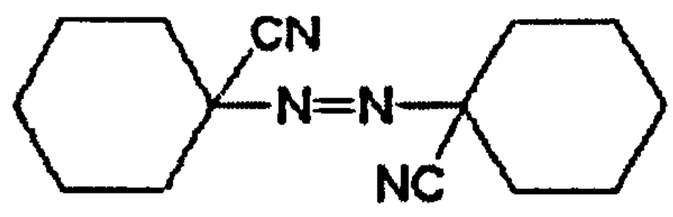	**Mol wt: 244.34** **soluble in toluene, benzene, insoluble in water**

III

CHARACTERISTIC VALUES OF IRON OXIDE SAMPLES

Table III-1 Samples prepared by precipitation from different starting materials at 25°C.

Sample	Intensity %	D spacing	Angle	Identification
$[Fe]^{2+}$	100	2.53238	35.6	Fe_3O_4
	34.7	1.47856	62.8	
	31.0	2.95811	30.2	
	27.8	1.61017	57.2	
	23.8	2.09361	43.2	
$[Fe]^{3+}:[Fe]^{2+}=1:9$	100	2.52848	35.5	Fe_3O_4
	49.7	2.10112	43.0	
	38.3	2.96093	30.2	
	38.3	1.48398	62.5	
	27.2	1.61273	57.1	
$[Fe]^{3+}:[Fe]^{2+}=1:2$	100	2.53264	35.6	Fe_3O_4
	37.4	1.47914	62.8	
	36.6	2.95799	30.2	
	30.6	1.60969	57.2	
	20.0	2.08923	43.3	
$[Fe]^{3+}:[Fe]^{2+}=1:1$	100	2.53057	35.6	Fe_3O_4
	45.4	1.47638	62.9	
	34.3	2.95738	30.2	
	29.5	1.60732	57.3	
	23.2	2.09208	43.2	
$[Fe]^{3+}:[Fe]^{2+}=2:1$	100	2.52558	35.7	Fe_3O_4
	36.6	1.47584	62.9	
	32.2	2.95313	30.2	
	29.7	1.60571	57.3	
	19.3	2.08811	43.3	
$[Fe]^{3+}:[Fe]^{2+}=3:2$	100	2.52730	35.6	Fe_3O_4
	44.3	1.47937	62.8	
	42.4	2.96614	30.1	
	41.4	2.08858	43.3	
	33.5	1.60853	57.2	

Table III-2 Iron oxide samples prepared by precipitation at different ripening temperatures for 2 hours.

Sample	Intensity %	D spacing	Angle	Identification
25 °C	/	/	/	Fe_3O_4
40°C	100	2.53222	35.4	Fe_3O_4
	59.5	1.48398	62.5	
	55.8	1.60853	57.2	
	52.5	2.96093	30.2	
	42.2	2.08858	43.3	
60 °C	100	2.53222	35.4	Fe_3O_4
	52.2	1.48282	62.6	
	51.8	2.96093	30.2	
	48.6	1.61133	57.1	
	43.4	2.09358	43.2	
90 °C	100	2.53180	35.4	Fe_3O_4
	55.1	1.47895	62.8	
	46.7	1.61508	57.0	
	39.4	2.96283	30.1	
	37.8	2.09546	43.1	

Table III-3 Iron oxide samples prepared by precipitation in different ripening times at 25°C.

Sample	Intensity	D spacing	Angle	Identification
25°C 2h	/	/	/	Fe_3O_4
25°C 12h	100	2.53098	35.4	Fe_3O_4
	55.3	1.48167	62.6	
	43.5	1.61695	56.9	
	38	2.96614	30.1	
	34	2.09108	43.2	
25°C 24h	100	2.52558	35.7	Fe_3O_4
	36.6	1.47584	62.9	
	32.2	2.95313	30.2	
	29.7	1.60571	57.3	
	19.3	2.08811	43.3	

Table III-4 Iron oxide samples prepared by precipitation in different ripening times at 60 °C

Sample	Intensity	D spacing	Angle	Identification
60°C 2h	/	/	/	Fe_3O_4
60°C 12h	100	2.52474	35.5	Fe_3O_4
	44.6	1.48282	62.6	
	44.2	2.95574	30.2	
	35.8	1.70552	53.7	
	35.6	1.61695	56.9	
60°C 24h	100	2.52150	35.6	γ-Fe_2O_3
	89.2	2.95023	30.4	
	86.1	1.47984	62.7	
	85.9	1.61302	57.1	
	82.6	1.70505	53.7	

Table III-5 Iron oxide samples prepared by precipitation in different ripening times at 90 °C

Sample	Intensity	D spacing	Angle	Identification
90°C 2h	/	/	/	Fe_3O_4
90°C 12h	100	2.51009	35.6	γ-Fe_2O_3
	87.9	1.47123	62.8	
	86	2.95117	30.3	
	85.2	1.60929	57.2	
	83.1	1.70525	53.7	
90°C 24h	100	2.51566	35.7	γ-Fe_2O_3
	88.5	1.47378	62.9	
	86.1	2.94749	30.3	
	84.6	1.60729	57.3	
	83.7	1.70561	53.7	

Table III-6 Iron oxide samples prepared by precipitation followed by hydrothermal at different temperatures for 12 hours.

Samples	Intensity	D spacing	Angle	Identification
No hydrothermal	/	/	/	Fe_3O_4
120°C	100	2.51360	35.7	γ - Fe_2O_3
	56.9	1.47588	62.9	
	50.2	2.94796	30.3	
	46.9	1.60859	57.2	
	43.8	2.09428	43.2	

140°C	100	2.51722	35.6	γ - Fe_2O_3
	39.3	1.47856	62.8	
	36.7	2.95002	30.3	
	36.0	1.61042	57.2	
	22.1	2.09315	43.2	
160°C	100	2.52431	35.5	γ - Fe203 & α - Fe203
	41.3	1.48120	62.7	
	33.5	2.96532	30.1	
	32.0	1.60924	57.2	
	22.2	2.08343	43.4	
200°C	100	2.69611	33.2	α - Fe203
	92.4	2.51783	35.6	
	50.4	1.69422	54.1	
	46.2	1.84052	49.5	
	42.4	1.48203	62.6	

Table III-7 Iron oxide samples prepared via w/o microemulsion system followed by hydrothermal in different temperatures for 12 hours.

Samples	Intensity	D spacing	Angle	Identification
No hydrothermal	/	/	/	Fe_3O_4
120°C	100	2.51140	35.7	γ - Fe_2O_3
	49.8	1.47473	63.0	
	43.2	2.95832	30.2	
	38.9	1.61139	57.1	
	31.2	1.70091	53.9	
140°C	100	2.70921	33.0	α - Fe_2O_3
	83.3	2.52032	35.6	
	63	3.68974	24.1	
	51.9	2.20113	41.0	
	50	1.81412	49.5	
160°C	100	2.70011	33.2	α – Fe_2O_3
	82.9	2.51325	35.7	
	62.6	1.69731	54.0	
	44.5	1.83902	49.5	
	43.1	3.66734	24.3	
200°C	100	2.70404	33.1	α - Fe_2O_3
	90	3.06810	29.1	
	76.2	2.52435	35.5	
	53.4	1.83527	50.0	

Table III-8 Iron oxide samples prepared by precipitation after hydrothermal at 120°C with different aging times.

Sample	Intensity	D spacing	Angle	Identification
No hydrothermal	/	/	/	Fe_3O_4
2 Hr	100	2.52102	35.6	
	51.0	1.47948	62.8	
	38.5	1.60803	57.2	γ-Fe_2O_3
	36.3	2.95056	30.3	
	34.3	2.09839	43.1	
12 Hr	/	/	/	γ-Fe_2O_3
24 Hr	100	2.52102	35.6	
	46.3	1.47937	62.8	
	32.9	1.61273	57.1	γ-Fe_2O_3
	31.0	2.96614	30.1	
	29.1	2.09860	43.1	
96 Hr	100	2.52474	35.5	
	56.7	1.48277	62.6	
	49.5	2.95313	30.2	γ-Fe_2O_3
	32.4	2.09178	43.2	
	29.7	1.61420	57.0	

Table III-9 Iron oxide samples prepared via precipitation process followed by calcinations with different temperatures.

Sample	Intensity	D spacing	Angle	Identification
140°C	100	2.51169	35.7	
	48.5	1.47394	63.0	
	42.3	2.93984	30.4	Fe_3O_4
	27.8	1.60353	57.4	
	20.4	2.08302	43.4	
200°C	100	2.51438	35.7	
	38.3	1.47446	63.0	
	36.6	2.94194	30.2	Fe_3O_4
	30.3	1.60484	57.4	
	20.3	2.08641	43.3	
250°C	100	2.51952	35.6	
	40.1	1.47664	62.9	
	35.7	2.94991	30.3	γ-Fe_2O_3
	32.6	1.60791	57.2	
	22.2	2.08750	43.3	
300°C	100	2.51113	35.7	
	68.1	1.47360	63.0	
	56.7	2.94796	30.3	γ-Fe_2O_3
	45.6	1.60303	57.4	
	34.3	2.07688	43.5	

	100	2.51232	35.7	
	55.8	1.47360	63.0	
400°C	42.6	2.08679	43.3	γ-Fe_2O_3
	40.0	1.60442	57.4	
	35.5	1.70091	53.9	
	100	2.50943	35.8	
	80.3	2.69154	33.3	
450°C	50.9	1.69124	54.2	α-Fe_2O_3
	41.6	1.48216	62.6	
	29.1	3.66920	24.2	
	100	2.69580	33.2	
	80.6	2.51416	35.7	
500°C	46.8	1.69335	54.1	α-Fe_2O_3
	41.9	3.67571	24.2	
	37.1	1.83844	49.5	

Table III-10 Iron oxide samples prepared via precipitation with different starting materials followed by calcination at 300°C.

Sample	Intensity	D spacing	Angle	Identification
	100	2.51208	35.7	
	36.5	2.94694	30.3	
$[Fe]^{2+}$	32	1.47384	63.0	γ-Fe_2O_3
	22.4	1.60433	57.4	
	17.4	2.08442	43.4	
	100	2.51463	35.7	
	34.9	2.69628	33.2	
$[Fe]^{3+}$:$[Fe]^{2+}$=1:2	31.4	1.47372	63.0	α-Fe_2O_3
	28.3	2.94983	30.3	
	26	1.60493	57.4	
	100	2.51009	35.7	
	39.9	1.47245	63.1	
$[Fe]^{3+}$:$[Fe]^{2+}$=1:1	34.6	2.93984	30.4	Fe_3O_4
	29.4	1.60377	57.4	
	18.3	2.07834	43.5	
$[Fe]^{3+}$:$[Fe]^{2+}$=2:1	/	/	/	γ-Fe_2O_3
	100	2.51804	35.6	
	66.9	2.69899	33.2	
$[Fe]^{3+}$	43.9	1.45287	64.0	α-Fe_2O_3
	33.6	2.19891	41.0	
	30.5	1.69173	54.2	